Université de Montréal

Genèse de l'immunopeptidome du CMH de classe I

par
Etienne Caron

Thèse présentée à la faculté de médecine
en vue de l'obtention du grade de Philosophiae Doctor
en sciences biomédicales

Avril 2011

Université de Montréal
Faculté des études supérieures

Cette thèse intitulée :

Genèse de l'immunopeptidome
du CMH de classe I

présentée par :

Etienne Caron

a été évaluée par un jury composé des personnes suivantes :

Jacques Thibodeau, Ph.D.
président-rapporteur

Claude Perreault, M.D., F.R.C.P. (C)
directeur de recherche

Pierre Thibault, Ph.D.
co-directeur de recherche

Stephen Michnick, Ph.D., F.R.S.C. (UK)
membre du jury

Anne-Claude Gingras, Ph.D.
examinateur externe

Michel Desjardins, Ph.D.
représentant du doyen

RÉSUMÉ

La différentiation entre le « soi » et le « non-soi » est un processus biologique essentiel à la vie. Les peptides endogènes présentés par les complexes majeurs d'histocompatibilité de classe I (CMH I) représentent le fondement du « soi » pour les lymphocytes T CD8+. On donne le nom d'immunopeptidome à l'ensemble des peptides présentés à la surface cellulaire par les molécules du CMH I. Nos connaissances concernant l'origine, la composition et la plasticité de l'immunopeptidome restent très limitées. Dans le cadre de cette thèse, nous avons développé une nouvelle approche par spectrométrie de masse permettant de définir avec précision : la nature et l'abondance relative de l'ensemble des peptides composant l'immunopeptidome. Nous avons trouvé que l'immunopeptidome, et par conséquent la nature du « soi » immun, est surreprésenté en peptides provenant de transcrits fortement abondants en plus de dissimuler une signature tissu-spécifique. Nous avons par la suite démontré que l'immunopeptidome est plastique et modulé par l'activité métabolique de la cellule. Nous avons en effet constaté que les modifications du métabolisme cellulaire par l'inhibition de mTOR (de l'anglais *mammalian Target Of Rapamycin*) provoquent des changements dynamiques dans la composition de l'immunopeptidome. Nous fournissons également la première preuve dans l'étude des systèmes que l'immunopeptidome communique à la surface cellulaire l'activité de certains réseaux biochimiques ainsi que de multiples événements métaboliques régulés à plusieurs niveaux à l'intérieur de la cellule. Nos découvertes ouvrent de nouveaux horizons dans les domaines de la biologie des systèmes et de l'immunologie. En effet, notre travail de recherche suggère que la composition de l'immunopeptidome est modulée dans l'espace et le temps. Il est par conséquent très important de poursuivre le développement de méthodes quantitatives au niveau des systèmes qui nous permettront de modéliser la plasticité de l'immunopeptidome. La simulation et la prédiction des variations dans l'immunopeptidome en réponse à différents facteurs cellulaires intrinsèques et extrinsèques seraient hautement pertinentes pour la conception de traitements immunothérapeutiques.

MOTS CLÉS : complexe majeur d'histocompatibilité, immunopeptidome, spectrométrie de masse, plasticité, mTOR

ABSTRACT

Self/non-self discrimination is a fundamental requirement of life. Endogenous peptides presented by major histocompatibility complex class I (MHC I) molecules represent the essence of self for CD8 T lymphocytes. These MHC I peptides (MIPs) are collectively referred to as the immunopeptidome. Very little is known about the origin, composition and plasticity of the immunopeptidome. Here, we developed a novel high-throughput mass spectrometry approach that yields an accurate definition of the nature and relative abundance of peptides presented by MHC I molecules. Surprisingly, we found that the immunopeptidome, and therefore the nature of the immune self, is biased toward peptides derived from highly abundant transcripts and conceals a tissue-specific signature. Then, we showed that the immunopeptidome is plastic and moulded by cellular metabolic activity. In fact, we found that altering cellular metabolism via the inhibition of the mammalian target of rapamycin (mTOR) results in dynamic changes in the cell surface MIPs landscape. Importantly, we provide the first systems-level evidence that the immunopeptidome projects at the cell surface a faithful representation of biochemical networks and metabolic events regulated at multiple levels inside the cell. Our discoveries open up new perspectives in systems biology and immunology. Indeed, our work suggests that the composition of the immunopeptidome is modulated in space and time. Therefore, it is imperative to further develop and exploit systems-level quantitative methods that will enable modelling of the immunopeptidome's plasticity. Simulating and predicting variations in the immunopeptidome in response to cell-intrinsic and -extrinsic factors could be relevant to numerous contexts, including the rational design of immunotherapeutic interventions.

KEYWORDS : major histocompatibility complex, immunopeptidome, mass spectrometry, plasticity, mTOR

TABLE DES MATIÈRES

LISTE DES FIGURES

CHAPITRE 1: Introduction

CHAPITRE 2: The structure and location of SIMP/STT3B account for its prominent imprint on the MHC I immunopeptidome

LISTE DES TABLEAUX

CHAPITRE 5: A comprehensive map of the mTOR signaling network

CHAPITRE 6: Discussion

LISTE DES ABRÉVIATIONS ET DES SYMBOLES

ABC	ATP-Binding Cassette transporter
ADN	Acide désoxyribonucléique
APC	Anaphse-promoting complex
AQUA	Absolute QUAntification
ARNm	Acide ribonucléique messager
ATF6	Activating transcription factor 6
ATP	Adénosine 5'-triphosphate
BioGrid	Biological general repository for interaction datasets
BIP	Immunoglobulin Binding Protein
c-CBL	Casitas B-lineage lymphoma
cCET	Cellules corticales épithéliales thymiques
CCR7	Chemokine (C-C motif) receptor 7
CCT	Chaperonin containing TCP1
Cdc48	Cell division cycle 48
CID	Collision-Induced Dissociation
CLIP	Class II associated Invariant chain Peptide
CMH I	Complexes majeurs d'histocompatibilité de classe I
CMH II	Complexes majeurs d'histocompatibilité de classe II
CPA	Cellule présentatrice d'antigène
Da	Dalton
DALIS	Dendritic cell Aggresome Like Induced Structures
DAVID	Database for Annotation, Visualization and Integrated Discovery
Derlin-1	Der1-like domain family, member 1
dNIC	deuterium-labeled nicotinoyloxy succinimide
DRiPs	Defective ribosomal products
E1	Ubiquitin activating enzyme
E2	Ubiquitin conjugating enzyme
E3	Ubiquitin ligase
E4	Ubiquitin chain assembly factor
EDEM	ER Degradation-Enhancing alpha-Mannosidase-like
eeF	Eukaryotic translation elongation factor
EGD	Enhancer of Gal4p DNA binding
eIF1A	Eukaryotic translation initiation factor 1A
eIF2	Eukaryotic translation initiation factor 2
eIF3	Eukaryotic Initiation factor 3
Eps1	ER protein with chaperone and co-chaperone activity
ERAAP/ERAP1	Endoplasmic reticulum aminopeptidase 1
ERAD	Endoplasmic Reticulum-Associated Degradation

ESI	Electrospray ionization
FT-ICR	Fourier-transform ion cyclotron resonance
Glc	Glucose
HECT	Homology to E6-AP C-terminus
HIV	Human immunodeficiency virus
HLA	Human Leucocyte Antigen
HSP	Heat Shock Protein
ICAT	Isotope-Coded Affinity Tag
IFI-6-16	Interferon, alpha-inducible protein 6
IFNγ	Interferon-γ
Int	Open source resource for molecular interaction data
IRE1	Inositol-requiring enzyme-1
iTRAQ	Isobaric Tag for Relative and Absolute Quantitation
JAK	Janus kinase
kDa	Kilodalton
LAP	Leucine aminopeptidase
Li	Chaîne invariante
LMP10	Proteasome subunit, beta type, 10
LMP2	Proteasome subunit, beta type, 9
LMP7	Proteasome subunit, beta type 8
LTQ	Linear trap quadupole
m/z	Mass-charge ratio
MALDI	Matrix-assisted laser desorption/ionization
Man	Mannose
MECL1	Proteasome subunit, beta type, 10
MINT	Molecular interaction database
MS	Mass spectrometry
MS/MS	Tandem mass spectrometry
MSC	Multi-Synthetase Complex
mTOR	mammalian target of rapamycin
Nac	N-acetyl cysteine
nanoLC	nano-liquid chromatography systems
NicNHS	Nicotinoyloxy succinimide
PA28	Proteasome (prosome, macropain) activator subunit
PAMP	Pathogen-Associated Molecular Patterns
PCR	Polymerase chain reaction
PDI	Protein Disulphide Isomerase

PERK	Eukaryotic translation initiation factor 2 alpha kinase 3
PLD	Protéine lentement dégradée
PRD	Protéine rapidement dégradée
PRR	Pattern-Recognition Receptors
PSMB10	Proteasome subunit, beta type, 10
PSMB8	Proteasome subunit, beta type 8
PSMB9	Proteasome subunit, beta type, 9
Q-q-Q	Triple quadrupole mass spectrometer
Q-q-TOF	Quadrupole time-of-flight-mass spectrometer
RCT	Récepteur des cellules T
RE	Réticulum endoplasmique
RING	Really Interesting New Gene
ROC1	Ring-box 1, E3 ubiquitin protein ligase
Rpt1	19S proteasome regulatory subunit Rpt1
SCF	Skp, Cullin, F-box
Sec61	Protein transport protein Sec61
SILAC	Stable Isotope Labelling by Amino acids in Cell culture
SIMP	Source of immunodominant MHC associated peptides
STITCH	Search Tool for Interactions of Chemicals
STRING	Search Tool for the Retrieval of Interacting Genes
STT3B	Oligosaccharyl transferase subunit STT3B
TAA	Tumor-associated antigen
TAP	Transporter associated with Antigen Processing
Th1	T helper 1
Th2	T helper 2
TLR	Toll-Like Receptor
TNF	Tumor necrosis factor
TOP	Thymet Oligopeptidase
TPPII	Tripeptidyl Peptidase II
Ubc1p	Ubiquitin-conjugating enzyme
UFR	Unusual folding regions
UPR	Unfolded protein response
UTR	Untranslated region
VBC	VHL-elongin, B-elongin, C-elongin
VCP	Valsolin Containing Protein
VDJ	Variable, Diverse, and Joining gene segments

À ma mère Chantal

À mon père Gilles

REMERCIEMENTS

Tout d'abord, je tiens à dire toute ma gratitude à Claude Perreault qui a eu la bienveillance de m'accueillir au sein de son équipe de recherche. Merci de nous avoir fait partager vos précieuses connaissances durant toutes ces années. Merci pour toute la liberté d'action que vous m'avez accordée. Cette liberté m'a permis de développer ma confiance, mon indépendance et ma créativité. Merci pour vos conseils avisés, vos sages proverbes et les merveilleuses opportunités que vous m'avez offertes. Grâce à vous, la recherche est devenue pour moi une véritable passion. Je vous en serai toujours reconnaissant.

Je remercie également mon codirecteur Pierre Thibault. Notre collaboration durant toutes ces années s'est avérée particulièrement fructueuse et je vous en suis pleinement reconnaissant. Vous et Claude m'avez ouvert les yeux sur l'immense richesse du travail multidisciplinaire et sur l'univers de la biologie des systèmes. Pour moi, ce fut une véritable révélation qui aura indéniablement modifié ma vision de la recherche et m'aura fait entrevoir nombre de nouvelles perspectives. Merci pour votre appui dans mes décisions et pour avoir grandement contribué à mon cheminement.

Je tiens à remercier Sébastien Lemieux, Philippe Roux, Hiroaki Kitano, Samik Gosh et Yukiko Matsuoka qui ont été de précieux collaborateurs dans l'achèvement de cette thèse. Merci pour vos utiles conseils et pour avoir pris le temps de partager votre expertise.

Merci également à Stephen Michnick d'avoir pris le temps de discuter du projet mTOR à diverses reprises avec moi. Merci pour votre aide lors de l'organisation du symposium en biologie des systèmes à l'IRIC. Nos quelques conversations auront eu une influence positive sur mes choix et mon cheminement.

En plus de mon directeur Claude Perreault et de mon codirecteur Pierre Thibault, je voudrais remercier cordialement les membres du jury, Jacques Thibodeau, Nathalie Labrecque, Stephen Michnick et Anne-Claude Gingras pour avoir accepté d'évaluer ma thèse. Je tiens également à exprimer mes remerciements à Michel Bouvier et Michel

Desjardins pour avoir siégé dans mes comités de formation. Je sais que votre temps est précieux et j'apprécie à sa juste valeur l'intérêt que vous me témoignez.

Je remercie les organismes subventionnaires qui m'ont permis de vivre pleinement durant mes études graduées, notamment les Instituts de Recherche en Santé du Canada (IRSC) et la fondation Cole.

Je voudrais également remercier tous les membres du laboratoire de Claude que j'ai côtoyé durant toutes ces années. Vous avez tous eu, de près ou de loin, une influence positive sur ma vie. J'ai tissé des liens d'amitié avec plusieurs d'entre vous et je vous en remercie. Un grand merci aux membres de l'équipe des « immunopeptidomeux » avec qui j'ai eu le bonheur de travailler : Diana, Danielle, Marie-Hélène, Krystel, Marie-Pierre, Grégory, Alexandre et Tara. Merci pour votre amitié, pour nos conversations enrichissantes et pour nos quelques « trippes » de vie (… saut en parachute!). Merci à Sylvie pour nos conversations philosophiques en salle de culture! Merci également à Caro pour ton humour, ton écoute, ta simplicité et ta « folie ».

Je souhaite également remercier tous ceux qui ont contribué à l'organisation et au succès du symposium sur la biologie des systèmes en immunologie et cancérologie (SysBio 2009). Un gros merci principalement à Martin Giroux, Jonas Dorn, Martin Sauvageau, Dariel Ashton-Beaucage, Marieke Rozendaal, Joëlle Mauffette et Michel Aubé.

Merci aux employés de l'administration de l'IRIC et M. Robert Turgeon en particulier, de m'avoir offert d'appréciables opportunités. Merci Robert de m'avoir fait partager ta passion de la multidisciplinarité.

Merci à Benoit Bolduc avec qui j'ai étudié l'anglais pendant près de deux ans. Ta passion pour l'enseignement a transformé mon apprentissage de l'anglais en une véritable expérience de vie. Avec toi, j'ai non seulement amélioré mon anglais, mais j'ai acquis des outils qui me permettent aujourd'hui de dépasser mes propres limites. Merci Ben!

J’aimerais remercier toute ma famille et mes amis pour leurs encouragements et leur intérêt pour mes études graduées. Votre soutien est très important pour moi. Merci pour votre présence dans ma vie.

J’adresse enfin mes plus vifs remerciements à ma tendre moitié et future épouse Valeria de Azcoitia. Merci pour ton grand coeur, tes encouragements, ton support inconditionnel, ta sagesse et ta formidable énergie. Merci d’enrichir ainsi ma vie au quotidien.

CHAPITRE 1

1. INTRODUCTION

1.1 HISTORIQUE : L'ORIGINE DE L'IMMUNOLOGIE

Les plus anciens témoignages connus d'observations d'ordre immunologique datent de 430 avant Jésus-Christ. À cette date, pendant l'épidémie de fièvre typhoïde qui sévit à Athènes durant la guerre du Péloponnèse, l'historien Thucydide nota que seules les personnes ayant déjà supporté et survécu à l'infection étaient aptes à s'occuper des malades.

Aux alentours de 6000 avant Jésus-Christ, il existait en Chine des pratiques de transmission volontaire de la variole dans un but de prévention. Cette technique, appelée « variolisation », consiste à prélever du pus sur un malade peu atteint par la maladie pour l'inoculer avec une aiguille à un sujet sain. Ce procédé se répandit à partir du quinzième siècle, notamment en Chine, en Inde et en Turquie. Par l'entremise de l'épouse de l'ambassadeur britannique à Constantinople, qui fit vacciner son fils de cette manière, la variolisation s'est fait connaître en Angleterre vers 1722, puis s'est propagée dans les années suivantes dans toute l'Europe.

À la même époque, le médecin de campagne Edward Jenner (Figure 1) constatait que les fermières en contact régulier, lors de la traite, avec la variole de la vache (vaccine ou *Cowpox*) qui est inoffensive pour les humains, étaient épargnées par les épidémies de variole ou ne montraient que de faibles symptômes. Après avoir minutieusement étudié le phénomène, il préleva le 14 mai 1796 du pus sur une pustule d'une jeune fille contaminée par la vaccine, et l'injecta à un jeune garçon de huit ans. Après que le garçon eut guéri de la maladie bénigne induite par la vaccine, Jenner lui injecta de la variole véritable. Le garçon surmonta également cette infection sans présenter de symptômes sérieux. Comparé à la variolisation, le procédé de Jenner offrait des avantages majeurs : les sujets qui avaient reçu de la vaccine ne présentaient pas les boutons et les cicatrices typiques induites habituellement par la variolisation; il n'y avait en outre, aucun risque de mortalité contrairement à la variolisation; et les personnes vaccinées ne représentaient aucun risque

de contagion. Le virus de la vaccine est à l'origine des noms de « vaccin » et « vaccination », et Edward Jenner est considéré aujourd'hui comme le fondateur de l'immunologie (Texte adapté de http://fr.wikipedia.org/wiki/Immunologie).

Figure 1. Edward Jenner, fondateur de l'immunologie.

1.2 L'IMMUNITÉ INNÉE ET ACQUISE

Le terme immunité réfère à tous mécanismes utilisés par l'organisme permettant de discriminer le « soi » du « non-soi » (Roitt, 1990). Ces mécanismes forment un système complexe procurant à l'organisme une protection contre les agents pathogènes étrangers tels que les virus, les bactéries, les levures et les champignons. Le système immunitaire est généralement divisé en deux grands sous-systèmes : l'immunité innée (ou *non spécifique*) et l'immunité acquise (ou *spécifique*).

1.2.1 L'immunité innée

L'immunité innée constitue la première ligne de défense contre les envahisseurs de l'environnement. L'immunité innée est conférée par un ensemble d'éléments physiques et chimiques présents chez l'individu dès la naissance. Ces éléments incluent les surfaces corporelles et leurs composantes internes, ainsi que le réflexe de toux. Le pH et la sécrétion d'acide gras constituent aussi des barrières chimiques contre l'invasion de plusieurs microorganismes. De nombreuses composantes internes caractérisent également le système immunitaire inné : la fièvre, l'interféron ainsi que plusieurs autres substances libérées par les granulocytes, les lymphocytes et les monocytes/macrophages. Certaines protéines sériques telles que la bêta-lysine, l'enzyme lysozyme, les polyamines et les kinines représentent également des éléments de l'immunité innée. Toutes ces composantes affectent directement les agents pathogènes ou encore stimulent l'efficacité du système immunitaire pour l'élimination de ces agents. L'immunité innée inclut également les cellules phagocytaires telles que les granulocytes, les macrophages et les cellules microgliales du système nerveux central. Tous ces éléments participent à la destruction et l'élimination des éléments étrangers ayant franchi les barrières physiques et chimiques de l'organisme (Coico et al, 2009).

1.2.2 L'immunité acquise

Le système immunitaire adaptatif, également nommé « immunité acquise », permet à l'organisme de riposter de façon spécifique aux menaces des antigènes étrangers. Cette immunité repose sur la sélection de clones lymphocytaires capables de cibler les antigènes étrangers. La réponse adaptative est lente, strictement dépendante des antigènes, et possède une mémoire immunitaire. Le système immunitaire adaptatif est divisé en deux catégories : la réponse immunitaire à médiation humorale et la réponse immunitaire à médiation cellulaire. On retrouve au sein de chacune de ces réponses un type de cellules spécialisées qui reconnaît spécifiquement un antigène particulier. Les lymphocytes B ont pour fonction de produire les immunoglobulines (ou anticorps) afin d'assurer la réponse à médiation humorale. Les lymphocytes T, préalablement activés par les cellules

présentatrices d'antigènes professionnelles (CPAs), assurent la réponse à médiation cellulaire (Paul, 2008).

1.2.2.1 Les cellules de la réponse à médiation cellulaire

Les cellules de la réponse à médiation cellulaire proviennent des cellules souches pluripotentes hématopoïétiques de la moelle osseuse (Figure 2). Ces cellules se différencient éventuellement en précurseurs lymphoïdes et myéloïdes. Ces précurseurs sont à l'origine des cellules de la réponse à médiation cellulaire incluant les cellules T, les monocytes/macrophages et les cellules dendritiques (Paul, 2008).

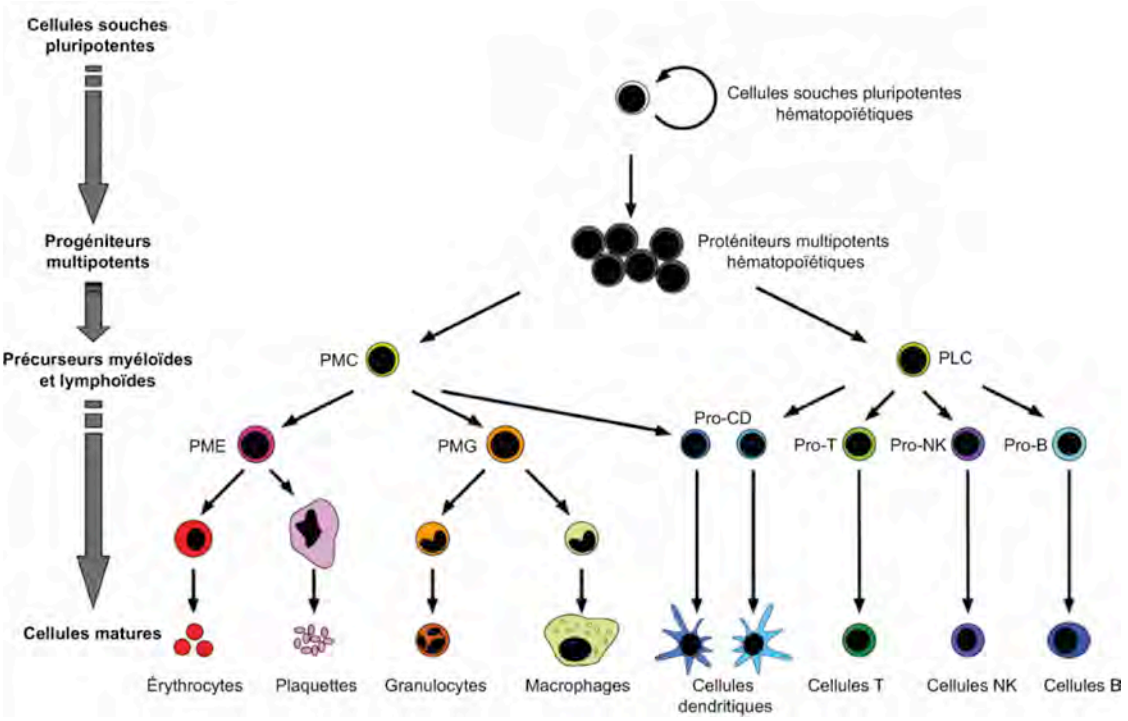

Figure 2. Hiérarchie des cellules hématopoïétiques. PMC, progéniteur myéloïde commun; PLC, progéniteur lymphoïde commun; PME, progéniteur mégakaryocyte-érythroïde; PMG, progéniteur macrophage-granulocyte; CD, cellule dendritique. Tiré de (Larsson & Karlsson, 2005).

1.2.2.1.1 Les lymphocytes T

Le développement des lymphocytes T se fait au niveau du thymus. Dans cet organe lymphoïde primaire, les lymphocytes T subissent une première étape de maturation et de prolifération (Silverstein, 1995). Tôt, durant leur développement, les loci codant pour les récepteurs des cellules T (RCTs) sont génétiquement réarrangés dans les domaines VDJ. Ces réarrangements engendrent des populations très diversifiées de RCTs (Lin & Desiderio, 1995). Les lymphocytes T qui comportent des RCTs auto-immuns ou silencieux sont éliminés par des mécanismes de sélection (Owen et al, 1990). La sélection des lymphocytes T se fait en deux étapes : la sélection positive et la sélection négative. La sélection positive se fait au niveau du cortex thymique. Cette sélection assure la survie des lymphocytes T possédant des RCTs capables d'interagir avec le CMH des cellules corticales épithéliales (Werlen et al, 2003). Les lymphocytes T qui n'interagissent pas avec les molécules du CMH sont éliminés par manque de signaux de survie. À ce stade de leur développement, les cellules T sélectionnées positivement peuvent réagir contre des antigènes/peptides du « soi » ou du « non-soi ». Les cellules qui réagissent trop fortement avec les peptides du « soi » sont néfastes pour l'organisme et entrainent le développement de réponses auto-immunes. Le rôle de la sélection négative est d'éliminer ces cellules hyperréactives (Nossal, 1994). La sélection négative s'effectue entre la zone corticale et la médulla du thymus (Fairchild & Austyn, 1990). Les lymphocytes T qui survivent à cette deuxième étape de sélection quittent le thymus et migrent vers les organes lymphoïdes secondaires. Les cellules T sortant du thymus sont des lymphocytes T naïfs. Les lymphocytes T naïfs prolifèrent et se différencient en lymphocytes T effecteurs suite à la rencontre d'un peptide du « non-soi » présenté par les CPAs. Les lymphocytes T sont divisés en deux grandes classes : les lymphocytes T CD4+ et les lymphocytes T CD8+.

1.2.2.1.1.1 Les lymphocytes T CD4+

Les cellules T CD4+ sont des médiateurs de la réponse immunitaire adaptative. Elles régulent les facettes de la réponse immunitaire à médiation humorales et cellulaires. Les cellules T CD4+ sont divisées en deux classes : les « T helper 1 » (Th1) et « T helper 2 » (Th2) (Annacker et al, 2001). L'activation des lymphocytes T CD4+ se fait suite à

l'interaction soutenue du complexe RCT-CD4-CD3 du lymphocyte et d'un peptide antigénique présenté par le CMH II à la surface d'une CPA (Figure 3) (Konig, 2002; Wang & Reinherz, 2002). Les lymphocytes T CD4+ effecteurs sécrètent des molécules qui stimulent les fonctions phagocytaires des macrophages (Th1) et/ou activent les lymphocytes B à produire des anticorps (Th2). Les lymphocytes CD4+ Th1 régulent donc la facette de la réponse immunitaire à médiation cellulaire alors que les lymphocytes CD4+ Th2 régulent la facette de la réponse immunitaire à médiation humorale (Romagnani, 1999).

1.2.2.1.1.2 Les lymphocytes T CD8+

Les lymphocytes T CD8+ cytotoxiques sont impliqués dans la réponse immunitaire adaptative à médiation cellulaire. Les lymphocytes T CD8+ effecteurs sont activés par l'interaction soutenue du complexe RCT-CD8-CD3 du lymphocyte et d'un peptide antigénique présenté par le CMH I à la surface d'une cellule cancéreuse ou infectée par un pathogène (Figure 3) (Masopust & Ahmed, 2004; Vallejo et al, 2004). Cette activation mène à la sécrétion de molécules toxiques (ex. Perforine) nécessaires à la destruction des cellules cibles. Les lymphocytes T CD8+ ont un rôle essentiel dans la protection de l'organisme contre les virus, les bactéries intracellulaires et l'élimination de cellules tumorales. Suivant l'élimination des cellules cibles, 90 à 95 % des lymphocytes T CD8+ effecteurs meurent par apoptose. Une petite fraction des lymphocytes T effecteurs survivent et se différencient en cellule mémoire, permettant ainsi à l'organisme de se défendre plus efficacement lors d'une réinfection (Crotty & Ahmed, 2004; Sprent & Surh, 2002).

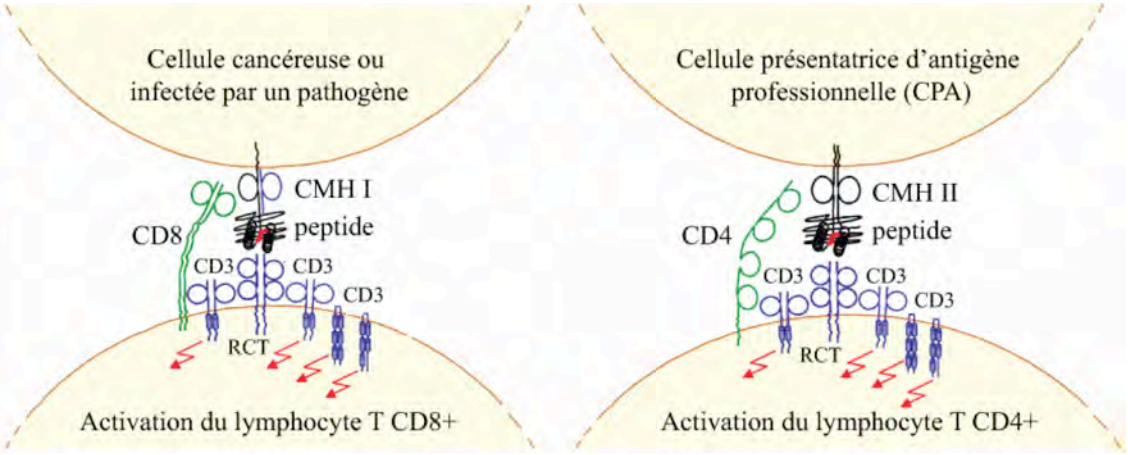

Figure 3. Représentation des complexes trimoléculaires RCT/peptide/CMH, des corécepteurs CD3 et des protéines associées CD4 et CD8 du lymphocyte T. Le cas du CMH I présentant un peptide antigénique au RCT d'un lymphocyte T CD8+ cytotoxique est schématisé par la figure de gauche. Le cas du CMH II présentant un peptide antigénique au RCT d'un lymphocyte T CD4+ auxiliaire (ou helper) est schématisé par la figure de droite. Le RCT interagit avec le peptide, mais aussi avec les domaines α1 et α 2 du CMH I ou avec les domaines α1 et β1 du CMH II. Le complexe CMH-peptide correspond à l'association d'une protéine du complexe majeur d'histocompatibilité avec un peptide. CD3 sont des corécepteurs participant à la transduction du signal de reconnaissance du complexe CMH-peptide au lymphocyte T. CD4 et CD8 sont des corécepteurs stabilisant les complexes RCT/peptide/CMH en réalisant des liaisons avec la région constante α1 du CMH I ou β2 du CMH II. Tiré de http://www.imgt.org/.

1.2.2.1.2 Les macrophages

Les macrophages sont des cellules infiltrant les tissus. Ils proviennent de la différenciation des monocytes (Bancroft et al, 1994; Paul, 2008). Les monocytes et les macrophages sont des phagocytes, c'est-à-dire des cellules capables de phagocytose. Ils participent à l'immunité innée en tant que défense non spécifique, mais participent également à l'immunité adaptative par le phénomène d'*opsonisation*. Leur rôle est de phagocyter les débris cellulaires et les pathogènes. La phagocytose est déclenchée par l'activation des récepteurs de reconnaissance des patrons PRRs (de l'anglais *Pattern-Recognition Receptors*). Lorsqu'un macrophage phagocyte un pathogène, la vésicule intracellulaire formée est nommée *Phagosome*. Le phagosome fusionne au lysosome. Les enzymes lysosomiales et les radicaux libres de l'oxygène (notamment l'hypochlorite) tuent et dégradent le pathogène. Après avoir dégradé un pathogène, un macrophage peut se comporter en CPA, c'est-à-dire présenter un peptide antigénique par les CMH II de manière à stimuler un lymphocyte T CD4+. La présentation de peptides antigéniques aux

lymphocytes T CD4+ est primordiale et permet de faire le pont entre la réponse immunitaire innée et adaptative.

Les macrophages sont attirés vers le lieu d'une inflammation par chimiotactisme. Les signaux d'appel sont constitués de différents stimuli provenant de cellules endommagées (par nécrose ou *apoptose*), de pathogènes, et de produits libérés (c.-à-d. histamine, chimiokines et cytokines) par les cellules présentes au niveau du site inflammatoire. La durée de vie d'un macrophage est de plusieurs mois. Comme il s'agit de cellules complètement différenciées, elles ne se divisent pas (Paul, 2008).

1.2.2.1.3 Les cellules dendritiques

Les cellules dendritiques sont des CPAs qui présentent dans certaines conditions, comme leur nom l'indique, des dendrites (Steinman & Witmer, 1978). Les cellules dendritiques ont deux fonctions principales : 1) le déclenchement de la réponse immunitaire adaptative par l'activation des lymphocytes T naïfs contre des peptides antigéniques du « non-soi » et, 2) le maintien de la tolérance centrale au « soi » dans le thymus par le processus de la sélection négative (Guermonprez et al, 2002).

En périphérie, les cellules dendritiques immatures détectent la présence de signaux inflammatoires et de motifs moléculaires microbiens ou « PAMP » (de l'anglais *Pathogen-Associated Molecular Patterns*) (Kapsenberg, 2003). Cette reconnaissance se fait par des PRRs comme les TLRs (de l'anglais *Toll-Like Receptor*). La réception de ces signaux, constituant des signaux de maturation, provoque une augmentation transitoire de l'activité phagocytaire; l'antigène est alors internalisé par phagocytose ou macropinocytose, dégradé et présenté sous forme de peptides antigéniques par les molécules du CMH.

Suite à la capture de l'antigène, les cellules dendritiques subissent un processus de maturation caractérisé par : 1) un changement de morphologie permettant la motilité de la cellule ainsi qu'une interaction accrue avec les lymphocytes, 2) une perte de la capacité à phagocyter, 3) l'augmentation de la capacité à présenter efficacement le peptide

antigénique (augmentation de l'expression du CMH et des molécules de costimulation telles que CD80, CD86, CD40) et, 4) l'acquisition de capacités migratoires. Les capacités migratoires sont liées à la modification de l'expression en surface des récepteurs des chemokines, notamment du récepteur CCR7, qui entraine la migration par chimiotactisme vers les organes lymphoïdes secondaires (Guermonprez et al, 2002).

1.3 LA PRÉSENTATION ANTIGÉNIQUE

Le développement d'une réponse immunitaire adaptative nécessite la présentation à la surface cellulaire de peptides antigéniques issus de protéines endogènes ou exogènes. Ces peptides sont respectivement présentés par les molécules du CMH I et II aux récepteurs des lymphocytes T CD8+ et CD4+ (Figure 3). Les molécules du CMH jouent un rôle essentiel dans la réponse immunitaire adaptative de tous les gnathostomes (vertébrés pourvus d'une mâchoire).

Les travaux d'Emil Unanue et Howard Grey, au début des années 1980, démontrent qu'une protéine exogène endocytée et dégradée représente la source des peptides antigéniques reconnus par les lymphocytes T CD4+ (Allen et al, 1984; Shimonkevitz et al, 1983). Quelques années plus tard, Alain Townsend et ses collaborateurs démontrent qu'une protéine endogène virale synthétisée et dégradée à l'intérieur d'une cellule infectée représente la source des peptides reconnus par les lymphocytes T CD8+ (Townsend et al, 1988; Townsend et al, 1986a; Townsend et al, 1985; Townsend et al, 1986b). Ces travaux pionniers sont à la base des voies dites classiques de la présentation antigénique par les molécules du CMH I et II.

1.3.1 La présentation des peptides endogènes par les CMH I

Les molécules du CMH I sont exprimées à la surface de presque toutes les cellules nucléées chez les vertébrés à mâchoires. La génération des peptides est initiée suivant la dégradation des protéines sources par le *protéasome* (Rock et al, 2002). Les peptides générés sont transloqués dans le réticulum endoplasmique (RE), associés aux molécules

du CMH I et exportés à la surface cellulaire (Figure 4) (Hammer et al, 2007b; Heemels & Ploegh, 1995; Pamer & Cresswell, 1998; Zhang & Williams, 2006). La présentation de peptides endogènes du « non-soi » (d'origine microbienne ou virale) ou du « soi » altéré (d'origine tumorale) par le CMH I est essentielle pour l'élimination des cellules anormales par les lymphocytes CD8+ effecteurs (Wong & Pamer, 2003). La voie de présentation des peptides antigéniques par les CMH I permet ainsi de communiquer l'état de santé des cellules de l'organisme aux lymphocytes T CD8+.

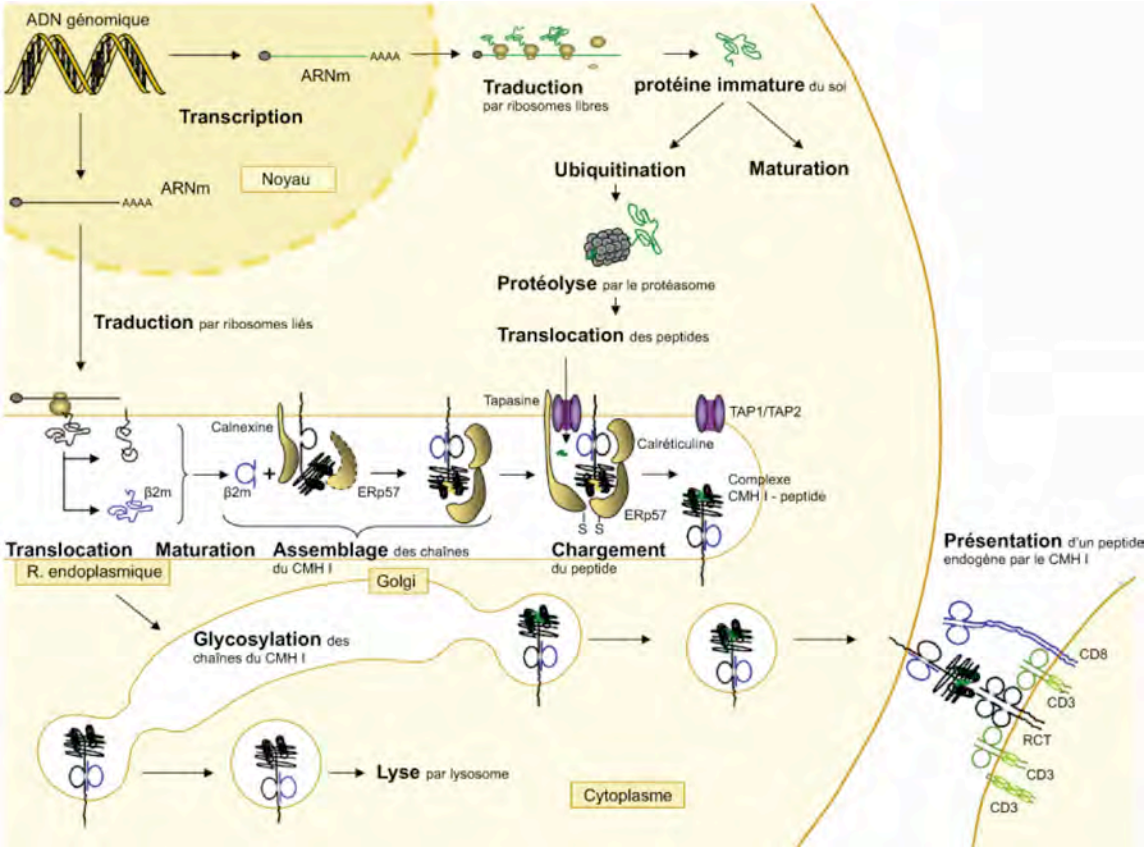

Figure 4. Voie classique de présentation antigénique par les CMH I. Étapes de la présentation d'un peptide endogène du « soi » par une molécule du CMH I au récepteur T d'un lymphocyte T CD8+. Tiré de http://www.imgt.org/.

En absence d'infection, les molécules du CMH I sont uniquement associées aux peptides du « soi ». Les peptides du « soi » jouent plusieurs rôles vitaux : ils sont nécessaires au développement des cellules T dans le thymus (Huseby et al, 2005; Starr et al, 2003), ils transmettent des signaux de survie aux lymphocytes T CD8+ matures en périphérie (Marrack & Kappler, 2004), ils amplifient les réponses contre les pathogènes intracellulaires (Anikeeva et al, 2006), ils sont responsables de l'immunosurveillance des

cellules néoplasiques (Dunn et al, 2004) et ils influencent le choix du partenaire sexuel (Leinders-Zufall et al, 2009; Slev et al, 2006). Les peptides du « soi » associés aux molécules du CMH I sont également impliqués dans de nombreuses pathologies. Ils sont en effet la cible des lymphocytes T auto-réactifs initiant les maladies auto-immunes et des lymphocytes T allo-réactifs provoquant le rejet de greffe et la maladie du greffon contre l'hôte (Liblau et al, 2002; Perreault et al, 1990).

1.3.1.1 Gènes, localisation chromosomique et structure des CMH I

Les molécules du CMH I sont divisées en deux sous-classes : les CMH I conventionnelles (CMH Ia) et les non-conventionnelles (CMH Ib). Chez l'humain, les molécules du CMH sont nommées HLA (de l'anglais *Human Leucocyte Antigen*). Six gènes localisés sur le chromosome 6 (6p21.3) codent pour différents allèles du CMH Ia (HLA-A, HLA-B et HLA-C) et du CMH Ib (HLA-E, HLA-F et HLA-G). Les molécules HLAs sont hautement polymorphiques. Près de 4721 allèles HLA sont présentement connus (1519 pour HLA-A, 2069 pour HLA-B et 1016 pour HLA-C; http://www.ebi.ac.uk/imgt/ hla/stats.html, mars 2011). Chez la souris, six gènes localisés sur le chromosome 17 (17p18.43 à 17p20.43) codent pour les molécules du CMH Ia (H2-K, H2-L et H2-D) et du CMH Ib (H2-Q, H2-M et H2-T).

Chaque gène du CMH I code pour une glycoprotéine transmembranaire : la chaîne lourde α. La chaîne lourde est composée de trois domaines : α1, α2 et α3 (Figure 5A) (Bjorkman et al, 1987). La chaîne lourde se lie de manière non covalente à la β2-microglobuline (β2m). Les molécules du CMH Ia et du CMH Ib chez l'humain et la souris ont de grandes similarités structurales. Leur structure se caractérise par la présence d'un sillon au niveau des domaines α1 et α2 (Figure 5B). Ce sillon au fond irrégulier est composé de 8 feuillets β et 2 hélices α (Bjorkman et al, 1987; Garrett et al, 1989; Madden et al, 1991). Généralement, le sillon des molécules du CMH I possède 6 poches de liaison. Ces poches de liaison sont hautement polymorphiques en termes de taille, de forme et de propriétés électrochimiques (Rudolph et al, 2006).

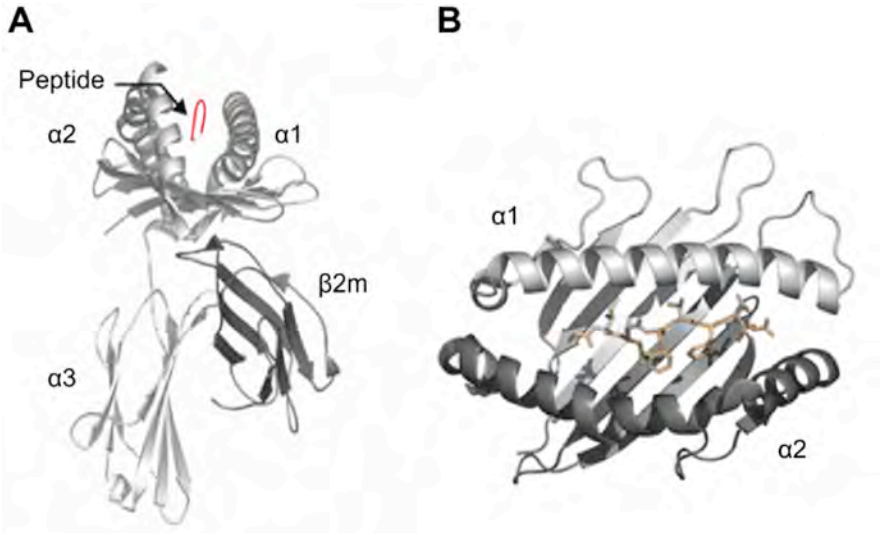

Figure 5. Représentation de la structure cristallographique du CMH I. (**A**) Les domaines α1, α2 et α3 de la chaîne lourde, la β2m et un peptide sont illustrés. (**B**) Sillon du CMH I présentant un peptide. La structure du sillon conditionne la taille des peptides antigéniques présentés, mais aussi le nombre et la localisation des liaisons entre les acides aminés du sillon et ceux des peptides. Les sites de liaison peptidique dans le sillon sont également nommés « sites de contact » ou « poche d'ancrage ». La stabilité du complexe CMH I-peptide dépend de ces sites de contact. Tiré de (Berman et al, 2000).

1.3.1.2 Les caractéristiques des peptides associés aux CMH I

Les peptides associés aux molécules du CMH I sont généralement d'une longueur variant entre 8 et 11 acides aminés (Madden et al, 1991; Rotzschke & Falk, 1991). Chaque allèle du CMH lie un ensemble spécifique de peptides. Les peptides spécifiques pour un allèle en particulier sont constitués d'acides aminés identiques ou fonctionnellement similaires. Ces acides aminés sont situés à des endroits bien précis dans la séquence peptidique. Ils correspondent aux résidus d'ancrage, ce qui permet aux peptides de s'associer aux sites de contact (ou poches d'ancrage) dans le sillon du CMH (Figure 5 et 6). L'ensemble de ces résidus d'ancrage constitue le motif de liaison du CMH. Les motifs de liaison ont été identifiés par l'équipe de Hans-Georg Rammensee en 1991 (Falk et al, 1991). En 1992, l'arrivée de la spectrométrie de masse dans le domaine propulse le séquençage des peptides, et par conséquent le raffinement des motifs de liaison (Hunt et al, 1992). Généralement, les résidus d'ancrage sont localisés à la position 2 et à l'extrémité C-terminale du peptide (Figure 6). Exceptionnellement, un de ces résidus est situé en position 3 de la molécule HLA-A*01 (DiBrino et al, 1993) et en position 5 de la molécule

HLA-B*08, $H2K^b$ et $H2D^b$ (Falk et al, 1991). Chez la souris, les peptides liant par exemple l'allèle $H2D^b$ ont comme résidus d'ancrage une asparagine en position 5 et une méthionine, isoleucine ou leucine à l'extrémité C-terminale du peptide (Rammensee et al, 1993). Des résidus d'ancrages auxiliaires peuvent également stabiliser la liaison du peptide à l'intérieur du sillon de certains CMH (Kondo et al, 1997; Kubo et al, 1994; Rammensee et al, 1999; Ruppert et al, 1993). D'autres exemples de résidus d'ancrage pour quelques allèles HLA sont illustrés à la Figure 6.

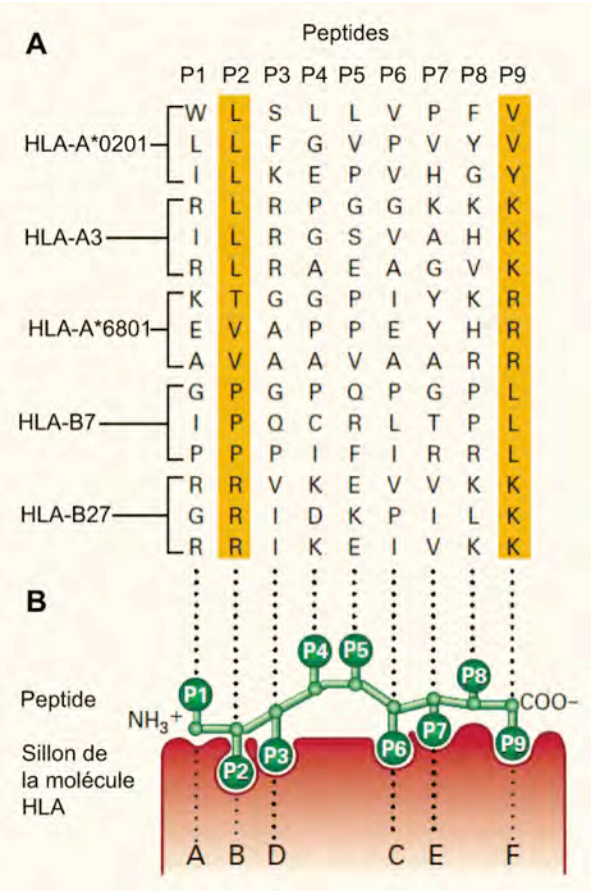

Figure 6. Interactions entre des molécules HLA et différents peptides. (**A**) Exemples de motifs de liaison. Les nonamères illustrés forment des complexes avec les molécules HLA de classe I indiquées. Les résidus d'ancrage sont surlignés avec la couleur orange. (**B**) Section longitudinale du sillon d'une molécule HLA de classe I liant un peptide. Les résidus composant le peptide (P1 à P9) lié à l'intérieur de la poche d'ancrage de la molécule HLA sont orientés vers le haut ou vers le bas. Une molécule HLA de classe I possède 6 poches d'ancrage (A à F). Deux ou trois sites de contact dans le sillon (généralement B et F) déterminent la spécificité du peptide lié. Des sites auxiliaires peuvent également stabiliser la liaison du peptide (D, C et E). Les acides aminés suivants sont illustrés : alanine (A), cystéine (C), acide aspartique (D), acide glutamique (E), phénylalanine (F), glycine (G), histidine (H), isoleucine (I), lysine (K), leucine (L), proline (P), glutamine (Q), arginine (R), serine (S), thréonine (T), valine (V), tryptophane (W) et tyrosine (Y). Tiré de (Klein & Sato, 2000).

Plusieurs centaines de peptides spécifiques pour les différents allèles du CMH sont maintenant répertoriés à travers différentes bases de données (Peters et al, 2005; Rammensee et al, 1999). La découverte de ces motifs a rapidement mené au développement d'algorithmes permettant de prédire la liaison et l'affinité des peptides pour différents allèles du CMH (Rotzschke et al, 1991). Plusieurs outils de prédiction sont maintenant publiquement disponibles (De Groot, 2006; Peters et al, 2006; Rammensee et al, 1999). Notre capacité de prédire les peptides présentés par les molécules du CMH représente un thème de recherche actif dans le domaine de la vaccinologie (Moise & De Groot, 2006; Moutaftsi et al, 2006; Sette & Rappuoli, 2010).

Bien que la vaste majorité des ligands associés aux CMH I soient de petits peptides canoniques dont la longueur varie entre 8 et 11 acides aminés, certains peptides contiennent des acides aminés modifiés. Plusieurs modifications post-traductionnelles ont été identifiées sur des peptides associés aux CMH I et II (Engelhard et al, 2006). Parmi les peptides du CMH I, ces modifications incluent la O-glycosylation (Haurum et al, 1999), l'acétylation (Zamvil et al, 1986), la phosphorylation sur une sérine ou une thréonine (Zarling et al, 2000), la déamidation (Skipper et al, 1996), la méthylation (Yague et al, 2000) et la cystéinylation (Meadows et al, 1997). Les modifications post-traductionnelles peuvent améliorer l'efficacité de présentation de certains peptides. Par exemple, certaines évidences démontrent qu'un phosphopeptide contenant des résidus d'ancrage sous-optimal peut être présenté par HLA-A*02 grâce à l'effet stabilisateur du groupement phosphate (Mohammed et al, 2008). L'analyse cristallographique révèle que ce groupement phosphate en position 4 du peptide peut compenser les interactions plus faibles à l'intérieur du sillon. L'identification des phosphopeptides est un domaine prometteur en immunothérapie puisque les lymphocytes T CD8+ ont la capacité de discriminer les peptides phosphorylés des peptides non phosphorylés *in vivo* (Andersen et al, 1999; Zarling et al, 2000; Zarling et al, 2006).

1.3.1.3 La voie de présentation classique des peptides endogènes associés aux CMH I

1.3.1.3.1 L'ubiquitination des protéines

La présentation classique des peptides par les CMH I débute lorsque les protéines endogènes sont reconnues et dégradées par le système ubiquitine-protéasome (Yewdell et al, 2003). Deux caractéristiques sont requises pour la dégradation de la grande majorité des protéines : la conjugaison de plusieurs molécules d'ubiquitine et la présence d'une région non structurée dans la protéine (Prakash et al, 2004). L'ubiquitination est une réaction dépendante de l'ATP nécessitant l'activité de trois classes de protéines : une E1, E2 et E3 (Figure 7) (Hershko et al, 1983). La E1 ou enzyme d'activation de l'ubiquitine est la protéine située la plus en amont dans le système. Cette enzyme active l'ubiquitine dans une réaction dépendante de l'ATP. L'ubiquitine est ensuite transférée sur une des E2 ou enzymes de conjugaison de l'ubiquitine. La réaction finale de transfert de l'ubiquitine sur le substrat est catalysée par les E3 ou ubiquitine ligases. Les E3 sont les enzymes responsables de la spécificité de la réaction d'ubiquitination. Ces enzymes interagissent à la fois avec une E2 et le substrat.

Les E3 sont globalement classées en deux groupes : les ligases à domaine HECT et les ligases à domaine RING (Pickart, 2001; Pickart & Eddins, 2004). Ces domaines interagissent spécifiquement avec les E2. Les séquences des E3 autres que ces domaines servent à lier directement ou indirectement le substrat. Les E3 reconnaissent un motif, un signal précis sur leur substrat généralement nommé *Dégron*. Le domaine HECT (de l'anglais *Homologous to E6-AP Carboxy-Terminus*) est responsable de la réaction d'ubiquitination. Ce domaine possède une cystéine conservée nécessaire pour la création d'un lien covalent thioester avec l'ubiquitine (Scheffner et al, 1995). Aucune évidence n'indique que le domaine RING (de l'anglais *Really Interesting New Gene*) forme ce type de lien covalent avec l'ubiquitine. Le domaine RING pourrait toutefois faciliter l'interaction entre le substrat et l'ubiquitine liée aux E2 (Borden, 2000). Les E3 ligases à domaine RING sont monomériques ou multimériques. Elles sont par conséquent sous-divisées en plusieurs sous-familles. Les E3 monomériques (ex. c-CBL) possèdent une région interagissant directement avec le substrat. À l'opposé, les E3 multimériques

(ex. ROC1) doivent s'associer avec d'autres protéines pour former les complexes SCF (Skp, Cullin, F-box), VBC (VHL-elongin, B-elongin, C-elongin) ou APC (anaphse-promoting complex). Ces complexes permettent aux E3 multimériques d'interagir avec leur substrat.

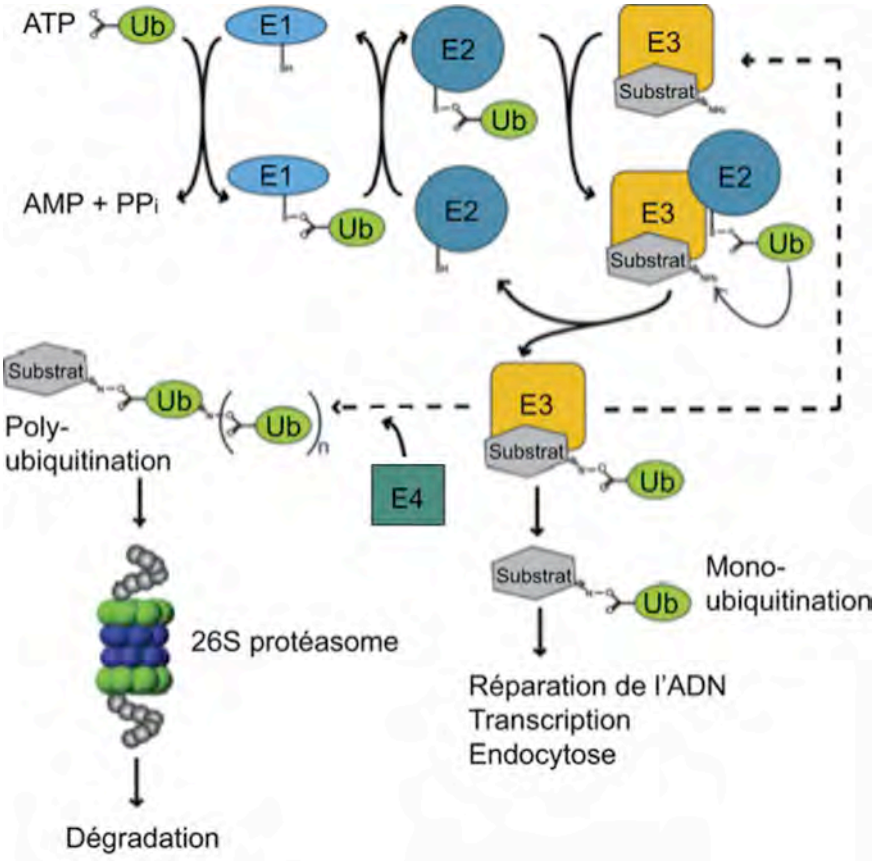

Figure 7. La réaction d'ubiquitination. L'ubiquitination est activée par l'action de la E1 ou enzyme d'activation de l'ubiquitine. L'activation de l'ubiquitination requiert de l'ATP et génère un intermédiaire thioester entre une cystéine de la E1 et la région C-terminale de l'ubiquitine. L'ubiquitine est ensuite transférée sur une E2 ou enzyme de conjugaison de l'ubiquitine. Avec une E3 ou ubiquitine ligase, l'ubiquitine est transféré sur le substrat. La polyubiquitination nécessite l'activité d'une E4 ou enzyme de polymérisation de l'ubiquitine. Tiré de http://faculty.ucr.edu/~karinel/index.html.

Généralement, la polyubiquitination des protéines requière seulement les enzymes E1, E2 et E3. Cependant, il a été démontré que certains substrats sont efficacement polyubiquitinés en présence d'un facteur de conjugaison additionnel : les E4 ou enzyme de polymérisation de l'ubiquitine (Hoppe, 2005). La première famille d'enzyme E4 à avoir été identifiée se caractérise par la présence d'un domaine C-terminal U-box. Le domaine

U-box est conservé et est structurellement relié au domaine RING des E3 ligases. Les enzymes E4 possèdent la capacité de prolonger la chaîne d'ubiquitine en collaboration avec les enzymes E1, E2 et E3. En effet, des études génétiques et biochimiques ont révélé que la protéine UFD2 chez la levure se lie à des substrats préalablement conjugués avec une à trois molécules d'ubiquitine. UFD2 catalyse ensuite l'ajout de plusieurs autres molécules d'ubiquitine en présence des enzymes E1, E2 et E3, menant ainsi à la polyubiquitination des substrats, lesquels sont subséquemment ciblés vers le 26S protéasome (Johnson et al, 1995; Koegl et al, 1999). UFD2 représente la première protéine identifiée avec ce type d'activité enzymatique, et par conséquent représente la première enzyme E4 à avoir été décrite. Chez l'humain, UFD2a fonctionne également comme une enzyme E4. Celle-ci est impliquée dans la dégradation des formes pathologiques de l'ataxin-3 (Matsumoto et al, 2004). D'autres enzymes E4 ont également été identifiées : CHIP (Imai et al, 2002), p300 (Grossman et al, 2003), BUL1-BUL2 (Helliwell et al, 2001) et UFD-2-CHN-1 (Hoppe et al, 2004). Tout comme les protéines à domaine RING, les enzymes E4 à domaine U-box pourraient fonctionner comme des E3. Il a en effet été démontré que certaines protéines à domaine U-box, incluant UFD2a, possédaient une activité E3 *in vitro* (Hatakeyama et al, 2001). Par ailleurs, la polyubiquitination de l'ataxin-3 par UFD2a requière une activité E3 additionnelle *in vivo*. UFD2a fonctionne donc comme une enzyme E4 et non comme une E3 sous conditions physiologiques (Matsumoto et al, 2004). Alternativement, les enzymes E4 pourraient être décrites comme des E3 ligases spécialisées dans l'élongation des chaînes d'ubiquitine. Cependant, l'incapacité des enzymes E4 à substituer une enzyme E3 *in vivo*, en plus de l'absence d'évidence concernant l'interaction entre les E4 et les E2 suggèrent fortement que les E4 représentent une autre classe d'enzymes dont l'activité se distingue de celle des E3 ligases.

Il est à noter que la monoubiquitination n'est pas un signal de dégradation reconnu par le 26S protéasome (Hicke, 2001). Cette modification post-traductionnelle est plutôt impliquée dans la réparation de l'ADN, la transcription et l'endocytose (Haglund et al, 2003).

1.3.1.3.2 Le 26S protéasome

Chez les eucaryotes, le protéasome est responsable de la dégradation des protéines conjuguées avec l'ubiquitine. Pour ce faire, le protéasome possède deux sous-complexes distincts : le 20S protéasome et le 19S protéasome. La combinaison de ces sous-complexes génère le 26S protéasome (Figure 8) (Kloetzel, 2001). Le 20 S protéasome est en forme de cylindre et possède l'activité protéolytique. Le 19 S protéasome contrôle ce qui entre dans la chambre centrale du 20S protéasome.

1.3.1.3.2.1 Le 20S protéasome

Le 20S protéasome est un complexe d'environ 700kDa en forme de cylindre de 15 x 10 nm (Groll et al, 1997). Le 20S protéasome est constitué de 28 sous-unités de petite taille. Ces sous-unités sont de deux types distincts, mais apparentés α et β 7 sous-unités de chaque type (α1 – α7 et β1 – β7) qui s'assemblent pour former un anneau. 2 anneaux de sous-unités α s'associent avec 2 anneaux β selon l'ordre αββα, générant ainsi le 20S protéasome (Figure 8). La chambre centrale est le siège de l'hydrolyse et est tapissée par les sous-unités β catalytiques. Trois sous-unités β (β1, β2 et β5) sur les 7 formant les anneaux centraux du 20S protéasome sont responsables de l'activité catalytique. Biochimiquement, le 20S protéasome possède trois types d'activité protéolytique : une activité semblable à la chymotrypsine (chymotrypsin-like), une semblable à la trypsine (trypsin-like) et une semblable aux caspases (caspase-like) (Bochtler et al, 1999). Ainsi, le protéasome clive du côté C-terminal des résidus hydrophobes (tyrosine et phenylalanine), basiques (arginine et lysine) et acides (acide aspartique et glutamine). À l'exception de la sous-unité β5, les activités protéolytiques des sous-unités β1 et β2 ne favorisent pas la génération de peptides pouvant s'associer parfaitement aux molécules du CMH I. En effet, les CMH I humain ont la capacité de lier des peptides contenant des acides aminés hydrophobes et occasionnellement basiques à leur extrémité C-terminale. Les CMH I du murin s'associent aux peptides contenant des acides aminés hydrophobes à leur extrémité C-terminale. De ce fait, un peptide à l'extrémité C-terminal acide généré par le protéasome 26S n'est pas en mesure de se lier à une molécule du CMH I tant chez l'humain que la souris (Rammensee et al, 1999).

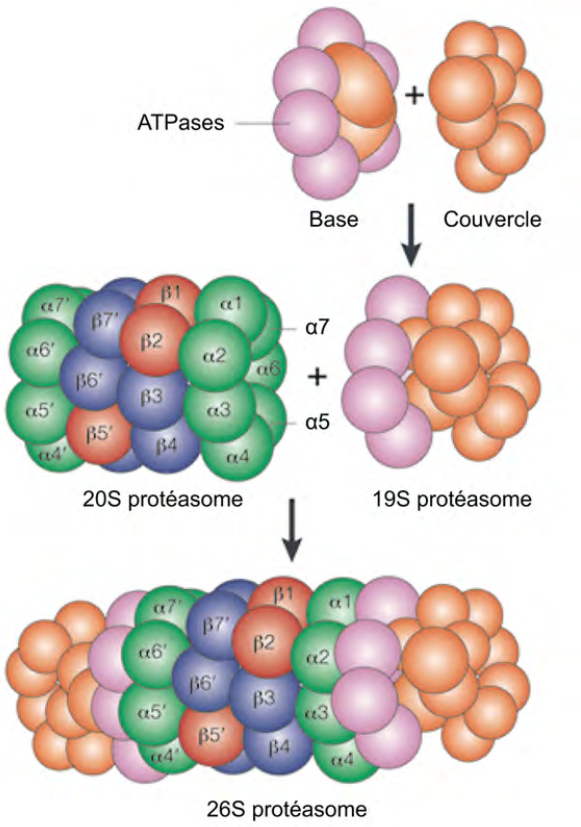

Figure 8. Composition du protéasome 26S. Le protéasome 20S est constitué de 28 (14 différentes) sous-unités, de 21 à 31kDa, organisés en quatre anneaux heptamériques. Les deux anneaux extérieurs sont composés des sous-unités α (α1- α7, vert). Les deux anneaux internes sont composés des sous-unités β (β1- β7, bleu et rouge). Les sous-unités β1, β2, β5 représentent les sous-unités catalytiques. La sous-unité 19S contient deux sous-structures : la base et le couvercle. La base est composée de six ATPase (mauve) et deux sous-unités non-ATPase (orange). La base s'attache à deux anneaux α. Le couvercle contient jusqu'à dix sous-unités non-ATPase (orange). Tiré de (Kloetzel, 2001).

Au début des années 1990, deux sous-unités β additionnelles du protéasome 20S sont identifiées : β1i (ou LMP2, PSMB9) et β5i (ou LMP7, PSMB8) (Brown et al, 1991; Kelly et al, 1991). Ces sous-unités, hautement similaires aux sous-unités β1 et β5, sont encodées par des gènes situés dans le locus chromosomique du CMH II, adjacents aux gènes codant pour TAP1 et TAP2 (de l'anglais *Transporter associated with Antigen Processing*). On notera que l'expression de β1i et β5i est fortement induite par les cytokines pro-inflammatoires IFNγ (de l'anglais *Interferon-γ*) et TNF (de l'anglais *Tumour Necrosis Factor*) (Aki et al, 1994). On va identifier quelques années plus tard une autre sous-unité β inductible par la présence de ces mêmes cytokines pro-inflammatoires : la sous-unité β2i (ou MECL1, PSMB10, LMP10) (Groettrup et al, 1996a; Hisamatsu et al,

1996). Suivant un traitement à l'IFNγ, l'expression de ces trois sous-unités inductibles est fortement accrue. Sous ces conditions, le protéasome 20S incorpore durant sa néosynthèse ces trois sous-unités alternatives et remplace graduellement les sous-unités constitutives pour donner naissance à l'immunoprotéasome (Figure 9) (Akiyama et al, 1994; Boes et al, 1994). Le protéasome constitutif et l'immunoprotéasome se localisent dans le noyau et le cytoplasme cellulaire (Palmer et al, 1994; Reits et al, 1997). Un enrichissement en immunoprotéasome a également été observé au niveau de la membrane du RE (Brooks et al, 2000).

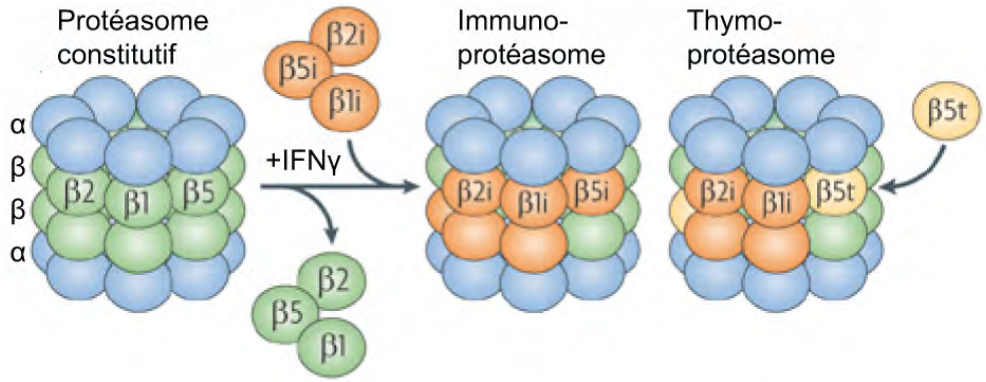

Figure 9. Composition des sous-unités protéolytiques du protéasome constitutif, de l'immunoprotéasome et du thymoprotéasome. Les sous-unités protéolytiques du protéasome constitutif sont β1 (ou PSMB9, LMP2), β2 (ou PSMB7, Z et MC14) et β5 (ou PSMB5, X, MB1 et ε). Les sous-unités protéolytiques de l'immunoprotéasome sont β1i (ou PSMB9, LMP2), β2i (ou PSMB10, LMP10 et MECL1) et β5i (ou PSMB8 et LMP7). Les sous-unités protéolytiques du thymoprotéasome son β1i, β2i et β5 t (ou PSMB11). Comparativement au protéasome constitutif, l'activité semblable à la caspase de l'immunoprotéasome est fortement diminuée et son activité semblable à la chymotrypsine est augmentée. L'activité semblable à la chymotrypsine est diminuée pour le thymoprotéasome. Tiré de (Groettrup *et al*, 2010).

Les peptides du CMH I produits par l'immunoprotéasome se distinguent et sont généralement mieux présentés que les peptides produits par le protéasome constitutif pour engager l'activation des lymphocytes T CD8+ (de Verteuil et al, 2010; Kloetzel, 2001). Ce résultat est en partie la conséquence de l'activité semblable à la caspase, fournie par la sous-unité β1, qui est remplacé par l'activité semblable à la chymotrypsine, fournie par la sous-unité β1i. L'immunoprotéasome est par conséquent plus actif contre les résidus hydrophobes et moins actif contre les résidus acides (Gaczynska et al, 1996). Des études chez la souris ont permis de mettre en évidence que l'immunoprotéasome jouait un rôle dans la génération du répertoire T CD8+ et dans l'élimination de pathogènes (Chen et al,

2001; Fehling et al, 1994; Van Kaer et al, 1994). La capacité de l'immunoprotéasome à diversifier le répertoire des cellules T cytotoxiques et à favoriser l'élimination de pathogènes a donc été attribuée aux sites de clivages alternatifs conférés par l'immunoprotéasome (de Verteuil et al, 2010; Toes et al, 2001). Des études ont suggéré très récemment un rôle alternatif pour l'immunoprotéasome. Certaines évidences laissent penser que l'immunoprotéasome aurait certains effets sur la production de cytokines (Muchamuel et al, 2009), la transcription de gènes (de Verteuil et al, 2010) et l'homéostasie des protéines (Seifert et al, 2010).

Les cellules corticales épithéliales thymiques (cCET) expriment un troisième type de protéasome surnommé thymoprotéasome. Le thymoprotéasome est composé des sous-unités β1i, β2i et β5 t (Figure 9). Cette dernière sous-unité est exclusivement exprimée par les cCET humain ou murin et semble essentielle à la sélection positive ainsi qu'au développement d'un répertoire en cellules T CD8+ approprié (Murata et al, 2007; Nitta et al, 2010). Contrairement aux sous-unités de l'immunoprotéasome, l'expression de β5 t n'est pas induite par l'IFNγ.

1.3.1.3.2.2 Le 19S protéasome

Le 20S protéasome est incapable de dégrader les protéines polyubiquitinées par lui-même. Son association avec le 19S protéasome (ou PA700) est essentielle. Le 19S protéasome se fixe aux extrémités du 20S protéasome formant ainsi le 26S protéasome observé *in vivo* (Voges et al, 1999). Le 19S protéasome est responsable de la dépendance de l'ATP du 26S protéasome et est composé de deux sous-complexes : le couvercle et la base (Figure 8) (Glickman et al, 1998a). Pour qu'une protéine polyubiquitinée soit dégradée, le 19S protéasome doit exécuter les fonctions suivantes : 1) le recrutement du substrat polyubiquitiné (Fu et al, 1998), 2) la dénaturation du substrat (Glickman et al, 1998a; Glickman et al, 1998b), 3) l'ouverture du 20S protéasome (Groll et al, 1997), 4) la translocation du substrat vers l'intérieur de la chambre catalytique (Larsen & Finley, 1997), 5) le recyclage de l'ubiquitine (Verma et al, 2002) et 6) l'activation catalytique du 20S protéasome (DeMartino et al, 1994).

Chez les mammifères, le régulateur PA28 (ou 11S REG) représente un complexe alternatif au protéasome 19S (Dubiel et al, 1992; Ma et al, 1992). Le régulateur PA28 est composé de deux sous-unités : PA28α et PA28β. L'expression de ces sous-unités est induite par l'IFNγ (Rechsteiner et al, 2000). Ce complexe se lie aux anneaux α à une des extrémités du 20S protéasome, formant alors un protéasome hybride 19S-20S-PA28 (Hendil et al, 1998; Tanahashi et al, 2000). Des évidences biochimiques et structurales ont démontré que le régulateur PA28 favoriserait : 1) l'ouverture du protéasome 20S (Knowlton et al, 1997; Whitby et al, 2000), 2) l'interaction du protéasome avec certaines chaperones ou composantes du RE (Rechsteiner et al., 2000) et 3) l'assemblage de l'immunoprotéasome (Preckel et al., 1999). Différentes études ont démontré que PA28 influence positivement la présentation de certains peptides associés aux CMH I (Groettrup et al, 1996b; Sun et al, 2002; van Hall et al, 2000). Néanmoins, le régulateur PA28 ne serait pas nécessaire à la génération de peptides antigéniques. Murata et ses collaborateurs ont en effet démontré que des souris PA28$\alpha\beta^{-/-}$ présentaient efficacement certains peptides de l'ovalbumine et développaient une réponse immunitaire normale suivant une infection par l'influenza (Murata et al, 2001). Le régulateur PA28 ne semble donc pas être un pré requis pour la présentation d'antigène. Considérant que PA28 est constitutivement exprimé dans presque tous les tissus et cellules analysées, il est considérable d'envisager que le rôle attribué à PA28 dans la présentation antigénique ne soit qu'un effet secondaire de sa fonction physiologique réelle (Sijts & Kloetzel, 2011).

1.3.1.3.3 La nature des substrats du protéasome

1.3.1.3.3.1 PRDs, DRiPs et PLDs

La génération des peptides associés aux molécules du CMH I est dépendante de la synthèse et de la dégradation des protéines (Yewdell et al, 2003). La génération de peptides cesse très rapidement suivant l'ajout de cycloheximide (inhibiteur de la synthèse protéique) ou l'ajout d'inhibiteurs du protéasome (ex. Lactacystine, MG-132, Epoxomicine) (Michalek et al, 1993; Qian et al, 2006b; Wherry et al, 2006). Plusieurs études dirigées par Jonathan Yewdell indiquent que les peptides présentés à la surface cellulaire par les CMH I proviennent préférentiellement de protéines rapidement

dégradées (PRDs; $t_{1/2}$ ~10 minutes) par rapport aux protéines lentement dégradées (PLDs; $t_{1/2}$ ~2000 minutes) (Figure 10) (Yewdell & Nicchitta, 2006). Les PRDs se divisent en deux classes : 1) les protéines matures et fonctionnelles possédant un temps de demi-vie très court (ex. ornithine decarboxylase; $t_{1/2}$ ~ 5 à 30 minutes) et 2) les protéines nouvellement synthétisées issues d'erreurs co-et/ou post-traductionnelles. Les PRDs de cette deuxième classe sont incorrectement repliées, instables, et rapidement acheminées vers le protéasome. On les nomme DRiPs (de l'anglais *Defective Ribosomal Products*) (Figure 11) (Reits et al, 2000b; Schubert et al, 2000; Yewdell et al, 1996; Yewdell et al, 2003). Les DRiPs représentent environ 30 % des protéines nouvellement synthétisées et sont dégradées par le protéasome en moins de 10 minutes (Schubert et al, 2000). Bien que les PLDs représentent également une source de peptides antigéniques (Dolan et al, 2011), les DRiPs/PRDs représentent la principale source de peptides présentés par les molécules du CMH I (Dolan et al, 2010b; Dolan et al, 2011; Qian et al, 2006a; Qian et al, 2006b). De cette façon, une cellule synthétisant des protéines virales peut être éliminée par un lymphocyte T CD8+ quelques minutes suivant l'infection (Bennink et al, 1984; Braciale et al, 1984; Esquivel et al, 1992; Yewdell et al, 1986).

Différents stimuli inflammatoires augmentent la proportion de DRiPs à l'intérieur des cellules dendritiques (Lelouard et al, 2002). Ces DRiPs s'accumulent de manière transitoire sous forme de corps cytosoliques lors de la maturation des cellules dendritiques. Ces structures cytosoliques enrichies en DRiPs sont surnommées DALIS (de l'anglais *Dendritic cell Aggresome Like Induced Structures*) (Lelouard et al, 2002). Les DALIS représentent des zones intracellulaires où s'effectuent l'ubiquitination et l'entreposage des DRiPs (Lelouard et al, 2004). La formation des DALIS durant le processus de maturation protège les DRiPs de la dégradation médiée par le système ubiquitine-protéasome, suggérant que les cellules dendritiques régulent finement la dégradation des DRiPs (Lelouard et al, 2004; Lelouard et al, 2002; Lelouard et al, 2007; Pierre, 2005; Pierre, 2009). La pertinence biologique de la formation des DALIS sur le système immunitaire n'a pas été évaluée à ce jour.

Figure 10. Les protéines dégradées par le protéasome se divisent en deux classes : les protéines avec un temps de demi-vie de ~10 minutes (PRDs) et celles avec un temps de demi-vie de ~2000 minutes (PLDs). Les PLDs ont des temps de demi-vie variant de plusieurs heures à plusieurs semaines. Les DRiPs appartiennent majoritairement à la classe des PRDs. Les peptides présentés par les CMH I semblent provenir préférentiellement des protéines de la classe des PRDs/DRiPs par rapport aux PLDs. Tiré de (Yewdell and Nicchitta, 2006).

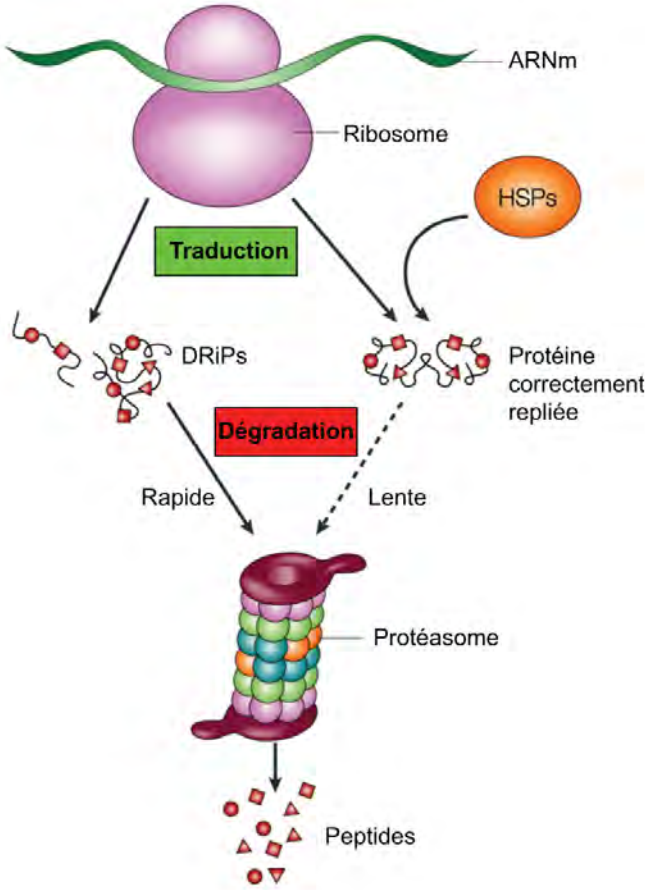

Figure 11. Synthèse et dégradation des protéines. Toutes les protéines sont synthétisées par les ribosomes. Les protéines nouvellement synthétisées sont fréquemment stabilisées par les HSPs (de l'anglais *Heat Shock Proteins*), ce qui facilite leur repliement et prévient leur agrégation (Thulasiraman *et al*, 1999). Malgré cela, certaines protéines sont défectueuses, ce qui mène à des protéines incorrectement repliées ou incorrectement assemblées. Ces protéines non fonctionnelles, ou DRiPs, sont acheminés au protéasome pour leur dégradation, ce qui permet une réponse rapide des lymphocytes T CD8+ contre des protéines virales nouvellement synthétisées. Tiré de (Yewdell *et al*, 2003).

1.3.3.3.3.2 L'ERAD

Les protéines résidentes du RE et les protéines sécrétées représentent environ 25 % du protéome cellulaire chez les mammifères (Istrail et al, 2004). À l'intérieur du RE, un mécanisme de « contrôle de qualité » impliquant plusieurs chaperones assure le repliement des protéines (Trombetta & Parodi, 2003). Les protéines aberrantes ou incorrectement repliées (c.-à-d. DRiPs) dans la lumière du RE sont des substrats de l'ERAD (de l'anglais *Endoplasmic Reticulum-Associated Degradation*) (Vembar & Brodsky, 2008). Les substrats de l'ERAD sont d'abord reconnus par certaines chaperonnes puis ensuite rétrotransloqués vers le cytoplasme pour être dégradé par le système ubiquitine-protéasome (Figures 12). Les substrats de l'ERAD contribuent donc à la génération de peptides antigéniques associés aux molécules du CMH I (Bacik et al, 1997; Golovina et al, 2002; Mosse et al, 1998; Selby et al, 1999).

1.3.3.3.3.2.1 La reconnaissance du substrat

Les substrats de l'ERAD sont des protéines solubles et membranaires incorrectement repliées. Les protéines solubles dont la conformation est inadéquate exposent généralement sur une période prolongée certaines de leurs séquences hydrophobes dans la lumière du RE, ce qui peut mener à leur agrégation (Trombetta & Parodi, 2003). Afin de minimiser cette problématique, les chaperones du RE [ex. BIP (de l'anglais *Immunoglobulin Binding Protein*)] se fixent aux motifs hydrophobiques des substrats de l'ERAD et assurent leur solubilité et leur rétrotranslation (Knittler et al, 1995; Nishikawa et al, 2001; Schmitz et al, 1995). Bien que le rôle de BIP dans la sélection du substrat soit toujours mitigé, il est possible que l'interaction prolongée entre le substrat et BIP soit suffisante pour initier le recrutement d'une ubiquitine ligase; lorsque le substrat est polyubiquitiné, son engagement dans la voie de l'ERAD est assuré (Denic et al, 2006). L'enzyme PDI (de l'anglais *Protein Disulphide Isomerase*) correspond à une oxidoréductase localisée dans la lumière du RE. Cette protéine est impliquée dans la formation des ponts disulfures durant le repliement des protéines. Lorsque les ponts disulfures sont imparfaits, les protéines défaillantes associées à PDI sont reconnues par

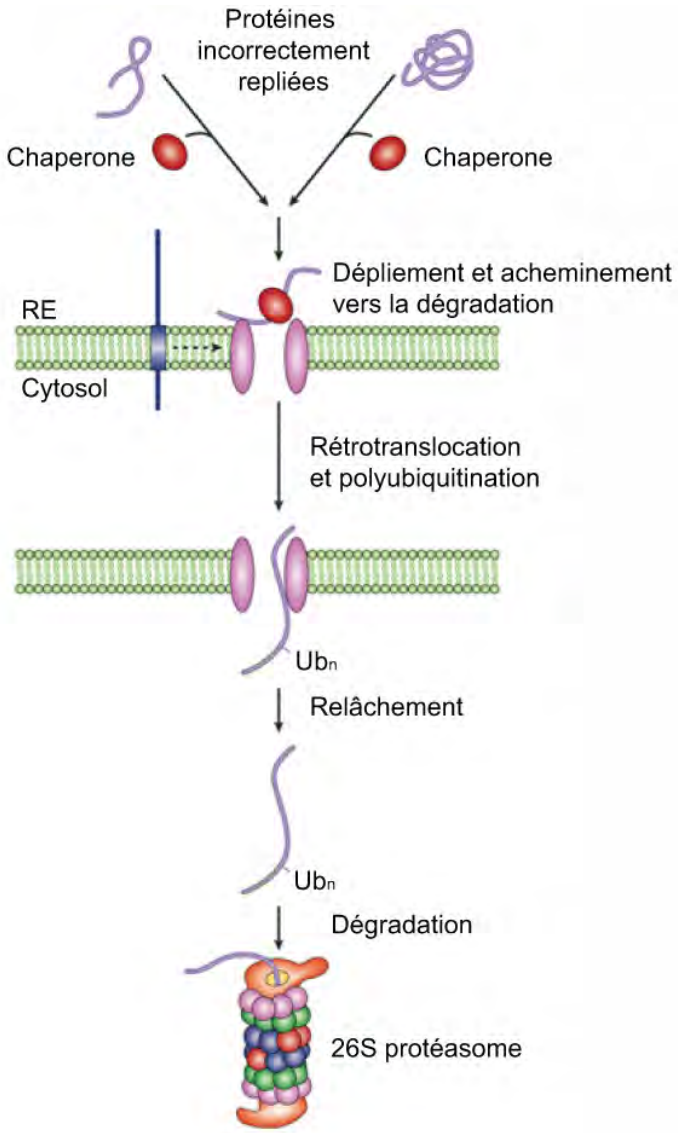

Figure 12. L'ERAD est un mécanisme en quatre étapes. À la première étape, les protéines incorrectement repliées dans la luminère du RE sont reconnues et dépliées par les chaperonnes résidentes du RE, et acheminées vers le canal de translocation. Les protéines membranaires incorrectement repliées pourraient être acheminées vers le canal par diffusion au niveau de la membrane (flèche pointillée). À la deuxième étape, les polypeptides sont transportés à travers le canal. La polyubiquitination débute lorsque la chaîne polypeptidique accède le cytosol. À la troisième étape, les polypeptides sont relâchés de la membrane du RE vers le cytosol. À la quatrième étape, les polypeptides sont dégradés par le protéasome. Tiré de (Tsai *et al*, 2002).

l'oxidoréductase Eps1. Cette reconnaissance permet aux substrats d'être ultimement dégradés (Wang & Chang, 2003).

La majorité des protéines transloquées à l'intérieur du RE sont co-traductionnellement modifiées par l'ajout d'un oligosaccharide $GlcNAc_2$-Man_9-Glc_3 (Alberts, 2008). Les glycoprotéines entrent dans le cycle calnexine-calréticuline suivant leur entrée dans la lumière du RE (Trombetta & Parodi, 2003). Les glycoprotéines constituées d'aberrations, cyclent plus longtemps et deviennent par conséquent la cible de la mannosidase I du RE. Cette mannosidase à action lente convertit les glycans $GlcNAc_2$-Man_9-Glc_3 des protéines aberrantes en $GlcNAc_2$-Man_8-Glc_3 (Trombetta & Parodi, 2003). Cette modification permet le recrutement spécifique de EDEM (de l'anglais *ER Degradation-Enhancing alpha-Mannosidase-like*) (Molinari et al, 2003; Oda et al, 2003). Ce recrutement est nécessaire pour que les glycoprotéines aberrantes soient ultimement dégradées.

1.3.3.3.3.2.2 La rétrotranslocation, dislocation et dégradation

Les protéines en voie d'être dégradées sont d'abord rétrotransloquées du RE vers le cytoplasme (Figure 12). Plusieurs évidences indirectes suggèrent que le translocon Sec61 correspond au canal impliqué dans le processus de rétrotranslocation (Pilon et al, 1997; Plemper et al, 1997; Schmitz et al, 2000). Certaines protéines sont cependant rétrotransloquées indépendamment de Sec61 (Hampton, 2002; Walter et al, 2001). La protéine transmembranaire Derlin-1 servirait également de canal dans le processus de rétrotranslocation (Lilley & Ploegh, 2004; Ye et al, 2004). Lorsque les substrats de l'ERAD font face au cytosol, ils sont disloqués du canal de rétrotranslocation et sont marqués pour leur dégradation. La polyubiquitination des protéines représente une étape clé pour leur dislocation (de Virgilio et al, 1998; Shamu et al, 2001). Quelques E2 (Ubc1p, Ubc6p et Ubc7p) et E3 ubiquitine-ligase (Hrd1p et Hrd3p) impliquées dans la dislocation des substrats de l'ERAD ont été identifiés (Bays et al, 2001; Jarosch et al, 2002a; Tsai et al, 2002). La monoubiquitination ne permet cependant pas la dislocation des substrats (Jarosch et al, 2002b).

La polyubiquitination des substrats de l'ERAD n'est pas suffisante pour leur dislocation vers le cytoplasme (Vembar & Brodsky, 2008). La dislocation est engendrée par l'activité ATPasique de Cdc48/VCP (de l'anglais *Valsolin Containing Protein*), une protéine cytosolique comportant un domaine AAA-ATPase (Jarosch et al, 2002b; Ye et al, 2004). Cdc48/VCP possède la capacité de lier le protéasome et les protéines polyubiquitinées (Jarosch et al, 2002b). Cdc48/VCP permet d'hydrolyser l'ATP, ce qui constitue la force motrice du processus de dislocation (Ye et al, 2003; Ye et al, 2004).

Suivant la dislocation des substrats de l'ERAD dans le cytosol, la N-glycanase effectue la déglycolysation des glycoprotéines (Suzuki et al, 2002). Tous les substrats de l'ERAD sont ensuite dégradés par le système ubiquitine-protéasome.

1.3.1.3.4 Les peptidases cytosoliques

Les fragments peptidiques générés par le protéasome ont généralement une longueur variant entre 3 et 20 acides aminés (Cascio et al, 2001; Kisselev et al, 1998; Reits et al, 2004). Ces fragments représentent des substrats pour les peptidases cytosoliques. Puisque le cytoplasme est composé exclusivement d'aminopeptidase, le protéasome représente le seul complexe protéolytique pouvant générer l'extrémité C-terminale des peptides (Cascio et al, 2001; Reits et al, 2003). En taillant l'extrémité N-terminale des peptides sortant du protéasome, les aminopeptidases génèrent des peptides de 9 acides aminés ou plus. La plupart des peptidases sont de larges structures protéiques dont la taille est parfois comparable à celle du protéasome. Par exemple, les images en microscopie électronique montrent que la peptidase TPPII (de l'anglais *Tripeptidyl Peptidase II*) est encore plus imposante que le 26S protéasome (Rockel et al, 2005). LAP (de l'anglais *Leucine aminopeptidase*) correspond pour sa part à un hexamer de 300 kDa (Geier et al, 1999; Turzynski & Mentlein, 1990). TPPII est probablement l'aminopeptidase la plus importante pour la génération de peptides antigéniques présentés par les CMH I. TPPII taille les fragments peptidiques de plus de 15 acides aminés (Reits et al, 2004). Son inhibition provoque une diminution de l'expression des molécules du CMH I à la surface cellulaire, suggérant ainsi que TPPII représente un intermédiaire clé dans la voie de présentation antigénique (Reits et al, 2004). Plusieurs autres aminopeptidases ont été

identifiées à ce jour incluant TOP (de l'anglais *Thymet Oligopeptidase*), neurolysine, aminopeptidase sensible à la puromycin et hydrolase bléomycine (Beninga et al, 1998; Bromme et al, 1996; Johnson & Hersh, 1990; Turzynski & Mentlein, 1990). Certaines chaperones cytoplasmiques telles que HSP70 (de l'anglais *Heat Shock Protein 70*) et HSP90 protègeraient néanmoins certains peptides contre la dégradation médiée par les protéases cytosoliques, favorisant ainsi la présentation de ces peptides à la surface cellulaire (Kunisawa & Shastri, 2003).

1.3.1.3.5 Le transport des peptides endogènes du cytosol vers le RE

Les peptides antigéniques générés dans le cytoplasme et le noyau traversent la membrane du RE, ce qui leur permet de s'associer aux molécules du CMH I. Les peptides sont transloqués dans la lumière du RE par l'intermédiaire du canal TAP (Neefjes et al, 1993; Shepherd et al, 1993). TAP appartient à la grande famille des transporteurs ABC (de l'anglais *ATP-Binding Cassette transporter*). TAP est composé de deux unités homologues, TAP1 et TAP2, formant trois sous-domaines distincts : 1) un domaine multimembranaire, 2) un domaine liant les peptides et 3) deux cassettes liant l'ATP (Figure 13) (Bauer & Tampe, 2002; Reits et al, 2000a). L'hydrolyse de l'ATP par une des cassettes liant l'ATP est nécessaire à l'ouverture du pore transmembranaire. L'hydrolyse de l'ATP par l'autre cassette est nécessaire à sa fermeture (Arora et al, 2001). TAP lie l'extrémité C-terminale des peptides (Nijenhuis & Hammerling, 1996; Vos et al, 2000; Vos et al, 1999). Le canal TAP transloque les peptides variant de 8 à 40 acides aminés en favorisant principalement les peptides de 9 à 12 acides aminés (Koopmann et al, 1996; Roelse et al, 1994). TAP humain diffère de la forme murine puisqu'il permet le transfert de peptides indépendamment du type d'acide aminé positionné à l'extrémité C-terminale du peptide. TAP murin effectue par contre le transfert de peptides exclusivement composés d'acides aminés hydrophobes ou aromatiques à l'extrémité C-terminale (Momburg et al, 1994; Schumacher et al, 1994).

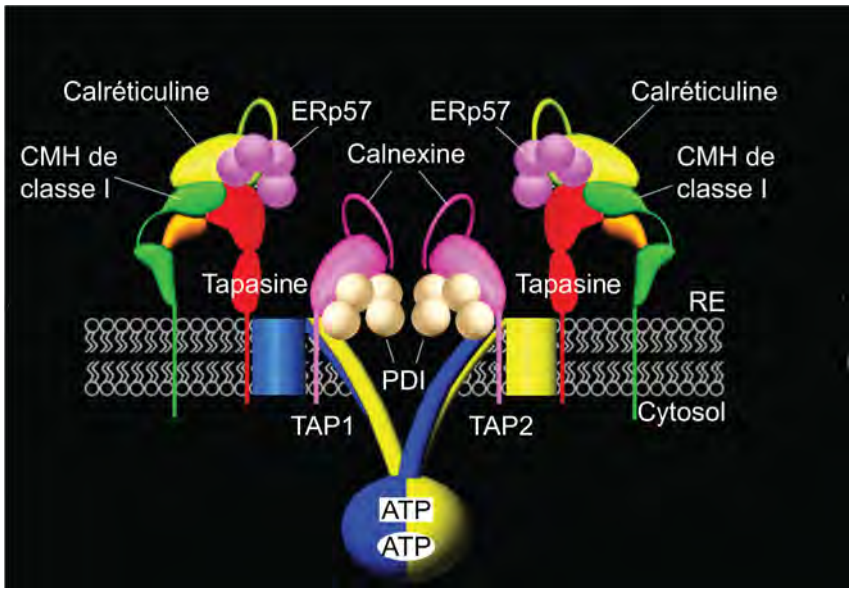

Figure 13. Composantes du complexe de chargement peptidique. Ces composantes favorisent la sélection et le chargement de peptides dans le sillon du CMH I. Ceci fourni un mécanisme de « contrôle de qualité » pour l'exportation préférentielle des complexes CMH I-peptides stables vers la surface cellulaire.

1.3.1.3.6 L'apprêtement des peptides endogènes dans la lumière du RE

Les peptides transloquées dans la lumière du RE par TAP sont majoritairement trop longs pour s'associer aux molécules du CMH I. Les peptides sont donc taillés par l'aminopeptidase ERAAP (ou ERAP1) (Saric et al, 2002; Serwold et al, 2002; York et al, 2002). Cette aminopeptidase est exprimée dans la lumière du RE de manière ubiquitaire. ERAAP reconnaît l'extrémité C-terminale des peptides et coupe ensuite leur extrémité N-terminale. Ce clivage permet de générer des peptides d'une longueur adéquate (8 à 11 acides aminés) pour leur liaison aux CMH I (Chang et al, 2005). Une étude a récemment démontré que les CPAs provenant de souris ERAAP KO avaient la propriété de stimuler une forte réponse T CD8+ lorsqu'elles étaient injectées chez des souris WT et vice et versa (Hammer et al, 2007a). Cette observation indique que plusieurs peptides sont uniquement présentés en présence ou en absence d'ERAAP. ERAAP a donc un rôle crucial sur la sélection du répertoire des cellules T CD8+.

Les peptides transloqués par TAP et taillés par ERAAP s'engagent dans un processus hautement orchestré par de multiples chaperonnes et molécules accessoires qui

résident dans le RE. Ces protéines facilitent la sélection des peptides optimaux pour leur chargement dans le sillon des molécules du CMH I. La molécule du CMH I nouvellement synthétisée est d'abord acheminée au RE et ensuite stabilisée par BIP et la calnexine. Lorsque la β2m s'associe à la chaîne lourde du CMH I, la calréticuline remplace la calnexine (Jensen, 2007). L'association du CMH I à la calréticuline est synchronisée avec le recrutement de la tapasine et d'ERp57 au niveau du complexe de chargement peptidique (Figure 13). ERp57 est une thiol oxidoréductase (Hughes & Cresswell, 1998) assurant la création des ponts disulfures sur la chaîne lourde nouvellement synthétisée du CMH I (Farmery et al, 2000). ERp57 et la calréticuline collaborent pour assurer le repliement adéquat des glycoprotéines (Maattanen et al, 2006).

Tapasine est une glycoprotéine reliant les molécules du CMH I mature au canal TAP. La colocalisation de tapasine et de TAP facilite le chargement des peptides dans le sillon des molécules du CMH I. De plus, tapasine stabilise l'association des CMH I et des peptides (Lehner et al, 1998). Cette stabilisation corrèle avec une augmentation de l'abondance du canal TAP (Bangia et al, 1999; Lehner et al, 1998) et une augmentation de la liaison des peptides à ce canal (Li et al, 2000). Tapasine prévient également le relâchement prématuré des molécules du CMH I vers l'extérieur du RE (Barnden et al, 2000). Tapasine s'associe de manière covalente à ERp57 par des ponts disulfures relativement stables. Des évidences obtenues *in vivo* suggèrent que le complexe hétérodimérique ERp57-tapasine représenterait l'unité fonctionnelle du complexe de chargement peptidique, facilitant ainsi la sélection et le chargement des peptides dans le sillon des CMH I (Kienast et al, 2007; Wearsch & Cresswell, 2007). L'enzyme PDI contrôlerait également le chargement des peptides en régulant l'état rédox des ponts disulfures dans le domaine α2 du CMH I (Park et al, 2006). Le chargement des peptides sur les molécules du CMH I permet aux molécules du CMH d'atteindre leur conformation finale. Les complexes CMH I-peptide quittent ensuite le complexe de chargement peptidique et sont transportées vers l'appareil de Golgi jusqu'à la surface cellulaire par la voie constitutive de sécrétion cellulaire.

1.3.1.4 L'inefficacité de la voie de présentation des peptides endogènes par les CMH I

On pourrait penser que la voie de présentation des peptides endogènes par les CMH I soit conçue pour optimiser la génération de peptides et leur chargement dans le sillon des molécules du CMH I. Cette voie de présentation est pourtant très inefficace. En moyenne, une cellule présente entre 20 000 et 50 000 molécules du CMH I associés à des peptides. Puisqu'une cellule contient en moyenne 2 milliards de protéines, chaque protéine ne peut contribuer également à la génération des peptides présentés par les CMH I. Plus précisément, ces 2 milliards de protéines sont continuellement exprimées et dégradées pour une durée d'environ 6h avant d'atteindre et de maintenir un équilibre (Yewdell, 2001). Quelques millions de protéines par cellule sont conséquemment dégradées chaque minute. Puisque le protéasome digère chaque protéine en plusieurs peptides, approximativement 100 millions de peptides par minute et par cellule sont générés. Cependant, seulement quelques centaines de molécules du CMH I sont générées par minute dans cette même cellule (Yewdell, 2001; Yewdell et al, 2003). Bien que la quantité de peptides générés soit toujours en excès, plusieurs molécules du CMH I sont incapables de s'associer à un peptide donné dans la lumière du RE (Neefjes & Ploegh, 1988). Le chargement peptidique des CMH I n'est donc pas un processus saturé. Ces chiffres suggèrent que la grande majorité des peptides sont perdus entre le protéasome et le site de chargement dans la lumière du RE.

En raison de l'activité excessive des peptidases cellulaires, un peptide possède en moyenne une demi-vie de 6 secondes *in vivo* (Reits et al, 2003). 99 % à 99.999 % de ces peptides cytosoliques sont détruits par les peptidases avant même de rencontrer le canal TAP (Reits et al, 2003; Yewdell et al, 2003). Pour qu'un peptide donné soit présenté par une molécule du CMH I, il doit être généré à plus de 10 000 copies par cellule. Sous ce seuil, la chance statistique d'obtenir un peptide ayant survécu aux attaques protéolytiques et à la liaison du CMH I est presque nulle.

Étant donné le nombre limité de CMH I exprimé en surface par rapport à l'énorme production de protéines, un mécanisme sélectif doit être utilisé pour éviter la présentation redondante de peptides provenant des protéines les plus abondantes (Yewdell et al, 2003). La cellule prévient cette problématique par l'utilisation prédominante de DRiPs comme

source de peptides (voir section 1.3.1.3.3.1). De récentes études ont de plus démontré que la compartimentalisation des peptides provenant des DRiPs leur permet d'être beaucoup plus compétitifs par rapport à des peptides cytosoliques plus abondants (Lev et al, 2010). L'efficacité de la présentation antigénique par les CMH I pourrait donc être modulable par certains mécanismes de compartimentalisation encore inconnus (Dolan et al, 2010a; Yewdell & Nicchitta, 2006). Ces mécanismes pourraient également expliquer l'efficacité de présentation des peptides endogènes cryptiques.

1.3.1.5 Les peptides endogènes cryptiques

Les DRiPs sont issus des processus conventionnels de la traduction et représentent la source principale de peptides antigéniques associés aux molécules du CMH I (Yewdell et al, 2003). Les peptides du CMH I peuvent également provenir des processus de la traduction cryptique. La traduction cryptique se réfère aux polypeptides synthétisés par des mécanismes non conventionnels de la traduction. Ceci inclut la génération de peptides provenant d'introns, de jonctions intron/exon, de régions 5' et 3' non traduites et de cadres de lecture alternatifs (Cardinaud et al, 2004; Mayrand & Green, 1998; Shastri et al, 2002). Bien que la présentation de peptides cryptique soit un phénomène rare, ces peptides sont capables d'induire une réponse T CD8+ chez une souris normale (Schwab et al, 2003). Les peptides cryptiques présentés par les molécules du CMH I ont donc un rôle significatif au niveau du système immunitaire.

Plusieurs peptides cryptiques sont encodés en aval de codons ATG. Ces codons alternatifs peuvent être utilisés par quelques ribosomes ayant échoué l'initiation de la traduction à partir de codons ATG authentiques (Bullock & Eisenlohr, 1996; Bullock et al, 1997). Certains peptides cryptiques proviennent même de cadre de lecture absent en codon ATG (Malarkannan et al, 1999; Shastri et al, 1995; Shastri et al, 2002). Le groupe de Nilabh Shastri a démontré l'existence d'un peptide antigénique provenant d'un polypeptide dont la traduction est initiée à partir d'un codon CTG (codant pour une leucine) plutôt qu'un codon ATG conventionnel (codant pour une méthionine) (Schwab et al, 2004). Contrairement aux peptides antigéniques provenant des processus de traduction conventionnels, la génération du peptide cryptique identifié par Schwab et ses

collaborateurs est indépendante du facteur d'initiation de la traduction eIF2. Cette observation est intrigante puisque eIF2 est un acteur clé de la synthèse protéique. Il est d'ailleurs fréquemment inhibé durant les infections virales et les stress cellulaires afin de ralentir la traduction conventionnelle (Mathews et al, 2007). Leurs résultats suggèrent que la traduction cryptique indépendante du facteur eIF2 permettrait aux cellules infectées de poursuivre efficacement la présentation de peptides viraux. Ce mécanisme assurerait la reconnaissance et l'élimination de ces cellules par les lymphocytes T CD8+ cytotoxiques.

Les peptides présentés par les CMH I proviennent habituellement d'une séquence continue et linéaire dans la séquence des protéines sources. Certains peptides proviennent cependant d'épissage peptidique catalysé par le protéasome (Dalet et al, 2010; Hanada et al, 2004; Vigneron et al, 2004; Warren et al, 2006). Ces peptides atypiques proviennent d'une fusion post-protéolytique entre deux fragments peptidiques produits par le protéasome. Cette fusion post-protéolytique s'effectue par une réaction de transpeptidation (Vigneron et al, 2004). Trois peptides du CMH I provenant de cette réaction ont été identifiés à ce jour.

1.3.1.6 La présentation croisée des peptides exogènes par les CMH I

Les cellules dendritiques et les macrophages sont les principales CPAs pouvant internaliser les antigènes provenant de l'environnement extracellulaire. Les peptides provenant de ces antigènes exogènes s'associent aux molécules du CMH I pour être présentés à la surface cellulaire. Ce processus est nommé « présentation croisée ». La présentation croisée de peptides provenant d'antigènes exogènes est essentielle à la génération d'une réponse T CD8+ pour l'élimination des cellules infectées ou de cellules tumorales (Heath & Carbone, 2001). Les mécanismes de phagocytose et d'endocytose jouent un rôle primordial dans la présentation croisée. Cinq modèles sont actuellement proposés : 1) la voie phagosome-au-cytosol, 2) la voie RE-phagosome-au-cytosol, 3) la voie endosome-RE 4) la voie vacuolaire et 5) les jonctions gap.

1.3.1.6.1 La voie phagosome-au-cytosol

Ce modèle de présentation croisée fût élaboré suivant l'identification d'une voie déchargeant les protéines phagocytées dans le cytosol (Figure 14) (Kovacsovics-Bankowski & Rock, 1995). Le transfert du contenu antigénique de la lumière du phagosome vers le cytosol a été observé chez des macrophages et des cellules dendritiques (Shen et al, 1997). Les protéines phagocytées qui ont accédé au cytosol sont dégradées par le système ubiquitine-protéasome (Kovacsovics-Bankowski & Rock, 1995; Oh et al, 1997; Rock et al, 1993; Shen et al, 1997). Les peptides générés empruntent la voie de la présentation classique des molécules CMH I pour être présentés à la surface cellulaire (Guermonprez et al, 1999; Rao et al, 1997). La membrane plasmique représente la source principale de membrane phagocytaire dans ce modèle (Touret et al, 2005). Le mécanisme impliqué dans le déchargement des protéines du phagosome vers le cytosol demeure inconnu dans ce modèle.

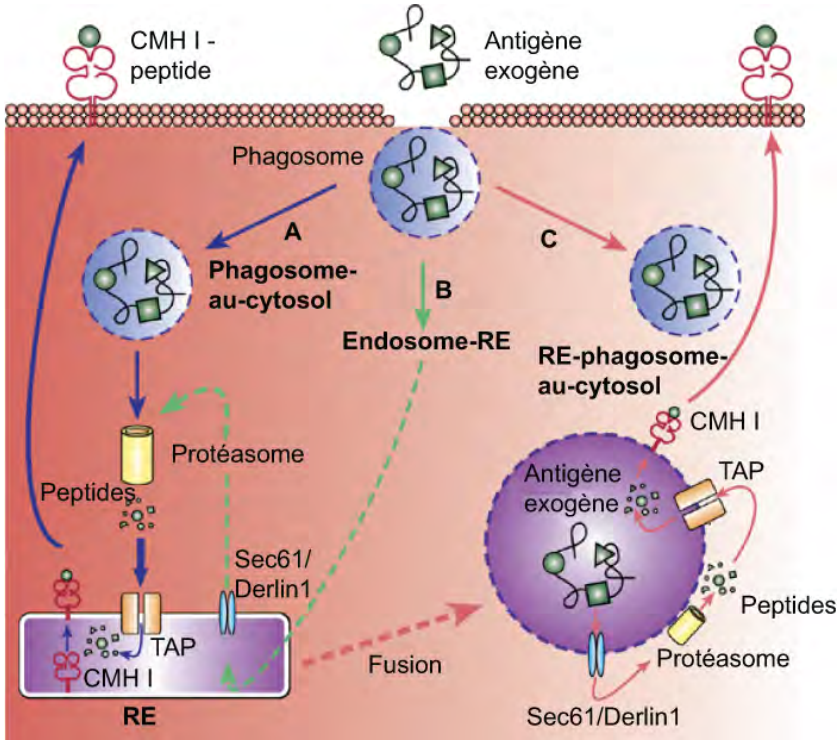

Figure 14. Trois modèles proposés de la présentation croisée sont illustrés. Voir le texte pour la description des différentes voies de présentation. Tiré de (Lin *et al*, 2008).

1.3.1.6.2 La voie du RE-phagosome-au-cytosol

Ce modèle propose que le RE fusionne avec le phagosome en formation, procurant ainsi une nouvelle source de membrane pour la génération du phagosome (Gagnon et al, 2002). Le phagosome est donc formé d'une membrane plasmique, de vacuoles endocytiques et de la membrane du RE. Cette fusion permet au phagosome de s'approprier certaines protéines résidentes du RE (CMH I, TAP, tapasin, chaperonnes, Sec61), créant ainsi un organel hybride autosuffisant pour exercer la présentation croisée des peptides associés aux CMH I (Figure 14) (Ackerman et al, 2003; Guermonprez et al, 2003; Houde et al, 2003). Les protéines phagocytées représentent des substrats de l'ERAD et sont ainsi rétrotransloquées vers le cytoplasme pour leur dégradation par le système ubiquitine-protéasome. Bien que controversé, le modèle RE-phagosome-au-cytosol fournit une explication intéressante permettant de rationaliser le déchargement des protéines antigéniques du phagosome vers le cytoplasme.

1.3.1.6.3 La voie endosome-RE

Selon ce modèle, les protéines exogènes solubles internalisées par macropinocytoses sont rétrogradées du Golgi vers le RE (Figure 14) (Ackerman et al, 2005). Ces protéines sont donc des substrats de l'ERAD et sont dégradées par le système ubiquitine-protéasome (Imai et al, 2005). Bien que le RE ne soit pas une destination typique du matériel endocytosé, l'intersection entre la voie endocytique et la voie de sécrétion est bien documentée (Bonifacino & Rojas, 2006).

1.3.1.6.4 La voie vacuolaire

Dans ce modèle, les peptides antigéniques sont générés à l'intérieur du phagosome par l'action de la protéase cystéine cathepsine S (Shen et al, 2004). Les peptides sont donc présentés par les CMH I indépendamment du système ubiquitine-protéasome et du canal TAP. Puisque les CMH I ne résident pas dans ce compartiment vacuolaire. Il a donc été proposé qu'un motif à base de tyrosine sur l'orientation cytoplasmique des molécules du CMH I puisse représenter un signal de reconnaissance pour l'acheminement des CMH I vers ce compartiment vacuolaire (Lizee et al, 2005).

1.3.1.6.5 Les jonctions gap

Neijssen et ses collaborateurs ont découvert plus récemment une autre voie de présentation croisée par laquelle des cellules transfèrent leurs peptides à des cellules voisines par l'intermédiaire de jonctions gap (Figure 15) (Neijssen et al, 2005). Ces jonctions sont de petits pores moléculaires formés entre les cellules par des protéines transmembranaires appelées *Connexines*. Ces pores sont généralement utilisés pour le transport intercellulaire de nutriments et d'autres petites molécules (Oviedo-Orta & Evans, 2002). Neijssen et ses collaborateurs démontrent que la connexine 43 peut former des canaux permettant aux peptides d'une longueur de 10 acides aminés d'être transférés d'une cellule à l'autre. Cette étude démontre que des monocytes peuvent utiliser les jonctions gap pour charger les molécules du CMH I avec des peptides viraux provenant de cellules infectées adjacentes.

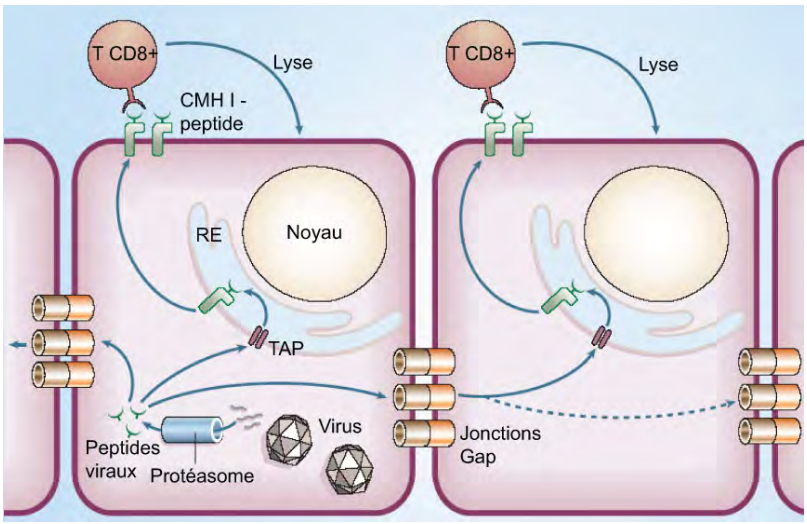

Figure 15. Présentation croisée par les jonctions gap. Voir le texte pour la description. Tiré de (Heath and Carbone, 2005).

1.3.2 La présentation antigénique par les CMH II

Les molécules du CMH II sont constitutivement exprimées à la surface des CPAs telles que les cellules dendritiques, les lymphocytes B et les macrophages. La voie de présentation classique par les CMH II a pour fonction de présenter des peptides de sources

exogènes aux lymphocytes T CD4+ (Figure 3 et 16). Les protéines endogènes contribuent également au répertoire peptidique des molécules du CMH II. La voie de présentation des CMH II joue un rôle primordial dans l'élaboration de la réponse à médiation humorale et cellulaire (Paul, 2008). Les peptides présentés par les CMH II proviennent généralement de la dégradation de protéines pathogéniques, de cellules infectées, de cellules altérées ou du « non-soi » endocyté par les CPAs.

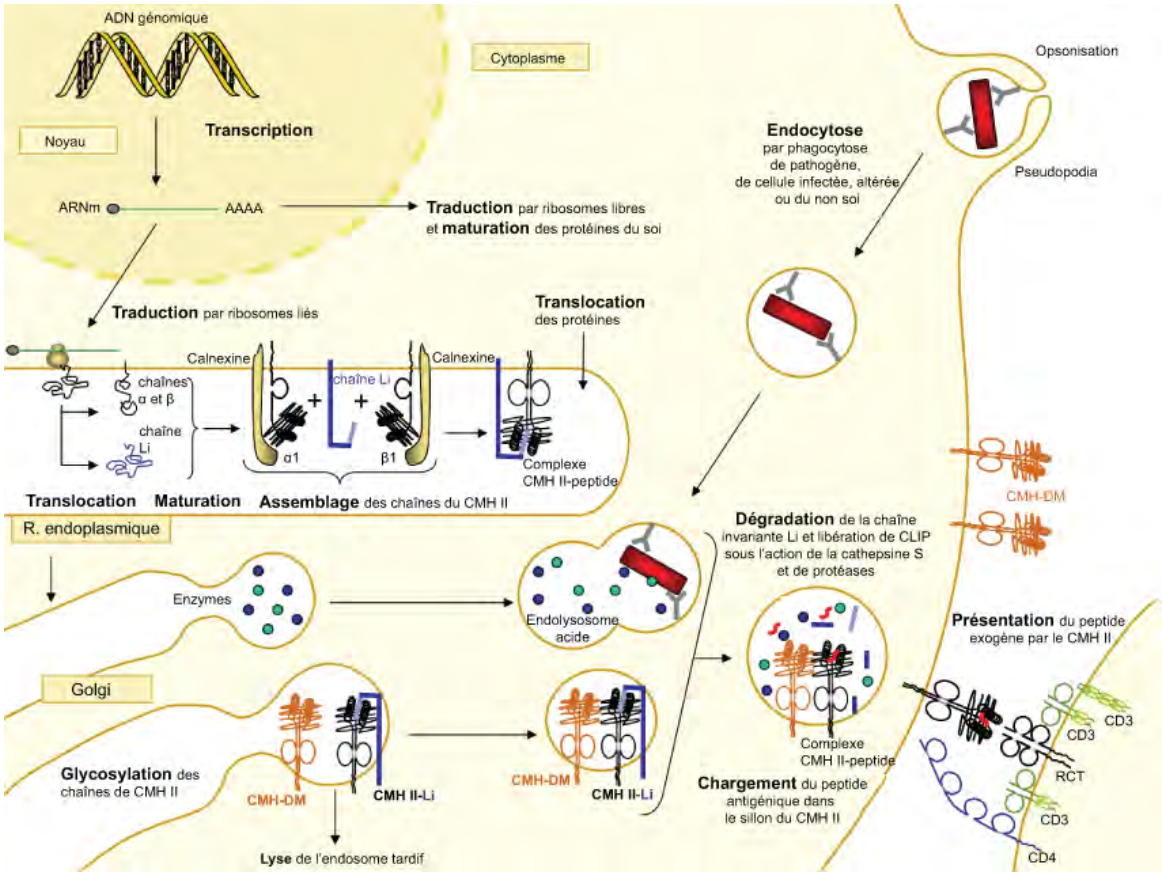

Figure 16. Voie classique de présentation antigénique par les CMH II. Étapes de la présentation d'un peptide exogène du « non-soi » par une molécule du CMH II au récepteur T d'un lymphocyte T CD4+. Tiré de http://www.imgt.org/.

1.3.2.1 Gènes, localisation chromosomique et structure des CMH II

Les molécules du CMH II sont divisées en deux sous-classes : les CMH II conventionnelles (CMH IIa) et les non-conventionnelles (CMH IIb). Chez l'humain, sept à onze gènes localisés sur le chromosome 6 (6p21.3) codent pour les molécules du CMH

IIa (HLA-DPA, HLA-DPB, HLA-DQA, HLA-DQB, HLA-DRA et plusieurs HLA-DRB). Quatre gènes dans la même région chromosomique codent pour les molécules du CMH IIb (HLA-DMA, HLA-DMB, HLA-DOA et HLA-DOB). Chez la souris, quatre gènes localisés sur le chromosome 17 (17p18.64 à 17p18.70) codent pour les molécules du CMH IIa (H2-AA, H2-AB, H2-EA, H2-EB). Quatre gènes sur le même chromosome (17p18.52 à 17p18.58) codent pour les molécules du CMH IIb (H2-DMA, H2-DMB, H2-DOA et H2-DOB).

Les gènes α et β du CMH II codent pour des chaînes d'un poids moléculaire respectif de 35kDa et 28kDa. Tout comme le CMH I, le CMH II est une glycoprotéine transmembraire composée d'une queue cytoplasmique et d'un domaine extracellulaire semblable aux immunoglobulines. Ces domaines sont nommés α_1, α_2, β_1 et β_2 (Figure 17). Tel que décrit pour les CMH I, les CMH II comprennent des régions polymorphiques et non polymorphiques. La molécule CD4 des lymphocytes T s'associe à la portion non polymorphique de toutes les molécules du CMH II.

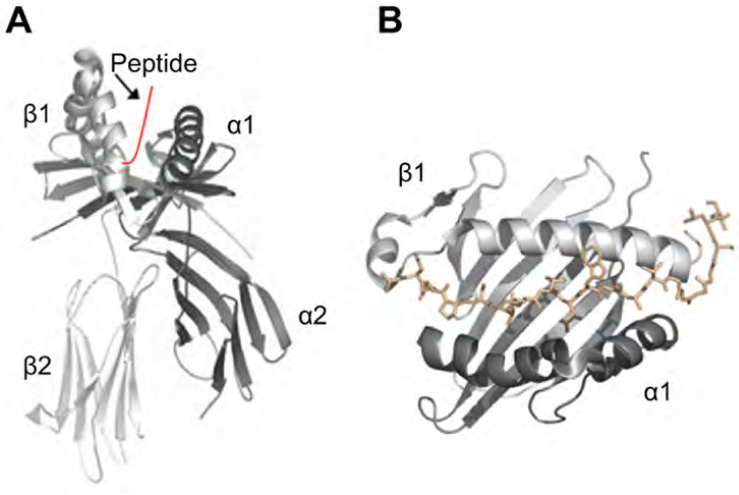

Figure 17. Représentation de la structure cristallographique du CMH II. (**A**) Les domaines α1, α2, β1, β2 et un peptide du CMH II sont illustrés. (**B**) Le sillon du CMH II est « ouvert » à ses deux extrémités, rendant possible la liaison d'un peptide dont la longueur peut varier entre 12 et 20 acides aminés. Tout comme pour le CMH I, la structure du sillon conditionne le nombre et la localisation des sites de contact entre les acides aminés du sillon et ceux du peptide. Tiré de (Berman *et al*, 2000).

La présence d'un sillon analogue à celui des CMH I est une caractéristique clé des molécules du CMH II (Figure 17). Pour les CMH II, ce sillon est formé par des interactions entre deux domaines de chaînes différentes, les domaines α_1 et β_1. La base du sillon est composée de 8 feuillets β (4 feuillets provenant du domaine α_1 et quatre autres du domaine β_1). Les hélices α constituent les parois du sillon. Contrairement au sillon du CMH I, celui de classe II montre une ouverture à ses deux extrémités, rendant possible la liaison d'un long peptide. Les peptides des CMH II ont une longueur pouvant varier approximativement entre 12 et 20 acides aminés. Les extrémités de ces peptides sont donc exposées à l'extérieur du sillon. Tout comme les peptides associés aux CMH I, les peptides s'associent aux classes II par des résidus d'ancrage qui constituent le motif de liaison. Étant donné la longueur relativement variable des peptides associés aux CMH II, leur motif est généralement situé dans la région centrale du peptide.

1.3.2.2 La voie de présentation classique des peptides exogènes par les CMH II

Les chaînes α et β du CMH II sont synthétisées au niveau du RE. La niche peptidique du CMH II est stabilisée par l'interaction de la chaîne invariante (Li) (Figure 16) (Ghosh et al, 1995). La chaîne invariante empêche temporairement toute fixation possible de peptide dans le sillon du CMH II. On retrouve Li sous forme trimérique. Cette forme trimérique promeut la formation de trois complexes Li-CMH II par l'interaction entre Li et plusieurs domaines des chaînes α et β du CMH (Castellino et al, 2001). La formation d'un nanomère composé de trois complexe trimériques $(\alpha\beta li)_3$ permet à la molécule du CMH II de quitter le RE et d'atteindre le compartiment trans-golgien (Jasanoff et al, 1998). Les complexes sont ensuite acheminés vers les endosomes par la présence d'un domaine de localisation cellulaire dans la région cytoplasmique de Li (Neefjes et al, 1990; Pieters et al, 1993; Wolf & Ploegh, 1995).

À l'intérieur des endolysosomes, Li est dégradé par certaines protéases telles que les cathepsines S et L. Cette dégradation est par contre incomplète et une portion de Li, nommée CLIP (de l'anglais *Class II associated Invariant chain Peptide*), demeure liée à l'intérieur du sillon du CMH II (Nakagawa et al, 1998; Riese & Chapman, 2000; Shi et al, 1999). La libération du sillon s'effectue par l'activité hydrolytique de HLA-DM (H2-M

chez la souris), une protéine transmembranaire de type II de la famille des CMH (Jensen et al, 1999; Mosyak et al, 1998). Les peptides d'origines exogènes générés à l'intérieur des lysosomes remplacent CLIP en s'associant au sillon du CMH II.

L'activité de HLA-DM est modulée par le pH, mais également par HLA-DO, un hétérodimère αβ similaire à la molécule du CMH II (Kropshofer et al, 1998; van Ham et al, 1997). Les molécules HLA-DO forment des complexes avec une importante fraction des molécules HLA-DM. Cette interaction provoque l'inhibition partielle ou complète de HLA-DM. L'activité de HLA-DO inhibe la fixation de peptides exogènes dans les endosomes naissants. Son activité est optimale à pH 6. Dans les endosomes matures, le pH plus acide favorise l'activité de HLA-DM. HLA-DO est exprimée chez les lymphocytes B, les cellules épithéliales thymiques et les cellules dendritiques (Chen et al, 2006; Fallas et al, 2007; Hornell et al, 2006; Karlsson et al, 1991). Son expression est réduite durant l'activation des cellules dendritiques, ce qui favorise la présentation de peptides par les CMH II (Chen et al, 2006; Hornell et al, 2006).

Lorsque le peptide exogène est logé dans le sillon du CMH II, le complexe CMH II-peptide est exporté à la membrane plasmique pour stimuler les lymphocytes T CD4+. Les mécanismes impliqués dans le transport des molécules du CMH II vers la membrane plasmique demeurent toujours mitigés.

L'ubiquitination des domaines cytoplasmiques des CMH II régule leur abondance à la surface cellulaire (Matsuki et al, 2007; Ohmura-Hoshino et al, 2006; Shin et al, 2006; van Niel et al, 2006). L'ubiquitination des CMH II en surface provoque leur l'internalisation et leur recyclage au niveau du compartiment endosomal.

1.3.2.3 La présentation des peptides endogènes par les CMH II

Bien que les peptides présentés par les molécules du CMH II soient principalement de sources exogènes, certains peptides sont générés à partir de sources endogènes virales ou cellulaires (Jacobson et al, 1989; Rudensky et al, 1991). Les principales sources de peptides endogènes associés aux CMH II proviennent des protéines vacuolaires qui

côtoient naturellement la voie de présentation des CMH II (Chicz et al, 1993; Lechler et al, 1996). Plusieurs études démontrent cependant que certaines protéines topologiquement isolées de la voie de présentation des CMH II, telles que les protéines localisées dans le cytosol et le noyau, sont également des sources de peptides présentés par les CMH II (Dorfel et al, 2005; Nimmerjahn et al, 2003; Paludan et al, 2005). Ceci s'explique par le fait que certaines protéines endogènes soient des substrats de l'autophagie cellulaire. Ces substrats de l'autophagie sont par conséquent transloqués à l'intérieur des compartiments de chargement des CMH II (Chicz et al, 1993; Crotzer & Blum, 2009; Dengjel et al, 2005; Dongre et al, 2001; Levine & Deretic, 2007; Nimmerjahn et al, 2003; Schmid & Munz, 2007). Il a d'ailleurs été démontré que le processus d'autophagie est nécessaire à la sélection du répertoire des lymphocytes T CD4+ dans le thymus (Nedjic et al, 2008). Une récente étude démontre également que l'autophagie pourrait réguler la présentation de peptides viraux par les CMH I (Chemali et al, 2011; English et al, 2009).

1.4 L'IMMUNOPEPTIDOME

1.4.1 Caractérisation de l'immunopeptidome par spectrométrie de masse

L'immunopeptidome constitue l'ensemble des peptides présenté par les molécules du CMH I et II (Istrail et al, 2004; Purcell & Gorman, 2004). Au début des années 1990, l'utilisation de la spectrométrie de masse en immunologie représente le premier pas vers la caractérisation de l'immunopeptidome (Hunt et al, 1992). Le chimiste Donald Hunt et l'immunologiste Victor Engelhard estiment qu'environ 10 000 peptides différents sont présentés par les molécules du CMH (Engelhard, 1994a; Engelhard, 1994b; Engelhard et al, 1993; Huczko et al, 1993; Hunt et al, 1992; Lippolis et al, 2002). On estime également que chaque peptide associé aux CMH I est présent dans des proportions variant environ entre 1 à 10 000 copies par cellule (Engelhard et al, 2002; Hunt et al, 1992; Realini et al, 1994; Stern, 2007). En plus de révéler le haut niveau de complexité de l'immunopeptidome, l'utilisation de la spectrométrie de masse mènera à d'importantes découvertes telles que l'identification de peptides tumoraux (Cox et al, 1994; Henderson et al, 1993; Huang et al, 1996), d'antigènes mineurs d'histocompatibilité (den Haan et al,

1998; den Haan et al, 1995) et de modifications post-traductionnelles dans la séquence des peptides (Meadows et al, 1997; Skipper et al, 1996; Zarling et al, 2000).

Nos connaissances actuelles sur la composition de l'immunopeptidome sont très limitées. Par conséquent, la spectrométrie de masse et les méthodes d'analyses développées dans le domaine de la protéomique sont indispensables pour la caractérisation qualitative et quantitative de l'immunopeptidome. De nombreuses stratégies décrites ci-dessous ont été ou peuvent être utilisées pour l'isolation, l'identification et la quantification de l'immunopeptidome du CMH I (Figure 18). Pour faciliter la lecture de cette thèse, le terme immunopeptidome sera utilisé pour désigner l'immunopeptidome du CMH I.

1.4.1.1 L'isolation des peptides composants l'immunopeptidome

1.4.1.1.1 Élution acide douce

L'élution acide douce des peptides à partir de cellules vivantes représente l'une des premières méthodes décrites (Storkus et al, 1993). Le tampon acide utilisé permet de dénaturer les molécules du CMH I par la dissociation de la β_2m. Le peptide est par conséquent libéré dans le tampon d'élution. Cette technique possède l'avantage d'identifier de manière non biaisée l'ensemble des peptides (de fortes et faibles affinités) présentés par les molécules du CMH I. Cette technique est efficace, rapide, peu dispendieuse et peut être appliquée à tous les modèles cellulaires (Tableau 1). La présence de peptides contaminants non spécifiques pour les molécules du CMH I représente le principal inconvénient de cette méthode. Suivant l'élution acide des peptides à la surface cellulaire, une étude suggère que 40 % des peptides ainsi élués, seraient spécifiques aux molécules du CMH I (Torabi-Pour et al, 2002). Cette approche est par conséquent très peu utilisée jusqu'à ce jour pour l'analyse des peptides du CMH I par nanoLC-MS. Pour surmontrer cet inconvénient, l'utilisation de cellules contrôles (β2m-/- ou CMH I-/-) est indispensable.

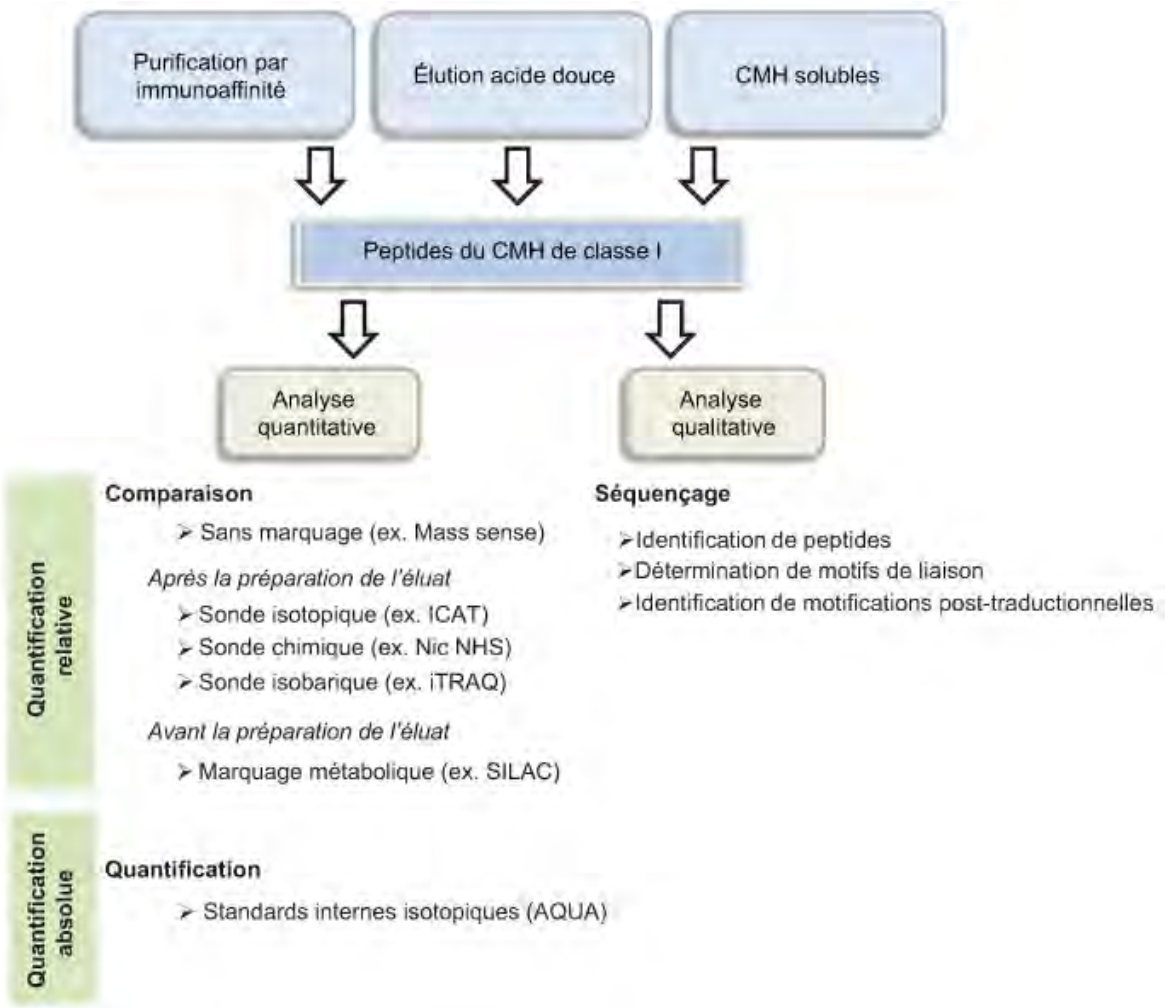

Figure 18. Approches pour isoler et quantifier l'immunopeptidome. Les peptides peuvent être isolés par élution acide douce, immunoaffinité ou à partir de complexes CMH I-peptide solubles et sécrétés. Les peptides isolés peuvent être analysés quantitativement ou qualitativement. L'évaluation qualitative des peptides associés aux CMH I est effectuée de nos jours presque exclusivement par LC-MS/MS. Les spectres obtenus par spectrométrie de masse permettent l'identification de peptides, la détermination de motifs de liaison et l'identification de modifications post-traductionnelles. Les analyses quantitatives peuvent être effectuées sans marquage, en comparant les changements de masse de peptides préalablement marqués par des isotopes stables, ou encore par l'ajout de peptides isotopiques (standards internes) dans l'échantillon pour une quantification absolue.

1.4.1.1.2 Immunoaffinité

La purification des complexes CMH I-peptide par immunoaffinité représente une approche plus ciblée par rapport à l'élution acide douce (Van Bleek & Nathenson, 1990). Les cellules sont d'abord lysées avec un détergent non dénaturant (zwitter-ionique

CHAPS ou non ionique NP-40). Les molécules du CMH sont ensuite précipitées en positionnant le lysat cellulaire sur une colonne d'affinité qui a préalablement été couplée à un anticorps spécifique contre l'allèle du CMH étudié. Les peptides sont ensuite élués avec un acide fort (ex. acide trifluoroacétique). Cette technique possède le grand avantage d'enrichir l'échantillon en peptides spécifiques pour le CMH en plus de pouvoir être appliquée à l'analyse de tous les modèles cellulaires (*in vitro* et *in vivo*) (Tableau 1). Par conséquent, cette technique est la plus couramment utilisée pour l'analyse des peptides du CMH en MS. Par contre, les détergents habituellement utilisés (CHAPS ou NP-40) pour la lyse cellulaire constituent une source de contamination pour la spectrométrie de masse. Cette approche peut également présenter certaines limitations pour l'étude de l'immunopeptidome de tissus humains puisque les rendements d'extraction sont faibles et les coûts relativement élevés (utilisation d'anticorps pour la purification). En effet, l'accès à une très grande quantité de cellules est nécessaire pour l'isolation d'un nombre suffisant de CMH I ($1x10^9$ à $1x10^{11}$ cellules). Les anticorps utilisés lors de la purification peuvent également provoquer un changement dans la conformation du CMH. Ce changement de conformation peut altérer l'affinité de liaison des peptides, et par conséquent, affecter l'intégrité de l'immunopeptidome à analyser (Bluestone et al, 1992; Solheim et al, 1993).

1.4.1.1.3 Les CMH solubles

Une autre méthode pour l'analyse de l'immunopeptidome implique l'utilisation de CMH solubles (Prilliman et al, 1997). Cette approche est basée sur l'utilisation de cellules transfectées exprimant des molécules du CMH sans domaine transmembranaire. Les complexes CMH I-peptide sont ainsi sécrétés dans le milieu de culture et peuvent être facilement purifiés par immunoprécipitation (Tableau 1). Cette méthode permet d'obtenir plusieurs milligrammes de peptides, ce qui représente un avantage significatif. En comparaison avec l'approche par lyse cellulaire, les préparations peptidiques ne contiennent pas de contaminations provenant de détergents ou de débris cellulaires, simplifiant ainsi l'analyse par nanoLC-MS. Cependant, cette technique s'applique uniquement à partir de modèles cellulaires *in vitro*. De plus, l'utilisation d'un CMH recombinant sécrété et surexprimé peut fausser considérablement la nature et l'abondance des peptides identifiés (Mester et al, 2011; Purcell & Gorman, 2001). Cette technique ne

permet donc pas d'étudier la nature de l'immunopeptidome sous des conditions physiologiques.

Tableau 1 : Comparaison des différentes méthodologies pour l'isolation des peptides du CMH I. Symboles : + (faible), ++ (modéré), +++ (élevé). IP : immunopurification. Adapté de (Fortier, 2009).

	Lysat cellulaire	**CMH soluble**	**Élution acide**
Purification par IP	Oui	Oui	Non
Rendement	+	+++	+++
Coût	+++	+++	+
Applicabilité	*in vitro, in vivo*	*in vitro*	*in vitro, in vivo*
Contaminant	Débris cellulaires, détergents et artéfacts IP	Artéfacts IP	Débris cellulaires
Débit	+	++	+++
Contrainte	Perte des peptides de faibles affinités	CMH artificiel	Nécessité un contrôle β2m-/- ou CMH -/-

1.4.1.2 L'identification de l'immunopeptidome par spectrométrie de masse

Le séquençage des peptides associés aux molécules du CMH I a principalement été effectué par deux méthodes : la dégradation Edman (Edman, 1949) et la spectrométrie de masse (Hillen & Stevanovic, 2006). Actuellement, l'identification des peptides s'effectue par spectrométrie de masse en tandem (MS/MS) couplée à la nano-chromatographie liquide (nanoLC) (Lemmel et al, 2004; Meiring et al, 2006). La technique la plus fréquemment utilisée pour la génération d'ions à partir des peptides est l'ionisation douce par électronébulisation (ESI) (Fenn et al, 1989) ou la désorption-ionisation laser assistée par matrice (MALDI) (Karas & Hillenkamp, 1988). La source ionisante ESI ou MALDI peut être couplée à différents analyseurs de masse. En appliquant des champs électromagnétiques, les analyseurs de masse trient les ions en fonction du ratio m/z. Les analyseurs de masse les plus fréquemment utilisés en protéomique sont les trappes ioniques [« linear trap quadupole » (LTQ)], le triple quadripôle (Q-q-Q), l'hybride quadripôle-temps d'envol (Q-q-TOF) ainsi que les instruments à haute résolution [FT-ICR (Han et al, 2008) et LTQ-Orbitrap (Makarov, 2000; Makarov et al, 2006a)]. Le LTQ-Orbitrap est un instrument de choix puisqu'il offre une sensibilité, une exactitude de masse et une résolution supérieure (Luber et al, 2010; Macek et al, 2006; Makarov et al,

2006b; Venable et al, 2007; Yates et al, 2006). Suivant la fragmentation des ions par CID (de l'anglais *Collision-Induced Dissociation*), les spectres de fragmentation sont détectés et analysés (Steen & Mann, 2004).

1.4.1.2.1 La fragmentation et le séquençage des peptides

Les types d'ions observés en MS/MS dépendent de plusieurs facteurs incluant la séquence primaire, la quantité d'énergie, l'état de charge, etc. La fragmentation par CID provoque le clivage au niveau de la liaison de la chaîne peptidique et génère des séries d'ions à partir de la région N- ou C-terminal du peptide. Les fragments sont détectés seulement s'ils portent au moins une charge. La nomenclature sur les séries d'ions a d'abord été proposée par Roepstorff et Fohlman (Roepstorff, 1984), pour ensuite être modifiée par Johnson et al. (Johnson, 1987). Si la charge est retenue sur le fragment en N-terminal, l'ion est de série *a*, *b* ou *c*. Si la charge est retenue sur le fragment en C-terminal, le type d'ion est de série *x*, *y* ou *z*. L'analyse du spectre MS/MS permet de déduire la séquence peptidique à partir des différences de masse observées entre les fragments consécutifs d'une même série. Une description exhaustive de la fragmentation et du séquençage des peptides va au delà de l'objectif de cette thèse mais a récemment été revue (Bramoullé, 2010).

1.4.1.2.2 L'identification des peptides à partir des banques de données

L'analyse des spectres MS/MS est principalement effectuée à partir des banques de données. Cette approche permet de maximiser l'identification à grande échelle des peptides. Le principe de cette approche consiste à établir une corrélation de similarité entre les spectres MS/MS expérimentaux et les spectres théoriques retrouvés dans les banques de données (Steen & Mann, 2004). Plusieurs algorithmes tels que SEQUEST (Craig & Beavis, 2003) et MASCOT (Perkins et al, 1999) sont utilisés pour effectuer une recherche basée sur le principe de la similarité spectrale. MASCOT simule la fragmentation et détermine la probabilité pour une séquence peptidique donnée de produire le spectre observé; SEQUEST se basent sur le comptage du nombre de pics partagés entre les spectres théoriques et expérimentaux (Bramoullé, 2010). Cette méthode de recherche est rapide, fiable et fréquemment utilisée. Lorsque les peptides ne sont pas

répertoriés à l'intérieur des banques de données, une autre méthode telle que le séquençage *de novo* doit être utilisée (Bramoullé, 2010).

1.4.1.2.3 Les méthodes de quantification par spectrométrie de masse

Plusieurs techniques dans le domaine de la protéomique ont été développées pour quantifier de manière relative ou absolue les signaux détectés par spectrométrie de masse (Gingras et al, 2007). Les techniques décrites ci-dessous peuvent être utilisé pour quantifier les peptides composants l'immunopeptidome (Lemmel et al, 2004; Meiring et al, 2006; Mester et al, 2011; Milner et al, 2006; Weinzierl et al, 2007). Parmi ces techniques, on compte le marquage isotopique chimique (ICAT, iTRAQ, AQUA) et métabolique (SILAC), ainsi que l'approche sans marquage. Le tableau 2 indique les avantages et les inconvénients de chacune des approches.

1.4.1.2.3.1 ICAT

La technique ICAT (de l'anglais *Isotope-Coded Affinity Tag*) permet de comparer l'abondance relative des peptides entre deux échantillons (Gygi et al, 1999). Cette méthode se base sur l'utilisation de réactifs chimiques de marquage. Les réactifs ICAT sont constituées de trois éléments : 1) un groupe réactif envers un thiol (le groupement thiol-SH des cystéines des peptides réagit avec l'iodoacétamide des réactifs ICAT), 2) une biotine et 3) une sonde isotopique lourde ou légère. Pour la quantification relative entre deux échantillons, un échantillon est marqué avec une sonde isotopique légère et l'autre échantillon avec une sonde isotopique lourde (Figure 19A). Pour minimiser les erreurs, les deux échantillons peptidiques sont combinés. Les peptides sont séparés par chromatographie d'affinité sur avidine par l'intermédiaire du groupement biotine. Les peptides identiques sont élués ensemble puisqu'ils ne diffèrent que par la présence de

l'isotope léger ou lourd. Les différences isotopiques provoquent un changement de masse entre chacun des peptides comparés. L'abondance relative est ensuite déterminée à partir des ratios d'intensité des signaux MS provenant des ions peptidiques légers et lourds. À

noter que la méthode ICAT n'a jamais été utilisée jusqu'à ce jour pour quantifier les peptides de l'immunopeptidome. Il est par ailleurs peu concevable d'opter pour cette méthode de quantification étant donné la faible présence de résidu cystéine dans la composition des peptides de l'immunopeptidome.

La structure imposante des réactifs ICAT influence cependant le spectre de fragmentation, ce qui représente un désavantage considérable pour l'identification des peptides. Plusieurs agents chimiques réagissant contre la partie N-terminale des peptides permet de contourner ce problème : 1) phenyl isocyanate (PIC): PIC réagit quantitativement à pH neutre sur les amines en position N-terminale des peptides. Le PIC deutéré (d_5) fourni une augmentation de masse suffisante pour permettre la quantification relative par MS. Ce réactif est disponible commercialement à faible coût (Mason & Liebler, 2003); 2) O-méthlisourea : ce réactif permet de convertir les résidus lysine en résidus homoarginine, introduisant ainsi une augmentation de masse de 42 dalton. Cette approche est cependant limitée pour les peptides contenant des lysines (Cagney & Emili, 2002); 3) acétylation : l'échantillon peptidique est séparé en deux parties, l'une est traitée avec le $^{1}H_6$-acetic anhydride, et l'autre avec le $^{2}D_6$-acetic anhydride. En conséquent, les variants peptidiques $^{1}H_3$-acétylés et $^{2}D_3$-acétylés diffèrent par une masse de 3Da. Cette approche est rapide, facile à effectuer et reproductible (Lemmel et al, 2004); 4) nicotinoyloxy succinimide (Nic NHS) : l'échantillon peptidique est séparé en deux parties, l'une est traité avec le $^{1}H_4$-Nic, et l'autre avec le $^{2}D_4$-Nic. En conséquent, les peptides de chacune des deux parties diffèrent par une masse de 4Da. La nicotinylation améliore la sensibilité lors de l'identification finale des peptides puisqu'elle maintient et renforcit

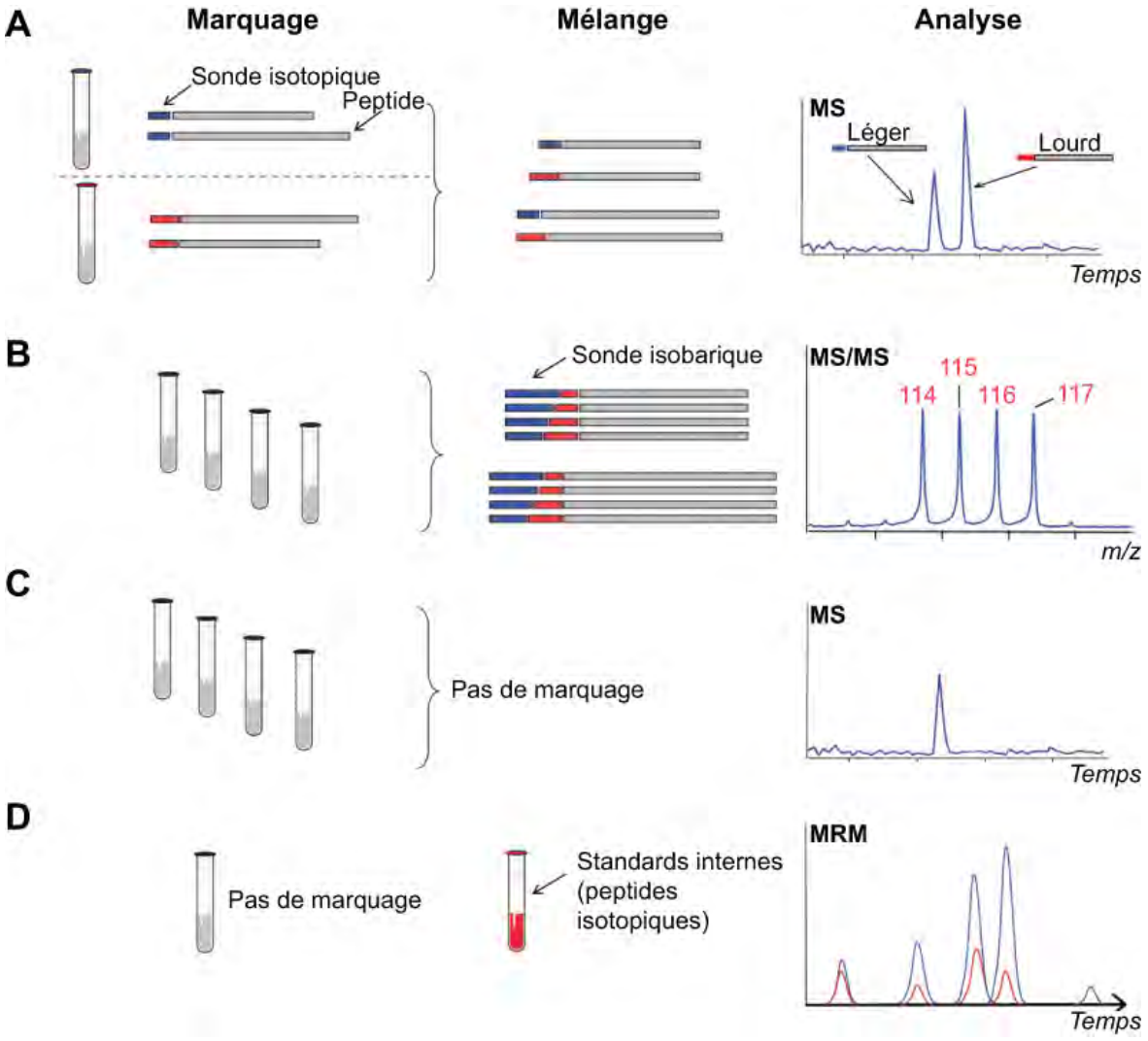

Figure 19. Stratégies pour la quantification relative ou absolue des peptides. (**A**) La technique ICAT est basée sur l'incorporation d'une sonde isotopique légère aux peptides du premier échantillon et de l'incorporation d'une sonde isotopique lourde dans le second échantillon. L'incorporation des isotopes stables s'effectue par réaction chimique. Les échantillons marqués sont ensuite mélangés et analysés. (**B**) La technique iTRAQ est basée sur le marquage des peptides avec une série de sondes composée de deux éléments. Ces sondes sont dites isobariques puisqu'elles possèdent toutes une masse constante. La quantification est effectuée en mode MS/MS en mesurant l'intensité relative du groupe rapporteur attaché en position N-terminale. (**C**) La quantification sans marquage est effectuée en comparant les intensités MS pour chacun des ions peptidiques entre les différents échantillons. La quantification sans marquage des échantillons au préalable nécessite l'utilisation de logiciels informatiques particuliers. (**D**) L'approche AQUA est utilisée pour la quantification absolue des peptides. Des standards internes, c.-à-d. des peptides isotopiques, sont ajoutés à différentes concentrations dans l'échantillon. Cette technique permet d'effectuer une quantification précise des peptides d'intérêt étudiés par l'utilisation de courbes de calibration.

l'état de charge des peptides (Lemmel et al, 2004; Munchbach et al, 2000; Schmidt et al, 2005). La quantification relative de l'immunopeptidome entre des tissus normaux et cancéreux a récemment été effectuée par nicotinylation (Lemmel et al, 2004; Weinzierl et al, 2007).

1.4.1.2.3.2 iTRAQ

L'approche iTRAQ (de l'anglais *Isobaric Tag for Relative and Absolute Quantitation*) se base sur l'incorporation chimique d'une sonde isobarique (Figure 19B) (Ross et al, 2004). Contrairement à l'approche ICAT, la quantification iTRAQ s'effectue en MS2 (MS/MS). En effet, les peptides provenant de sources différentes ne sont pas distingués par un changement de masse, mais plutôt par la présence d'ions rapporteurs dans le spectre de fragmentation. Jusqu'à huit ions rapporteurs MS/MS différents, sont disponibles pour quantifier l'expression des protéines ou peptides dans une seule analyse (Choe et al, 2007), augmentant ainsi la cadence analytique.

Le principe de la méthode iTRAQ repose sur le marquage de peptides avec une série de réactifs formant un lien covalent avec les amines primaires de l'extrémité N-terminale. Ces différents réactifs sont dits isobariques car ils possèdent tous une masse moléculaire de 145 Da. Lors de l'analyse MS, les peptides marqués (précurseurs) sont détectés avec la masse intrinsèque du peptide plus 145 Da provenant du réactif iTRAQ. Ce n'est qu'à l'étape de fragmentation du peptide (MS/MS) que l'on peut apprécier la contribution de chacun des quatre peptides qui se traduit par la libération d'ions ayant des masses de 114, 115, 116 ou 117 Da. L'intégration de l'aire sous la courbe des pics émanant de ces ions rapporteurs permet la quantification relative puisqu'un ratio des valeurs d'intégration peut-être calculé pour chaque peptide détecté. D'autres méthodes de quantification en MS2 ont plus récemment été développées (ex. iMSTIQ) (Yan *et al*, 2011). À noter que les approches de quantification en MS2 n'ont jamais été utilisée jusqu'à ce jour pour la quantification des peptides composant l'immunopeptidome.

Tableau 2. Comparaison des différentes approches utilisées pour la quantification relative de l'immunopeptidome. Adapté de (Fortier, 2009).

	Marquage métabolique	Marquage chimique	Sans marquage
Applicabilité	*in vitro, in vivo*	*in vitro, in vivo*	*in vitro, in vivo*
Complexité des échantillons	+++	+++	++
Coût : préparation	+++	+++	+
Débit : préparation	+	++	+++
Débit : analyse MS	+++	+++	++
Contrainte	Limité pour les applications *in vivo*	Réactions secondaires chimiques possibles	Besoin de méthodes LC-MS reproductibles et outils bioinformatiques efficaces

1.4.1.2.3.3 SILAC

L'approche SILAC (de l'anglais *Stable Isotope Labelling by Amino acids in Cell culture*) se base sur l'incorporation métabolique d'isotopes stables lors de la synthèse des protéines (Ong et al, 2002). Les cellules sont cultivées dans un milieu contenant soit des acides aminés naturels (synthèse de protéines « légères »), soit leurs équivalents isotopiquement marqués (synthèse de protéines « lourdes »). L'arginine et la lysine sont les acides aminés les plus fréquemment utilisés pour le marquage. Les populations cellulaires à comparer sont mélangées et traitées comme un seul échantillon, ce qui permet de préparer les peptides d'intérêt sans risquer d'introduire des erreurs de quantification. À l'analyse, l'abondance relative entre les échantillons biologiques peut être calculée pour chaque peptide en comparant l'intensité des peptides légers et lourds. Des études *in vivo* peuvent également être effectuées à partir de souris SILAC (Kruger et al, 2008). L'approche SILAC a récemment été utilisée pour évaluer la corrélation entre le protéome cellulaire et l'immunopeptidome (Milner et al, 2006).

1.4.1.2.3.4 Sans marquage

En plus des nombreuses stratégies de marquages mentionnées ci-dessus, certains efforts ont été déployés pour développer des méthodes de quantification sans marquage. Dans ce

cas, la comparaison de différents échantillons est possible sans aucune modification préalable (Figure 19C). La quantification relative est effectuée en comparant les intensités MS pour chacun des ions peptidiques entre les différents échantillons. Le développement et l'utilisation de programmes informatiques (ex. Mass sense) est indispensable au succès de cette approche (Bonneil, 2007). L'utilisation de cette méthode permet la comparaison d'un nombre infini d'échantillons. Contrairement aux méthodes de marquage, les différents échantillons peptidiques ne sont pas manipulés avant leur analyse, offrant ainsi des avantages considérables au niveau de l'intégrité des échantillons peptidiques à analyser. La quantification relative sans marquage exige cependant des méthodes LC-MS hautement reproductibles. À noter que dans le cadre de cette thèse, cette méthode a été utilisée pour quantifier les peptides composant l'immunopeptidome.

1.4.1.2.3.5 AQUA

La technique des peptides AQUA (de l'anglais *Absolute QUAntification*) permet de réaliser la quantification absolue de protéines ou de peptides contenus dans un échantillon biologique (Papaioannou et al, 2010). Cette technique repose sur le principe du standard interne marqué par des isotopes stables (Figure 19D). Un peptide AQUA est un peptide synthétique qui possède la même séquence d'acides aminés que le peptide natif sélectionné, mais qui comporte un acide aminé alourdi par plusieurs isotopes stables (13C, 15N, 2D) permettant d'augmenter la masse du peptide de 6 à 10 Da. Après la préparation de l'éluat dans lequel est contenu les peptides à quantifier, les peptides AQUA sont ajoutés en quantité connue en tant que standard interne. L'échantillon est ensuite analysé par spectrométrie de masse. Les peptides natifs et les peptiques AQUA sont détectés au même temps de rétention et possèdent les mêmes propriétés d'ionisation. Ils sont toutefois facilement distingués en spectrométrie de masse par la différence de masse due au marquage isotopique. La quantité de peptide natif peut alors être déterminée à partir du rapport d'intensité observé entre le signal correspondant au peptide natif et le signal correspondant au peptide AQUA présent en quantité connue. Puisque les peptides AQUA doivent être identifiés et synthétisés, cette méthode est considérablement ciblée et limitée à un nombre beaucoup plus restreint de peptides. L'utilisation de cette stratégie prévient

par conséquent les analyses quantitatives à grande échelle en plus d'être uniquement applicable aux peptides du CMH déjà connus et répertoriés. À noter que la méthode AQUA n'a jamais été utilisée, jusqu'à ce jour pour quantifier les peptides de l'immunopeptidome.

1.4.2 Analyse systématique sur l'origine de l'immunopeptidome

Les approches réductionnistes utilisées au cours des vingt dernières années ont permis de dévoiler de nombreux mécanismes régulant la présentation des peptides par les CMH I (Yewdell, 2007). L'utilisation d'approches systématiques modernes a pour objectif d'accélérer et d'approfondir nos connaissances sur l'origine de l'immunopeptidome.

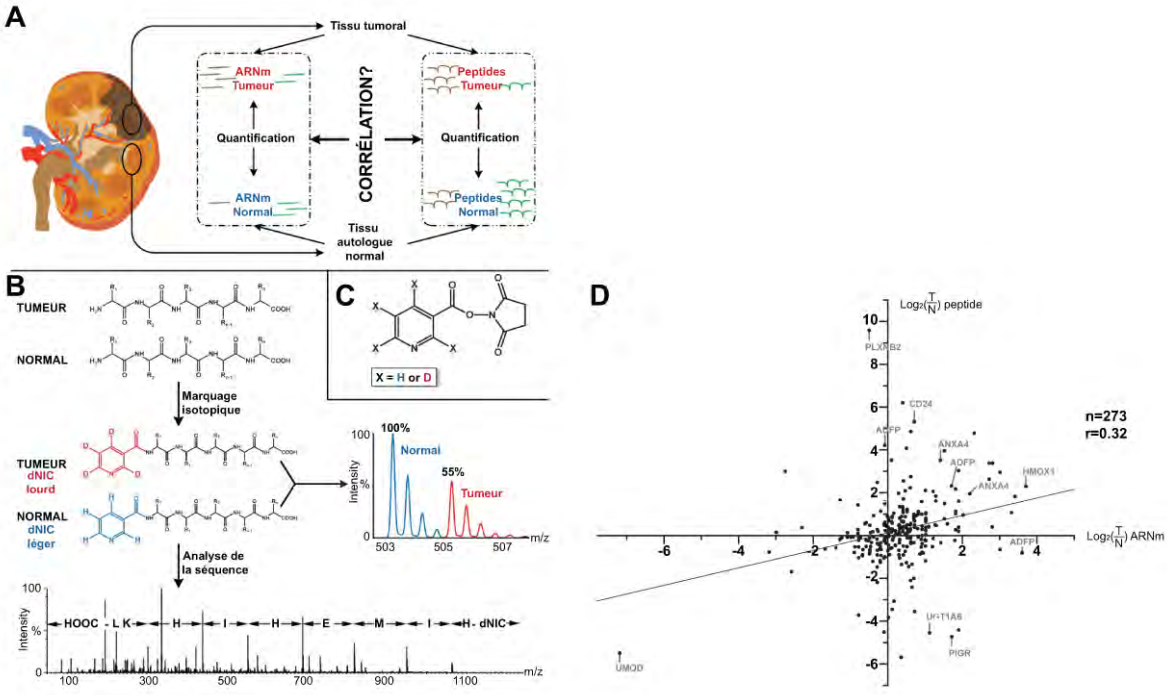

Figure 20. Stratégie pour l'analyse de corrélation entre l'abondance relative des peptides du CMH I et des ARNm sources. (A) L'ARNm et les peptides ont été isolés à partir de tissus humain rénaux seins et cancéreux. La quantification relative a été effectuée à partir des deux échantillons et la corrélation entre les données quantitatives a été déterminée. (B) Les peptides du CMH I ont été modifiés avec la version lourde et légère du réactif dNIC. Pour l'analyse des ratios, les deux échantillons ont été mélangés dans un ratio peptidique de 1:1. (C) Réactif dNIC. X représente la position du marquage isotopique stable. D représente deutérium. (D) Corrélation entre l'expression relative des ARNm sources de peptides et l'abondance relative de leur peptide correspondant. Tiré de (Weinzierl *et al.*, 2007).

En 2004, une analyse systématique de l'immunopeptidome révèle pour la première fois que les protéines sources de peptides proviennent de presque tous les compartiments cellulaires (Hickman et al, 2004). Les auteurs observent que chaque peptide identifié provient généralement de protéines sources différentes. Leurs résultats indiquent donc que l'immunopeptidome représente une vue d'ensemble du protéome cellulaire. Hickman et ses collaborateurs notent de plus que les protéines liant l'ARN et l'ADN semblent contribuer davantage à la génération de l'immunopeptidome.

En 2006, une analyse à partir de 51 peptides associés aux CMH I indique que l'abondance d'environ 6 % des peptides corrèle avec l'abondance relative de leur protéine source correspondante (Milner et al, 2006). Ce faible pourcentage appuie donc les évidences actuelles, générées par des approches réductionnistes classiques, indiquant que les peptides proviennent majoritairement de protéines rapidement dégradées (PRDs/DRiPs) (voir section 1.3.1.3.3.1). L'immunopeptidome serait donc davantage une représentation du dégradome plutôt que du protéome cellulaire.

En 2007, le groupe de Stefan Stevanovic effectue à partir de tissus rénaux normaux et cancéreux une corrélation entre l'abondance relative des peptides et leur ARNm source correspondant (Weinzierl et al, 2007). L'analyse suivant la quantification relative de 273 peptides par nicotinylation et ARNm sources par puces d'ADN n'indique aucune corrélation stricte ($r = 0.32$) (Figure 20). Le niveau d'expression relatif des transcrits aurait donc un faible pouvoir prédictif sur l'abondance des peptides présentés.

Bien que l'immunopeptidome joue un rôle vital dans le développement et la réponse du système immunitaire, nos connaissances sur sa composition et sa genèse demeurent donc très limitées jusqu'à ce jour (Perreault, 2010).

1.5 OBJECTIFS DU PROJET DE RECHERCHE

Article 1 : The structure and location of SIMP/STT3B account for its prominent imprint on the MHC I immunopeptidome

Ce premier projet tentait de répondre à la question fondamentale suivante : pourquoi certaines protéines contribuent plus fortement à la composition de l'immunopeptidome? Pour répondre à cette question, nous avons choisi d'étudier les caractéristiques intrinsèques de la protéine SIMP/STT3B. Cette protéine représente un modèle de choix puisqu'elle correspond à un « phénotype extrême » en générant une très grande quantité de peptides associés aux molécules du CMH I. En effet, chez la souris $H2^b$, environ 1% des molécules $H2D^b$ des cellules de la rate sont occupées par KAPDNRETL, un peptide provenant de SIMP/STT3B. De la même manière, les peptides de SIMP/STT3B DERVFVALY et NLYDKAGKV, sont parmi les plus abondants dans l'immunopeptidome des cellules exprimant respectivement HLA-B*1801 et HLA-A2.

Article 2 : The MHC class I peptide repertoire is molded by the transcriptome

Ce deuxième projet avait comme objectif de comprendre la structure et la genèse de l'immunopeptidome. En collaboration avec l'équipe du Dr. Pierre Thibault, notre objectif consistait d'abord à développer une nouvelle approche analytique par spectrométrie de masse pour identifier et quantifier les peptides composant l'immunopeptidome. En collaboration avec l'équipe du Dr. Sébastien Lemieux, nous avons également posé quatre questions plus spécifiques : 1) est-ce que l'immunopeptidome reflète la composition du transcriptome? 2) est-ce que certaines familles de gènes sont surreprésentées dans l'immunopeptidome? 3) quel est l'impact de la transformation néoplasique sur la composition de l'immunopeptidome? et 4) est-ce qu'une plate-forme de séquençage de peptides à grande échelle pourrait être utilisée pour l'identification d'épitopes immunogènes associés aux tumeurs?

Article 3 : The MHC I immunopeptidome conveys to the cell surface an integrative view of cellular regulation

Ce troisième projet avait pour objectif de répondre à la question fondamentale suivante : l'immunopeptidome est-il plastique (ou dynamique) et est-il affecté par l'état métabolique de la cellule? Cette question est d'ordre fondamentale puisque les cellules ciblées par les lymphocytes T CD8 sont métaboliquement perturbées par les virus/pathogènes ou encore par différents événements impliqués dans la transformation néoplasique. Pour répondre à cette question, nous devions quantifier les peptides composant l'immunopeptidome de cellules traitées avec l'inhibiteur classique de mTOR : la rapamycine. Nous avons sélectionné ce modèle en collaboration avec le Dr. Philippe Roux puisque la rapamycine inhibe exclusivement mTOR et parce que mTOR est un régulateur central de l'homéostasie cellulaire en promouvant et en inhibant respectivement des processus anaboliques et cataboliques.

Article 4 : A comprehensive map of the mTOR signaling network

Dans le troisième projet mentionné ci-dessus, une question additionnelle s'est posée en cours de route: les changements dans l'immunopeptidome suivant le traitement des cellules à la rapamycine sont-ils fonctionnellement reliés au réseau de signalisation mTOR? Pour répondre à cette question, il était nécessaire d'amorcer un quatrième projet en parallèle. En collaboration avec l'équipe du Dr. Hiroaki Kitano, notre objectif était de construire une carte illustrant de manière exhaustive l'ensemble du réseau de signalisation mTOR.

CHAPITRE 2

MISE EN SITUATION:

Les protéines montrent des divergences drastiques dans leur contribution à la composition de l'immunopeptidome. Pour mieux comprendre pourquoi certaines protéines contribuent plus activement à la génération de peptides associés aux molécules du CMH I, nous avons choisi d'étudier les caractéristiques intrinsèques de SIMP/STT3B car cette protéine génère des quantités très élevées de peptides associés au CMH I chez la souris et les humains. En utilisant des approches réductionnistes classiques, nous avons étudié les propriétés biochimiques, la localisation intracellulaire de SIMP/STT3B, en plus de caractériser un domaine particulier dans la séquence primaire de la protéine.

Dans le cadre de cette étude, nous montrons que les caractéristiques clés de SIMP/STT3B sont 1) sa région riche en lysine, 2) sa propension à mal se replier, et 3) sa localisation dans la membrane du réticulum endoplasmique à proximité de l'immunoprotéasome. De plus, nous montrons que le couplage de SIMP/STT3B peut être utilisé pour favoriser la présentation d'un peptide sélectionné, le peptide OVA SIINFEKL dans cette étude. Ces données fournissent de nouvelles connaissances sur la relation entre le protéome des cellules et l'immunopeptidome du CMH I. Nos résultats suggèrent que la contribution d'une protéine donnée à l'immunopeptidome du CMH I résulte de l'interaction d'au moins trois facteurs: la présence de dégrons (signaux de dégradation), la tendance de la protéine au mauvais repliement et sa localisation subcellulaire. Finalement, nos travaux indiquent que les substrats de la voie de dégradation du réticulum endoplasmique pourraient contribuer préférentiellement à la composition de l'immunopeptidome du CMH I.

2. ARTICLE 1:

The structure and location of SIMP/STT3B account for its prominent imprint on the MHC I immunopeptidome

Étienne Caron[1,2‡], Renée Charbonneau[1,2‡], Gabrielle Huppé[1], Sylvie Brochu[1] and Claude Perreault[1,2*]

Institute for Research in Immunology and Cancer[1], and Department of Medicine[2], University of Montreal, CP 6128, Downtown Station, Montreal, Quebec, Canada, H3C 3J7

Manuscript information: Abstract: 199 words
Total length: 58 458 characters (incl. spaces)
Materials and Methods: 993 words
Introduction, Results and Discussion section: 4 576 words

Running title: STT3B imprints on the MHC I immunopeptidome

‡EC and RC contributed equally to this work

*Corresponding authors:

Dr. Claude Perreault

Article publié dans: **International Immunology, Volume 17, p. 1583-1596 (2005).**

CONTRIBUTIONS DES AUTEURS:

Etienne Caron a participé à la conception du projet, à l'analyse des résultats et aux figures 1, 2, 7, 8, 9 et 10. Renée Charbonneau a participé à la microscopie électronique et aux figures 4, 5, 6 et 7. Gabrielle Huppé a participé aux figures 4 et 5. Sylvie Brochu a participé à la figure 3. Claude Perreault a participé à la conception du projet, à l'analyse des résultats et à l'écriture du manuscrit.

2.1 Abstract

Proteins show drastic discrepancies in their contribution to the collection of self-peptides that shape the repertoire of CD8 T cells (MHC I self-immunopeptidome). To decipher why selected proteins are the foremost sources of MHC I-associated self-peptides, we chose to study SIMP/STT3B because this protein generates very high amounts of MHC I-associated peptides in mice and humans. We show that the endoplasmic reticulum-associated degradation pathway and MHC I processing intersect at SIMP/STT3B. Relevant key features of SIMP/STT3B are its lysine-rich region, its propensity to misfold, and its location in the endoplasmic reticulum membrane in close proximity to the immunoproteasome. Moreover, we show that coupling to SIMP/STT3B can be used to foster MHC I presentation of a selected peptide, here the OVA peptide SIINFEKL. These data yield novel insights into relations between the cell proteome and the MHC I immunopeptidome. They suggest that the contribution of a given protein to the MHC I immunopeptidome results from the interplay of at least three factors: the presence of degrons (degradation signals), the tendency of the protein to misfold and its subcellular localization. Furthermore, they indicate that substrates of the endoplasmic reticulum-associated degradation pathway may have a prominent imprint on the MHC I self-immunopeptidome.

2.2 Introduction

The role of classical MHC class I molecules is to display a small sample of the cell proteome, referred to as the immunopeptidome, for scrutiny by CD8 T cells (Pamer and Cresswell, 1998; Rock *et al*, 2002; Yewdell and Bennink, 2001a). Under basal conditions, the immunopeptidome is composed of short peptides, typically nonamers, derived from 'self'-proteins. The self-immunopeptidome molds T cell development and homeostasis by regulating intrathymic positive and negative selection, as well as peripheral T cell survival and expansion (Goldrath and Bevan, 1999). Moreover, those among self-peptides that display inter-individual polymorphism (i.e. minor histocompatibility antigens) represent a major barrier in transplantation (Perreault *et al*, 1990; Simpson and Roopenian, 1997), while those that are expressed selectively or preferentially on neoplastic cells are potential targets for cancer immunotherapy (Boon and van der Bruggen, 1996). Studies based on sequencing of MHC-associated peptides by mass spectrometry suggest that some proteins supply much more MHC-associated peptides than others (Engelhard *et al*, 2002; Hickman *et al*, 2004).

To decipher why selected proteins are foremost sources of MHC I-associated self-peptides, we chose to study SIMP/STT3B because this protein displays an 'extreme phenotype' in that it generates exceedingly high amounts of MHC I-associated peptides in mice and humans. In $H2^b$ mice, ~1% of D^b molecules on spleen cells are occupied by KAPDNRETL, a peptide derived from SIMP/STT3B (Fontaine *et al*, 2001; McBride *et al*, 2002; Pion *et al*, 1999; Pion *et al*, 1997) (Figure 1). Likewise, following comprehensive proteomic analyses of the HLA-B*1801 immunopeptidome, the SIMP/STT3B DERVFVALY peptide emerged as one of the most abundant peptides (Hickman *et al*, 2004). Moreover, we recently found that the SIMP/STT3B NLYDKAGKV peptide was a major constituent of the HLA-A2 immunopeptidome (C. Perreault, unpublished observation). SIMP (source of immunodominant MHC-associated peptides) was originally identified as the gene encoding the immunodominant $B6^{dom1}/H7^a$ minor histocompatibility antigen ($H2D^b$-associated KAPDNRETL peptide) (McBride *et al*, 2002). SIMP was later shown to represent one of the two functional homologs of the yeast STT3 protein found in multi-cellular eukaryotes and was thus named STT3B (Annexe 1) (Kelleher *et al*, 2003).

STT3 homologs, large polytopic glycoproteins located in the endoplasmic reticulum (ER) membrane, contain the active site of the oligosaccharyltransferase complex that catalyzes N-linked glycosylation of nascent proteins in the lumen of the ER (Nilsson *et al*, 2003).

Current evidence suggests that the MHC I immunopeptidome derives from the rapid degradation of newly synthesized proteins (Reits *et al*, 2000; Schubert *et al*, 2000). Rapidly degraded proteins are of two types: normal short-lived proteins and defective ribosomal products (DRiPs) (Ostankovitch *et al*, 2005; Shastri *et al*, 2002; Yewdell, 2003). As defined by Yewdell (Yewdell, 2003), DRiPs 'include properly translated but misfolded proteins and misbegotten polypeptides resulting from mistakes in the fidelity of transcription or translation'. The processing of antigens to generate MHC I-associated antigenic peptides occurs predominantly, though not exclusively, by proteasome-mediated degradation (Kessler *et al*, 2003; Rock *et al*, 2002). Proteasomes are present in the cytoplasm and nuclei of all eukaryotic cells, but with highly variable relative abundance within those compartments (Wojcik and DeMartino, 2003). Several studies have shown proteasome enrichment in the vicinity of the microtubule organizing center (MTOC) and on the cytosolic side of the ER (Anton *et al*, 1999; Brooks *et al*, 2000; Lacaille and Androlewicz, 2000). This raises the interesting possibility that subcellular localization of proteins might influence their proteasomal degradation. Because of the lack of proteasome inside the ER (Reits *et al*, 2003), degradation of ER proteins must be preceded by their retrotranslocation (or dislocation) from the ER to the cytosol for degradation by the proteasome in a process called endoplasmic reticulum-associated degradation (ERAD) (Sitia and Braakman, 2003). In our quest to understand why STT3B has a prominent contribution to the MHC I immunopeptidome, we found that MHC I processing and ERAD intersect at STT3B. The results of our studies suggest that three features render STT3B a major ERAD substrate: its location in the ER membrane, its propensity to form DRiPs and its conserved lysine-rich region that functions as a degradation signal (degron). Furthermore, we found that coupling to STT3B can be used to increase MHC I presentation of a selected peptide.

2.3 Methods

Plasmid constructs

STT3B construct was generated by inserting the coding sequence of mouse STT3B (McBride *et al*, 2002) in pcDNA3 vector (Invitrogen, Burlington, Canada). EGFP-STT3B and c-myc-STT3B were constructed by inserting the STT3B ORF into pEGFP-C2 (Clontech, Mountain View, USA) and pCMV-Tag3C (Stratagene, Cedar Creek, USA), respectively. STT3B-FLAG was produced following PCR amplification to create a mutation into the stop codon, and then inserted into the pFLAG-CMV5a vector (Sigma-Aldrich, Oakville, Canada). EGFP-STT3B construct encoding SIINFEKL instead of KAPDNRETL peptide (EGFP-STT3B-SIINFEKL) was inserted into pEGFP-C1 (Clontech). EGFP-STT3B-SIINFEKL was created by PCR using a reverse primer extended by the SIINFEKL coding sequence to produce $STT3B_{1-780}$-SIINFEKL. $STT3B_{789-823}$ was excised and inserted with $STT3B_{1-780}$-SIINFEKL in the same ORF into pEGFP-C1. EGFP-SIINFEKL was created following insertion of the SIINFEKL coding sequence into pEGFP-C1. The $STT3B_{790-823}$ coding sequence was excised to produce EGFP-$STT3B_{\Delta 790-823}$-SIINFEKL. To create EGFP-$STT3B_{\Delta 612-662}$-SIINFEKL, $STT3B_{1-611}$ and $STT3B_{663-823}$ coding region were amplified by PCR and inserted in the same ORF into pEGFP-C1 vector. EGFP-OVA-$STT3B_{790-823}$ was created following insertion of OVA_{61-386} and $STT3B_{790-823}$ in the same ORF into pEGFP-C1 vector. HA-ubiquitin was a gift from Dr. S. Meloche (Institute of Research in Immunology and Cancer, University of Montreal, Qc, Canada). pIRES2-EGFP cloning vector (Clontech) was used to insert the OVA and MSIINFEKL ORF excised from pcDNA3.1 (kindly provided from Dr. K. Rock, Department of Pathology, University of Massachusetts Medical School, Worcester, Massachusetts), and STT3B-SIINFEKL from pEGFP-C1. To create OVA-$STT3B_{790-823}$ into pIRES2-EGFP vector, the OVA coding sequence was amplified by PCR to create a mutation into the stop codon, and then inserted with the $STT3B_{790-823}$ coding region in the same ORF. To generate EGFP-SIINFEKL, two oligonucleotides encoding SIINFEKL peptide were annealed and inserted into pEGFP-C1. $STT3B_{790-823}$ coding sequence was added to EGFP-SIINFEKL to generate EGFP-SIINFEKL-$STT3B_{790-823}$.

Reagents and Abs

Clasto-lactacystin β-lactone was purchased from Calbiochem (San Diego, USA), 3-methyl-adenine and bafilomycin A1 from Sigma-Aldrich, and recombinant human IFN-γ from Peprotech (Rocky Hill, USA). Rabbit polyclonal Ab against the following molecules was used: anti-calnexin and anti-calreticulin from Stressgen (Victoria, Canada), anti-c-myc from Abcam (Cambridge, USA), anti-Sec61β from Upstate Biotechnology (Waltham, USA), anti-LMP2 from Affiniti **(**Exeter, UK**)**, and anti-HA from Santa Cruz Biotechnology (Santa Cruz, USA). Mouse monoclonal anti-γ-tubulin (clone GTU-88) and anti-FLAG (clone M2) Abs were from Sigma-Aldrich. Goat anti-mouse and anti-rabbit Cy3-labeled Abs were from Jackson ImmunoResearch (West Grove, USA). Dr. J. Yewdell (National Institute of Allergy and Infectious Diseases, Bethesda, MD) kindly provided the 25-D1.16 hybridoma (Porgador *et al*, 1997) as well as Alexa-labeled 25-D1.16 mAb (anti-K^b-SIINFEKL).

Membrane preparation, SDS-PAGE and Western Blotting

COS-7-K^b cells were transfected with c-myc-STT3B construct. After 48 h, growth media was removed, and cells were washed twice with TBS containing protease inhibitor cocktail (PIC, Roche, Laval, Canada) and 20 mM N-ethylmaleimide (NEM, Sigma-Aldrich). The cells were harvested with TBS containing 2mM EDTA, 20 mM NEM, 20mM MG-132 (Calbiochem), PIC and 1mM PMSF, recovered by centrifugation, quick frozen in liquid nitrogen and stored at –80C. After thawing, the cell pellet was suspended in buffer A (25mM Tris-Cl, 0.25M sucrose, 5 mM $MgCl_2$, 2 mM EDTA, 20 mM NEM, 20 mM MG-132, PIC and 1 mM PMSF) and cells were broken with an Ultra Turrax T-25 homogenizer (Janke and Kunkel, Markham, Canada). After removing the nuclei, the homogenate was centrifuged for 2 h at 150 000 X g to pellet the membrane fraction. The pellet was resuspended in buffer B (25 mM Tris-Cl, 0.25 M sucrose, 500 mM NaCl, 5 mM EDTA and PIC) at a concentration of 0.5-2.0 mg/ml, and then 10 mg of membrane protein were extracted with one of the following detergent: 1.5% digitonin (w/v) or 1% CHAPS + 0.2% deoxycholate (w/v) or 1% n-dodecyl-B-D-maltoside (w/v) for 1 h on ice with regular gentle vortexing. Detergent-soluble proteins were separated from detergent-insoluble proteins by centrifugation at 150,000 X g for 40 min. Before mixing to loading buffer, the insoluble fraction was suspended with buffer B containing 4M urea. Samples

resolved in 8% SDS-PAGE under reducing conditions were transferred with staking gel onto nitrocellulose sheets (Amersham Pharmacia Biotech, Piscataway, USA) and probed with anti-myc and anti-calnexin Abs. The reaction was developed by using the ECL + system (Amersham Pharmacia Biotech).

Cell culture and transfection

HeLa-K^b and COS-7-K^b cells were kindly provided by Drs. T. van Hall (Leiden University Medical Center, The Netherlands) and K. Rock, respectively. Cells were maintained in DME supplemented with 10% FBS and antibiotics. Transient transfection was performed according to the manufacturer's instructions using FuGENE 6 transfection reagent (Roche) for COS-7, COS-7-K^b and HEK 293 cells, and Lipofectamine reagent (Invitrogen) for HeLa-K^b cells.

Cytofluorography

Cells were analyzed on a FACSCalibur flow cytometer using CellQuest software and sorted on a FACSVantage SE system with FACSDiVa option (BD Biosciences, Mississauga, Canada). Cell surface K^b-SIINFEKL labeling was carried out as described using Alexa-labeled 25-D1.16 mAb (Porgador *et al*, 1997).

Immunocytochemistry

Cells on coverslips were fixed in 4% formaldehyde in PBS for 30 min or in methanol at –20°C for 20 min, then washed twice in PBS and permeabilized with 0.1% triton X-100 in PBS for 30 min at RT. Cells were then washed thrice in PBS, blocked with 10% FBS in PBS for 1 h, and incubated with primary Ab diluted in 1% BSA 0.01% triton X-100 in PBS for 1 h at RT. After washing thrice in PBS, coverslips were incubated with secondary Ab diluted in 1% BSA 0.01% triton X-100 in PBS for 1 h at RT. Cells were washed five times in PBS, mounted with Vectashield with DAPI (Vector Laboratories Inc., Burlingame, USA) and analysed under a Zeiss LSM 510 confocal microscope (Zeiss, North York, Canada).

Electron Microscopy

Trypsinized cells were collected in a pellet by centrifugation at 2000 *g*, fixed in 2.5% glutaraldehyde in 0.1M cacodylate buffer for 1 h at 4°C, postfixed in 1% osmium acid and embedded in epon. Lead citrate stained thin sections were examined under a Hitachi (Rexdale , Canada) H-7500 transmission electron microscope and photographs were taken with a Hamamatsu (Markham , Canada) digital camera model C4742-95.

2.4 Results

STT3B enhances MHC I presentation of OVA-derived peptide

In theory, the prominent contribution of STT3B to the immunopeptidome could be due solely to the high affinity of selected STT3B peptides for several MHC I allelic products. The STT3B derived peptide presented by $H2D^b$ (KAPDNRETL) has indeed a high affinity for $H2D^b$ (Pion *et al*, 1999). However, the fact that the STT3B-derived peptide (NLYDKAGKV) presented by HLA-A2 has a low affinity for HLA-A2 (data not shown) argues against this contention and suggests that other factor(s) account for the major contribution of STT3B to the immunopeptidome. A likely explanation would be that STT3B is processed more efficiently than other proteins along the MHC I pathway. To test this hypothesis, we transfected Hela-K^b cells with two chimeras: EGFP-SIINFEKL and EGFP-STT3B-SIINFEKL (Figure 2A). We postulated that with these constructs, EGFP fluorescence would be proportional to the quantity of intracellular protein containing the SIINFEKL peptide. We then assessed 25-D1.16 MFI in discrete cell populations expressing various levels of EGFP intensity. This strategy allowed us to correlate the amount of K^b-SIINFEKL complexes at the cell surface with intracellular SIINFEKL. In cells expressing EGFP-STT3B-SIINFEKL, the intensity of 25-D1.16 staining increased in a linear fashion as a function of EGFP MFI up to an EGFP MFI of 80 where a plateau was reached (Figure 2B). The notable point was that until this plateau was reached, EGFP-STT3B-SIINFEKL generated 6 times more K^b-SIINFEKL complexes than EGFP-SIINFEKL (Figure 2B). Thus, the amount of K^b-SIINFEKL complexes was dramatically increased by coupling SIINFEKL to STT3B.

STT3B tends to adopt a non-native conformation and induces ER biogenesis

Because of growing evidence that, at least for viral proteins, DRiPs represent an important source of MHC I-associated peptides (Yewdell *et al*, 2003), we asked whether synthesis of STT3B would generate high amounts of DRiPs. DRiPs tend to adopt a non-native (misfolded) conformation and their insoluble nature makes quantitative analysis difficult and prevents precise estimation of the DRiP rate. To estimate the propensity of STT3B to generate DRiPs, we therefore adopted a two-pronged strategy based on biochemistry and cell biology.

Biochemistry. A general feature of misfolded proteins is that they are insoluble and resistant to extraction with relatively mild detergents (Illing *et al*, 2002; Yewdell *et al*, 2001b). We therefore wished to determine whether this was the case for STT3B. We extracted membrane proteins from COS-7-K^b cells transfected with c-myc-STT3B using three detergents: digitonin, CHAPS + deoxycholate, and n-dodecyl-B-D-maltoside. The soluble and insoluble fractions were resolved in 8% SDS-PAGE and probed with anti-myc and anti-calnexin Abs. Like STT3B, calnexin is an integral ER membrane protein. While calnexin partitioned in similar amounts in the soluble and insoluble fractions, STT3B mainly partitioned into the detergent-insoluble fractions (Figure 3). Furthermore, STT3B, but not calnexin, migrated for the most part as high M_r complexes (150-250 kDa) rather than monomers (~ 75 kDa). These complexes are evidence of a non-native conformation (misfolded oligomers), because STT3B is monomeric in its native membrane (Karaoglu *et al*, 1997). Of note, yeast HA-tagged STT3 was also found to be poorly soluble and showed an anomalous electrophoretic migration that persisted after deglycolysation (Yewdell *et al*, 2001b).

Cell biology. Misfolded proteins found in the ER become ERAD substrates whose disposal is limited by two bottlenecks: dislocation across the membrane and actual degradation by the proteasome (Vashist and Ng, 2004). Inefficient proteolysis results in the formation of pericentriolar membrane-free cytoplasmic inclusions called aggresomes (Johnston *et al*, 1998). By contrast, inefficient dislocation results in substrate accumulation in the ER which leads to an XBP1-dependent biogenesis of ER membranes (Cox *et al*, 1997; Raposo *et al*, 1995; Sriburi *et al*, 2004; Szczesna-Skorupa *et al*, 2004). Aggresomes and accretion of ER arrays can be detected by fluorescence and electron microcoscopy. To determine whether STT3B would induce formation of aggresomes or accumulation of ER membranes, we studied COS-7 cells transfected with EGFP-STT3B constructs. From 24 to 48 h after transfection, STT3B appeared in most cells in a disperse ER pattern in close proximity to calnexin and calreticulin (Figure 4A). The STT3B pattern showed significant though not complete overlap with Sec61 (Figure 4A) but none with COP II (data not shown). Notably, in about 40% of EGFP-STT3B transfected COS-7 cells, fluorescence accumulated in a juxtanuclear compartment (Figure 5A,B) not seen in cells transfected with EGFP (data not shown). Accumulation in a tight paranuclear pattern

was not cell-type specific since it was also observed, albeit at lower frequency, in HEK 293 and NIH 3T3 cells transfected with EGFP-STT3B (Figure 5B). The pattern was not EGFP-dependent since it was also induced by constructs in which STT3B was tagged with c-myc or FLAG epitope (Figure 5C). Juxtanuclear accumulation of EGFP-STT3B was impaired by the microtubule-depolymerizing drug nocodazole (Figure 5D). Nocodazole-treated cells showed dispersed small protein clusters rather than the sequestration of one major juxtanuclear pattern.

Confocal microscopy revealed that three ER markers calnexin, calreticulin and Sec61, but not ubiquitin, concentrated to the same paranuclear compartment where STT3B accumulated (Figure 5A). In mammalian cells, the immunoproteasome is associated primarily with the cytosolic side of the ER membrane (Anton *et al*, 1999; Wojcik *et al*, 2003), and staining with anti-LMP2 Ab shows a dispersed ER-like pattern in IFN-γ-treated cells (Figure 4B,C). Immunostaining for LMP2 disclosed a striking enrichment of immunoproteasome in the same juxtanuclear compartment where STT3B accumulated (Figure 4D). That subcellular compartment was adjacent to the centrioles as visualized by staining of γ–tubulin (Figure 5A). Consistent with colocalization of STT3B with ER markers, transmission electron microscopy showed bulky accumulation of anastomosing smooth ER tubules in about 30% of cells transfected with EGFP-STT3B (Figure 6). Accumulation of ER tubules was not observed in untransfected cells (Figure 6) or cells transfected with EGFP alone (data not shown). The latter observation indicates that accumulation of STT3B leads to massive ER biogenesis and paranuclear accretion of ER membranes. On the whole, the ER compartment where STT3B accumulates shares the features of the yeast "ER-associated compartment" (Huyer *et al*, 2004) and the mammalian "ER quality control compartment" (Kamhi-Nesher *et al*, 2001). The prevailing view is that these ER subdomains serve as repositories for misfolded proteins that have not been translocated to the cytosol. Together, STT3B insolubility and tendency to adopt a non-native conformation (high M_r forms), and its ability to induce a massive ER biogenesis provide compelling evidence that STT3B is prone to misfolding.

STT3B is degraded by the proteasome system and not by autophagy

The major pathways for degradation of cellular constituents are autophagy and cytosolic turnover by the proteasome (Cuervo, 2004; Glickman and Ciechanover, 2002). Intracellular levels of EGFP-STT3B were significantly increased following treatment with *clasto*-lactacystin β-lactone but not with inhibitors of autophagy (3-methyl-adenine and bafilomycin) (Figure 7A). Thus, degradation of STT3B is mediated primarily, if not exclusively, by the proteasome.

We showed above that when the SIINFEKL peptide is inserted into STT3B (between aa 769 and 779) it is efficiently processed along the MHC I pathway and presented by $H2K^b$ (Figure 2B). In our next experiment we wished to determine whether this processing was proteasome dependent. COS-7-K^b cells were transfected with three constructs: OVA, STT3B-SIINFEKL, and an MSIINFEKL minigene. Cells were treated with citric acid to elute MHC-associated peptides, then cultured in the presence of graded concentrations of *clasto*-lactacystin β-lactone for 4 h, and stained with 25-D1.16 Ab (Figure 7B). Proteasome inhibition by *clasto*-lactacystin β-lactone induced a dose dependent decrease of cell surface levels of K^b-SIINFEKL complexes in cells transfected with OVA but, as expected (Anton *et al*, 1999), not in cells transfected with the MSIINFEKL minigene. The key finding was that in cells expressing STT3B-SIINFEKL, generation of K^b-SIINFEKL complexes was abrogated at exceedingly low concentrations of *clasto*-lactacystin β-lactone. Thus, MHC I presentation of peptides embedded in STT3B is proteasome-dependent.

Retrotranslocation of STT3B is coupled to its degradation and is facilitated by N-linked glycans

Proteasomal degradation of proteins present in the ER lumen requires their retrotranslocation to the cytosol (Lilley and Ploegh, 2004; Mosse *et al*, 1998). It has been hypothesized however, that proteasomal degradation of integral ER membrane proteins, such as STT3B, might be initiated prior to retrotranslocation (Jarosch *et al*, 2002). Nevertheless, the predicted location of two STT3B-derived MHC I-associated peptides on the lumenal side of ER membrane (Figure 1) suggests that retrotranslocation of STT3B is important for proteasomal degradation. In many cases, dislocation of ERAD substrates is

tightly coupled to proteasomal degradation and so they accumulate in the ER following proteasome inhibition (Elkabetz *et al*, 2004; Kamhi-Nesher *et al*, 2001). We found that this was the case for STT3B. Indeed, following transfection with EGFP-STT3B, the percentage of cells showing juxtanuclear accumulation of fluorescence in ER arrays was more than doubled in the presence of *clasto*-lactacystin β-lactone (Figure 7C). Of note, in the latter conditions, EGFP fluorescence was limited to the juxtanuclear ER arrays and was not detected in the cytosol (data not shown). Thus, as for many ERAD substrates, degradation of STT3B is linked to its retrotranslocation.

ER to cytosol dislocation of at least some glycoproteins is critically dependent on the recognition of specific glycosylation intermediates of N-linked glycans by the EDEM lectin (Helenius and Aebi, 2004; Spear and Ng, 2005). To determine whether this was the case for STT3B we expressed a mutant form of STT3B in which the region containing N-glycosylation sites (aa 612-662, cf Figure 1) was deleted. We then compared COS-7-K^b cells transfected with EGFP-STT3B-SIINFEKL versus EGFP-STT3B$_{\Delta 612\text{-}662}$-SIINFEKL constructs. Deletion of N-glycosylation sites caused a threefold increase in the proportion of cells with paranuclear STT3B accretion in ER arrays (Figure 7D) that could be due to two factors: an increased proportion of unfolded protein and decreased protein retrotranslocation. Notably, deletion of the glycosylation sequon decreased the generation of K^b-SIINFEKL epitopes by about 20% (Figure 7E; $p < 0.05$, Student's *t*-test). Thus, protein accumulation was due at least in part to impairment of retrotranslocation and was not due solely to an increased proportion of unfolded protein. Nonetheless, the fact that loss of N-glycosylation sites has a relatively modest impact on the generation of STT3B-derived MHC I presented peptides suggests that N-linked glycans have a contributory but not essential role in STT3B retrotranslocation and degradation.

STT3B retrotranslocation is a limiting step in peptide generation

We reported in Figure 2B that generation of K^b-SIINFEKL complexes from EGFP-STT3B-SIINFEKL was a saturable process that reached a plateau when EGFP attained a MFI of ~ 80. We wished to elucidate the nature of the limiting step in STT3B processing. Cells with low and high EGFP fluorescence (Figure 8A) were electronically sorted and the percentage of cells with EGFP accumulation in juxtanuclear ER arrays was determined by

fluorescence microscopy. More than 80% of cells with high EGFP levels, but none with low EGFP levels, showed paranuclear EGFP accumulation (Figure 8B). These data suggest that retrotranslocation is a limiting step in STT3B processing by the ERAD pathway and that ER biogenesis occurs when the ER membrane contains more STT3B than it can dislocate. The idea that STT3B is difficult to retrotranslocate but is rapidly degraded once in the cytosol is supported by two observations: i) under no circumstances did we detect STT3B in the cytosol, even in cells with massive accumulation of EGFP-STT3B in the ER (e.g., in cells treated with *clasto*-lactacystin β-lactone as in Figure 7C) and ii) *in vivo* STT3B accumulates only in non-ubiquitinated form(s) (Figure 5A). No plateau in the generation of K^b-SIINFEKL complexes was observed with the EGFP-OVA-$STT3B_{790-823}$ construct (Figure 8C). The latter chimera contains only a 34 aa sequence from STT3B and its product diffuses in the cytosol (data not shown). The absence of a plateau with the latter construct suggests that there is no additional bottleneck involved in MHC processing of SIINFEKL downstream of retrotranslocation [e.g. proteolysis by the proteasome, interaction with TAP, and MHC binding].

IFN-g enhances generation of K^b-SIINFEKL complexes in cells transfected with EGFP-STT3B-SIINFEKL

One striking feature of STT3B is its subcellular localization in close proximity to the proteasomes. Being located in the ER membrane, STT3B locates in the vicinity of the immunoproteasome which is primarily found on the cytosolic side of the ER (Figure 4C, D) (Brooks *et al*, 2000; Wojcik *et al*, 2003). Furthermore, STT3B can induce ER biogenesis and accumulation of ER arrays in close proximity to the MTOC (Figure 5A), a major site of proteasomal degradation in the cytosol (Anton *et al*, 1999).

To determine whether subcellular localization of STT3B influenced its processing along the MHC I pathway, we first asked whether preventing recruitment of STT3B to the MTOC would influence the generation of MHC I-associated peptides. We showed above that among cells expressing EGFP-STT3B-SIINFEKL, more than 80% of "EGFP high" cells showed juxtanuclear accumulation of $EGFP^+$ ER arrays (Figure 8B). Treatment with nocodazole completely abrogates formation of this paracentriolar compartment (Figure 9A). The microtubule-depolymerizing effect of nocodazole treatment does not abrogate

ER biogenesis but prevents recruitment of ER arrays to the MTOC (Figure 5D). Thus, we asked whether nocodazole would influence the amount of K^b-SIINFEKL complexes presented at the surface of EGFP high cells (i.e., the cells with paracentriolar accumulation of ER arrays) and found that it was not the case (Figure 9B). Preventing recruitment of ER arrays towards the MTOC with nocodazole had no discernible effect on the generation of K^b-SIINFEKL complexes.

We next wished to evaluate whether the close proximity between STT3B and the immunoproteasome might be functionally important for STT3B processing. We therefore asked whether increasing the levels of immunoproteasome in cells expressing STT3B-SIINFEKL would influence the MHC presentation of SIINFEKL. Thus, Hela-K^b cells transfected with EGFP-STT3B-SIINFEKL were treated with IFN-γ and the amount of intracellular proteins was correlated with the cell surface density of K^b-SIINFEKL complexes. As depicted in Figure 9C, IFN-γ treatment dramatically raised the plateau in the generation of K^b-SIINFEKL complexes. Indeed, the maximal amount of K^b-SIINFEKL complexes was increased by 2- to 3-fold in IFN-γ treated cells relative to controls. The effects of IFN-γ are not limited to induction of the immunoproteasome and encompass upregulation of molecules such as TAP and MHC I (Fruh and Yang, 1999). However, that retrotranslocation is the sole limiting step in MHC processing of STT3B peptides and is tightly coupled to proteasome degradation (Figure 7, 8C) provide indirect evidence that the effect of IFN-γ in these experiments was due to immunoproteasome mediated enhancement of STT3B retrotranslocation.

The lysine-rich region of STT3B enhances the generation of MHC I-associated peptides

In general, ubiquitination is a prerequisite for proteasomal degradation and is initiated by formation of an isopeptide bond between ubiquitin C-terminal glycine residue and the ε-NH_2 group of an internal lysine of the substrate (Glickman *et al*, 2002). Is the conserved lysine-rich region found at the C-terminus of STT3B ($STT3B_{790-823}$) important for generation of MHC I-associated peptides? Compared with cells transfected with OVA, those transfected with OVA-$STT3B_{790-823}$ fusion constructs displayed about 2-fold increase in the cell surface density of K^b-SIINFEKL complexes at the cell surface (Figure

10A). STT3B$_{790\text{-}823}$ had a similar effect when coupled to EGFP-SIINFEKL (Figure 10B). Thus, the lysine-rich region of STT3B is sufficient to promote MHC presentation of OVA-derived peptides. Moreover, deletion of STT3B lysine-rich region (△790-823) decreased by 30-35% the amount of K^b-SIINFEKL complexes at the surface of cells transfected with EGFP-STT3B-SIINFEKL constructs (Figure 10C). These data indicate that while about two-thirds of MHC peptides complexes can be generated in the absence of STT3B lysine-rich region, this region is necessary for optimal presentation of STT3B-derived peptides by MHC I molecules.

2.5 Discussion

A typical mammalian cell contains about 2 x 10^9 copies of ~3 x 10^4 different proteins with an average length of 466 amino acid residues (Princiotta *et al*, 2003). Its complexity being greater than that of microbial pathogens, the self proteome represents per se the most complex entity to which the mammalian MHC processing pathway is confronted. Considering the fierce competition among self-proteins for being represented in the immunopeptidome, the prominent imprint of STT3B on the mouse and human MHC I immunopeptidome (cf introduction) is no small achievement.

The prevailing view is that in cases of viral infection, virus MHC I-associated peptides derive largely if not mainly from DRiPs. Our work provides strong evidence that STT3B, a major source of MHC I-associated peptides, has a high propensity to misfold. This conclusion is based on the following evidence: the demonstration that STT3B is resistant to extraction with several detergents and tends to form high *M*r complexes, and the tendency of overexpressed STT3B to induce ER biogenesis. These data suggest that the MHC I self-immunopeptidome like its viral counterpart, is moulded by proteins with a high DRiP rate. Anastomosing ER arrays are thought to represent holding sites to which misfolded proteins are specifically diverted so as not to interfere with normal cellular functions (Huyer *et al*, 2004). These structures form when mutant membrane proteins accumulate in the ER due to defects in their ability to be dislocated to the cytosol (Dickson *et al*, 2002; Okiyoneda *et al*, 2004). However, in some situations ER biogenesis may also be induced by the increased accumulation of nonmutant resident proteins (Szczesna-Skorupa *et al*, 2004). While the high DRiP rate of STT3B leaves practically no doubt, further studies are needed to determine whether all nonmutant proteins that can induce ER biogenesis share a similar DRiP rate. These considerations underscore the unavoidable imprecision in the current definition of DRiPs and the need to investigate to what extent DRiPs result from defects in transcription, splicing, translation, assembly or folding. In the case of STT3B, our data lead us to infer that the high DRiP rate is mainly due to inherent difficulties in protein folding. This is consistent with studies of tyrosinase mutants showing that protein misfolding increases proteasomal degradation and generation of MHC I-associated epitopes (Ostankovitch *et al*, 2005).

Retrotranslocation is a bottleneck for several ERAD substrates (Sitia *et al*, 2003). Our data indicate that the limiting step in STT3B processing is retrotranslocation and that this can be alleviated by increasing expression of the immunoproteasome. The latter finding is consistent with the fact that the proteasome located on the cytosolic side of the ER (i.e., mainly the immunoproteasome in jawed vertebrates) is sufficient to retrotranslocate and degrade an ERAD substrate (Lee *et al*, 2004). With few exceptions, proteasomal substrates are degraded in a ubiquitin-dependent manner and di-lysine sequences are preferred ubiquitination sites (Catic *et al*, 2004; Glickman *et al*, 2002). The conserved lysine–rich region at the C-terminus of STT3B contains four di-lysine sequences. We therefore postulate that STT3B lysine-rich region is a degron because it is a preferred target for ubiquitin conjugation. This would explain why this region is sufficient to enhance generation of MHC-associated OVA peptides and is required for optimal STT3B degradation and processing along the MHC I pathway (Figure 10). Nevertheless, about two-thirds of MHC peptide complexes could be generated in the absence of the lysine-rich region (Figure 10B). This suggests that STT3B may contain other ubiquitination sites and/or that proteasomal degradation of STT3B may be to some extent ubiquitin-independent. Indeed, experimental evidence suggests that the sole function of polyubiquitin chains in proteasomal degradation is in tethering substrates to the proteasome (Janse *et al*, 2004). Bringing proteins in close proximity to the proteasome while bypassing the ubiquitination step is sufficient to initiate degradation (Janse *et al*, 2004). Thus, the close proximity between the immunoproteasome and STT3B (Figure 4D) could lessen the need for ubiquitination.

Once in the cytoplasm, peptides derived from proteasomal degradation have a very short half-life *in vivo*: around 7 s for 9-mer peptides (Reits *et al*, 2003). More than 99% of peptides are degraded by cytosolic peptidases before they bind TAP (on the cytosolic side of the ER) and thereby enter the MHC I presentation pathway. Thus, the competition for peptides between peptidases and TAP drastically decreases the efficiency of MHC I epitope generation. As a corollary, the probability that a peptide generated by the proteasome will associate with an MHC I molecule should be maximal when the proteasome is located closest to TAP, that is, on the cytosolic face of the ER. Recent data even suggest that proteasomes on the cytosolic side of the ER interact with TAP, thereby

supporting the concept of direct targeting of antigenic peptides to the ER via a TAP–proteasome association (Begley *et al*, 2005). These data lead us to propose that location of STT3B in the ER membrane is crucial for its contribution to the immunopeptidome because it brings STT3B in close proximity to both the immunoproteasome and TAP. Moreover, preferential degradation by the immunoproteasome, as opposed to the constitutive proteasome, may increase the contribution of STT3B to the immunopeptidome. Indeed, bioinformatic studies predict that the immunoproteasome generates peptides that are better ligands for MHC binding than peptides generated by the constitutive proteasome (Kesmir *et al*, 2003). In contrast with the housekeeping proteasome, the immunoproteasome is found only in vertebrates with an adaptive immune system (gnathostomes) and has co-evolved with the MHC to optimize antigen presentation in gnathostome cells (Kesmir *et al*, 2003; Klein and Nikolaidis, 2005).

One fundamental question raised by our work is whether the behavior of STT3B can be extended to other ERAD substrates. In other words, are ERAD substrates a preferential source of MHC I-associated peptides? We anticipate that the answer to this question will be dependent on cell type. First, because the content in housekeeping proteasome and immunoproteasome are dependent on cell type. Second, because the quantity of ERAD substrates produced varies as a function of the cell's rate of protein synthesis and secretion (Brewer and Hendershot, 2005). Nonetheless, we envision at least two reasons why the contribution of ERAD substrates to the MHC I immunopeptidome might have considerable biologic relevance: i) central tolerance to self is induced strictly by peptides produced by the immunoproteasome because this is the only proteasome expressed by cells in the thymic medulla (Nil *et al*, 2004), ii) the immunoproteasome is the dominant type of proteasome found in dendritic cells, the most important antigen-presenting cells (Morel *et al*, 2000). Moreover, one could even see the crucial contribution of ER membranes in antigen cross-presentation (Ackerman and Cresswell, 2004; Desjardins, 2003) as a means to use the ERAD machinery to quickly modify the MHC I immunopeptidome.

Seminal studies by other groups strongly suggest that the contribution of a protein to the immunopeptidome is not determined by a single factor. Thus, the extent of protein

misfolding, the degradation rate and localization in the cytosol versus the secretory pathway were relevant for some but not all proteins (Golovina *et al*, 2005; Golovina *et al*, 2002; Ostankovitch *et al*, 2005; Princiotta *et al*, 2003). Our work suggests that the prominent imprint of STT3B on the MHC I immunopeptidome results from the interplay of three factors that render STT3B an optimal ERAD substrate: its propensity to misfold, its lysine-rich degron and its location in the ER membrane. Moreover, our analyses show that coupling to STT3B can be used to foster MHC I presentation of a specific peptide. Preliminary work suggests that the same effect can also be achieved with STT3A and with truncated STT3B constructs (data not shown). Given the recent demonstration that a substantial portion of the MHC II immunopeptidome is generated by a proteasome- and TAP-dependent pathway (Tewari *et al*, 2005), it will be interesting to evaluate whether coupling to STT3B could be used to generate not only MHC I but also MHC II epitopes. This approach could be relevant for application in developing vaccines against selected proteins such as oncoproteins.

2.6 Acknowledgements

We thank Drs. S. Meloche, K. Rock, T. van Hall and J. Yewdell for reagents. We also thank Dr. J. Ferrara and B. Morin for help with electron microscopy and J.A. Kashul for editorial assistance. This work was supported by grants to CP from the National Cancer Institute of Canada and the Canadian Network for Vaccines and Immunotherapeutics. RC was supported by a training grant from the Fonds de la Recherche en Santé du Québec. CP holds a Canada Research Chair in Immunobiology.

2.7 References

Ackerman AL, Cresswell P (2004) Cellular mechanisms governing cross-presentation of exogenous antigens. *Nat Immunol* **5:** 678-684.

Anton LC, Schubert U, Bacik I, Princiotta MF, Wearsch PA, Gibbs J, Day PM, Realini C, Rechsteiner MC, Bennink JR, Yewdell JW (1999) Intracellular localization of proteasomal degradation of a viral antigen. *J Cell Biol* **146:** 113-124.

Begley GS, Horvath AR, Taylor JC, Higgins CF (2005) Cytoplasmic domains of the transporter associated with antigen processing and P-glycoprotein interact with subunits of the proteasome. *Mol Immunol* **42:** 137-141.

Boon T, van der Bruggen P (1996) Human tumor antigens recognized by T lymphocytes. *J Exp Med* **183:** 725-729.

Brewer JW, Hendershot LM (2005) Building an antibody factory: a job for the unfolded protein response. *Nat Immunol* **6:** 23-29.

Brooks P, Murray RZ, Mason GG, Hendil KB, Rivett AJ (2000) Association of immunoproteasomes with the endoplasmic reticulum. *Biochem J* **352 Pt 3:** 611-615.

Catic A, Collins C, Church GM, Ploegh HL (2004) Preferred in vivo ubiquitination sites. *Bioinformatics* **20:** 3302-3307.

Cox JS, Chapman RE, Walter P (1997) The unfolded protein response coordinates the production of endoplasmic reticulum protein and endoplasmic reticulum membrane. *Mol Biol Cell* **8:** 1805-1814.

Cuervo AM (2004) Autophagy: in sickness and in health. *Trends Cell Biol* **14:** 70-77.

Desjardins M (2003) ER-mediated phagocytosis: a new membrane for new functions. *Nat Rev Immunol* **3:** 280-291.

Dickson KM, Bergeron JJ, Shames I, Colby J, Nguyen DT, Chevet E, Thomas DY, Snipes GJ (2002) Association of calnexin with mutant peripheral myelin protein-22 ex vivo: a basis for "gain-of-function" ER diseases. *Proc Natl Acad Sci U S A* **99:** 9852-9857.

Elkabetz Y, Shapira I, Rabinovich E, Bar-Nun S (2004) Distinct steps in dislocation of luminal endoplasmic reticulum-associated degradation substrates: roles of endoplamic reticulum-bound p97/Cdc48p and proteasome. *J Biol Chem* **279:** 3980-3989.

Engelhard VH, Brickner AG, Zarling AL (2002) Insights into antigen processing gained by direct analysis of the naturally processed class I MHC associated peptide repertoire. *Mol Immunol* **39:** 127-137.

Fontaine P, Roy-Proulx G, Knafo L, Baron C, Roy DC, Perreault C (2001) Adoptive transfer of minor histocompatibility antigen-specific T lymphocytes eradicates leukemia cells without causing graft-versus-host disease. *Nat Med* **7:** 789-794.

Fruh K, Yang Y (1999) Antigen presentation by MHC class I and its regulation by interferon gamma. *Curr Opin Immunol* **11:** 76-81.

Glickman MH, Ciechanover A (2002) The ubiquitin-proteasome proteolytic pathway: destruction for the sake of construction. *Physiol Rev* **82:** 373-428.

Goldrath AW, Bevan MJ (1999) Selecting and maintaining a diverse T-cell repertoire. *Nature* **402:** 255-262.

Golovina TN, Morrison SE, Eisenlohr LC (2005) The impact of misfolding versus targeted degradation on the efficiency of the MHC class I-restricted antigen processing. *J Immunol* **174:** 2763-2769.

Golovina TN, Wherry EJ, Bullock TN, Eisenlohr LC (2002) Efficient and qualitatively distinct MHC class I-restricted presentation of antigen targeted to the endoplasmic reticulum. *J Immunol* **168:** 2667-2675.

Helenius A, Aebi M (2004) Roles of N-linked glycans in the endoplasmic reticulum. *Annu Rev Biochem* **73:** 1019-1049.

Hickman HD, Luis AD, Buchli R, Few SR, Sathiamurthy M, VanGundy RS, Giberson CF, Hildebrand WH (2004) Toward a definition of self: proteomic evaluation of the class I peptide repertoire. *J Immunol* **172:** 2944-2952.

Hirokawa T, Boon-Chieng S, Mitaku S (1998) SOSUI: classification and secondary structure prediction system for membrane proteins. *Bioinformatics* **14:** 378-379.

Huyer G, Longsworth GL, Mason DL, Mallampalli MP, McCaffery JM, Wright RL, Michaelis S (2004) A striking quality control subcompartment in Saccharomyces cerevisiae: the endoplasmic reticulum-associated compartment. *Mol Biol Cell* **15:** 908-921.

Illing ME, Rajan RS, Bence NF, Kopito RR (2002) A rhodopsin mutant linked to autosomal dominant retinitis pigmentosa is prone to aggregate and interacts with the ubiquitin proteasome system. *J Biol Chem* **277:** 34150-34160.

Janse DM, Crosas B, Finley D, Church GM (2004) Localization to the proteasome is sufficient for degradation. *J Biol Chem* **279:** 21415-21420.

Jarosch E, Geiss-Friedlander R, Meusser B, Walter J, Sommer T (2002) Protein dislocation from the endoplasmic reticulum--pulling out the suspect. *Traffic* **3:** 530-536.

Johnston JA, Ward CL, Kopito RR (1998) Aggresomes: a cellular response to misfolded proteins. *J Cell Biol* **143:** 1883-1898.

Kamhi-Nesher S, Shenkman M, Tolchinsky S, Fromm SV, Ehrlich R, Lederkremer GZ (2001) A novel quality control compartment derived from the endoplasmic reticulum. *Mol Biol Cell* **12:** 1711-1723.

Karaoglu D, Kelleher DJ, Gilmore R (1997) The highly conserved Stt3 protein is a subunit of the yeast oligosaccharyltransferase and forms a subcomplex with Ost3p and Ost4p. *J Biol Chem* **272:** 32513-32520.

Kelleher DJ, Karaoglu D, Mandon EC, Gilmore R (2003) Oligosaccharyltransferase isoforms that contain different catalytic STT3 subunits have distinct enzymatic properties. *Mol Cell* **12:** 101-111.

Kesmir C, van Noort V, de Boer RJ, Hogeweg P (2003) Bioinformatic analysis of functional differences between the immunoproteasome and the constitutive proteasome. *Immunogenetics* **55:** 437-449.

Kessler B, Hong X, Petrovic J, Borodovsky A, Dantuma NP, Bogyo M, Overkleeft HS, Ploegh H, Glas R (2003) Pathways accessory to proteasomal proteolysis are less efficient in major histocompatibility complex class I antigen production. *J Biol Chem* **278:** 10013-10021.

Klein J, Nikolaidis N (2005) The descent of the antibody-based immune system by gradual evolution. *Proc Natl Acad Sci U S A* **102:** 169-174.

Lacaille VG, Androlewicz MJ (2000) Targeting of HIV-1 Nef to the centrosome: implications for antigen processing. *Traffic* **1:** 884-891.

Lee RJ, Liu CW, Harty C, McCracken AA, Latterich M, Romisch K, DeMartino GN, Thomas PJ, Brodsky JL (2004) Uncoupling retro-translocation and degradation in the ER-associated degradation of a soluble protein. *EMBO J* **23:** 2206-2215.

Lilley BN, Ploegh HL (2004) A membrane protein required for dislocation of misfolded proteins from the ER. *Nature* **429:** 834-840.

McBride K, Baron C, Picard S, Martin S, Boismenu D, Bell A, Bergeron J, Perreault C (2002) The model B6(dom1) minor histocompatibility antigen is encoded by a mouse homolog of the yeast STT3 gene. *Immunogenetics* **54:** 562-569.

Morel S, Levy F, Burlet-Schiltz O, Brasseur F, Probst-Kepper M, Peitrequin AL, Monsarrat B, Van Velthoven R, Cerottini JC, Boon T, Gairin JE, Van den Eynde BJ (2000) Processing of some antigens by the standard proteasome but not by the immunoproteasome results in poor presentation by dendritic cells. *Immunity* **12:** 107-117.

Mosse CA, Meadows L, Luckey CJ, Kittlesen DJ, Huczko EL, Slingluff CL, Shabanowitz J, Hunt DF, Engelhard VH (1998) The class I antigen-processing pathway for the membrane protein tyrosinase involves translation in the endoplasmic reticulum and processing in the cytosol. *J Exp Med* **187:** 37-48.

Nil A, Firat E, Sobek V, Eichmann K, Niedermann G (2004) Expression of housekeeping and immunoproteasome subunit genes is differentially regulated in positively and negatively selecting thymic stroma subsets. *Eur J Immunol* **34:** 2681-2689.

Nilsson I, Kelleher DJ, Miao Y, Shao Y, Kreibich G, Gilmore R, von Heijne G, Johnson AE (2003) Photocross-linking of nascent chains to the STT3 subunit of the oligosaccharyltransferase complex. *J Cell Biol* **161:** 715-725.

Okiyoneda T, Harada K, Takeya M, Yamahira K, Wada I, Shuto T, Suico MA, Hashimoto Y, Kai H (2004) Delta F508 CFTR pool in the endoplasmic reticulum is increased by calnexin overexpression. *Mol Biol Cell* **15:** 563-574.

Ostankovitch M, Robila V, Engelhard VH (2005) Regulated folding of tyrosinase in the endoplasmic reticulum demonstrates that misfolded full-length proteins are efficient substrates for class I processing and presentation. *J Immunol* **174:** 2544-2551.

Pamer E, Cresswell P (1998) Mechanisms of MHC class I--restricted antigen processing. *Annu Rev Immunol* **16:** 323-358.

Perreault C, Decary F, Brochu S, Gyger M, Belanger R, Roy D (1990) Minor histocompatibility antigens. *Blood* **76:** 1269-1280.

Pion S, Christianson GJ, Fontaine P, Roopenian DC, Perreault C (1999) Shaping the repertoire of cytotoxic T-lymphocyte responses: explanation for the immunodominance effect whereby cytotoxic T lymphocytes specific for immunodominant antigens prevent recognition of nondominant antigens. *Blood* **93:** 952-962.

Pion S, Fontaine P, Desaulniers M, Jutras J, Filep JG, Perreault C (1997) On the mechanisms of immunodominance in cytotoxic T lymphocyte responses to minor histocompatibility antigens. *Eur J Immunol* **27:** 421-430.

Porgador A, Yewdell JW, Deng Y, Bennink JR, Germain RN (1997) Localization, quantitation, and in situ detection of specific peptide-MHC class I complexes using a monoclonal antibody. *Immunity* **6:** 715-726.

Princiotta MF, Finzi D, Qian SB, Gibbs J, Schuchmann S, Buttgereit F, Bennink JR, Yewdell JW (2003) Quantitating protein synthesis, degradation, and endogenous antigen processing. *Immunity* **18:** 343-354.

Raposo G, van Santen HM, Leijendekker R, Geuze HJ, Ploegh HL (1995) Misfolded major histocompatibility complex class I molecules accumulate in an expanded ER-Golgi intermediate compartment. *J Cell Biol* **131:** 1403-1419.

Reits E, Griekspoor A, Neijssen J, Groothuis T, Jalink K, van Veelen P, Janssen H, Calafat J, Drijfhout JW, Neefjes J (2003) Peptide diffusion, protection, and degradation in nuclear and cytoplasmic compartments before antigen presentation by MHC class I. *Immunity* **18:** 97-108.

Reits EA, Vos JC, Gromme M, Neefjes J (2000) The major substrates for TAP in vivo are derived from newly synthesized proteins. *Nature* **404:** 774-778.

Rock KL, York IA, Saric T, Goldberg AL (2002) Protein degradation and the generation of MHC class I-presented peptides. *Adv Immunol* **80:** 1-70.

Schubert U, Anton LC, Gibbs J, Norbury CC, Yewdell JW, Bennink JR (2000) Rapid degradation of a large fraction of newly synthesized proteins by proteasomes. *Nature* **404:** 770-774.

Shastri N, Schwab S, Serwold T (2002) Producing nature's gene-chips: the generation of peptides for display by MHC class I molecules. *Annu Rev Immunol* **20:** 463-493.

Simpson E, Roopenian D (1997) Minor histocompatibility antigens. *Curr Opin Immunol* **9:** 655-661.

Sitia R, Braakman I (2003) Quality control in the endoplasmic reticulum protein factory. *Nature* **426:** 891-894.

Spear ED, Ng DT (2005) Single, context-specific glycans can target misfolded glycoproteins for ER-associated degradation. *J Cell Biol* **169:** 73-82.

Sriburi R, Jackowski S, Mori K, Brewer JW (2004) XBP1: a link between the unfolded protein response, lipid biosynthesis, and biogenesis of the endoplasmic reticulum. *J Cell Biol* **167:** 35-41.

Storkus WJ, Zeh HJ, 3rd, Salter RD, Lotze MT (1993) Identification of T-cell epitopes: rapid isolation of class I-presented peptides from viable cells by mild acid elution. *J Immunother Emphasis Tumor Immunol* **14:** 94-103.

Szczesna-Skorupa E, Chen CD, Liu H, Kemper B (2004) Gene expression changes associated with the endoplasmic reticulum stress response induced by microsomal cytochrome p450 overproduction. *J Biol Chem* **279:** 13953-13961.

Tewari MK, Sinnathamby G, Rajagopal D, Eisenlohr LC (2005) A cytosolic pathway for MHC class II-restricted antigen processing that is proteasome and TAP dependent. *Nat Immunol* **6:** 287-294.

Vashist S, Ng DT (2004) Misfolded proteins are sorted by a sequential checkpoint mechanism of ER quality control. *J Cell Biol* **165:** 41-52.

Wojcik C, DeMartino GN (2003) Intracellular localization of proteasomes. *Int J Biochem Cell Biol* **35:** 579-589.

Yewdell JW (2003) Immunology. Hide and seek in the peptidome. *Science* **301:** 1334-1335.

Yewdell JW, Bennink JR (2001a) Cut and trim: generating MHC class I peptide ligands. *Curr Opin Immunol* **13:** 13-18.

Yewdell JW, Reits E, Neefjes J (2003) Making sense of mass destruction: quantitating MHC class I antigen presentation. *Nat Rev Immunol* **3:** 952-961.

Yewdell JW, Schubert U, Bennink JR (2001b) At the crossroads of cell biology and immunology: DRiPs and other sources of peptide ligands for MHC class I molecules. *J Cell Sci* **114:** 845-851.

2.8 Figure Legends

Figure 1: **Proposed mouse STT3B topology in the ER membrane.**
The model is based on SOSUI (Hirokawa *et al*, 1998) and TOPO2 (http://www.sacs.ucsf.edu/TOPO2/) prediction methods. Human and mouse STT3B proteins share 97% amino acid identity (McBride *et al*, 2002). Lysine residues in the C-terminal lysine-rich region (aa 780-823) are in black and predicted *N*-glycosylation sites in red. Three STT3B peptides presented in large amounts by MHC I molecules are depicted in blue: 1) DERVFVALY (aa 438-446) is presented by HLA-B18; 2) NLYDKAGKV (aa 509-517) by HLA-A2; and 3) KAPDNRETL (aa 770-778) by $H2D^b$.

Figure 2: STT3B enhances presentation of K^b-SIINFEKL complexes.
(**A**) HeLa-K^b cells were transfected with two EGFP constructs. In the EGFP-STT3B-SIINFEKL chimera, the KAPDNRETL peptide of STT3B (aa 770-778, cf Figure 1) was replaced by SIINFEKL (the OVA peptide presented by $H2K^b$). (**B**). Following analysis with the CellQuest software, cell surface levels of K^b-SIINFEKL complexes (labeling with 25-D1.16 mAb) were correlated with intracellular protein levels (EGFP MFI). Data to the left of the dotted lines (plateau reached with the EGFP-STT3B-SIINFEKL construct) were used to calculate the slope of the lines (m).

Figure 3: STT3-B is highly insoluble.
Total cellular membranes from nontransfected and c-myc-STT3B transfected COS-7-K^b cells were isolated and extracted with three different detergents (see Methods). The detergent-soluble (S) and -insoluble (I) fractions were separated and immunoblotted (IB) with either anti-myc or anti-calnexin Ab. DDM, n-dodecyl-B-D-maltoside; DOC, deoxycholate.

Figure 4: EGFP-STT3B is located in the ER.
(**A**) COS-7 cells were transfected with EGFP-STT3B, and after 40 h were stained with Ab to calnexin, calreticulin and sec61β, and imaged to localize EGFP-STT3B. (**B**) Immunoproteasome induction by IFN-γ. COS-7 cells cultured for 88 h with or without 250U/ml IFN-γ were stained for LMP-2. (**C**) Higher magnification view of a COS-7 cell

treated with IFN-γ. (**D**) Colocalization of EGFP-STT3B and LMP-2 in IFN-γ treated COS-7 cells. Bar for A, C and D = 5 μm, and for B = 10 μm.

Figure 5: EGFP-STT3B accumulates in a juxtanuclear ER compartment.

(**A**) At 40 h after transfection with EGFP-STT3B, COS-7 cells were stained with Ab to calnexin, calreticulin, sec61β and γ-tubulin and imaged to localize EGFP-STT3B. For ubiquitin colocalization, cells were co-transfected with HA-ubiquitin and EGFP-STT3B vectors and immunostained for HA. (**B**) Juxtanuclear accumulation of EGFP-STT3B in 3 cell lines 24 h after transfection with EGFP-STT3B. The number of cells with juxtanuclear accumulation of EGFP-STT3B is reported as a percentage of transfected cells. 600 cells were counted for each condition. (**C**) Juxtanuclear accumulation of STT3B is not EGFP-dependent. At 40 h after transfection with c-myc-STT3B or STT3B-FLAG, COS-7 cells were immunostained with anti-c-myc or ant-FLAG Ab. (**D**) COS-7 cells were transfected with EGFP-STT3B and treated or not with nocodazole (10 μM) 6 h after transfection. Bar = 5 μm.

Figure 6: Cells transfected with STT3B show bulky accumulation of anastomosing smooth ER arrays.

Transmission electron microscopy analysis of COS-7 cells transfected (**A, C**) or not (**B, D**) with EGFP-STT3B. **C** and **D** are higher magnification views of sections indicated by white boxes in **A** and **B**, respectively. N, nucleus. Bar for A and B, 2 μm; C and D, 500 nm.

Figure 7: Degradation of STT3B by the proteasome.

(**A**) HEK 293 cells were transfected with EGFP-STT3B and were incubated 24 h later with *clasto*-lactacystin β-lactone (10 mM, 16 h), bafilomycin (1.6 mM, 16 h) or 3-methyl-adenine (10 mM, 8 h). Results are expressed as ratios between MFI of cells treated with drug versus diluent. (**B**) 24 h after transfection with MSIINFEKL, OVA or STT3B-SIINFEKL, COS-7-K^b cells were treated with *clasto*-lactacystin β-lactone for 90 min and cell surface MHC I-associated peptides were eluted by treatment with citrate-phosphate buffer (pH 3.3) for 1 min (Storkus *et al*, 1993). Cells were then washed, incubated for 4 h in presence of graded concentrations of *clasto*-lactacystin β-lactone, and stained with 25-

D1.16 mAb. For each construct, surface K^b-SIINFEKL levels are expressed as the percent of expression relative to cells cultured in the absence of *clasto*-lactacystin β-lactone. (**C**) Juxtanuclear accumulation of STT3B is enhanced by proteasome inhibition. HEK 293 cells were transfected with EGFP-STT3B and cultured for 16 h in the presence of *clasto*-lactacystin β-lactone or its diluent (DMSO). (**D** and **E**) Regulation of STT3B degradation by N-linked glycans. (**D**) Percentage of cells showing juxtanuclear accumulation of EGFP and (**E**) relative levels of K^b-SIINFEKL complexes in COS-7-K^b cells transfected with constructs in which the STT3B region containing N-glycosylation sites was deleted ($\Delta_{612-662}$) or not. Data (mean ± SD) are representative of 3 independent experiments.* $p < 0.05$ (Student's *t*-test). *Clasto.*: *clasto*-lactacystin β-lactone.

Figure 8: Correlation between protein levels, juxtanuclear pattern, and cell surface levels of K^b-SIINFEKL complexes.

(**A**) HeLa-K^b cells transfected with EGFP-STT3B-SIINFEKL construct were assessed for EGFP fluorescence and labeling with 25-D1.16 mAb (K^b-SIINFEKL MFI) as in Figure 2C. (**B**) Cell populations with low or high EGFP fluorescence were sorted on a FACSVantage SE system and prepared for fluorescent microscopy. The percentage of cells showing juxtanuclear accumulation of EGFP was calculated after counting 200 cells. (**C**) HeLa-K^b cells transfected with two EGFP constructs were assessed for EGFP fluorescence and labeling with 25-D1.16 mAb.

Figure 9: IFN-γ but not nocodazole influences the efficacy of K^b-SIINFEKL presentation.

(**A**) COS-7-K^b cells were transfected for 6 h with EGFP-STT3B-SIINFEKL construct and then incubated with nocodazole for 16 h to block juxtanuclear accumulation of EGFP-labeled protein. (**B**) Cells cultured with nocodazole or its diluent were analyzed for EGFP fluorescence and labeling with 25-D1.16 mAb (K^b-SIINFEKL MFI). (**C**) Hela-K^b cells were transfected with EGFP-STT3B-SIINFEKL and incubated for 48 h with or without IFN-γ (500 U/mL). Data to the left of the dotted line were used to calculate the slope of the lines (m).

Figure 10: The lysine-rich region of STT3B regulates the generation of cell surface K^b-SIINFEKL complexes.

Cells surface levels of K^b-SIINFEKL complexes (evaluated by staining with 25-D1.16 mAb) were assessed in cells transfected with various constructs. (**A**) COS-7-K^b cells were transfected with OVA or OVA-STT3B$_{790\text{-}823}$ fusion constructs. (**B**) Hela-K^b cells were transfected with EGFP-SIINFEKL or EGFP-SIINFEKL-STT3B$_{790\text{-}823}$. (**C**) COS-7-K^b cells were transfected with EGFP-STT3B-SIINFEKL constructs in which the lysine-rich region of STT3B was deleted ($\Delta_{790\text{-}823}$) or not. Data (mean + SD) are representative of three independent experiments. * $p < 0.05$, ** $p < 0.005$ (Student's *t*-test).

Figure 1

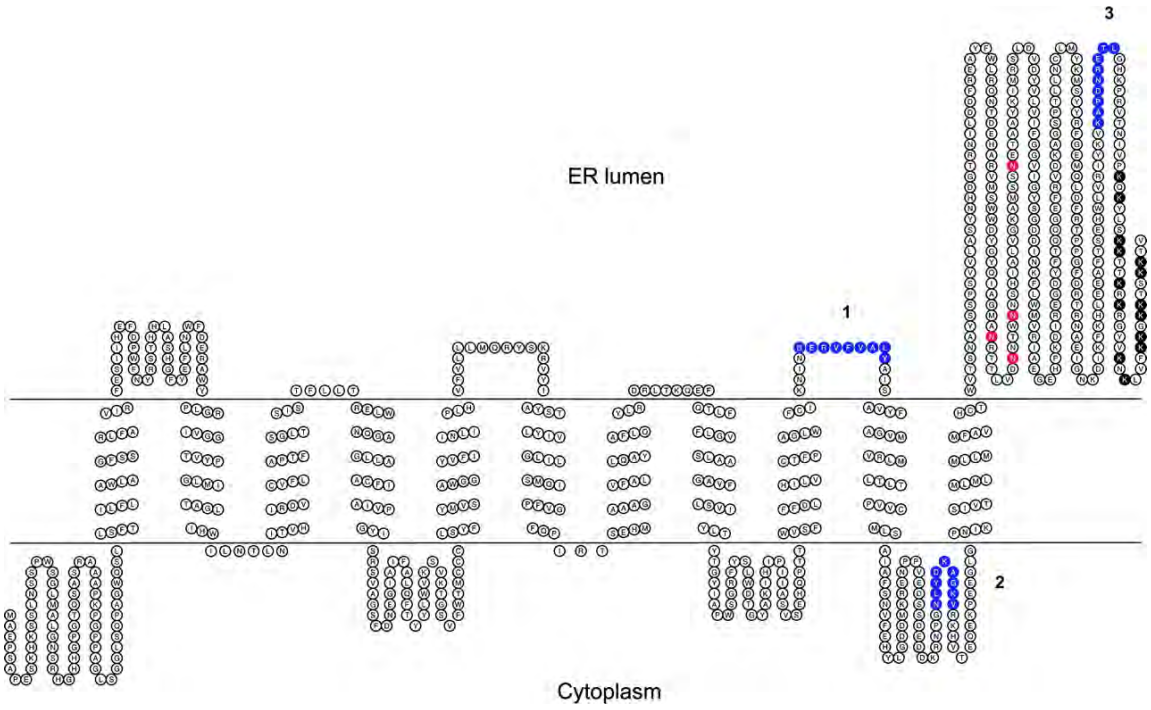

Figure 2

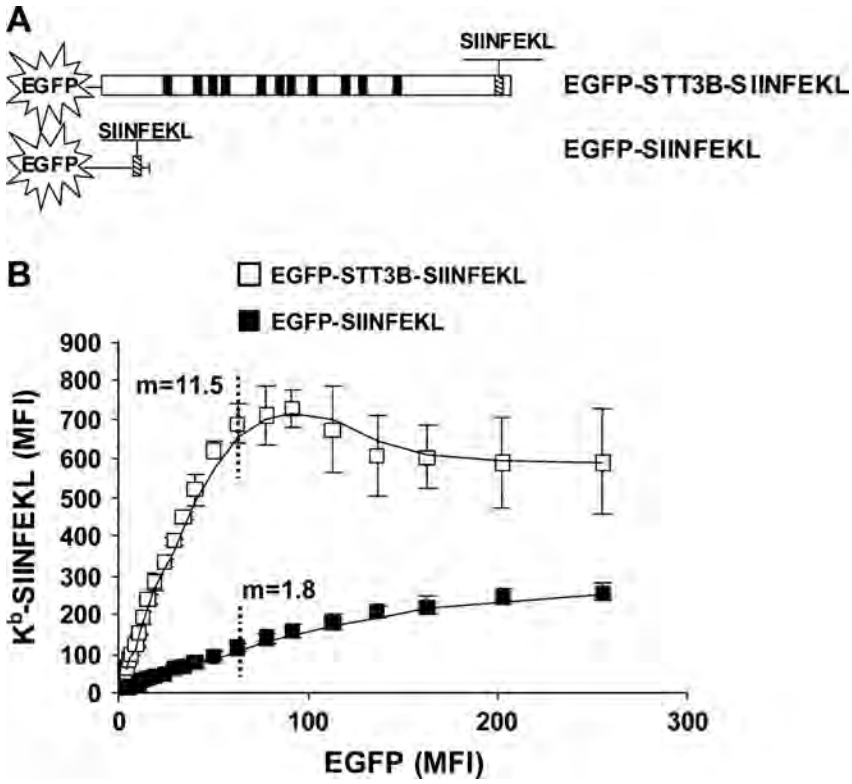
A
SIINFEKL
EGFP
EGFP-STT3B-SIINFEKL
SIINFEKL
EGFP
EGFP-SIINFEKL
B
EGFP-STT3B-SIINFEKL
EGFP-SIINFEKL
m=11.5
m=1.8
Kb-SIINFEKL (MFI)
EGFP (MFI)
0
100
200
300
400
500
600
700
800
900

Figure 3

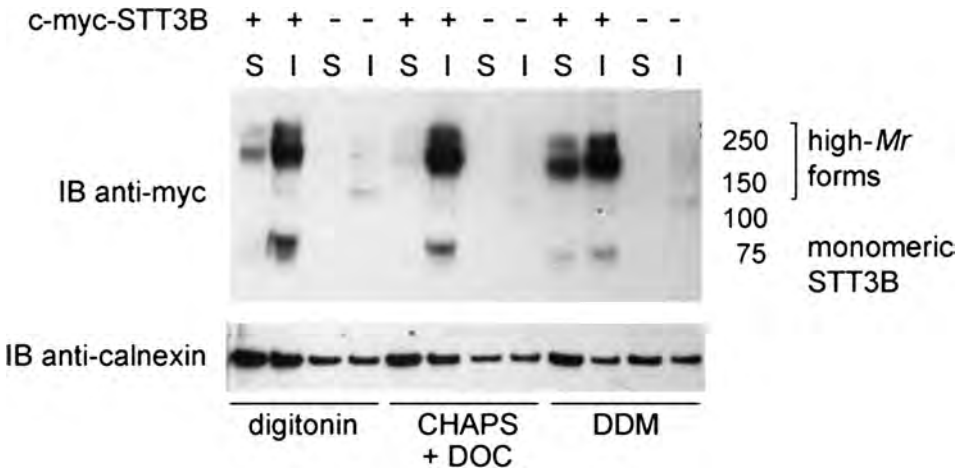
c-myc-STT3B
+ + - - + + - - + + - -
S I S I S I S I S I S I
IB anti-myc
IB anti-calnexin
250
150
100
75
high-Mr forms
monomeric STT3B
digitonin
CHAPS + DOC
DDM

Figure 4

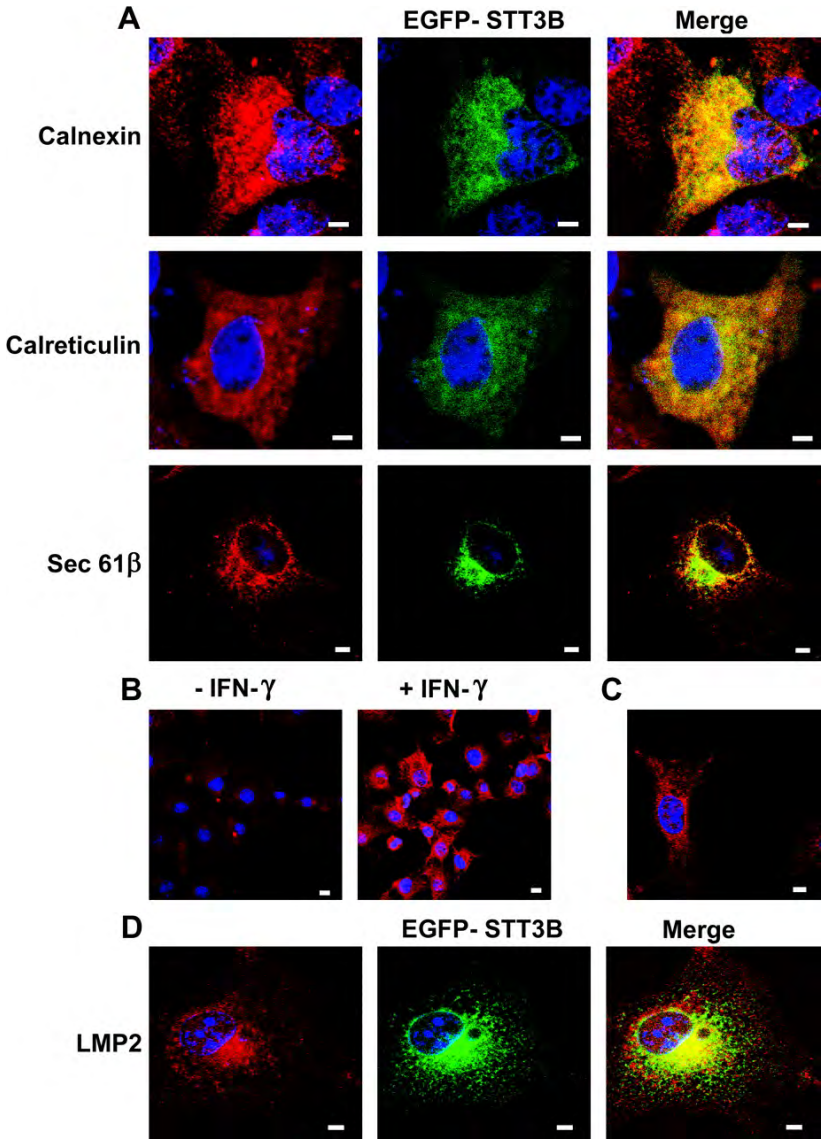
A
EGFP- STT3B
Merge
Calnexin
Calreticulin
Sec 61β
B
- IFN-γ
+ IFN-γ
C
D
EGFP- STT3B
Merge
LMP2

Figure 5

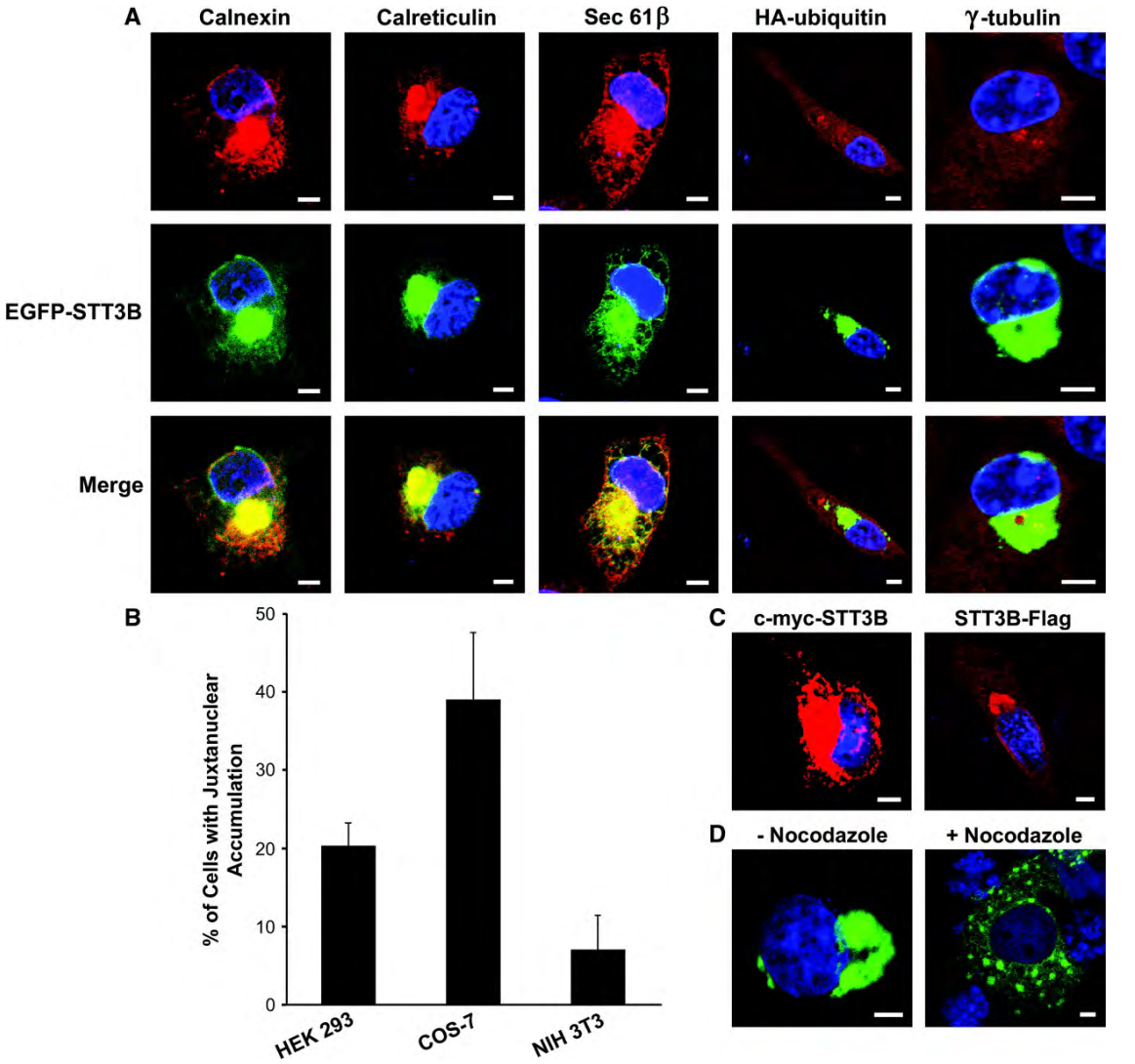
A
Calnexin
Calreticulin
Sec 61β
HA-ubiquitin
γ-tubulin
EGFP-STT3B
Merge
B
% of Cells with Juxtanuclear Accumulation
50
40
30
20
10
0
HEK 293
COS-7
NIH 3T3
C
c-myc-STT3B
STT3B-Flag
D
- Nocodazole
+ Nocodazole

Figure 6

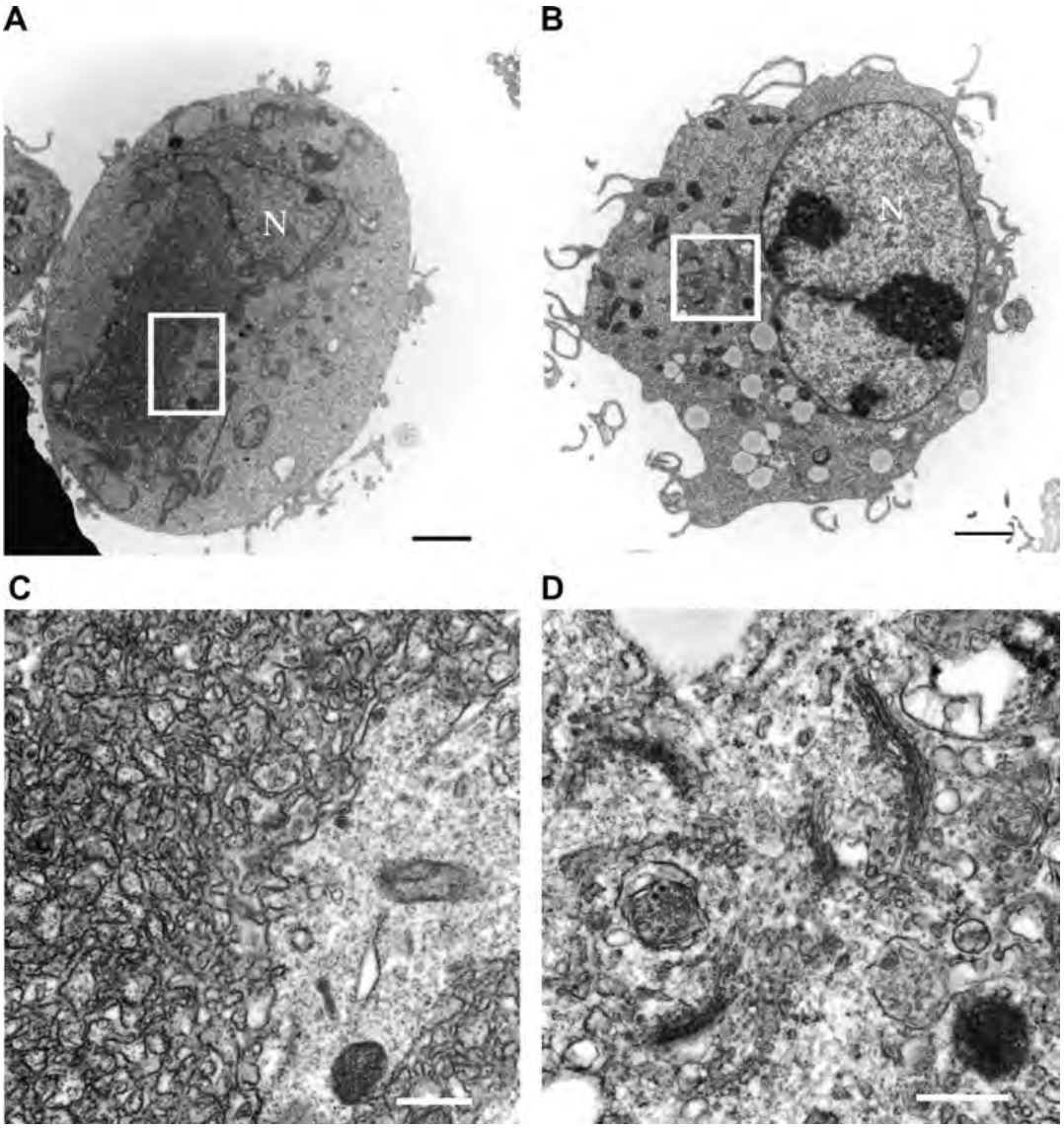

Figure 7

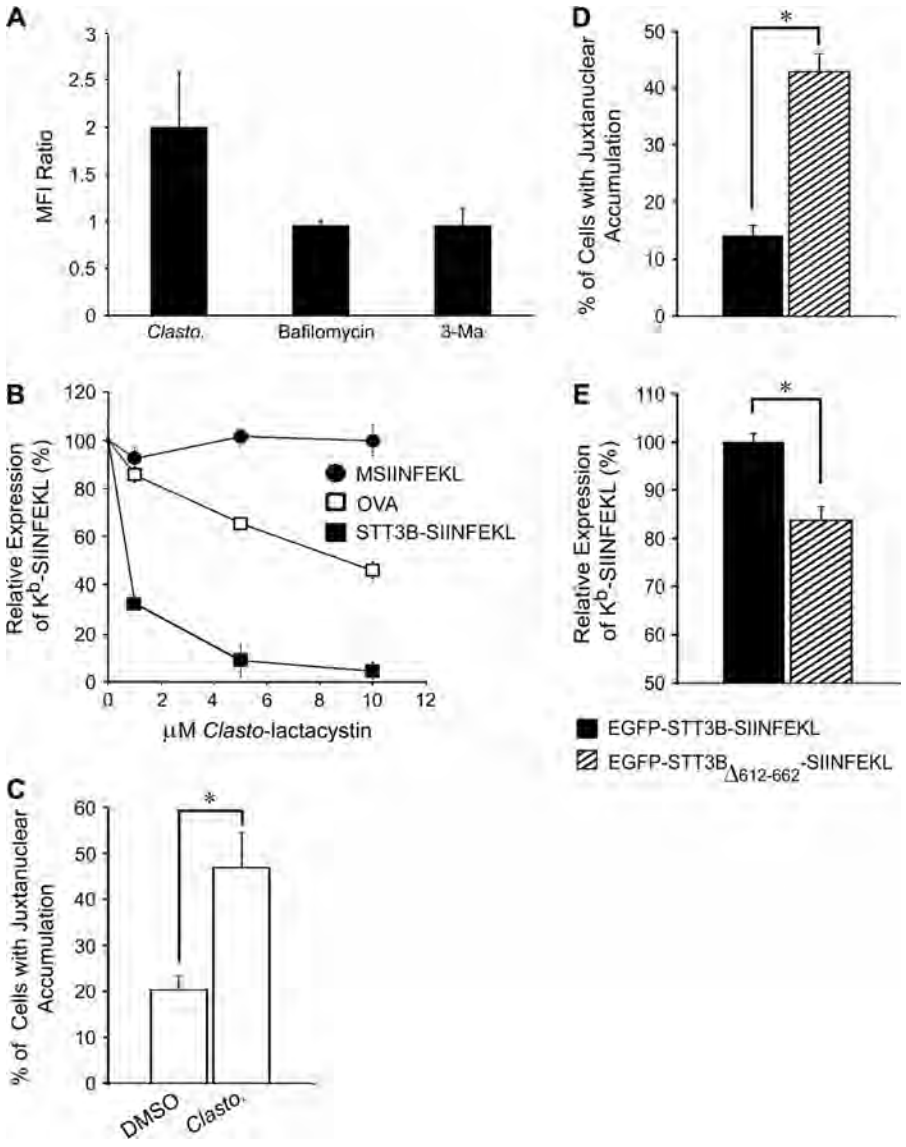
A
MFI Ratio
3
2.5
2
1.5
1
0.5
0
Clasto.
Bafilomycin
3-Ma
B
Relative Expression of K^b-SIINFEKL (%)
120
100
80
60
40
20
0
0
2
4
6
8
10
12
μM Clasto-lactacystin
MSIINFEKL
OVA
STT3B-SIINFEKL
C
% of Cells with Juxtanuclear Accumulation
60
50
40
30
20
10
0
*
DMSO
Clasto.
D
% of Cells with Juxtanuclear Accumulation
50
40
30
20
10
0
*
E
Relative Expression of K^b-SIINFEKL (%)
110
100
90
80
70
60
50
*
EGFP-STT3B-SIINFEKL
EGFP-STT3B Δ612-662 -SIINFEKL

Figure 8

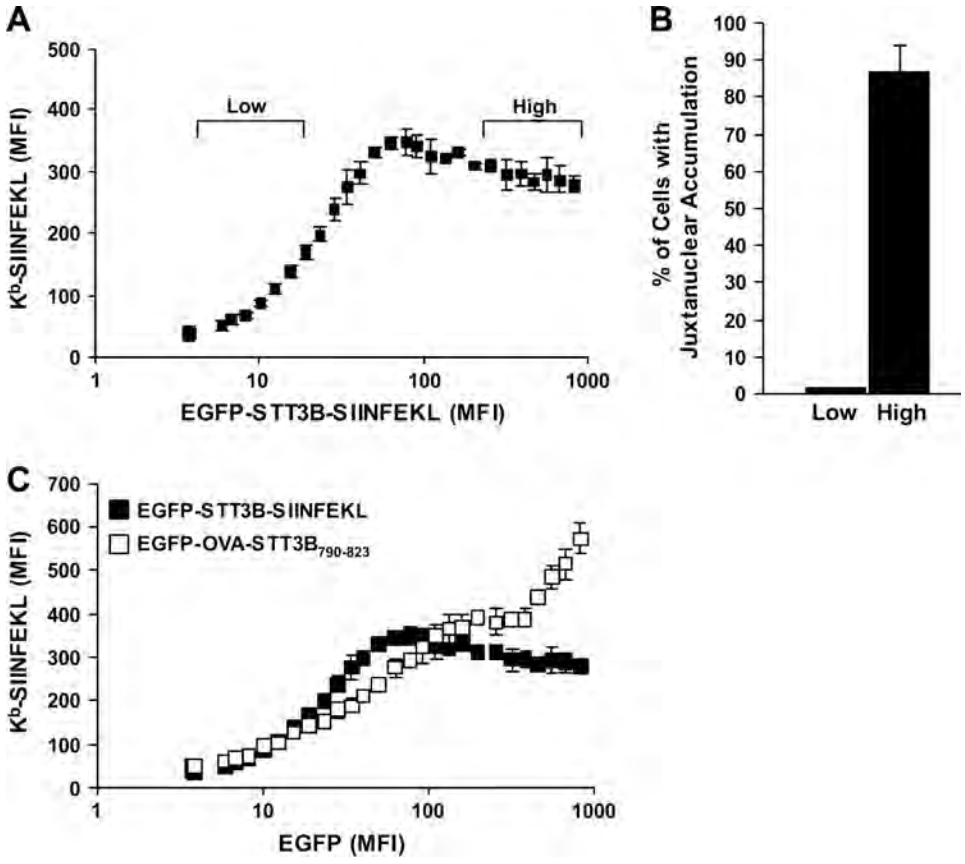
A
Low
High
K^b-SIINFEKL (MFI)
EGFP-STT3B-SIINFEKL (MFI)
B
% of Cells with Juxtanuclear Accumulation
Low
High
C
EGFP-STT3B-SIINFEKL
EGFP-OVA-STT3B$_{790-823}$
K^b-SIINFEKL (MFI)
EGFP (MFI)

Figure 9

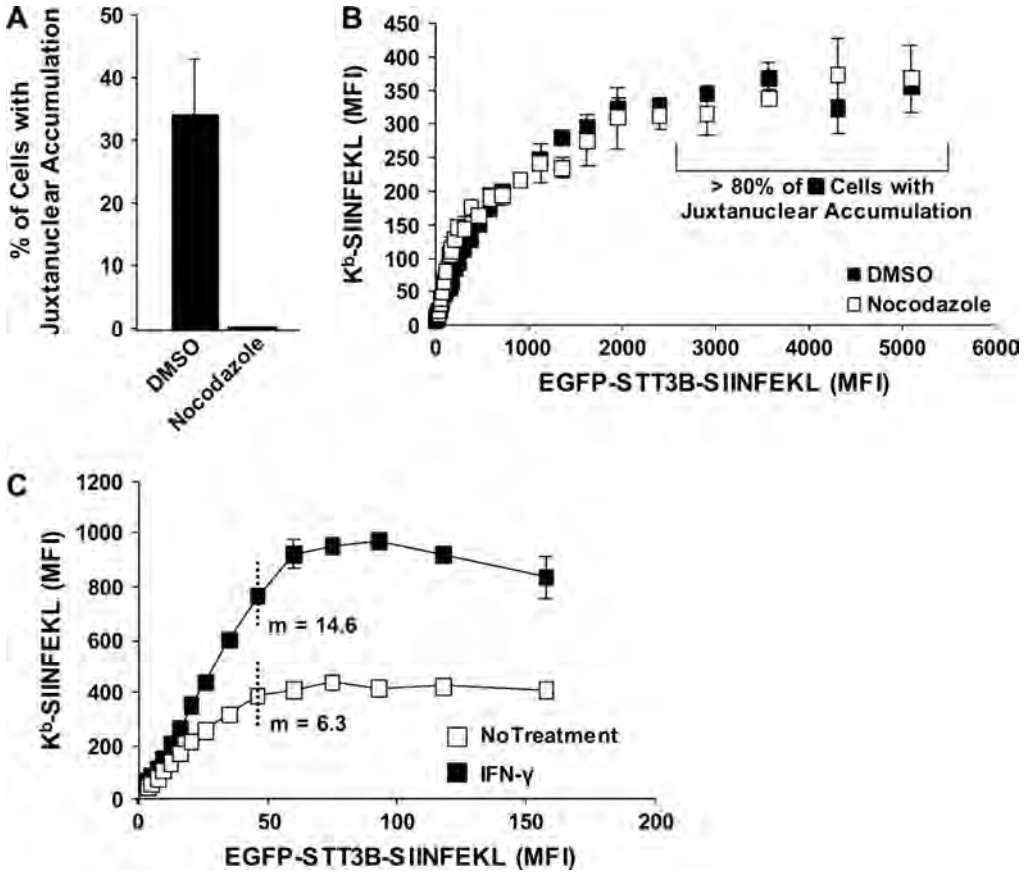
A
% of Cells with Juxtanuclear Accumulation
50
40
30
20
10
0
DMSO
Nocodazole
B
Kb-SIINFEKL (MFI)
450
400
350
300
250
200
150
100
50
0
0
1000
2000
3000
4000
5000
6000
EGFP-STT3B-SIINFEKL (MFI)
> 80% of ■ Cells with Juxtanuclear Accumulation
■ DMSO
□ Nocodazole
C
Kb-SIINFEKL (MFI)
1200
1000
800
600
400
200
0
0
50
100
150
200
EGFP-STT3B-SIINFEKL (MFI)
m = 14.6
m = 6.3
□ NoTreatment
■ IFN-γ

Figure 10

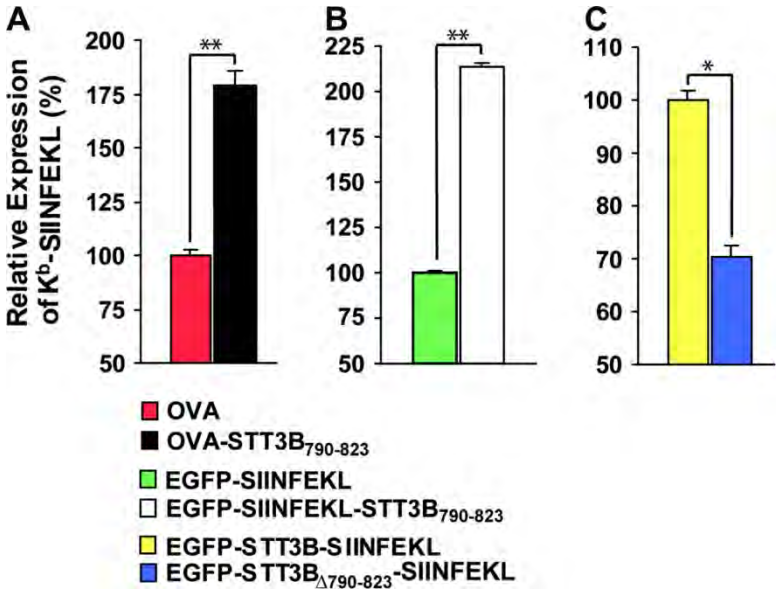
A
B
C
Relative Expression of Kb-SIINFEKL (%)
200
175
150
125
100
75
50
225
110
90
80
70
60
**
*
OVA
OVA-STT3B790-823
EGFP-SIINFEKL
EGFP-SIINFEKL-STT3B790-823
EGFP-STT3B-SIINFEKL
EGFP-STT3BΔ790-823-SIINFEKL

CHAPITRE 3

MISE EN SITUATION:

Dans le chapitre précédent, des approches réductionnistes classiques ont été utilisées pour mieux comprendre pourquoi certaines protéines contribuent plus activement à la génération de peptides associés aux molécules du CMH I. De nos jours, ces approches réductionnistes permettent d'identifier et d'étudier un nombre plutôt limité de peptides antigéniques. Le développement des technologies dans le domaine de la protéomique a récemment propulsé notre façon d'identifier les peptides composant l'immunopeptidome.

Dans ce présent chapitre, nous avons développé une nouvelle approche à haut débit par spectrométrie de masse permettant de définir la nature et l'abondance relative des peptides présentés par les molécules du CMH I. Nous avons identifié 189 et 196 peptides du CMH I provenant respectivement de thymocytes normaux et néoplasiques de souris. En intégrant nos données peptidomiques au transcriptome, nous sommes arrivés à deux conclusions : 1) l'immunopeptidome de thymocytes primaires est biaisé en faveur des peptides provenant de transcrits fortement abondants et 2) l'immunopeptidome est enrichi en peptides provenant de cyclines / kinases dépendantes des cyclines et des hélicases. De plus, nous avons constaté que 25% des peptides associés aux CMH I ont été exprimés de manière différentielle entre les thymocytes normaux et néoplasiques. Environ la moitié de ces peptides provenaient de protéines directement impliquées dans la transformation néoplasique (par exemple, les composantes de la voie PI3K-AKT-mTOR). Dans la plupart des cas, nos résultats montrent que la surexpression des peptides à la surface des cellules cancéreuses provient de mécanismes post-transcriptionnels. Globalement, notre étude indique que l'analyse à haut débit et le séquençage de peptides associés aux molécules du CMH I apporte des connaissances uniques sur la genèse de l'immunopeptidome de cellules normales et néoplasiques.

3. ARTICLE 2:

The MHC class I peptide repertoire is molded by the transcriptome

Marie-Hélène Fortier[1,2†], Étienne Caron[1,3†], Marie-Pierre Hardy[1], Grégory Voisin[1], Sébastien Lemieux[1], Claude Perreault[1,3‡*] and Pierre Thibault[1,2‡]

Institute for Research in Immunology and Cancer[1], Department of Chemistry[2], and Department of Medicine[3], University of Montreal, CP 6128, Downtown Station, Montreal, Quebec, Canada, H3C 3J7

Manuscript information: Abstract: 207 words
Total length: 79 343 characters (incl. spaces)
Materials and Methods: 1 725 words
Introduction, Results and Discussion section: 5 230 words

Running title: Genesis of the MHC I Immunopeptidome

[†]MHF and EC contributed equally to this work

[‡]Corresponding authors:

Dr. Claude Perreault
Dr. Pierre Thibault

Article publié dans: **Journal of Experimental Medicine, Volume 205, p. 595-610 (2008).**

CONTRIBUTIONS DES AUTEURS:

Marie-Hélène Fortier a effectué les expériences en spectrométrie de masse, a conçu les figures 1 et 6, et a écrit la première version du manuscrit. Etienne Caron a participé à la conception du projet, à l'analyse des données, aux figures 2, 3, 4, 5, 6 et à l'écriture de la première version du manuscrit. Marie-Pierre Hardy a participé à la figure 7. Grégory Voisin et Sébastien Lemieux ont effectué des analyses bioinformatiques. Claude Perreault et Pierre Thibault ont participé à la conception du projet, à l'analyse des résultats et à l'écriture du manuscrit.

3.1 Abstract

Under steady-state conditions, major histocompatibility complex (MHC) I molecules are associated with self-peptides that are collectively referred to as the MHC class I peptide (MIP) repertoire. Very little is known about the genesis and molecular composition of the MIP repertoire. We developed a novel high-throughput mass spectrometry approach that yields an accurate definition of the nature and relative abundance of unlabeled peptides presented by MHC I molecules. We identified 189 and 196 MHC I – associated peptides from normal and neoplastic mouse thymocytes, respectively. By integrating our peptidomic data with global profiling of the transcriptome, we reached two conclusions. The MIP repertoire of primary mouse thymocytes is biased toward peptides derived from highly abundant transcripts and is enriched in peptides derived from cyclins/cyclin-dependent kinases and helicases. Furthermore, we found that 25% of MHC I – associated peptides were differentially expressed on normal versus neoplastic thymocytes. Approximately half of those peptides are derived from molecules directly implicated in neoplastic transformation (e.g., components of the PI3K – AKT – mTOR pathway). In most cases, overexpression of MHC I peptides on cancer cells entailed posttranscriptional mechanisms. Our results show that high-throughput analysis and sequencing of MHC I – associated peptides yields unique insights into the genesis of the MIP repertoire in normal and neoplastic cells.

3.2 Introduction

MHC class I molecules present short peptides at the cell surface, typically 8 – 11 mers, for scrutiny by CD8 T lymphocytes (Rammensee *et al*, 1993; Yewdell *et al*, 2003). Generation of peptide – MHC I complexes is initiated by proteasomal degradation of source proteins in the cytosol (Rock *et al*, 2002). Peptides generated by the proteasome are translocated in the endoplasmic reticulum, where they are subjected to N-terminal trimming, and then incorporated in MHC I proteins and exported at the cell surface (Hammer *et al*, 2007/4; Heemels and Ploegh, 1995; Pamer and Cresswell, 1998; Zhang and Williams, 2006). Presentation of microbial peptides by MHC I is required to elicit CD8 T cell responses against intracellular pathogens (Wong and Pamer, 2003). Under steady-state conditions, i.e., in the absence of infection, cell surface MHC I molecules are associated solely with self-peptides. These peptides, collectively referred to as the MHC class I peptide (MIP) repertoire (Weinzierl *et al*, 2007), play vital roles. They shape the repertoire of developing thymocytes (Huseby *et al*, 2005; Starr *et al*, 2003), transmit survival signals to mature CD8 T cells (Marrack and Kappler, 2004), amplify responses against intracellular pathogens (Anikeeva *et al*, 2006), allow immunosurveillance of neoplastic cells (Dunn *et al*, 2004), and influence mating preferences in mice (Slev *et al*, 2006). The MIP repertoire is also involved in immunopathology because it can be targeted by autoreactive T cells that initiate autoimmune diseases and alloreactive T cells that cause graft rejection and graft-versus-host disease (Liblau *et al*, 2002; Perreault *et al*, 1990).

Despite the tremendous importance of the MIP repertoire, we know very little about its genesis and molecular composition. Proteomic analysis of the MIP repertoire is a daunting task because estimates suggest that it encompasses thousands of peptides that are present in low copy numbers per cell (Hunt *et al*, 1992; Rammensee *et al*, 1993). Each MHC molecule recognizes peptides through a broadly defined consensus motif of amino acids serving as anchors to the appropriate binding pockets on the MHC molecules. Such motifs were first established by pool Edman sequencing of unfractionated peptide mixtures eluted from MHC molecules (Falk *et al*, 1991). Direct biochemical characterization of specific MHC I – associated peptides has typically involved

immunoaffinity purification of MHC molecules after cell lysis, fractionation of the peptides by chromatography, and sequencing, initially by Edman' s method and, more recently, by mass spectrometry (MS). Refinements in MS methods pioneered by Hunt et al. and Falk et al. represented major progress and led to the characterization of several MHC I – associated peptides (Huczko *et al*, 1993; Hunt *et al*, 1992; McBride *et al*, 2002), in spite of limitations such as low peptide yield, preferential loss of peptides with low affinity for MHC I, and contamination of the MHC molecules by cellular debris and detergents (Admon *et al*, 2003; Gebreselassie *et al*, 2006).

Two high-throughput strategies were therefore implemented to provide comprehensive molecular definition of the MIP repertoire. The first is based on transfection of cell lines with expression vectors coding soluble secreted MHCs (lacking a functional transmembrane domain) and elution of peptides associated with secreted MHCs (Barnea *et al*, 2002; Hickman *et al*, 2004). This interesting approach improves MHC I peptide recovery, but presents some limitations, as follows: (a) it cannot be used on freshly explanted cells; (b) cell transfection by itself may perturb the MIP repertoire (26); and (c) the MIP repertoire associated with soluble MHC corresponds to the repertoire of peptides that can bind the transfected MHC allele (what "can be presented"), but not necessarily to peptides that are normally presented at the cell surface (what "is presented"). The second approach hinges on chemical or metabolic labeling to provide quantitative profiles of MHC I – associated peptides (Lemmel *et al*, 2004; Meiring *et al*, 2006; Milner *et al*, 2006; Weinzierl *et al*, 2007). Although chemical derivatization suffers from variable modification yields and unexpected side reaction products, metabolic labeling is only applicable to certain MHC I allelic products and to cell culture model systems (Mann, 2006; Ong *et al*, 2003). Nonetheless, high-throughput peptide sequencing analyses have provided crucial insights into the structure of the MIP repertoire. First, the source proteins for the MIP repertoire are found in almost every compartment of the cell (Hickman *et al*, 2004). Second, only a limited correlation is observed between the amounts of the MHC I – associated peptides presented by cells and the relative expression of source proteins from which these peptides are derived (Milner *et al*, 2006). A likely explanation for this discrepancy is that the MIP repertoire preferentially derives from defective ribosomal products (DRiPs) and short-lived proteins relative to slowly degraded

proteins (Caron *et al*, 2005; Yewdell and Nicchitta, 2006; Yewdell *et al*, 2003). Third, for peptides differentially expressed on normal versus neoplastic cells, no clear correlation was found between mRNA levels and corresponding MHC peptide levels (Weinzierl *et al*, 2007).

The goal of our work was to understand the structure and genesis of the MIP repertoire. In accordance with a recent advocacy for " systems immunology " (Benoist *et al*, 2006), we used novel bioinformatics tools based on peptide mapping and segmentation to obtain a global and accurate quantification of native unlabeled peptides present in the MIP repertoire (unpublished data) (Fortier *et al*, 2005; Kearney and Thibault, 2003). In particular, we addressed four specific questions. Does the MIP repertoire reflect the composition of the transcriptome? Are some gene families overrepresented in the MIP repertoire? What is the impact of neoplastic transformation on the MIP repertoire? Can a high-throughput, unlabeled-peptide – sequencing platform provide valuable insights for the identification of immunogenic tumor-associated epitopes?

3.3 Materials and Methods

Chemicals and materials

Citric Acid, aprotinin, iodoacetamide and sodium phosphate dibasic (Na_2HPO_4) were purchased from Sigma-Aldrich; high performance liquid chromatography grade water, methanol (MeOH) and acetonitrile (ACN) from Fisher Scientific; formic acid (FA) and ammonium acetate from EM Science; fused-silica capillaries from Polymicro Technologies; and teflon and PEEK tubing from Supelco. The Jupiter Proteo C18 4μm material used for packing home made precolumn and column was obtained from Phenomenex. Strong cation exchange (SCX) material was purchased from PolyLC.

Cell lines and flow cytometry

The EL4 ($\beta2m^+$ wildtype), C4.4-25$^-$ ($\beta2m^-$ mutant) and E50.16$^+$ ($\beta2m^+$ transfectant of C4.4-25$^-$) cell lines were kindly provided by Dr. Rickard Glas (Karolinska Institutet, Karolinska University Hospital, Huddinge, Sweden). T2-K^b and T2-D^b cell lines (gifts from Sebastian. Joyce, Vanderbilt University School of Medicine, Nashville, TN) were maintained, as described (Yoshimura *et al*, 2004). MHC class I molecules at the cell surface were stained with PE-conjugated anti-H-2K^b (clone AF6-88.5, BD Pharmingen), FITC-conjugated anti-H-2D^b (clone KH95, BD Pharmingen), and biotin-conjugated anti-Qa-2 (clone 1-1-2, BD Pharmingen) and analyzed on a BD LSR II flow cytometer using FACSDiva software (BD Biosciences).

Peptide extraction and mass spectrometry analysis

Freshly isolated thymocytes were obtained from 4-6 wk-old C57BL/6 female mice purchased from The Jackson Laboratory. Thymocytes were separated from stroma according to standard procedures (Louis *et al*, 2003). For isolation of EL4 cells grown *in vivo*, mice were injected intraperitoneally with 200,000 EL4 cells, and ascites fluid was harvested 17 days later. Purity of EL4 cells was assessed by flow cytometry (Meunier *et al*, 2003). Three biological replicates were prepared and analyzed for normal thymocytes and EL4 cells. Cell surface MHC I peptides were isolated from viable cells as described using a slightly modified protocol (Storkus *et al*, 1993). Briefly, 4 mL of citrate-phosphate buffer at pH 3.3 (0.131 M citric acid/0.066 M Na_2HPO_4, isoosmotic) containing aprotinin

and iodoacetamide (1:100) was added to each flask and cell pellets were resuspended by gentle pipetting for 1 min to denature MHC I complexes. Cell suspensions were then pelletted and the resulting supernatant was isolated. Peptides extracts were desalted using Oasis HLB cartridges (30mg, Waters) and bound material was eluted with 1 mL H_2O/80% MeOH/0.2% FA (v/v) and diluted to H_2O/40% MeOH/0.2% FA (v/v). Peptides were then passed through ultrafiltration devices (Amicon Ultra, Millipore) to isolate peptides < 5000 Da and to remove β2m proteins. The resulting flowthrough was then lyophilized and stored at -30°C or -80°C until analysis.

To extract equivalent amount of MHC I peptide from EL4 cells and normal thymocytes we assessed the amount of MHC I molecules on both cell populations using previously described methods (Pion *et al*, 1995). Equivalent amount of MHC I material from neoplastic (8×10^7) and normal (2.3×10^9) thymocytes were separated by on-line two-dimensional separation (SCX/C18 Jupiter Proteo 4μm) using an Eksigent nanoLC-2D system. Samples were diluted in H_2O/2% ACN/0.2% FA prior to LC-MS analyses. The home made SCX column (0.3 mm i.d. X 45 mm) was connected directly to the switching valve. During sample loading, SCX column was positioned off-line of C_{18} precolumn to remove interfering species. Salt fractions (10 μL each) were loaded on SCX column at 5 μL/min for 6 min to sequentially elute peptides onto the C_{18} precolumn using pulsed fractions of 0, 75, 300, 1000 mM of ammonium acetate (pH 3.0). A 69 min gradient from 3-60% acetonitrile (0.2% FA) was used to elute peptides from home made reversed-phase column (150 μm i.d. X 100 mm) with a flow rate set at 600 nL/min. On-line 2D-nanoLC-MS system was used to provide enhanced selectivity as well as a higher capacity to detect low abundance MHC I peptides. To achieve high mass accuracy and sensitivity from limited amount of starting material, expression profile measurements and tandem MS experiments were performed simultaneously using a LTQ-Orbitrap mass spectrometer (Thermo Electron) equipped with a nanoelectrospray ion source (voltage 1.5-1.7 kV). MS scans were acquired in the FT mode (Orbitrap) with a resolution set at 60,000 (m/z 400). Each full MS spectrum was followed by three MS/MS spectra (four scan events), where the three most abundant multiply charged ions were selected for MS/MS sequencing. Tandem MS experiments were performed using collision-induced dissociation (CID) in the linear ion trap (IT mode). Target ions already selected for MS/MS fragmentation were

dynamically excluded for 80 seconds and a minimal intensity value of 10,000 was fixed for precursor ion selection.

Peptide detection and Clustering

Raw data files generated from the Orbitrap were processed using in-house peptide detection software (Mass Sense) to identify all ions according to their corresponding m/z values, charge state, retention time and intensity. From this process, lists of detected peptides ions were generated to define individual LC-MS analysis. A user defined intensity threshold above the background noise (typically between 5,000–15,000) was fixed to limit false-positive identification. Segmentation analyses were performed across sample sets using hierarchical clustering to generate lists of non-redundant peptide clusters (Fortier *et al*, 2005). User-specified tolerances were fixed to typically ± 0.04 m/z, ± 1.5 min and ± 1 fraction for 2D-LC-MS Orbitrap experiments. Identification files from Mascot were converted in excel format and sequenced peptides were aligned with their corresponding peptide clusters using in-house clustering software.

MS/MS sequencing and protein identification

The data were searched against International Protein Index (IPI) mouse database using Mascot (Matrix Science) search engine. The peptide and MS/MS tolerances were set to ± 0.1 Da and ± 0.4 Da, respectively. Searches were performed without enzyme specificity. All relevant hits were checked manually and were validated according to their complete sequence coverage with MS/MS fragments. From MHC I peptide structures identified, 85% were sequenced at least twice across replicate injections. To estimate the false-positive rate across peptide identification, 100 randomly chosen MHC I peptides identified from EL4 cells were searched against a concatenated forward/reverse IPI mouse database to establish a cutoff score threshold for a false-positive rate of less than two percent ($P < 0.02$). All identified peptides were blasted against non-redundant NCBInr (restricted to mouse entries) to identify their corresponding source proteins (Gene ID).

Quantitative real-time PCR

Freshly isolated thymocytes and EL4 cells were homogenized in TRIzol RNA preparation reagent (Invitrogen) and total RNA was isolated as instructed by the manufacturer. Then 1

µg of total RNA was converted to cDNA using random hexamer priming (Thermoscript RT-PCR System; Invitrogen). Gene expression level was determined using primer and probe sets from Universal ProbeLibrary (Table S7) https://www.roche-applied-science.com/sis/rtpcr/upl/index.jsp. PCR reactions for 384 well plate formats were performed using 2 µl of cDNA samples (50 ng), 5 µl of the TaqMan PCR Master Mix (Applied Biosystems), 2 µM of each primer and 1 µM of the Universal TaqMan probe in a total volume of 10 µl. The ABI PRISM® 7900HT Sequence Detection System (Applied Biosystems) was used to detect the amplification level and was programmed to an initial step of 10 minutes at 95˚C, followed by 40 cycles of 15 seconds at 95˚C and 1 minute at 60˚C. All reactions were run in triplicate and the average values were used for quantification. The mouse GAPDH or 18S ribosomal RNA were used as endogenous controls.

Microarray dataset crosscomparison

Normalized mRNA expression data (Su *et al*, 2004) (http://symatlas.gnf.org/SymAtlas/) used in this study were visualized with TIGR MultiExperiment Viewer (http://www.tigr.org/software/microarray.shtml). Normalized average expression values were calculated as follows for each tissue: average expression value of 180 peptide source genes / average expression value of 36,182 transcripts.

EASE Analysis and statistical methods

The Expression Analysis Systemic Explorer (EASE) software (Hosack *et al*, 2003) was downloaded from the Database for Annotation, Visualization, and Integrated Discovery (http://david.niaid.nih.gov/david/ease.htm) (Dennis *et al*, 2003). For gene enrichment analysis, statistical P-values and corrected P-values were calculated from the Fisher exact test and the global false-discovery rate, respectively.

Z score transformation

Raw intensity data for each tissue were log2 transformed and then used for the calculation of Z scores. Z scores were calculated by subtracting the overall average tissue intensity (for a single gene) from the raw intensity data within a given tissue, and dividing that result by the SD of the overall tissue intensities: Z score = (intensity G_{Th} – mean intensity

$G_{T1...Tn}$)/ SD $G_{T1...Tn}$ where G_{Th} is any gene on the microarray from the thymus tissue and T1…Tn represents the aggregate measure of all tissues.

Peptide-binding and *in vitro* cytolytic assay

Peptides were synthesized by the CHUL research center (Quebec) and purified by high performance liquid chromatography (purity > 90%). Rescue of class I expression in T2-D^b and T2-K^b cells by allele-specific peptides was determined, as described (Pion *et al*, 1997). Bone-marrow derived DCs were generated as previously described (Galea-Lauri *et al*, 2004). On day 9 of culture, peptides were added at a concentration of 2 x 10^{-6}M and incubated with DCs for 3h at 37°C. For mice immunization, 10^6 peptide-pulsed DCs were injected i.v. in C57BL/6 females at day 0 and 7. At day 14, splenocytes were harvested from the spleens of immunized mice and depleted of red blood cells using 0.83% NH_4CL. Cells were plated at 5 x 10^6 cells/well in 24-well plates and restimulated with 2 x 10^{-6}M peptide at 37°C. After 6 days, cytotoxicity was evaluated by a CFSE-based assay (Jedema *et al*, 2004). The % specific lysis was calculated as follows: (number of $CFSE^+$ remaining cells after incubation of target cells alone – number of $CFSE^+$ remaining cells after incubation with effector cells / number of $CFSE^+$ cells after incubation of target cells alone) x100.

Online Supplemental Material

Supplementary Figure 1 illustrates that 95% of peptide ions showed a variation of less than ± 1.4-fold and ± 2.2-fold in abundance across 2D-nanoLC-MS instrumental and biological replicates, respectively. Table S1 shows the relative abundance of peptides eluted from WT, $\beta2m^-$ and $\beta2m^+$ EL4 cell lines. Table S2 shows the computed MHC binding affinity of MHC I-associated peptides eluted from EL4 cells. Table S3 shows the computed MHC binding affinity of MHC I-associated peptides eluted from primary mouse thymocytes. Table S4 shows the computed MHC binding affinity of MHC I-associated peptides eluted from *in vivo* grown EL4 cells. Table S5 shows the relative abundance of MHC I-associated peptides eluted from primary thymocytes versus *in vivo* grown EL4 cells. Table S6 is a list (with references) of cancer related genes coding for MHC I peptides differentially expressed in neoplastic (EL4) versus normal thymocytes. Table S7 is a list of primers used for quantitative RT PCR analyses.

3.4 Results

Experimental approach for the identification and quantification of MHC I – associated peptides

Mild acid elution (MAE) of MHC I – associated peptides from living cells presents several advantages over immunoprecipitation of peptide – MHC I complexes. Because it involves fewer purification steps and no detergents, MAE yields 10 times more MHC I – associated peptides than the latter and introduces no bias linked to preferential loss of low-affi nity peptides (Perreault *et al*, 1996; Purcell, 2004; Storkus *et al*, 1993). However, MAE has never been used for highthroughput sequencing of the MIP repertoire because it is assumed that eluted peptides contain not only MHC I – associated peptides, but also "contaminant" peptides. We reasoned that this problem could be overcome by using MHC I – deficient cells as a negative control. Because β2-microglobulin (β2m) is essential for formation of stable peptide – MHC I complexes, β2m-deficient cells are MHC I deficient. We therefore compared peptides eluted from three cell populations, as follows: WT EL4 thymoma cell line, a β2m-deficient EL4 mutant cell line (C4.4-25^{-}), and C4.4-25^{-} cells transfected with a genomic clone of murine β2m (E50.16^{+}) (40). Flow cytometry analysis showed that expression of H2D^{b}, H2K^{b}, and Qa2 MHC I molecules were abrogated in β2m-deficient EL4 cells, but were restored in β2m transfectants (Figure 1A).

Samples obtained by MAE of peptides from 8×10^{7} cells were analyzed using an on-line 2D-nanoLC-MS system (see Materials and methods for more details). Each individual LCMS run was visualized as a three-dimensional map where each isotopic profile (dot) corresponds to a given ion that is defined by its specific abundance, m/z, and retention time coordinates (Figure 1 B). We first assessed the reproducibility of data obtained with our method using peptide eluates from WT EL4 cells. We found that 95% of peptide ions showed a variation of less than ± 1.4- and ± 2.2-fold in abundance across 2DnanoLC- MS instrumental and biological replicates, respectively (Supplementary Figure 1, available at http://www.jem.org/cgi/content/full/ jem.20071985/DC1). Therefore, peptides were considered to be differentially expressed when the fold difference in abundance was ≥ 2.5 ($P < 0.05$). We next compared profiles from WT and β2m-deficient EL4 cells. Contour profiles obtained after computational analyses showed a

higher level of peptide complexity for WT compared with β2m-deficient EL4 cells (Figure 1 B). We assessed the proportion of MHC I – associated versus contaminant peptides using in-house peptide detection software (unpublished data). To identify and define individual peptide clusters, peptide lists generated by Mass Sense were compared through replicate injections from both WT- and $\beta 2m^-$ mutant-derived samples using segmentation analyses with hierarchical clustering. Heat map representation was used to visualize differences in peptide cluster expression between WT- and $\beta 2m^-$ mutant derived samples (Figure 1B). Peptides that were recovered only from WT EL4 cells were considered to be part of the MIP repertoire. Because β2m-deficient cells express low amounts of incomplete MHC I molecules at the cell surface (Williams *et al*, 1989), we also considered that peptides significantly more abundant on WT relative to β2m-deficient cells were MHC I associated. In the latter case, we used a very stringent criterion; to be considered as MHC I associated, a peptide had to be at least five times more abundant on WT relative to β2m-deficient cells. Out of 3,716 unique peptide clusters that were reproducibly detected across three biological replicates, 1,487 peptide clusters were overexpressed or uniquely detected within the WT EL4 sample. Thus, we estimated that 40% of acid-eluted materials correspond to specific-MHC I peptides.

We obtained MS/MS assignments for 881 of the 3,716 peptide clusters, all of which had a characteristic fragmentation associated to peptide backbone cleavages. Although these identifications correspond to 24% of the entire ion population detected, other MS/MS spectra were assigned to modified residues, de novo peptide sequences, or spectra of poor quality. Peptide coordinates were computationally related to their corresponding sequenced peptides. Out of 881 sequenced peptides, 383 had a consensus motif for $H2D^b$, $H2K^b$, Qa1, or Qa2 MHC I molecules. Stringent validation criteria were next applied to select peptide ions showing mass accuracy of < 30 parts per million (ppm), with MS/MS spectra displaying consistent sets of b- and/or y-type fragment ion series corresponding to the MHC I peptide sequence. This manual validation enabled the identification of 178 unique MS/MS corresponding to MHC I – associated peptides: 158 were detected uniquely in eluates from WT EL4 cells, whereas 20 were overexpressed at least 5-fold on WT relative to β2m-deficient EL4 cells (Figure 1 C). To confirm that differences between WT and β2m-deficient EL4 cells were truly β2m dependent, we

analyzed peptides recovered from E50.16 + cells (β2m-deficient EL4 cells transfected with a genomic clone of murine β2m). As expected, we observed that 95% of MHC I peptides were expressed at the cell surface of $\beta2m^+$ transfectants. Absence of a few MHC I peptides on β2m transfectants is probably explained by the lower expression of $H2D^b$ and $H2K^b$ on β2m transfectants compared with WT cells (Figure 1A). For the 178 sequenced MHC I – associated peptides, relative abundance in the three EL4 cell variants (WT, $\beta2m^-$ mutants, and $\beta2m^+$ transfectants) is presented in Table S1 (available at http://www.jem.org/cgi/content/full/jem.20071985/DC1). Data for a representative set of peptides is shown in Table I. Notably, although MHC I peptides were 8 – 13 mers, the length of contaminant peptides was more variable, ranging from 6 to 26 amino acids with a median value of 13 residues (unpublished data).

Definition of the MIP repertoire presented by discrete MHC I allelic products

Large databases of MHC I peptides and computational binding methods are now part of emerging biomedical resources (Moutaftsi *et al*, 2006; Peters *et al*, 2006; Peters and Sette, 2007; Rammensee *et al*, 1999). Information in these databases concerns mainly, though not exclusively, viral and bacterial-derived peptides presented by MHC I allelic products in humans and mice. Each MHC I peptide in Table S1 was manually classified according to restriction size and binding motif favored by D^b , K^b , Qa1, and Qa2 class I molecules (Aldrich *et al*, 1994; Falk *et al*, 1991; Rotzschke *et al*, 1993). From 178 MHC I peptides identified from variant EL4 cell lines, 92% were presented by classical MHC Ia allelic products $H2D^b$ and $H2K^b$, and 8% were presented by MHC Ib molecules Qa1 and Qa2 (Figure 2A and Table S2, available at http://www.jem.org/cgi/content/full/jem.20071985/DC1).When viewed *in toto*, peptide pools presented by $H2D^b$, $H2K^b$, and Qa2 displayed the canonical binding motifs documented for these MHC I molecules (Figure 2B).

A priori, two factors may determine whether specific peptides are presented by MHC I: peptide affinity for MHC molecules and the processing of source proteins along the MHC I presentation pathway. Protein attributes that are relevant to MHC I processing include rates of protein translation, DRiP formation, and degradation (Caron *et al*, 2005; Qian *et al*, 2006a; Qian *et al*, 2006b; Yewdell *et al*, 2006). To evaluate the importance of

peptide binding affinity, each of the 164 source proteins of peptides presented by $H2D^b$ (n = 96) or $H2K^b$ (n = 68) was analyzed with the smm algorithm. We scored and ranked the predicted binding affinity of all peptides from individual proteins for $H2D^b$ or $H2K^b$ (for example, a protein of 400 amino acids contains 392 nonapeptide sequences). We then asked how each peptide that we had sequenced by MS/MS would rank relative to other peptides from its source protein. Remarkably, 91% of $H2D^b$-associated peptides eluted from EL4 cells ranked in the top 1% in terms of $H2D^b$ binding affinity (Figure 2C and Table S2). Similar results were obtained from the SYFPEITHI database (unpublished data). That some peptide sequences predicted to be top MHC I binders were not found in the MIP repertoire of EL4 cells is not surprising. This means either that proteases involved in MHC I processing do not generate these specific "degradation products" or that they are present in subthreshold amounts. For $H2K^b$, 85% of peptides ranked in the top 5% for predicted $H2K^b$ binding affinity (Figure 2C and Table S2). These data support the concept that MHC I binding affinity plays a dominant role in shaping the content of the MIP repertoire.

Discrimination between MHC I – associated peptides and contaminant peptides using bioinformatic tools

In the aforementioned experiments, we used β2m-deficient cells as negative control to discriminate MHC I – associated peptides from contaminant peptides. The need for an MHC I – deficient negative control would nevertheless represent a significant hurdle for high-throughput sequencing of the MIP repertoire of primary cells. We therefore asked whether bioinformatic tools could be used to identify MHC I – associated peptides among a peptide mixture obtained by MAE. We first ranked the 164 $H2D^b$- and $H2K^b$-associated peptides eluted from EL4 cells as a function of their MHC binding score estimated with smm and SYFPEITHI algorithms (Figure 3, red bars). We found that 97% of MHC I – associated peptides were scored below an smm binding threshold of 1,000 nM (IC 50) and above a SYFPEITHI binding threshold of 22 for $H2D^b$ and 13 for $H2K^b$ (Figure 3). The aforementioned thresholds therefore provided a 3% false-negative rate (3% of MHC I – associated peptides were wrongly classified as contaminants). To estimate the false-positive rate obtained with these thresholds, we analyzed the 215 contaminant peptides eluted from EL4 cells representing high-quality assignment (Mascot score > 45, mass

accuracy < 30 ppm, MS/MS manually inspected) from a list of 498 candidates that were not significantly overexpressed on WT relative to β2m-deficient EL4 cells. Only 56 out of the 215 contaminant peptides had the canonical length for binding $H2D^b$ or $H2K^b$, and very few of them satisfied our smm and SYFPEITHI thresholds (Figure 3, blue bars). Overall, the false-positive rate was < 2% (< 2% of contaminants were wrongly classified as MHC I – associated peptides). Similar results were obtained for Qa2 peptides using the Rankpep algorithm with a binding threshold of 120. We synthesized nine peptides across the predicted affinity spectrum and tested their ability to bind $H2K^b$ or $H2D^b$. Peptides classified as MHC I associated according to their smm score did bind to MHC I, whereas peptides classified as contaminants did not (Supplementary Figure 2). These experimental data further validate bioinformatic discrimination between MHC I – associated peptides and contaminant peptides. We therefore conclude that peptides obtained by MAE can be categorized as MHC I – associated versus contaminant peptides with 1 – 3% false-positive and -negative rates using publicly available algorithms.

Global portrayal of the MIP repertoire of primary mouse thymocytes

In the next series of experiments, peptides eluted from primary mouse thymocytes by MAE were analyzed by on-line 2D-nanoLC-MS/MS. Of the sequenced peptides, 189 were classified as MHC I associated based on the smm, SYFPEITHI, and Rankpep thresholds selected above: 84 $H2D^b$-, 91 $H2K^b$-, 13 Qa2-, and 1 Qa1-associated peptides (TableS3, available at http://www.jem.org/cgi/content/full/jem.20071985/DC1). Based on analyses described in the previous paragraph, we estimate that the false-positive rate for the 189 thymocyte peptides is < 2%. GO term enrichment analysis was performed on the 189 genes coding for those peptides by applying stringent criteria from 772 functional annotations (Figure 4A). In accordance with a study on HLA-B*1801 – associated peptides (25), the MIP repertoire of primary thymocytes showed a modest but significant two fold enrichment in proteins located in the cytoplasm and the nucleus. More interestingly, we found an 11 – 19-fold enrichment in proteins related to cyclin and cyclin-dependent kinases (Ccng1, Cdkn1b, Chek1, Bccip, Cul2, Ccnd3, and CcnF), which regulate the cell cycle. We also found an 11 – 17-fold enrichment in helicases (Dhx15, Ddx5, Ddx6, Hells, and Ddx47), which are required for efficient and accurate replication, repair, and recombination of the genome.

MHC I – associated peptides derive preferentially from highly abundant mRNAs

We next sought to determine whether the MIP repertoire of thymocytes was molded at the mRNA level. To this end, we compared the relative abundance of two sets of thymic transcripts: (a) those encoding MHC I peptides eluted from primary thymocytes (Table S3), and (b) 36,182 transcripts encoded by the mouse genome (Su *et al*, 2004). We found a dramatic enrichment in highly abundant mRNAs among transcripts coding for MHC I peptides (Figure 4, B and C). Thus, although 9% of total mRNAs are expressed at high levels, 42% of those coding MHC I peptides did so (Figure 4C). Conversely, 62% of total mRNAs showed low abundance, but only 20% of those coding MHC I peptides were expressed at low levels. Nonetheless, some MHC I peptides are coded by low abundance mRNAs (Figure 4, B and C). We hypothesized that low abundance mRNAs may contribute to the MIP repertoire because they code peptides with very high affinity for MHC I. Our data did not support that assertion. We found no correlation between the computed MHC I binding affinity of peptides and the abundance of their mRNAs (Figure 4D). MHC I peptides derived from low-abundance transcripts did not display superior computed MHC binding affinity. Although the ability to detect MHC I peptides is limited by the MS sensitivity (high attomole range) and dynamic range of detection (13 orders of magnitude on log 2 scale of Figure 4), our results demonstrate that MHC I peptides derived preferentially, but not exclusively, from highly abundant mRNAs.

Evidence that the MIP repertoire of thymocytes conceals a tissue-specific signature

Because MHC I peptides derived preferentially from highly abundant mRNAs, and abundance of discrete mRNAs varies among different tissues and organs, we hypothesized the MIP repertoire might harbor a tissue-specific signature. Using the SymAtlas database (http://symatlas.gnf.org/SymAtlas/) (Su *et al*, 2004), we analyzed the relative expression in 58 mouse tissues of mRNAs encoding thymocyte MHC I – associated peptides (see Materials and methods for details on calculation). Remarkably, the mean expression of the 180 mRNAs coding thymocyte MHC I peptides was higher in the thymus than in all other tissues and organs (Figure 5A).

Large-scale quantitative analyses of transcriptional expression profiles across different tissues have revealed broadly expressed and tissue-specific groupings (Su *et al*,

2004; Zhang *et al*, 2004). To determine whether the MIP repertoire of thymocytes is imprinted by tissue-specific genes, we attributed a z score to individual source mRNAs (Virtaneva *et al*, 2001). Genes with high z score (from 2.5 to 7) correspond to those that are preferentially overexpressed in the thymus. Among the 180 genes encoding thymocyte MHC I peptides, 30 showed a high z score (Figure 5, B and C). The z score distribution of genes encoding thymocyte MHC I peptides is illustrated in Figure 5B, and a heat map representation of the 30 genes with high z scores is depicted in Figure 5C. Next, we estimated how additive removal of high z score genes would affect the thymus specificity of the gene set. Thymus specificity of the gene set was lost after removal of the 30 high z score genes (Figure 5 D). In contrast, removal of up to 70 random genes did not affect the thymus specificity of the gene set. These results suggest that the MIP repertoire of thymocytes conceals a tissue-specific signature that is constituted by 30 genes, i.e., 17% of genes that are represented in the thymocytes' MIP repertoire.

Among the 30 genes with high thymic z score, 16 are expressed, albeit at lower levels than in other organs, whereas 14 genes are expressed almost exclusively in hematolymphoid organs: Rhoh, Centb1, Cxcr4, Depdc1a, Foxp1, Dnmt1, 9230105E10Rik, Cd3e, C330027C09Rik, Igtp, Mns1, Dock2, Actr2, and Vps13d (Figure 5C). In accordance with the concept that tissue-specific expression is indicative of gene function in mammals (Zhang *et al*, 2004), we noted that hematolymphoid genes represented in the thymocytes' MIP repertoire play critical roles in T cell development. For example, Rhoh is important for positive thymocyte selection, Cxcr4 for migration of T cell progenitors, and CD3e for migration of T cell development (Dorn *et al*, 2007; Malissen *et al*, 1995; Plotkin *et al*, 2003). Further studies are needed to cogently assess the functional importance of genes that impart tissue specificity to the thymocytes' MIP repertoire. However, evidence suggests that many, if not all, of these genes are functionally important for thymocyte function. In conclusion, two major and related points can be made regarding the connection between the transcriptome and the MIP repertoire. First, the MIP repertoire is enriched in peptides derived from highly abundant transcripts. Second, our data suggest that thymocytes' MIP repertoire conceals a tissue-specific signature that derives from 17% of MHC I – associated peptides.

The MIP repertoire of normal versus neoplastic thymocytes

Ultimately, the genesis of MHC I peptides must be regulated by mRNA translation and protein degradation by the proteasome (Qian *et al*, 2006b; Yewdell *et al*, 2003), two processes that are profoundly perturbed in neoplastic cells (Nakayama and Nakayama, 2006; Richter and Sonenberg, 2005). To evaluate the impact of neoplastic transformation on the MIP repertoire, we compared the MIP repertoire of primary thymocytes from C57BL/6 female mice to that of neoplastic thymocytes. As a source of neoplastic thymocytes, we used in vivo grown EL4 cells. EL4 cells were originally derived from a C57BL/6 female mouse. Based on aforementioned experiments on the reproducibility of estimation of peptide abundance by MS analyses (Supplementary Figure 1), peptides were considered to be differentially expressed when the fold difference in abundance was ≥ 2.5 ($P < 0.05$). Table S3 and S4 (available at http://www.jem.org/cgi/content/full/jem.20071985/DC1) present the complete list of peptides eluted from primary thymocytes and in vivo grown EL4 cells and their computed MHC binding score. Overall, 25% of MHC I peptides were differentially expressed on normal versus neoplastic thymocytes (Table II and Figure 6A). Thus, 22 peptides were underexpressed and 21 were overexpressed on neoplastic relative to normal thymocytes (Table II). Differentially expressed peptides derived from genes implicated in several biological processes, such as cell cycle progression, apoptosis, signal transduction, cytoskeleton assembly, and differentiation, as well as regulation of transcription and translation (Table II). As an example, the X-linked lymphocyte-regulated 3 (Xlr3a/b) gene encoded a peptide found only on EL4 cells (Figure 6B and Table II). Xlr genes are important for T cell differentiation and are overexpressed in several lymphoid malignancies (Siegel *et al*, 1987). In contrast, an MHC I peptide from cyclin dependent kinase inhibitor 1B (Cdkn1b) was underexpressed on neoplastic cells (Figure 6C, Table II). Cdkn1b is known to act as a potent tumor suppressor gene in a variety of cancers (Nakayama *et al*, 2006). Remarkably, 50% of differentially expressed peptides derived from genes that are known to be involved in tumorigenesis (Table II and Table S5). For example, 10 differentially expressed peptides (Bach2, Cdkn1b, Cxcr4, Eif3s2, Eif3s10, Igtp, Pa2g4, Pi3kap1, Ptpn6, and Sgk) originated from genes related to the PI3K–AKT–mTOR pathway, which is the oncogenic signalling pathway most commonly targeted by genomic aberrations in cancer (Hennessy *et al*, 2005; Mamane *et al*, 2006).

Genesis of peptides overexpressed on tumor cells

An important question is whether differential expression of MHC I peptides on neoplastic relative to normal thymocytes correlates with changes in mRNA levels of source transcripts. To test this, we selected 19 peptides overexpressed on EL4 cells relative to primary thymocytes, 15 that were underexpressed, and 13 that were not differentially expressed. Then, we analyzed the level of expression of their source mRNAs in neoplastic versus primary thymocytes using quantitative real-time PCR. Scatterplot representation of the correlation between relative mRNA expression and relative MHC I peptide expression is depicted in Figure 6D. From the linear regression, a Spearman coefficient of 0.63 was calculated, showing a significant but moderate correlation between peptide and mRNA expression ratios. The strength of the correlation was conspicuously decreased by a set of 14 peptides that were more abundant on neoplastic cells, but whose mRNA levels were not overexpressed (Figure 6D, dotted box). Exclusion of these 14 genes increased the correlation coefficient to 0.78. Remarkably, for the 19 peptides overexpressed on EL4 cells, increased transcript levels were present in EL4 cells in only 5 cases (Figure 6D). Peptides overexpressed on neoplastic cells are particularly important because they can be used as targets in cancer immunotherapy (Purcell *et al*, 2007; Singh-Jasuja *et al*, 2004). Thus, the salient finding here is that 74% (14 of 19) of peptides overexpressed on EL4 cells would have been missed by studies of mRNA expression levels. An important implication is that, at least in our model, overexpression of MHC I – associated peptides on neoplastic cells generally entails posttranscriptional mechanisms.

Testing the immunogenicity of peptides overexpressed on neoplastic cells

Finally, we wished to determine whether peptides overexpressed on neoplastic thymocytes (in vivo grown EL4 cells) would be able to elicit specific CD8 T cell response. To test this, we used the following two peptides: (a) STLTYSRM, which is derived from serum/glucocorticoid-regulated kinase (Sgk) and presented by $H2K^b$, and (b) VAAANREVL derived from X-linked lymphocyte-regulated 3 (Xlr3a/b) and presented by $H2D^b$. One important difference between the two peptides is that VAAANREVL was not found on primary thymocytes (fold difference relative to EL4 cells $\geq$ 85), whereas low levels of STLTYSRM were present on primary thymocytes (fold difference = 10; Table II and Table S6, available at http://www.jem.org/cgi/content/full/jem.20071985/DC1). TAP-

deficientT2-D^b and T2-K^b cells were first incubated with titrated amounts of synthetic peptides to evaluate their ability to bind and stabilize $H2K^b$ and $H2D^b$. In contrast to the L^d-restricted peptide RPQASGVYM, both STLTYSRM and VAAANREVL peptide loading resulted in an increase in cell surface expression of H2-K^b or H2-D^b (Supplementary Figure 2), thereby confirming their ability to bind their respective MHC allele. We next immunized C57BL/6 mice with DCs coated or not coated with VAAANREVL and STLTYSRM synthetic peptides. Splenocytes from immunized mice were tested for in vitro cytotoxicity against primary thymocytes and EL4 target cells that were not loaded with exogenous peptides. Splenocytes from mice primed with unloaded DCs showed no cytotoxic activity. In contrast, splenocytes primed with coated DCs killed EL4 cells, but not primary thymocytes (Figure 7). Thus, peptides overexpressed by 10- to $\geq$ 85-fold on neoplastic cells elicited specific cytotoxic activity against endogenously presented epitopes.

3.5 Discussion

We have developed a novel method for high-throughput analysis of MHC I peptides and performed a comprehensive study of the MIP repertoire of normal and neoplastic thymocytes. Our studies yielded important insights into the genesis of the MIP repertoire and how it is modified by neoplastic transformation.

A novel method for high-throughput, MS-based analysis of MHC I peptides

In the last few years, high-throughput screening methods coupled with bioinformatics tools have helped to figure out the complexity of biological matrices. Thus, emerging technologies in mass spectrometry have led to the development of peptide detection algorithms that can be used, in combination with segmentation analyses, to compare unlabeled peptide populations (unpublished data) (Kearney *et al*, 2003). This powerful approach allowed us to obtain an accurate quantification of native unlabeled MHC I peptides without any chemical or metabolic labeling modifications. Because preparation of samples does not require different purification steps, higher sensitivity can be achieved from limiting the amount of materials compared with chemical derivatization where peptide recovery can be affected by variable modification yields or side reaction products (Ong *et al*, 2003). Thus, by combining our MS strategy with MAE, we were able to generate a comprehensive portrayal of the MIP repertoire of EL4 cells from $< 10^8$ cells. The ability to identify large numbers of MHC I peptides from limiting amounts of cells is a noteworthy advantage. Moreover, our quantification method can be used to analyze any type of cell population, whereas metabolic labeling strategies can only be applied to cell culture model systems. Nevertheless, low abundance peptides (< 100 copies/cell) remain challenging to identify in view of the sensitivity of present high-throughput, MS-based methods. The portrayal of the MIP repertoire described in this study and others is far from complete, and low-abundance peptides that may be biologically relevant could remain elusive to current detection methods.

We took advantage of EL4 variant cell lines (WT, $\beta 2m^-$ mutant, and $2m^+$ transfectant) to unambiguously discriminate between MHC I – associated peptides and contaminants in peptide mixtures obtained by MAE. A large proportion of contaminants

was made of long peptides derived from the C-terminal end of source proteins (unpublished data). We noted that some of these contaminants have previously been considered as MHC I – associated peptides in studies where peptides were obtained by MAE or immunoaffinity purification (Gebreselassie *et al*, 2006; Suri *et al*, 2006). The need to have an MHC I – deficient negative control to distinguish MHC I peptides from contaminants would be a cumbersome limitation for analysis of primary cells. However, we showed that the use of computational models such as SYFPEITHI and smm obviated this need. Thus, thresholds used herein yielded false-positive and –negative rates of 2% in identification of MHC I peptides.

The MIP repertoire of primary cells

High-throughput analysis of peptides obtained by MAE provided us with a global portrayal of peptides presented by different MHC I allelic products (in this study: $H2D^b$, $H2K^b$, Qa1, and Qa2). We found that, with rare exceptions, discrete MHC I molecules presented peptides derived from different sets of source proteins (Table S2 and S3). A corollary is that expression of multiple MHC I allelic products (a consequence of gene duplication and diversification (Gleimer and Parham, 2003)) favors representation of largely nonoverlapping sets of source proteins in the MIP repertoire. By integrating global profiling of the mouse protein-encoding transcriptome (Su *et al*, 2004) with the MIP repertoire of thymocytes, we found that the thymocytes' MIP repertoire is enriched in peptides derived from highly abundant transcripts. Furthermore, our data suggest that the repertoire of MHC I – associated peptides conceals a tissue-specific signature that derives from 17% of genes represented in the MIP repertoire. Cogent evaluation of this exciting concept will require comprehensive analyses of MHC I – associated peptides eluted from various tissues and organs. Why would the MIP repertoire show a stronger correlation with the transcriptome (this study) than the proteome (Milner *et al*, 2006)? Probably because the proteome is enriched in slowly degraded proteins (with a mean $t_{1/2}$ of > 1,000 min), whereas the MIP repertoire originates mainly from rapidly degraded proteins (with a mean $t_{1/2}$ of 10 min) that have recently been translated and degraded (Milner *et al*, 2006; Qian *et al*, 2006a). In other words, MHC I molecules sample what is being translated rather than what has been translated (Qian *et al*, 2006b). Considering the pervasive roles of MIPs, particularly in CD8 T cell development and function, it will be extremely

interesting to determine whether the MIP repertoire of specialized cell types does conceal a tissue-specific signature. Of particular interest are thymus cortical epithelial cells, which support thymocyte positive selection, and thymus medullary epithelial cells, which express promiscuous transcripts involved in tolerance induction. Besides, although the MIP repertoire is enriched in peptides derived from highly abundant mRNAs, some peptides presented by MHC class I molecules derive from low abundance mRNAs (Figure 4). How can low-abundance transcripts successfully compete with more abundant transcripts for representation in the MIP repertoire? Attractive possibilities would be that successful transcripts generate more DRiPs than others or that they are translated by special "immunoribosomes" (Qian *et al*, 2006b; Yewdell *et al*, 2006).

The proteasome, which is the primary source of MHC I peptides, is much more ancient than the MHC. The MHC appeared in gnathostomes, whereas proteasomes are found in all eukaryotes. Fundamental functions of the proteasome are to regulate cell cycle, proliferation, and apoptosis (Glickman and Ciechanover, 2002). In line with this, we found that the MIP repertoire of primary thymocytes was enriched in peptides derived from cyclins, cyclindependent kinases, and helicases (Figure 4A). These highly conserved proteins regulate cell proliferation, cell cycle arrest, and apoptosis. Peptides derived from cyclin, cyclin-dependent kinase, and helicase gene families have also been found in other studies of MHC I peptides (Hickman *et al*, 2004; Suri *et al*, 2006; Weinzierl *et al*, 2007). We surmise that the presence of these peptide families in the MIP repertoire may represent an imprint of primordial functions of the proteasome. Nevertheless, an alternative hypothesis would be that overrepresentation of peptide-derived proteins regulating proliferation and apoptosis is a thymocyte-specific feature because thymocytes display particularly high rates of proliferation and apoptosis.

The MIP repertoire of neoplastic cells

Neoplastic transformation is associated with many genomic and proteomic changes. How these changes may impinge on the MIP repertoire and thereby be perceived by CD8 T cells, is a fundamental question in cancer immunology that can be addressed directly only by MS-based analysis of the MIP repertoire. Weinzierl et al. recently reported a seminal study in which they integrated mass spectrometry and microarray data on renal cell

carcinomas and autologous normal kidney tissues (Weinzierl *et al*, 2007). They found a poor correlation between changes in peptide expression and changes in the abundance of mRNA levels in normal versus cancer cells (r = 0.32). We found a better correlation between mRNA levels and expression of corresponding MHC I peptides in normal and neoplastic thymocytes (Figure 6D ; r = 0.63). We surmise that the stronger correlation in our case may be caused by estimation of transcript levels with quantitative real-time PCR analyses rather than microarrays. Indeed, quantitative real-time PCR provides a more accurate estimation of quantitative differences than microarrays (Matos *et al*, 2004). However, our data support the main conclusion of Weinzierl et al., which is that a majority of peptides overexpressed on neoplastic cells (74% in our case) would have been missed by estimation of transcript levels. Together with data from Weinzierl et al., our results suggest that in general, overexpression of MHC I peptides on neoplastic cells is caused by posttranscriptional mechanisms and can be detected only by MS-based expression profiling approaches. Further studies on diverse cancer types are needed to test the generality of these observations. Relevant mechanisms may include dysregulation of microRNA expression, protein translation, and proteasomal degradation (Lu *et al*, 2005; Nalepa *et al*, 2006; Ruggero and Pandolfi, 2003).

Our data suggest that the MIP repertoire gives a unique perspective into the mechanisms of carcinogenesis. Approximately 50% of peptides differentially expressed on normal versus neoplastic cells are coded by genes involved in neoplastic transformation (Table II and Table S5). It is quite remarkable that 10 of the differentially expressed peptides derived from genes related to the PI3K–AKT–mTOR pathway. The PI3K–AKT–mTOR pathway is the most prominent pathway regulating protein translation, cell growth, and cell proliferation, and is activated in most cancers (Hennessy *et al*, 2005). In addition, our data lead us to speculate that the MIP repertoire might give unique insights into acquired epigenetic abnormalities that are so important in cancer. Indeed, Dnmt1, which regulates DNA methylation and prevents genomic instability (Eden *et al*, 2003), is expressed at high levels in thymocytes (Figure 5C). We found that a Dnmt1-derived peptide was overexpressed 9-fold on neoplastic relative to primary thymocytes (Table II). This raises the enticing possibility that enhanced proteasomal degradation of Dnmt1 might be responsible for the genomic instability of EL4 cells. Finally, we were

able to generate specific cytotoxic T cell responses against EL4 cells by priming WT mice with two peptides overexpressed on EL4 cells (Figure 7). The finding that efficient cytotoxic responses could be elicited against endogenously expressed tumor peptides identified with our MS-based expression analyses validates the analytical potential of the present approach. Though further work is needed to evaluate the therapeutic value of vaccination with these peptides, our results strongly support the concept that high-throughput analysis of the MIP repertoire is a promising discovery platform for the identification of immunogenic tumor-associated peptides (Lemmel *et al*, 2004; Purcell *et al*, 2007; Singh-Jasuja *et al*, 2004).

3.6 Acknowledgements

We are grateful to the staff of the following core facilities at the Institute for Research in Immunology and Cancer for their outstanding support: Animal facility, Bioinformatics, Flow cytometry, and Proteomics. We thank Dr. R. Glas for kindly providing us with WT EL4, C4.4-25^{-} and E50.16^{+} cell lines. This work was supported by funds from the Canadian Cancer Society and the Terry Fox Foundation through the National Cancer Institute of Canada. MHF and EC are supported by training grants from the Natural Sciences and Engineering Research Council of Canada and the Canadian Institutes of Health Research, respectively. CP and PT hold Canada Research Chairs in Immunobiology, and Proteomics and Bioanalytical Spectrometry, respectively. The authors have no conflicting financial interests.

3.7 References

Admon A, Barnea E, Ziv T (2003) Tumor antigens and proteomics from the point of view of the major histocompatibility complex peptides. *Mol Cell Proteomics* **2:** 388-398.

Aldrich CJ, DeCloux A, Woods AS, Cotter RJ, Soloski MJ, Forman J (1994) Identification of a Tap-dependent leader peptide recognized by alloreactive T cells specific for a class Ib antigen. *Cell* **79:** 649-658.

Anikeeva N, Lebedeva T, Clapp AR, Goldman ER, Dustin ML, Mattoussi H, Sykulev Y (2006) Quantum dot/peptide-MHC biosensors reveal strong CD8-dependent cooperation between self and viral antigens that augment the T cell response. *Proceedings of the National Academy of Sciences of the United States of America* **103:** 16846-16851.

Barnea E, Beer I, Patoka R, Ziv T, Kessler O, Tzehoval E, Eisenbach L, Zavazava N, Admon A (2002) Analysis of endogenous peptides bound by soluble MHC class I molecules: a novel approach for identifying tumor-specific antigens. *European journal of immunology* **32:** 213-222.

Benoist C, Germain RN, Mathis D (2006) A plaidoyer for 'systems immunology'. *Immunological reviews* **210:** 229-234.

Caron E, Charbonneau R, Huppe G, Brochu S, Perreault C (2005) The structure and location of SIMP/STT3B account for its prominent imprint on the MHC I immunopeptidome. *International immunology* **17:** 1583-1596.

Dennis G, Jr., Sherman BT, Hosack DA, Yang J, Gao W, Lane HC, Lempicki RA (2003) DAVID: Database for Annotation, Visualization, and Integrated Discovery. *Genome biology* **4:** P3.

Dorn T, Kuhn U, Bungartz G, Stiller S, Bauer M, Ellwart J, Peters T, Scharffetter-Kochanek K, Semmrich M, Laschinger M, Holzmann B, Klinkert WE, Straten PT, Kollgaard T, Sixt M, Brakebusch C (2007) RhoH is important for positive thymocyte selection and T-cell receptor signaling. *Blood* **109:** 2346-2355.

Dunn GP, Old LJ, Schreiber RD (2004) The immunobiology of cancer immunosurveillance and immunoediting. *Immunity* **21:** 137-148.

Eden A, Gaudet F, Waghmare A, Jaenisch R (2003) Chromosomal instability and tumors promoted by DNA hypomethylation. *Science (New York, NY* **300:** 455.

Falk K, Rotzschke O, Stevanovic S, Jung G, Rammensee HG (1991) Allele-specific motifs revealed by sequencing of self-peptides eluted from MHC molecules. *Nature* **351:** 290-296.

Fortier MH, Bonneil E, Goodley P, Thibault P (2005) Integrated microfluidic device for mass spectrometry-based proteomics and its application to biomarker discovery programs. *Anal Chem* **77:** 1631-1640.

Galea-Lauri J, Wells JW, Darling D, Harrison P, Farzaneh F (2004) Strategies for antigen choice and priming of dendritic cells influence the polarization and efficacy of antitumor T-cell responses in dendritic cell-based cancer vaccination. *Cancer Immunol Immunother* **53:** 963-977.

Gebreselassie D, Spiegel H, Vukmanovic S (2006) Sampling of major histocompatibility complex class I-associated peptidome suggests relatively looser global association of HLA-B*5101 with peptides. *Human immunology* **67:** 894-906.

Gleimer M, Parham P (2003) Stress management: MHC class I and class I-like molecules as reporters of cellular stress. *Immunity* **19:** 469-477.

Glickman MH, Ciechanover A (2002) The ubiquitin-proteasome proteolytic pathway: destruction for the sake of construction. *Physiol Rev* **82:** 373-428.

Hammer GE, Kanaseki T, Shastri N (2007/4) The final touches make perfect the peptide-MHC class I repertoire. *Immunity* **26:** 397-406.

Heemels MT, Ploegh H (1995) Generation, translocation, and presentation of MHC class I-restricted peptides. *Annu Rev Biochem* **64:** 463-491.

Hennessy BT, Smith DL, Ram PT, Lu Y, Mills GB (2005) Exploiting the PI3K/AKT pathway for cancer drug discovery. *Nature reviews* **4:** 988-1004.

Hickman HD, Luis AD, Buchli R, Few SR, Sathiamurthy M, VanGundy RS, Giberson CF, Hildebrand WH (2004) Toward a definition of self: proteomic evaluation of the class I peptide repertoire. *J Immunol* **172:** 2944-2952.

Hosack DA, Dennis G, Jr., Sherman BT, Lane HC, Lempicki RA (2003) Identifying biological themes within lists of genes with EASE. *Genome biology* **4:** R70.

Huczko EL, Bodnar WM, Benjamin D, Sakaguchi K, Zhu NZ, Shabanowitz J, Henderson RA, Appella E, Hunt DF, Engelhard VH (1993) Characteristics of endogenous peptides eluted from the class I MHC molecule HLA-B7 determined by mass spectrometry and computer modeling. *J Immunol* **151:** 2572-2587.

Hunt DF, Henderson RA, Shabanowitz J, Sakaguchi K, Michel H, Sevilir N, Cox AL, Appella E, Engelhard VH (1992) Characterization of peptides bound to the class I MHC molecule HLA-A2.1 by mass spectrometry. *Science (New York, NY* **255:** 1261-1263.

Huseby ES, White J, Crawford F, Vass T, Becker D, Pinilla C, Marrack P, Kappler JW (2005) How the T cell repertoire becomes peptide and MHC specific. *Cell* **122:** 247-260.

Jedema I, van der Werff NM, Barge RM, Willemze R, Falkenburg JH (2004) New CFSE-based assay to determine susceptibility to lysis by cytotoxic T cells of leukemic precursor cells within a heterogeneous target cell population. *Blood* **103:** 2677-2682.

Kearney P, Thibault P (2003) Bioinformatics meets proteomics--bridging the gap between mass spectrometry data analysis and cell biology. *J Bioinform Comput Biol* **1:** 183-200.
Lemmel C, Weik S, Eberle U, Dengjel J, Kratt T, Becker HD, Rammensee HG, Stevanovic S (2004) Differential quantitative analysis of MHC ligands by mass spectrometry using stable isotope labeling. *Nature biotechnology* **22:** 450-454.

Liblau RS, Wong FS, Mars LT, Santamaria P (2002) Autoreactive CD8 T cells in organ-specific autoimmunity: emerging targets for therapeutic intervention. *Immunity* **17:** 1-6.

Louis I, Dulude G, Corneau S, Brochu S, Boileau C, Meunier C, Cote C, Labrecque N, Perreault C (2003) Changes in the lymph node microenvironment induced by oncostatin M. *Blood* **102:** 1397-1404.

Lu J, Getz G, Miska EA, Alvarez-Saavedra E, Lamb J, Peck D, Sweet-Cordero A, Ebert BL, Mak RH, Ferrando AA, Downing JR, Jacks T, Horvitz HR, Golub TR (2005) MicroRNA expression profiles classify human cancers. *Nature* **435:** 834-838.

Malissen M, Gillet A, Ardouin L, Bouvier G, Trucy J, Ferrier P, Vivier E, Malissen B (1995) Altered T cell development in mice with a targeted mutation of the CD3-epsilon gene. *The EMBO journal* **14:** 4641-4653.

Mamane Y, Petroulakis E, LeBacquer O, Sonenberg N (2006) mTOR, translation initiation and cancer. *Oncogene* **25:** 6416-6422.

Mann M (2006) Functional and quantitative proteomics using SILAC. *Nat Rev Mol Cell Biol* **7:** 952-958.

Marrack P, Kappler J (2004) Control of T cell viability. *Annual review of immunology* **22:** 765-787.

Matos M, Park R, Mathis D, Benoist C (2004) Progression to islet destruction in a cyclophosphamide-induced transgenic model: a microarray overview. *Diabetes* **53:** 2310-2321.

McBride K, Baron C, Picard S, Martin S, Boismenu D, Bell A, Bergeron J, Perreault C (2002) The model B6(dom1) minor histocompatibility antigen is encoded by a mouse homolog of the yeast STT3 gene. *Immunogenetics* **54:** 562-569.

Meiring HD, Soethout EC, Poelen MC, Mooibroek D, Hoogerbrugge R, Timmermans H, Boog CJ, Heck AJ, de Jong AP, van Els CA (2006) Stable isotope tagging of epitopes: a highly selective strategy for the identification of major histocompatibility complex class I-associated peptides induced upon viral infection. *Mol Cell Proteomics* **5:** 902-913.

Meunier MC, Roy-Proulx G, Labrecque N, Perreault C (2003) Tissue distribution of target antigen has a decisive influence on the outcome of adoptive cancer immunotherapy. *Blood* **101:** 766-770.

Milner E, Barnea E, Beer I, Admon A (2006) The turnover kinetics of major histocompatibility complex peptides of human cancer cells. *Mol Cell Proteomics* **5:** 357-365.

Moutaftsi M, Peters B, Pasquetto V, Tscharke DC, Sidney J, Bui HH, Grey H, Sette A (2006) A consensus epitope prediction approach identifies the breadth of murine T(CD8+)-cell responses to vaccinia virus. *Nature biotechnology* **24:** 817-819.

Nakayama KI, Nakayama K (2006) Ubiquitin ligases: cell-cycle control and cancer. *Nat Rev Cancer* **6:** 369-381.

Nalepa G, Rolfe M, Harper JW (2006) Drug discovery in the ubiquitin-proteasome system. *Nature reviews* **5:** 596-613.

Ong SE, Foster LJ, Mann M (2003) Mass spectrometric-based approaches in quantitative proteomics. *Methods* **29:** 124-130.

Pamer E, Cresswell P (1998) Mechanisms of MHC class I--restricted antigen processing. *Annual review of immunology* **16:** 323-358.

Perreault C, Decary F, Brochu S, Gyger M, Belanger R, Roy D (1990) Minor histocompatibility antigens. *Blood* **76:** 1269-1280.

Perreault C, Jutras J, Roy DC, Filep JG, Brochu S (1996) Identification of an immunodominant mouse minor histocompatibility antigen (MiHA). T cell response to a single dominant MiHA causes graft-versus-host disease. *The Journal of clinical investigation* **98:** 622-628.

Peters B, Bui HH, Frankild S, Nielson M, Lundegaard C, Kostem E, Basch D, Lamberth K, Harndahl M, Fleri W, Wilson SS, Sidney J, Lund O, Buus S, Sette A (2006) A community resource benchmarking predictions of peptide binding to MHC-I molecules. *PLoS computational biology* **2:** e65.

Peters B, Sette A (2007) Integrating epitope data into the emerging web of biomedical knowledge resources. *Nat Rev Immunol* **7:** 485-490.

Pion S, Fontaine P, Baron C, Gyger M, Perreault C (1995) Immunodominant minor histocompatibility antigens expressed by mouse leukemic cells can serve as effective targets for T cell immunotherapy. *The Journal of clinical investigation* **95:** 1561-1568.

Pion S, Fontaine P, Desaulniers M, Jutras J, Filep JG, Perreault C (1997) On the mechanisms of immunodominance in cytotoxic T lymphocyte responses to minor histocompatibility antigens. *European journal of immunology* **27:** 421-430.

Plotkin J, Prockop SE, Lepique A, Petrie HT (2003) Critical role for CXCR4 signaling in progenitor localization and T cell differentiation in the postnatal thymus. *J Immunol* **171:** 4521-4527.

Purcell AW (2004) Isolation and characterization of naturally processed MHC-bound peptides from the surface of antigen-presenting cells. *Methods Mol Biol* **251:** 291-306.

Purcell AW, McCluskey J, Rossjohn J (2007) More than one reason to rethink the use of peptides in vaccine design. *Nature reviews* **6:** 404-414.

Qian SB, Princiotta MF, Bennink JR, Yewdell JW (2006a) Characterization of rapidly degraded polypeptides in mammalian cells reveals a novel layer of nascent protein quality control. *The Journal of biological chemistry* **281:** 392-400.

Qian SB, Reits E, Neefjes J, Deslich JM, Bennink JR, Yewdell JW (2006b) Tight linkage between translation and MHC class I peptide ligand generation implies specialized antigen processing for defective ribosomal products. *J Immunol* **177:** 227-233.

Rammensee H, Bachmann J, Emmerich NP, Bachor OA, Stevanovic S (1999) SYFPEITHI: database for MHC ligands and peptide motifs. *Immunogenetics* **50:** 213-219.

Rammensee HG, Falk K, Rotzschke O (1993) Peptides naturally presented by MHC class I molecules. *Annual review of immunology* **11:** 213-244.

Richter JD, Sonenberg N (2005) Regulation of cap-dependent translation by eIF4E inhibitory proteins. *Nature* **433:** 477-480.

Rock KL, York IA, Saric T, Goldberg AL (2002) Protein degradation and the generation of MHC class I-presented peptides. *Advances in immunology* **80:** 1-70.

Rotzschke O, Falk K, Stevanovic S, Grahovac B, Soloski MJ, Jung G, Rammensee HG (1993) Qa-2 molecules are peptide receptors of higher stringency than ordinary class I molecules. *Nature* **361:** 642-644.

Ruggero D, Pandolfi PP (2003) Does the ribosome translate cancer? *Nat Rev Cancer* **3:** 179-192.

Siegel JN, Turner CA, Klinman DM, Wilkinson M, Steinberg AD, MacLeod CL, Paul WE, Davis MM, Cohen DI (1987) Sequence analysis and expression of an X-linked, lymphocyte-regulated gene family (XLR). *The Journal of experimental medicine* **166:** 1702-1715.

Singh-Jasuja H, Emmerich NP, Rammensee HG (2004) The Tubingen approach: identification, selection, and validation of tumor-associated HLA peptides for cancer therapy. *Cancer Immunol Immunother* **53:** 187-195.

Slev PR, Nelson AC, Potts WK (2006) Sensory neurons with MHC-like peptide binding properties: disease consequences. *Current opinion in immunology* **18:** 608-616.

Starr TK, Jameson SC, Hogquist KA (2003) Positive and negative T cell selection. *Annual review of immunology* **21:** 139-176.

Storkus WJ, Zeh HJ, 3rd, Salter RD, Lotze MT (1993) Identification of T-cell epitopes: rapid isolation of class I-presented peptides from viable cells by mild acid elution. *J Immunother Emphasis Tumor Immunol* **14:** 94-103.

Su AI, Wiltshire T, Batalov S, Lapp H, Ching KA, Block D, Zhang J, Soden R, Hayakawa M, Kreiman G, Cooke MP, Walker JR, Hogenesch JB (2004) A gene atlas of the mouse and human protein-encoding transcriptomes. *Proceedings of the National Academy of Sciences of the United States of America* **101:** 6062-6067.

Suri A, Walters JJ, Levisetti MG, Gross ML, Unanue ER (2006) Identification of naturally processed peptides bound to the class I MHC molecule H-2Kd of normal and TAP-deficient cells. *European journal of immunology* **36:** 544-557.

Virtaneva K, Wright FA, Tanner SM, Yuan B, Lemon WJ, Caligiuri MA, Bloomfield CD, de La Chapelle A, Krahe R (2001) Expression profiling reveals fundamental biological differences in acute myeloid leukemia with isolated trisomy 8 and normal cytogenetics. *Proceedings of the National Academy of Sciences of the United States of America* **98:** 1124-1129.

Weinzierl AO, Lemmel C, Schoor O, Muller M, Kruger T, Wernet D, Hennenlotter J, Stenzl A, Klingel K, Rammensee HG, Stevanovic S (2007) Distorted relation between mRNA copy number and corresponding major histocompatibility complex ligand density on the cell surface. *Mol Cell Proteomics* **6:** 102-113.

Williams DB, Barber BH, Flavell RA, Allen H (1989) Role of beta 2-microglobulin in the intracellular transport and surface expression of murine class I histocompatibility molecules. *J Immunol* **142:** 2796-2806.

Wong P, Pamer EG (2003) CD8 T cell responses to infectious pathogens. *Annual review of immunology* **21:** 29-70.

Yewdell JW, Nicchitta CV (2006) The DRiP hypothesis decennial: support, controversy, refinement and extension. *Trends in immunology* **27:** 368-373.

Yewdell JW, Reits E, Neefjes J (2003) Making sense of mass destruction: quantitating MHC class I antigen presentation. *Nat Rev Immunol* **3:** 952-961.

Yoshimura Y, Yadav R, Christianson GJ, Ajayi WU, Roopenian DC, Joyce S (2004) Duration of alloantigen presentation and avidity of T cell antigen recognition correlate with immunodominance of CTL response to minor histocompatibility antigens. *J Immunol* **172:** 6666-6674.

Zhang W, Morris QD, Chang R, Shai O, Bakowski MA, Mitsakakis N, Mohammad N, Robinson MD, Zirngibl R, Somogyi E, Laurin N, Eftekharpour E, Sat E, Grigull J, Pan Q, Peng WT, Krogan N, Greenblatt J, Fehlings M, van der Kooy D, Aubin J, Bruneau BG,

Rossant J, Blencowe BJ, Frey BJ, Hughes TR (2004) The functional landscape of mouse gene expression. *Journal of biology* **3:** 21.

Zhang Y, Williams DB (2006) Assembly of MHC class I molecules within the endoplasmic reticulum. *Immunologic research* **35:** 151-162.

3.8 Figure Legends

Figure 1: Experimental design for identification and relative quantification of native unlabeled MHC I-associated peptides.

(**A**) Cell surface MHC I expression on EL4 WT, β2m^{-} mutant and β2m^{+} transfectant cell lines. Cells were stained with antibodies against H2D^{b}, H2K^{b} and Qa2 (black) or the corresponding isotype control antibody (grey). (**B**) Peptides obtained by MAE were analyzed by on-line 2D-nanoLC-MS (three biological replicates for each cell population). Contour profiles of m/z versus retention time versus intensity were used to visualize differences between MS profiles (middle panel). A logarithmic intensity scale distinguishes between low (dark red) and highly (bright yellow) abundant species. Examples of peptides that were differentially expressed (blue line) or not (green line) between WT and β2m^{-} EL4 cells are highlighted in boxes. Dendrogram representation shows differential peptide expression between WT and β2m^{-} EL4 cells where each horizontal line corresponds to a unique peptide cluster (n = 3716) (lower panel). A logarithmic scale depicts peptides that are expressed at high (red) or low (green) level in each cell population. (**C**) Volcano plot representation showing reproducibly detected peptides ions across three replicate analyses. Peptide clusters (n = 1236) highlighted in dashed box were considered as class I-restricted ($P \leq 0.05$ and fold change ≥ 5). Peptides that were sequenced by MS/MS are represented by colored dots: green for contaminants, and blue for MHC I-associated peptides.

Figure 2: Allelic distribution and binding scores of 178 MHC I-associated peptides eluted from EL4 cells.

(**A**) Pie chart shows distribution of 178 MHC I-associated peptides eluted from EL4 cells. The smm, SYFPEITHI (H2D^{b} and H2K^{b}) and Rankpep (Qa2) computational models were used to link individual peptides to MHC I allelic products. (**B**) Logo showing the profile motif for peptides presented by H2-D^{b}, H2-K^{b} and Qa2 molecules. Acidic (red), basic (blue), hydrophobic (black) and neutral (green) amino acids are illustrated. (**C**) Individual source proteins for peptides presented by H2D^{b} and H2K^{b} (n = 164) were entered in the smm binding algorithm. We assessed the predicted MHC I binding affinity of all peptides contained in individual proteins. Pie charts show the proportion of peptides eluted from

EL4 cells that ranked in the top 1% (blue), top 5% (green), top 10% (yellow), or below the 90th percentile of peptides (red).

Figure 3: Discrimination between MHC I-associated peptides and contaminant peptides using bioinformatic tools.

(**A-E**) For peptides eluted from EL4 cells, the y axis shows computed MHC binding scores determined with the smm (**A, C**), SYFPEITHI (**B, D**) and Rankpep (**E**) computational methods. The x axis cut at the selected binding thresholds. Each bar represents a sequenced peptide. Individual H2D^{b}-, H2K^{b}-, Qa2-associated peptides (red) and contaminant peptides (blue) were scored as illustrated.

Figure 4: Analyses of genes and transcripts coding MHC I-associated peptides eluted from primary thymocytes.

(**A**) GO term enrichment analysis of 189 genes coding MHC I peptides eluted from thymocytes. Exact P-values and global false-discovery rates were < 0.05 for each listed GO term. Values in parentheses indicate the fold enrichment relative to the whole mouse genome. (**B**) We compared the relative abundance of two sets of thymic transcripts using previously reported microarray data (Su *et al*, 2004): 1) mRNAs coding MHC I peptides eluted from primary thymocytes (red), and 2) 36,182 thymus-derived transcripts (grey). Original mRNA expression data on the x axis were plotted on a log2 scale. The y axes represent the number of transcripts for each sample set. (**C**) Frequency distributions for the two sets of thymic transcripts defined in (B) were plotted using a bin increment of 0.2. Three distinct mRNA expression groups are shown (low-, medium- and high-abundance mRNA). Graph shows the proportion of mRNAs with low- (black), medium- (red), and high- (blue) abundance among the two sets of transcripts. * $P < 0.05$, ** $P < 0.0001$. (**D**) Predicted MHC binding score (determined with smm) for peptides whose mRNA are expressed at low, medium or high level. Spearman linear correlation coefficient (r) was calculated for H2K^{b}- (dashed line; white squares) and H2D^{b}- (solid line; black squares) associated peptides.

Figure 5: Peptide source mRNAs expression patterns reveal an organ-specific signature in the immunopeptidome of thymocytes.

(**A**) Comparison of normalized average expression values (y axis) across 58 different tissues (x axis) including the thymus (red). Normalized average expression values were calculated as follows: average expression value from 180 peptide source genes / average expression value of 36,182 transcripts for each particular tissue. Calculated values were ranked from left to right in a decreasing order. (**B**) Z scores were calculated for each of the 180 peptide source genes to identify transcripts preferentially expressed in the thymus. Graph shows frequency distributions of calculated Z scores with a bin increment of 0.05. (**C**) Heat map shows the relative mRNA expression in 58 tissues of the 30 peptide source genes with highest thymic Z scores. (**D**) High Z score genes determine the thymus-specificity of the gene set encoding MHC I-associated peptides. Genes preferentially overexpressed in the thymus (high thymic Z scores; blue) were additively removed (x axis). Normalized average expression values and thymus rank (y axis) were determined following removal of each individual gene. Removal of the 30 genes with a high thymic Z score had a drastic impact on thymus rank ($P < 0.005$). Removal of up to 70 randomly selected genes (100,000 permutations; green) had no significant impact on thymus rank.

Figure 6: Relative quantification of differentially expressed MHC I peptides and source mRNAs from thymocytes and EL4 cells.

(**A**) Volcano Plot representation illustrates MHC I peptides reproducibly detected across biological replicates ($n = 3$). Peptides over- and underexpressed on EL4 cells relative to thymocytes ($P \leq 0.05$; fold change ≥ 2.5) were highlighted in blue and red, respectively. MS-MS spectra of circled peptides are shown in B and C. (**B, C**) Illustration of two differentially expressed MHC I peptides. Reconstructed ion chromatograms show differential abundance for m/z 471.74^{2+} (VAAANREVL) and 521.22^{2+} (FGPVNHEEL) in EL4 cells versus thymocytes. MS-MS spectra confirm MHC I peptide sequences and the identification of the cognate source proteins. (**D**) Scatter plot shows the correlation between relative expression of mRNA and that of MHC I peptide. Expression ratios for source mRNA (x axis) and MHC I peptide (y axis) between EL4 cells and thymocytes were plotted on a log 2 scale for 47 pairs. A Spearman correlation coefficient was calculated from the linear regression. MHC I peptides overexpressed in EL4 cells or

normal thymocytes are highlighted in blue and red, respectively; peptides that were not differentially expressed are in grey. Dashed box includes peptides whose overexpression on EL4 cells did not correlate with increased mRNA levels of their source protein.

Figure 7: Splenocytes primed against peptides overexpressed on EL4 cells selectively kill EL4 cells.

(**A, B**) T2-D^b and T2-K^b cells maintained at 26°C for 18–20 h were pulsed with graded concentrations of the indicated peptides for 45 min at 26°C, washed, and incubated at 37°C for 4 h. $H2L^d$-restricted RPQASGVYM was used as a negative control. Cells were stained with PE-conjugated anti-$H2K^b$ or FITC-conjugated anti-$H2D^b$ antibody and analyzed by flow cytometry. Mean ± SD of three experiments. (**C, D**) Mice were immunized with STLTYSRM- or VAAANREVL-loaded DCs. Splenocytes from primed mice were restimulated *in vitro* with the corresponding peptide for 6 days, and tested for *in vitro* cytotoxic activity against CFSE-labeled target cells (EL4 cells and primary mouse thymocytes) at different E/T ratios. Number of effectors represents the number of unfractionated splenocytes used in the cytotoxicity assay. Mice immunized with unloaded DCs were used as negative control. Data represent the mean ± SD for 4 mice per group.

3.9 Supplementary Figure Legends

Supplementary Figure 1: Reproducibility of intensity measurements for instrumental and biological replicates.

(**A**) Log–log plot of individual ion intensity versus the average intensity for replicate 2D-LC analysis (n = 3). (**B**) Expression plot for 2D-LC instrumental replicates (n = 5,568 peptide clusters). Distribution indicates that 95% of peptide ions show a variation of <1.4-fold change in intensity. (**C**) Scatter plot of intensities for biological replicates (n = 3). (**D**) Expression plot from different biological preparations (n = 4,046 peptide clusters). Peptide ions (95%) show variation in intensity within ± 2.2-fold change.

Supplementary Figure 2: Evaluation of MHC binding affinity of nine peptides.

(**A**) For peptides eluted from WT EL4 cells, the y axis shows computed MHC binding scores determined with the smm computational method. The x axis cut at the selected binding thresholds. Each bar represents a sequenced peptide. Individual H2Kb- or H2Db-associated peptides (red) and contaminant peptides (blue) were scored as illustrated. (**B–D**) We synthesized nine peptides across the predicted affinity spectrum and tested their ability to bind H2Kb or H2Db. T2-Kb or T2-Db cells maintained at 26°C for 18–20 h were pulsed with graded concentrations of the indicated peptides for 45 min at 26°C, washed, and incubated at 37°C for 4 h. Cells were stained with PE-conjugated anti-H2Kb or FITC-conjugated anti-H2Db antibody and analyzed by flow cytometry. Mean ± the SD of three experiments. Experimental results correlated perfectly with bioinformatic predictions: peptides classified as MHC I associated did bind to MHC I, whereas peptides classified as contaminants did not. (**B**) Stabilization of H2Kb by seven peptides. (**C** and **D**) Stabilization of H2Kb or H2Db by two peptides used in cytotoxicity assays (Figure 7). The RPQASGVYM peptide was used as negative control.

Figure 1

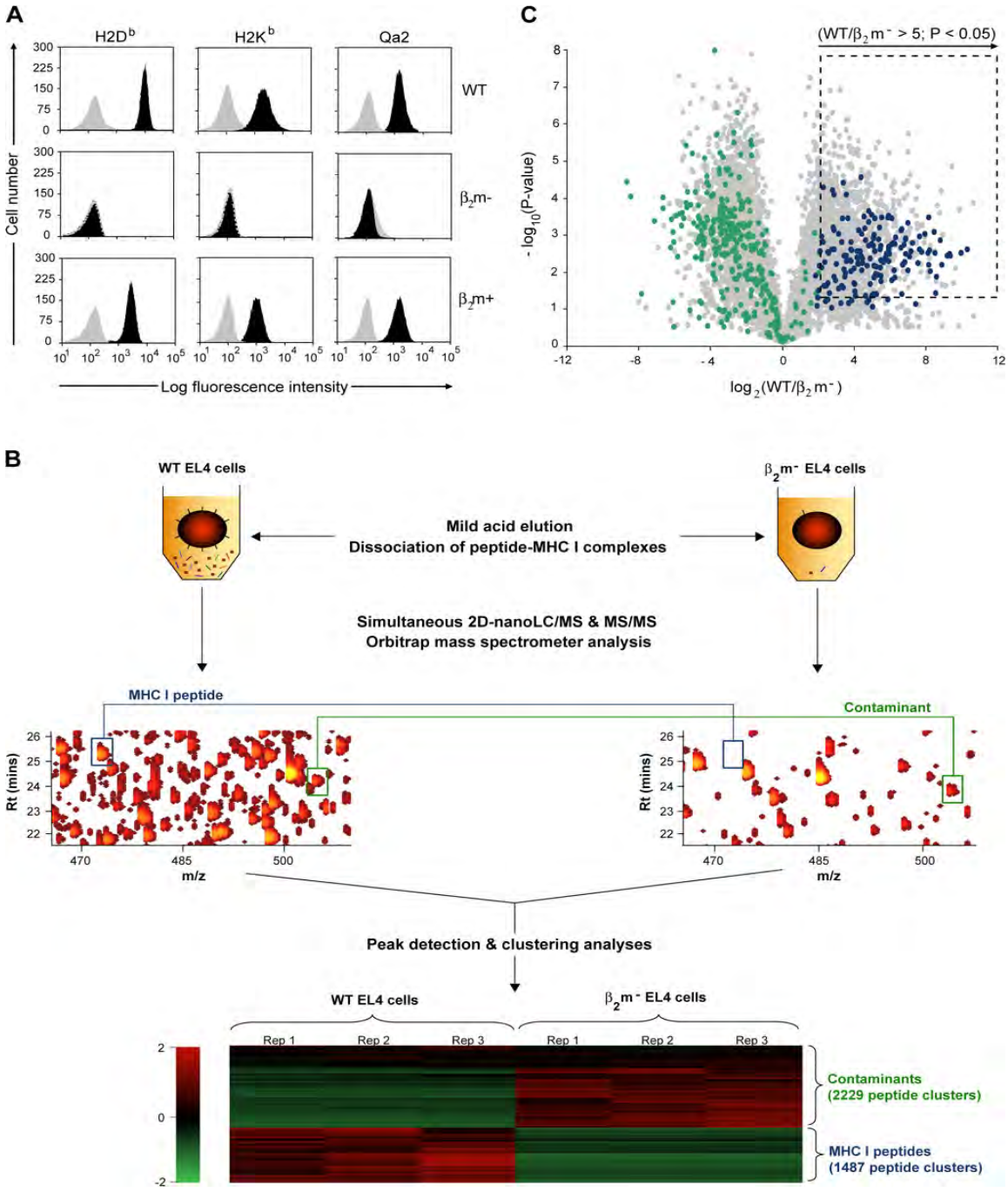
A
H2D^b
H2K^b
Qa2
WT
β2m-
β2m+
Cell number
Log fluorescence intensity
C
(WT/β2m- > 5; P < 0.05)
- log10(P-value)
log2(WT/β2m-)
B
WT EL4 cells
β2m- EL4 cells
Mild acid elution
Dissociation of peptide-MHC I complexes
Simultaneous 2D-nanoLC/MS & MS/MS
Orbitrap mass spectrometer analysis
MHC I peptide
Contaminant
Rt (mins)
m/z
Peak detection & clustering analyses
WT EL4 cells
β2m- EL4 cells
Rep 1
Rep 2
Rep 3
Contaminants
(2229 peptide clusters)
MHC I peptides
(1487 peptide clusters)

Figure 2

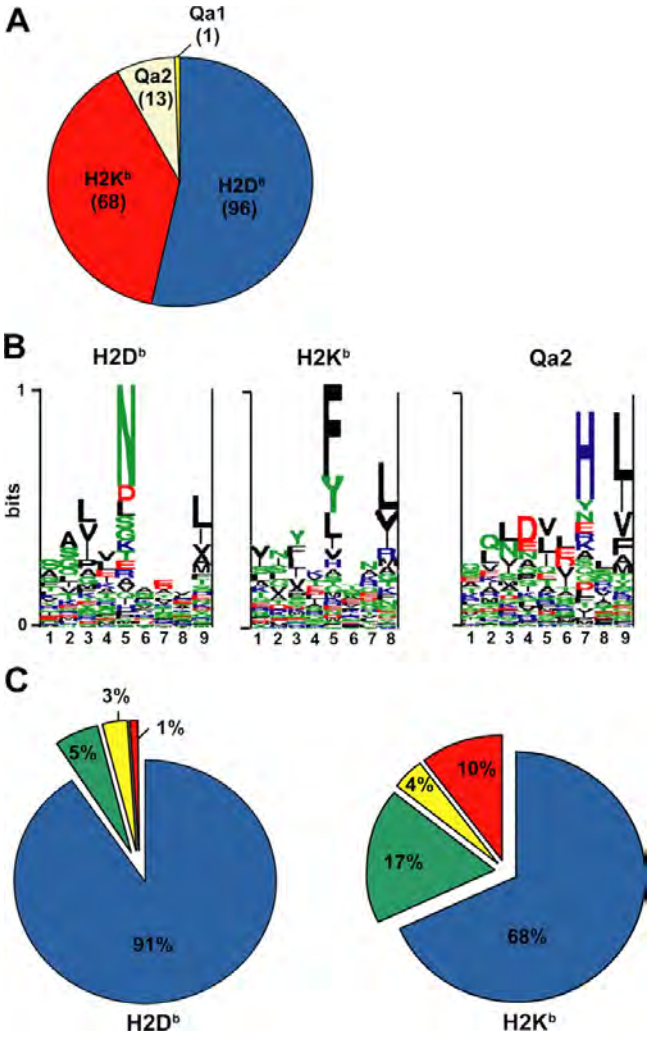
A
Qa1
(1)
Qa2
(13)
H2K^b
(68)
H2D^b
(96)
B
H2D^b
H2K^b
Qa2
bits
1
0
1 2 3 4 5 6 7 8 9
1 2 3 4 5 6 7 8
1 2 3 4 5 6 7 8 9
C
3%
1%
5%
91%
H2D^b
10%
4%
17%
68%
H2K^b

Figure 3

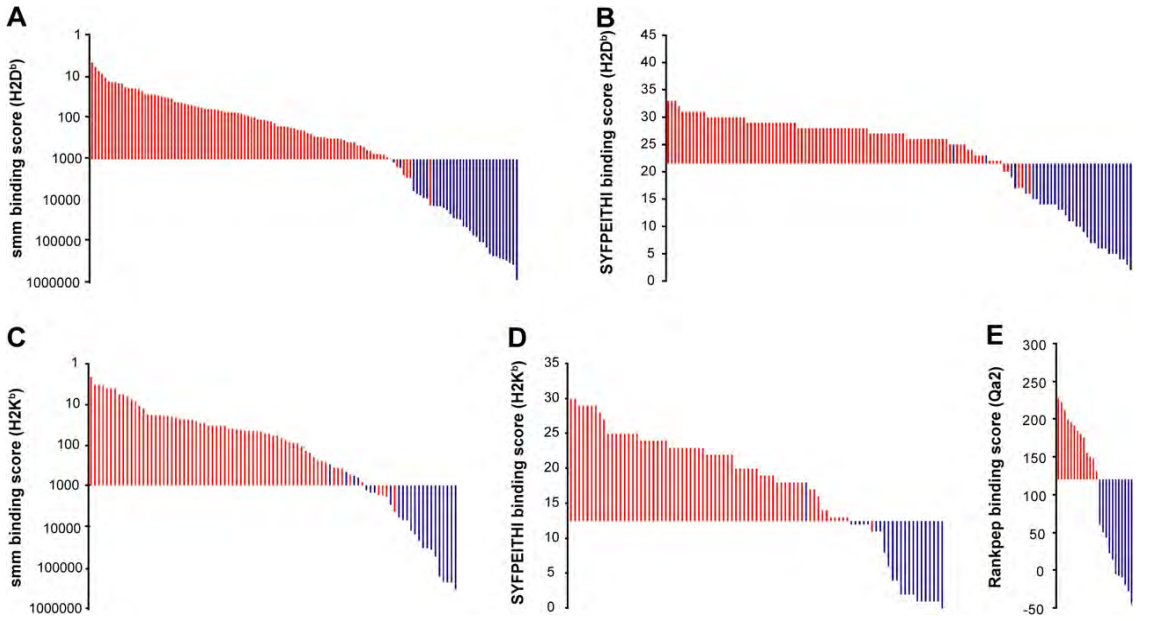
A
smm binding score (H2D^b)
1
10
100
1000
10000
100000
1000000
B
SYFPEITHI binding score (H2D^b)
45
40
35
30
25
20
15
10
5
0
C
smm binding score (H2K^b)
1
10
100
1000
10000
100000
1000000
D
SYFPEITHI binding score (H2K^b)
35
30
25
20
15
10
5
0
E
Rankpep binding score (Qa2)
300
250
200
150
100
50
0
-50

Figure 4

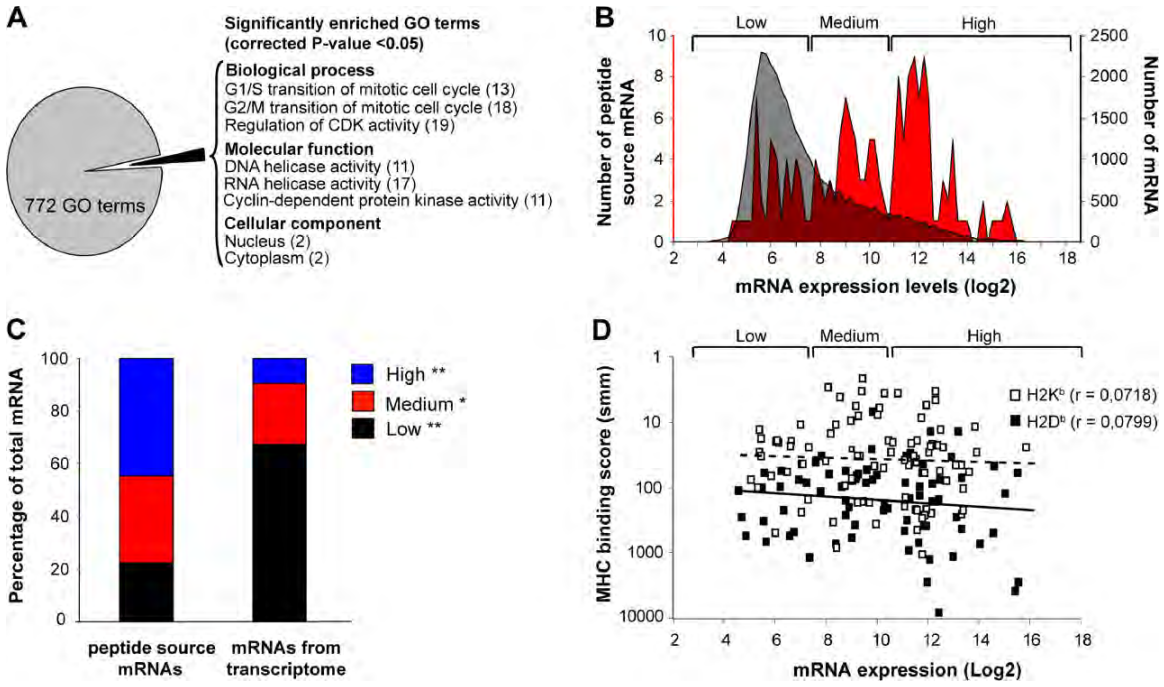
A
Significantly enriched GO terms
(corrected P-value <0.05)
Biological process
G1/S transition of mitotic cell cycle (13)
G2/M transition of mitotic cell cycle (18)
Regulation of CDK activity (19)
Molecular function
DNA helicase activity (11)
RNA helicase activity (17)
Cyclin-dependent protein kinase activity (11)
Cellular component
Nucleus (2)
Cytoplasm (2)
772 GO terms
B
Low
Medium
High
Number of peptide source mRNA
Number of mRNA
mRNA expression levels (log2)
C
Percentage of total mRNA
High **
Medium *
Low **
peptide source mRNAs
mRNAs from transcriptome
D
Low
Medium
High
MHC binding score (smm)
H2Kb (r = 0,0718)
H2Db (r = 0,0799)
mRNA expression (Log2)

Figure 5

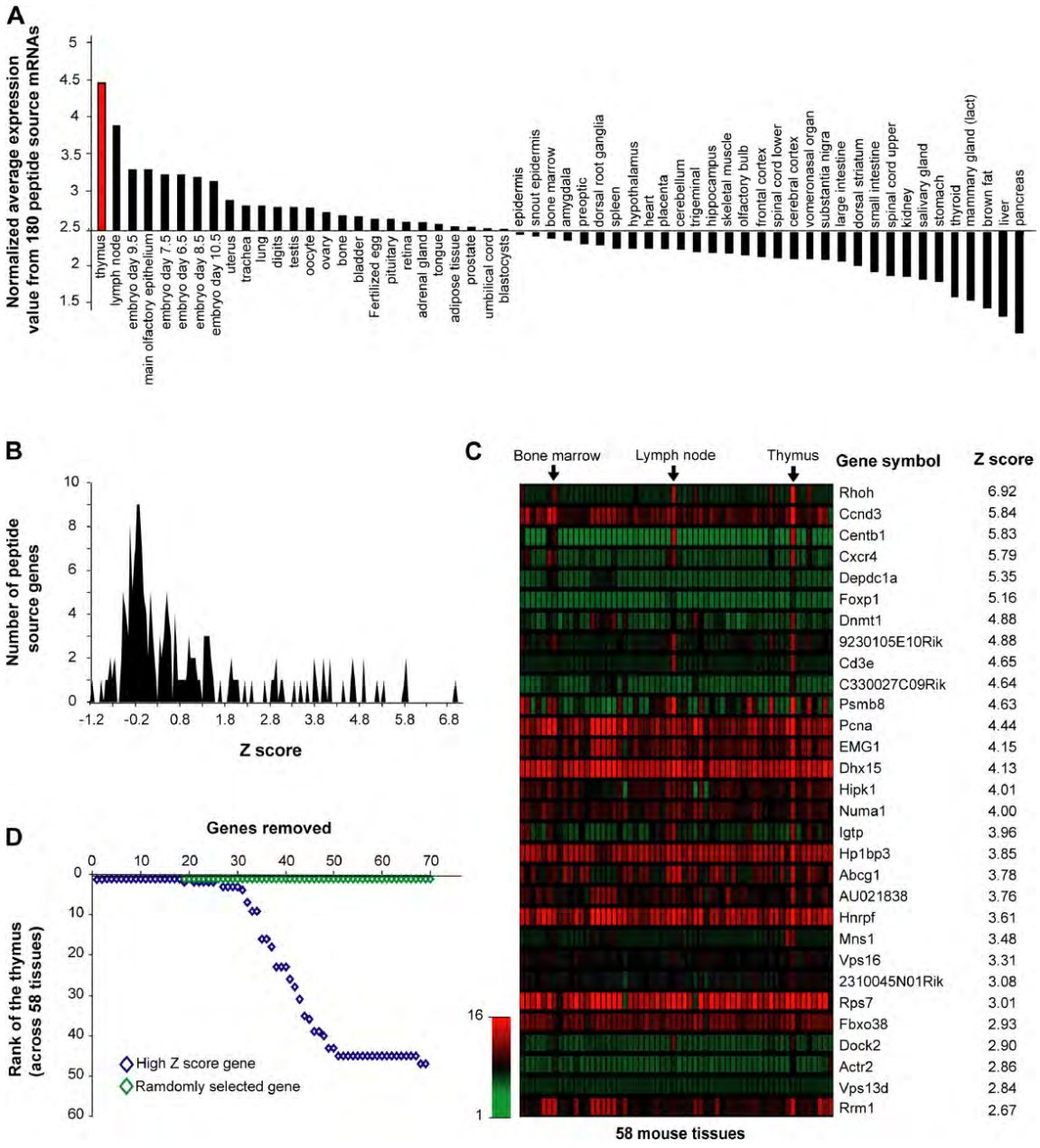
A
Normalized average expression value from 180 peptide source mRNAs
5
4.5
4
3.5
3
2.5
2
1.5
thymus
lymph node
embryo day 9.5
main olfactory epithelium
embryo day 7.5
embryo day 6.5
embryo day 8.5
embryo day 10.5
uterus
trachea
lung
digits
testis
oocyte
ovary
bone
bladder
Fertilized egg
pituitary
retina
adrenal gland
tongue
adipose tissue
prostate
umbilical cord
blastocysts
epidermis
snout epidermis
bone marrow
amygdala
preoptic
dorsal root ganglia
spleen
hypothalamus
heart
placenta
cerebellum
trigeminal
hippocampus
skeletal muscle
olfactory bulb
frontal cortex
spinal cord lower
cerebral cortex
vomeronasal organ
substantia nigra
large intestine
dorsal striatum
small intestine
spinal cord upper
kidney
salivary gland
stomach
thyroid
mammary gland (lact)
brown fat
liver
pancreas
B
Number of peptide source genes
10
8
6
4
2
0
-1.2
-0.2
0.8
1.8
2.8
3.8
4.8
5.8
6.8
Z score
C
Bone marrow
Lymph node
Thymus
Gene symbol
Z score
Rhoh 6.92
Ccnd3 5.84
Centb1 5.83
Cxcr4 5.79
Depdc1a 5.35
Foxp1 5.16
Dnmt1 4.88
9230105E10Rik 4.88
Cd3e 4.65
C330027C09Rik 4.64
Psmb8 4.63
Pcna 4.44
EMG1 4.15
Dhx15 4.13
Hipk1 4.01
Numa1 4.00
Igtp 3.96
Hp1bp3 3.85
Abcg1 3.78
AU021838 3.76
Hnrpf 3.61
Mns1 3.48
Vps16 3.31
2310045N01Rik 3.08
Rps7 3.01
Fbxo38 2.93
Dock2 2.90
Actr2 2.86
Vps13d 2.84
Rrm1 2.67
16
1
58 mouse tissues
D
Genes removed
0
10
20
30
40
50
60
70
Rank of the thymus (across 58 tissues)
High Z score gene
Ramdomly selected gene

Figure 6

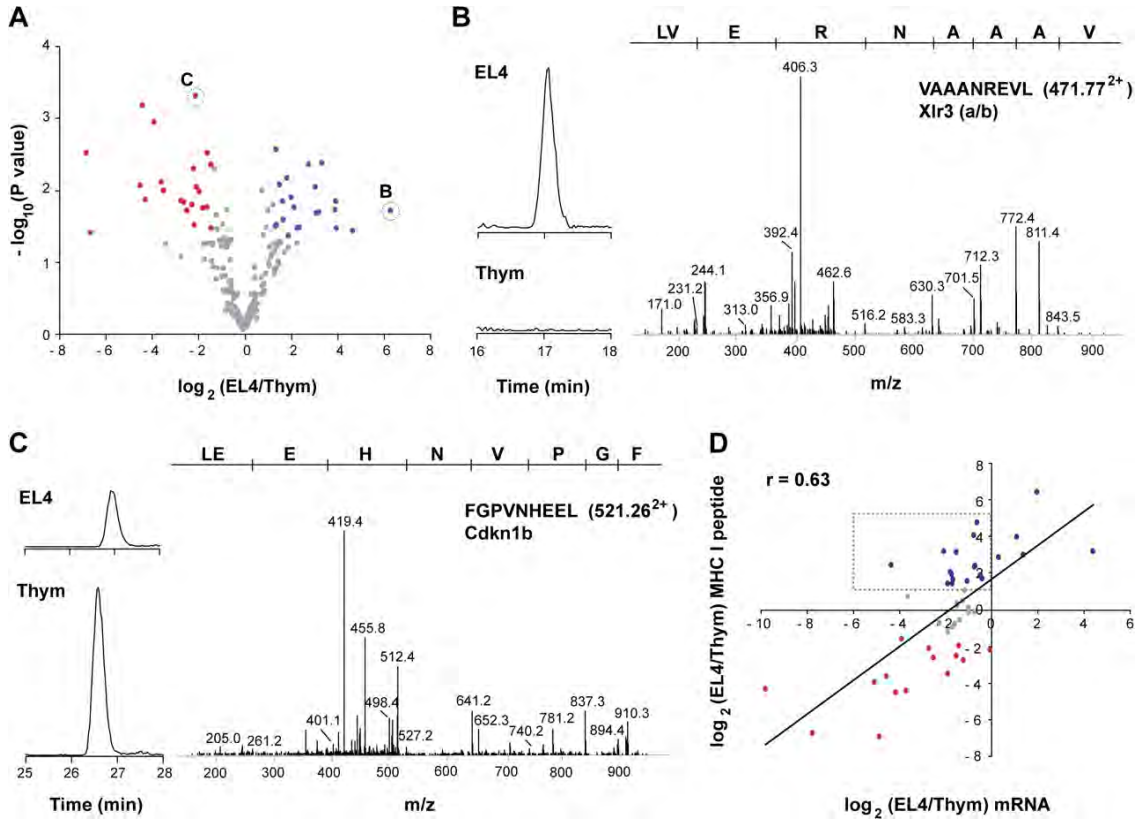
A
C
B
- log10(P value)
log2 (EL4/Thym)
B
EL4
Thym
Time (min)
LV E R N A A A V
VAAANREVL (471.77 2+)
Xlr3 (a/b)
406.3
392.4
772.4
811.4
712.3
701.5
462.6
244.1
231.2
171.0
313.0
356.9
630.3
516.2
583.3
843.5
m/z
C
LE E H N V P G F
EL4
Thym
FGPVNHEEL (521.26 2+)
Cdkn1b
419.4
455.8
512.4
498.4
401.1
527.2
641.2
652.3
740.2
781.2
837.3
894.4
910.3
205.0
261.2
Time (min)
m/z
D
r = 0.63
log2 (EL4/Thym) MHC I peptide
log2 (EL4/Thym) mRNA

Figure 7

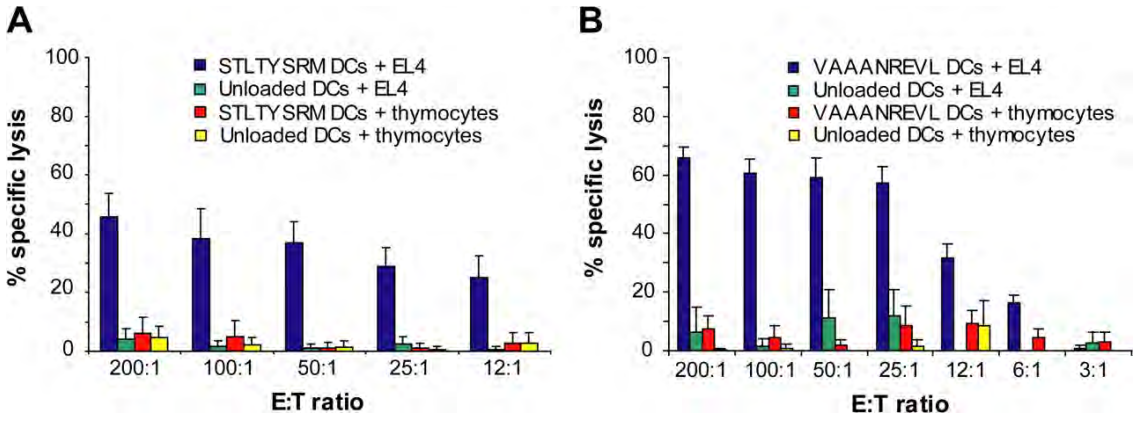
A
100
80
60
40
20
0
% specific lysis
STLTYSRM DCs + EL4
Unloaded DCs + EL4
STLTYSRM DCs + thymocytes
Unloaded DCs + thymocytes
200:1
100:1
50:1
25:1
12:1
E:T ratio
B
100
80
60
40
20
0
% specific lysis
VAAANREVL DCs + EL4
Unloaded DCs + EL4
VAAANREVL DCs + thymocytes
Unloaded DCs + thymocytes
200:1
100:1
50:1
25:1
12:1
6:1
3:1
E:T ratio

Table 1: Relative Abundance of a Representative Set of Peptides Recovered in Eluates from Three EL4 Cell Variants: WT, β2m^{-} Mutants and β2m^{+} Transfectants

Gene ID	Gene Symbol	Sequence	WT	β2m-	β2m+	WT/β2m-
20848	*Stat3*	ATLVFHNL	4,023,137	12,000	6,208,130	335
66165	*Bccip*	KAPVNTAEL	1,741,908	12,000	998,607	145
15016	*H2-Q5*	AMAPRTLLL	5,436,819	12,000	12,941,105	453
67755	*Ddx47*	KTFLFSATM	70,059	12,000	289,017	6
12649	*Chek1*	TGPSNVDKL	6,545,497	112,308	14,733,333	58
267019	*Rps15a*	VIVRFLTV	514,406	12,000	12,000	43
71745	*Cul2*	VINSFVHV	67,372	12,000	244,370	6
233489	*Picalm*	NGVINAAFM	265,420	12,000	438,191	22
26413	*Mapk1*	VGPRYTNL	39,166,667	149,969	45,832,060	261
108655	*Foxp1*	QQLQQQHLL	705,266	12,000	1,054,408	59
170755	*Sgk3*	YSIVNASVL	255,048	38,491	151,335	7
326622	*Upf2*	SAVIFRTL	244,247	12,000	1,102,686	20
12877	*Cpeb1*	SMLQNPLGNVL	185,198	12,000	528,268	15
94176	*Dock2*	SMVQNRVFL	895,081	12,000	671,603	75
16913	*Psmb8*	GGVVNMYHM	3,332,728	12,000	2,116,510	277

Gene ID and Gene Symbol description refer to NCBI gene entries. Intensities for each EL4 variant cell line correspond to the average MS signal calculated from triplicate experiments. An intensity threshold value of 12,000 was fixed when no signal was detected. To be considered as MHC I-associated, a peptide had to be at least 5 times more abundant on WT relative to β2m-deficient cells.

Table 2: Peptides Differentially Expressed on EL4 Cells vs. Primary Thymocytes

Functional Classification	Gene Symbol	Gene ID	Function	Sequence	P-value	EL4/ Thy
Transcription	*Pa2g4*[a]	18813	Growth regulation	AQFKFTVL	0.02	4.6
	Top2a[a]	21973	DNA topoisomerase	NSMVLFDHV	0.02	15.6
	Dnmt1[a]	13433	DNA methylation	LSLENGTHTL	0.02	8.9
	Pfdn5[a]	56612	Protein binding/Folding	SMYVPGKL	0.04	16.6
	Per1[a]	18626	Transcription regulator	YTLRNQDTF	0.04	5.0
	Foxp1[a]	108655	Transcription factor	QQLQQQHLL	0.01	-4.3
	Bach2[a]	12014	Transcription factor	EQLEFIHDI	0.02	-20.2
	Pbrm1	66923	DNA binding	SQVYNDAHI	0.02	-3.5
	Ddx5[a]	13207	RNA helicase	NQAINPKLLQL	0.02	-5.7
	Jhdm1d	338523	Histone demethylase	SSIQNGKYTL	0.02	-4.9
Cell Differentiation	*Ptpn6*[a]	15170	Key role in hematopoiesis	AQYKFIYV	0.03	3.3
	Mark2	13728	Maintenance of cell polarity	ASIQNGKDSL	0.03	2.7
	Pi3kap1[a]	83490	Role in BCR-mediated Pi3K activation	YGLKNLTAL	0.001	-21.8
	Xlr3a/b	22446	Role in lymphocyte development	VAAANREVL	0.02	84.9
	RhoH[a]	74734	Small GTPase/thymocyte maturation	YSVANHNSFL	0.02	-3.1
Cell Cycle	*Rcc2*	108911	Required in mitosis and cytokinesis	AAYRNLGQNL	0.04	27.0
	Cdkn1b[a]	12576	Involved in G1 arrest	FGPVNHEEL	0.003	-3.1
Apoptosis	*Sgk*[a]	20393	Response to DNA damage stimulus	STLTYSRM	0.02	9.7
	Pdcd10[a]	56426	Role in apoptotic pathways	ILQTFKTVA	0.001	-4.3
Signal Transduction	*Cxcr4*[a]	12767	Receptor for the chemokine CXCL12/SDF1	VVFQFQHI	0.003	2.6
	CD97[a]	26364	Involved in adhesion and signaling process	KLLSNINSVF	0.03	-4.6
Translation	*Eif3s10*[a]	13669	Translation initiation factor	QSIEFSRL	0.02	3.2
	Eif3s2[a]	54709	Translation initiation factor	FGPINSVAF	0.04	5.3
Transport	*Tmed9*	67511	Intracellular protein transport	VIGNYRTQL	0.02	-6.9
	Copb1	70349	ER to Golgi vesicle-mediated transport	IALRYVAL	0.01	2.9
Cytoskeleton	*Tmod1*	21916	Cytoskeleton organization	SSIVNKEGL	0.004	10.5
	Mylc2b	67938	Cytoskeleton organization and	SLGKNPTDAYL	0.01	4.2

			biogenesis			
	Mns1	17427	Involved in cell division and motility	KIIEFANI	0.01	-12.4
	Krt5	110308	Strutural constituent of cytoskeleton	AAYMNKVEL	0.04	-106.7
	Krt7	110310	Strutural constituent of cytoskeleton	AAYTNKVEL	0.003	-121.5
Miscellaneous	*Igtp*[a]	16145	IFN gamma induced GTPase	IVAENTKTSL	0.001	-15.5
	Nup205	70699	Outer membrane exporter porin	VNNEFEKL	0.005	-4.6
	Dhx15[a]	13204	RNA helicase	TLLNVYHAF	0.02	-11.5
	Stk11ip	71728	Serine/Threonine kinase	SALRFLNL	0.01	-3.9
	Pde2a	207728	Catalytic activity	IKNENQEVI	0.02	16.0
	Gtpbp4[a]	69237	GTP binding	QILSDFPKL	0.03	2.6
	Narfl	67563	Prelamin recognition	VAYGFRNI	0.01	8,7
	Rmnd5a	68477	Hypothetic role for meiotic nuclear division	WAVSNREML	0.02	-6.2
Unknown	*Specc1*	432572		TSLAFESRL	0,01	7.1
	Ccdc41	77048		AQVENVQRI	0.01	-2.8
	2900073G15Rik	67268		SMGKNPTDEYL	0.05	3.8
	D14Ertd436e	218978		SQHVNLDQL	0.04	-2.7
	9230105E10Rik	319236		FISDVEHQL	0.01	-23.2

Gene ID and Gene Symbol description refer to NCBI gene entries. Fold change and P-values were calculated from biological replicate experiments (n = 3). Functional classification is based upon bibliographic searches. [a]Indicate genes that are involved in neoplastic transformation (See Table S6 for references).

Supplementary Figure 1

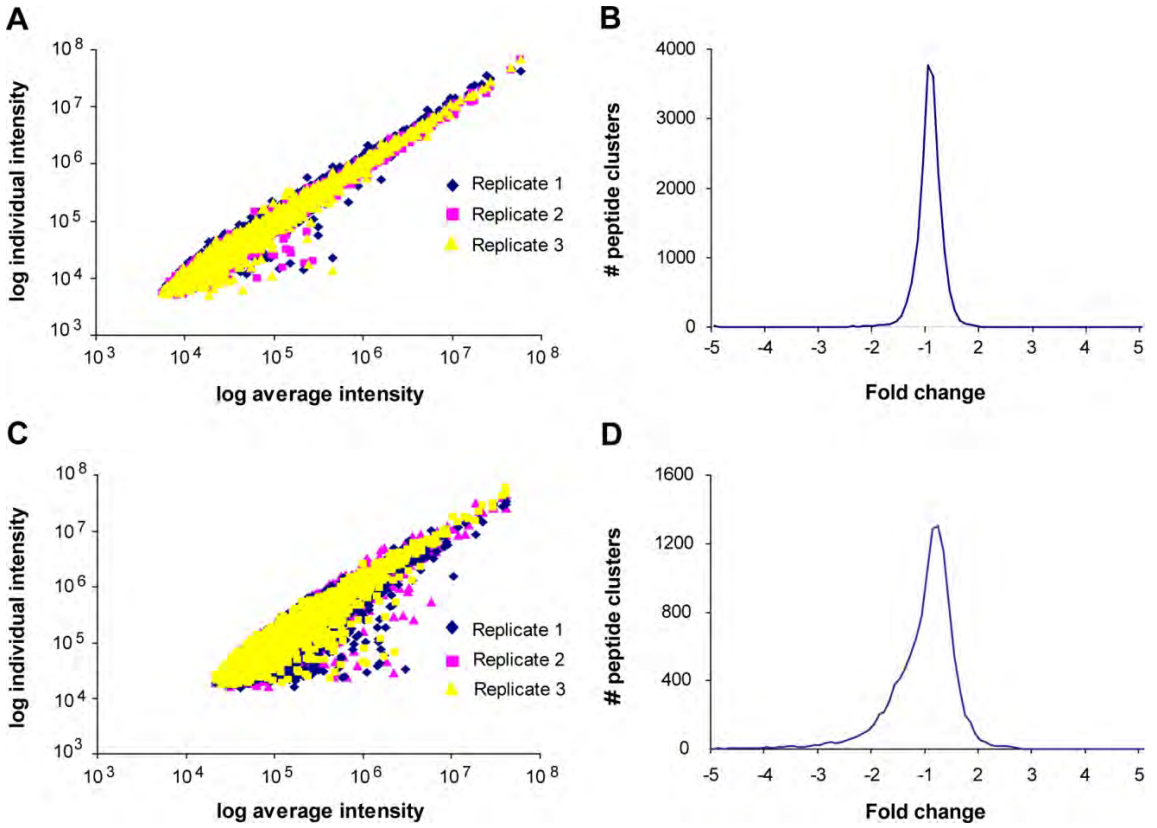

Supplementary Figure 2

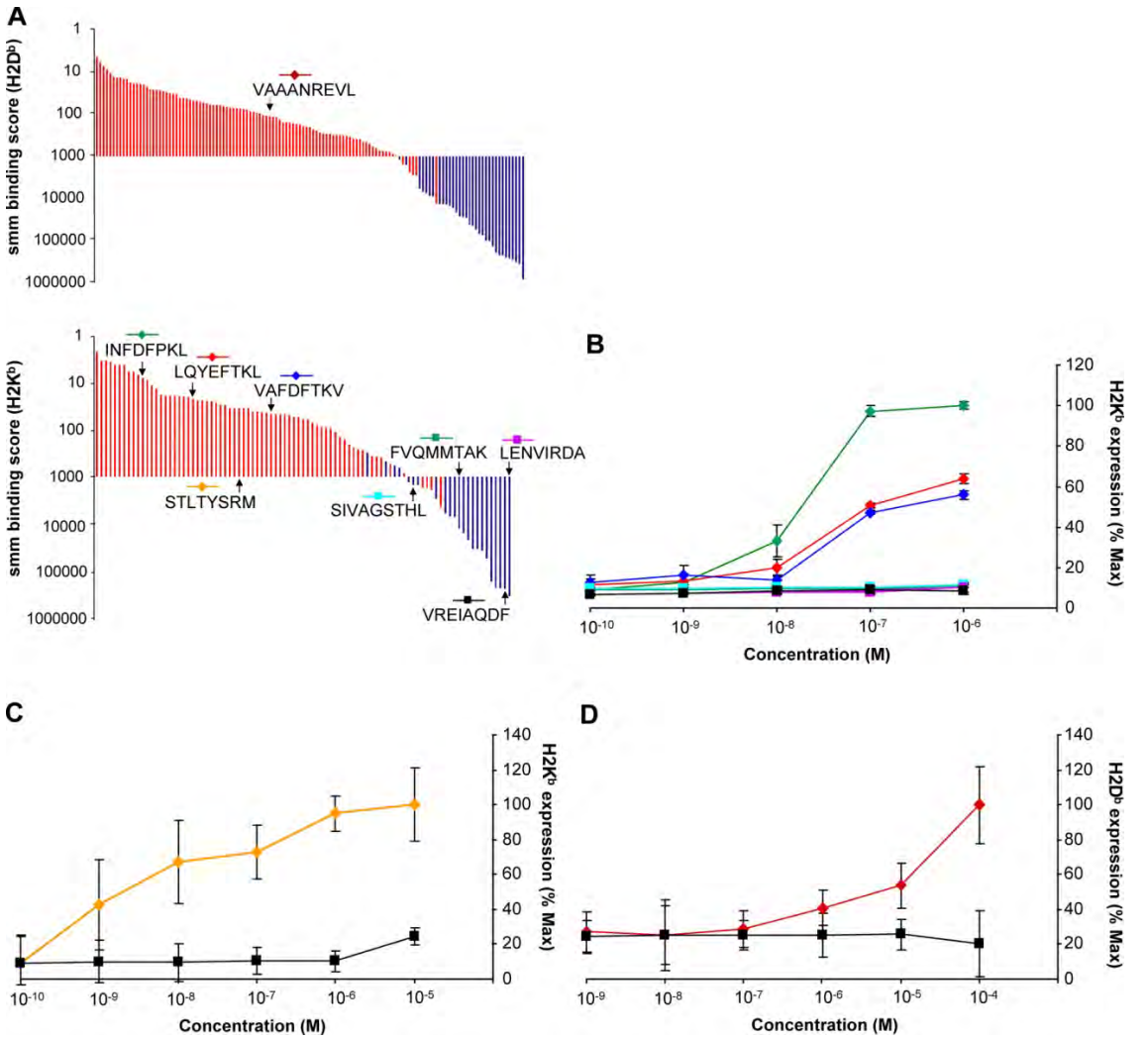

Supplementary Table 1

Relative abundance of peptides eluted from WT, b2m- and b2m+ EL4 cell lines

			Intensities from			Fold change
Gene ID	**Gene Symbol**	**Peptide**	**WT**	**b2m-**	**b2m+**	**WT/b2m-**
68523	*1110019N10Rik*	AALENTHLL	160364	12000	39986	13
66185	*1110037F02Rik*	RQILNADAM	364055	12000	227326	30
67463	*1200014M14Rik*	GALENAKAEI	191356	12000	381782	16
74174	*1700006H03Rik*	NSPANNIVM	68002	12000	1534480	6
100910	*2010209O12Rik*	AQIRNLTVL	212465	12000	106874	18
76559	*2410024A21Rik*	AGPENSSKI	216979	12000	649743	18
75425	*2610036D13Rik*	QTVENVEHL	356744	52221	827933	7
67268	*2900073G15Rik*	SMGKNPTDEYL	4278255	12000	11467376	357
77877	*6030458C11Rik*	KVLDVLHSL	63278	12000	71265	5
338523	*A630082K20Rik*	SSIQNGKYTL	1351220	12000	480198	113
18671	*Abcb1a*	STVRNADVI	3232678	12000	12000	269
11307	*Abcg1*	VNIEFKDL	838637	12000	2348761	70
104112	*Acly*	SIANFTNV	59580	12000	225167	5
66713	*Actr2*	YAGSNFPEHI	5117498	12000	6554584	426
67019	*Actr6*	SGYSFTHI	428791	12000	996812	36
226747	*Ahctf1*	TSVENHEFL	676119	12000	1115879	56
223774	*Alg12*	AAMLNYTHI	121626	12000	450762	10
81702	*Ankrd17*	ASVLNVNHI	7537305	12000	14073365	628
11765	*Ap1g1*	FALVNGNNI	238448	12000	508707	20
71435	*Arhgap21*	TGVTNRDLI	421388	12000	194111	35
11984	*Atp6v0c*	SAMVFSAM	100221	12000	314743	8
328099	*AU021838*	VSYLFSHV	163732	12000	285904	14
66165	*Bccip*	KAPVNTAEL	1741908	12000	998607	145
213895	*Bms1l*	YQNQEIHNL	1272300	12000	1633700	106
12176	*Bnip3*	LSMRNTSVM	133906	12000	371093	11
12181	*Bop1*	EQVALVHRL	306162	12000	1219215	26
107976	*Bre*	ATQVYPKL	1147903	12000	3484401	96
224171	*C330027C09Rik*	AQNDIEHLF	1329747	12000	1373696	111
76740	*C920006C10Rik*	SAIINEDNL	899101	12000	1629693	75
69719	*Cad*	RQAENGMYI	92562	12000	1267863	8
12340	*Capza1*	ISFKFDHL	35372	12000	56253	3
26885	*Casp8ap2*	VTVLNVDHL	285120	12000	299518	24
12449	*Ccnf*	SQAVNKQQI	236020	68580	828654	3
12465	*Cct5*	SMMDVDHQI	1326343	12000	2363592	111
12468	*Cct7*	RAIKNDSVV	930640	12000	1300660	78
12576	*Cdkn1b*	FGPVNHEEL	11267481	12000	17543161	939
229841	*Cenpe*	SALQNAESDRL	1125746	12000	2349902	94
216859	*Centb1*	INQIYEARV	691884	12000	1065038	58
12649	*Chek1*	TGPSNVDKL	6545497	112308	14733333	58
214901	*Chtf18*	QLSDTLHSL	61094	12000	190594	5
80986	*Ckap2*	TLNDLIHNI	136301	12000	345332	11
234594	*Cnot1*	IAFIFNNL	46952	12000	74559	4
12847	*Copa*	SQLPVDHIL	404318	12000	676882	34
12877	*Cpeb1*	SMLQNPLGNVL	185198	12000	528268	15
68975	*Crsp8*	SGLLNQQSL	978436	99069	1634916	10
71745	*Cul2*	VINSFVHV	67372	12000	244370	6
215821	*D10Bwg1379e*	AVLTNQETI	158503	12000	747537	13
52635	*D12Ertd551e*	RQLENGTTL	1477468	12000	1284587	123

218978	*D14Ertd436e*	SQHVNLDQL	322974	12000	690276	27
229473	*D930015E06Rik*	ASLVNSPSYL	160789	12000	1730981	13
208846	*Daam1*	AAKVNMTEL	2278053	12000	1980628	190
68087	*Dcakd*	VIQVFQQL	241295	12000	464584	20
67755	*Ddx47*	KTFLFSATM	70060	12000	289017	6
13209	*Ddx6*	INFDFPKL	207697	12000	58611	17
72121	*Dennd2d*	VIYPFMQGL	507408	28423	12000	18
217207	*Dhx8*	QLYTLGAL	185369	12000	505758	15
94176	*Dock2*	SMVQNRVFL	895081	12000	671603	75
233115	*Dpy19l3*	SVVAFHNL	2131426	12000	1928879	178
76843	*Dtl*	SSPENKNWL	2840050	12000	10831315	237
13424	*Dync1h1*	ASYEFVQRL	2201922	33937	1946008	65
66967	*Edem3*	FMATNPEHL	255530	12000	303884	21
13669	*Eif3s10*	QSIEFSRL	3331791	12000	6269562	278
15569	*Elavl2*	GAVTNVKVI	120705	12000	327586	10
14791	*Emg1*	VSVEYTEKM	133779	12000	214864	11
66366	*Ergic3*	QQLDVEHNL	1458352	12000	807276	122
13877	*Erh*	YQPYNKDWI	108556	12000	29068	9
14050	*Eya3*	TIIIFHSL	465796	12000	216132	39
212377	*F730047E07Rik*	VGVTYRTL	84194	12000	462448	7
70611	*Fbxo33*	SSLSNPIANTM	127288	12000	69463	11
14137	*Fdft1*	ISLEFRNL	523739	12000	130109	44
57778	*Fmnl1*	LQYEFTHL	770529	12000	1208086	64
22379	*Fmnl3*	LQYEFTKL	642004	12000	934003	54
108655	*Foxp1*	QQLQQQHLL	705266	12000	1054408	59
239554	*Foxred2*	LGVTNFVHM	168986	12000	118096	14
56784	*Garnl1*	GAIVNGKVL	83646	12000	315141	7
14751	*Gpi1*	KNLVNKEVM	318694	12000	560091	27
14790	*Grcc10*	SAPENAVRM	3768572	12000	48595185	314
68153	*Gtf2e2*	SGYKFGVL	537587	12000	2451306	45
69237	*Gtpbp4*	QILSDFPKL	395416	12000	225758	33
15016	*H2-Q5*	AMAPRTLLL	5436819	12000	12941105	453
15201	*Hells*	KVLVFSQM	475943	12000	1183394	40
319189	*Hist2h2bb*	SVYVYKVL	871990	12000	3175247	73
382522	*Hist3h2bb*	VNDIFERI	91065	12000	63614	8
15368	*Hmox1*	IQAENAEFM	531189	12000	12000	44
15387	*Hnrpk*	DQIQNAQYL	99408	12000	43071	8
23918	*Impdh2*	GGIQNVGHI	932864	90438	5379787	10
16867	*Lhcgr*	SILLLNAVAF	185982	12000	1613907	15
545270	*LOC545270*	YALYNNWEHM	118954	12000	102363	10
72416	*Lrpprc*	AAIENIEHL	384743	12000	385640	32
99470	*Magi3*	SGLTNRDTL	159958	12000	3688747	13
56692	*Map2k1ip1*	QVVQFNRL	114970	12000	140373	10
26413	*Mapk1*	VGPRYTNL	39166667	149969	45832060	261
212307	*Mapre2*	QLNEQVHSL	493384	12000	1547458	41
17168	*Mare*	SAVKNLQQL	4185921	12000	2766551	349
17169	*Mark3*	TSIAFKNI	57818	12000	289972	5
17427	*Mns1*	KIIEFANI	65858	12000	12000	5
17863	*Myb*	NAIKNHWNSTM	668372	12000	338244	56
67938	*Mylc2b*	SLGKNPTDAYL	503898	12000	4119401	42
74838	*Narg1*	SAVENLNEM	615625	12000	297903	51
17992	*Ndufa4*	VNVDYSKL	14338076	12000	29429606	1195

227197	*Ndufs1*	AKLVNQEVL	503868	12000	908787	42
64652	*Nisch*	TNQDFIQRL	123915	12000	948264	10
68979	*Nol11*	TQLIQTHVL	515769	62667	1499186	8
66394	*Nosip*	TSVRFTQL	3518404	12000	7472080	293
18145	*Npc1*	VAVVNKVDI	243630	12000	356718	20
101706	*Numa1*	VSILNRQVL	365089	12000	799609	30
69482	*Nup35*	AQYGNILKHVM	78184	12000	610648	7
18519	*Pcaf*	VQYKFSHL	7220707	12000	5160299	602
14827	*Pdia3*	FAHTNIESL	7732607	107365	2392144	72
23986	*Peci*	SSYTFPKM	1349403	12000	12000	112
75725	*Phf14*	VNYYFERNM	48515	12000	12000	4
236539	*Phgdh*	TGVVNAQAL	324963	12000	1003626	27
233489	*Picalm*	NGVINAAFM	265420	12000	438191	22
233489	*Picalm*	VAFDFTKV	622109	12000	1026908	52
224938	*Pja2*	SSVQNGIML	186205	33856	525538	5
59047	*Pnkp*	YVHVNRDTL	1160230	12000	178123	97
231329	*Polr2b*	IGPTYYQRL	393502	12000	716661	33
218832	*Polr3a*	VTIQNSELM	206677	12000	12000	17
19015	*Ppard*	ASIVNKDGL	144953	12000	217899	12
170826	*Ppargc1b*	LSVRNGATL	218140	12000	267046	18
54397	*Ppt2*	SSYSFRHL	283225	12000	919892	24
106042	*Prickle1*	LNYKFPGL	376026	12000	124373	31
23992	*Prkra*	ISPENHISL	84113	12000	1206217	7
16913	*Psmb8*	GGVVNMYHM	3322728	12000	185723	277
15170	*Ptpn6*	AQYKFIYV	1303118	12000	1598969	109
78697	*Pus7*	TSIKNQTQL	84865	12000	160379	7
110816	*Pwp2*	FAYRFSNL	218474	12000	126002	18
70314	*Rabep2*	AQVQNSEQL	1384849	46060	843925	30
74734	*Rhoh*	YSVANHNSFL	1605054	82775	2637549	19
68477	*Rmnd5a*	WAVSNREML	79683	12000	116624	7
22644	*Rnf103*	KTIYNVEHL	54697	12000	148600	5
66480	*Rpl15*	STYKFFEV	423190	12000	263479	35
19942	*Rpl27*	KTVVNKDVF	783897	12000	3144986	65
67891	*Rpl4*	VNFVHTNL	2514370	12000	1519392	210
267019	*Rps15a*	VIVRFLTV	514406	12000	12000	43
267019	*Rps15a*	VIVRFLTVM	388796	12000	57863	32
20115	*Rps7*	QQNNVEHKV	1979899	12000	2175109	165
20133	*Rrm1*	FQIVNPHLL	2977570	400671	1830528	7
20133	*Rrm1*	YGIRNSLLI	1677107	174840	647604	10
269254	*Setx*	SQLENKTII	204933	12000	137119	17
81898	*Sf3b1*	KAIVNVIGM	78160	12000	335976	7
170755	*Sgk3*	YSIVNASVL	255048	38491	151335	7
20425	*Shmt1*	RNLDYARL	147317	12000	921297	12
63959	*Slc29a1*	SAIFNNVMTL	61949	12000	295795	5
20527	*Slc2a3*	TGVINAPETI	6643529	12000	5706248	554
20586	*Smarca4*	TQVLNTHYV	276940	12000	121529	23
20740	*Spna2*	KALINADEL	4393266	12000	1485888	366
20815	*Srpk1*	ISGVNGTHI	1109459	12000	1330242	92
67437	*Ssr3*	VAFAYKNV	413665	12000	1416589	34
20448	*St6galnac4*	QVYTFTERM	233788	12000	170957	19
20848	*Stat3*	ATLVFHNL	4023137	12000	6208130	335
58523	*Statip1*	SAPRNFVENF	7865121	248931	13541769	32

16430	*Stt3a*	AVLSFSTRL	42362	12000	41291	4
21687	*Tek*	NDIKFQDV	43651	12000	142042	4
22042	*Tfrc*	KAFTYINL	435591	12000	480537	36
21894	*Tln1*	SVMENSKVLGEAM	522658	12000	352355	44
70549	*Tln2*	SVMENSKVLGESM	52094	12000	41337	4
66074	*Tmem167*	SAIFNFQSL	56289	12000	320506	5
67878	*Tmem33*	QSIAFISRL	394668	12000	166467	33
21916	*Tmod1*	SSIVNKEGL	689429	12000	96959	57
217351	*Tnrc6c*	TSPINPQHM	341556	12000	1238666	28
22142	*Tuba1a*	DIERPTYTNL	656598	157480	1267632	4
22142	*Tuba1a*	ERPTYTNL	816936	86447	698017	9
53382	*Txnl1*	FQNVNSVTL	1199864	12000	1713670	100
67123	*Ubap1*	KSLSFPKL	255902	12000	697677	21
19704	*Upf1*	SGYIYHKL	1545046	12000	391481	129
326622	*Upf2*	SAVIFRTL	244247	12000	1102686	20
216825	*Usp22*	FAVVNHQGTL	711737	12000	12000	59
230895	*Vps13d*	INIHYTQL	188518	12000	90025	16
80743	*Vps16*	VSFTYRYL	794606	57587	689203	14
233405	*Vps33b*	ASLVNADKL	2323671	12000	2376572	194
65114	*Vps35*	FSEENHEPL	345757	12000	562939	29
241627	*Wdr76*	FSPTNPAHL	164815	12000	599612	14
22446	*Xlr3b*	VAAANREVL	1654355	12000	1362836	138
103573	*Xpo1*	TILEFSQNM	561596	12000	2010930	47
68090	*Yif1a*	SGYKYVGM	300842	12000	1171758	25
66980	*Zdhhc6*	SVIKFENL	863986	12000	734576	72
67187	*Zmynd19*	ESYSFEARM	132049	12000	253228	11

Supplementary Table 2

Computed MHC binding affinity of MHC I-associated peptides eluted from EL4 cells

MHC Ia-associated peptides

GeneID	Gene symbol	Peptide	Restriction size	SYFPEITHI	smm	smm-rank
68523	*1110019N10Rik*	AALENTHLL	Db 9-mer	30	327	1/309
66185	*1110037F02Rik*	RQILNADAM	Db 9-mer	25	13	1/3705
67463	*1200014M14Rik*	GALENAKAEI	Db 10-mer	30	286	2/1099
74174	*1700006H03Rik*	NSPANNIVM	Db 9-mer	25	28	1/317
100910	*2010209O12Rik*	AQIRNLTVL	Db 9-mer	30	20	1/713
76559	*2410024A21Rik*	AGPENSSKI	Db 9-mer	30	2402	110/4133
75425	*2610036D13Rik*	QTVENVEHL	Db 9-mer	27	635	15/2153
67268	*2900073G15Rik*	SMGKNPTDEYL	Db 11-mer	20	344	3/327
338523	*A630082K20Rik*	SSIQNGKYTL	Db 10-mer	29	273	9/1761
18671	*Abcb1a*	STVRNADVI	Db 9-mer	28	10	1/2535
11307	*Abcg1*	VNIEFKDL	Kb 8-mer	23	107	16/1177
104112	*Acly*	SIANFTNV	Kb 8-mer	20	198	33/2167
66713	*Actr2*	YAGSNFPEHI	Db 10-mer	29	386	4/771
67019	*Actr6*	SGYSFTHI	Kb 8-mer	25	39	4/777
226747	*Ahctf1*	TSVENHEFL	Db 9-mer	30	67	1/2235
223774	*Alg12*	AAMLNYTHI	Db 9-mer	28	4	1/753
81702	*Ankrd17*	ASVLNVNHI	Db 9-mer	27	87	5/5189
11765	*Ap1g1*	FALVNGNNI	Db 9-mer	29	23	1/1633
71435	*Arhgap21*	TGVTNRDLI	Db 9-mer	29	392	7/3875
11984	*Atp6v0c*	SAMVFSAM	Kb 8-mer	19	84	3/295
328099	*AU021838*	VSYLFSHV	Kb 8-mer	24	3	1/487
66165	*Bccip*	KAPVNTAEL	Db 9-mer	31	43	1/615
12176	*Bnip3*	LSMRNTSVM	Db 9-mer	24	14	1/357
107976	*Bre*	ATQVYPKL	Kb 8-mer	22	67	7/751
76740	*C920006C10Rik*	SAIINEDNL	Db 9-mer	29	19	1/1621
69719	*Cad*	RQAENGMYI	Db 9-mer	24	732	26/4433
12340	*Capza1*	ISFKFDHL	Kb 8-mer	23	6	1/557
26885	*Casp8ap2*	VTVLNVDHL	Db 9-mer	26	30	1/3907
12449	*Ccnf*	SQAVNKQQI	Db 9-mer	26	588	4/1537
12468	*Cct7*	RAIKNDSVV	Db 9-mer	22	27	1/1071
12576	*Cdkn1b*	FGPVNHEEL	Db 9-mer	33	77	1/377
229841	*Cenpe*	SALQNAESDRL	Db 11-mer	22	76	1/4925
216859	*Centb1*	INQIYEARV	Kb 9-mer	13	268	243/1265
12649	*Chek1*	TGPSNVDKL	Db 9-mer	29	784	7/935
234594	*Cnot1*	IAFIFNNL	Kb 8-mer	23	5	1/4751
12877	*Cpeb1*	SMLQNPLGNVL	Db 11-mer	23	456	10/1105
68975	*Crsp8*	SGLLNQQSL	Db 9-mer	28	118	1/605
71745	*Cul2*	VINSFVHV	Kb 8-mer	17	527	92/1397
215821	*D10Bwg1379e*	AVLTNQETI	Db 9-mer	28	73	4/4323
52635	*D12Ertd551e*	RQLENGTTL	Db 9-mer	28	33	1/1673
218978	*D14Ertd436e*	SQHVNLDQL	Db 9-mer	29	61	1/967
229473	*D930015E06Rik*	ASLVNSPSYL	Db 10-mer	31	730	48/3177
208846	*Daam1*	AAKVNMTEL	Db 9-mer	30	171	4/2137
68087	*Dcakd*	VIQVFQQL	Kb 8-mer	22	33	2/447
67755	*Ddx47*	KTFLFSATM	Kb 9-mer	11	33	14/755

13209	*Ddx6*	INFDFPKL	Kb 8-mer	24	7	1/811
72121	*Dennd2d*	VIYPFMQGL	Kb 9-mer	18	4	4/923
217207	*Dhx8*	QLYTLGAL	Kb 8-mer	16	1953	332/2473
94176	*Dock2*	SMVQNRVFL	Db 9-mer	29	7	2/3639
233115	*Dpy19l3*	SVVAFHNL	Kb 8-mer	22	44	6/1417
76843	*Dtl*	SSPENKNWL	Db 9-mer	29	291	2/1441
13424	*Dync1h1*	ASYEFVQRL	Kb 9-mer	20	18	4/9133
66967	*Edem3*	FMATNPEHL	Db 9-mer	28	32	1/1845
22446	*Xlr3b*	VAAANREVL	Db 9-mer	26	111	1/435
13669	*Eif3s10*	QSIEFSRL	Kb 8-mer	24	28	1/1267
15569	*Elavl2*	GAVTNVKVI	Db 9-mer	26	42	1/703
14791	*Emg1*	VSVEYTEKM	Kb 9-mer	13	58	8/473
13877	*Erh*	YQPYNKDWI	Db 9-mer	26	48	1/191
14050	*Eya3*	TIIIFHSL	Kb 8-mer	22	45	4/1005
212377	*F730047E07Rik*	VGVTYRTL	Kb 8-mer	23	28	2/1911
70611	*Fbxo33*	SSLSNPIANTM	Db 11-mer	17	107	1/575
14137	*Fdft1*	ISLEFRNL	Kb 8-mer	25	3	1/677
57778	*Fmnl1*	LQYEFTHL	Kb 8-mer	29	19	1/2173
22379	*Fmnl3*	LQYEFTKL	Kb 8-mer	30	25	2/2011
239554	*Foxred2*	LGVTNFVHM	Db 9-mer	28	247	3/1313
56784	*Garnl1*	GAIVNGKVL	Db 9-mer	27	27	2/4149
14751	*Gpi1*	KNLVNKEVM	Db 9-mer	27	198	2/1099
14790	*Grcc10*	SAPENAVRM	Db 9-mer	33	165	2/235
68153	*Gtf2e2*	SGYKFGVL	Kb 8-mer	29	18	1/569
69237	*Gtpbp4*	QILSDFPKL	Kb 9-mer	23	231	19/1253
15201	*Hells*	KVLVFSQM	Kb 8-mer	18	254	22/1627
319189	*Hist2h2bb*	SVYVYKVL	Kb 8-mer	27	46	1/237
382522	*Hist3h2bb*	VNDIFERI	Kb 8-mer	18	1748	43/293
15368	*Hmox1*	IQAENAEFM	Db 9-mer	27	308	3/561
15387	*Hnrpk*	DQIQNAQYL	Db 9-mer	28	52	1/909
23918	*Impdh2*	GGIQNVGHI	Db 9-mer	26	291	5/1011
16867	*Lhcgr*	SILLLNAVAF	Db 10-mer	22	2815	564/1383
545270	*LOC545270*	YALYNNWEHM	Db 10-mer	28	45	2/165
72416	*Lrpprc*	AAIENIEHL	Db 9-mer	32	64	4/2595
99470	*Magi3*	SGLTNRDTL	Db 9-mer	31	14	1/2235
56692	*Map2k1ip1*	QVVQFNRL	Kb 8-mer	20	368	14/233
26413	*Mapk1*	VGPRYTNL	Kb 8-mer	25	12	2/701
17168	*Mare*	SAVKNLQQL	Db 9-mer	31	85	1/1121
17169	*Mark3*	TSIAFKNI	Kb 8-mer	19	88	5/1473
17427	*Mns1*	KIIEFANI	Kb 8-mer	20	20	1/967
17863	*Myb*	NAIKNHWNSTM	Db 11-mer	17	309	2/1255
67938	*Mylc2b*	SLGKNPTDAYL	Db 11-mer	16	13242	31/327
74838	*Narg1*	SAVENLNEM	Db 9-mer	33	94	2/1713
17992	*Ndufa4*	VNVDYSKL	Kb 8-mer	24	40	1/149
227197	*Ndufs1*	AKLVNQEVL	Db 9-mer	28	175	1/1437
64652	*Nisch*	TNQDFIQRL	Kb 9-mer	14	358	98/3171
66394	*Nosip*	TSVRFTQL	Kb 8-mer	24	33	1/447
18145	*Npc1*	VAVVNKVDI	Db 9-mer	29	73	3/2537
101706	*Numa1*	VSILNRQVL	Db 9-mer	26	14	1/4171
69482	*Nup35*	AQYGNILKHVM	Db 11-mer	20	1543	42/633
18519	*Pcaf*	VQYKFSHL	Kb 8-mer	28	4	1/1611
14827	*Pdia3*	FAHTNIESL	Db 9-mer	29	19	1/993

23986	*Peci*	SSYTFPKM	Kb 8-mer	25	8	1/561
75725	*Phf14*	VNYYFERNM	Kb 9-mer	18	18	6/1603
236539	*Phgdh*	TGVVNAQAL	Db 9-mer	29	203	2/1049
233489	*Picalm*	NGVINAAFM	Db 9-mer	26	192	4/1303
233489	*Picalm*	VAFDFTKV	Kb 8-mer	20	45	6/1305
224938	*Pja2*	SSVQNGIML	Db 9-mer	26	15	1/1397
59047	*Pnkp*	YVHVNRDTL	Db 9-mer	25	9	1/1027
231329	*Polr2b*	IGPTYYQRL	Kb 9-mer	20	23	15/2319
218832	*Polr3a*	VTIQNSELM	Db 9-mer	27	503	13/2763
19015	*Ppard*	ASIVNKDGL	Db 9-mer	30	117	3/863
170826	*Ppargc1b*	LSVRNGATL	Db 9-mer	27	41	1/2011
54397	*Ppt2*	SSYSFRHL	Kb 8-mer	29	4	1/589
106042	*Prickle1*	LNYKFPGL	Kb 8-mer	29	5	1/1509
23992	*Prkra*	ISPENHISL	Db 9-mer	28	109	2/609
16913	*Psmb8*	GGVVNMYHM	Db 9-mer	27	135	2/535
15170	*Ptpn6*	AQYKFIYV	Kb 8-mer	25	23	1/1039
78697	*Pus7*	TSIKNQTQL	Db 9-mer	28	159	2/1303
110816	*Pwp2*	FAYRFSNL	Kb 8-mer	30	2	1/1823
70314	*Rabep2*	AQVQNSEQL	Db 9-mer	28	382	2/1005
74734	*Rhoh*	YSVANHNSFL	Db 10-mer	26	767	7/365
68477	*Rmnd5a*	WAVSNREML	Db 9-mer	27	158	1/765
22644	*Rnf103*	KTIYNVEHL	Db 9-mer	26	308	4/1349
66480	*Rpl15*	STYKFFEV	Kb 8-mer	24	51	3/393
19942	*Rpl27*	KTVVNKDVF	Db 9-mer	25	54	1/255
67891	*Rpl4*	VNFVHTNL	Kb 8-mer	13	51	1/823
267019	*Rps15a*	VIVRFLTV	Kb 8-mer	19	33	1/245
267019	*Rps15a*	VIVRFLTVM	Kb 9-mer	19	33	9/245
20133	*Rrm1*	FQIVNPHLL	Db 9-mer	28	71	2/1567
20133	*Rrm1*	YGIRNSLLI	Db 9-mer	26	452	7/1567
269254	*Setx*	SQLENKTII	Db 9-mer	28	61	2/5275
81898	*Sf3b1*	KAIVNVIGM	Db 9-mer	28	70	2/2591
170755	*Sgk3*	YSIVNASVL	Db 9-mer	28	6	1/975
20425	*Shmt1*	RNLDYARL	Kb 8-mer	23	22	2/941
63959	*Slc29a1*	SAIFNNVMTL	Db 10-mer	29	886	16/899
20527	*Slc2a3*	TGVINAPETI	Db 10-mer	30	2873	57/969
20586	*Smarca4*	TQVLNTHYV	Db 9-mer	22	94	3/3211
20740	*Spna2*	KALINADEL	Db 9-mer	31	19	1/4817
20815	*Srpk1*	ISGVNGTHI	Db 9-mer	28	55	1/1279
67437	*Ssr3*	VAFAYKNV	Kb 8-mer	18	18	1/355
20448	*St6galnac4*	QVYTFTERM	Kb 9-mer	17	137	13/589
20848	*Stat3*	ATLVFHNL	Kb 8-mer	22	23	1/1429
58523	*Statip1*	SAPRNFVENF	Db 10-mer	30	315	11/1645
16430	*Stt3a*	AVLSFSTRL	Kb 9-mer	13	154	66/1695
21687	*Tek*	NDIKFQDV	Kb 8-mer	18	4583	645/2231
22042	*Tfrc*	KAFTYINL	Kb 8-mer	23	11	2/1371
21894	*Tln1*	SVMENSKVLGEAM	Db 13-mer	23	60	5/5065
70549	*Tln2*	SVMENSKVLGESM	Db 13-mer	23	60	5/5069
66074	*Tmem167*	SAIFNFQSL	Db 9-mer	30	48	1/127
67878	*Tmem33*	QSIAFISRL	Kb 9-mer	13	75	28/479
21916	*Tmod1*	SSIVNKEGL	Db 9-mer	30	228	3/701
217351	*Tnrc6c*	TSPINPQHM	Db 9-mer	28	158	5/3783
22142	*Tuba1a*	ERPTYTNL	Kb 8-mer	23	1759	134/889

22142	*Tuba1a*	DIERPTYTNL	Kb 10-mer	23	849	134/889
53382	*Txnl1*	FQNVNSVTL	Db 9-mer	28	27	1/561
67123	*Ubap1*	KSLSFPKL	Kb 8-mer	22	42	3/867
19704	*Upf1*	SGYIYHKL	Kb 8-mer	29	18	2/2211
326622	*Upf2*	SAVIFRTL	Kb 8-mer	24	57	4/2523
216825	*Usp22*	FAVVNHQGTL	Db 10-mer	31	985	7/1033
230895	*Vps13d*	INIHYTQL	Kb 8-mer	25	39	10/8753
80743	*Vps16*	VSFTYRYL	Kb 8-mer	22	3	1/1663
233405	*Vps33b*	ASLVNADKL	Db 9-mer	31	25	1/1217
65114	*Vps35*	FSEENHEPL	Db 9-mer	27	33	3/1575
241627	*Wdr76*	FSPTNPAHL	Db 9-mer	29	18	1/1031
103573	*Xpo1*	TILEFSQNM	Kb 9-mer	14	88	81/2127
68090	*Yif1a*	SGYKYVGM	Kb 8-mer	25	17	1/571
66980	*Zdhhc6*	SVIKFENL	Kb 8-mer	25	44	3/811
67187	*Zmynd19*	ESYSFEARM	Kb 9-mer	18	386	2/439

MHC Ib-associated peptides

GeneID	Gene symbol	Peptide	Restriction size	Rankpep
77877	*6030458C11Rik*	KVLDVLHSL	Qa2 9-mer	228
213895	*Bms1l*	YQNQEIHNL	Qa2 9-mer	131
12181	*Bop1*	EQVALVHRL	Qa2 9-mer	199
224171	*C330027C09Rik*	AQNDIEHLF	Qa2 9-mer	155
12465	*Cct5*	SMMDVDHQI	Qa2 9-mer	223
214901	*Chtf18*	QLSDTLHSL	Qa2 9-mer	184
80986	*Ckap2*	TLNDLIHNI	Qa2 9-mer	192
12847	*Copa*	SQLPVDHIL	Qa2 9-mer	196
66366	*Ergic3*	QQLDVEHNL	Qa2 9-mer	212
108655	*Foxp1*	QQLQQQHLL	Qa2 9-mer	148
15016	*H2-Q5*	AMAPRTLLL	Qa1 9-mer	
212307	*Mapre2*	QLNEQVHSL	Qa2 9-mer	176
68979	*Nol11*	TQLIQTHVL	Qa2 9-mer	150
20115	*Rps7*	QQNNVEHKV	Qa2 9-mer	180

Supplementary Table 3

Computed MHC binding affinity of MHC I-associated peptides from primary mouse thymocytes

MHC Ia-associated peptides

GeneID	Gene symbol	Peptides	Restriction size	smm	SYFPEITHI
68295	*0610011L14Rik*	ISILYHQL	Kb 8-mer	20	24
68523	*1110019N10Rik*	AALENTHLL	Db 9-mer	327	30
72368	*2310045N01Rik*	SSVYFRSV	Kb 8-mer	51	19
75425	*2610036D13Rik*	QTVENVEHL	Db 9-mer	635	27
72722	*2810405J04Rik*	ASPEFTKL	Kb 8-mer	60	26
72747	*2810439F02Rik*	SGYDFENRL	Kb 9-mer	19	21
67268	*2900073G15Rik*	SMGKNPTDEYL	Db 11-mer	344	20
67392	*4833420G17Rik*	FVISNYREQL	Db 11-mer	1238	26
218989	*6720456H20Rik*	TGIRNLEWL	Db 9-mer	574	30
11307	*Abcg1*	VNIEFKDL	Kb 8-mer	107	23
66713	*Actr2*	YAGSNFPEHI	Db 10-mer	386	29
67019	*Actr6*	SGYSFTHI	Kb 8-mer	39	25
57869	*Adck2*	SGPTYIKL	Kb 8-mer	78	25
81702	*Ankrd17*	ASVLNVNHI	Db 9-mer	87	27
329154	*Ankrd44*	ASVINGHTL	Db 9-mer	60	28
73341	*Arhgef6*	AIIAFKTL	Kb 8-mer	45	24
54208	*Arl6ip1*	IILKYIGM	Kb 8-mer	11	20
192195	*Ash1l*	VGLINKDSV	Db 9-mer	412	24
11906	*Atbf1*	VAIGNPVHL	Db 9-mer	292	28
Q9JKK8	*Atr*	FQALNAEKL	Db 9-mer	208	26
54138	*Atxn10*	NSIRNLDTI	Db 9-mer	13	31
328099	*AU021838*	VSYLFSHV	Kb 8-mer	3	24
213550	*AV340375*	FSNKNLEEL	Db 9-mer	53	31
235461	*B230380D07Rik*	VNVRFTGV	Kb 8-mer	36	19
224727	*Bat3*	SIAAFIQRL	Kb 9-mer	199	14
66165	*Bccip*	KAPVNTAEL	Db 9-mer	43	31
107976	*Bre*	ATQVYPKL	Kb 8-mer	67	22
26885	*Casp8ap2*	VTVLNVDHL	Db 9-mer	30	26
76041	*Ccdc125*	NAVLNQRYL	Db 9-mer	32	27
77048	*Ccdc41*	AQVENVQRI	Db 9-mer	498	29
12445	*Ccnd3*	AAVIAHDFL	Db 9-mer	46	20
12449	*Ccnf*	SQAVNKQQI	Db 9-mer	588	26
12450	*Ccng1*	TAFQFLQL	Kb 8-mer	80	22
12501	*Cd3e*	YSGLNQRAV	Db 9-mer	406	19
26364	*Cd97*	KLLSNINSVF	Db 10-mer	9292	23
12576	*Cdkn1b*	FGPVNHEEL	Db 9-mer	77	33
229841	*Cenpe*	SALQNAESDRL	Db 12-mer	76	22
216859	*Centb1*	INQIYEARV	Kb 9-mer	268	13
12649	*Chek1*	TGPSNVDKL	Db 9-mer	784	29
243764	*Chrm2*	TVIGYWPL	Kb 8-mer	196	21
70349	*Copb1*	IALRYVAL	Kb 8-mer	22	23
67876	*Coq10b*	ISFEFRSL	Kb 8-mer	2	24
68975	*Crsp8*	SGLLNQQSL	Db 9-mer	118	28
71745	*Cul2*	VINSFVHV	Kb 8-mer	527	17
12767	*Cxcr4*	VVFQFQHI	Kb 8-mer	56	16
52635	*D12Ertd551e*	RQLENGTTL	Db 9-mer	33	28
218978	*D14Ertd436e*	SQHVNLDQL	Db 9-mer	61	29

71919	*D15Ertd682e*	TNVLFNHL	Kb 8-mer	169	21
69601	*Dab2ip*	VSPTNPTKL	Db 9-mer	98	29
67755	*Ddx47*	KTFLFSATM	Kb 9-mer	33	11
13207	*Ddx5*	NQAINPKLLQL	Db 11-mer	4239	22
13209	*Ddx6*	INFDFPKL	Kb 8-mer	7	24
76131	*Depdc1a*	FSQENTEKI	Db 9-mer	231	28
13433	*Dnmt1*	LSLENGTHTL	Db 10-mer	758	28
94176	*Dock2*	SMVQNRVFL	Db 9-mer	7	29
233115	*Dpy19l3*	SVVAFHNL	Kb 8-mer	44	22
13424	*Dync1h1*	ASYEFVQRL	Kb 9-mer	18	20
13669	*Eif3s10*	QSIEFSRL	Kb 8-mer	28	24
73830	*Eif3s12*	VGITYQHI	Kb 8-mer	100	18
170439	*Elovl6*	KSFLFSAL	Kb 8-mer	10	22
10436	*EMG1*	VSVEYTEKM	Kb 9-mer	58	13
13819	*Epas1*	SNYLFTKL	Kb 8-mer	10	30
212377	*F730047E07Rik*	VGVTYRTL	Kb 8-mer	28	23
107035	*Fbxo38*	SAFSFRTL	Kb 8-mer	22	24
14137	*Fdft1*	ISLEFRNL	Kb 8-mer	3	25
57778	*Fmnl1*	LQYEFTHL	Kb 8-mer	19	29
22379	*Fmnl3*	LQYEFTKL	Kb 8-mer	25	30
14359	*Fxr1h*	EIVTFERL	Kb 8-mer	464	22
14790	*Grcc10*	SAPENAVRM	Db 9-mer	165	33
68153	*Gtf2e2*	SGYKFGVL	Kb 8-mer	18	29
69237	*Gtpbp4*	QILSDFPKL	Kb 9-mer	231	23
14976	*H2-Ke2*	SNVVFKLL	Kb 9-mer	145	22
15019	*H2-Q8*	FAYEGRDYI	Db 9-mer	12	21
15201	*Hells*	KVLVFSQM	Kb 8-mer	254	18
15257	*Hipk1*	SLLTNHVTL	Db 9-mer	167	28
319189	*Hist2h2bb*	SVYVYKVL	Kb 8-mer	46	27
98758	*Hnrpf*	FSPLNPVRV	Db 9-mer	127	25
15441	*Hp1bp3*	VSQYYPKL	Kb 8-mer	29	22
16145	*Igtp*	IVAENTKTSL	Db 10-mer	3059	24
23918	*Impdh2*	GGIQNVGHI	Db 9-mer	291	26
16329	*Inpp1*	YMGTNIHSL	Db 9-mer	84	25
76582	*Ipo11*	TIILFTKV	Kb 8-mer	95	20
338523	*Jhdm1d*	SSIQNGKYTL	Db 10-mer	273	29
16211	*Kpnb1*	AALQNLVKI	Db 9-mer	77	31
110308	*Krt5*	AAYMNKVEL	Db 9-mer	63	28
110310	*Krt7*	AAYTNKVEL	Db 9-mer	66	28
72416	*Lrpprc*	AAIENIEHL	Db 9-mer	64	32
26413	*Mapk1*	VGPRYTNL	Kb 8-mer	12	25
17168	*Mare*	SAVKNLQQL	Db 9-mer	85	31
13728	*Mark2*	ASIQNGKDSL	Db 10-mer	1344	30
217615	*Mgea6*	RNQVYTQL	Kb 8-mer	224	24
67014	*Mina*	VVYIYHSL	Kb 8-mer	9	26
17427	*Mns1*	KIIEFANI	Kb 8-mer	20	20
121022	*Mrps6*	SAVENILEHL	Db 10-mer	178	32
219135	*Mtmr6*	VGIENIHVM	Db 9-mer	150	27
17886	*Myh9*	RVAEFTTNL	Kb 9-mer	228	14
67938	*Mylc2b*	SLGKNPTDAYL	Db 11-mer	344	16
67608	*Narf*	AAYGFRNI	Kb 8-mer	32	26
17992	*Ndufa4*	VNVDYSKL	Kb 8-mer	40	24

227197	*Ndufs1*	AKLVNQEVL	Db 9-mer	175	28
18034	*Nfkb2*	AALQNLEQL	Db 9-mer	98	32
64652	*Nisch*	TNQDFIQRL	Kb 9-mer	358	14
97895	*Nlrp4f*	TPVKNIDTV	Db 9-mer	509	24
68979	*Nol11*	IAVSFREL	Kb 8-mer	48	23
211548	*Nomo1*	SSLVNKEDV	Db 9-mer	99	26
66394	*Nosip*	TSVRFTQL	Kb 8-mer	33	24
18145	*Npc1*	VAVVNKVDI	Db 9-mer	73	29
101706	*Numa1*	VSILNRQVL	Db 9-mer	14	26
70699	*Nup205*	VNNEFEKL	Kb 8-mer	1138	24
66923	*Pbrm1*	SQVYNDAHI	Db 9-mer	111	26
18538	*Pcna*	RAEDNADTLAL	Db 11-mer	59	27
56426	*Pdcd10*	ILQTFKTVA	Kb 9-mer	5	18
207728	*Pde2a*	IKNENQEVI	Db 9-mer	1260	24
23986	*Peci*	SSYTFPKM	Kb 8-mer	8	25
73739	*Pgea1*	ASLSNLHSL	Db 9-mer	218	30
233489	*Picalm*	VAFDFTKV	Kb 8-mer	45	20
83490	*Pik3ap1*	YGLKNLTAL	Db 9-mer	40	29
18950	*Pnp*	SLITNKVVM	Db 9-mer	104	26
231329	*Polr2b*	IGPTYYQRL	Kb 9-mer	23	20
66385	*Ppp1r7*	RAIENIDTL	Db 9-mer	7	30
51792	*Ppp2r1a*	IIPMFSNL	Kb 8-mer	4	25
73699	*Ppp2r1b*	VADKFSEL	Kb 8-mer	375	23
214572	*Prmt7*	VIVEFRDL	Kb 8-mer	28	23
19167	*Psma3*	KAVENSSTAI	Db 10-mer	517	30
16913	*Psmb8*	GGVVNMYHM	Db 9-mer	135	27
15170	*Ptpn6*	AQYKFIYV	Kb 8-mer	23	25
19696	*Rel*	TTLIFQKL	Kb 8-mer	58	21
26374	*Rfwd2*	YVVDNIDHL	Db 9-mer	156	25
74734	*Rhoh*	YSVANHNSFL	Db 10-mer	767	26
68477	*Rmnd5a*	WAVSNREML	Db 9-mer	158	27
20054	*Rps15*	VGVYNGKTF	Db 9-mer	3132	25
267019	*Rps15a*	ISPRFDVQL	Kb 9-mer	172	14
267019	*Rps15a*	VIVRFLTV	Kb 8-mer	33	19
20115	*Rps7*	VNFEFPEF	Kb 8-mer	24	12
20133	*Rrm1*	FQIVNPHLL	Db 9-mer	71	28
20133	*Rrm1*	YGIRNSLLI	Db 9-mer	452	26
235623	*Scap*	SGYDFSRL	Kb 8-mer	5	30
13722	*Scye1*	SGLVNHVPL	Db 9-mer	59	29
20338	*Sel1l*	QALKYFNL	Kb 8-mer	171	23
20393	*Sgk*	STLTYSRM	Kb 8-mer	38	18
20740	*Spna2*	KALINADEL	Db 9-mer	19	31
20815	*Srpk1*	ISGVNGTHI	Db 9-mer	55	28
20443	*St3gal4*	GAVKNLTYF	Db 9-mer	81	30
20848	*Stat3*	ATLVFHNL	Kb 8-mer	23	22
71728	*Stk11ip*	SALRFLNL	Kb 8-mer	23	24
16430	*Stt3a*	AVLSFSTRL	Kb 9-mer	154	13
108143	*Taf9*	SGLKYVNV	Kb 8-mer	45	20
216198	*Tcp11l2*	KATTNIVEM	Db 9-mer	225	27
217353	*Tmc6*	ASYLFRGL	Kb 8-mer	3	29
67511	*Tmed9*	VIGNYRTQL	Kb 9-mer	271	14
72759	*Tmem135*	KGFTFSAL	Kb 8-mer	23	22

66074	*Tmem167*	AIFNFQSL	Kb 8-mer	8	22
67878	*Tmem33*	QSIAFISRL	Kb 9-mer	75	13
21916	*Tmod1*	SSIVNKEGL	Db 9-mer	228	30
22057	*Tob1*	ISYLYNKL	Kb 8-mer	4	29
21990	*Tph1*	FSLENEVGGL	Db 10-mer	728	28
21990	*Tph1*	WGTIFREL	Kb 8-mer	309	22
12751	*Tpp1*	IQRVNTEFM	Db 9-mer	100	25
100683	*Trrap*	QDPVFQKL	Kb 8-mer	885	22
73710	*Tubb2b*	VNMVPFPRL	Kb 9-mer	252	20
56085	*Ubqln1*	RALSNLESI	Db 9-mer	87	30
224826	*Ubr2*	VAYKFPELL	Kb 9-mer	6	28
59025	*Usp14*	VKYLFTGL	Kb 8-mer	20	27
216825	*Usp22*	FAVVNHQGTL	Db 10-mer	985	31
271564	*Vps13a*	VSIQFYHL	Kb 8-mer	3	22
230895	*Vps13d*	INIHYTQL	Kb 8-mer	39	25
80743	*Vps16*	VSFTYRYL	Kb 8-mer	3	22
77573	*Vps33a*	GSLANHTSI	Db 9-mer	161	27
233405	*Vps33b*	ASLVNADKL	Db 9-mer	25	31
65114	*Vps35*	FSEENHEPL	Db 9-mer	33	27
22375	*Wars*	YTVENAKDII	Db 10-mer	492	26
69544	*Wdr5b*	AALENDKTI	Db 9-mer	56	31
74781	*Wipi2*	SGYKFFSL	Kb 8-mer	14	29
68090	*Yif1a*	SGYKYVGM	Kb 8-mer	17	25
66980	*Zdhhc6*	SVIKFENL	Kb 8-mer	44	25

MHC Ib-associated peptides

GeneID	Gene symbol	Peptides	Restriction size	Rankpep
319236	*9230105E10Rik*	FISDVEHQL	Qa2 9-mer	181
12014	*Bach2*	EQLEFIHDI	Qa2 9-mer	183
224171	*C330027C09Rik*	AQNDIEHLF	Qa2 9-mer	155
75565	*Ccdc101*	ELLTELHQL	Qa2 9-mer	198
13204	*Dhx15*	TLLNVYHAF	Qa2 9-mer	215
66366	*Ergic3*	QQLDVEHNL	Qa2 9-mer	212
108655	*Foxp1*	QQLQQQHLL	Qa2 9-mer	148
15016	*H2-Q5*	AMAPRTLLL	Qa1 9-mer	
212307	*Mapre2*	QLNEQVHSL	Qa2 9-mer	176
68979	*Nol11*	TQLIQTHVL	Qa2 9-mer	150
69608	*Sec24d*	ESQSVIHNL	Qa2 9-mer	185
319565	*Syne2*	DLIQTIHEL	Qa2 9-mer	213
50875	*Tmod3*	AAILGMHNL	Qa2 9-mer	134
320938	*Tnpo3*	GLLEIAHSL	Qa2 9-mer	237

Supplementary Table 4

Computed MHC binding affinity of MHC I-associated peptides in vivo grown EL4 cells

MHC Ia-associated peptides

GeneID	Gene symbol	Peptides	Restriction size	smm	SYFPEITHI
68295	*0610011L14Rik*	ISILYHQL	Kb 8-mer	20	24
68523	*1110019N10Rik*	AALENTHLL	Db 9-mer	327	30
72368	*2310045N01Rik*	SSVYFRSV	Kb 8-mer	51	19
75425	*2610036D13Rik*	QTVENVEHL	Db 9-mer	635	27
72722	*2810405J04Rik*	ASPEFTKL	Kb 8-mer	60	26
72747	*2810439F02Rik*	SGYDFENRL	Kb 9-mer	19	21
67268	*2900073G15Rik*	SMGKNPTDEYL	Db 11-mer	344	20
67392	*4833420G17Rik*	FVISNYREQL	Db 11-mer	1238	26
218989	*6720456H20Rik*	TGIRNLEWL	Db 9-mer	574	30
11307	*Abcg1*	VNIEFKDL	Kb 8-mer	107	23
66713	*Actr2*	YAGSNFPEHI	Db 10-mer	386	29
67019	*Actr6*	SGYSFTHI	Kb 8-mer	39	25
57869	*Adck2*	SGPTYIKL	Kb 8-mer	78	25
81702	*Ankrd17*	ASVLNVNHI	Db 9-mer	87	27
329154	*Ankrd44*	ASVINGHTL	Db 9-mer	60	28
75415	*Arhgap12*	YGLLNVTKI	Db 9-mer	60	26
73341	*Arhgef6*	AIIAFKTL	Kb 8-mer	45	24
54208	*Arl6ip1*	IILKYIGM	Kb 8-mer	11	20
192195	*Ash1l*	VGLINKDSV	Db 9-mer	412	24
11906	*Atbf1*	VAIGNPVHL	Db 9-mer	292	28
Q9JKK8	*Atr*	FQALNAEKL	Db 9-mer	208	26
54138	*Atxn10*	NSIRNLDTI	Db 9-mer	13	31
328099	*AU021838*	VSYLFSHV	Kb 8-mer	3	24
213550	*AV340375*	FSNKNLEEL	Db 9-mer	53	31
235461	*B230380D07Rik*	VNVRFTGV	Kb 8-mer	36	19
224727	*Bat3*	SIAAFIQRL	Kb 9-mer	199	14
66165	*Bccip*	KAPVNTAEL	Db 9-mer	43	31
107976	*Bre*	ATQVYPKL	Kb 8-mer	67	22
26885	*Casp8ap2*	VTVLNVDHL	Db 9-mer	30	26
76041	*Ccdc125*	NAVLNQRYL	Db 9-mer	32	27
77048	*Ccdc41*	AQVENVQRI	Db 9-mer	498	29
12445	*Ccnd3*	AAVIAHDFL	Db 9-mer	46	20
12449	*Ccnf*	SQAVNKQQI	Db 9-mer	588	26
12450	*Ccng1*	TAFQFLQL	Kb 8-mer	80	22
12501	*Cd3e*	YSGLNQRAV	Db 9-mer	406	19
26364	*Cd97*	KLLSNINSVF	Db 10-mer	9292	23
12576	*Cdkn1b*	FGPVNHEEL	Db 9-mer	77	33
229841	*Cenpe*	SALQNAESDRL	Db 12-mer	76	22
216859	*Centb1*	INQIYEARV	Kb 9-mer	268	13
12649	*Chek1*	TGPSNVDKL	Db 9-mer	784	29
243764	*Chrm2*	TVIGYWPL	Kb 8-mer	196	21
70349	*Copb1*	IALRYVAL	Kb 8-mer	22	23
67876	*Coq10b*	ISFEFRSL	Kb 8-mer	2	24
68975	*Crsp8*	SGLLNQQSL	Db 9-mer	118	28
71745	*Cul2*	VINSFVHV	Kb 8-mer	527	17
12767	*Cxcr4*	VVFQFQHI	Kb 8-mer	56	16
52635	*D12Ertd551e*	RQLENGTTL	Db 9-mer	33	28

218978	*D14Ertd436e*	SQHVNLDQL	Db 9-mer	61	29
71919	*D15Ertd682e*	TNVLFNHL	Kb 8-mer	169	21
69601	*Dab2ip*	VSPTNPTKL	Db 9-mer	98	29
67755	*Ddx47*	KTFLFSATM	Kb 9-mer	33	11
13209	*Ddx6*	INFDFPKL	Kb 8-mer	7	24
76131	*Depdc1a*	FSQENTEKI	Db 9-mer	231	28
13433	*Dnmt1*	LSLENGTHTL	Db 10-mer	758	28
94176	*Dock2*	SMVQNRVFL	Db 9-mer	7	29
233115	*Dpy19l3*	SVVAFHNL	Kb 8-mer	44	22
13424	*Dync1h1*	ASYEFVQRL	Kb 9-mer	18	20
13669	*Eif3s10*	QSIEFSRL	Kb 8-mer	28	24
73830	*Eif3s12*	VGITYQHI	Kb 8-mer	100	18
54709	*Eif3s2*	FGPINSVAF	Db 9-mer	1976	26
170439	*Elovl6*	KSFLFSAL	Kb 8-mer	10	22
10436	*EMG1*	VSVEYTEKM	Kb 9-mer	58	13
13819	*Epas1*	SNYLFTKL	Kb 8-mer	10	30
212377	*F730047E07Rik*	VGVTYRTL	Kb 8-mer	28	23
14104	*Fasn*	TALENLSTL	Db 9-mer	48	33
107035	*Fbxo38*	SAFSFRTL	Kb 8-mer	22	24
14137	*Fdft1*	ISLEFRNL	Kb 8-mer	3	25
57778	*Fmnl1*	LQYEFTHL	Kb 8-mer	19	29
22379	*Fmnl3*	LQYEFTKL	Kb 8-mer	25	30
14359	*Fxr1h*	EIVTFERL	Kb 8-mer	464	22
14790	*Grcc10*	SAPENAVRM	Db 9-mer	165	33
68153	*Gtf2e2*	SGYKFGVL	Kb 8-mer	18	29
69237	*Gtpbp4*	QILSDFPKL	Kb 9-mer	231	23
14976	*H2-Ke2*	SNVVFKLL	Kb 9-mer	145	22
15019	*H2-Q8*	FAYEGRDYI	Db 9-mer	12	21
15201	*Hells*	KVLVFSQM	Kb 8-mer	254	18
15257	*Hipk1*	SLLTNHVTL	Db 9-mer	167	28
319189	*Hist2h2bb*	SVYVYKVL	Kb 8-mer	46	27
20585	*Hltf*	SGFVFTRL	Kb 8-mer	7	23
98758	*Hnrpf*	FSPLNPVRV	Db 9-mer	127	25
15441	*Hp1bp3*	VSQYYPKL	Kb 8-mer	29	22
23918	*Impdh2*	GGIQNVGHI	Db 9-mer	291	26
16329	*Inpp1*	YMGTNIHSL	Db 9-mer	84	25
76582	*Ipo11*	TIILFTKV	Kb 8-mer	95	20
338523	*Jhdm1d*	SSIQNGKYTL	Db 10-mer	273	29
16211	*Kpnb1*	AALQNLVKI	Db 9-mer	77	31
76130	*Las1l*	ALVRFVNL	Kb 8-mer	74	23
72416	*Lrpprc*	AAIENIEHL	Db 9-mer	64	32
26413	*Mapk1*	VGPRYTNL	Kb 8-mer	12	25
17168	*Mare*	SAVKNLQQL	Db 9-mer	85	31
13728	*Mark2*	ASIQNGKDSL	Db 10-mer	1344	30
217615	*Mgea6*	RNQVYTQL	Kb 8-mer	224	24
67014	*Mina*	VVYIYHSL	Kb 8-mer	9	26
121022	*Mrps6*	SAVENILEHL	Db 10-mer	178	32
219135	*Mtmr6*	VGIENIHVM	Db 9-mer	150	27
17886	*Myh9*	RVAEFTTNL	Kb 9-mer	228	14
67938	*Mylc2b*	SLGKNPTDAYL	Db 11-mer	344	16
67608	*Narf*	AAYGFRNI	Kb 8-mer	32	26
67563	*Narfl*	VAYGFRNI	Kb 8-mer	15	25

17992	*Ndufa4*	VNVDYSKL	Kb 8-mer	40	24
227197	*Ndufs1*	AKLVNQEVL	Db 9-mer	175	28
18034	*Nfkb2*	AALQNLEQL	Db 9-mer	98	32
64652	*Nisch*	TNQDFIQRL	Kb 9-mer	358	14
97895	*Nlrp4f*	TPVKNIDTV	Db 9-mer	509	24
68979	*Nol11*	IAVSFREL	Kb 8-mer	48	23
211548	*Nomo1*	SSLVNKEDV	Db 9-mer	99	26
66394	*Nosip*	TSVRFTQL	Kb 8-mer	33	24
18145	*Npc1*	VAVVNKVDI	Db 9-mer	73	29
101706	*Numa1*	VSILNRQVL	Db 9-mer	14	26
70699	*Nup205*	VNNEFEKL	Kb 8-mer	1138	24
18813	*Pa2g4*	AQFKFTVL	Kb 8-mer	59	23
66923	*Pbrm1*	SQVYNDAHI	Db 9-mer	111	26
18538	*Pcna*	RAEDNADTLAL	Db 11-mer	59	27
56426	*Pdcd10*	ILQTFKTVA	Kb 9-mer	5	18
207728	*Pde2a*	IKNENQEVI	Db 9-mer	1260	24
23986	*Peci*	SSYTFPKM	Kb 8-mer	8	25
18626	*Per1*	YTLRNQDTF	Db 9-mer	55	25
56612	*Pfdn5*	SMYVPGKL	Kb 8-mer	293	18
73739	*Pgea1*	ASLSNLHSL	Db 9-mer	218	30
233489	*Picalm*	VAFDFTKV	Kb 8-mer	45	20
83490	*Pik3ap1*	YGLKNLTAL	Db 9-mer	40	29
18950	*Pnp*	SLITNKVVM	Db 9-mer	104	26
231329	*Polr2b*	IGPTYYQRL	Kb 9-mer	23	20
18985	*Pou2af1*	SGPQFVQL	Kb 8-mer	172	24
66385	*Ppp1r7*	RAIENIDTL	Db 9-mer	7	30
51792	*Ppp2r1a*	IIPMFSNL	Kb 8-mer	4	25
73699	*Ppp2r1b*	VADKFSEL	Kb 8-mer	375	23
106042	*Prickle1*	LNYKFPGL	Kb 8-mer	5	29
214572	*Prmt7*	VIVEFRDL	Kb 8-mer	28	23
19167	*Psma3*	KAVENSSTAI	Db 10-mer	517	30
16913	*Psmb8*	GGVVNMYHM	Db 9-mer	135	27
15170	*Ptpn6*	AQYKFIYV	Kb 8-mer	23	25
108911	*Rcc2*	AAYRNLGQNL	Db 10-mer	924	29
19696	*Rel*	TTLIFQKL	Kb 8-mer	58	21
26374	*Rfwd2*	YVVDNIDHL	Db 9-mer	156	25
74734	*Rhoh*	YSVANHNSFL	Db 10-mer	767	26
20054	*Rps15*	VGVYNGKTF	Db 9-mer	3132	25
267019	*Rps15a*	VIVRFLTV	Kb 8-mer	33	19
267019	*Rps15a*	ISPRFDVQL	Kb 9-mer	172	14
20115	*Rps7*	VNFEFPEF	Kb 8-mer	24	12
20133	*Rrm1*	FQIVNPHLL	Db 9-mer	71	28
20133	*Rrm1*	YGIRNSLLI	Db 9-mer	452	26
235623	*Scap*	SGYDFSRL	Kb 8-mer	5	30
13722	*Scye1*	SGLVNHVPL	Db 9-mer	59	29
20338	*Sel1l*	QALKYFNL	Kb 8-mer	171	23
20393	*Sgk*	STLTYSRM	Kb 8-mer	38	18
432572	*Specc1*	TSLAFESRL	Kb 9-mer	97	12
20740	*Spna2*	KALINADEL	Db 9-mer	19	31
20815	*Srpk1*	ISGVNGTHI	Db 9-mer	55	28
20443	*St3gal4*	GAVKNLTYF	Db 9-mer	81	30
20848	*Stat3*	ATLVFHNL	Kb 8-mer	23	22

71728	*Stk11ip*	SALRFLNL	Kb 8-mer	23	24
16430	*Stt3a*	AVLSFSTRL	Kb 9-mer	154	13
108143	*Taf9*	SGLKYVNV	Kb 8-mer	45	20
245638	*Tbc1d8b*	TAFRFSEL	Kb 8-mer	23	23
216198	*Tcp11l2*	KATTNIVEM	Db 9-mer	225	27
217353	*Tmc6*	ASYLFRGL	Kb 8-mer	3	29
72759	*Tmem135*	KGFTFSAL	Kb 8-mer	23	22
66074	*Tmem167*	AIFNFQSL	Kb 8-mer	8	22
67878	*Tmem33*	QSIAFISRL	Kb 9-mer	75	13
21916	*Tmod1*	SSIVNKEGL	Db 9-mer	228	30
22057	*Tob1*	ISYLYNKL	Kb 8-mer	4	29
21973	*Top2a*	NSMVLFDHV	Db 9-mer	228	14
21990	*Tph1*	FSLENEVGGL	Db 10-mer	728	28
21990	*Tph1*	WGTIFREL	Kb 8-mer	309	22
12751	*Tpp1*	IQRVNTEFM	Db 9-mer	100	25
100683	*Trrap*	QDPVFQKL	Kb 8-mer	885	22
73710	*Tubb2b*	VNMVPFPRL	Kb 9-mer	252	20
56085	*Ubqln1*	RALSNLESI	Db 9-mer	87	30
224826	*Ubr2*	VAYKFPELL	Kb 9-mer	6	28
59025	*Usp14*	VKYLFTGL	Kb 8-mer	20	27
216825	*Usp22*	FAVVNHQGTL	Db 10-mer	985	31
271564	*Vps13a*	VSIQFYHL	Kb 8-mer	3	22
230895	*Vps13d*	INIHYTQL	Kb 8-mer	39	25
80743	*Vps16*	VSFTYRYL	Kb 8-mer	3	22
77573	*Vps33a*	GSLANHTSI	Db 9-mer	161	27
233405	*Vps33b*	ASLVNADKL	Db 9-mer	25	31
65114	*Vps35*	FSEENHEPL	Db 9-mer	33	27
218035	*Vps41*	IGLAYVNHL	Kb 9-mer	17	13
22375	*Wars*	YTVENAKDII	Db 10-mer	492	26
69544	*Wdr5b*	AALENDKTI	Db 9-mer	56	31
74781	*Wipi2*	SGYKFFSL	Kb 8-mer	14	29
22446	*Xlr3b*	VAAANREVL	Db 9-mer	111	26
68090	*Yif1a*	SGYKYVGM	Kb 8-mer	17	25
66980	*Zdhhc6*	SVIKFENL	Kb 8-mer	44	25

MHC Ib-associated peptides

GeneID	Gene symbol	Peptides	Restriction size	Rankpep
224171	*C330027C09Rik*	AQNDIEHLF	Qa2 9-mer	155
75565	*Ccdc101*	ELLTELHQL	Qa2 9-mer	198
13204	*Dhx15*	TLLNVYHAF	Qa2 9-mer	215
66366	*Ergic3*	QQLDVEHNL	Qa2 9-mer	212
108655	*Foxp1*	QQLQQQHLL	Qa2 9-mer	148
15016	*H2-Q5*	AMAPRTLLL	Qa1 9-mer	
212307	*Mapre2*	QLNEQVHSL	Qa2 9-mer	176
68979	*Nol11*	TQLIQTHVL	Qa2 9-mer	150
69608	*Sec24d*	ESQSVIHNL	Qa2 9-mer	185
319565	*Syne2*	DLIQTIHEL	Qa2 9-mer	213
50875	*Tmod3*	AAILGMHNL	Qa2 9-mer	134

Supplementary Table 5

List of genes coding for MHC I peptides differentially expressed in neoplastic (EL4) versus normal thymocytes and involved in carcinogenesis.

Functional Classification	Gene Symbol	Gene ID	Sequence	p-values	EL4/Thy
Transcription	*Pa2g4* (1-4)	18813	AQFKFTVL	0.018	4.6
	Top2a (5)	21973	NSMVLFDHV	0.020	15.6
	Dnmt1 (6, 7)	13433	LSLENGTHTL	0.022	8.9
	Pfdn5 (8, 9)	56612	SMYVPGKL	0.036	16.6
	Per1 (10, 11)	18626	YTLRNQDTF	0.036	5.0
	Foxp1 (12, 13)	108655	QQLQQQHLL	0.010	-4.3
	Bach2 (14, 15)	12014	EQLEFIHDI	0.015	-20.2
	Ddx5 (16, 17)	13207	NQAINPKLLQL	0.021	-5.7
Cell Differentiation	*Ptpn6* (18, 19)	15170	AQYKFIYV	0.028	3.3
	RhoH (20, 21)	74734	YSVANHNSFL	0.019	-3.1
	Pi3kap1 (22, 23)	83490	YSVANHNSFL	0.001	-21.8
Cell Cycle	*Cdkn1b* (24-26)	12576	FGPVNHEEL	0.003	-3.1
Apoptosis	*Sgk* (27-29)	20393	STLTYSRM	0.022	9.7
	Pdcd10 (30)	56426	ILQTFKTVA	0.001	-4.3
Signal Transduction	*Cxcr4* (31, 32)	12767	VVFQFQHI	0.003	2.6
	CD97 (33, 34)	26364	KLLSNINSVF	0.033	-4.6
Translation	*Eif3s10* (35, 36)	13669	QSIEFSRL	0.015	3.2
	Eif3s2 (35, 36)	54709	FGPINSVAF	0.035	5.3
Miscellaneous	*Dhx15* (37)	13204	TLLNVYHAF	0.017	-11.5
	Gtpbp4 (38)	69237	QILSDFPKL	0.034	2.6
	Igtp (39)	16145	IVAENTKTSL	0.001	-15.5

Supplementary Table 6

Relative abundance of MHC I peptides eluted from primary thymocytes versus in vivo grown EL4

			Average intensities from			
GeneID	Gene symbol	Peptide	EL4	Thymocytes	p-values	EL4/Thy
68295	*0610011L14Rik*	ISILYHQL	810647	1248361	0.10	-1.5
68523	*1110019N10Rik*	AALENTHLL	116372	145359	0.63	-1.2
72368	*2310045N01Rik*	SSVYFRSV	94609	42165	0.09	2.2
75425	*2610036D13Rik*	QTVENVEHL	268223	422026	0.20	-1.6
72722	*2810405J04Rik*	ASPEFTKL	1928424	879573	0.07	2.2
72747	*2810439F02Rik*	SGYDFENRL	55031	123324	0.13	-2.2
67268	*2900073G15Rik*	SMGKNPTDEYL	2911106	762807	0.05	3.8
218989	*6720456H20Rik*	TGIRNLEWL	197157	149305	0.56	1.3
319236	*9230105E10Rik*	FISDVEHQL	12000	278323	0.01	-23.2
11307	*Abcg1*	VNIEFKDL	2074080	1805346	0.54	1.1
66713	*Actr2*	YAGSNFPEHI	2319817	1277449	0.04	1.8
67019	*Actr6*	SGYSFTHI	436804	141915	0.06	3.1
57869	*Adck2*	SGPTYIKL	86469	161672	0.26	-1.9
81702	*Ankrd17*	ASVLNVNHI	5882733	5485733	0.65	1.1
329154	*Ankrd44*	ASVINGHTL	385034	353775	0.79	1.1
54208	*Arl6ip1*	IILKYIGM	246911	127103	0.16	1.9
192195	*Ash1l*	VGLINKDSV	241257	132489	0.28	1.8
Q9JKK8	*Atr*	FQALNAEKL	60707	89418	0.20	-1.5
54138	*Atxn10*	NSIRNLDTI	11787170	22819844	0.03	-1.9
328099	*AU021838*	VSYLFSHV	432991	356073	0.63	1.2
235461	*B230380D07Rik*	VNVRFTGV	54488	74969	0.31	-1.4
12014	*Bach2*	EQLEFIHDI	12000	242371	0.01	-20.2
224727	*Bat3*	SIAAFIQRL	133395	93668	0.45	1.4
66165	*Bccip*	KAPVNTAEL	210648	387950	0.17	-1.8
107976	*Bre*	ATQVYPKL	626010	343031	0.21	1.8
224171	*C330027C09Rik*	AQNDIEHLF	296259	355661	0.61	-1.2
26885	*Casp8ap2*	VTVLNVDHL	112568	295624	0.06	-2.6
75565	*Ccdc101*	ELLTELHQL	109977	377688	0.06	-3.4
76041	*Ccdc125*	NAVLNQRYL	53422	80693	0.05	-1.5
77048	*Ccdc41*	AQVENVQRI	77635	214892	0.005	-2.8
12445	*Ccnd3*	AAVIAHDFL	195002	116726	0.31	1.7
12449	*Ccnf*	SQAVNKQQI	46629	75687	0.48	-1.6
12501	*Cd3e*	YSGLNQRAV	92673	193576	0.05	-2.1
26364	*Cd97*	KLLSNINSVF	177758	812560	0.03	-4.6
12576	*Cdkn1b*	FGPVNHEEL	2765989	8474581	0.003	-3.1
216859	*Centb1*	INQIYEARV	242126	288600	0.58	-1.2
12649	*Chek1*	TGPSNVDKL	5073167	2489307	0.02	2.0
243764	*Chrm2*	TVIGYWPL	57092	112673	0.17	-2.0
70349	*Copb1*	IALRYVAL	579237	197990	0.01	2.9
67876	*Coq10b*	ISFEFRSL	46870	41415	0.74	1.1
71745	*Cul2*	VINSFVHV	163398	55024	0.06	3.0
12767	*Cxcr4*	VVFQFQHI	165482	63047	0.003	2.6
52635	*D12Ertd551e*	RQLENGTTL	405701	580254	0.28	-1.4
218978	*D14Ertd436e*	SQHVNLDQL	274085	752598	0.04	-2.7
69601	*Dab2ip*	VSPTNPTKL	148633	180896	0.52	-1.2
67755	*Ddx47*	KTFLFSATM	76238	60088	0.50	1.3
13207	*Ddx5*	NQAINPKLLQL	20171	115009	0.02	-5.7

13209	*Ddx6*	INFDFPKL	867416	2016311	0.02	-2.3
13204	*Dhx15*	TLLNVYHAF	72069	827769	0.01	-11.5
13433	*Dnmt1*	LSLENGTHTL	1108884	124482	0.02	8.9
94176	*Dock2*	SMVQNRVFL	182029	261777	0.56	-1.4
233115	*Dpy19l3*	SVVAFHNL	114097	81273	0.53	1.4
13424	*Dync1h1*	ASYEFVQRL	2301414	1013239	0.08	2.3
13669	*Eif3s10*	QSIEFSRL	3422637	1081266	0.02	3.2
73830	*Eif3s12*	VGITYQHI	1223275	1317577	0.88	-1.1
54709	*Eif3s2*	FGPINSVAF	63523	12000	0.03	5.3
10436	*Emg1*	VSVEYTEKM	82838	67514	0.30	1.2
13819	*Epas1*	SNYLFTKL	704947	1387353	0.05	-2.0
66366	*Ergic3*	QQLDVEHNL	193740	378788	0.07	-2.0
212377	*F730047E07Rik*	VGVTYRTL	152126	70387	0.12	2.2
107035	*Fbxo38*	SAFSFRTL	270808	192573	0.34	1.4
14137	*Fdft1*	ISLEFRNL	198436	214993	0.81	-1.1
57778	*Fmnl1*	LQYEFTHL	1190978	933913	0.45	1.3
22379	*Fmnl3*	LQYEFTKL	1171553	1937711	0.05	-1.7
108655	*Foxp1*	QQLQQQHLL	518392	2217859	0.01	-4.3
14359	*Fxr1h*	EIVTFERL	336814	132963	0.08	2.5
14790	*Grcc10*	SAPENAVRM	3734208	2535151	0.66	1.5
68153	*Gtf2e2*	SGYKFGVL	972201	381917	0.06	2.5
69237	*Gtpbp4*	QILSDFPKL	1361649	526685	0.03	2.6
15016	*H2-Q5*	AMAPRTLLL	2156626	5661232	0.06	-2.6
15019	*H2-Q8*	FAYEGRDYI	2248785	1616977	0.29	1.4
15201	*Hells*	KVLVFSQM	263746	52922	0.06	5.0
15257	*Hipk1*	SLLTNHVTL	504676	412123	0.63	1.2
319189	*Hist2h2bb*	SVYVYKVL	5932574	2470423	0.02	2.4
98758	*Hnrpf*	FSPLNPVRV	101312	82387	0.49	1.2
16145	*Igtp*	IVAENTKTSL	12000	185606	0.001	-15.5
23918	*Impdh2*	GGIQNVGHI	29380844	17244971	0.01	1.7
16329	*Inpp1*	YMGTNIHSL	37800	259193	0.09	-6.9
76582	*Ipo11*	TIILFTKV	99616	76723	0.41	1.3
338523	*Jhdm1d*	SSIQNGKYTL	182192	886026	0.02	-4.9
110308	*Krt5*	AAYMNKVEL	12000	1280013	0.04	-106.7
110310	*Krt7*	AAYTNKVEL	12000	1458071	0.00	-121.5
72416	*Lrpprc*	AAIENIEHL	159927	163843	0.95	-1.0
26413	*Mapk1*	VGPRYTNL	15419971	25982309	0.02	-1.7
212307	*Mapre2*	QLNEQVHSL	130503	225894	0.28	-1.7
17168	*Mare*	SAVKNLQQL	2084131	2315130	0.64	-1.1
13728	*Mark2*	ASIQNGKDSL	358351	132344	0.03	2.7
217615	*Mgea6*	RNQVYTQL	179246	186263	0.89	-1.0
67014	*Mina*	VVYIYHSL	86825	230698	0.10	-2.7
17427	*Mns1*	KIIEFANI	12000	149382	0.01	-12.4
219135	*Mtmr6*	VGIENIHVM	46307	499479	0.06	-10.8
17886	*Myh9*	RVAEFTTNL	469290	706492	0.28	-1.5
67938	*Mylc2b*	SLGKNPTDAYL	4571127	1100520	0.01	4.2
67608	*Narf*	AAYGFRNI	141414	67434	0.11	2.1
67563	*Narfl*	VAYGFRNI	104022	12000	0.01	8.7
17992	*Ndufa4*	VNVDYSKL	6565000	10705177	0.06	-1.6
227197	*Ndufs1*	AKLVNQEVL	502906	132505	0.07	3.8
18034	*Nfkb2*	AALQNLEQL	275269	482669	0.53	-1.8
64652	*Nisch*	TNQDFIQRL	395004	137997	0.12	2.9

97895	*Nlrp4f*	TPVKNIDTV	44098	40329	0.72	1.1
68979	*Nol11*	TQLIQTHVL	344889	793732	0.04	-2.3
211548	*Nomo1*	SSLVNKEDV	45468	76970	0.07	-1.7
66394	*Nosip*	TSVRFTQL	3233929	3880050	0.30	-1.2
18145	*Npc1*	VAVVNKVDI	337841	629999	0.13	-1.9
101706	*Numa1*	VSILNRQVL	678568	917089	0.33	-1.4
70699	*Nup205*	VNNEFEKL	109609	505624	0.01	-4.6
18813	*Pa2g4*	AQFKFTVL	55142	12000	0.02	4.6
66923	*Pbrm1*	SQVYNDAHI	70006	242803	0.02	-3.5
18538	*Pcna*	RAEDNADTLAL	49024	73938	0.24	-1.5
56426	*Pdcd10*	ILQTFKTVA	71543	309466	0.001	-4.3
207728	*Pde2a*	IKNENQEVI	308207	19230	0.02	16.0
23986	*Peci*	SSYTFPKM	274504	246774	0.82	1.1
18626	*Per1*	YTLRNQDTF	59957	12000	0.04	5.0
56612	*Pfdn5*	SMYVPGKL	199322	12000	0.04	16.6
73739	*Pgea1*	ASLSNLHSL	284222	107706	0.13	2.6
233489	*Picalm*	VAFDFTKV	1026391	970576	0.78	1.1
83490	*Pik3ap1*	YGLKNLTAL	74055	1614342	0.001	-21.8
231329	*Polr2b*	IGPTYYQRL	152006	456565	0.06	-3.0
66385	*Ppp1r7*	RAIENIDTL	1371985	2449039	0.06	-1.8
73699	*Ppp2r1b*	VADKFSEL	123409	43924	0.10	2.8
214572	*Prmt7*	VIVEFRDL	127033	144217	0.65	-1.1
16913	*Psmb8*	GGVVNMYHM	312549	367796	0.77	-1.2
15170	*Ptpn6*	AQYKFIYV	2532589	774524	0.03	3.3
108911	*Rcc2*	AAYRNLGQNL	323760	12000	0.04	27.0
19696	*Rel*	TTLIFQKL	52627	69335	0.46	-1.3
26374	*Rfwd2*	YVVDNIDHL	103204	182323	0.17	-1.8
74734	*Rhoh*	YSVANHNSFL	257883	790683	0.02	-3.1
68477	*Rmnd5a*	WAVSNREML	12000	74507	0.02	-6.2
20054	*Rps15*	VGVYNGKTF	94776	119204	0.32	-1.3
267019	*Rps15a*	VIVRFLTV	561265	225633	0.15	2.5
267019	*Rps15a*	ISPRFDVQL	487134	141860	0.08	3.4
20115	*Rps7*	VNFEFPEF	315064	460959	0.42	-1.5
20133	*Rrm1*	YGIRNSLLI	2099554	1995074	0.76	1.1
20133	*Rrm1*	FQIVNPHLL	8238219	6013528	0.18	1.4
235623	*Scap*	SGYDFSRL	215152	296647	0.35	-1.4
13722	*Scye1*	SGLVNHVPL	121736	137771	0.81	-1.1
69608	*Sec24d*	ESQSVIHNL	154217	185515	0.71	-1.2
20338	*Sel1l*	QALKYFNL	342436	120117	0.06	2.9
20393	*Sgk*	STLTYSRM	301908	67793	0.02	9.7
432572	*Specc1*	TSLAFESRL	84991	12000	0.005	7.1
20740	*Spna2*	KALINADEL	4367025	7898847	0.05	-1.8
20815	*Srpk1*	ISGVNGTHI	1498558	1233136	0.46	1.2
20443	*St3gal4*	GAVKNLTYF	84768	217591	0.12	-2.6
20848	*Stat3*	ATLVFHNL	8702796	6298873	0.13	1.4
71728	*Stk11ip*	SALRFLNL	64125	250911	0.01	-3.9
319565	*Syne2*	DLIQTIHEL	64700	102995	0.25	-1.6
108143	*Taf9*	SGLKYVNV	1888511	964010	0.04	2.0
216198	*Tcp11l2*	KATTNIVEM	39337	92718	0.19	-2.4
217353	*Tmc6*	ASYLFRGL	42599	104982	0.01	-2.5
67511	*Tmed9*	VIGNYRTQL	12000	82097	0.01	-6.8
67878	*Tmem33*	QSIAFISRL	312693	175900	0.23	1.8

21916	*Tmod1*	SSIVNKEGL	676206	64142	0.004	10.5
320938	*Tnpo3*	GLLEIAHSL	12000	40153	0.10	-3.3
22057	*Tob1*	ISYLYNKL	137897	149667	0.87	-1.1
21973	*Top2a*	NSMVLFDHV	187186	12000	0.02	15.6
21990	*Tph1*	WGTIFREL	57225	54992	0.90	1.0
21990	*Tph1*	FSLENEVGGL	614142	228500	0.07	2.7
12751	*Tpp1*	IQRVNTEFM	56506	48388	0.66	1.2
100683	*Trrap*	QDPVFQKL	63687	47544	0.41	1.3
56085	*Ubqln1*	RALSNLESI	402950	278602	0.31	1.4
224826	*Ubr2*	VAYKFPELL	36262	33865	0.62	1.1
216825	*Usp22*	FAVVNHQGTL	264021	179805	0.52	1.5
230895	*Vps13d*	INIHYTQL	81820	133304	0.41	-1.6
80743	*Vps16*	VSFTYRYL	1178420	1298769	0.70	-1.1
77573	*Vps33a*	GSLANHTSI	235063	137938	0.23	1.7
233405	*Vps33b*	ASLVNADKL	1141391	750579	0.41	1.5
65114	*Vps35*	FSEENHEPL	100228	72330	0.36	1.4
22375	*Wars*	YTVENAKDII	164659	97161	0.18	1.7
69544	*Wdr5b*	AALENDKTI	995387	846431	0.64	1.2
74781	*Wipi2*	SGYKFFSL	108304	60742	0.28	1.8
22446	*Xlr3b*	VAAANREVL	1019171	12000	0.02	84.9
68090	*Yif1a*	SGYKYVGM	172942	68389	0.14	2.5
66980	*Zdhhc6*	SVIKFENL	57125	76621	0.59	-1.3

Supplementary Table 7

List of primers for quantitative real-time PCR analyses

.	Ref Seq	Gene ID	Primer_A	Primer_B	Probe
2900073G15RIK	NM_026064	67268	cgcttgctttgatgaggaa	gtcagcagctccctcaggt	Universal ProbeLibrary probe: #79
9230105E10RIK	NM_175677	319236	ggccacaaaacagctctcat	cagcctttgcagaactacctg	Universal ProbeLibrary probe: #68
Atxn10	NM_016843.2	54138	gagcctcacaccgaggataa	tggacgtcatttcacacaaga	Universal ProbeLibrary probe: #92
Bach2	NM_007521	12014	catctcttcctctgcccagt	agacatgccgttcaaaccat	Universal ProbeLibrary probe: #89
Ccnd3	NM_007632.2	12445	gcatactggatgctggaggt	ggtagcgatccaggtagttca	Universal ProbeLibrary probe: #88
Ccnf	NM_007634.2	12449	cggaaacacagggactacg	tccacctgcacaggcttt	Universal ProbeLibrary probe: #3
Cd97	NM_011925	26364	atccagccacggtcaactac	ttgttgggtttgagtctccat	Universal ProbeLibrary probe: #11
Cdkn1b	NM_009875	12576	gagcagtgtccagggatgag	tctgttggccctttgtttt	Universal ProbeLibrary probe: #62
Chek1	NM_007691.2	12649	gagggaaggccatatccagt	ttgttcaggcatccctatgtc	Universal ProbeLibrary probe: #25
Copb1	NM_033370.3	70349	ccgcttggtggaattaaaag	ggatgtccatgaccagatcc	Universal ProbeLibrary probe: #15
Cxcr4	NM_009911.3	12767	tggaaccgatcagtgtgagt	gggcaggaagatcctattga	Universal ProbeLibrary probe: #38
Ddx47	NM_026360	67755	tgggaaggccattacttttg	agcttctttccaatcaagtgct	Universal ProbeLibrary probe: #11
Ddx5	NM_007840	13207	agaggtgatgggcctatttg	caagcgacaagctcgaca	Universal ProbeLibrary probe: #66
Ddx6	NM_007841.3	13209	caaaaagtgcactgcctcaa	ggagttgcagaaaatgatgga	Universal ProbeLibrary probe: #80
Dhx15	NM_007839.2	13204	tcggacagtgatccaaatacat	caggcctcatcaatttcctc	Universal ProbeLibrary probe: #12
Dnmt1	NM_010066.3	13433	ctcattggcttctccactgc	gcccaaatattggctcatactc	Universal ProbeLibrary probe: #107
Eif3s10	NM_010123	13669	gattcagaaggcacctggag	catcccgagtttctcgtctc	Universal ProbeLibrary probe: #93
Eif3s12	NM_028659	73830	gctcaagggtatcgacaggt	tttggcttgtgtctccacat	Universal ProbeLibrary probe: #1
Eif3s2	NM_018799	54709	gaagccatggatgtgacca	tcaaaagccaaatggaagaac	Universal ProbeLibrary probe: #22
Gtpbp4	NM_027000.2	69237	tgggagatgattacattttgga	gccttcccaaatttctggtat	Universal ProbeLibrary probe: #95
Igtp	NM_018738	16145	cggagagctgtggagagaga	tgccatgtttatgaaaagtgtaaaa	Universal ProbeLibrary probe: #108
Krt5	NM_027011.2	110308	ccttcgaaacaccaagcac	gttctggaggttggcacact	Universal ProbeLibrary probe: #110
Krt7	NM_033073	110310	ggagatggccaaccacag	ggcctggagtgtctcaaactt	Universal ProbeLibrary probe: #41
Mapk1	NM_011949.3	26413	gacagagtacgtagccacacgtt	agcccacagaccaaatatcaa	Universal ProbeLibrary probe: #50
Mark2	NM_007928.2	13728	gaaagggacacggagcag	agcagaggtggctgagttg	Universal ProbeLibrary probe: #3
Mns1	NM_008613	17427	gaggcagagacccatcctg	gctcaaagctctcttttggtc	Universal ProbeLibrary probe: #63
Mylc2b	NM_023402	67938	aggaggacctgcacgaca	gtccaggtaggcatcagtgg	Universal ProbeLibrary probe: #60
Narf1	NM_026238	67563	gcagttacttccaagtgaaccaa	gcagtcattcagggagacct	Universal ProbeLibrary probe: #78
Pa2g4	NM_011119	18813	ggtcgtgaccaagtataagatgg	cagacacacctgagctggaa	Universal ProbeLibrary probe: #22
Pcna	NM_011045.2	18538	ctagccatgggcgtgaac	gaatactagtgctaaggtgtctgcat	Universal ProbeLibrary probe: #41
Pdcd10	NM_019745.2	56426	tggcagctgatgacgtagaa	tgccttttcatttaggtcctg	Universal ProbeLibrary probe: #21
Pde2a	NM_001008548	207728	tcggacctactgggaaagc	caggggtatgaccagcactt	Universal ProbeLibrary probe: #64
Per1	NM_011065	18626	tggacttgacacctcttctgtg	tgctttagatcggcagtggt	Universal ProbeLibrary probe: #71
Pfdn5	NM_027044	56612	aggagaagcatgccatgaag	agtgcactctcaggctttgac	Universal ProbeLibrary probe: #100
Pik3ap1	NM_031376	83490	cacggtctctgtgaaagcac	ccaggtccccagaatagacc	Universal ProbeLibrary probe: #91
Psmb8	NM_010724	16913	gttggccaaggagtgcag	cagcatcatgttggaaagca	Universal ProbeLibrary probe: #89
Ptpn6	NM_013545.2	15170	tctggatgccacagtcaatg	ggccagtatgggacacattt	Universal ProbeLibrary probe: #51
Rcc2	NM_173867	108911	ctatcagttggggtccatcg	agaagatgccatccagagtctt	Universal ProbeLibrary probe: #79
Rmnd5a	NM_024288	68477	ttcttccgacaaggaatgct	ttgggtctacagacagaccaga	Universal ProbeLibrary probe: #73
Specc1	NM_001029936.2	432572	aaatgccaggctgcagaa	ctctggctcttcattcacagg	Universal ProbeLibrary probe: #33
Stat3	NM_213659.2	20848	agtctcgcctcctccagac	gctgcttctctgtcactacgg	Universal ProbeLibrary probe: #26
Stk11ip	NM_027886.2	71728	ggtgccccagtttttctacc	aacagggacacaggacaggt	Universal ProbeLibrary probe: #41
Tmed9	NM_026211	67511	taaaagaccccgaggacaag	tgtgggaggtgaaggtgaac	Universal ProbeLibrary probe: #21
Tmod1	NM_021883	21916	ctggtcgagctgaaaatcg	tctccatttccactttgttgc	Universal ProbeLibrary probe: #21
Top2a	NM_011623	21973	aatggaaatatgctgccagtg	cctgttcatgtatcaccttcagtg	Universal ProbeLibrary probe: #48
Tpp1	NM_009906.2	12751	cggatcctagctctcctcaa	gtcaggggtgatggttgaa	Universal ProbeLibrary probe: #88
Ubr2	NM_146078.2	224826	cagcagctctgaagttgtgg	tgtaagttctggcgatcacatc	Universal ProbeLibrary probe: #101

3.10 Supplementary References (see supplementary table 5)

1. Squatrito, M., M. Mancino, M. Donzelli, L.B. Areces, and G.F. Draetta. 2004. EBP1 is a nucleolar growth-regulating protein that is part of pre-ribosomal ribonucleoprotein complexes. *Oncogene*. 23:4454-4465.

2. Zhang, Y., X.W. Wang, D. Jelovac, T. Nakanishi, M.H. Yu, D. Akinmade, O. Goloubeva, D.D. Ross, A. Brodie, and A.W. Hamburger. 2005. The ErbB3-binding protein Ebp1 suppresses androgen receptor-mediated gene transcription and tumorigenesis of prostate cancer cells. *Proc. Natl. Acad. Sci. USA*. 102:9890-9895.

3. Ahn, J.Y., X. Liu, Z. Liu, L. Pereira, D. Cheng, J. Peng, P.A. Wade, A.W. Hamburger, and K. Ye. 2006. Nuclear Akt associates with PKC-phosphorylated Ebp1, preventing DNA fragmentation by inhibition of caspase-activated DNase. *EMBO J.* 25:2083-2095.

4. Liu, Z., J.Y. Ahn, X. Liu, and K. Ye. 2006. Ebp1 isoforms distinctively regulate cell survival and differentiation. *Proc. Natl. Acad. Sci. USA*. 103:10917-10922.

5. Murphy, A.J., C.A. Hughes, C. Barrett, H. Magee, B. Loftus, J.J. O'Leary, and O. Sheils. 2007. Low-level TOP2A amplification in prostate cancer is associated with HER2 duplication, androgen resistance, and decreased survival. *Cancer Res*. 67:2893-2898.

6. Brown, K.D., and K.D. Robertson. 2007. DNMT1 knockout delivers a strong blow to genome stability and cell viability. *Nat. Genet*. 39:289-290.

7. Rhee, I., K.E. Bachman, B.H. Park, K.W. Jair, R.W. Yen, K.E. Schuebel, H. Cui, A.P. Feinberg, C. Lengauer, K.W. Kinzler, S.B. Baylin, and B. Vogelstein. 2002. DNMT1 and DNMT3b cooperate to silence genes in human cancer cells. *Nature*. 416:552-556.

8. Fujioka, Y., T. Taira, Y. Maeda, S. Tanaka, H. Nishihara, S.M. Iguchi-Ariga, K. Nagashima, and H. Ariga. 2001. MM-1, a c-Myc-binding protein, is a candidate for a tumor suppressor in leukemia/lymphoma and tongue cancer. *J. Biol. Chem*. 276:45137-45144.

9. Hoffman, B., A. Amanullah, M. Shafarenko, and D.A. Liebermann. 2002. The proto-oncogene c-myc in hematopoietic development and leukemogenesis. *Oncogene*. 21:3414-3421.

10. Chen, S.T., K.B. Choo, M.F. Hou, K.T. Yeh, S.J. Kuo, and J.G. Chang. 2005. Deregulated expression of the PER1, PER2 and PER3 genes in breast cancers. *Carcinogenesis*. 26:1241-1246.

11. Gery, S., N. Komatsu, N. Kawamata, C.W. Miller, J. Desmond, R.K. Virk, A. Marchevsky, R. McKenna, H. Taguchi, and H.P. Koeffler. 2007. Epigenetic silencing of the candidate tumor suppressor gene Per1 in non-small cell lung cancer. *Clin*. *Cancer Res*. 13:1399-1404.

12. Banham, A.H., N. Beasley, E. Campo, P.L. Fernandez, C. Fidler, K. Gatter, M. Jones, D.Y. Mason, J.E. Prime, P. Trougouboff, K. Wood, and J.L. Cordell. 2001. The FOXP1 winged helix transcription factor is a novel candidate tumor suppressor gene on chromosome 3p. *Cancer Res*. 61:8820-8829.

13. Wlodarska, I., E. Veyt, P. De Paepe, P. Vandenberghe, P. Nooijen, I. Theate, L. Michaux, X. Sagaert, P. Marynen, A. Hagemeijer, and C. De Wolf-Peeters. 2005. FOXP1, a gene highly expressed in a subset of diffuse large B-cell lymphoma, is recurrently targeted by genomic aberrations. *Leukemia*. 19:1299-1305.

14. Gutierrez, N.C., E.M. Ocio, J. de Las Rivas, P. Maiso, M. Delgado, E. Ferminan, M.J. Arcos, M.L. Sanchez, J.M. Hernandez, and J.F. San Miguel. 2007. Gene expression profiling of B lymphocytes and plasma cells from Waldenstrom's macroglobulinemia: comparison with expression patterns of the same cell counterparts from chronic lymphocytic leukemia, multiple myeloma and normal individuals. *Leukemia*. 21:541-549.

15. Yoshida, C., F. Yoshida, D.E. Sears, S.M. Hart, D. Ikebe, A. Muto, S. Basu, K. Igarashi, and J.V. Melo. 2007. Bcr-Abl signaling through the PI-3/S6 kinase pathway inhibits nuclear translocation of the transcription factor Bach2, which represses the antiapoptotic factor heme oxygenase-1. *Blood*. 109:1211-1219.

16. Causevic, M., R.G. Hislop, N.M. Kernohan, F.A. Carey, R.A. Kay, R.J. Steele, and F.V. Fuller-Pace. 2001. Overexpression and poly-ubiquitylation of the DEAD-box RNA helicase p68 in colorectal tumours. *Oncogene*. 20:7734-7743.

17. Yang, L., C. Lin, and Z.R. Liu. 2005. Phosphorylations of DEAD box p68 RNA helicase are associated with cancer development and cell proliferation. *Mol*. *Cancer Res*. 3:355-363.

18. Cuevas, B., Y. Lu, S. Watt, R. Kumar, J. Zhang, K.A. Siminovitch, and G.B. Mills. 1999. SHP-1 regulates Lck-induced phosphatidylinositol 3-kinase phosphorylation and activity. *J*. *Biol*. *Chem*. 274:27583-27589.

19. Zhang, Q., H.Y. Wang, M. Marzec, P.N. Raghunath, T. Nagasawa, and M.A. Wasik. 2005. STAT3- and DNA methyltransferase 1-mediated epigenetic silencing of SHP-1 tyrosine phosphatase tumor suppressor gene in malignant T lymphocytes. *Proc*. *Natl*. *Acad*. *Sci*. *USA*. 102:6948-6953.

20. Duquette, M.L., M.D. Huber, and N. Maizels. 2007. G-rich proto-oncogenes are targeted for genomic instability in B-cell lymphomas. *Cancer Res*. 67:2586-2594.

21. Pasqualucci, L., P. Neumeister, T. Goossens, G. Nanjangud, R.S. Chaganti, R. Kuppers, and R. Dalla-Favera. 2001. Hypermutation of multiple proto-oncogenes in B-cell diffuse large-cell lymphomas. *Nature*. 412:341-346.

22. Okada, T., A. Maeda, A. Iwamatsu, K. Gotoh, and T. Kurosaki. 2000. BCAP: the tyrosine kinase substrate that connects B cell receptor to phosphoinositide 3-kinase activation. *Immunity*. 13:817-827.

23. Yamazaki, T., K. Takeda, K. Gotoh, H. Takeshima, S. Akira, and T. Kurosaki. 2002. Essential immunoregulatory role for BCAP in B cell development and function. *J. Exp. Med*. 195:535-545.

24. Chien, W.M., S. Rabin, E. Macias, P.L. Miliani de Marval, K. Garrison, J. Orthel, M. Rodriguez-Puebla, and M.L. Fero. 2006. Genetic mosaics reveal both cell-autonomous and cell-nonautonomous function of murine p27Kip1. *Proc. Natl. Acad. Sci. USA*. 103:4122-4127.

25. Fu, Y., Z. Fang, Y. Liang, X. Zhu, P. Prins, Z. Li, L. Wang, L. Sun, J. Jin, Y. Yang, and X. Zha. 2007. Overexpression of integrin beta1 inhibits proliferation of hepatocellular carcinoma cell SMMC-7721 through preventing Skp2-dependent degradation of p27 via PI3K pathway. *J. Cell. Biochem*.

26. Nakayama, K.I., and K. Nakayama. 2006. Ubiquitin ligases: cell-cycle control and cancer. *Nat. Rev. Cancer*. 6:369-381.

27. Buse, P., S.H. Tran, E. Luther, P.T. Phu, G.W. Aponte, and G.L. Firestone. 1999. Cell cycle and hormonal control of nuclear-cytoplasmic localization of the serum- and glucocorticoid-inducible protein kinase, Sgk, in mammary tumor cells. A novel convergence point of anti-proliferative and proliferative cell signaling pathways. *J. Biol. Chem*. 274:7253-7263.

28. Sakoda, H., Y. Gotoh, H. Katagiri, M. Kurokawa, H. Ono, Y. Onishi, M. Anai, T. Ogihara, M. Fujishiro, Y. Fukushima, M. Abe, N. Shojima, M. Kikuchi, Y. Oka, H. Hirai, and T. Asano. 2003. Differing roles of Akt and serum- and glucocorticoid-regulated kinase in glucose metabolism, DNA synthesis, and oncogenic activity. *J. Biol. Chem*. 278:25802-25807.

29. Tessier, M., and J.R. Woodgett. 2006. Serum and glucocorticoid-regulated protein kinases: variations on a theme. *J. Cell. Biochem*. 98:1391-1407.

30. Chen, P.Y., W.S. Chang, R.H. Chou, Y.K. Lai, S.C. Lin, C.Y. Chi, and C.W. Wu. 2007. Two non-homologous brain diseases-related genes, SERPINI1 and PDCD10, are tightly linked by an asymmetric bidirectional promoter in an evolutionarily conserved manner. *BMC Mol. Biol*. 8:2.

31. Spoo, A.C., M. Lubbert, W.G. Wierda, and J.A. Burger. 2007. CXCR4 is a prognostic marker in acute myelogenous leukemia. *Blood*. 109:786-791.

32. Tavor, S., I. Petit, S. Porozov, A. Avigdor, A. Dar, L. Leider-Trejo, N. Shemtov, V. Deutsch, E. Naparstek, A. Nagler, and T. Lapidot. 2004. CXCR4 regulates migration and development of human acute myelogenous leukemia stem cells in transplanted NOD/SCID mice. *Cancer Res*. 64:2817-2824.

33. Aust, G., W. Eichler, S. Laue, I. Lehmann, N.E. Heldin, O. Lotz, W.A. Scherbaum, H. Dralle, and C. Hoang-Vu. 1997. CD97: a dedifferentiation marker in human thyroid carcinomas. *Cancer Res*. 57:1798-1806.

34. Wobus, M., O. Huber, J. Hamann, and G. Aust. 2006. CD97 overexpression in tumor cells at the invasion front in colorectal cancer (CC) is independently regulated of the canonical Wnt pathway. *Mol*. *Carcinog*. 45:881-886.

35. Dong, Z., and J.T. Zhang. 2006. Initiation factor eIF3 and regulation of mRNA translation, cell growth, and cancer. *Crit*. *Rev*. *Oncol*. *Hematol*. 59:169-180.

36. Zhang, L., X. Pan, and J.W. Hershey. 2007. Individual overexpression of five subunits of human translation initiation factor eIF3 promotes malignant transformation of immortal fibroblast cells. *J*. *Biol*. *Chem*. 282:5790-5800.

37. Nakagawa, Y., A. Yoshida, K. Numoto, T. Kunisada, D. Wai, N. Ohata, K. Takeda, A. Kawai, and T. Ozaki. 2006. Chromosomal imbalances in malignant peripheral nerve sheath tumor detected by metaphase and microarray comparative genomic hybridization. *Oncol*. *Rep*. 15:297-303.

38. Lee, H., D. Kim, H.C. Dan, E.L. Wu, T.M. Gritsko, C. Cao, S.V. Nicosia, E.A. Golemis, W. Liu, D. Coppola, S.S. Brem, J.R. Testa, and J.Q. Cheng. 2007. Identification and characterization of putative tumor suppressor NGB, a GTP-binding protein that interacts with the neurofibromatosis 2 protein. *Mol*. *Cell*. *Biol*. 27:2103-2119.

39. Zhang, H.M., J. Yuan, P. Cheung, H. Luo, B. Yanagawa, D. Chau, N. Stephan-Tozy, B.W. Wong, J. Zhang, J.E. Wilson, B.M. McManus, and D. Yang. 2003. Overexpression of interferon-gamma-inducible GTPase inhibits coxsackievirus B3-induced apoptosis through the activation of the phosphatidylinositol 3-kinase/Akt pathway and inhibition of viral replication. *J*. *Biol*. *Chem*. 278:33011-33019.

CHAPITRE 4

MISE EN SITUATION:

Dans le chapitre précédent, nous avons développé une nouvelle approche à haut débit par spectrométrie de masse pour définir la nature et l'abondance relative des peptides présentés par les molécules du CMH I.

Dans ce présent chapitre, nous avons étudié la plasticité de l'immunopeptidome. Nous nous sommes donc posé la question suivante : la composition de l'immunopeptidome est-elle modulable dans le temps? Pour répondre à cette question, nous avons perturbé le métabolisme cellulaire en ciblant la voie de signalisation mTOR par la rapamycine. Suivant le traitement des cellules à la rapamycine, nous avons quantifié les changements dans l'immunopeptidome à travers le temps. Dans cette étude, nous montrons que l'immunopeptidome est plastique en fonction de l'activité métabolique de la cellule. De plus, nous apportons pour la première fois des évidences au niveau des systèmes que l'immunopeptidome projète à la surface cellulaire une représentation de réseaux biochimiques et d'événements métaboliques régulés à plusieurs niveaux à l'intérieur de la cellule. Nos résultats ouvrent de nouveaux horizons en immunologie et en biologie des systèmes. En effet, prédire les variations de l'immunopeptidome en réponse à différents facteurs intrinsèques et extrinsèques pourrait être fort utile pour la conception de nouvelles stratégies immunothérapeutiques.

4. ARTICLE 3:

The MHC I immunopeptidome conveys to the cell surface an integrative view of cellular regulation

Etienne Caron[1,2]*, Krystel Vincent[1]*, Marie-Hélène Fortier[1,3]*, Jean-Philippe Laverdure[1], Alexandre Bramoullé[1], Marie-Pierre Hardy[1], Grégory Voisin[1], Philippe P. Roux[1,4], Sébastien Lemieux[1,5], Pierre Thibault[1,3†], Claude Perreault[1,2†]

Institute for Research in Immunology and Cancer (IRIC), Université de Montréal, Montreal, Canada[1], Department of Medicine, Faculty of Medicine, Université de Montréal, Montreal, Quebec, Canada[2], Department of Chemistry, Université de Montréal, Montreal, Quebec, Canada[3], Department of Pathology and Cell biology, Faculty of Medicine, Université de Montréal, Montreal, Quebec, Canada[4], Department of Computer Science and Operations Research, Faculty of Arts and Sciences, Université de Montréal, Montreal, Quebec, Canada[5]

*These authors contributed equally to this work.
[†]Corresponding authors

Manuscript information: Abstract: 175 words
Total length: 54 246 characters (incl. spaces)
Materials and Methods: 1 656 words
Introduction, Results and Discussion section: 3 452 words

*Corresponding authors:

Dr. Claude Perreault
Dr. Pierre Thibault

Article soumis à: **Molecular Systems Biology (en révision)**.

CONTRIBUTIONS DES AUTEURS:

Etienne Caron a participé à la conception du projet, à l'analyse des données, aux figures 1, 2, 3, 4, 5 et 6, et à l'écriture de la première version du manuscrit. Marie-Hélène Fortier a effectué les expériences en spectrométrie de masse. Krystel Vincent a effectué les expériences menant aux figures 1 et 7. Jean-Philippe Laverdure, Alexandre Bramoullé, Grégory Voisin et Sébastien Lemieux ont effectué des analyses bioinformatiques. Marie-Pierre Hardy a participé à la figure 7. Philippe Roux a analysé les résultats et commenté le manuscrit. Pierre Thibault et Claude Perreault ont analysé les résultats et participé à l'écriture du manuscrit.

4.1 Abstract

Self/non-self discrimination is a fundamental requirement of life. Endogenous peptides presented by major histocompatibility complex class I (MHC I) molecules represent the essence of self for CD8 T lymphocytes. These MHC I peptides (MIPs) are collectively referred to as the immunopeptidome. Very little is known about the origin, composition and plasticity of the immunopeptidome. Here, we show that the immunopeptidome, and therefore the nature of the immune self, is plastic and moulded by cellular metabolic activity. By using a quantitative high throughput mass spectrometry-based approach, we found that altering cellular metabolism via the inhibition of the mammalian target of rapamycin (mTOR) results in dynamic changes in the cell surface MIPs landscape. Moreover, we provide systems-level evidence that the immunopeptidome projects at the cell surface a faithful representation of biochemical networks and metabolic events regulated at multiple levels inside the cell. Our findings open up new perspectives in systems immunology and predictive biology. Indeed, predicting variations in the immunopeptidome in response to cell-intrinsic and -extrinsic factors could be relevant to the rational design of immunotherapeutic interventions.

4.2 Introduction

While unicellular eukaryotes primarily employ self/nonself discrimination to avoid self-mating, multicellular organisms use self/nonself discrimination primarily in immune defence (Boehm, 2006). Failure to respond to non-self can lead to death from infection whereas untoward response to self paves the way to autoimmunity. Peptides presented by major histocompatibility complex class I (MHC I) molecules represent the essence of self for CD8 T lymphocytes (Klein *et al.*, 2009; Rammensee *et al.*, 1993). These MHC I-associated peptides (MIPs) regulate all key events that occur during the lifetime of CD8 T cells in the thymus and the periphery (Goldrath and Bevan, 1999; Klein *et al.*, 2009). MIPs are presented at the surface of most nucleated cells in jawed vertebrates and are collectively referred to as the MHC I immunopeptidome (Istrail *et al.*, 2004).

Classic reductionist approaches have established the broad outlines of the MIP processing system and shown that MIPs derive from proteasomal degradation of endogenous proteins (Yewdell *et al.*, 2003). In-depth mechanistic understanding of the immunopeptidome biogenesis would allow prediction of its molecular composition and would therefore be highly relevant to the development of immunotherapies (Sette and Rappuoli, 2010; Zarling *et al.*, 2006). Therefore, high throughput technologies and integrative approaches have recently been used in order to elucidate the mechanisms that mould the immunopeptidome (Perreault, 2010). Such systematic studies have revealed that 1) the immunopeptidome derives from degradation of proteins found in all cell compartments (Hickman *et al.*, 2004; Sette *et al.*, 2010; Zarling *et al.*, 2006); 2) changes in MIP abundance cannot be predicted from the expression of their source mRNA (Weinzierl *et al.*, 2007); and 3) the immunopeptidome is not a random sample of the proteome: many abundant proteins do not generate MIPs, while some low-abundance proteins generate large amounts of MIPs (Milner *et al.*, 2006). Therefore, despite its tremendous importance, we still know very little about the genesis and molecular composition of the immunopeptidome.

A key unresolved question is whether the immunopeptidome of a particular cell is plastic and affected by its metabolic state. This issue is of fundamental importance

because cells targeted by CD8 T lymphocytes (i.e., infected and neoplastic cells) are metabolically perturbed by intracellular parasite/viruses or various transforming events. We addressed this question by studying the immunopeptidome of a mouse lymphoma cell line (EL4) treated with the classic mTOR inhibitor, rapamycin. We selected this model because rapamycin is an exquisitely specific inhibitor of the serine/threonine kinase mTOR, and because mTOR is a central regulator of cellular homeostasis through its involvement in promoting anabolic and inhibiting catabolic processes (Sengupta *et al.*, 2010). Furthermore, mTOR signaling is regulated in numerous physiological and pathological conditions in all cell types, including neoplastic and immune cells (Chapitre 5) (Araki *et al.*, 2009; Sengupta *et al.*, 2010).

4.3 Results

The effect of rapamycin on mTOR signaling in EL4 cells

As a prelude to our peptidomic studies, we first assessed the effects of rapamycin on EL4 cells. The first mTOR complex, mTORC1, phosphorylates both S6K1 and 4E-BP1 (Dowling *et al.*, 2010). Recent studies have shown that rapamycin, previously thought to completely inhibit mTORC1 activity, differentially affects 4E-BP1 and S6K1 (Choo and Blenis, 2009; Choo *et al.*, 2008; Thoreen *et al.*, 2009). While rapamycin treatment completely and sustainably inhibits S6K1 activation, it partly and variably inhibits 4E-BP1 phosphorylation (Choo *et al.*, 2008). To evaluate how rapamycin affected mTORC1 signaling in EL4 cells, we treated EL4 cells with rapamycin for different time durations up to 48h. As expected, Thr-389 on S6K1 was fully dephosphorylated upon rapamycin treatment, correlating with a decrease in cell size (Figure 1A and B). In contrast, Ser-65 and Thr-37/46 on 4E-BP1 were partially dephosphorylated by rapamycin (Figure 1A). As previously reported, we also noted that abundance of 4E-BP1 was decreased after 24h of rapamycin treatment (Figure 1A) (Dilling *et al.*, 2002). Because 4E-BP1 is critically involved in cap-dependant translation via regulation of eIF4E, these results suggested that translation was maintained in EL4 cells in the presence of rapamycin. Accordingly, we observed that protein synthesis decreased during the first 12h of rapamycin treatment, but progressively recovered thereafter (Figure 1C). Prolonged rapamycin treatment for up to 24h has also been shown to inhibit the assembly of mTORC2, the second mTOR complex (Sarbassov *et al.*, 2006). Here, we observed that mTORC2-mediated phosphorylation of AKT at Ser-473 was transiently decreased but recovered and was increased after treatment for 48h. Thus, rapamycin treatment for 48h inhibited mTORC1, but activated mTORC2 in EL4 cells. Collectively, these results showed that rapamycin-mediated mTORC1 inhibition perturbed protein synthesis and cell size by differentially inhibiting S6K1 and 4E-BP1 in EL4 cells (Figure 1D). Of direct relevance to our analyses of the MIP landscape, rapamycin treatment did not affect expression levels of key proteins involved in the MHC I antigen processing and presentation pathway (Supplementary Figure 1).

High throughput mass spectrometry (MS)-based studies unveil the plasticity of the immunopeptidome

The plasticity of the immunopeptidome can only be estimated by systems-level analyses (Benoist *et al.*, 2006; Germain *et al.*, 2011), and MS with high accuracy analyzers is the most comprehensive and versatile tool in large-scale proteomics (Yates *et al.*, 2009). We therefore used a high throughput mass spectrometry-based approach (de Verteuil *et al.*, 2010; Fortier *et al.*, 2008) to profile in a time-sequential manner the abundance of MIPs presented by EL4 cells exposed to rapamycin for up to 48h (Figure 2A). This resulted in identification and quantification of the relative abundance of 422 unique MIPs associated to different MHC I allelic products (Figure 2B and Supplementary Table 1). The salient finding was that the abundance of most peptides presented by classical MHC Ia molecules ($H2D^b$ and $H2K^b$) increased over time after 12h to 48h of rapamycin treatment (Figure 2B). In contrast, the abundance of most peptides associated to non-classical MHC Ib molecules (Qa1 and Qa2) was not augmented after treatment with rapamycin for 48h. Accordingly, exposure to rapamycin led to an increase in cell surface levels of $H2D^b$ and $H2K^b$ but not Qa1 and Qa2 (Supplementary Figure 2B). Clustering analysis of the time-series data sets revealed that the abundance of numerous MIPs increased progressively in response to rapamycin (Supplementary Figure 2A). In general, the dynamic range of this response was modest with a median fold-change in MIP abundance of 2.1 relative to untreated cells (calculated from Supplementary Table 1). Nonetheless, a subset of 222 MIPs showed fold-changes between 2 to 15, including 6 MIPs detected exclusively on rapamycin-treated cells (Supplementary Table 1). Perturbation of cellular metabolic activity with rapamycin therefore unveiled the plasticity of the immunopeptidome, by increasing both the abundance and the diversity of MIPs at the cell surface in a time-dependent manner.

mTOR inhibition induces functionally coherent changes in the transcriptome and the immunopeptidome

Whether the immunopeptidome accurately projects intracellular metabolic changes to the cell surface is a fundamental question that has not been addressed yet. More precisely, we asked herein whether variations in the immunopeptidome specifically reflected perturbations of rapamycin-sensitive metabolic processes regulated at the transcript level.

To address this question, we first define the impact of rapamycin on the transcriptome of EL4 cells. Using NimbleGen MM8 385K microarrays, we compared the transcriptome of untreated EL4 cells to that of EL4 cells treated with rapamycin for 48h. A total of 1353 differentially expressed transcripts were identified (fold change > 2.0; $P < 0.05$), which represents about 3% of transcripts in EL4 cells (Figure 3A). Among these, 903 and 450 mRNAs were under- and overexpressed, respectively. Analysis of Gene Ontology (GO) annotations revealed that 101 and 70 genes (Figure 3C and Supplementary Figure 3B and C) coding for under- and overexpressed mRNAs were associated to 7 and 8 (Figure 3D) significantly enriched cellular processes, respectively ($P < 0.05$) (Supplementary Table 2). These genes are hereafter referred to as differentially expressed genes (DEGs). We next performed a GO term analysis on 98 unique source genes coding for the most differentially expressed MIPs (DEMs) [fold change > 2.5; $P < 0.05$: as described in (Fortier *et al.*, 2008)] (Figure 3B and Supplementary Table 1). We found a significant ($P < 0.05$) enrichment for 6 cellular processes (Figure 3D) implicating 38 DEM source genes (Figure 3C, Supplementary Figure 3A and Supplementary Table 2). Analysis of DEGs and DEM source genes involved in enriched cellular processes yielded several findings. First, there was no overlap between DEGs and DEM source genes (Figure 3C). In other words, DEMs did not originate from DEGs. Second, cross-comparison of the overrepresented functional groups identified four distinct cellular processes (protein transport, cell cycle/proliferation, DNA replication, and transcription), that were enriched in both DEGs and DEM source genes (Figure 3D). In order to determine whether this result implies a significant functional relationship between transcriptome and immunopeptidome variations, we developed an all-pairs-shortest-path matrix, which scores the functional connectivity between two lists of genes (Figure 4A). Using this matrix, we first calculated a connectivity score between the 171 DEGs and the 38 DEM source genes identified above. We then calculated control connectivity scores from 10^5 sets of 38 randomly selected MIP source genes from a database of 891 unique source genes encoding $H2^b$-associated peptides (Supplementary Table 3). These analyses revealed that the 38 DEM source genes were tightly interconnected to the 171 DEGs (bootstrapping, $P = 0.004$) (Figure 4B). Hence, though DEGs and DEM sources genes are different, their functions are tightly connected. In other words, this systems-level analysis demonstrates that rapamycin-mediated mTOR inhibition induces functionally coherent changes in the

transcriptome and the immunopeptidome. Thus, the immunopeptidome projects at the cell surface a faithful representation of intracellular metabolic processes regulated at the transcript level. Given the tremendous complexity of the transcriptome, this finding suggests that the immunopeptidome of the cell is more complex than anticipated and that its plasticity might be extensive.

DEMs arise from biochemical networks specifically connected to mTOR

To explore whether the plasticity of the immunopeptidome originates from specific intracellular biochemical networks, we conducted an analysis on the 98 DEM source genes (Figure 3B and Supplementary Table 1) using the interaction network database STITCH (Kuhn *et al.*, 2010). This analysis uncovered a network containing 30 DEM source genes that were interconnected and organized within discrete functional modules (Supplementary Figure 4). Strikingly, the network included the chemicals rapamycin and everolimus (rapamycin analog) in addition to components (e.g.: Rictor, Sgk1) and modules (e.g.: mTOR signaling, translation, lipid biosynthesis) known to be regulated by mTOR (Chapitre 5). Therefore, we reasoned that specific changes in the immunopeptidome might selectively reflect a rapamycin-regulatory network whose components were likely to participate into intracellular processes governed by mTOR. To systematically evaluate this assumption, we measured the connectivity score between the 30 DEM source genes and components extracted from a comprehensive map of the mTOR interactome and signaling network [Supplementary Table 4 based on (Chapitre 5)]. By using the all-pair-shortest-path matrix described above, we calculated that the 30 DEM source genes were highly interconnected to the mTOR network components relative to random assignments (bootstrapping, $P < 10^{-5}$) (Figure 4C). Thus, this systems-level analysis demonstrates that rapamycin-induced variations in the immunopeptidome arise from biochemical networks specifically connected to the target of rapamycin (i.e. mTOR).

To gain deeper insights about the origin of rapamycin-induced variations in the immunopeptidome, we integrated in a global network the mTOR interactome and signaling network [Supplementary Table 4 based on (Chapitre 5)], the 98 DEM source genes (Figure 3B and Supplementary Table 1), and the 171 DEGs (Figure 3C and Supplementary Figure 3B and C). We found that 33 DEM source genes were constituents

of 7 discrete functional subnetworks (Figure 5A). All modules included components of the mTOR network. Integration of microarray data revealed that DEGs were found in 5 out of the 7 modules containing DEM source genes. Notably, two modules contained DEM source genes but no DEGs: the proteasome and the core mTOR signaling modules. Overall, 82% of the DEM source genes (27 of 33) were localized within subnetworks transcriptionally regulated by DEGs. These data indicate that rapamycin-induced variations in the immunopeptidome arise from biochemical networks specifically connected to the target of rapamycin (i.e. mTOR).

The immunopeptidome integrates events occurring at the transcriptional and co- or post-translational level

Generation of MIPs exploits generic cellular processes including transcription, translation and protein degradation (de Verteuil *et al.*, 2010; Fortier *et al.*, 2008; Yewdell *et al.*, 2003). However, the relative contribution of these different regulatory processes in moulding the immunopeptidome remains elusive. Here, we first sought to determine whether the 33 DEM source genes depicted in Figure 5A were translationally and/or transcriptionally regulated in response to rapamycin. After 48h of rapamycin treatment, polysome-associated RNA as well as total RNA from both rapamycin-treated and -untreated cells, were analyzed using quantitative real-time PCR. Translation of a large number of genes is reduced following rapamycin treatment (Grolleau *et al.*, 2002). Accordingly, analysis of normalized polysomal mRNAs (NPR) (see Materials and methods) showed that, in rapamycin-treated cells, ribosomal loading efficiency was decreased for 36% (12 out of 33), and increased for 6% (2 out of 33) of the DEM source mRNAs (Figure 5B). In contrast, we observed that 36% (12 out of 33) of the source genes were upregulated at the transcript level. Two points can be made from these data. First, while transcriptional activation could explain the increased abundance of about 36% of MIPs in rapamycin-treated cells, the role of translational activation appears negligible. As a corollary, increased levels of 20 out of 33 MIPs can neither be ascribed to enhanced transcription or translation of their source genes. From this, we infer that increased MIP levels on rapamycin-treated cells are caused mainly by co- and/or post-translational mechanisms.

In order to probe the role of co- and/or post-translational mechanisms, we first assessed the abundance and stability of 8 DEM source proteins by Western blotting on total lysates from EL4 cells treated or not with rapamycin and cycloheximide (Figure 6 and Supplementary Table 5). The abundance of two proteins was increased (Myb and Tfdp2) while that of the other six proteins was unchanged (Rfc2, Psmb9, Psmb8, Pabpc1, Rictor, and Sgk1). Notably, the eight DEM source proteins were relatively stable with a half-life ≥ 8h in the presence or absence of rapamycin. Myb was the only DEM source protein degraded more rapidly (2-fold; half-life from 8h to 4h) in the presence of rapamycin. These data strongly suggest that MIP levels do not correlate with the abundance or stability of the native form of DEM source proteins. However, up to 30% of proteins are so rapidly degraded (with a mean $t_{1/2}$ of ~10min) by the ubiquitin-proteasome that they escape detection in standard cycloheximide chase experiments(Qian et al., 2006). Most of these rapidly degraded proteins are defective ribosomal products (DRiPs) resulting from imperfections of protein synthesis or assembly (Yewdell and Nicchitta, 2006). Accordingly, most protein species have two half-lives: a longer one for the well-conformed native protein and a short one for DRiPs. Importantly, MIPs are generated at higher efficiency from rapidly degraded proteins than from old proteins (Yewdell *et al.*, 2006; Yewdell *et al.*, 2003). Western blotting experiments on whole EL4 cell extracts revealed that rapamycin increased the amount of proteasomal substrates, that is, ubiquitinated proteins that accumulate in lactacystin-treated cells (Figure 7A). We focused on Rictor, a DEM source protein that is a component of the mTOR complex 2, to evaluate more specifically whether rapamycin enhances proteasomal substrates generation from DEM source proteins. Rictor is coding for the KALSYASL peptide, which was exclusively detected after 48h of rapamycin treatment (Supplementary Table 1). EL4 cells were treated or not with rapamycin for 48h, with or without lactacystin for the last 8h. In the presence of lactacystin, we observed a substantial accumulation of polyubiquitinated Rictor proteins in rapamycin-treated cells relative to untreated cells (Figure 7B). This result indicates that more polyubiquitinated Rictor proteins are subjected to proteasome-mediated degradation upon rapamycin treatment. Because steady-state levels of the native Rictor protein were not affected by rapamycin (Figure 6), we infer that the overabundant Rictor MIP derives from a rapidly degraded pool of Rictor and not from the long-lived native form of Rictor. Collectively, our data indicate that changes in the

immunopeptidome integrate events occurring at the transcriptional and co- or post-translational level. Furthermore, consistent with the fact that mTOR links protein quality and quantity control (Qian *et al.*, 2010), our work suggests that enhanced generation of rapidly degraded proteasomal substrates is instrumental to rapamycin-induced changes in the immunopeptidome. Altogether, our results show that the immunopeptidome projects at the cell surface a representation of biochemical networks and metabolic events regulated at multiple levels inside the cell.

MIPs appearing *de novo* on rapamycin-treated cells elicit cytotoxic T-cell responses

Finally, we wished to determine whether MIPs that were exclusively detected on rapamycin-treated cells could be immunogenic. To test this, we selected the KALSYASL and the VNTHFSHL peptide, which are encoded by Rictor and Ttc21b, respectively (Supplementary Table 1). We immunized C57BL/6 mice with dendritic cells coated with KALSYASL or VNTHFSHL synthetic peptide. Splenocytes from immunized mice did not kill untreated EL4 cells, but they showed specific cytotoxicity for EL4 cells treated with rapamycin or EL4 cells coated with the peptide used for T-cell priming (Figure 7C and D). Further studies are needed to evaluate the proportion of rapamycin-specific or overabundant MIPs that are immunogenic. Nevertheless, the immunogenicity of KALSYASL and VNTHFSHL is consistent with the notion that the immune system is tolerant to MIPs expressed at physiological levels but can mount biologically relevant immune responses toward self MIPs present in excessive amounts (Schild *et al.*, 1990).

4.4 Discussion

Early proteomic studies of the immunopeptidome have led scientists to believe that MIPs were derived from housekeeping genes and presented minimal if any differences among different cell types (Barnea *et al.*, 2002; Engelhard *et al.*, 2002; Hughes and Hughes, 1995; Marrack *et al.*, 1993). In other words, they suggested that, at the organismal level, the immune self was practically invariant. However, these studies were conducted with analyzers whose sensitivity (dynamic range) and accuracy were orders of magnitude inferior to that of MS analyzers that are now available (Depontieu *et al.*, 2009; Nilsson *et al.*, 2010; Yates *et al.*, 2009). More recently, high-throughput MS-based analyses have shown that immunopeptidome conceals a cell type-specific signature. Thus, though the immunopeptidome of dendritic cells and thymocytes partially overlap, no less than 40% of their MIPs are cell type-specific (de Verteuil *et al.*, 2010; Fortier *et al.*, 2008). The present study demonstrates that perturbation of a single signaling pathway can lead to significant changes in the composition of the immunopeptidome. More specifically, our work shows that dynamic changes of mTOR signals are reflected in MHC I presentation of numerous peptides associated with the mTOR interactome and its signaling network. The connectivity between DEM source genes and mTOR network components was amazingly strong ($P < 10^{-5}$). A bootstrap procedure (500,000 iterations) failed to reveal a single set of peptide source genes that were so tightly connected to component of the mTOR network (Figure 4C). An important implication for the immune system is that, at the peptide level, the immune self is plastic and its molecular composition is influenced by the cell's metabolic activity. Furthermore, since mTOR integrates environmental cues in terms of nutrients and growth factors, it is reasonable to infer that cell-extrinsic factors modulate the repertoire of self peptides presented by MHC I. That means the nature of the immune self is much more complex than anticipated. Moreover, the notion that MIPs presented specifically on metabolically stressed cells can be immunogenic (e.g., KALSYASL and VNTHFSHL) could have several implications that need to be explored: immune responses against metabolic stress-associated MIPs could contribute to elimination of infected or transformed cells (Gleimer and Parham, 2003), but might also elicit autoimmunity (Todd *et al.*, 2008).

From a more general perspective, our data provide a proof of concept that acquisition and integration of large-scale, quantitative biological data from multiple regulatory layers (i.e. –omics) may enable prediction of variations in the composition of the immunopeptidome. The notion that the immunopeptidome is plastic and conveys at the cell surface an integrative view of cellular protein metabolism opens up new perspectives in systems immunology and predictive biology (Benoist *et al.*, 2006; Germain *et al.*, 2011). The immune system has co-evolved with pathogens and positive selection imposed by pathogens has hastened the evolution of immune genes and thereby increased the complexity of the immune system (Hedrick, 2004; Waterston *et al.*, 2002). Given the complexity of the immune system and the quintessential importance of self/nonself discrimination, it is imperative to further develop and exploit systems-level quantitative methods that will enable modelling of the immunopeptidome's plasticity. Such systems-oriented approaches will help to simulate and predict how cell-autonomous and -extrinsic elements modulate the composition of the immunopeptidome in health and disease.

4.5 Materials and methods

Cell culture, flow cytometry, and determination of cell size

EL4 cell lines were cultured as previously reported (Fortier *et al.*, 2008). Rapamycin, lactacystin, and cycloheximide were purchased from Sigma-Aldrich. For MHC I labeling, cells were stained with anti-$H2D^b$ (B22–249.R1; Cedarlane), anti-$H2K^b$ (Y3; ATCC), anti-Qa2 (clone 1-1-2, BD Pharmingen), anti-Qa1b (6A8.6F10.1A6) antibodies and analyzed on a BD LSR II flow cytometer using FACSDiva software (BD Biosciences) (Meunier et al., 2005). Cell number and cell size were measured by light microscopy using an Axio Imager microscope (Zeiss) and the Northern Eclipse software (Empix Imaging Inc.).

Western blotting and isolation of polyubiquitinated proteins

EL4 cells were harvested and lysed in RIPA buffer, samples were resolved by SDS-PAGE and immunoblotted with the following antibodies: ERAAP (gift from N. Shastri, University of California, Berkeley, CA); Tapasin (gift from T.H. Hansen, Washington Univ Sch of Med, St Louis, MO); Lmp7, Lmp2, β1, β5, ERp57, Sgk1, β2m, PDI (Abcam); Calnexin, Calreticulin, β-actin (Sigma); PA28, S6K1, p-S6K1 (Thr389), 4E-BP1, p-4E-BP1 (Ser65), p-4E-BP1 (Thr37/46), α-tubulin, Rictor, Akt, p-Akt (S473), Ubiquitin (Cell Signaling); Myb (Upstate, Millipore); Mecl1, β2 (Biomol International); Rfc2 (Proteintech Group, PTG); Tfdp2 (Proteintech Group, PTG); Pabpc1 (Cell Signaling); $H2K^b$/$H2D^b$ (2G5; Thermo Scientific); Tap1, Tap2 (Santa Cruz Biotechnology). Isolation of polyubiquitinated proteins was achieved by using Tandem Ubiquitin Binding Entities (TUBEs) (LifeSensors, Inc.) according to the manufacturer's instruction.

Metabolic radiolabeling

To measure protein synthesis, EL4 cells were cultured in absence or presence of rapamycin (20 ng/ml) for 0h (ctrl), 6h, 12h, 24h, and 48h. During the last hour, cells were transferred to 96-well plates (0.5×10^6 cells per well, 12 replicates per conditions) and [3H]-Leucine (10 μCi/mL) (Perkin Elmer) was added to each well. At the end of the culture period, cells were harvested with a Cell Harvester (Perkin Elmer) on a fiber glass filter (Packard) for washing. Filters were dried for 24 hours and 20 μL of scintillation

liquid per well (MicroScint-O, Perkin Elmer) was added. Radioactivity incorporation was determined with the TopCount-NXT microplate scintillation and luminescence counter (Packard).

Peptide extraction and mass spectrometry analysis

EL4 cells were treated with 20ng/mL of rapamycin for 0h, 6h, 12h, 24h, and 48h. MIPs were then isolated from EL4 cells as described previously using mild acid elution (de Verteuil *et al.*, 2010; Fortier *et al.*, 2008). Three biological replicates (5×10^8 EL4 cells per replicate) were prepared. MIPs obtained after acid elution were separated using an off-line 1100 series binary LC system (Agilent Technologies) to remove contaminating species. Peptides were loaded on a homemade SCX column (0.3 mm internal diameter x 50 mm length) packed with strong cation exchange (SCX) bulk material (Polysulfoethyl ATM, PolyLC). Peptides were fractionated with a gradient of 0-25% B after 25 minutes, 25-60% B after 35 minutes (Solvent A = 5mmol/L ammonium formate, 15% acetonitrile, pH 3.0; Solvent B = 2 mol/L ammonium formate, 15% acetonitrile, pH 3.0). MIPs were collected in five consecutive fractions and brought to dryness using a speedvac. MIP fractions were resuspended in 2% aqueous acetonitrile (0.2% formic acid) and analyzed by nanoLC-MS/MS on a LTQ-Orbitrap mass spectrometer (Thermo Fisher Scientific) (Fortier *et al.*, 2008). Full mass spectra were acquired with the Orbitrap analyzer operated at a resolving power of 60,000 (at m/z 400) and collision-activated dissociation tandem mass spectra were acquired in data-dependent mode with the quadrupole linear ion trap analyzer. Mass calibration used an internal lock mass [protonated (Si(CH3)2O))6; m/z 445.12057] and typically provided mass accuracy within 5 ppm for all nanoLC-MS/MS experiments.

MS/MS sequencing, hierarchical clustering and identification of MIP source proteins

Peptidomic data were analyzed using Xcalibur software and peak lists were generated using Mascot distiller (version 2.1.1, www.matrixscience.com). Database searches were performed against the International Protein Index mouse database (version 3.23 containing 51,536 sequences and 24,497,860 residues) using Mascot (version 2.2, www.matrixscience.com) with a mass precursor tolerance of ± 0.05 Da and a fragment tolerance of ± 0.5 Da. Searches were performed without enzyme specificity and a variable

modification of oxidized Met. All search results were filtered using an MHC motif filter based on the predicted mouse MHC I allele motifs. Raw data files were converted to peptide maps comprising m/z values, charge state, retention time and intensity for all detected ions above a threshold of 10,000 counts using in-house software (Mass Sense) (de Verteuil *et al.*, 2010; Fortier *et al.*, 2008). Peptide maps were aligned and clustered together to profile the abundance of Mascot identified peptides using hierarchical clustering with criteria based on m/z and time tolerance (±0.02 m/z and ±1min). This resulted in a list of non-redundant peptide clusters for all replicates of all samples to be compared. Subtraction of "contaminant peptides" eluted from β2m$^-$ mutant EL4 cells allowed specific identification of genuine MIPs(de Verteuil *et al.*, 2010; Fortier *et al.*, 2008). MIPs were further inspected for mass accuracy and MS/MS spectra were validated manually. The Sidekick resource (http://www.bioinfo.iric.ca/sidekick/Main) was used to identify MIP source proteins. The list of MIPs reported in the present work has been provided to The Immune Epitope Database and Analysis Resource (http://beta.immuneepitope.org/) (Vita *et al.*, 2010).

MIP classification and abundance profiling

Each MIP listed in Supplementary Table 1 was classified according to restriction size and binding motif (de Verteuil *et al.*, 2010; Fortier *et al.*, 2008). The raw ratios for the time profiles of detected MIPs were then clustered using the TIGR MultiExperiment Viewer (TMEV) software. Hierarchical clustering with euclidean distances and average linkage was used.

Microarray analysis

EL4 cells were treated or not with 20ng/mL of rapamycin for 48h. Three biological replicates were prepared. Total RNA was extracted from EL4 cells with TRIzol RNA reagent (Invitrogen) as instructed by the manufacturer. Samples were purified using DNase (Qiagen) and the RNeasy Mini kit (Qiagen), and the overall quality was analyzed with the 2100 Bioanalyzer (Agilent Technologies). Purified RNA (10 µg/sample) was hybridized on MM8 385K NimbleGen chips according to the manufacturer's instruction. Arrays were scanned using a GenePix4000B scanner (Axon Instruments) at 5 µm resolution. Data were extracted and normalized using the NimbleScan 2.4 extraction

software (NimbleGen Systems). Further microarray analyses were performed using GeneSpring GX 7.3.1. The complete microarray datasets have been deposited in ArrayExpress (http://www.ebi.ac.uk/arrayexpress) under accession number E-MEXP-3007.

Isolation of total and polysomal RNA for quantitative real-time PCR

EL4 cells were treated or not with 20ng/mL of rapamycin for 48h. Three biological replicates were prepared. Total RNA was extracted as described above. Polysomal RNA was extracted from 2 $x10^8$ EL4 cells as described previously (Rajasekhar et al., 2003). Gene expression level was determined using primer and probe sets from Universal ProbeLibrary (https://www.roche-applied-science.com/sis/rtpcr/upl/index.jsp). Primer sequences are given in Supplementary Table 6. PCR reactions for 384-well plate format were performed as described in (Baron *et al.*, 2007). All reactions were run in triplicate, and the mean values were used for quantification. The mouse Hprt1 and Tbp genes were used as endogenous controls for total RNA and polysomal RNA, respectively. In order to obtain an unbiased profile of the normalized ribosomal loading efficiencies for cells, we calculated the net polysomal mRNA to total mRNA ratios. Such data are presented in the manuscript as normalized polysomal mRNA (NPR) (Rajasekhar *et al.*, 2003).

GO enrichment and connectivity score

The Database for Annotation, Visualization, and Integrated Discovery (DAVID) Bioinformatics Resource (Peters and Sette, 2007) was used to identify significantly enriched GO terms associated to DEM source genes and DEGs from untreated and rapamycin-treated EL4 cells. To calculate connectivity scores between two lists of nodes (genes/proteins), computed scores from STRING (http://string-db.org/) (Szklarczyk et al., 2011) were used. By using computed scores in STRING, functional associations between two lists of nodes were integrated into an all-pairs-shortest-path distance matrix. Each functional association in the all-pairs-shortest-path matrix was transformed into a "distance" (D), defined as -ln(S), where S is the computed STRING score. The all-pairs-shortest path matrix contains the length of the shortest path (distance) between every pair of nodes in the network. A connectivity score was then obtained by calculating the mean of the shortest path distance between every pair of nodes in a given matrix.

STITCH network

The 98 DEM source genes highlighted in Figure 3B were used to build the DEM network (Supplementary Figure 4). The 98 source genes encoding DEMs, the 171 DEGs classified within the enriched GO terms ($P < 0.05$) in Supplementary Figure 3B and C and the mTOR network components in Supplementary Table 4 were used to build the global rapamycin-regulatory network. Subnetworks (Figure 5A) were manually extracted based on the modular organization of the total network (Hartwell *et al.*, 1999; Rives and Galitski, 2003). Each of these molecules was individually searched in the STITCH (http://stitch.embl.de/) (Kuhn *et al.*, 2010) database for its functional associations. The parameters used to elucidate the network were as follows: forty additional nodes, a network depth = 1, and interactions with a minimum STITCH combined score of 0.400. Functional associations identified for all of the molecules were then imported into Adobe Illustrator as a Scalable Vector Graphics (SVG) image (action view configuration).

In vitro cytoxicity assay

Bone marrow–derived dendritic cells (DCs) were generated as previously described (de Verteuil *et al.*, 2010; Fortier *et al.*, 2008). On day 9 of culture, peptides were added at a concentration of 2×10^{-6} M and incubated with DCs for 3 h at 37°C. For mouse immunization, 10^6 peptide-pulsed DCs were injected i.v. in C57BL/6 females at day 0 and 7. On day 14, splenocytes were harvested from the spleens of immunized mice and depleted of red blood cells using 0.83% NH4CL. Cells were plated at 5×10^6 cells/well in 24-well plates and restimulated with 2×10^{-6} M peptide at 37°C. After 6 d, cytotoxicity was evaluated by a 4h CFSE-based assay[18]. The percentage of specific lysis was calculated as follows: (number of remaining CFSE+ cells after incubation of target cells alone - number of remaining CFSE+ cells after incubation with effector cells)/number of CFSE+ cells after incubation of target cells alone × 100.

4.6 Acknowledgments

We thank Raphaëlle Lambert and Mathieu Courcelles (IRIC, Montreal, Canada) for technical support. We also thank Stephen W. Michnick (Université de Montréal, Montreal, Canada) and Valeria de Azcoitia for comments on the manuscript. This work was supported by grants from the Canadian Institutes for Health Research (MOP 42384) and the Canadian Cancer Society (019475). E.C. and K.V. are supported by training grants from the Cole Foundation. M.H.F. was supported by a studentship from the Fonds de la Recherche en Santé du Québec (FRSQ). C.P., P.T., and P.P.R. are supported by the Canada Research Chairs Program. IRIC is supported in part by the Canadian Center of Excellence in Commercialization and Research, the Canada Foundation for Innovation, and the FRSQ.

Author contributions: E.C. designed the study, carried out experiments, analysed the data, prepared figures and wrote the first draft of the manuscript. K.V. and M.-P.H. carried out experiments and prepared figures. M.-H.F. carried out experiments and the mass spectrometry analysis. J.-P.L., A.B. and G.V. carried out bioinformatics analysis. C.P. and P.T. designed the study, analysed data, discussed results and wrote the manuscript. S.L. and P.P.R. contributed to the study design, discussed results and commented on the manuscript.

4.7 References

Araki K, Turner AP, Shaffer VO, Gangappa S, Keller SA, Bachmann MF, Larsen CP, and Ahmed R (2009) mTOR regulates memory CD8 T-cell differentiation. *Nature*, **460:** 108-112.

Barnea E, Beer I, Patoka R, Ziv T, Kessler O, Tzehoval E, Eisenbach L, Zavazava N, and Admon A (2002) Analysis of endogenous peptides bound by soluble MHC class I molecules: a novel approach for identifying tumor-specific antigens. *Eur J Immunol,* **32:** 213-222.

Baron C, Somogyi R, Greller LD, Rineau V, Wilkinson P, Cho CR, Cameron MJ, Kelvin DJ, Chagnon P, Roy DC, Busque L, Sékaly RP, and Perreault C (2007) Prediction of graft-versus-host disease in humans by donor gene expression profiling. *PLoS Med*, **4:** e23.

Benoist C, Germain RN, and Mathis D (2006) A plaidoyer for 'systems immunology'. *Immunol Rev*, **210:** 229-234.

Boehm T (2006) Quality control in self/nonself discrimination. *Cell*, **125:** 845-858

Choo AY and Blenis J (2009) Not all substrates are treated equally: implications for mTOR, rapamycin-resistance and cancer therapy. *Cell Cycle*, **8:** 567-572.

Choo AY, Yoon SO, Kim SG, Roux PP, and Blenis J (2008) Rapamycin differentially inhibits S6Ks and 4E-BP1 to mediate cell-type-specific repression of mRNA translation. *Proc Natl Acad Sci U S A*, **105:** 17414-17419.

de Verteuil D, Muratore-Schroeder TL, Granados DP, Fortier MH, Hardy MP, Bramoullé A, Caron E, Vincent K, Mader S, Lemieux S, Thibault P, and Perreault C (2010) Deletion of immunoproteasome subunits imprints on the transcriptome and has a broad impact on peptides presented by major histocompatibility complex I molecules. *Mol Cell Proteomics*, **9:** 2034-2047.

Depontieu FR, Qian J, Zarling AL, McMiller TL, Salay TM, Norris A, English AM, Shabanowitz J, Engelhard VH, Hunt DF, and Topalian SL (2009) Identification of tumor-associated, MHC class II-restricted phosphopeptides as targets for immunotherapy. *Proc Natl Acad Sci U S A*, **106:** 12073-12078.

Dilling MB, Germain GS, Dudkin L, Jayaraman AL, Zhang X, Harwood FC, and Houghton PJ (2002) 4E-binding proteins, the suppressors of eukaryotic initiation factor 4E, are down-regulated in cells with acquired or intrinsic resistance to rapamycin. *J Biol Chem*, **277:** 13907-13917.

Dowling RJ, Topisirovic I, Alain T, Bidinosti M, Fonseca BD, Petroulakis E, Wang X, Larsson O, Selvaraj A, Liu Y, Kozma SC, Thomas G, and Sonenberg N (2010) mTORC1-mediated cell proliferation, but not cell growth, controlled by the 4E-BPs. *Science*, **328:** 1172-1176.

Engelhard V, Brickner A, and Zarling A (2002) Insights into antigen processing gained by direct analysis of the naturally processed class I MHC associated peptide repertoire. *Mol Immunol*, **39:** 127.

Fortier MH, Caron E, Hardy MP, Voisin G, Lemieux S, Perreault C, and Thibault P (2008) The MHC class I peptide repertoire is molded by the transcriptome. *J Exp Med*, **205:** 595-610.

Germain RN, Meier-Schellersheim M, Nita-Lazar A, and Fraser ID (2011) Systems biology in immunology: a computational modeling perspective. *Annu Rev Immunol*, **29:** 527-585.

Gleimer M and Parham P (2003) Stress management: MHC class I and class I-like molecules as reporters of cellular stress. *Immunity*, **19:** 469-477.

Goldrath AW and Bevan MJ (1999) Selecting and maintaining a diverse T-cell repertoire. *Nature*, **402:** 255-262.

Grolleau A, Bowman J, Pradet-Balade B, Puravs E, Hanash S, Garcia-Sanz JA, and Beretta L (2002) Global and specific translational control by rapamycin in T cells uncovered by microarrays and proteomics. *J Biol Chem*, **277:** 22175-22184.

Hartwell LH, Hopfield JJ, Leibler S, and Murray AW (1999) From molecular to modular cell biology. *Nature*, **402:** C47-C52.

Hedrick SM (2004) The acquired immune system; a vantage from beneath. *Immunity*, **21:** 607-615.

Hickman HD, Luis AD, Buchli R, Few SR, Sathiamurthy M, VanGundy RS, Giberson CF, and Hildebrand WH (2004) Toward a definition of self: proteomic evaluation of the class I peptide repertoire. *J Immunol*, **172:** 2944-2952.

Hughes AL and Hughes MK (1995) Self peptides bound by HLA class I molecules are derived from highly conserved regions of a set of evolutionarily conserved proteins. *Immunogenetics*, **41:** 257-262.

Istrail S, Florea L, Halldorsson B, V, Kohlbacher O, Schwartz RS, Yap VB, Yewdell JW, and Hoffman SL (2004) Comparative immunopeptidomics of humans and their pathogens. *Proc Natl Acad Sci U S A*, **101:** 13268-13272.

Klein L, Hinterberger M, Wirnsberger G, and Kyewski B (2009) Antigen presentation in the thymus for positive selection and central tolerance induction. *Nat Rev Immunol*, **9:** 833-844.

Kuhn M, Szklarczyk D, Franceschini A, Campillos M, von MC, Jensen LJ, Beyer A, and Bork P (2010) STITCH 2: an interaction network database for small molecules and proteins. *Nucleic Acids Res*, **38:** D552-D556.

Marrack P, Ignatowicz L, Kappler JW, Boymel J, and Freed JH (1993) Comparison of peptides bound to spleen and thymus class II. *J Exp Med*, **178:** 2173-2183.

Meunier MC, Delisle JS, Bergeron J, Rineau V, Baron C, and Perreault C (2005) T cells targeted against a single minor histocompatibility antigen can cure solid tumors. *Nat Med*, **11:** 1222-1229.

Milner E, Barnea E, Beer I, and Admon A (2006) The turnover kinetics of MHC peptides of human cancer cells. *Mol Cell Proteomics*, **5:** 357-365.

Nilsson T, Mann M, Aebersold R, Yates JR, III, Bairoch A, and Bergeron JJ (2010) Mass spectrometry in high-throughput proteomics: ready for the big time. *Nat Methods*, **7:** 681-685.

Perreault C (2010) The origin and role of MHC class I-associated self-peptides. *Prog Mol Biol Transl Sci*, **92C:** 41-60.

Peters B and Sette A (2007) Integrating epitope data into the emerging web of biomedical knowledge resources. *Nat Rev Immunol*, **7:** 485-490.

Qian SB, Princiotta MF, Bennink JR, and Yewdell JW (2006) Characterization of rapidly degraded polypeptides in mammalian cells reveals a novel layer of nascent protein quality control. *J Biol Chem*, **281:** 392-400.

Qian SB, Zhang X, Sun J, Bennink JR, Yewdell JW, and Patterson C (2010) mTORC1 links protein quality and quantity control by sensing chaperone availability. *J Biol Chem*, **285:** 27385-27395.

Rajasekhar VK, Viale A, Socci ND, Wiedmann M, Hu X, and Holland EC (2003) Oncogenic Ras and Akt signaling contribute to glioblastoma formation by differential recruitment of existing mRNAs to polysomes. *Mol Cell*, **12:** 889-901.

Rammensee HG, Falk K, and Rotzschke O (1993) Peptides naturally presented by MHC class I molecules. *Annu Rev Immunol*, **11:** 213-244.

Rives AW and Galitski T (2003) Modular organization of cellular networks. *Proc Natl Acad Sci U S A*, **100:** 1128-1133.

Sarbassov DD, Ali SM, Sengupta S, Sheen JH, Hsu PP, Bagley AF, Markhard AL, and Sabatini DM (2006) Prolonged rapamycin treatment inhibits mTORC2 assembly and Akt/PKB. *Mol Cell*, **22:** 159-168.

Schild H, Rotzschke O, Kalbacher H, and Rammensee HG (1990) Limit of T cell tolerance to self proteins by peptide presentation. *Science*, **247:** 1587-1589.

Sengupta S, Peterson TR, and Sabatini DM (2010) Regulation of the mTOR complex 1 pathway by nutrients, growth factors, and stress. *Mol Cell*, **40:** 310-322.

Sette A and Rappuoli R (2010) Reverse vaccinology: developing vaccines in the era of genomics. *Immunity*, **33:** 530-541.

Szklarczyk D, Franceschini A, Kuhn M, Simonovic M, Roth A, Minguez P, Doerks T, Stark M, Muller J, Bork P, Jensen LJ, and von MC (2011) The STRING database in 2011: functional interaction networks of proteins, globally integrated and scored. *Nucleic Acids Res*, **39:** D561-D568.

Thoreen CC, Kang SA, Chang JW, Liu Q, Zhang J, Gao Y, Reichling LJ, Sim T, Sabatini DM, and Gray NS (2009) An ATP-competitive mammalian target of rapamycin inhibitor reveals rapamycin-resistant functions of mTORC1. *J Biol Chem*, **284:** 8023-8032.

Todd DJ, Lee AH, and Glimcher LH (2008) The endoplasmic reticulum stress response in immunity and autoimmunity. *Nat Rev Immunol*, **8:** 663-674.

Vita R, Zarebski L, Greenbaum JA, Emami H, Hoof I, Salimi N, Damle R, Sette A, and Peters B (2010) The immune epitope database 2.0. *Nucleic Acids Res*, **38:** D854-D862.

Waterston RH, Lindblad-Toh K, Birney E, Rogers J, Abril JF, Agarwal P, Agarwala R, Ainscough R, Alexandersson M, An P, Antonarakis SE, Attwood J, Baertsch R, Bailey J, Barlow K, Beck S, Berry E, Birren B, Bloom T, Bork P et al. (2002) Initial sequencing and comparative analysis of the mouse genome. *Nature*, **420:** 520-562.

Weinzierl AO, Lemmel C, Schoor O, Muller M, Kruger T, Wernet D, Hennenlotter J, Stenzl A, Klingel K, Rammensee HG, and Stevanovic S (2007) Distorted relation between mRNA copy number and corresponding major histocompatibility complex ligand density on the cell surface. *Mol Cell Proteomics*, **6:** 102-113.

Yates JR, Ruse CI, and Nakorchevsky A (2009) Proteomics by mass spectrometry: approaches, advances, and applications. *Annu Rev Biomed Eng*, **11:** 49-79.

Yewdell JW and Nicchitta CV (2006) The DRiP hypothesis decennial: support, controversy, refinement and extension. *Trends Immunol*, **27:** 368-373.

Yewdell JW, Reits E, and Neefjes J (2003) Making sense of mass destruction: quantitating MHC class I antigen presentation. *Nature Rev Immunol*, **3:** 952-961.

Zarling AL, Polefrone JM, Evans AM, Mikesh LM, Shabanowitz J, Lewis ST, Engelhard VH, and Hunt DF (2006) Identification of class I MHC-associated phosphopeptides as targets for cancer immunotherapy. *Proc Natl Acad Sci U S A*, **103:** 14889-14894.

4.8 Figure Legends

Figure 1: Rapamycin differentially inhibits S6K1 versus 4E-BP1 in EL4 cells.

Cells were treated with 20ng/mL of rapamycin for the indicated time periods. (**A**) Levels of the indicated proteins were determined by western blotting. β-actin served as a loading control. Data are representative of three independent experiments. (**B**) EL4 cells were treated or not (ctrl) with rapamycin for 48h. One thousand cells were counted for each condition. Cell size was measured by light microscopy. The red line corresponds to the average cell size. Data are representative of three independant experiments. * $P < 0.0005$ (student *t*-test). (**C**) Relative protein synthesis was measured by [3H]-leucine incorporation. Data (mean ± SD) are representative of three independent experiments. * $P < 0.01$, ** $P < 0.005$ (student *t*-test). (**D**) Model for effects of rapamycin-mediated mTORC1 inhibition in EL4 cells. Proteins and reactions were curated from the literature. Color code is based on results in Figure 1 after 48h of rapamycin treatment. Activation and inhibition of components/reactions are depicted in green and red, respectively. Partial inactivation is represented by the thinner green lines.

Figure 2: Rapamycin increases the abundance of MIPs presented by MHC Ia molecules.

(**A**) Experimental design for identification and relative quantification of MIPs. EL4 cells were incubated with 20ng/mL of rapamycin for 0h (ctrl), 6h, 12h, 24h, and 48h. Cells from all experimental conditions were harvested simultaneously. MIPs from rapamycin-treated and ctrl EL4 cells were isolated by mild acid elution and analyzed by nanoLC-MS-MS/MS. Heat maps displaying m/z, retention time and abundance were generated. A logarithmic intensity scale distinguishes between low (dark red) and high (bright yellow) abundance species. Analysis of β2m- mutant EL4 cells allows discrimination of genuine MIPs from contaminants(de Verteuil *et al.*, 2010; Fortier *et al.*, 2008). Examples of peptides that were differentially expressed (red line) or not (green line) between WT and β2m- mutant EL4 cells are highlighted in the boxes. (**B**) Volcano plots show the relative abundance of 416 $H2^b$-associated peptides identified in three biological replicates at each time point. Six MIPs were detected uniquely after 48h of rapamycin treatment.

Figure 3: Rapamycin-mediated mTOR inhibition induces functionally coherent changes in the transcriptome and the immunopeptidome.

(**A**) Volcano plot representation of the relative abundance of 42,586 transcripts after 48h of rapamycin treatment. Transcripts were considered to be differentially expressed when the fold difference in abundance was > 2.0 (P < 0.05). Transcripts over- and underexpressed in rapamycin-treated cells relative to ctrl cells are depicted in the red and green boxes, respectively. (**B**) Volcano plot representation of the relative abundance of 422 MIPs after 48h of rapamycin treatment. MIPs that were the most differentially expressed [fold difference relative to untreated cells > 2.5; P < 0.05; fold difference and P value based on (Fortier *et al.*, 2008)] are highlighted in the blue boxes. **(C, D)** GO enrichment analyses were performed for DEM source genes and DEGs. 38 DEM source genes (blue) were associated to 6 significantly enriched cellular processes. 101 (green) and 70 (red) genes coding for under- and overexpressed mRNAs were associated to 7 and 8 significantly enriched cellular processes, respectively. (**C**) Venn diagram showing no overlap between DEM source genes and DEGs. Dashed boxes show representative genes that contributed to enrichment of four cellular processes both in DEM source genes and DEGs. (**D**) Venn diagram showing functional overlap between cellular processes overrepresented in DEM source genes and DEGs. The four cellular processes overrepresented both in DEM source genes and DEGs are listed in the dashed boxes**.**

Figure 4: DEM source genes are tightly connected to transcriptomic changes and the mTOR network.

(**A**) An all-pairs-shortest-path matrix was developed by using computed scores (S) in the STRING database (http://string-db.org/). The all-pairs-shortest-path matrix was used to calculate functional associations between 1) DEM source genes and DEGs, and 2) DEM source genes and mTOR network components. Each functional association in the all-pairs-shortest-path matrix was transformed into a distance (D). The matrix shows DEM source genes (rows), DEGs or mTOR network components (columns), and the shortest path distance between every pair of nodes (genes/proteins) in the association network (e.g.: Dw-z and Dx-y). A connectivity score corresponds to the mean of the shortest path distance between every pair of nodes in a given matrix. (**B, C**) The all-pairs-shortest-path matrix was used to calculate functional connectivity scores. The red lines represent the

connectivity score between DEM source genes and DEGs (**B**), and between DEM source genes and mTOR network components (**C**). A bootstrap procedure was used to calculate control connectivity scores represented by the gaussian distributions.

Figure 5: DEM source genes are regulated at multiple layers within specific mTOR subnetworks.

(**A**) The STITCH database (http://stitch.embl.de/) was used to generate a network from protein-protein interactions and functional associations involving identified DEM source genes, DEGs, and mTOR network components. From the total network, subnetworks of DNA replication/transcription, cell cycle/proliferation, apoptosis, lipid biosynthesis, translation, proteasome and mTOR signaling were extracted. Legend for functional associations (edges) is depicted in Supplementary Figure 4. **(B)** EL4 cells were treated or not with rapamycin for 48h. Total mRNA and normalized polysomal mRNA (NPR) levels of the DEM source genes depicted in (A) were assessed by quantitative real-time PCR (see also Supplementary Table 5).

Figure 6: Relative abundance and stability of 8 DEM source proteins in the presence or absence of rapamycin.

EL4 cells were treated or not (ctrl) with 20ng/mL of rapamycin for 48h. Levels of DEM source proteins were determined by western blotting and quantified by densitometry. Fold change indicates the rapamycin/ctrl protein abundance ratio. To estimate the half-life of DEM source proteins, cells were treated with cycloheximide (CHX) for 0h, 4h, and 8h in the presence and absence of rapamycin. Results in the graphs are expressed as a percentage of the remaining protein abundance in CHX-treated cells relative to CHX-untreated cells. β-actin served as a loading control. One representative western blot out of three is shown for individual proteins (*P* value: Student *t*-test).

Figure 7: Rapamycin-treated cells contain increased levels of proteasomal substrates and express immunogenic MIPs.

(**A, B**) EL4 cells were treated or not with 20 ng/mL rapamycin for 48h, combined or not with 10 μM of lactacystin for the last 8h. (**A**) Accumulation of ubiquitinated proteins was measured on total cell lysates by western blotting. (**B**) Polyubiquitinated proteins from

total cell lysates were isolated with Tandem Ubiquitin Binding Entities (TUBEs) and levels of polyubiquitinated Rictor were then determined by western blotting. One representative western blot out of three is shown. (**C, D**) Mice were immunized with dendritic cells coated with VNTHFSHL (**C**) or KALSYASL (**D**) peptide. Splenocytes from primed mice were tested for cytotoxic activity against CFSE-labeled target EL4 cells at different E/T ratios. EL4 cells coated with VNTHFSHL or KALSYASL were used as positive control. Data represent the mean ± SD for three mice per group.

4.9 Supplementary Figure Legends

Supplementary Figure 1 : Rapamycin does not affect levels of proteins involved in the antigen processingand presentation pathway (Jensen et al., 2007).

Levels of the indicated proteins were determinedby western blotting. β-actin and α-tubulin served as loading controls. Data are representative of three independent experiments.

Supplementary Figure 2 : Rapamycin increases the abundance of MIPs presented by MHC Ia molecules.

(**A**) Representation of unsupervised hierarchical clustering of 416 MIPs detected and quantified at different time points. 6 MIPs were detected exclusively after 48h of rapamycin treatment and were not included in the clustering analysis. MIPs are represented vertically, and experimental conditions (i.e., rapamycin time course) are displayed horizontally. Clusters for $H2K^b$-, $H2D^b$-, and Qa1/2-associated peptides are shown with the mean temporal profile in A1-A8. The number of MIPs per cluster is indicated in parenthesis. Clusters A1,2,4,5 and 7 show MIPs that were progressively overexpressed upon rapamycin treatment. (**B**) Cell surface expression of MHC I allelic products was evaluated by flow cytometry after 48h of rapamycin treatment. Histogram shows the rapamycin/ctrl mean fluorescence intensity ratio for $H2K^b$, $H2D^b$, Qa1, and Qa2. (n=6, *$P < 0.005$, Student t-test).

Supplementary Figure 3 : Cellular processes enriched in the DEM source genes or the DEGs.

(**A**) Representation of 38 genes encoding DEMs (rows) in 6 cellular processes (columns) that were enriched in the GO analysis. (**B**) Representation of 101 underexpressed genes (rows) in 7 cellular processes (columns) that were enriched in the GO analysis. (**C**) Representation of 70 overexpressed genes (rows) in 8 functional classes (columns) that were enriched in the GO analysis. See also Supplementary Table 2.

Supplementary Figure 4 : DEM source genes are involved in cellular processes and signaling events governed by the mTOR network.

Source genes encoding DEMs were analyzed with the STITCH database (http://stitch.embl.de/) and the network was elucidated based upon protein-protein interactions, protein-chemical associations, and functional associations. The emerging network elucidates a total of 30 DEM source genes distributed within different subnetworks, such as apoptosis, cell cycle/proliferation, DNA replication, lipid biosynthesis, proteasome, transcription, translation, mTOR signaling and tyrosine kinase receptors (TKRs) signaling. Rapamycin and everolimus (rapamycin analog) are the 2 unique chemicals that were revealed in the network. Symbols and arrows in the network are illustrated in the legend.

Figure 1

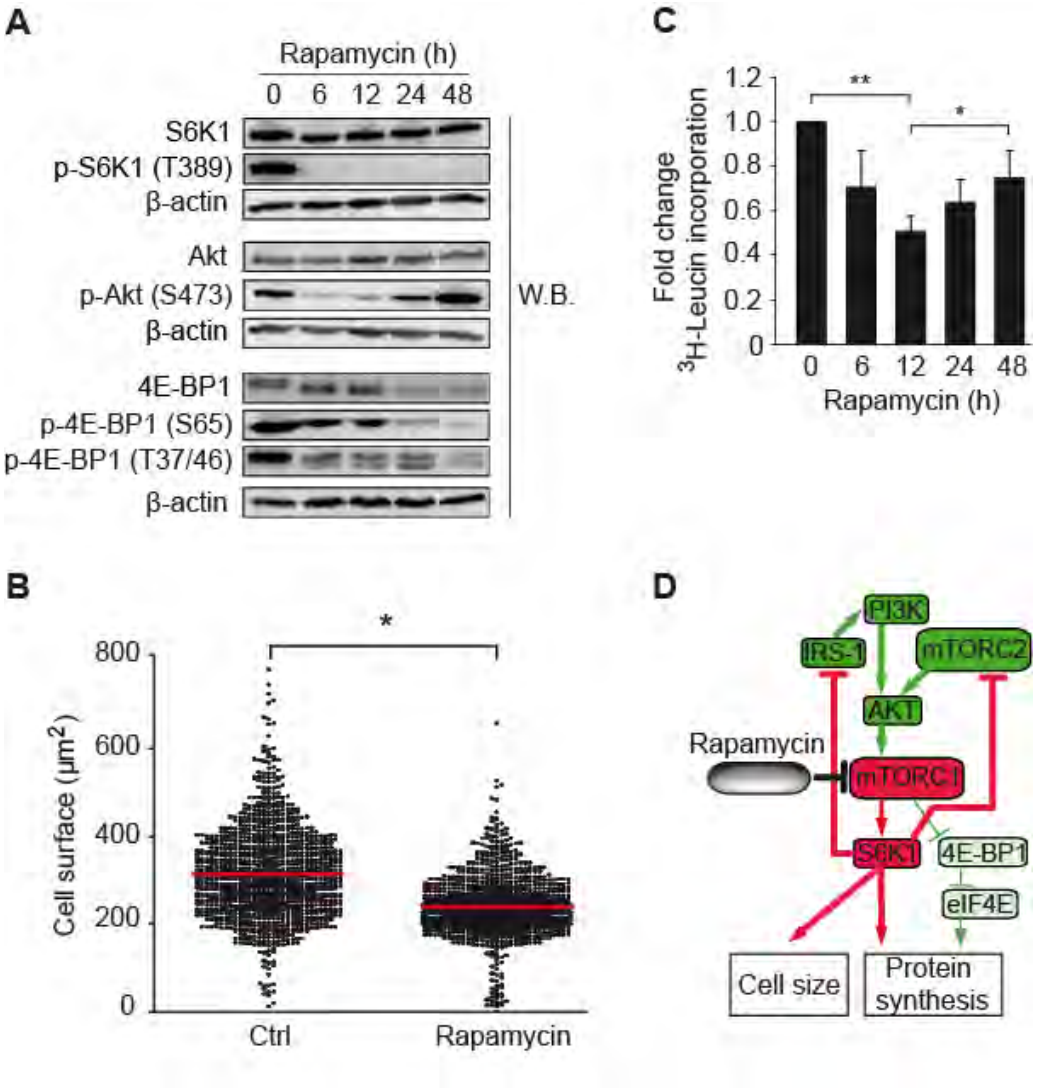
A
Rapamycin (h)
0 6 12 24 48
S6K1
p-S6K1 (T389)
β-actin
Akt
p-Akt (S473)
β-actin
4E-BP1
p-4E-BP1 (S65)
p-4E-BP1 (T37/46)
β-actin
W.B.
C
Fold change
3H-Leucin incorporation
1.2
1.0
0.8
0.6
0.4
0.2
0
**
*
0 6 12 24 48
Rapamycin (h)
B
Cell surface (μm2)
800
600
400
200
0
*
Ctrl
Rapamycin
D
PI3K
IRS-1
mTORC2
AKT
Rapamycin
mTORC1
S6K1
4E-BP1
eIF4E
Cell size
Protein synthesis

Figure 2

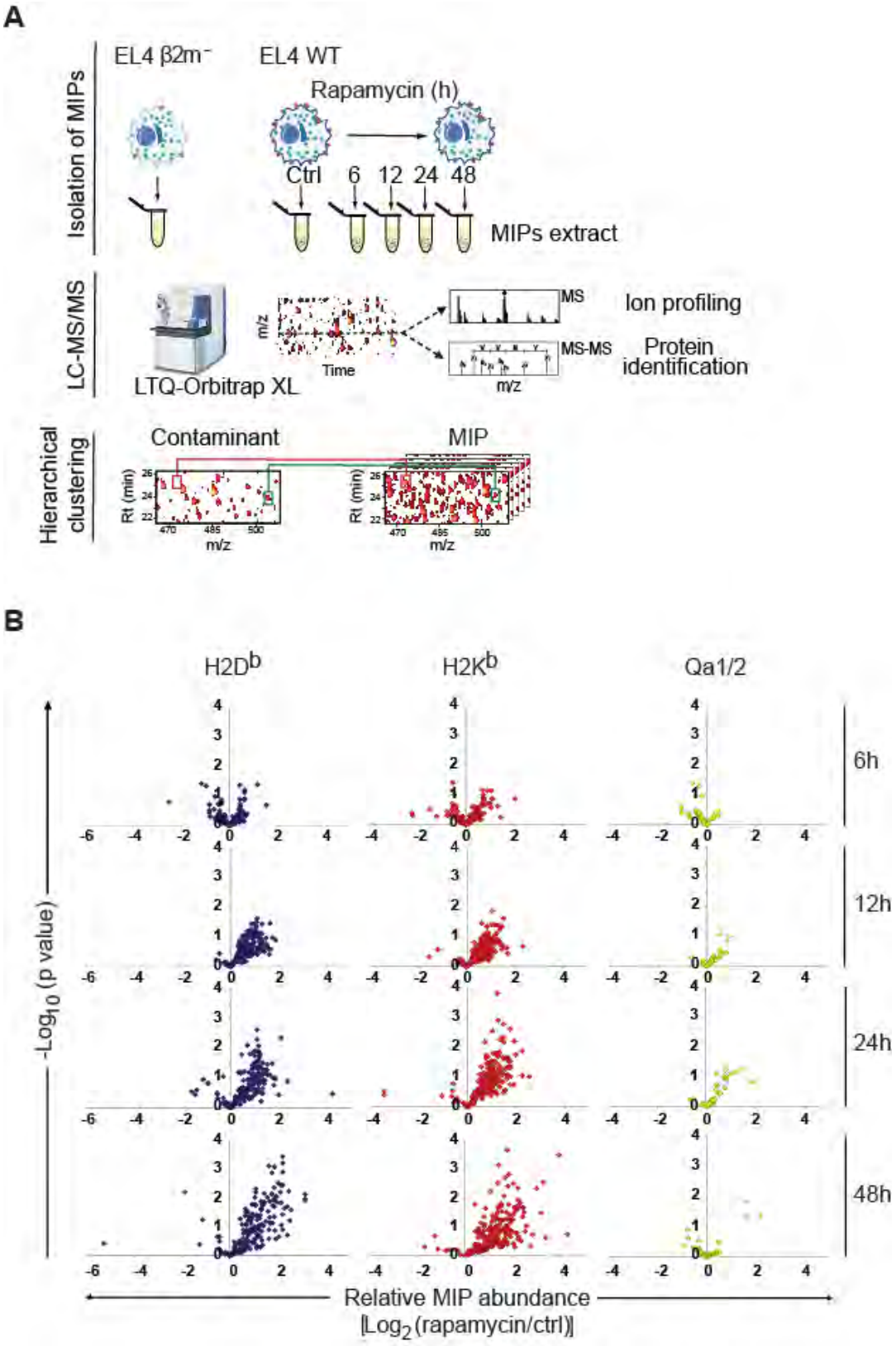
A
Isolation of MIPs
EL4 β2m⁻
EL4 WT
Rapamycin (h)
Ctrl
6
12
24
48
MIPs extract
LC-MS/MS
LTQ-Orbitrap XL
Time
m/z
MS
MS-MS
Ion profiling
Protein identification
Hierarchical clustering
Contaminant
MIP
Rt (min)
m/z
B
H2D^b
H2K^b
Qa1/2
6h
12h
24h
48h
-Log10 (p value)
Relative MIP abundance
[Log2 (rapamycin/ctrl)]

Figure 3

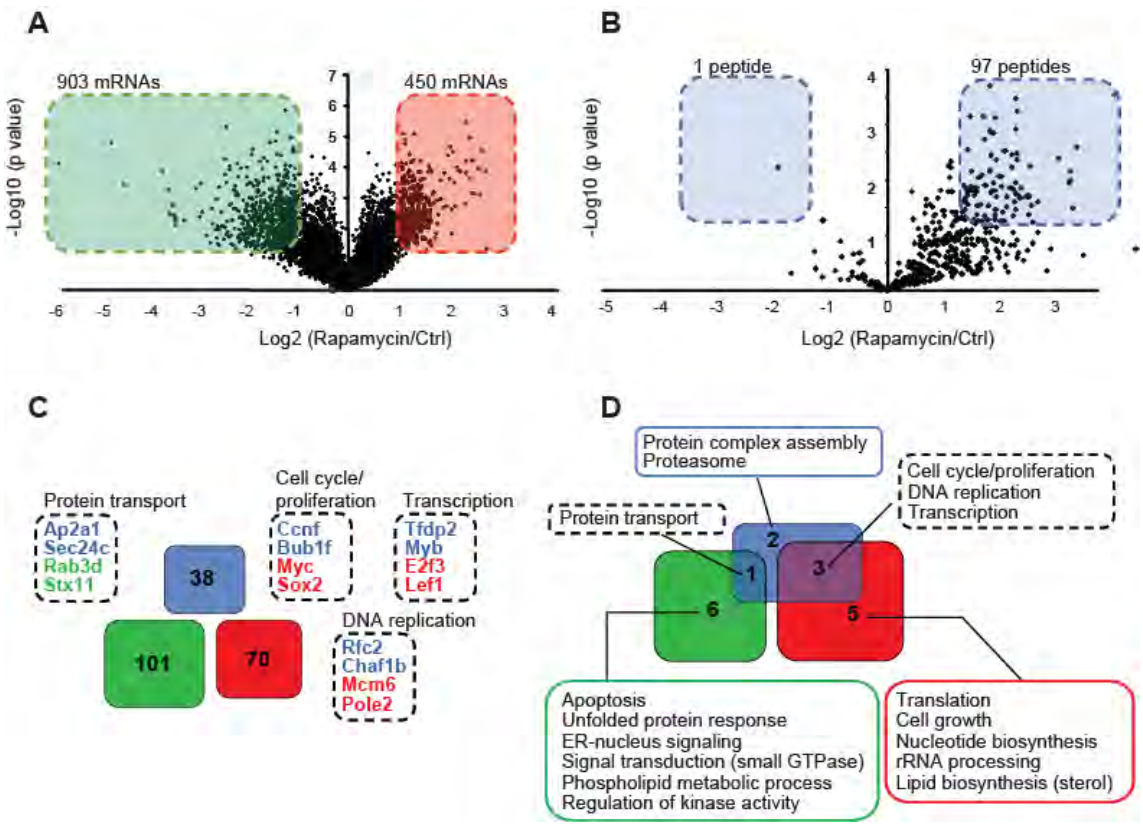
A
903 mRNAs
450 mRNAs
-Log10 (p value)
Log2 (Rapamycin/Ctrl)
B
1 peptide
97 peptides
-Log10 (p value)
Log2 (Rapamycin/Ctrl)
C
Protein transport
Ap2a1
Sec24c
Rab3d
Stx11
38
Cell cycle/
proliferation
Ccnf
Bub1f
Myc
Sox2
Transcription
Tfdp2
Myb
E2f3
Lef1
DNA replication
Rfc2
Chaf1b
Mcm6
Pole2
101
70
D
Protein complex assembly
Proteasome
Protein transport
Cell cycle/proliferation
DNA replication
Transcription
1
2
3
6
5
Apoptosis
Unfolded protein response
ER-nucleus signaling
Signal transduction (small GTPase)
Phospholipid metabolic process
Regulation of kinase activity
Translation
Cell growth
Nucleotide biosynthesis
rRNA processing
Lipid biosynthesis (sterol)

Figure 4

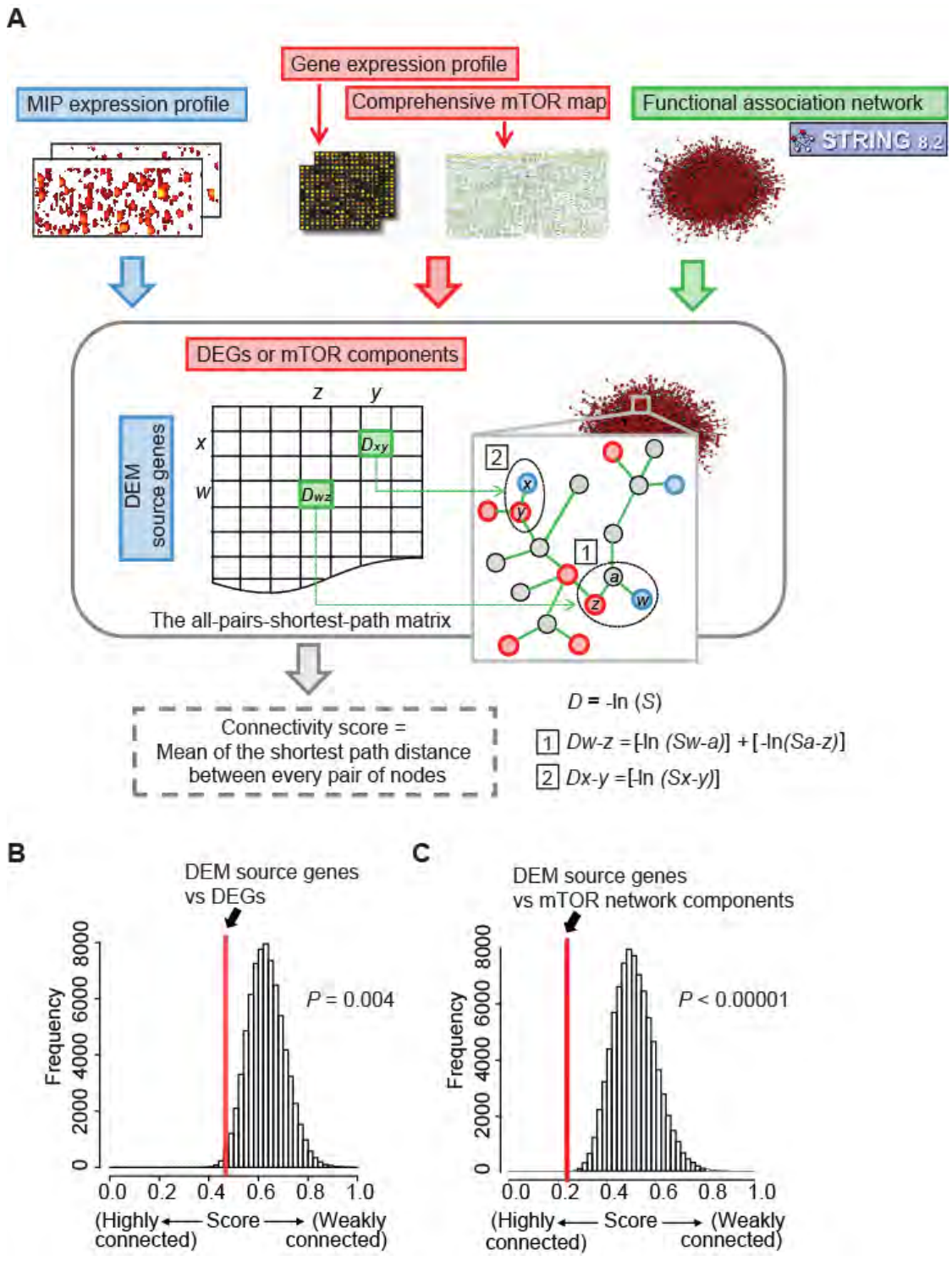
A
Gene expression profile
MIP expression profile
Comprehensive mTOR map
Functional association network
STRING 8.2
DEGs or mTOR components
DEM source genes
z
y
x
w
Dxy
Dwz
2
1
The all-pairs-shortest-path matrix
Connectivity score =
Mean of the shortest path distance
between every pair of nodes
D = -ln (S)
1 Dw-z = [-ln (Sw-a)] + [-ln(Sa-z)]
2 Dx-y = [-ln (Sx-y)]
B
DEM source genes
vs DEGs
P = 0.004
Frequency
0 2000 4000 6000 8000
0.0 0.2 0.4 0.6 0.8 1.0
(Highly connected) Score (Weakly connected)
C
DEM source genes
vs mTOR network components
P < 0.00001
Frequency
0 2000 4000 6000 8000
0.0 0.2 0.4 0.6 0.8 1.0
(Highly connected) Score (Weakly connected)

Figure 5

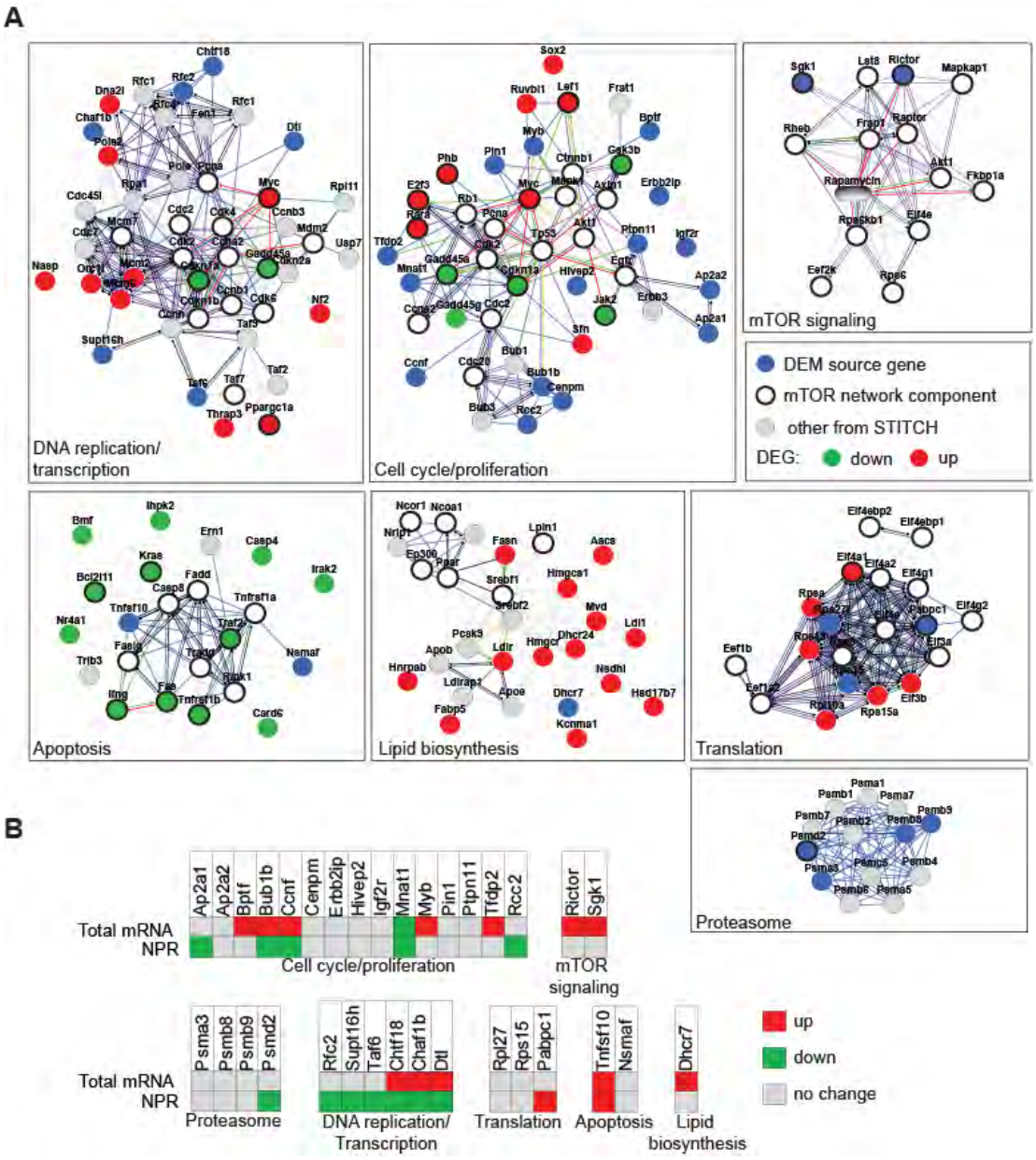
A
DNA replication/ transcription
Cell cycle/proliferation
mTOR signaling
DEM source gene
mTOR network component
other from STITCH
DEG: down up
Apoptosis
Lipid biosynthesis
Translation
Proteasome
B
Total mRNA
NPR
Ap2a1 Ap2a2 Bptf Bub1b Ccnf Cenpm Erbb2ip Hivep2 Igf2r Mnat1 Myb Pin1 Ptpn11 Tfdp2 Rcc2
Cell cycle/proliferation
Rictor Sgk1
mTOR signaling
Psma3 Psmb8 Psmb9 Psmd2
Proteasome
Rfc2 Supt16h Taf6 Chtf18 Chaf1b Dtl
DNA replication/ Transcription
Rpl27 Rps15 Pabpc1
Translation
Tnfsf10 Nsmaf
Apoptosis
Dhcr7
Lipid biosynthesis
up
down
no change

Figure 6

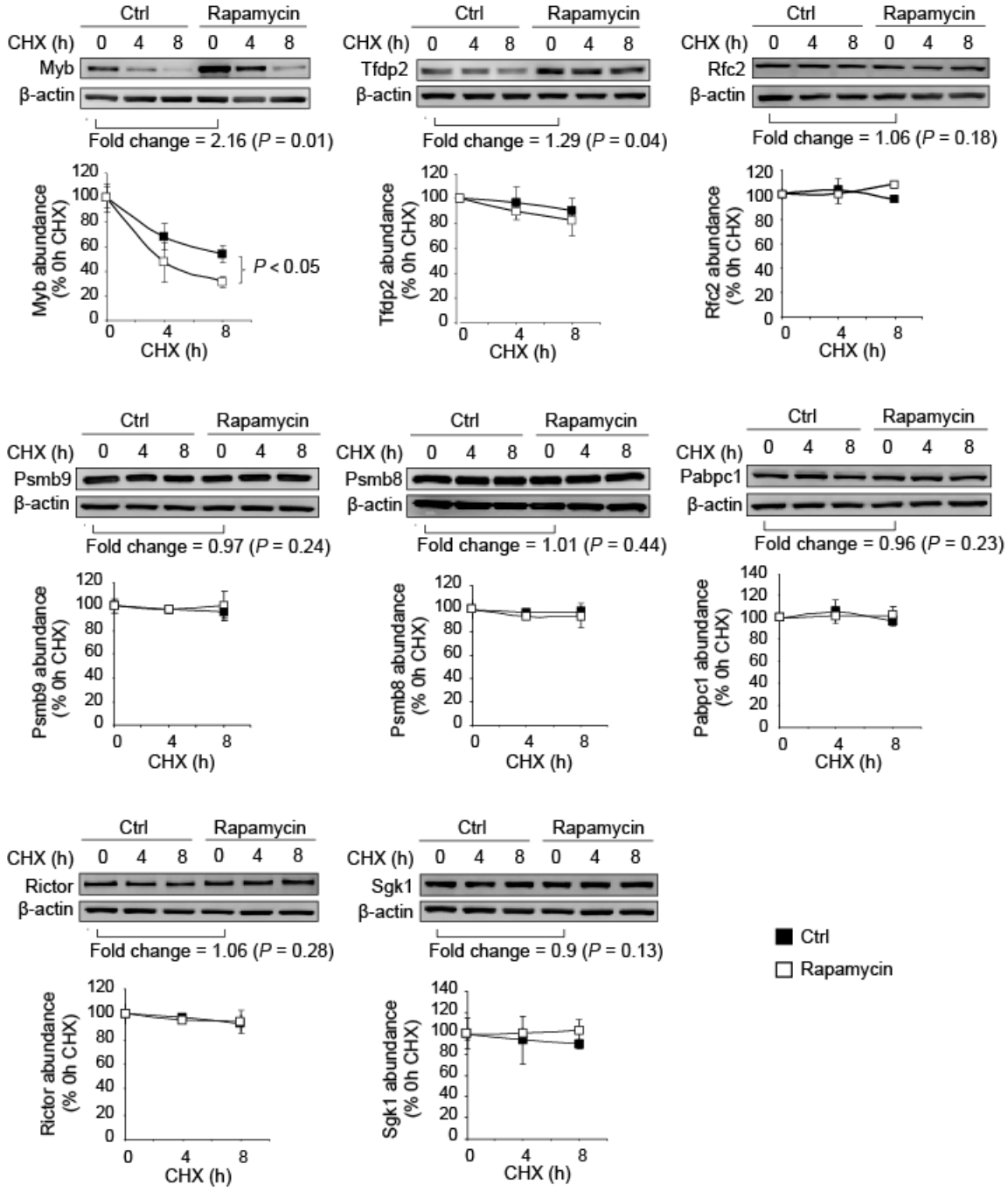
Ctrl
Rapamycin
CHX (h) 0 4 8 0 4 8
Myb
β-actin
Fold change = 2.16 (P = 0.01)
Myb abundance (% 0h CHX)
P < 0.05
CHX (h)
Tfdp2
Fold change = 1.29 (P = 0.04)
Tfdp2 abundance (% 0h CHX)
Rfc2
Fold change = 1.06 (P = 0.18)
Rfc2 abundance (% 0h CHX)
Psmb9
Fold change = 0.97 (P = 0.24)
Psmb9 abundance (% 0h CHX)
Psmb8
Fold change = 1.01 (P = 0.44)
Psmb8 abundance (% 0h CHX)
Pabpc1
Fold change = 0.96 (P = 0.23)
Pabpc1 abundance (% 0h CHX)
Rictor
Fold change = 1.06 (P = 0.28)
Rictor abundance (% 0h CHX)
Sgk1
Fold change = 0.9 (P = 0.13)
Sgk1 abundance (% 0h CHX)
Ctrl
Rapamycin

Figure 7

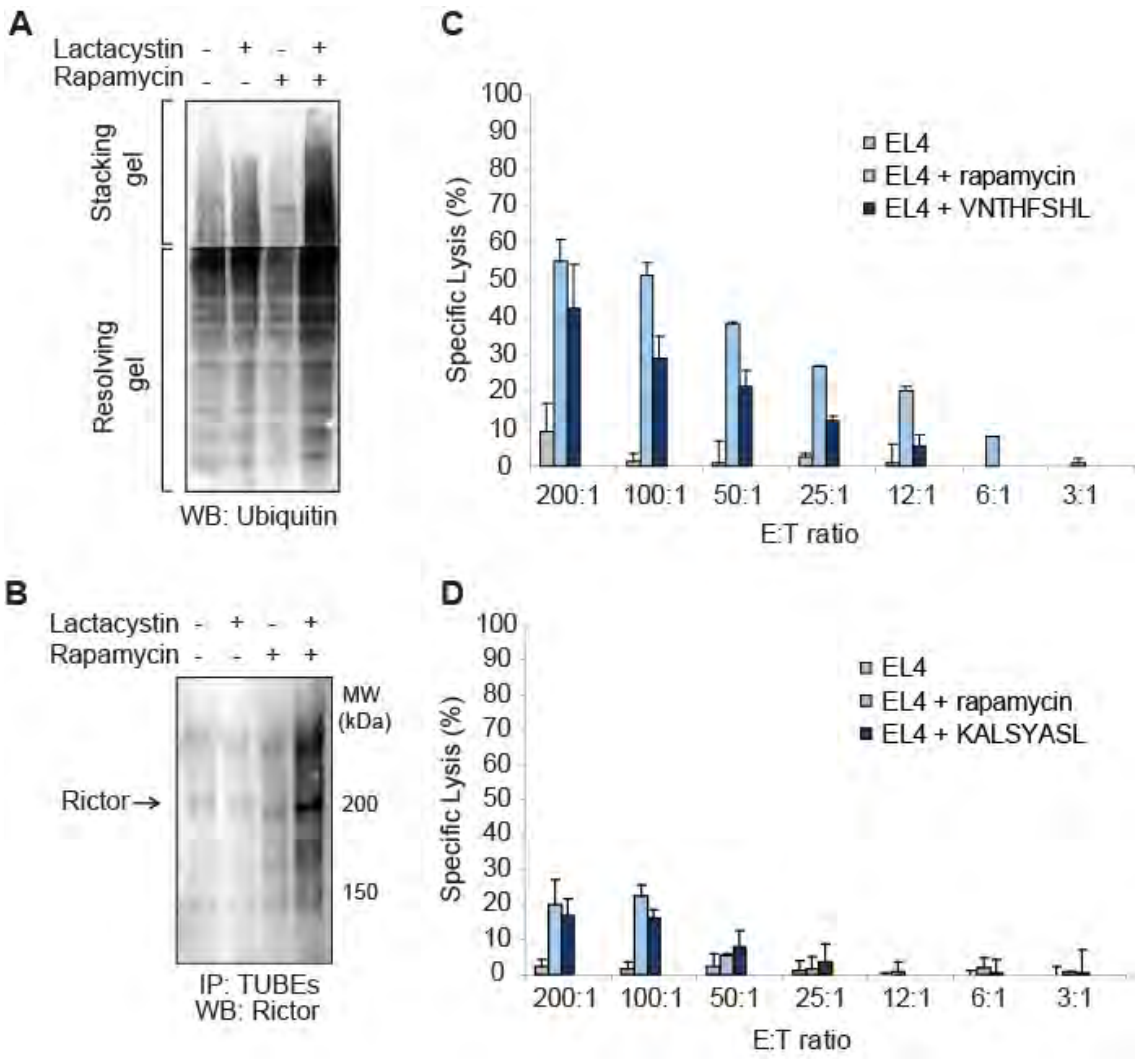
A
Lactacystin - + - +
Rapamycin - - + +
Stacking gel
Resolving gel
WB: Ubiquitin
B
Lactacystin - + - +
Rapamycin - - + +
MW (kDa)
Rictor→
200
150
IP: TUBEs
WB: Rictor
C
Specific Lysis (%)
EL4
EL4 + rapamycin
EL4 + VNTHFSHL
200:1 100:1 50:1 25:1 12:1 6:1 3:1
E:T ratio
D
Specific Lysis (%)
EL4
EL4 + rapamycin
EL4 + KALSYASL
200:1 100:1 50:1 25:1 12:1 6:1 3:1
E:T ratio

Supplementary Figure 1

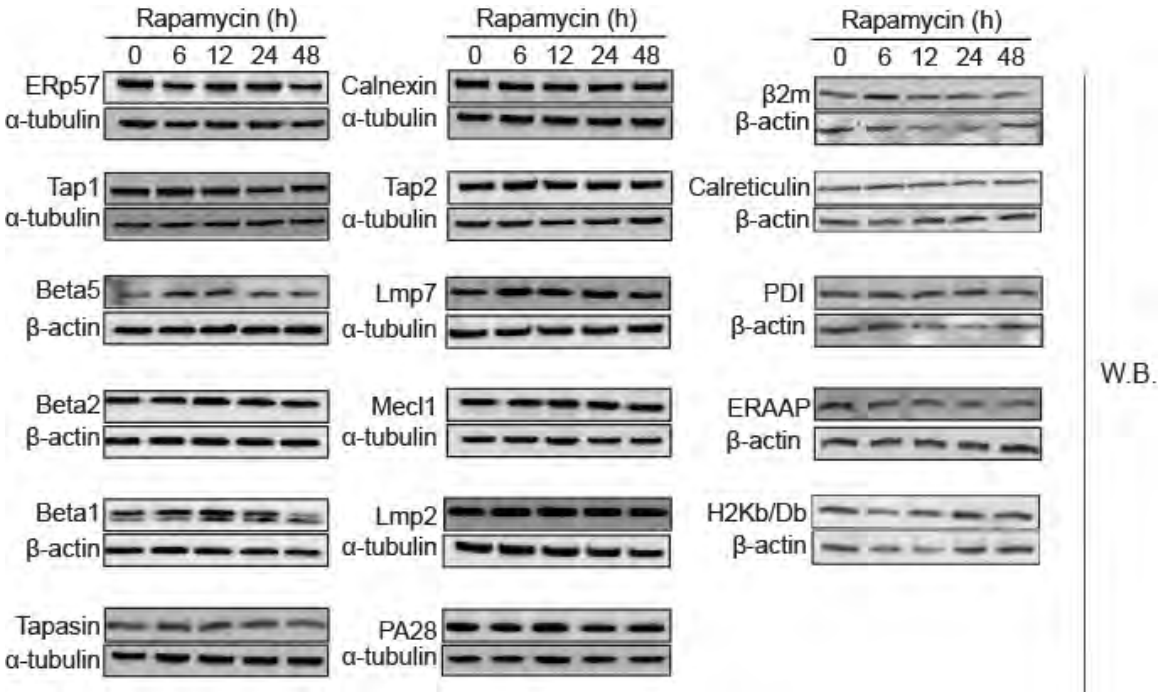

Supplementary Figure 2

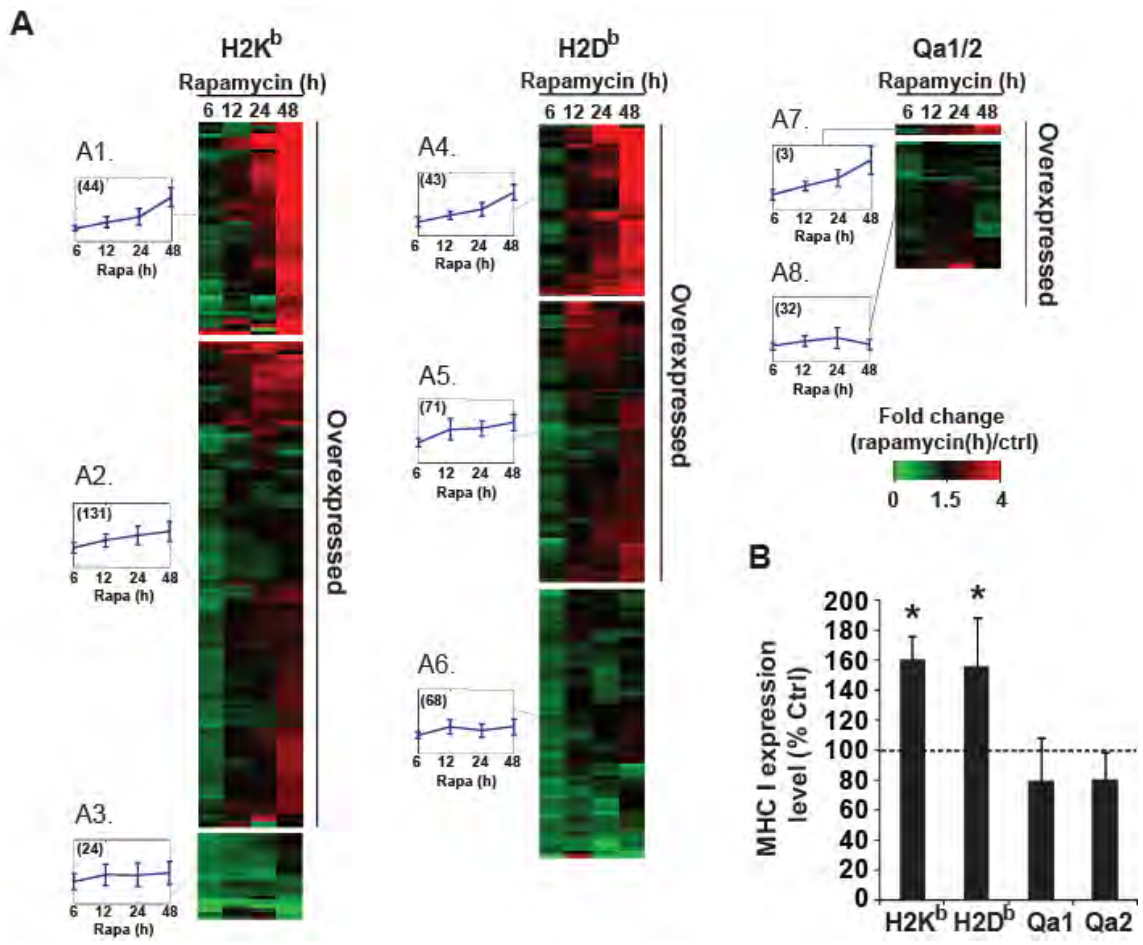

Supplementary Figure 3

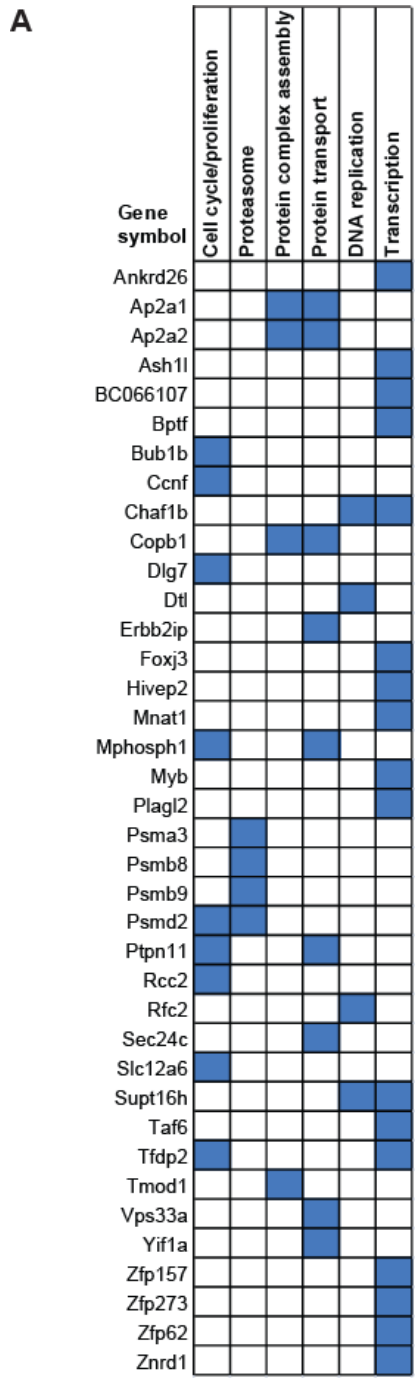

Supplementary Figure 3 (continued)

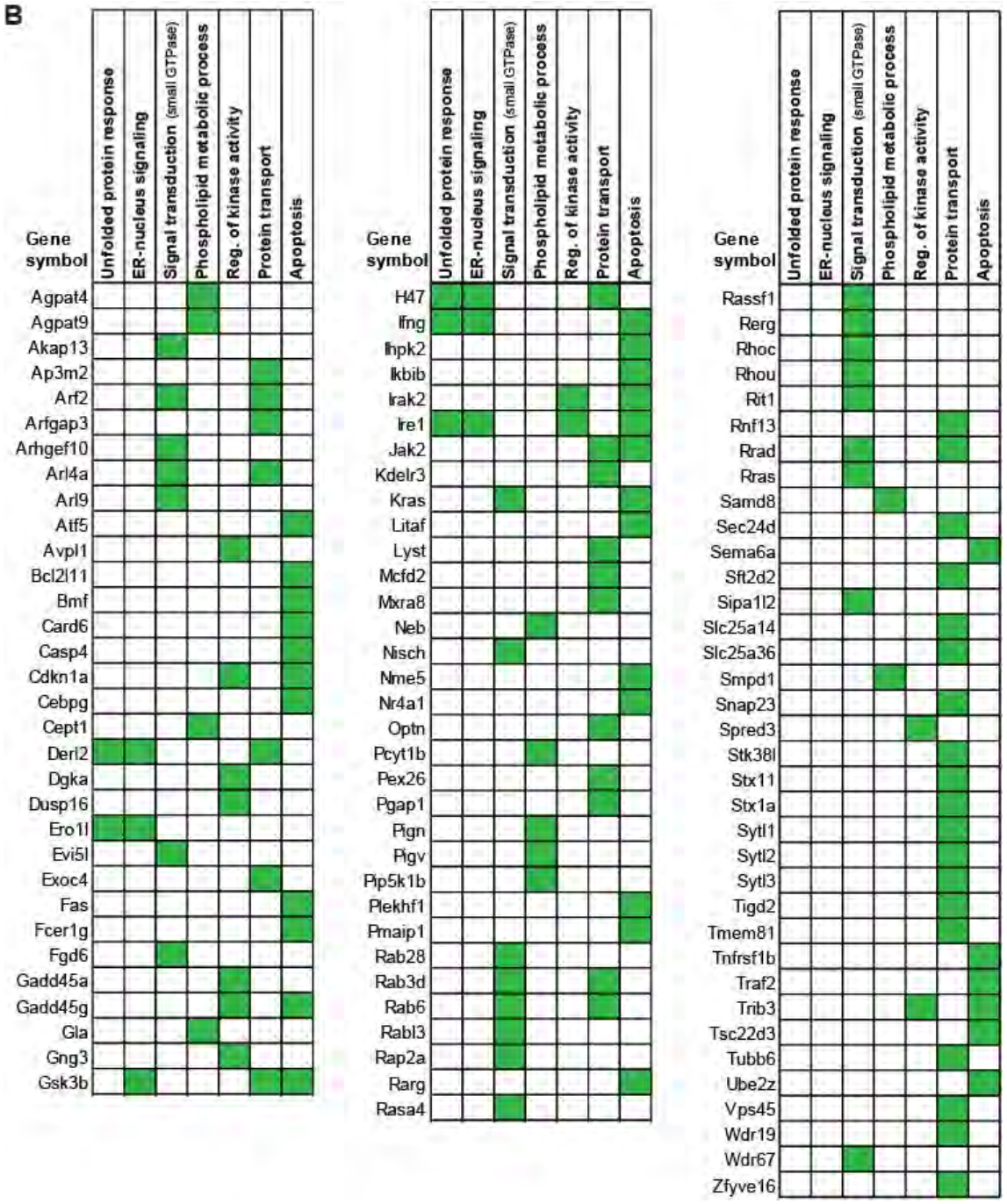

Supplementary Figure 3 (continued)

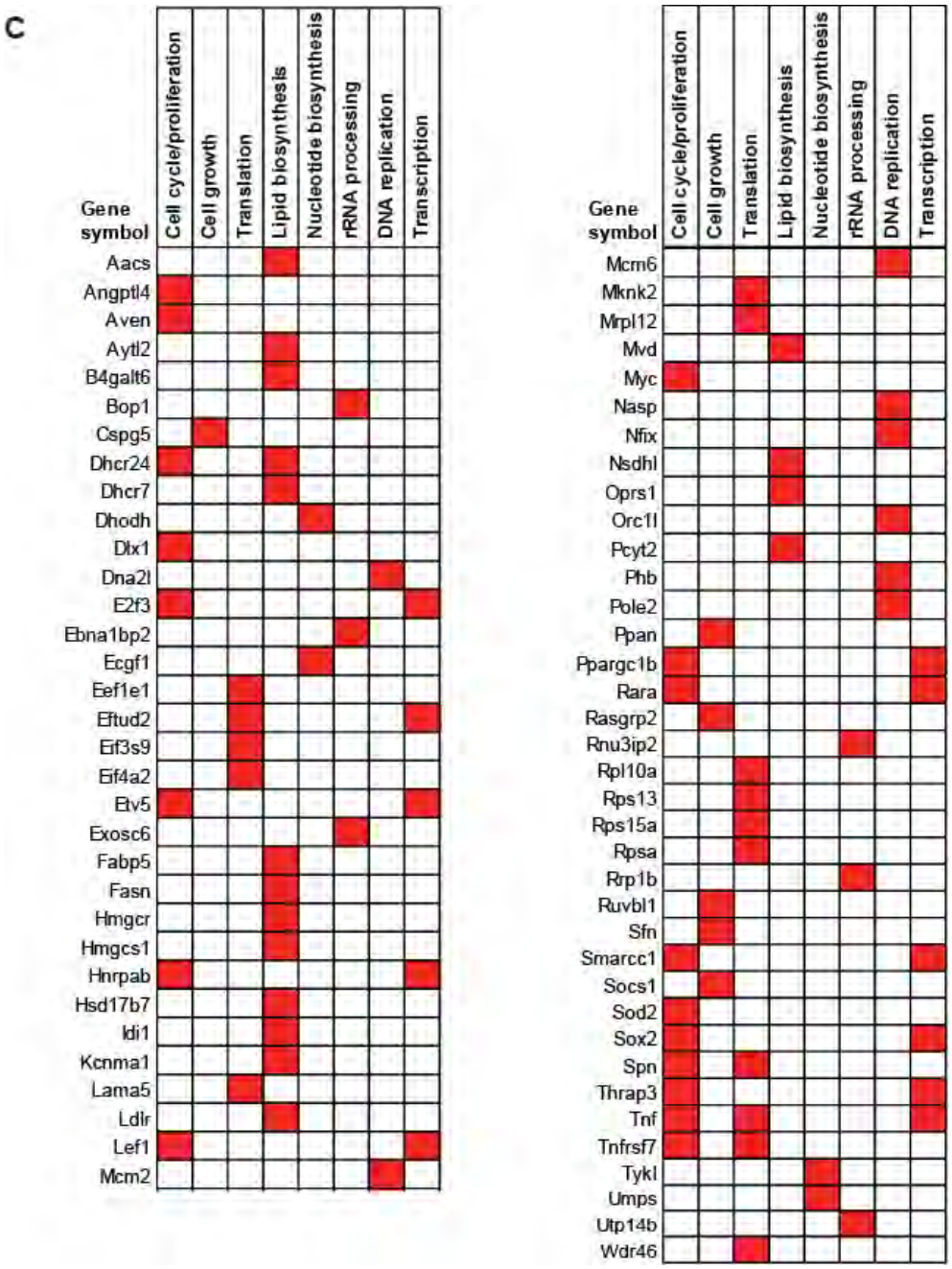

Supplementary Figure 4

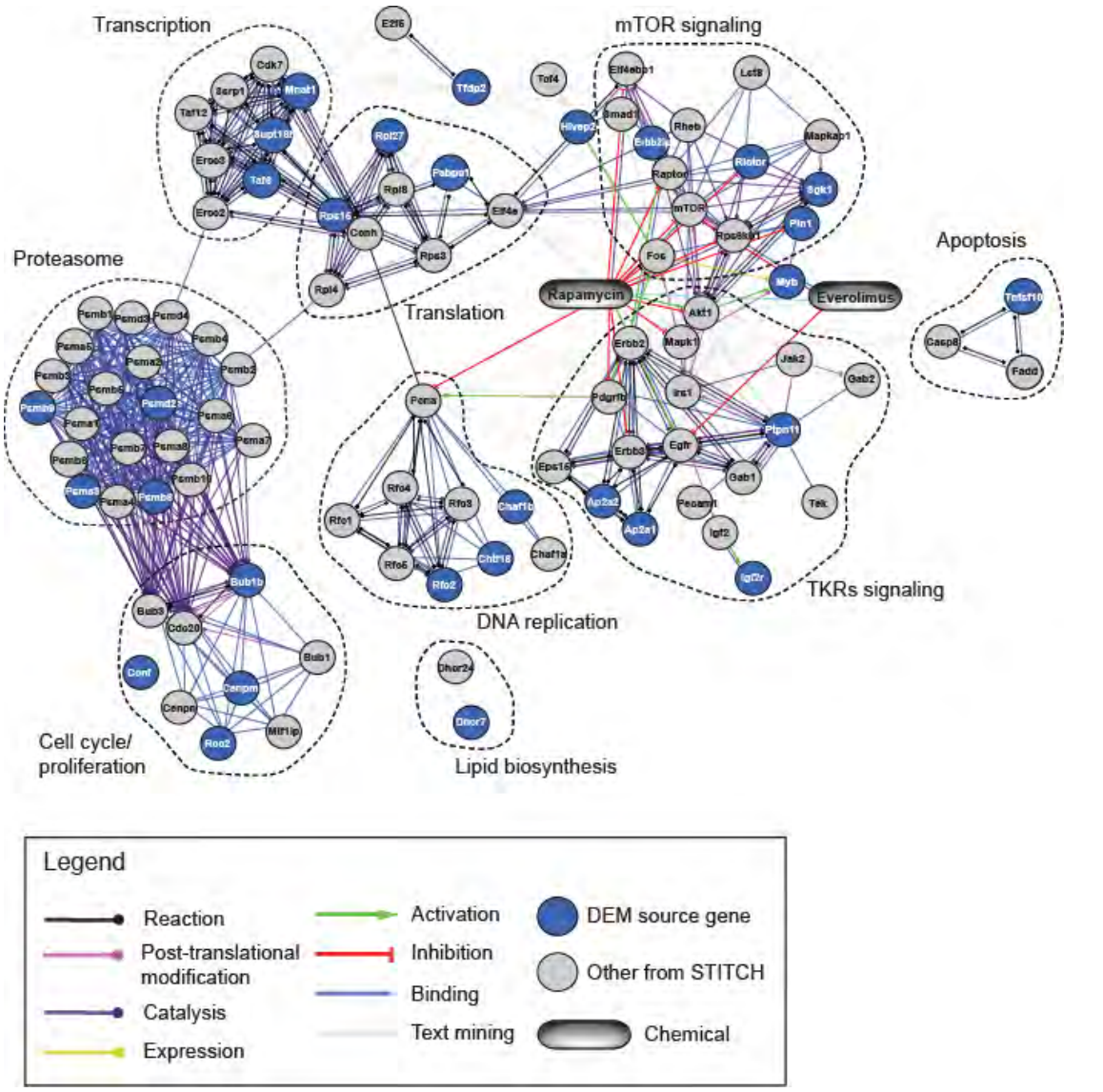

Supplementary Table 1

Relative abundance of 422 MIPs upon rapamycin treatment for 6h, 12h, 24h, and 48h. Fold change (FC) represents the rapamycin/ctrl peptide abundance ratio. Source proteins coding for the most differentially expressed MIPs (DEMs) are highlighted in blue (FC≥2.5, p<0.05). "ND" corresponds to not detected.

GeneID	Gene symbol	Peptide	MHCI allele	Relative MIP abundance (rapamycin/ctrl)							
				6h		12h		24h		48h	
				FC	p value	FC	p value	FC	p value	FC	p value
56700	0610031J06Rik	SALVFTRL	H2Kb	1.23	0.629	1.38	0.217	1.63	0.085	2.39	0.312
68523	1110019N10Rik	AALENTHLL	H2Db	0.93	0.858	1.08	0.743	0.53	0.142	1.52	0.437
66185	1110037F02Rik	RQILNADAM	H2Db	1.01	0.977	1.30	0.420	1.43	0.219	1.70	0.148
74133	1200011M11Rik	KSYNFHTGL	H2Kb	0.91	0.537	1.60	0.313	1.77	0.020	2.61	0.242
67463	1200014M14Rik	GALENAKAEI	H2Db	0.96	0.916	1.66	0.215	1.47	0.333	2.09	0.009
67490	1810074P20Rik	KQLEVVHTL	Qa2	0.78	0.456	1.04	0.916	1.02	0.961	0.98	0.949
100910	2010209O12Rik	AQIRNLTVL	H2Db	0.73	0.186	1.45	0.264	1.34	0.375	1.86	0.121
268721	**2310021P13Rik**	**RAPAFHQL**	**H2Kb**	**1.38**	**0.438**	**2.59**	**0.143**	**2.46**	**0.102**	**4.61**	**0.018**
227446	2310035C23Rik	SSVSNKTTL	H2Db	0.73	0.473	1.38	0.575	0.95	0.893	1.63	0.549
72368	**2310045N01Rik**	**SSVYFRSV**	**H2Kb**	**1.54**	**0.418**	**2.32**	**0.297**	**2.14**	**0.180**	**4.16**	**0.030**
75425	**2610036D13Rik**	**QTVENVEHL**	**H2Db**	**0.92**	**0.810**	**1.74**	**0.057**	**2.08**	**0.105**	**2.99**	**0.009**
72722	**2810405J04Rik**	**ASPEFTKL**	**H2Kb**	**1.41**	**0.412**	**2.08**	**0.122**	**2.48**	**0.214**	**3.98**	**0.038**
67268	2900073G15Rik	SMGKNPTDEYL	H2Db	1.13	0.673	1.63	0.279	1.89	0.167	2.18	0.037
67392	4833420G17Rik	FVISNYREQL	H2Db	0.83	0.741	2.31	0.214	2.24	0.083	1.65	0.279
382051	4833426J09Rik	MAHVNGVHL	H2Db	0.86	0.487	1.11	0.767	1.16	0.428	2.12	0.005
75007	4930504E06Rik	VNVRFTGV	H2Kb	0.90	0.816	1.43	0.320	1.82	0.326	1.87	0.235
232853	5730403M16Rik	SSYNFIRHM	H2Db	0.88	0.792	1.22	0.707	1.32	0.436	0.99	0.989
74741	5730419I09Rik	AAVLNPRFL	H2Db	1.00	0.990	1.58	0.238	2.13	0.002	2.25	0.056
77877	6030458C11Rik	KVLDVLHSL	Qa2	1.37	0.503	0.93	0.801	3.55	0.150	1.03	0.966
218989	6720456H20Rik	TGIRNLEWL	H2Db	0.18	0.160	3.06	0.382	0.38	0.248	0.42	0.401
382252	**A830080D01Rik**	**VSYNHTNI**	**H2Db**	**1.43**	**0.344**	**1.86**	**0.037**	**2.17**	**0.049**	**3.63**	**0.0007**
56321	Aatf	RAVKNQIAL	H2Db	0.66	0.105	0.96	0.899	0.99	0.945	2.15	0.006
320631	Abca15	VEFFLDAL	H2Kb	0.99	0.981	1.75	0.225	1.34	0.383	2.21	0.186
18671	Abcb1a	STVRNADVI	H2Db	1.05	0.922	1.26	0.542	0.95	0.898	1.24	0.588
11666	Abcd1	RVVANSEEI	H2Db	2.88	0.204	2.51	0.152	3.94	0.359	4.19	0.217
11307	Abcg1	VNIEFKDL	H2Kb	1.16	0.697	1.70	0.215	2.44	0.079	2.25	0.452
27405	**Abcg3**	**SSYFFGKL**	**H2Kb**	**0.88**	**0.718**	**1.30**	**0.512**	**2.81**	**0.006**	**5.71**	**0.139**
99382	**Abtb2**	**NTYKYAKI**	**H2Kb**	**0.76**	**0.253**	**1.23**	**0.451**	**1.69**	**0.019**	**3.39**	**0.0002**
11432	Acp2	RSIQNAQFL	H2Db	0.80	0.164	1.35	0.251	1.38	0.017	1.67	0.028
66713	Actr2	YAGSNFPEHI	H2Db	0.90	0.684	1.37	0.207	1.00	0.987	0.99	0.967
67019	Actr6	SGYSFTHI	H2Kb	1.00	0.995	1.59	0.107	1.36	0.140	2.17	0.067
57869	Adck2	SGPTYIKL	H2Kb	0.99	0.976	1.40	0.205	1.47	0.264	2.26	0.038
11566	**Adss**	**VSLKYAHM**	**H2Kb**	**1.63**	**0.179**	**1.93**	**0.096**	**3.26**	**0.042**	**2.83**	**0.053**
226747	Ahctf1	TSVENHEFL	H2Db	0.97	0.914	2.05	0.041	1.54	0.257	2.15	0.016
380959	Alg10b	GVLRFVNL	H2Kb	1.04	0.949	1.71	0.453	2.05	0.139	2.91	0.445
223774	Alg12	AAMLNYTHI	H2Db	1.16	0.672	1.08	0.831	1.35	0.380	2.03	0.335
109674	Ampd2	VGYRYETL	H2Kb	0.86	0.681	1.18	0.626	1.16	0.644	2.78	0.057
81702	Ankrd17	ASVLNVNHI	H2Db	0.93	0.860	1.21	0.534	1.11	0.770	1.22	0.605
232339	**Ankrd26**	**AVYSYKRL**	**H2Kb**	**1.04**	**0.872**	**1.25**	**0.544**	**1.95**	**0.028**	**3.59**	**0.016**
329154	Ankrd44	ASVINGHTL	H2Db	1.38	0.217	2.14	0.024	2.39	0.081	2.34	0.121
237615	Ankrd52	SSLSNEHVL	Qa2	1.08	0.706	1.45	0.094	1.42	0.359	1.37	0.323
11761	Aox1	NAYKFPNL	H2Kb	0.85	0.600	1.18	0.626	1.30	0.399	1.11	0.668

11771	Ap2a1	TNLRYLAL	H2Kb	1.37	0.316	1.82	0.398	3.10	0.087	2.82	0.149
11771	**Ap2a1**	**SQLRNADVEL**	**H2Db**	**1.00**	**0.999**	**1.58**	**0.193**	**2.00**	**0.017**	**2.58**	**0.015**
11772	**Ap2a2**	**SQLKNADVEL**	**H2Db**	**1.10**	**0.754**	**1.58**	**0.202**	**3.05**	**0.076**	**3.39**	**0.007**
66884	Appbp2	RLLQEAHDL	Qa2	0.66	0.039	0.88	0.759	1.11	0.747	0.86	0.732
75415	Arhgap12	YGLLNVTKI	H2Db	0.99	0.974	1.72	0.311	1.93	0.157	1.71	0.437
71435	Arhgap21	TGVTNRDLI	H2Db	1.26	0.705	0.87	0.719	1.87	0.423	2.04	0.255
54208	Arl6ip1	IILKYIGM	H2Kb	1.53	0.675	0.82	0.521	2.54	0.096	19.53	0.177
192195	**Ash1l**	**VGLINKDSV**	**H2Db**	**0.94**	**0.859**	**1.54**	**0.142**	**1.56**	**0.236**	**3.64**	**0.042**
320817	Atad2b	YGIQNHHEV	H2Db	0.75	0.323	0.93	0.790	1.25	0.514	1.85	0.058
67972	Atp2b1	KVYTFNSV	H2Kb	0.96	0.899	1.32	0.395	1.18	0.586	2.04	0.132
54670	Atp8b1	KNFAFTLV	H2Kb	1.17	0.720	1.50	0.414	2.67	0.082	2.40	0.312
54138	Atxn10	NSIRNLDTI	H2Db	0.84	0.651	1.21	0.506	1.01	0.966	1.28	0.362
231874	AU022870	KIQSFINRM	H2Kb	1.33	0.600	1.61	0.540	2.64	0.057	3.40	0.088
228850	B230339M05Rik	KSYVNPTEL	H2Db	0.94	0.831	1.70	0.293	1.18	0.739	2.42	0.084
226562	Bat2d	SQLIDTHLL	Qa2	1.24	0.511	1.84	0.142	1.93	0.080	1.21	0.802
217578	Baz1a	SALENGRYEL	H2Db	0.51	0.047	1.55	0.244	1.17	0.566	1.30	0.309
80744	BC003993	ASPIFTHV	H2Kb	1.27	0.522	1.67	0.085	1.68	0.138	1.69	0.485
224823	BC011248	KTYQFLNDI	H2Kb	1.12	0.739	1.47	0.424	1.35	0.410	1.14	0.851
105203	**BC016423**	**SSSLNQEKI**	**H2Db**	**1.18**	**0.560**	**2.00**	**0.055**	**1.81**	**0.106**	**2.61**	**0.017**
231123	BC023882	TSYRFLAL	H2Kb	1.10	0.740	1.50	0.189	1.65	0.125	2.27	0.301
231123	BC023882	SQLNELHHL	H2Db	0.75	0.390	1.09	0.771	1.12	0.669	1.22	0.620
217216	BC030867	SALENAENHV	H2Db	0.95	0.845	1.46	0.185	1.53	0.322	2.48	0.025
231128	**BC037112**	**AAPRNSPTGL**	**H2Db**	**0.96**	**0.885**	**1.42**	**0.090**	**1.96**	**0.072**	**3.39**	**0.007**
240066	**BC066107**	**SSFQFHNRM**	**H2Kb**	**1.13**	**0.550**	**1.21**	**0.694**	**1.99**	**0.029**	**3.55**	**0.001**
12211	Birc6	VNYHYMSQV	H2Kb	1.04	0.920	1.58	0.429	1.51	0.248	1.42	0.473
213895	Bms1	YQNQEIHNL	Qa2	0.88	0.743	1.13	0.716	1.09	0.795	0.95	0.874
12176	Bnip3	LSMRNTSVM	H2Db	0.86	0.690	0.73	0.377	0.46	0.114	0.70	0.214
12181	Bop1	EQVALVHRL	Qa2	0.86	0.563	1.08	0.786	1.03	0.896	0.58	0.238
207165	**Bptf**	**KAVDFDGRL**	**H2Kb**	**1.29**	**0.252**	**1.89**	**0.266**	**3.20**	**0.028**	**4.70**	**0.004**
12190	Brca2	HAIENIDTF	H2Db	0.96	0.913	1.62	0.062	1.29	0.263	1.80	0.121
107976	Bre	ATQVYPKL	H2Kb	0.90	0.752	1.13	0.657	1.32	0.415	2.29	0.052
107182	Btaf1	GQIQNKEVL	H2Db	1.19	0.776	2.16	0.081	2.25	0.067	1.16	0.821
12236	**Bub1b**	**IITGFRNV**	**H2Kb**	**0.59**	**0.487**	**1.86**	**0.229**	**1.72**	**0.243**	**3.62**	**0.051**
67832	Bxdc2	FLVQNIHTL	H2Db	1.34	0.130	1.74	0.063	2.79	0.055	3.11	0.121
277939	C2cd3	VITKFDHL	H2Kb	1.11	0.830	1.58	0.504	2.32	0.158	3.21	0.119
77480	C330002I19Rik	RANQNFDEI	H2Db	0.74	0.684	0.90	0.876	1.06	0.922	1.45	0.549
224171	C330027C09Rik	AQNDIEHLF	Qa2	1.02	0.972	1.14	0.688	1.26	0.567	0.82	0.697
69719	Cad	RQAENGMYI	H2Db	1.52	0.541	2.35	0.306	3.65	0.105	3.13	0.256
227541	Camk1d	KIFEFKETL	H2Kb	0.68	0.462	1.11	0.814	4.76	0.086	4.09	0.366
12340	Capza1	ISFKFDHL	H2Kb	0.68	0.474	1.03	0.956	2.33	0.105	0.63	0.621
26885	Casp8ap2	VTVLNVDHL	H2Db	0.95	0.847	1.30	0.137	1.39	0.356	1.27	0.739
234309	Cbr4	AAGINRDSL	H2Db	1.41	0.637	1.38	0.643	1.70	0.497	1.46	0.570
73739	Cby1	ASLSNLHSL	H2Db	1.57	0.464	2.47	0.124	2.44	0.129	3.18	0.068
75565	Ccdc101	ELLTELHQL	Qa2	1.20	0.621	1.45	0.399	1.72	0.114	1.30	0.766
12449	**Ccnf**	**SQAVNKQQI**	**H2Db**	**1.50**	**0.710**	**2.55**	**0.280**	**5.12**	**0.129**	**6.05**	**0.025**
56706	Ccnl1	VINVFHHL	H2Kb	0.88	0.690	1.26	0.540	2.21	0.017	2.74	0.436
12465	Cct5	SMMDVDHQI	Qa2	0.93	0.888	0.93	0.888	0.99	0.988	0.68	0.533
12468	Cct7	RAIKNDSVV	H2Db	0.74	0.192	0.95	0.866	0.52	0.154	1.19	0.708
12501	Cd3e	YSGLNQRAV	H2Db	1.08	0.728	1.44	0.270	1.78	0.111	2.16	0.017
12530	Cdc25a	KGYLFNTV	H2Kb	1.70	0.415	0.90	0.884	0.96	0.949	1.20	0.756

12537	Cdc2l1	VMNYVEHDL	Qa2	0.59	0.441	0.65	0.523	0.70	0.550	0.88	0.784
12576	Cdkn1b	FGPVNHEEL	H2Db	0.86	0.537	1.09	0.686	1.24	0.250	1.95	0.036
229841	Cenpe	SALQNAESDRL	H2Db	1.25	0.672	2.24	0.105	1.82	0.262	1.97	0.139
229841	Cenpe	EQNESAHTL	Qa2	0.49	0.391	1.03	0.955	0.64	0.583	0.53	0.433
66570	**Cenpm**	**RSPENPPSKEL**	**H2Db**	**1.07**	**0.916**	**2.04**	**0.335**	**2.13**	**0.084**	**3.90**	**0.013**
216859	**Centb1**	**INQIYEARV**	**H2Kb**	**0.95**	**0.820**	**1.49**	**0.119**	**1.77**	**0.073**	**2.89**	**0.016**
110749	**Chaf1b**	**SNIHYHTL**	**H2Kb**	**1.36**	**0.437**	**2.06**	**0.321**	**2.04**	**0.058**	**2.62**	**0.028**
12649	Chek1	TGPSNVDKL	H2Db	0.72	0.577	0.83	0.750	1.23	0.548	1.23	0.723
27967	Cherp	KSYSFIARM	H2Kb	0.96	0.893	1.02	0.968	2.09	0.015	2.56	0.117
214901	**Chtf18**	**QLSDTLHSL**	**Qa2**	**1.00**	**0.996**	**1.56**	**0.394**	**1.64**	**0.095**	**4.47**	**0.044**
80986	Ckap2	TLNDLIHNI	Qa2	0.94	0.919	1.76	0.358	1.67	0.228	1.42	0.723
53321	**Cntnap1**	**SGVRFNNV**	**H2Kb**	**1.45**	**0.272**	**2.51**	**0.041**	**2.37**	**0.019**	**5.56**	**0.029**
12847	Copa	SQLPVDHIL	Qa2	0.89	0.745	1.21	0.473	1.20	0.601	0.77	0.526
70349	**Copb1**	**IALRYVAL**	**H2Kb**	**1.32**	**0.498**	**1.78**	**0.144**	**2.79**	**0.002**	**4.35**	**0.154**
70349	Copb1	KMLEVFHAI	Qa2	0.97	0.949	1.11	0.842	1.50	0.341	0.92	0.912
26893	Cops6	NQFVNKFNVL	H2Db	1.04	0.968	1.37	0.755	1.82	0.466	1.84	0.566
23790	**Coro1c**	**ASVQNEAKL**	**H2Db**	**1.53**	**0.447**	**3.15**	**0.034**	**1.66**	**0.112**	**1.96**	**0.350**
74114	Crot	IQLMNTAHL	H2Db	0.99	0.987	1.60	0.358	2.51	0.324	4.73	0.124
12387	Ctnnb1	RTYTYEKL	H2Kb	0.71	0.260	1.00	0.999	1.05	0.832	1.83	0.022
51797	Ctps	AVVEFSRNV	H2Kb	0.96	0.803	1.80	0.042	1.48	0.044	2.08	0.005
71745	Cul2	VINSFVHV	H2Kb	1.01	0.976	1.23	0.534	1.57	0.161	1.83	0.356
12767	Cxcr4	VVFQFQHI	H2Kb	1.01	0.978	1.56	0.176	1.63	0.072	2.67	0.304
320714	**D030016E14Rik**	**VSTKFEHL**	**H2Kb**	**1.00**	**0.992**	**1.81**	**0.183**	**1.74**	**0.034**	**2.61**	**0.003**
52635	**D12Ertd551e**	**VAVKNSGGFL**	**H2Db**	**0.86**	**0.571**	**1.63**	**0.106**	**1.46**	**0.597**	**4.45**	**0.003**
52635	**D12Ertd551e**	**RQLENGTTL**	**H2Db**	**1.34**	**0.660**	**2.42**	**0.076**	**2.68**	**0.063**	**3.68**	**0.004**
218978	**D14Ertd436e**	**SQHVNLDQL**	**H2Db**	**0.96**	**0.862**	**1.50**	**0.155**	**2.18**	**0.028**	**4.68**	**0.001**
67789	**Dalrd3**	**TAPQYYRL**	**H2Kb**	**1.10**	**0.715**	**1.71**	**0.083**	**1.82**	**0.034**	**2.82**	**0.019**
104721	Ddx1	ASVLNKWQM	H2Db	0.89	0.791	1.69	0.175	1.46	0.472	1.31	0.585
67755	Ddx47	KTFLFSATM	H2Kb	1.31	0.516	1.29	0.585	1.82	0.147	1.51	0.522
13209	Ddx6	INFDFPKL	H2Kb	0.98	0.983	2.02	0.509	2.95	0.266	2.90	0.477
76131	**Depdc1a**	**FSQENTEKI**	**H2Db**	**0.93**	**0.892**	**1.85**	**0.280**	**2.02**	**0.311**	**2.71**	**0.013**
13360	**Dhcr7**	**AGVVNKYEV**	**H2Db**	**0.91**	**0.749**	**1.36**	**0.202**	**1.53**	**0.315**	**3.81**	**0.009**
69192	Dhx16	AAIANHQVL	H2Db	1.02	0.961	1.40	0.308	0.81	0.675	1.32	0.339
23856	Dido1	EQQPQQHNL	Qa2	0.93	0.838	1.16	0.694	1.05	0.885	1.06	0.857
218977	**Dlg7**	**VNQKFNNL**	**H2Kb**	**0.79**	**0.361**	**1.46**	**0.234**	**1.51**	**0.131**	**2.69**	**0.001**
66861	Dnajc10	AALIYGKL	H2Kb	1.12	0.501	1.57	0.035	2.03	0.003	3.20	0.265
13430	Dnm2	YAIKNIHGV	H2Db	1.03	0.873	1.62	0.377	1.72	0.015	2.27	0.043
13433	Dnmt1	LSLENGTHTL	H2Db	1.46	0.343	2.48	0.078	2.35	0.117	1.94	0.115
94176	Dock2	SMVQNRVFL	H2Db	0.94	0.864	1.09	0.845	1.31	0.417	1.41	0.417
233115	Dpy19l3	SVVAFHNL	H2Kb	0.98	0.963	1.31	0.424	1.63	0.162	2.42	0.050
76843	**Dtl**	**SSPENKNWL**	**H2Db**	**1.03**	**0.933**	**2.46**	**0.036**	**2.01**	**0.039**	**2.52**	**0.021**
13424	Dync1h1	ASYEFVQRL	H2Kb	1.07	0.779	1.61	0.180	1.60	0.006	1.34	0.604
66967	Edem3	FMATNPEHL	H2Db	0.98	0.946	1.03	0.939	18.64	0.356	1.23	0.605
223691	Eif3eip	TTYKYEMI	H2Kb	2.12	0.136	1.97	0.333	3.00	0.054	3.26	0.088
13669	Eif3s10	QSIEFSRL	H2Kb	1.05	0.884	1.68	0.083	1.24	0.355	1.09	0.741
15568	Elavl1	GAVTNVKVI	H2Db	1.31	0.448	2.12	0.033	2.04	0.031	2.86	0.060
13709	Elf1	LVYQFKEM	H2Kb	0.37	0.307	1.50	0.654	0.48	0.411	2.79	0.481
170439	Elovl6	KSFLFSAL	H2Kb	0.86	0.831	1.63	0.476	2.02	0.184	3.03	0.402
58523	Elp2	SAPRNFVENF	H2Db	0.85	0.453	1.41	0.214	1.24	0.066	1.13	0.503
14791	Emg1	VSVEYTEKM	H2Kb	1.25	0.491	1.74	0.152	2.01	0.164	2.09	0.094

13849	Ephx1	LGYTEKDL	H2Kb	0.21	0.418	1.84	0.520	1.03	0.975	0.31	0.475
59079	**Erbb2ip**	**GSLKNVTTL**	**H2Db**	**1.28**	**0.526**	**2.03**	**0.069**	**2.16**	**0.049**	**4.64**	**0.034**
50505	Ercc4	NQVKNIAEL	H2Db	1.03	0.875	1.36	0.558	1.32	0.474	2.17	0.174
67458	Ergic1	YTVANKEYV	H2Db	0.85	0.590	1.28	0.385	1.17	0.510	1.97	0.036
66366	**Ergic3**	**QQLDVEHNL**	**Qa2**	**0.62**	**0.580**	**1.92**	**0.100**	**2.25**	**0.071**	**2.90**	**0.014**
13877	Erh	YQPYNKDWI	H2Db	0.91	0.892	2.87	0.181	2.21	0.165	2.02	0.360
14049	Eya2/3	TIIIFHSL	H2Kb	1.40	0.525	1.68	0.318	1.94	0.193	1.14	0.894
212377	**F730047E07Rik**	**VGVTYRTL**	**H2Kb**	**1.26**	**0.487**	**1.87**	**0.073**	**2.37**	**0.052**	**4.78**	**0.019**
14104	Fasn	TSVQFMKL	H2Kb	0.97	0.939	1.72	0.253	1.68	0.190	2.30	0.271
107035	Fbxo38	SAFSFRTL	H2Kb	1.07	0.852	1.44	0.187	1.34	0.256	2.41	0.288
74015	**Fcho1**	**SALRFQAM**	**H2Kb**	**1.40**	**0.264**	**1.86**	**0.290**	**3.23**	**0.023**	**5.41**	**0.020**
14137	Fdft1	ISLEFRNL	H2Kb	0.80	0.657	1.28	0.598	1.25	0.526	1.45	0.728
14155	Fem1b	GANVNHTTV	H2Db	0.70	0.701	1.84	0.421	1.32	0.768	2.60	0.425
218952	**Fermt2**	**KTWRFSNM**	**H2Kb**	**1.05**	**0.863**	**2.34**	**0.144**	**2.53**	**0.005**	**4.56**	**0.154**
57778	Fmnl1	LQYEFTHL	H2Kb	1.20	0.837	2.09	0.126	1.68	0.257	1.76	0.197
71409	Fmnl2	LQYEFTKL	H2Kb	1.01	0.966	1.38	0.198	1.70	0.023	2.47	0.143
110606	Fntb	SSYKFNHL	H2Kb	0.71	0.233	0.89	0.692	1.19	0.438	1.59	0.072
230700	**Foxj3**	**NTVTNKVTL**	**H2Db**	**1.39**	**0.290**	**1.99**	**0.150**	**2.70**	**0.052**	**4.70**	**0.003**
239554	Foxred2	LGVTNFVHM	H2Db	0.93	0.846	1.35	0.561	2.58	0.118	3.81	0.250
72313	Fryl	YSGTNTGNVHI	H2Db	1.03	0.945	2.63	0.330	2.32	0.310	1.51	0.248
14359	Fxr1h	EIVTFERL	H2Kb	2.09	0.273	2.08	0.156	2.72	0.150	3.23	0.261
27041	G3bp1	GSVANKFYV	H2Db	0.83	0.777	1.41	0.512	1.39	0.505	1.45	0.516
56784	Garnl1	GAIVNGKVL	H2Db	1.14	0.671	1.27	0.215	1.17	0.659	1.50	0.120
170772	**Glcci1**	**SRVSFTSL**	**H2Kb**	**1.67**	**0.132**	**2.18**	**0.246**	**2.99**	**0.022**	**4.58**	**0.025**
433864	Gm1040	KVVEFSEL	H2Kb	0.94	0.859	1.42	0.327	1.48	0.151	2.24	0.126
14571	Gpd2	AAVKFHNL	H2Kb	0.96	0.865	1.72	0.188	1.21	0.365	1.34	0.016
14751	Gpi1	KNLVNKEVM	H2Db	0.79	0.134	0.93	0.827	0.81	0.087	1.45	0.077
58245	Gpr180	SALANYIHL	H2Db	1.05	0.933	1.55	0.440	1.62	0.268	1.38	0.769
14790	**Grcc10**	**SAPENAVRM**	**H2Db**	**1.31**	**0.309**	**1.92**	**0.072**	**2.85**	**0.079**	**4.42**	**0.006**
232906	Grlf1	SQLQAEHTL	Qa2	0.99	0.982	1.00	0.995	1.21	0.692	0.88	0.818
68153	Gtf2e2	SGYKFGVL	H2Kb	1.03	0.927	1.66	0.136	1.28	0.452	1.58	0.147
14964	**H2-D1**	**AMAPRTLLL**	**Qa1**	**1.38**	**0.350**	**1.41**	**0.523**	**2.63**	**0.053**	**2.92**	**0.043**
14972	H2-K1	AVVAFVMKM	H2Kb	1.71	0.132	2.28	0.175	2.17	0.114	1.78	0.079
320487	Heatr5a	IGPRYSSV	H2Kb	0.86	0.638	1.30	0.241	1.27	0.295	3.11	0.055
207304	Hectd1	IFYYVQKL	H2Kb	1.35	0.552	2.05	0.038	2.34	0.000	2.39	0.297
15201	Hells	RNFIFSRL	H2Kb	0.58	0.376	0.77	0.634	2.16	0.126	1.69	0.634
15201	Hells	KVLVFSQM	H2Kb	1.11	0.778	1.28	0.653	1.37	0.387	1.54	0.422
15257	Hipk1	SLLTNHVTL	H2Db	1.21	0.819	2.55	0.238	3.50	0.100	5.33	0.189
319178	Hist1h2bb	SVYVYKVL	H2Kb	1.04	0.911	1.84	0.118	1.87	0.062	1.99	0.363
319178	Hist1h2bb	VNDIFERI	H2Kb	1.70	0.183	1.20	0.641	2.22	0.310	1.45	0.510
15273	**Hivep2**	**KSFDYGNL**	**H2Kb**	**1.01**	**0.967**	**1.45**	**0.239**	**1.86**	**0.131**	**2.94**	**0.029**
98758	Hnrpf	FSPLNPVRV	H2Db	0.84	0.829	0.83	0.792	0.36	0.358	0.88	0.887
15441	**Hp1bp3**	**VSQYYPKL**	**H2Kb**	**1.09**	**0.818**	**1.36**	**0.427**	**1.96**	**0.169**	**3.65**	**0.035**
53415	Htatip2	YKNVNQEVV	H2Db	0.81	0.572	1.19	0.695	1.27	0.499	1.76	0.043
15978	Ifng	ELIRVVHQL	Qa2	0.79	0.048	0.90	0.669	1.34	0.190	0.57	0.128
16004	**Igf2r**	**VSYKYSKV**	**H2Kb**	**0.68**	**0.319**	**0.82**	**0.558**	**1.12**	**0.692**	**3.18**	**0.002**
23918	Impdh2	GGIQNVGHI	H2Db	0.99	0.980	1.22	0.502	1.15	0.667	1.66	0.134
16329	Inpp1	YMGTNIHSL	H2Db	0.95	0.885	1.21	0.653	1.49	0.309	1.82	0.148
76582	Ipo11	TIILFTKV	H2Kb	1.18	0.776	1.63	0.396	1.82	0.275	4.26	0.472
76582	Ipo11	QQFIYEKL	H2Kb	0.94	0.801	1.29	0.550	2.05	0.068	1.22	0.617

338523	Jhdm1d	SNPEFRQL	H2Kb	1.12	0.700	1.58	0.298	2.08	0.044	3.09	0.008
338523	Jhdm1d	SSIQNGKYTL	H2Db	0.86	0.594	1.14	0.634	1.45	0.118	1.73	0.030
16551	Kif11	AAVANQHSSFV	H2Db	0.81	0.491	1.44	0.215	1.13	0.644	1.49	0.163
71778	Klhl5	IQYAYTGRL	H2Kb	1.43	0.360	2.38	0.078	0.63	0.446	1.56	0.510
16211	Kpnb1	AALQNLVKI	H2Db	1.09	0.889	2.41	0.145	2.44	0.068	2.18	0.555
226519	Lamc1	EIIKDIHNL	Qa2	0.86	0.104	1.17	0.529	1.36	0.082	0.91	0.838
76130	Las1l	ALVRFVNL	H2Kb	0.86	0.839	1.51	0.662	1.60	0.403	3.45	0.405
16828	Ldha	QAPQNKITV	H2Db	0.87	0.431	1.28	0.225	0.97	0.898	1.36	0.051
75660	Lin37	STLIYRNM	H2Kb	2.09	0.074	2.62	0.056	3.37	0.047	2.76	0.079
1E+08	LOC100040505	VSPQNVHHSYL	H2Db	0.91	0.764	1.12	0.724	1.23	0.442	1.25	0.649
57913	Lrdd	VALEFTHL	H2Kb	1.19	0.666	1.67	0.238	1.92	0.048	2.12	0.470
72416	Lrpprc	AAIENIEHL	H2Db	0.86	0.727	0.99	0.972	0.68	0.317	1.46	0.458
16977	Lrrc23	KSLQYLNL	H2Kb	1.00	0.995	1.50	0.255	1.77	0.050	2.37	0.102
241296	Lrrc8a	EIISFQHL	H2Kb	0.95	0.943	1.30	0.723	1.18	0.802	0.87	0.886
116748	Lsm10	QQLQIIHRV	Qa2	0.73	0.318	1.10	0.740	1.12	0.674	0.92	0.818
11426	Macf1	QAIKNGQAL	H2Db	1.08	0.736	1.82	0.063	2.00	0.013	1.60	0.023
56692	Map2k1ip1	QVVQFNRL	H2Kb	4.10	0.133	5.11	0.207	1.38	0.353	6.04	0.089
26413	Mapk1	VGPRYTNL	H2Kb	0.90	0.818	1.05	0.888	0.94	0.881	1.33	0.385
212307	Mapre2	QLNEQVHSL	Qa2	0.94	0.890	1.25	0.528	1.21	0.612	0.93	0.855
17168	Mare	SAVKNLQQL	H2Db	0.83	0.609	1.15	0.610	1.08	0.790	1.52	0.159
226778	Mark1	TSIAFKNI	H2Kb	1.20	0.598	2.11	0.013	1.88	0.068	2.63	0.019
216443	Mars	VSPLFQKL	H2Kb	1.17	0.638	1.68	0.202	1.44	0.205	1.74	0.098
17184	Matr3	KNLRYQLL	H2Kb	0.93	0.862	1.53	0.447	2.41	0.001	1.30	0.724
17246	Mdm2	YAMIYRNL	H2Kb	1.23	0.604	0.99	0.153	0.95	0.115	10.37	0.231
192191	Med9	QQQQQLHSL	Qa2	0.86	0.667	1.13	0.711	1.25	0.518	1.04	0.894
17276	Mela	AGLQNAGRSPTNL	H2Db	0.86	0.694	0.97	0.934	0.95	0.885	1.18	0.725
29808	Mga	SNLKYILV	H2Kb	0.71	0.527	1.31	0.622	1.22	0.640	2.04	0.396
67014	Mina	VVYIYHSL	H2Kb	0.92	0.890	3.26	0.367	1.52	0.359	3.96	0.139
17420	Mnat1	YQKENKDVI	H2Db	0.73	0.694	1.65	0.431	2.01	0.131	3.56	0.011
17427	Mns1	KIIEFANI	H2Kb	0.94	0.905	1.25	0.154	1.29	0.329	2.00	0.327
240641	Mphosph1	QSVAFTKL	H2Kb	1.01	0.983	1.85	0.169	1.97	0.231	4.07	0.003
64659	Mrps14	SRIVFRHL	H2Kb	1.44	0.701	3.23	0.244	3.08	0.113	1.54	0.703
17685	Msh2	AIVSFAHV	H2Kb	0.95	0.917	1.21	0.637	1.68	0.269	2.93	0.351
17758	Mtap4	KVAEFNNV	H2Kb	0.43	0.549	0.77	0.852	0.09	0.291	0.46	0.565
17769	Mthfr	AAIRNYGIEL	H2Db	0.88	0.648	1.18	0.566	1.00	1.000	0.46	0.053
219135	Mtmr6	VGIENIHVM	H2Db	1.07	0.822	1.44	0.282	1.88	0.080	2.00	0.103
17863	Myb	NAIKNHWNSTM	H2Db	1.04	0.914	1.66	0.320	2.24	0.008	4.34	0.014
18432	Mybbp1a	RAIAFQHL	H2Kb	1.28	0.377	1.37	0.280	2.16	0.029	1.78	0.206
17865	Mybl2	NAVKNHWNSTI	H2Db	0.74	0.579	1.67	0.333	1.33	0.465	1.72	0.302
17886	Myh9	RVAEFTTNL	H2Kb	1.63	0.067	1.94	0.204	2.26	0.016	2.00	0.248
67938	Mylc2b	SLGKNPTDAYL	H2Db	1.21	0.667	1.40	0.701	2.65	0.123	3.66	0.020
234664	Nae1	AAVGNHVAKL	H2Db	1.40	0.571	2.80	0.114	2.42	0.048	4.64	0.0003
67608	Narf	AAYGFRNI	H2Kb	1.36	0.343	2.26	0.087	2.47	0.014	2.95	0.057
67563	Narfl	VAYGFRNI	H2Kb	0.90	0.808	1.05	0.893	0.99	0.971	1.38	0.495
20185	Ncor1	YAMENTRQTI	H2Db	1.15	0.615	1.33	0.376	2.19	0.231	2.41	0.047
17992	Ndufa4	VNVDYSKL	H2Kb	0.98	0.958	1.21	0.356	1.46	0.181	2.54	0.034
227197	Ndufs1	AKLVNQEVL	H2Db	0.99	0.975	1.86	0.058	1.18	0.457	2.09	0.094
64652	Nisch	TNQDFIQRL	H2Kb	1.54	0.500	2.05	0.425	3.37	0.180	4.96	0.014
64652	Nisch	VGYRFVTAI	H2Kb	0.93	0.882	1.73	0.309	1.54	0.218	2.15	0.393
52633	Nit2	RAVDNQVYV	H2Db	0.98	0.961	1.66	0.184	1.38	0.328	3.23	0.012

195046	Nlrp1a	LSYSFAHL	H2Kb	1.08	0.871	1.03	0.942	1.53	0.360	5.10	0.285
68979	Nol11	IAVSFREL	H2Kb	1.00	0.998	1.40	0.623	1.92	0.075	0.83	0.653
68979	Nol11	TQLIQTHVL	Qa2	0.92	0.805	1.17	0.629	1.18	0.603	0.79	0.553
230082	Nol6	SSVRFSYM	H2Kb	1.19	0.619	1.49	0.426	1.49	0.382	2.76	0.117
211548	Nomo1	SSLVNKEDVL	H2Db	1.07	0.851	1.74	0.101	0.98	0.963	1.01	0.966
211548	Nomo1	SSLVNKEDV	H2Db	0.78	0.449	1.06	0.782	0.81	0.473	0.91	0.781
66394	Nosip	TSVRFTQL	H2Kb	0.87	0.688	1.32	0.260	1.22	0.398	1.73	0.044
244879	Npat	KQVNNLTNL	H2Db	1.23	0.758	1.51	0.673	2.53	0.076	2.44	0.502
19155	Npepps	RQATNQIVM	H2Db	1.06	0.854	1.32	0.425	1.97	0.075	1.60	0.403
18201	**Nsmaf**	**RSISFSNM**	**H2Kb**	**1.29**	**0.676**	**2.25**	**0.038**	**2.17**	**0.071**	**3.47**	**0.004**
101706	Numa1	VSILNRQVL	H2Db	0.45	0.039	1.73	0.256	2.32	0.017	2.29	0.104
59015	Nup160	AAPTNRQIEIL	H2Db	0.88	0.657	1.26	0.348	1.10	0.672	0.74	0.214
69482	Nup35	AQYGNILKHVM	H2Db	1.18	0.694	1.32	0.575	2.14	0.005	1.15	0.877
66844	**Ormdl2**	**AMYIFLHTV**	**H2Kb**	**2.49**	**0.243**	**2.65**	**0.189**	**3.81**	**0.006**	**2.94**	**0.444**
73162	Otud3	QLNVVIHQL	Qa2	0.89	0.651	1.46	0.308	1.37	0.183	1.10	0.876
54644	Otud5	NSVVNPNKATI	H2Db	1.02	0.954	1.83	0.187	1.96	0.230	1.60	0.029
18458	**Pabpc1**	**AGVRNPQQHL**	**H2Db**	**1.13**	**0.599**	**1.68**	**0.188**	**2.21**	**0.013**	**3.41**	**0.001**
54624	Paf1	YGISNEKPEV	H2Db	1.00	0.992	1.44	0.371	1.45	0.336	1.04	0.913
214230	Pak6	YQHLNVVEM	H2Db	0.82	0.604	1.04	0.932	1.32	0.384	0.89	0.726
56330	Pdcd5	KAVENYLIQM	H2Db	1.64	0.426	2.17	0.235	2.29	0.071	1.29	0.664
14827	Pdia3	FAHTNIESL	H2Db	0.91	0.842	0.90	0.781	0.87	0.724	1.00	0.999
23986	Peci	SSYTFPKM	H2Kb	0.91	0.889	0.96	0.957	1.19	0.788	1.47	0.603
56612	Pfdn5	KLHDVEHVL	Qa2	0.82	0.489	0.96	0.936	1.16	0.793	1.30	0.715
75725	Phf14	VNYYFERNM	H2Kb	1.30	0.517	1.77	0.497	2.53	0.137	4.03	0.055
74016	Phf19	QGPEYIERL	H2Kb	1.74	0.224	2.15	0.111	2.81	0.327	3.32	0.051
213109	Phf3	RAPQFINL	H2Kb	0.95	0.822	1.36	0.239	1.68	0.203	2.17	0.108
68770	Phtf2	AQLLHVHEI	Qa2	0.72	0.105	1.06	0.865	0.97	0.847	0.78	0.285
233489	Picalm	VAFDFTKV	H2Kb	1.44	0.341	1.85	0.067	1.98	0.032	2.54	0.247
18693	Pick1	VTIHYNKL	H2Kb	0.78	0.339	1.00	0.989	1.15	0.484	1.38	0.139
68845	**Pih1d1**	**VNSNFYLRM**	**H2Db**	**ND**	**-**	**ND**	**-**	**ND**	**-**	**8.96**	**0.010**
23988	**Pin1**	**RVYYFNHI**	**H2Kb**	**1.10**	**0.840**	**1.35**	**0.643**	**3.02**	**0.023**	**1.57**	**0.694**
241035	**Pkhd1**	**ILSVFPKV**	**H2Kb**	**0.91**	**0.894**	**1.89**	**0.348**	**3.08**	**0.048**	**7.09**	**0.178**
54711	**Plagl2**	**ANVDFSHL**	**H2Kb**	**1.26**	**0.630**	**1.52**	**0.558**	**2.75**	**0.021**	**3.78**	**0.208**
18950	**Pnp**	**SLITNKVVM**	**H2Db**	**1.25**	**0.723**	**1.78**	**0.405**	**3.34**	**0.101**	**4.91**	**0.021**
69693	Pof1b	KNVVYERV	H2Kb	0.72	0.099	0.94	0.913	1.41	0.079	1.67	0.445
20020	Polr2a	VNYRHLAL	H2Kb	0.73	0.242	1.15	0.722	1.79	0.033	2.39	0.317
231329	Polr2b	IGPTYYQRL	H2Kb	0.61	0.482	0.80	0.731	0.70	0.579	0.97	0.964
19015	Ppard	ASIVNKDGL	H2Db	0.99	0.979	1.25	0.350	0.87	0.650	0.74	0.315
170826	Ppargc1b	LSVRNGATL	H2Db	0.64	0.291	1.16	0.695	1.17	0.640	2.57	0.139
66385	Ppp1r7	RAIENIDTL	H2Db	1.20	0.750	1.63	0.293	0.90	0.868	1.40	0.633
73699	**Ppp2r1b**	**VADKFSEL**	**H2Kb**	**1.17**	**0.731**	**1.69**	**0.312**	**2.10**	**0.178**	**3.37**	**0.029**
54397	Ppt2	SSYSFRHL	H2Kb	0.70	0.192	1.27	0.592	0.72	0.500	2.61	0.185
50907	Preb	TGIKNGVHFL	H2Db	0.92	0.816	1.38	0.547	2.29	0.039	2.27	0.176
74182	Prei4	FGIHNGVETL	H2Db	0.97	0.921	1.91	0.116	1.38	0.242	1.61	0.145
106042	Prickle1	LNYKFPGL	H2Kb	1.00	0.993	1.35	0.335	1.95	0.064	3.25	0.152
18760	**Prkcm**	**SQLRNEVAI**	**H2Db**	**1.10**	**0.731**	**1.66**	**0.199**	**1.92**	**0.033**	**2.73**	**0.007**
19167	**Psma3**	**KAVENSSTAI**	**H2Db**	**1.29**	**0.627**	**1.95**	**0.095**	**1.67**	**0.204**	**2.60**	**0.016**
16913	**Psmb8**	**GGVVNMYHM**	**H2Db**	**0.99**	**0.977**	**1.38**	**0.463**	**2.61**	**0.155**	**5.39**	**0.019**
16912	**Psmb9**	**VNRVFDKL**	**H2Kb**	**0.90**	**0.541**	**1.35**	**0.329**	**2.73**	**0.004**	**4.67**	**0.011**
21762	**Psmd2**	**YVLHNSNTM**	**H2Db**	**1.53**	**0.407**	**1.83**	**0.380**	**2.51**	**0.219**	**3.46**	**0.017**

19206	Ptch1	SNVKYVML	H2Kb	1.05	0.899	1.26	0.692	1.50	0.553	3.55	0.113
19247	**Ptpn11**	**AQYRFIYM**	**H2Kb**	**1.45**	**0.273**	**1.50**	**0.421**	**2.79**	**0.024**	**2.45**	**0.234**
104831	Ptpn23	RALENPDTASL	H2Db	1.34	0.042	2.83	0.207	1.93	0.040	1.57	0.040
15170	Ptpn6	AQYKFIYV	H2Kb	1.14	0.721	1.79	0.129	1.90	0.071	2.14	0.305
78697	Pus7	TSIKNQTQL	H2Db	1.08	0.808	1.44	0.383	1.69	0.166	1.65	0.128
110816	Pwp2	FAYRFSNL	H2Kb	1.28	0.621	1.34	0.439	1.51	0.260	1.77	0.309
110078	Pygb	SNYRVSLL	H2Kb	1.14	0.592	1.65	0.428	1.76	0.282	2.52	0.352
19395	Rasgrp2	VITHFVHV	H2Kb	1.05	0.826	1.67	0.155	1.94	0.052	2.00	0.113
240168	**Rasgrp3**	**VITKFINV**	**H2Kb**	**1.43**	**0.593**	**1.98**	**0.136**	**3.35**	**0.048**	**4.78**	**0.214**
108911	**Rcc2**	**AAYRNLGQNL**	**H2Db**	**1.54**	**0.065**	**2.26**	**0.143**	**2.88**	**0.035**	**3.24**	**0.073**
19718	**Rfc2**	**AVLRYTKL**	**H2Kb**	**1.29**	**0.511**	**2.04**	**0.356**	**3.36**	**0.029**	**5.31**	**0.020**
74734	Rhoh	YSVANHNSFL	H2Db	0.86	0.524	1.35	0.308	1.35	0.066	1.62	0.077
78757	**Rictor**	**KALSYASL**	**H2Kb**	**ND**	**-**	**ND**	**-**	**ND**	**-**	**9.73**	**0.003**
78757	Rictor	LSPINHNTL	H2Db	0.92	0.759	1.53	0.152	1.67	0.115	2.06	0.016
51869	Rif1	KQLVNKEHL	H2Db	0.85	0.560	1.04	0.921	1.36	0.327	1.72	0.057
68477	**Rmnd5a**	**WAVSNREML**	**H2Db**	**1.50**	**0.138**	**2.17**	**0.236**	**4.24**	**0.005**	**5.55**	**0.006**
22644	Rnf103	KTIYNVEHL	H2Db	0.97	0.894	1.87	0.216	2.05	0.345	3.47	0.069
109331	Rnf20	SSLQNHNHQL	H2Db	1.23	0.492	1.74	0.438	1.88	0.037	1.98	0.044
68275	Rpa1	SAVKNDYEM	H2Db	0.56	0.313	1.08	0.866	0.85	0.788	1.08	0.894
71919	Rpap3	TNVLFNHL	H2Kb	1.57	0.217	2.62	0.167	2.21	0.108	2.48	0.092
66480	Rpl15	STYKFFEV	H2Kb	1.22	0.575	1.71	0.097	1.21	0.444	1.48	0.479
19899	Rpl18	KILTFDQL	H2Kb	1.53	0.245	0.89	0.824	2.16	0.139	3.69	0.183
19942	**Rpl27**	**KVYNYNHL**	**H2Db**	**1.00**	**0.991**	**1.65**	**0.350**	**1.67**	**0.115**	**4.63**	**0.001**
19942	Rpl27	KTVVNKDVF	H2Db	0.79	0.182	1.41	0.109	0.96	0.725	1.15	0.324
19943	Rpl28	NSFRYNGL	H2Kb	1.08	0.858	1.07	0.881	2.14	0.128	2.12	0.164
67891	Rpl4	VNFVHTNL	H2Kb	0.91	0.797	0.78	0.607	0.66	0.162	1.48	0.147
20054	**Rps15**	**VGVYNGKTF**	**H2Db**	**1.28**	**0.525**	**1.07**	**0.851**	**2.09**	**0.257**	**2.52**	**0.023**
267019	Rps15a	VIVRFLTVM	H2Kb	1.40	0.553	1.37	0.563	1.59	0.221	1.65	0.666
267019	Rps15a	VIVRFLTV	H2Kb	0.81	0.621	1.38	0.413	1.18	0.710	1.49	0.683
73086	Rps6ka5	QLLTVKHEL	Qa2	1.00	0.995	1.04	0.906	1.77	0.126	1.13	0.844
20133	Rrm1	FQIVNPHLL	H2Db	1.07	0.861	1.97	0.203	2.23	0.024	1.33	0.668
20133	Rrm1	YGIRNSLLI	H2Db	0.90	0.746	1.55	0.373	1.71	0.064	1.33	0.729
106298	Rrn3	AAITNKYQL	H2Db	0.84	0.511	1.27	0.178	1.16	0.538	1.62	0.085
66409	Rsl1d1	QIIPFKTL	H2Kb	1.86	0.071	1.90	0.266	2.51	0.096	2.07	0.200
319934	Sbf2	QAIHFANL	H2Kb	0.96	0.882	1.42	0.250	1.20	0.456	1.46	0.224
235623	Scap	SGYDFSRL	H2Kb	0.86	0.636	1.14	0.639	1.19	0.466	2.08	0.096
13722	Scye1	SGLVNHVPL	H2Db	0.88	0.745	1.15	0.657	0.91	0.798	1.13	0.715
218811	**Sec24c**	**KVLHFYNV**	**H2Kb**	**1.24**	**0.447**	**1.45**	**0.456**	**3.35**	**0.002**	**1.92**	**0.533**
235626	Setd2	SSPSNKFFF	H2Db	1.09	0.790	1.19	0.675	1.40	0.269	1.71	0.205
81898	Sf3b1	KAIVNVIGM	H2Db	1.21	0.609	1.33	0.536	1.82	0.160	2.13	0.120
20393	**Sgk1**	**STLTYSRM**	**H2Kb**	**1.42**	**0.597**	**0.85**	**0.338**	**1.90**	**0.176**	**9.21**	**0.032**
20425	Shmt1	RNLDYARL	H2Kb	0.87	0.630	1.26	0.506	1.60	0.072	1.71	0.457
107723	**Slc12a6**	**SAARFALL**	**H2Kb**	**1.18**	**0.697**	**1.97**	**0.167**	**1.86**	**0.088**	**2.52**	**0.047**
63959	Slc29a1	ATKYFTNRL	H2Kb	1.16	0.492	1.47	0.432	1.69	0.091	2.74	0.141
26570	Slc7a11	VAVTFSERL	H2Kb	1.11	0.713	1.19	0.281	2.35	0.361	3.40	0.319
13990	Smarcad1	YQHINSYQL	H2Db	1.56	0.075	2.45	0.083	2.24	0.014	1.90	0.016
70099	Smc4	AALDFKNV	H2Kb	1.68	0.142	2.01	0.236	3.12	0.082	3.23	0.136
57319	Smpdl3a	KVYFIAHV	H2Kb	0.70	0.038	0.89	0.613	1.50	0.172	0.70	0.616
75627	Snapc1	AAFVFRKL	H2Kb	0.80	0.615	1.48	0.314	1.95	0.099	2.01	0.336
244962	Snx14	IGPKNYEFL	H2Db	0.89	0.511	1.30	0.360	1.34	0.069	1.09	0.734

244962	Snx14	EQLFQEHRL	Qa2	0.79	0.415	1.13	0.760	1.32	0.278	0.68	0.468
20740	Spna2	KALINADEL	H2Db	0.97	0.945	1.04	0.905	0.97	0.943	1.44	0.349
20747	Spop	KVVKFSYM	H2Kb	1.14	0.707	1.52	0.296	2.04	0.051	2.52	0.053
20815	Srpk1	ISGVNGTHI	H2Db	1.05	0.913	1.19	0.582	1.37	0.351	2.30	0.092
67437	Ssr3	VAFAYKNV	H2Kb	0.98	0.953	1.18	0.584	1.15	0.700	1.57	0.180
20443	St3gal4	GAVKNLTYF	H2Db	1.03	0.955	2.06	0.095	1.96	0.117	5.66	0.057
20448	St6galnac4	QVYTFTERM	H2Kb	1.02	0.956	1.24	0.565	1.55	0.242	2.97	0.117
20846	Stat1	KFLEQVHQL	Qa2	0.83	0.379	0.99	0.971	1.71	0.058	0.75	0.613
20848	Stat3	ATLVFHNL	H2Kb	0.93	0.839	1.19	0.468	1.18	0.488	1.48	0.398
20868	Stk10	HQLQERHQL	Qa2	0.90	0.840	1.26	0.647	1.48	0.373	1.32	0.654
71728	Stk11ip	SALRFLNL	H2Kb	0.99	0.993	1.48	0.543	2.00	0.122	2.57	0.355
16430	Stt3a	AVLSFSTRL	H2Kb	0.76	0.507	1.12	0.806	1.88	0.287	1.52	0.630
68292	Stt3b	KAPDNRETL	H2Db	0.58	0.511	0.67	0.612	0.33	0.295	0.80	0.788
114741	**Supt16h**	**VSYKNPSLM**	**H2Db**	**ND**	**-**	**ND**	**-**	**ND**	**-**	**8.91**	**0.011**
21335	Tacc3	AQMQNHSLEM	H2Db	0.56	0.377	1.57	0.675	1.48	0.061	1.05	0.894
21343	**Taf6**	**AQQVNRTTL**	**H2Db**	**2.24**	**0.042**	**2.14**	**0.388**	**3.30**	**0.032**	**4.07**	**0.003**
108143	Taf9	SGLKYVNV	H2Kb	0.86	0.778	0.99	0.982	0.97	0.940	1.36	0.408
66860	**Tanc1**	**FQAINAGHI**	**H2Db**	**1.10**	**0.744**	**1.64**	**0.120**	**2.79**	**0.053**	**2.76**	**0.015**
21355	Tap2	HTVQNADQV	H2Db	1.55	0.128	2.21	0.074	3.44	0.177	2.55	0.295
75812	Tasp1	SGIKNPVSV	H2Db	1.10	0.774	3.32	0.104	1.38	0.331	2.46	0.038
72238	Tbc1d5	KTLLNPEYL	H2Db	1.26	0.406	2.55	0.171	2.50	0.030	2.17	0.244
211586	**Tfdp2**	**QQIAFKNL**	**H2Kb**	**ND**	**-**	**ND**	**-**	**ND**	**-**	**7.92**	**0.004**
22042	Tfrc	KAFTYINL	H2Kb	0.85	0.652	1.25	0.501	1.26	0.459	1.42	0.697
76355	Tgds	RAFEFTYV	H2Kb	2.05	0.202	2.82	0.192	1.92	0.431	3.06	0.312
21822	**Tgtp**	**SKYDFPKL**	**H2Kb**	**0.85**	**0.770**	**1.29**	**0.659**	**2.59**	**0.048**	**1.77**	**0.613**
57314	Th1l	KAIETVHNL	Qa2	0.74	0.392	0.98	0.963	0.90	0.741	1.03	0.919
21894	Tln1	SVMENSKVLGEAM	H2Db	0.92	0.855	0.98	0.962	1.45	0.381	1.73	0.304
70549	Tln2	SVMENSKVLGESM	H2Db	0.57	0.193	1.07	0.875	1.18	0.690	1.17	0.704
217353	Tmc6	ASYLFRGL	H2Kb	0.22	0.510	0.34	0.463	0.67	0.724	0.57	0.634
67878	Tmem33	QSIAFISRL	H2Kb	0.94	0.889	1.61	0.389	1.64	0.218	0.42	0.199
230770	Tmem39b	RTYSFLNL	H2Kb	0.76	0.576	1.53	0.482	1.84	0.219	1.87	0.600
21916	**Tmod1**	**SSIVNKEGL**	**H2Db**	**0.93**	**0.827**	**1.59**	**0.082**	**0.69**	**0.338**	**0.27**	**0.006**
22035	**Tnfsf10**	**VSVTNEHLM**	**H2Db**	**ND**	**-**	**ND**	**-**	**ND**	**-**	**8.97**	**0.007**
22057	Tob1	ISYLYNKL	H2Kb	0.81	0.571	0.91	0.747	0.89	0.730	1.37	0.515
67095	Trak1	SSVQNYFHL	H2Db	0.91	0.788	1.57	0.320	1.87	0.050	2.20	0.483
212528	Trmt1	VITEFARI	H2Kb	1.16	0.728	1.74	0.128	1.97	0.116	2.11	0.253
83922	Tsga14	KVTTFAQL	H2Kb	0.86	0.851	1.39	0.655	2.03	0.242	1.19	0.846
73668	**Ttc21b**	**VNTHFSHL**	**H2Kb**	**ND**	**-**	**ND**	**-**	**ND**	**-**	**15.25**	**0.0003**
56085	Ubqln1	RALSNLESI	H2Db	1.15	0.748	1.55	0.082	1.41	0.215	1.87	0.073
22222	Ubr1	STFEFHSI	H2Kb	1.14	0.725	1.48	0.308	1.27	0.548	1.17	0.691
19704	Upf1	SGYIYHKL	H2Kb	0.95	0.864	1.18	0.588	1.48	0.104	1.48	0.106
326622	Upf2	SAVIFRTL	H2Kb	1.22	0.583	1.55	0.111	1.57	0.146	1.66	0.224
22224	Usp10	VGPKNKTSI	H2Db	0.87	0.714	0.96	0.925	0.69	0.469	0.76	0.657
216825	Usp22	FAVVNHQGTL	H2Db	0.83	0.547	1.19	0.453	1.16	0.589	1.37	0.307
20955	Vamp7	IMVRNIDLV	H2Db	0.93	0.869	1.38	0.629	1.67	0.436	2.24	0.437
271564	Vps13a	VSIQFYHL	H2Kb	0.96	0.910	1.43	0.414	1.67	0.131	1.11	0.909
666173	Vps13b	SNFHFAVL	H2Kb	0.92	0.869	1.46	0.432	1.46	0.390	1.86	0.491
230895	Vps13d	INIHYTQL	H2Kb	2.73	0.571	1.89	0.658	0.09	0.388	6.75	0.440
80743	Vps16	VSFTYRYL	H2Kb	0.96	0.910	1.27	0.436	1.21	0.398	1.59	0.525
77573	**Vps33a**	**GSLANHTSI**	**H2Db**	**0.90**	**0.793**	**1.71**	**0.271**	**1.99**	**0.095**	**3.90**	**0.008**

233405	Vps33b	ASLVNADKL	H2Db	0.94	0.880	1.19	0.524	1.09	0.779	1.94	0.138
65114	Vps35	FSEENHEPL	H2Db	1.03	0.915	1.82	0.036	1.25	0.433	1.17	0.452
218035	Vps41	IGLAYVNHL	H2Kb	1.07	0.836	1.59	0.225	2.21	0.075	2.64	0.384
22375	Wars	YTVENAKDII	H2Db	1.38	0.316	3.19	0.263	2.57	0.118	1.57	0.369
73828	**Wdr21**	**KAPTFEVQM**	**H2Kb**	**1.67**	**0.101**	**2.93**	**0.024**	**3.97**	**0.018**	**5.41**	**0.042**
54636	Wdr45	SSPKFSEI	H2Kb	1.02	0.939	1.64	0.113	1.16	0.559	1.69	0.145
140858	Wdr5	AALENDKTI	H2Db	1.03	0.956	1.25	0.549	0.96	0.914	1.21	0.619
210544	Wdr67	GIMRFVNI	H2Kb	1.33	0.625	1.95	0.359	0.77	0.640	3.30	0.192
223499	Wdsof1	SSVKFNPV	H2Kb	0.72	0.431	0.89	0.719	0.64	0.290	1.31	0.549
234135	Whsc1l1	KGIGNKTEI	H2Db	0.98	0.879	1.39	0.427	1.34	0.225	2.44	0.213
74781	Wipi2	SGYKFFSL	H2Kb	1.13	0.788	1.58	0.376	2.07	0.110	2.22	0.427
232341	Wnk1	KSISNPPGSNL	H2Db	1.31	0.273	2.09	0.046	2.05	0.012	2.58	0.081
574437	**Xlr3a**	**VAAANREVL**	**H2Db**	**1.05**	**0.887**	**1.78**	**0.088**	**1.88**	**0.044**	**4.51**	**0.014**
70120	Yars2	SGYEFIHKL	H2Kb	1.09	0.922	1.66	0.535	2.08	0.321	1.79	0.625
208146	Yeats2	SGVSNPHVI	H2Db	0.97	0.925	1.43	0.215	1.45	0.206	2.49	0.012
68090	**Yif1a**	**SGYKYVGM**	**H2Kb**	**1.39**	**0.449**	**2.78**	**0.045**	**3.41**	**0.096**	**4.16**	**0.020**
106369	Ypel1	RAYLFNSV	H2Kb	1.19	0.256	1.84	0.096	2.67	0.069	3.88	0.055
22628	Ywhag	AAMKNVTEL	H2Db	0.66	0.560	0.87	0.776	0.97	0.960	1.49	0.342
214290	Zcchc6	TTYKYFAL	H2Kb	1.34	0.366	1.03	0.942	1.92	0.070	1.46	0.496
66980	Zdhhc6	SVIKFENL	H2Kb	0.93	0.876	1.06	0.862	1.10	0.785	1.10	0.818
11906	Zfhx3	VAIGNPVHL	H2Db	1.34	0.190	1.55	0.252	2.30	0.018	3.71	0.129
22640	Zfp1	KTFSFKSL	H2Kb	0.81	0.663	0.90	0.717	1.06	0.873	1.03	0.965
65020	Zfp110	NMISVEHHF	Qa2	0.48	0.260	1.05	0.916	0.89	0.862	0.83	0.765
72154	**Zfp157**	**IQVRNPVAL**	**H2Db**	**0.72**	**0.454**	**1.54**	**0.202**	**1.90**	**0.014**	**3.06**	**0.027**
67911	Zfp169	VMLENYSHL	H2Db	1.21	0.541	1.23	0.555	1.55	0.284	2.27	0.216
212569	**Zfp273**	**VNLIYHQRI**	**H2Kb**	**1.48**	**0.487**	**2.78**	**0.270**	**4.73**	**0.013**	**4.68**	**0.253**
22720	**Zfp62**	**SSLINHKSV**	**H2Db**	**1.10**	**0.494**	**1.34**	**0.229**	**1.61**	**0.008**	**3.13**	**0.0007**
52521	Zfp622	SLVKNVAHM	H2Db	0.97	0.959	1.39	0.634	1.89	0.118	4.52	0.087
67187	Zmynd19	ESYSFEARM	H2Kb	1.27	0.570	1.63	0.274	2.04	0.103	3.72	0.124
66136	**Znrd1**	**TSVVFNKL**	**H2Kb**	**1.11**	**0.761**	**1.41**	**0.300**	**1.67**	**0.191**	**2.86**	**0.015**

Supplementary Table 2

GO terms enriched in DEM source genes and DEGs. DAVID bioinformatics resources (http://david.abcc.ncifcrf.gov/) were used to identify enriched biological processes (P<0.05) associated to DEGs and to genes coding for DEMs. Functionally related GO terms were annoted within unique cellular processes (last column). Biological processes enriched in DEM source genes are highlighted in blue. Biological processes enriched in over- and underexpressed mRNAs are highlighted in red and green, respectively.

Biological processes enriched in DEM source genes

GO term	GO number	Genes in sample	p value	Gene symbol	Cellular processes in Figure 3 and Supplementary Figure S3
Regulation of progression through cell cycle	GO:0000074	7	0.007	Bub1b, Ccnf, Ptpn11, Psmd2, Slc12a6, Tfdp2, Dlg7	Cell cycle/proliferation
M phase of mitotic cell cycle	GO:0000087	5	0.012	Bub1b, Ccnf, Rcc2, Dlg7, Mphosph1	
DNA replication	GO:0006260	4	0.044	Rfc2, Dtl, Chaf1b, Supt16h	DNA replication
Transcription, DNA-dependent	GO:0006351	17	0.042	Hivep2, Mnat1, Myb, Taf6, Zfp62, Plagl2, Znrd1, Zfp157, Chaf1b, Supt16h, Ash1l, Bptf, Tfdp2, Zfp273, Foxj3, Ankrd26, BC066107	Transcription
Regulation of transcription, DNA-dependent	GO:0006355	17	0.038	Hivep2, Mnat1, Myb, Taf6, Zfp62, Plagl2, Znrd1, Zfp157, Chaf1b, Supt16h, Ash1l, Bptf, Tfdp2, Zfp273, Foxj3, Ankrd26, BC066107	
Protein complex assembly	GO:0006461	4	0.047	Ap2a1, Ap2a2, Tmod1, Copb1	Protein complex assembly
Intracellular transport	GO:0046907	8	0.048	Ptpn11, Erbb2ip, Sec24c, Mphosph1, Ap2a1, Ap2a2, Yif1a, Copb1	Protein transport
Protein transport	GO:0015031	8	0.043	Ptpn11, Erbb2ip, Sec24c, Vps33a, Ap2a1, Ap2a2, Yif1a, Copb1	
Proteasome complex	GO:0000502	4	0.011	Psma3, Psmb8, Psmb9, Psmd2	Proteasome

Biological processes enriched in DEGs (overexpressed mRNAs)

Translation	GO:0006412	15	0.012	Lama5, Rpl10a, Eif3s9, Mknk2, Wdr46, Rpsa, Eif4a2, Rps15a, Mrpl12, Eftud2, Tnf, Eef1e1, Spn, Tnfrsf7, Rps13	Translation
DNA replication	GO:0006260	8	0.010	Pole2, Mcm2, Mcm6, Dna2l, Nfix, Orc1l, Phb, Nasp	DNA replication
Positive regulation of cellular metabolic process	GO:0031325	19	0.037	E2f3, Lef1, Ppargc1b, Smarcc1, Etv5, Hnrpab, Thrap3, Tnf, Tnfrsf7, Rara, Spn, Sox2, Myc, Dhcr24, Aven, Sod2, Tnfrsf7, Dlx1, Angptl4	Cell cycle/proliferation
Steroid biosynthetic process	GO:0006694	9	0.00001	Dhcr7, Dhcr24, Hmgcr, Idi1, Oprs1, Hsd17b7, Mvd, Nsdhl, Hmgcs1	Lipid biosynthesis (sterol)
Steroid metabolic process	GO:0008202	11	0.00006	Kenma1, Ldlr, Dhcr7, Dhcr24, Hmgcr, Idi1, Oprs1, Hsd17b7, Mvd, Nsdhl, Hmgcs1	
Cholesterol metabolic process	GO:0008203	9	0.00001	Dhcr7, Hmgcr, Hsd17b7, Ldlr, Nsdhl, Dhcr24, Mvd, Hmgcs1, Idi1	
Lipid biosynthetic process	GO:0008610	15	0.00001	Dhcr7, Fasn, Hmgcr, Hsd17b7, Fabp5, Nsdhl, Oprs1, B4galt6, Pcyt2, Dhcr24, Aacs, Mvd, Hmgcs1, Aytl2, Idi1	
Sterol metabolic process	GO:0016125	10	0.000001	Dhcr7, Hmgcr, Hsd17b7, Ldlr, Nsdhl, Oprs1, Dhcr24, Mvd, Hmgcs1, Idi1	
Sterol biosynthetic process	GO:0016126	9	0.000000001	Dhcr7, Hmgcr, Hsd17b7, Nsdhl, Oprs1, Dhcr24, Mvd, Hmgcs1, Idi1	
rRNA processing	GO:0006364	6	0.001	Rrp1b, Exosc6, Utp14b, Bop1, Rnu3ip2, Ebna1bp2	rRNA processing
RNA processing	GO:0006396	17	0.0001	Sf3b3, Rrp1b, Ppih, 6720458F09Rik, Syncrip, Hnrpab, Magoh, Bop1, Rnu3ip2, Ddx54, Pus1l, Lsm7, Exosc6, Eftud2, Utp14b, Lsm2, Ebna1bp2	
Positive regulation of transcription, DNA-dependent	GO:0045893	9	0.043	E2f3, Hnrpab, Lef1, Rara, Smarcc1, Eftud2, Tnf, Ppargc1b, Thrap3	Transcription
Positive regulation of transcription	GO:0045941	10	0.047	Etv5, E2f3, Hnrpab, Lef1, Rara, Smarcc1, Eftud2, Tnf, Ppargc1b, Thrap3	

Supplementary Table 2 (continued)

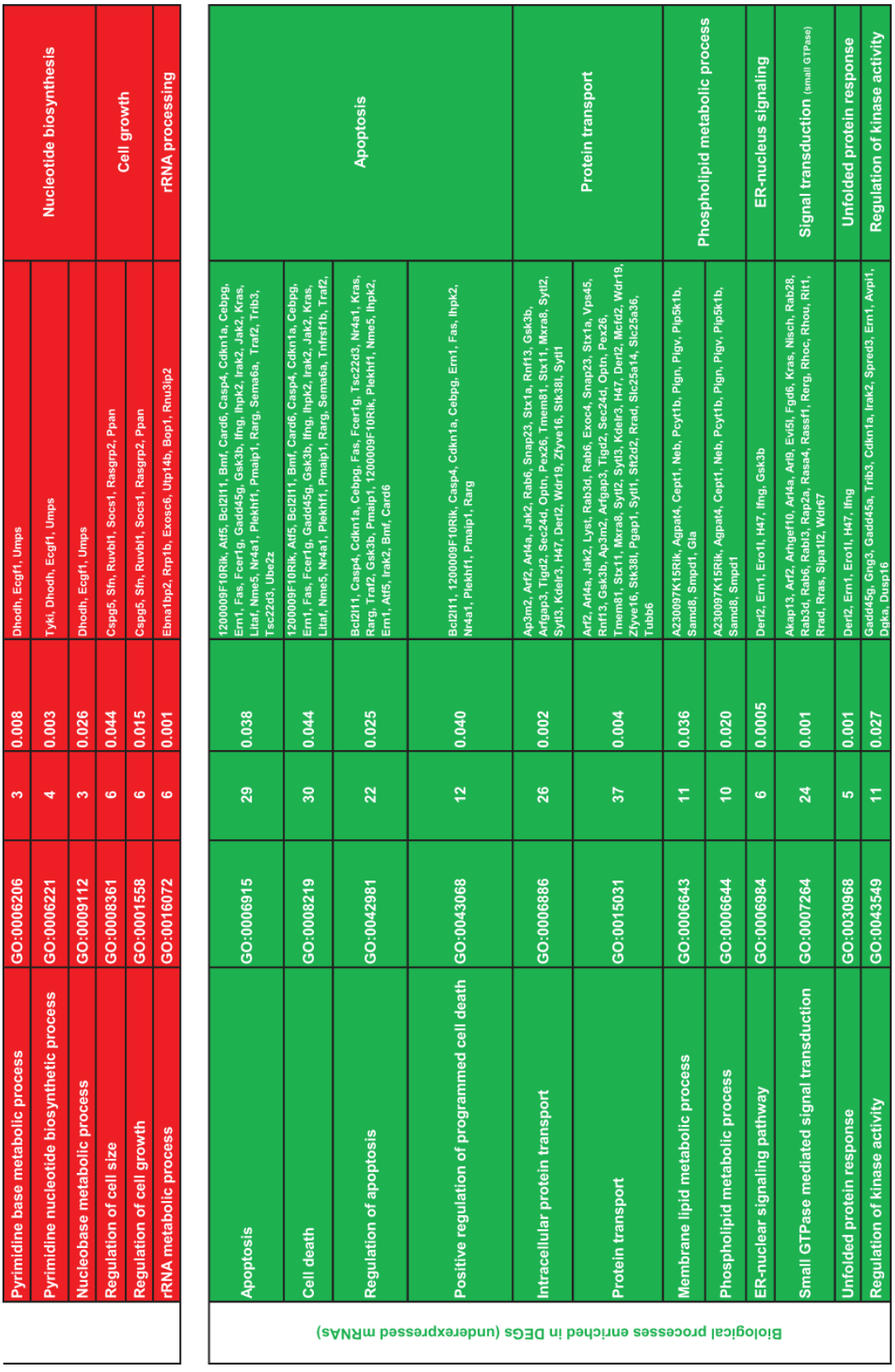

Biological processes enriched in DEGs (underexpressed mRNAs)							
Pyrimidine base metabolic process	GO:0006206	3	0.008	Dhodh, Ecgf1, Umps	Nucleotide biosynthesis		
Pyrimidine nucleotide biosynthetic process	GO:0006221	4	0.003	Tyki, Dhodh, Ecgf1, Umps			
Nucleobase metabolic process	GO:0009112	3	0.026	Dhodh, Ecgf1, Umps			
Regulation of cell size	GO:0008361	6	0.044	Csps5, Sfn, Ruvbl1, Socs1, Rasgrp2, Ppan	Cell growth		
Regulation of cell growth	GO:0001558	6	0.015	Csps5, Sfn, Ruvbl1, Socs1, Rasgrp2, Ppan			
rRNA metabolic process	GO:0016072	6	0.001	Ebna1bp2, Rrp1b, Exosc6, Utp14b, Bop1, Rnu3ip2	rRNA processing		
Apoptosis	GO:0006915	29	0.038	1200009F10Rik, Atf5, Bcl2l11, Bmf, Card6, Casp4, Cdkn1a, Cebpg, Ern1, Fas, Fcer1g, Gadd45g, Gsk3b, Ifng, Ihpk2, Irak2, Jak2, Kras, Litaf, Nme5, Nr4a1, Plekhf1, Pmaip1, Rarg, Sema6a, Traf2, Trib3, Tsc22d3, Ube2z	Apoptosis		
Cell death	GO:0008219	30	0.044	1200009F10Rik, Atf5, Bcl2l11, Bmf, Card6, Casp4, Cdkn1a, Cebpg, Ern1, Fas, Fcer1g, Gadd45g, Gsk3b, Ifng, Ihpk2, Irak2, Jak2, Kras, Litaf, Nme5, Nr4a1, Plekhf1, Pmaip1, Rarg, Sema6a, Tnfrsf1b, Traf2,			
Regulation of apoptosis	GO:0042981	22	0.025	Bcl2l11, Casp4, Cdkn1a, Cebpg, Fas, Fcer1g, Tsc22d3, Nr4a1, Kras, Rarg, Traf2, Gsk3b, Pmaip1, 1200009F10Rik, Plekhf1, Nme5, Ihpk2, Ern1, Atf5, Irak2, Bmf, Card6			
Positive regulation of programmed cell death	GO:0043068	12	0.040	Bcl2l11, 1200009F10Rik, Casp4, Cdkn1a, Cebpg, Ern1, Fas, Ihpk2, Nr4a1, Plekhf1, Pmaip1, Rarg			
Intracellular protein transport	GO:0006886	26	0.002	Ap3m2, Arf2, Arl4a, Jak2, Rab6, Snap23, Stx1a, Rnf13, Gsk3b, Arfgap3, Tigd2, Sec24d, Optn, Pex26, Tmem81, Stx11, Mxra8, Sytl2, Sytl3, Kdelr3, H47, Derl2, Wdr19, Zfyve16, Stk38l, Sytl1	Protein transport		
Protein transport	GO:0015031	37	0.004	Arf2, Arl4a, Jak2, Lyst, Rab3d, Rab6, Exoc4, Snap23, Stx1a, Vps45, Rnf13, Gsk3b, Ap3m2, Arfgap3, Tigd2, Sec24d, Optn, Pex26, Tmem81, Stx11, Mxra8, Sytl2, Sytl3, Kdelr3, H47, Derl2, Mcfd2, Wdr19, Zfyve16, Stk38l, Pgap1, Sytl1, Sft2d2, Rrad, Slc25a14, Slc25a36, Tubb6			
Membrane lipid metabolic process	GO:0006643	11	0.036	A230097K15Rik, Agpat4, Cept1, Neb, Pcyt1b, Plgn, Pigv, Pip5k1b, Samd8, Smpd1, Gla	Phospholipid metabolic process		
Phospholipid metabolic process	GO:0006644	10	0.020	A230097K15Rik, Agpat4, Cept1, Neb, Pcyt1b, Plgn, Pigv, Pip5k1b, Samd8, Smpd1			
ER-nuclear signaling pathway	GO:0006984	6	0.0005	Derl2, Ern1, Ero1l, H47, Ifng, Gsk3b	ER-nucleus signaling		
Small GTPase mediated signal transduction	GO:0007264	24	0.001	Akap13, Arf2, Arhgef10, Arl4a, Arl9, Evi5l, Fgd6, Kras, Nisch, Rab28, Rab3d, Rab6, Rabl3, Rap2a, Rasa4, Rassf1, Rerg, Rhoc, Rhou, Rit1, Rrad, Rras, Sipa1l2, Wdr67	Signal transduction (small GTPase)		
Unfolded protein response	GO:0030968	5	0.001	Derl2, Ern1, Ero1l, H47, Ifng	Unfolded protein response		
Regulation of kinase activity	GO:0043549	11	0.027	Gadd45g, Gng3, Gadd45a, Trib3, Cdkn1a, Irak2, Spred3, Ern1, Avpi1, Dgka, Dusp16	Regulation of kinase activity		

Supplementary Table 3

List of 891 unique peptide source genes encoding H2b-peptides (Fortier et al, 2008; de Verteuil et al, 2010; Caron E et al, current study) deposited in the Immune Epitope Database and Analysis Resource (http://beta.immuneepitope.org)

Gene number	Gene ID	Source gene (gene symbol)	Peptide sequence	MHC I allele (Kb, Db, Qa1/2)	Source tissue
1	11307	Abcg1	VNIEFKDL	Kb	EL4 cell line
	11307	Abcg1	VNIEFKDL	Kb	Dendritic cell
	11307	Abcg1	VNIEFKDL	Kb	Thymocyte
2	11426	Macf1	QAIKNGQAL	Db	EL4 cell line
3	11432	Acp2	RSIQNAQFL	Db	EL4 cell line
	11432	Acp2	RSIQNAQFL	Db	Dendritic cell
4	11566	Adss	VSLKYAHM	Kb	EL4 cell line
5	11605	Gla	NGYKYMAL	Kb	Dendritic cell
6	11630	Aim1	QSIVFKSL	Kb	Dendritic cell
7	11666	Abcd1	RVVANSEEI	Db	EL4 cell line
	11666	Abcd1	RVVANSEEI	Db	Dendritic cell
8	11674	Aldoa	ELSDIAHRI	Qa2	Dendritic cell
9	11690	Alox5ap	AGILNHYLI	Db	Dendritic cell
10	11745	Anxa3	DLLDIRHEF	Qa2	Dendritic cell
11	11750	Anxa7	ATRSFPQL	Kb	Dendritic cell
12	11761	Aox1	NAYKFPNL	Kb	EL4 cell line
13	11771	Ap2a1	SQLRNADVEL	Db	EL4 cell line
	11771	Ap2a1	TNLRYLAL	Kb	EL4 cell line
	11771	Ap2a1	SQLRNADVEL	Db	Dendritic cell
14	11772	Ap2a2	SQLKNADVEL	Db	EL4 cell line
	11772	Ap2a2	TNLRYLAL	Kb	EL4 cell line
	11772	Ap2a2	SQLKNADVEL	Db	Dendritic cell
	11772	Ap2a2	RNPTFMGL	Kb	Dendritic cell
15	11774	Ap3b1	GQVVIIHML	Qa2	Dendritic cell
16	11787	Apbb2	ATLRYASL	Kb	Dendritic cell
17	11906	Zfhx3	VAIGNPVHL	Db	EL4 cell line
	11906	Atbf1	VAIGNPVHL	Db	Thymocyte
18	11933	Atp1b3	VGYRQPLV	Kb	Dendritic cell
19	11941	Atp2b2	KVYTFNSV	Kb	EL4 cell line
	11941	Atp2b2	KVYTFNSV	Kb	Dendritic cell
20	12014	Bach2	EQLEFIHDI	Qa2	Thymocyte
21	12033	Bcap29	SAFEHTQM	Kb	EL4 cell line
22	12044	Bcl2a1a	ARIIFNQV	Kb	Dendritic cell
23	12045	Bcl2a1b	ARIIFNQV	Kb	Dendritic cell
24	12047	Bcl2a1d	ARIIFNQV	Kb	Dendritic cell
25	12122	Bid	SQEEIIHNI	Qa2	Dendritic cell
26	12143	Blk	RSLDNGGYYI	Db	Dendritic cell
27	12176	Bnip3	LSMRNTSVM	Db	EL4 cell line
	12176	Bnip3	LSMRNTSVM	Db	Dendritic cell
28	12181	Bop1	EQVALVHRL	Qa2	EL4 cell line
	12181	Bop1	EQVALVHRL	Qa2	Dendritic cell
29	12190	Brca2	HAIENIDTF	Db	EL4 cell line
30	12211	Birc6	SGLTYIKI	Kb	EL4 cell line
	12211	Birc6	VNYHYMSQV	Kb	EL4 cell line
	12211	Birc6	SGLTYIKI	Kb	Dendritic cell
	12211	Birc6	VNYHYMSQV	Kb	Dendritic cell
31	12236	Bub1b	IITGFRNV	Kb	EL4 cell line
32	12340	Capza1	ISFKFDHL	Kb	EL4 cell line
	12340	Capza1	ISFKFDHL	Kb	Dendritic cell

33	12387	Ctnnb1	RTYTYEKL	Kb	EL4 cell line
	12387	Ctnnb1	RTYTYEKL	Kb	Dendritic cell
	12387	Ctnnb1	VALLNKTNV	Db	Dendritic cell
34	12445	Ccnd3	AAVIAHDFL	Db	Thymocyte
35	12449	Ccnf	SQAVNKQQI	Db	EL4 cell line
	12449	Ccnf	SQAVNKQQI	Db	Thymocyte
36	12450	Ccng1	TAFQFLQL	Kb	Thymocyte
37	12452	Ccng2	TALNFLHL	Kb	Dendritic cell
38	12455	Ccnt1	ALIGVDHSL	Qa2	Dendritic cell
39	12464	Cct4	AQIRFSNI	Kb	EL4 cell line
40	12465	Cct5	SMMDVDHQI	Qa2	EL4 cell line
	12465	Cct5	SMMDVDHQI	Qa2	Dendritic cell
41	12468	Cct7	RAIKNDSVV	Db	EL4 cell line
42	12492	Scarb2	KSVINTTLV	Db	EL4 cell line
43	12501	Cd3e	YSGLNQRAV	Db	EL4 cell line
	12501	Cd3e	YSGLNQRAV	Db	Thymocyte
44	12508	Cd53	YGVLFRNL	Kb	Dendritic cell
45	12530	Cdc25a	KGYLFNTV	Kb	EL4 cell line
46	12537	Cdc2l1	VMNYVEHDL	Qa2	EL4 cell line
47	12566	Cdk2	KSYLFQLL	Kb	Dendritic cell
48	12567	Cdk4	VTLVFEHI	Kb	EL4 cell line
49	12576	Cdkn1b	FGPVNHEEL	Db	EL4 cell line
	12576	Cdkn1b	FGPVNHEEL	Db	Dendritic cell
	12576	Cdkn1b	FGPVNHEEL	Db	Thymocyte
50	12648	Chd1	RVLIFSQM	Kb	EL4 cell line
	12648	Chd1	RVLIFSQM	Kb	Dendritic cell
51	12649	Chek1	TGPSNVDKL	Db	EL4 cell line
	12649	Chek1	TGPSNVDKL	Db	Dendritic cell
	12649	Chek1	TGPSNVDKL	Db	Thymocyte
52	12751	Tpp1	IQRVNTEFM	Db	EL4 cell line
	12751	Tpp1	IQRVNTEFM	Db	Thymocyte
53	12767	Cxcr4	VVFQFQHI	Kb	EL4 cell line
	12767	Cxcr4	VVFQFQHI	Kb	Thymocyte
54	12847	Copa	SQLPVDHIL	Qa2	EL4 cell line
	12847	Copa	SQLPVDHIL	Qa2	Dendritic cell
55	12914	Crebbp	YSYQNRYHF	Db	EL4 cell line
56	12978	Csf1r	FAPKNIYSI	Db	Dendritic cell
57	13006	Smc3	KAILNGIDSI	Db	EL4 cell line
58	13121	Cyp51	KNIFYKAI	Kb	EL4 cell line
59	13162	Slc6a3	NVWRFPYL	Kb	Dendritic cell
60	13204	Dhx15	TLLNVYHAF	Qa2	Dendritic cell
	13204	Dhx15	TLLNVYHAF	Qa2	Thymocyte
61	13207	Ddx5	NQAINPKLLQL	Db	Thymocyte
62	13209	Ddx6	INFDFPKL	Kb	EL4 cell line
	13209	Ddx6	NQLKNTSTI	Db	EL4 cell line
	13209	Ddx6	INFDFPKL	Kb	Dendritic cell
	13209	Ddx6	NQLKNTSTI	Db	Dendritic cell
	13209	Ddx6	INFDFPKL	Kb	Thymocyte
63	13244	Degs1	SMTLAIHEI	Qa2	Dendritic cell
64	13360	Dhcr7	AGVVNKYEV	Db	EL4 cell line
65	13424	Dync1h1	ASYEFVQRL	Kb	EL4 cell line
	13424	Dync1h1	ASYEFVQRL	Kb	Dendritic cell
	13424	Dync1h1	ASYEFVQRL	Kb	Thymocyte
67	13430	Dnm2	YAIKNIHGV	Db	EL4 cell line
68	13433	Dnmt1	LSLENGTHTL	Db	EL4 cell line
	13433	Dnmt1	LSLENGTHTL	Db	Dendritic cell
	13433	Dnmt1	LSLENGTHTL	Db	Thymocyte

69	13654	Egr2	SAPRNQTFTYM	Db	Dendritic cell
70	13660	Ehd1	FALANHLIKV	Db	EL4 cell line
	13660	Ehd1	FALANHLIKV	Db	Dendritic cell
71	13669	Eif3s10	QSIEFSRL	Kb	EL4 cell line
	13669	Eif3s10	QSIEFSRL	Kb	Dendritic cell
	13669	Eif3s10	QSIEFSRL	Kb	Thymocyte
72	13709	Elf1	LVYQFKEM	Kb	EL4 cell line
	13709	Elf1	LVYQFKEM	Kb	Dendritic cell
73	13722	Scye1	SGLVNHVPL	Db	EL4 cell line
	13722	Scye1	SGLVNHVPL	Db	Thymocyte
74	13728	Mark2	ASIQNGKDSL	Db	Thymocyte
75	13819	Epas1	SNYLFTKL	Kb	Thymocyte
76	13849	Ephx1	LGYTEKDL	Kb	EL4 cell line
77	13877	Erh	YQPYNKDWI	Db	EL4 cell line
78	13990	Smarcad1	YQHINSYQL	Db	EL4 cell line
79	14000	Rnasen	IGVIFTHV	Kb	EL4 cell line
80	14049	Eya2	TIIIFHSL	Kb	EL4 cell line
	14049	Eya2	TIIIFHSL	Kb	Dendritic cell
81	14050	Eya3	TIIIFHSL	Kb	EL4 cell line
	14050	Eya3	TIIIFHSL	Kb	Dendritic cell
82	14104	Fasn	FGGSNVHVI	Db	EL4 cell line
	14104	Fasn	TSVQFMKL	Kb	EL4 cell line
83	14137	Fdft1	ISLEFRNL	Kb	EL4 cell line
	14137	Fdft1	ISLEFRNL	Kb	Dendritic cell
	14137	Fdft1	ISLEFRNL	Kb	Thymocyte
84	14155	Fem1b	GANVNHTTV	Db	EL4 cell line
85	14359	Fxr1h	EIVTFERL	Kb	EL4 cell line
	14359	Fxr1h	EIVTFERL	Kb	Dendritic cell
	14359	Fxr1h	EIVTFERL	Kb	Thymocyte
86	14411	Slc6a12	SQVRNNVYM	Db	EL4 cell line
	14411	Slc6a12	SQVRNNVYM	Db	Dendritic cell
	14411	Slc6a12	NVWRFPYL	Kb	Dendritic cell
87	14412	Slc6a13	SLYKLRTL	Kb	EL4 cell line
	14412	Slc6a13	NVWRFPYL	Kb	Dendritic cell
88	14468	Gbp1	KSYLMNKL	Kb	Dendritic cell
89	14469	Gbp2	KSYLMNKL	Kb	Dendritic cell
90	14534	Gcn5l2	VQYKFSHL	Kb	EL4 cell line
91	14571	Gpd2	AAVKFHNL	Kb	EL4 cell line
92	14664	Slc6a9	NVWRFPYL	Kb	Dendritic cell
93	14727	Gp49a	VSISFKSL	Kb	EL4 cell line
	14727	Gp49a	VSISFKSL	Kb	Dendritic cell
94	14751	Gpi1	KNLVNKEVM	Db	EL4 cell line
95	14790	Grcc10	GVLKFARL	Kb	EL4 cell line
	14790	Grcc10	SAPENAVRM	Db	EL4 cell line
	14790	Grcc10	SAPENAVRM	Db	Dendritic cell
	14790	Grcc10	SAPENAVRM	Db	Thymocyte
96	14791	Emg1	VSVEYTEKM	Kb	EL4 cell line
97	14824	Grn	VSPTGTHTL	Qa2	Dendritic cell
98	14827	Pdia3	FAHTNIESL	Db	EL4 cell line
	14827	Pdia3	FAHTNIESL	Db	Dendritic cell
99	14897	Trip12	NIAETLHFL	Qa2	Dendritic cell
100	14964	H2-D1	AMAPRTLLL	Qa1	EL4 cell line
	14964	H2-D1	AMAPRTLLL	Qa1	Dendritic cell
101	14972	H2-K1	AVVAFVMKM	Kb	EL4 cell line
	14972	H2-K1	AVVAFVMKM	Kb	Dendritic cell
102	14976	H2-Ke2	SNVVFKLL	Kb	EL4 cell line
	14976	H2-Ke2	SNVVFKLL	Kb	Thymocyte

103	15007	H2-Q10	AMAPRTLLL	Qa1	EL4 cell line
	15007	H2-Q10	AMAPRTLLL	Qa1	Dendritic cell
104	15016	H2-Q5	AMAPRTLLL	Qa1	EL4 cell line
	15016	H2-Q5	AMAPRTLLL	Qa1	Dendritic cell
	15016	H2-Q5	AMAPRTLLL	Qa1	Thymocyte
105	15019	H2-Q8	FAYEGRDYI	Db	Thymocyte
106	15108	Hsd17b10	IGTFNVIRL	Db	Dendritic cell
107	15170	Ptpn6	AQYKFIYV	Kb	EL4 cell line
	15170	Ptpn6	AQYKFIYV	Kb	Dendritic cell
	15170	Ptpn6	AQYKFIYV	Kb	Thymocyte
108	15201	Hells	KVLVFSQM	Kb	EL4 cell line
	15201	Hells	RNFIFSRL	Kb	EL4 cell line
	15201	Hells	KVLVFSQM	Kb	Thymocyte
109	15257	Hipk1	SLLTNHVTL	Db	EL4 cell line
	15257	Hipk1	SLLTNHVTL	Db	Thymocyte
110	15273	Hivep2	KSFDYGNL	Kb	EL4 cell line
111	15441	Hp1bp3	VSQYYPKL	Kb	EL4 cell line
	15441	Hp1bp3	VSQYYPKL	Kb	Dendritic cell
	15441	Hp1bp3	VSQYYPKL	Kb	Thymocyte
112	15463	Hrb	RGPTYVNM	Kb	Dendritic cell
113	15568	Elavl1	GAVTNVKVI	Db	EL4 cell line
	15568	Elavl1	GAVTNVKVI	Db	Dendritic cell
114	15569	Elavl2	GAVTNVKVI	Db	EL4 cell line
	15569	Elavl2	GAVTNVKVI	Db	Dendritic cell
115	15571	Elavl3	GAVTNVKVI	Db	EL4 cell line
	15571	Elavl3	GAVTNVKVI	Db	Dendritic cell
116	15978	Ifng	ELIRVVHQL	Qa2	EL4 cell line
117	16004	Igf2r	VSYKYSKV	Kb	EL4 cell line
118	16145	Igtp	IVAENTKTSL	Db	EL4 cell line
	16145	Igtp	IVAENTKTSL	Db	Thymocyte
119	16149	Cd74	TQDHVMHLL	Qa2	Dendritic cell
120	16211	Kpnb1	AALQNLVKI	Db	EL4 cell line
	16211	Kpnb1	AALQNLVKI	Db	Dendritic cell
	16211	Kpnb1	AALQNLVKI	Db	Thymocyte
121	16329	Inpp1	YMGTNIHSL	Db	EL4 cell line
	16329	Inpp1	YMGTNIHSL	Db	Dendritic cell
	16329	Inpp1	YMGTNIHSL	Db	Thymocyte
122	16364	Irf4	AQQNTGHFL	Qa2	Dendritic cell
123	16428	Itk	GVFSFSRL	Kb	EL4 cell line
124	16430	Stt3a	AVLSFSTRL	Kb	EL4 cell line
	16430	Stt3a	AVLSFSTRL	Kb	Thymocyte
125	16438	Itpr1	SSYNYRVV	Kb	EL4 cell line
	16438	Itpr1	SSYNYRVV	Kb	Dendritic cell
126	16480	Jup	RNYSYEKL	Kb	Dendritic cell
127	16551	Kif11	AAVANQHSSFV	Db	EL4 cell line
128	16828	Ldha	QAPQNKITV	Db	EL4 cell line
129	16834	Cog1	SQIRFGLL	Kb	Dendritic cell
130	16912	Psmb9	TAVVNRVFDKL	Db	EL4 cell line
	16912	Psmb9	VNRVFDKL	Kb	EL4 cell line
	16912	Psmb9	TAVVNRVFDKL	Db	Dendritic cell
131	16913	Psmb8	GGVVNMYHM	Db	EL4 cell line
	16913	Psmb8	GGVVNMYHM	Db	Dendritic cell
	16913	Psmb8	GGVVNMYHM	Db	Thymocyte
132	16950	Loxl3	NVIEVEHQL	Qa2	Dendritic cell
133	16977	Lrrc23	KSLQYLNL	Kb	EL4 cell line
134	17096	Lyn	RSLDNGGYYI	Db	Dendritic cell
135	17101	Lyst	TNFEYLTHL	Kb	Dendritic cell

136	17168	Mare	SAVKNLQQL	Db	EL4 cell line
	17168	Mare	SAVKNLQQL	Db	Dendritic cell
	17168	Mare	SAVKNLQQL	Db	Thymocyte
137	17169	Mark3	TSIAFKNI	Kb	EL4 cell line
	17169	Mark3	TSIAFKNI	Kb	Dendritic cell
138	17184	Matr3	KNLRYQLL	Kb	EL4 cell line
139	17246	Mdm2	YAMIYRNL	Kb	EL4 cell line
140	17276	Mela	AGLQNAGRSPTNL	Db	EL4 cell line
141	17420	Mnat1	YQKENKDVI	Db	EL4 cell line
142	17427	Mns1	KIIEFANI	Kb	EL4 cell line
	17427	Mns1	KIIEFANI	Kb	Thymocyte
143	17685	Msh2	AIVSFAHV	Kb	EL4 cell line
	17685	Msh2	AVIKFLEL	Kb	EL4 cell line
	17685	Msh2	AIVSFAHV	Kb	Dendritic cell
	17685	Msh2	AVIKFLEL	Kb	Dendritic cell
144	17758	Mtap4	KVAEFNNV	Kb	EL4 cell line
145	17769	Mthfr	AAIRNYGIEL	Db	EL4 cell line
	17769	Mthfr	AAIRNYGIEL	Db	Dendritic cell
146	17863	Myb	NAIKNHWNSTM	Db	EL4 cell line
147	17865	Mybl2	NAVKNHWNSTI	Db	EL4 cell line
148	17874	Myd88	SILRFITI	Kb	Dendritic cell
149	17886	Myh9	RVAEFTTNL	Kb	EL4 cell line
	17886	Myh9	RVAEFTTNL	Kb	Dendritic cell
	17886	Myh9	RVAEFTTNL	Kb	Thymocyte
150	17969	Ncf1	STIRNAQSI	Db	EL4 cell line
	17969	Ncf1	STIRNAQSI	Db	Dendritic cell
	17969	Ncf1	EIYEFHKM	Kb	Dendritic cell
151	17979	Ncoa3	ALLDQLHTL	Qa2	Dendritic cell
152	17992	Ndufa4	VNVDYSKL	Kb	EL4 cell line
	17992	Ndufa4	VNVDYSKL	Kb	Dendritic cell
	17992	Ndufa4	VNVDYSKL	Kb	Thymocyte
153	18024	Nfe2l2	SNYHFYSSI	Kb	Dendritic cell
154	18034	Nfkb2	AALQNLEQL	Db	Thymocyte
155	18126	Nos2	FQKQNVTIM	Db	Dendritic cell
156	18145	Npc1	VAVVNKVDI	Db	EL4 cell line
	18145	Npc1	VAVVNKVDI	Db	Dendritic cell
	18145	Npc1	VAVVNKVDI	Db	Thymocyte
157	18201	Nsmaf	RSISFSNM	Kb	EL4 cell line
	18201	Nsmaf	RSISFSNM	Kb	Dendritic cell
158	18292	Sebox	AIVTNVDHF	Db	EL4 cell line
159	18432	Mybbp1a	RAIAFQHL	Kb	EL4 cell line
160	18458	Pabpc1	AGVRNPQQHL	Db	EL4 cell line
	18458	Pabpc1	AGVRNPQQHL	Db	Dendritic cell
161	18519	Pcaf	VQYKFSHL	Kb	EL4 cell line
162	18538	Pcna	RAEDNADTLAL	Db	Thymocyte
163	18572	Pdcd11	VIVKFAQL	Kb	EL4 cell line
	18572	Pdcd11	VIVKFAQL	Kb	Dendritic cell
164	18626	Per1	YTLRNQDTF	Db	Dendritic cell
165	18655	Pgk1	KVLNNMEIGTSL	Db	EL4 cell line
166	18669	Abcb1b	STVRNADVI	Db	EL4 cell line
167	18671	Abcb1a	STVRNADVI	Db	EL4 cell line
168	18693	Pick1	VTIHYNKL	Kb	EL4 cell line
169	18753	Prkcd	KNHEFIATF	Kb	Dendritic cell
	18753	Prkcd	ENFTFQKV	Kb	Dendritic cell
170	18760	Prkcm	SQLRNEVAI	Db	EL4 cell line
171	18777	Lypla1	KALINPANVTF	Db	Dendritic cell
172	18796	Plcb2	TQPLNHYFI	Db	EL4 cell line

173	18803	Plcg1	VNYRVPNM	Kb	EL4 cell line
174	18813	Pa2g4	AQFKFTVL	Kb	EL4 cell line
	18813	Pa2g4	VAHTFVIGV	Kb	EL4 cell line
	18813	Pa2g4	AQFKFTVL	Kb	Dendritic cell
175	18950	Pnp	SLITNKVVM	Kb	EL4 cell line
	18950	Pnp	SLITNKVVM	Db	Dendritic cell
	18950	Pnp	SLITNKVVM	Db	Thymocyte
176	19015	Ppard	ASIVNKDGL	Db	EL4 cell line
	19015	Ppard	ASIVNKDGL	Db	Dendritic cell
177	19084	Prkar1a	KNVLFSHL	Kb	Dendritic cell
178	19085	Prkar1b	KNVLFSHL	Kb	Dendritic cell
179	19139	Prps1	VSYLFSHV	Kb	EL4 cell line
	19139	Prps1	VSYLFSHV	Kb	Dendritic cell
180	19155	Npepps	RQATNQIVM	Db	EL4 cell line
	19155	Npepps	RQATNQIVM	Db	Dendritic cell
181	19167	Psma3	KAVENSSTAI	Db	EL4 cell line
	19167	Psma3	KAVENSSTAI	Db	Thymocyte
182	19179	Psmc1	EFIRNQEQM	Db	EL4 cell line
183	19206	Ptch1	SNVKYVML	Kb	EL4 cell line
184	19224	Ptgs1	IAMEFNHL	Kb	Dendritic cell
185	19225	Ptgs2	TTPEFLTRI	Kb	Dendritic cell
186	19247	Ptpn11	AQYRFIYM	Kb	EL4 cell line
187	19252	Dusp1	VNVRFSTI	Kb	Dendritic cell
188	19299	Abcd3	RLITNSEEI	Db	EL4 cell line
	19299	Abcd3	RLITNSEEI	Db	Dendritic cell
189	19309	Pygm	SNYRVSLL	Kb	EL4 cell line
	19309	Pygm	SNYRVSLL	Kb	Dendritic cell
190	19395	Rasgrp2	VGFRFPIL	Kb	EL4 cell line
	19395	Rasgrp2	VITHFVHV	Kb	EL4 cell line
191	19645	Rb1	SIQNFSKL	Kb	EL4 cell line
192	19696	Rel	TTLIFQKL	Kb	Dendritic cell
	19696	Rel	TTLIFQKL	Kb	Thymocyte
193	19704	Upf1	SGYIYHKL	Kb	EL4 cell line
	19704	Upf1	SGYIYHKL	Kb	Dendritic cell
194	19718	Rfc2	AVLRYTKL	Kb	EL4 cell line
195	19899	Rpl18	KILTFDQL	Kb	EL4 cell line
	19899	Rpl18	KILTFDQL	Kb	Dendritic cell
196	19921	Rpl19	ILMEHIHKL	Qa2	EL4 cell line
197	19942	Rpl27	KTVVNKDVF	Db	EL4 cell line
	19942	Rpl27	KVYNYNHL	Kb	EL4 cell line
	19942	Rpl27	KTVVNKDVF	Db	Dendritic cell
198	19943	Rpl28	NSFRYNGL	Kb	EL4 cell line
	19943	Rpl28	NSFRYNGL	Kb	Dendritic cell
199	19989	Rpl7	RQIFNGTFV	Db	Dendritic cell
200	20020	Polr2a	VNYRHLAL	Kb	EL4 cell line
201	20054	Rps15	VGVYNGKTF	Db	EL4 cell line
	20054	Rps15	VGVYNGKTF	Db	Thymocyte
202	20068	Rps17	KLLDFGSL	Kb	EL4 cell line
203	20115	Rps7	VNFEFPEF	Kb	Thymocyte
204	20133	Rrm1	FQIVNPHLL	Db	EL4 cell line
	20133	Rrm1	YGIRNSLLI	Db	EL4 cell line
	20133	Rrm1	YGIRNSLLI	Db	Dendritic cell
	20133	Rrm1	FQIVNPHLL	Db	Dendritic cell
	20133	Rrm1	FQIVNPHLL	Db	Thymocyte
	20133	Rrm1	YGIRNSLLI	Db	Thymocyte
205	20185	Ncor1	YAMENTRQTI	Db	EL4 cell line
	20185	Ncor1	YAMENTRQTI	Db	Dendritic cell

206	20336	Exoc4	KILANADTM	Db	EL4 cell line
207	20338	Sel1l	QALKYFNL	Kb	EL4 cell line
	20338	Sel1l	QALKYFNL	Kb	Dendritic cell
	20338	Sel1l	QALKYFNL	Kb	Thymocyte
208	20393	Sgk1	STLTYSRM	Kb	EL4 cell line
	20393	Sgk1	VFYAVKVL	Kb	EL4 cell line
	20393	Sgk1	VFYAVKVL	Kb	Dendritic cell
	20393	Sgk1	STLTYSRM	Kb	Dendritic cell
	20393	Sgk1	STLTYSRM	Kb	Thymocyte
209	20425	Shmt1	RNLDYARL	Kb	EL4 cell line
210	20442	St3gal1	VSYWFDQRF	Kb	Dendritic cell
211	20443	St3gal4	GAVKNLTYF	Db	EL4 cell line
	20443	St3gal4	GAVKNLTYF	Db	Dendritic cell
	20443	St3gal4	GAVKNLTYF	Db	Thymocyte
212	20448	St6galnac4	QVYTFTERM	Kb	EL4 cell line
213	20525	Slc2a1	GALGTLHQL	Qa2	Dendritic cell
214	20526	Slc2a2	GALGTLHQL	Qa2	Dendritic cell
215	20538	Slc6a2	NVWRFPYL	Kb	Dendritic cell
216	20544	Slc9a1	VIAAFTSRF	Kb	Dendritic cell
217	20585	Hltf	SGFVFTRL	Kb	EL4 cell line
	20585	Hltf	VGLRYYTGV	Kb	EL4 cell line
218	20620	Plk2	SAVENKQQI	Db	Dendritic cell
219	20740	Spna2	KALINADEL	Db	EL4 cell line
	20740	Spna2	KALINADEL	Db	Dendritic cell
	20740	Spna2	KALINADEL	Db	Thymocyte
220	20747	Spop	KVVKFSYM	Kb	EL4 cell line
221	20815	Srpk1	ISGVNGTHI	Db	EL4 cell line
	20815	Srpk1	ISGVNGTHI	Db	Dendritic cell
	20815	Srpk1	ISGVNGTHI	Db	Thymocyte
222	20842	Stag1	YTIQNRVDI	Db	EL4 cell line
223	20846	Stat1	KFLEQVHQL	Qa2	EL4 cell line
	20846	Stat1	KFLEQVHQL	Qa2	Dendritic cell
224	20848	Stat3	ATLVFHNL	Kb	EL4 cell line
	20848	Stat3	IVELFRNL	Kb	EL4 cell line
	20848	Stat3	ATLVFHNL	Kb	Dendritic cell
	20848	Stat3	ATLVFHNL	Kb	Thymocyte
225	20850	Stat5a	INQRFEEL	Kb	Dendritic cell
226	20868	Stk10	HQLQERHQL	Qa2	EL4 cell line
227	20955	Vamp7	IMVRNIDLV	Db	EL4 cell line
228	21335	Tacc3	AQMQNHSLEM	Db	EL4 cell line
229	21343	Taf6	AQQVNRTTL	Db	EL4 cell line
230	21355	Tap2	HTVQNADQV	Db	EL4 cell line
231	21366	Slc6a6	NVWRFPYL	Kb	Dendritic cell
232	21428	Mlx	IVIGVLHQL	Qa2	Dendritic cell
233	21762	Psmd2	YVLHNSNTM	Db	EL4 cell line
	21762	Psmd2	YVLHNSNTM	Db	Dendritic cell
234	21781	Tfdp1	QQIAFKNL	Kb	EL4 cell line
235	21821	Ift88	IGLTYKKL	Kb	EL4 cell line
236	21822	Tgtp	SKYDFPKL	Kb	EL4 cell line
237	21894	Tln1	SVMENSKVLGEAM	Db	EL4 cell line
	21894	Tln1	SVMENSKVLGEAM	Db	Dendritic cell
238	21916	Tmod1	SSIVNKEGL	Db	EL4 cell line
	21916	Tmod1	SSIVNKEGL	Db	Thymocyte
239	21990	Tph1	FSLENEVGGL	Db	Thymocyte
	21990	Tph1	WGTIFREL	Kb	Thymocyte
240	22029	Traf1	SQLDREHIL	Qa2	Dendritic cell
241	22035	Tnfsf10	VSVTNEHLM	Db	EL4 cell line

	22035	Tnfsf10	VSVTNEHLM	Db	Dendritic cell
242	22042	Tfrc	KAFTYINL	Kb	EL4 cell line
	22042	Tfrc	KAFTYINL	Kb	Dendritic cell
243	22057	Tob1	ISYLYNKL	Kb	EL4 cell line
	22057	Tob1	ISYLYNKL	Kb	Dendritic cell
	22057	Tob1	ISYLYNKL	Kb	Thymocyte
244	22137	Ttk	NAIKYVNL	Kb	EL4 cell line
245	22151	Tubb2a	IREEYPDRI	Kb	EL4 cell line
	22151	Tubb2a	QGFQLTHSL	Qa2	EL4 cell line
	22151	Tubb2a	VQNKNSSYF	Db	EL4 cell line
246	22152	Tubb3	QGFQLTHSL	Qa2	EL4 cell line
247	22153	Tubb4	QGFQLTHSL	Qa2	EL4 cell line
248	22154	Tubb5	IREEYPDRI	Kb	EL4 cell line
	22154	Tubb5	QGFQLTHSL	Qa2	EL4 cell line
	22154	Tubb5	VQNKNSSYF	Db	EL4 cell line
249	22200	Ube1c	VSNLNRQFL	Db	Dendritic cell
250	22201	Uba1	VSISFKSL	Kb	EL4 cell line
	22201	Uba1	VSISFKSL	Kb	Dendritic cell
251	22222	Ubr1	STFEFHSI	Kb	EL4 cell line
252	22224	Usp10	VGPKNKTSI	Db	EL4 cell line
253	22375	Wars	YTVENAKDII	Db	EL4 cell line
	22375	Wars	YTVENAKDII	Db	Dendritic cell
	22375	Wars	YTVENAKDII	Db	Thymocyte
254	22379	Fmnl3	LQYEFTKL	Kb	EL4 cell line
	22379	Fmnl3	LQYEFTKL	Kb	Dendritic cell
	22379	Fmnl3	LQYEFTKL	Kb	Thymocyte
255	22599	Slc6a20b	NVWRFPYL	Kb	Dendritic cell
256	22628	Ywhag	AAMKNVTEL	Db	EL4 cell line
	22628	Ywhag	AAMKNVTEL	Db	Dendritic cell
257	22640	Zfp1	KTFSFKSL	Kb	EL4 cell line
258	22644	Rnf103	KTIYNVEHL	Db	EL4 cell line
259	22693	Zfp30	VMLENYSHL	Db	EL4 cell line
	22693	Zfp30	VMLENYSHL	Db	Dendritic cell
260	22720	Zfp62	SSLINHKSV	Db	EL4 cell line
261	22746	Zfp85-rs1	VNLIYHQRI	Kb	EL4 cell line
262	22754	Zfp92	VMLENYSHL	Db	EL4 cell line
	22754	Zfp92	VMLENYSHL	Db	Dendritic cell
263	23790	Coro1c	ASVQNEAKL	Db	EL4 cell line
264	23856	Dido1	EQQPQQHNL	Qa2	EL4 cell line
	23856	Dido1	EQQPQQHNL	Qa2	Dendritic cell
265	23881	G3bp2	YTLLNKAPEYL	Db	EL4 cell line
266	23918	Impdh2	GGIQNVGHI	Db	EL4 cell line
	23918	Impdh2	GGIQNVGHI	Db	Dendritic cell
	23918	Impdh2	GGIQNVGHI	Db	Thymocyte
267	23983	Pcbp1	YSIQGQHTI	Qa2	Dendritic cell
268	23986	Peci	SSYTFPKM	Kb	EL4 cell line
	23986	Peci	SSYTFPKMM	Kb	EL4 cell line
	23986	Peci	SSYTFPKM	Kb	Thymocyte
269	23988	Pin1	RVYYFNHI	Kb	EL4 cell line
270	23992	Prkra	ISPENHISL	Db	Dendritic cell
271	24136	Zeb2	TSPINPYKDHM	Db	Dendritic cell
272	26364	Cd97	KLLSNINSVF	Db	Thymocyte
273	26374	Rfwd2	YVVDNIDHL	Db	EL4 cell line
	26374	Rfwd2	YVVDNIDHL	Db	Dendritic cell
	26374	Rfwd2	YVVDNIDHL	Db	Thymocyte
274	26413	Mapk1	VGPRYTNL	Kb	EL4 cell line
	26413	Mapk1	VGPRYTNL	Kb	Dendritic cell

	26413	Mapk1	VGPRYTNL	Kb	Thymocyte
275	26417	Mapk3	VGPRYTQL	Kb	Dendritic cell
278	26562	Ncdn	VGFTFPNRL	Kb	EL4 cell line
279	26570	Slc7a11	VAVTFSERL	Kb	EL4 cell line
280	26885	Casp8ap2	VTVLNVDHL	Db	EL4 cell line
	26885	Casp8ap2	VTVLNVDHL	Db	Dendritic cell
	26885	Casp8ap2	VTVLNVDHL	Db	Thymocyte
281	26893	Cops6	NQFVNKFNVL	Db	EL4 cell line
282	26949	Vat1	RTVENVTVF	Db	Dendritic cell
283	27041	G3bp1	GSVANKFYV	Db	EL4 cell line
284	27060	Tcirg1	IVYKWVNV	Kb	Dendritic cell
	27060	Tcirg1	SQNPTNHLL	Qa2	Dendritic cell
285	27405	Abcg3	AVLSFHNI	Kb	EL4 cell line
	27405	Abcg3	SSYFFGKL	Kb	EL4 cell line
286	27967	Cherp	KSYSFIARM	Kb	EL4 cell line
287	29808	Mga	SNLKYILV	Kb	EL4 cell line
	29808	Mga	SNLKYILV	Kb	Dendritic cell
288	29875	Iqgap1	TALKNPNAML	Db	Dendritic cell
289	30930	Vps26a	RSYDFEFM	Kb	Dendritic cell
290	50505	Ercc4	NQVKNIAEL	Db	EL4 cell line
291	50771	Atp9b	AGPWYRNL	Kb	Dendritic cell
292	50875	Tmod3	AAILGMHNL	Qa2	Thymocyte
293	50884	Nckap1	VILSFRSL	Kb	Dendritic cell
294	50907	Preb	TGIKNGVHFL	Db	EL4 cell line
295	50995	Uba2	VSNLNRQFL	Db	Dendritic cell
296	51792	Ppp2r1a	IIPMFSNL	Kb	Thymocyte
297	51797	Ctps	AVVEFSRNV	Kb	EL4 cell line
298	51869	Rif1	KQLVNKEHL	Db	EL4 cell line
299	52521	Zfp622	SLVKNVAHM	Db	EL4 cell line
300	52551	Sgta	AGLLNNPHFI	Db	Dendritic cell
301	52633	Nit2	RAVDNQVYV	Db	EL4 cell line
302	52635	D12Ertd551e	RQLENGTTL	Db	EL4 cell line
	52635	D12Ertd551e	VAVKNSGGFL	Db	EL4 cell line
	52635	D12Ertd551e	VAVKNSGGFL	Db	Dendritic cell
	52635	D12Ertd551e	RQLENGTTL	Db	Dendritic cell
	52635	D12Ertd551e	STFSFTKV	Kb	Dendritic cell
	52635	D12Ertd551e	RQLENGTTL	Db	Thymocyte
303	52858	Cdipt	SVISVIHLI	Qa2	Dendritic cell
304	53321	Cntnap1	SGVRFNNV	Kb	EL4 cell line
305	53415	Htatip2	YKNVNQEVV	Db	EL4 cell line
	53415	Htatip2	YKNVNQEVV	Db	Dendritic cell
306	53417	Hif3a	SAYEYIHAL	Kb	EL4 cell line
307	54138	Atxn10	NSIRNLDTI	Db	EL4 cell line
	54138	Atxn10	NSIRNLDTI	Db	Dendritic cell
	54138	Atxn10	NSIRNLDTI	Db	Thymocyte
308	54208	Arl6ip1	IILKYIGM	Kb	EL4 cell line
	54208	Arl6ip1	IILKYIGM	Kb	Dendritic cell
	54208	Arl6ip1	IILKYIGM	Kb	Thymocyte
309	54325	Elovl1	GQVTFLHVF	Kb	Dendritic cell
310	54397	Ppt2	SSYSFRHL	Kb	EL4 cell line
	54397	Ppt2	SSYSFRHL	Kb	Dendritic cell
311	54405	Ndufa1	ISGVNRYYV	Db	Dendritic cell
312	54624	Paf1	YGISNEKPEV	Db	EL4 cell line
313	54636	Wdr45	SSPKFSEI	Kb	EL4 cell line
314	54644	Otud5	NSVVNPNKATI	Db	EL4 cell line
	54644	Otud5	NSVVNPNKATI	Db	Dendritic cell
315	54670	Atp8b1	KNFAFTLV	Kb	EL4 cell line

316	54711	Plagl2	ANVDFSHL	Kb	EL4 cell line
	54711	Plagl2	ANVDFSHL	Kb	Dendritic cell
317	56085	Ubqln1	RALSNLESI	Db	EL4 cell line
	56085	Ubqln1	RALSNLESI	Db	Thymocyte
318	56321	Aatf	RAVKNQIAL	Db	EL4 cell line
319	56330	Pdcd5	KAVENYLIQM	Db	EL4 cell line
320	56335	Mettl3	NQLDGIHLL	Qa2	Dendritic cell
321	56347	Eif3c	KMIINEELM	Db	EL4 cell line
324	56426	Pdcd10	ILQTFKTVA	Kb	Thymocyte
325	56501	Elf4	LVYQFKEM	Kb	EL4 cell line
	56501	Elf4	LVYQFKEM	Kb	Dendritic cell
326	56612	Pfdn5	KLHDVEHVL	Qa2	EL4 cell line
	56612	Pfdn5	SMYVPGKL	Kb	EL4 cell line
327	56692	Map2k1ip1	QVVQFNRL	Kb	EL4 cell line
	56692	Map2k1ip1	QVVQFNRL	Kb	Dendritic cell
328	56697	Akap10	SNLYYKYL	Kb	EL4 cell line
	56697	Akap10	SNLYYKYL	Kb	Dendritic cell
329	56700	0610031J06Rik	SALVFTRL	Kb	EL4 cell line
	56700	0610031J06Rik	SALVFTRL	Kb	Dendritic cell
330	56706	Ccnl1	VINVFHHL	Kb	EL4 cell line
	56706	Ccnl1	DVINVFHHL	Qa2	Dendritic cell
331	56715	Rabgef1	SNIQYITRF	Kb	Dendritic cell
332	56717	Frap1	ITFIFKSL	Kb	Dendritic cell
334	56774	Slc6a14	NVWRFPYL	Kb	Dendritic cell
335	56784	Garnl1	GAIVNGKVL	Db	EL4 cell line
	56784	Garnl1	GAIVNGKVL	Db	Dendritic cell
336	57028	Pdxp	GVFSFSRL	Kb	EL4 cell line
337	57259	Tob2	ISYLYNKL	Kb	EL4 cell line
	57259	Tob2	ISYLYNKL	Kb	Dendritic cell
338	57314	Th1l	KAIETVHNL	Qa2	EL4 cell line
	57314	Th1l	KAIETVHNL	Qa2	Dendritic cell
339	57440	Ehd3	FALANHLIKV	Db	EL4 cell line
	57440	Ehd3	FALANHLIKV	Db	Dendritic cell
340	57778	Fmnl1	LQYEFTHL	Kb	EL4 cell line
	57778	Fmnl1	LQYEFTHL	Kb	EL4 cell line
	57778	Fmnl1	LQYEFTHL	Kb	Dendritic cell
	57778	Fmnl1	LQYEFTHL	Kb	Thymocyte
341	57869	Adck2	SGPTYIKL	Kb	EL4 cell line
	57869	Adck2	SGPTYIKL	Kb	Dendritic cell
	57869	Adck2	SGPTYIKL	Kb	Thymocyte
342	57913	Lrdd	VALEFTHL	Kb	EL4 cell line
343	58180	Hic2	SSIYFKSL	Kb	EL4 cell line
344	58245	Gpr180	SALANYIHL	Db	EL4 cell line
	58245	Gpr180	SALANYIHL	Db	Dendritic cell
345	58523	Elp2	SAPRNFVENF	Db	EL4 cell line
	58523	Elp2	SAPRNFVENF	Db	Dendritic cell
346	58801	Pmaip1	NAPVNPTRAEL	Db	Dendritic cell
347	59013	Hnrph1	FSPLNPVRV	Db	EL4 cell line
	59013	Hnrph1	FSPLNPVRVHI	Db	Dendritic cell
	59013	Hnrph1	FSPLNPVRV	Db	Dendritic cell
348	59015	Nup160	AAPTNRQIEIL	Db	EL4 cell line
349	59022	Edf1	RAIPNNQVL	Db	EL4 cell line
	59022	Edf1	RAIPNNQVL	Db	Dendritic cell
350	59025	Usp14	VKYLFTGL	Kb	EL4 cell line
	59025	Usp14	VKYLFTGL	Kb	Dendritic cell
	59025	Usp14	VKYLFTGL	Kb	Thymocyte
351	59027	Pbef1	KSYSFDEV	Kb	Dendritic cell

352	59047	Pnkp	YVHVNRDTL	Db	Dendritic cell
353	59079	Erbb2ip	GSLKNVTTL	Db	EL4 cell line
	59079	Erbb2ip	GSLKNVTTL	Db	Dendritic cell
354	59287	Ncstn	KALANVATV	Db	Dendritic cell
355	60409	Trappc4	FALKNPFYSL	Db	Dendritic cell
356	60595	Actn4	VIASFKVL	Kb	Dendritic cell
357	63959	Slc29a1	ATKYFTNRL	Kb	EL4 cell line
358	64652	Nisch	TNQDFIQRL	Kb	EL4 cell line
	64652	Nisch	VGYRFVTAI	Kb	EL4 cell line
	64652	Nisch	TNQDFIQRL	Kb	Thymocyte
359	64659	Mrps14	SRIVFRHL	Kb	EL4 cell line
360	65020	Zfp110	NMISVEHHF	Qa2	EL4 cell line
361	65114	Vps35	FSEENHEPL	Db	EL4 cell line
	65114	Vps35	FSEENHEPL	Db	Dendritic cell
	65114	Vps35	FSEENHEPL	Db	Thymocyte
362	65969	Cubn	KSLTFTNL	Kb	Dendritic cell
363	66067	Gtpbp8	SAVTNSGVHL	Db	EL4 cell line
364	66074	Tmem167	AIFNFQSL	Kb	Thymocyte
365	66090	Ypel3	RAYLFNSV	Kb	EL4 cell line
	66090	Ypel3	RAYLFNSV	Kb	Dendritic cell
366	66136	Znrd1	TSVVFNKL	Kb	EL4 cell line
367	66165	Bccip	KAPVNTAEL	Db	EL4 cell line
	66165	Bccip	KAPVNTAEL	Db	Thymocyte
368	66185	1110037F02Rik	RQILNADAM	Db	EL4 cell line
	66185	1110037F02Rik	RQILNADAM	Db	Dendritic cell
	66185	1110037F02Rik	DLLGTLHNL	Qa2	Dendritic cell
369	66366	Ergic3	QQLDVEHNL	Qa2	EL4 cell line
	66366	Ergic3	QQLDVEHNL	Qa2	Dendritic cell
	66366	Ergic3	QQLDVEHNL	Qa2	Thymocyte
370	66385	Ppp1r7	RAIENIDTL	Db	EL4 cell line
	66385	Ppp1r7	RAIENIDTL	Db	Dendritic cell
	66385	Ppp1r7	RAIENIDTL	Db	Thymocyte
371	66394	Nosip	TSVRFTQL	Kb	EL4 cell line
	66394	Nosip	TSVRFTQL	Kb	Dendritic cell
	66394	Nosip	TSVRFTQL	Kb	Thymocyte
372	66405	Mcts2	IGIENIHYL	Db	Dendritic cell
373	66409	Rsl1d1	QIIPFKTL	Kb	EL4 cell line
374	66413	Psmd6	EILEVLHSL	Qa2	Dendritic cell
375	66480	Rpl15	STYKFFEV	Kb	EL4 cell line
	66480	Rpl15	STYKFFEV	Kb	Dendritic cell
376	66540	3110001A13Rik	LAPQNKPEL	Db	EL4 cell line
377	66570	Cenpm	RSPENPPSKEL	Db	EL4 cell line
378	66590	Farsa	YGINNIREL	Db	EL4 cell line
379	66610	Abi3	YQVGNLAGHTL	Db	EL4 cell line
380	66637	5730449L18Rik	STIVYYKL	Kb	EL4 cell line
381	66689	Klhl28	YMLANLTHL	Db	EL4 cell line
	66689	Klhl28	YMLANLTHL	Db	Dendritic cell
382	66713	Actr2	YAGSNFPEHI	Db	EL4 cell line
	66713	Actr2	YAGSNFPEHI	Db	Dendritic cell
	66713	Actr2	YAGSNFPEHI	Db	Thymocyte
383	66844	Ormdl2	AMYIFLHTV	Kb	EL4 cell line
	66844	Ormdl2	TLTNVIHNL	Qa2	Dendritic cell
384	66855	Tcf25	RNYEYLIRL	Kb	EL4 cell line
385	66860	Tanc1	FQAINAGHI	Db	EL4 cell line
386	66861	Dnajc10	AALIYGKL	Kb	EL4 cell line
387	66884	Appbp2	NQYENAEKL	Db	EL4 cell line
	66884	Appbp2	RLLQEAHDL	Qa2	EL4 cell line

	66884	Appbp2	RLLQEAHDL	Qa2	Dendritic cell
388	66923	Pbrm1	SQVYNDAHI	Db	EL4 cell line
	66923	Pbrm1	SQVYNDAHI	Db	Dendritic cell
	66923	Pb1	SQVYNDAHI	Db	Thymocyte
389	66967	Edem3	FMATNPEHL	Db	EL4 cell line
390	66980	Zdhhc6	SVIKFENL	Kb	EL4 cell line
	66980	Zdhhc6	SVIKFENL	Kb	Dendritic cell
	66980	Zdhhc6	SVIKFENL	Kb	Thymocyte
391	66997	Psmd12	EQSDLVHRI	Qa2	Dendritic cell
392	67014	Mina	VVYIYHSL	Kb	EL4 cell line
	67014	Mina	VVYIYHSL	Kb	Dendritic cell
	67014	Mina	VVYIYHSL	Kb	Thymocyte
393	67019	Actr6	SGYSFTHI	Kb	EL4 cell line
	67019	Actr6	SGYSFTHI	Kb	Dendritic cell
	67019	Actr6	SGYSFTHI	Kb	Thymocyte
394	67048	2610030H06Rik	KAYIFEGAL	Kb	EL4 cell line
395	67095	Trak1	SSVQNYFHL	Db	EL4 cell line
396	67134	Nol5a	YGYHFPEL	Kb	EL4 cell line
397	67144	Lrrc40	INLSFNKL	Kb	EL4 cell line
398	67187	Zmynd19	ESYSFEARM	Kb	EL4 cell line
399	67222	Srfbp1	RLLEEIHAM	Qa2	Dendritic cell
400	67241	Smc6	TMKTNLEYL	Db	EL4 cell line
401	67249	Tbc1d19	AVFAFRAV	Kb	EL4 cell line
402	67268	2900073G15Rik	SMGKNPTDEYL	Db	EL4 cell line
	67268	2900073G15Rik	SMGKNPTDEYL	Db	Dendritic cell
	67268	2900073G15Rik	SMGKNPTDEYL	Db	Thymocyte
403	67300	Cltc	SAIMNPASKV	Db	Dendritic cell
404	67392	4833420G17Rik	FVISNYREQL	Db	EL4 cell line
	67392	4833420G17Rik	FVISNYREQL	Db	Dendritic cell
	67392	4833420G17Rik	FVISNYREQL	Db	Thymocyte
405	67437	Ssr3	VAFAYKNV	Kb	EL4 cell line
	67437	Ssr3	VAFAYKNV	Kb	Dendritic cell
406	67458	Ergic1	YTVANKEYV	Db	EL4 cell line
	67458	Ergic1	YTVANKEYV	Db	Dendritic cell
407	67463	1200014M14Rik	GALENAKAEI	Db	EL4 cell line
408	67465	Sf3a1	RNYQFDFL	Kb	EL4 cell line
	67465	Sf3a1	RNYQFDFL	Kb	Dendritic cell
409	67490	1810074P20Rik	KQLEVVHTL	Qa2	EL4 cell line
	67490	1810074P20Rik	KQLEVVHTL	Qa2	Dendritic cell
410	67493	Mett10d	TAIENSWIHL	Db	EL4 cell line
411	67511	Tmed9	VIGNYRTQL	Kb	Thymocyte
412	67563	Narfl	VAYGFRNI	Kb	EL4 cell line
	67563	Narfl	VAYGFRNI	Kb	Dendritic cell
413	67608	Narf	AAYGFRNI	Kb	EL4 cell line
	67608	Narf	AAYGFRNI	Kb	Dendritic cell
	67608	Narf	AAYGFRNI	Kb	Thymocyte
414	67755	Ddx47	KTFLFSATM	Kb	EL4 cell line
	67755	Ddx47	KTFLFSATM	Kb	Thymocyte
415	67763	Prpsap1	MAYLFRNI	Kb	EL4 cell line
416	67789	Dalrd3	TAPQYYRL	Kb	EL4 cell line
417	67832	Bxdc2	FLVQNIHTL	Db	EL4 cell line
418	67876	Coq10b	ISFEFRSL	Kb	EL4 cell line
	67876	Coq10b	ISFEFRSL	Kb	Dendritic cell
	67876	Coq10b	ISFEFRSL	Kb	Thymocyte
419	67878	Tmem33	QSIAFISRL	Db	EL4 cell line
	67878	Tmem33	QSIAFISRL	Kb	Dendritic cell
	67878	Tmem33	QSIAFISRL	Kb	Thymocyte

420	67891	Rpl4	VNFVHTNL	Kb	EL4 cell line
	67891	Rpl4	VNFVHTNL	Kb	Dendritic cell
421	67911	Zfp169	VMLENYSHL	Db	EL4 cell line
	67911	Zfp169	VMLENYSHL	Db	Dendritic cell
422	67938	Mylc2b	SLGKNPTDAYL	Db	EL4 cell line
	67938	Mylc2b	SLGKNPTDAYL	Db	Dendritic cell
	67938	Mylc2b	SLGKNPTDAYL	Db	Thymocyte
423	67951	Tubb6	IREEYPDRI	Kb	EL4 cell line
	67951	Tubb6	QGFQLTHSL	Qa2	EL4 cell line
424	67972	Atp2b1	KVYTFNSV	Kb	EL4 cell line
	67972	Atp2b1	KVYTFNSV	Kb	Dendritic cell
425	68090	Yif1a	SGYKYVGM	Kb	EL4 cell line
	68090	Yif1a	SGYKYVGM	Kb	Dendritic cell
	68090	Yif1a	SGYKYVGM	Kb	Thymocyte
426	68135	Eif3h	ASITFEHM	Kb	EL4 cell line
427	68145	Etaa1	VAVSNLEKV	Db	EL4 cell line
428	68153	Gtf2e2	SGYKFGVL	Kb	EL4 cell line
	68153	Gtf2e2	SGYKFGVL	Kb	Dendritic cell
	68153	Gtf2e2	SGYKFGVL	Kb	Thymocyte
429	68275	Rpa1	SAVKNDYEM	Db	EL4 cell line
430	68292	Stt3b	KAPDNRETL	Db	EL4 cell line
431	68295	0610011L14Rik	ISILYHQL	Kb	EL4 cell line
	68295	0610011L14Rik	ISILYHQL	Kb	Dendritic cell
	68295	0610011L14Rik	ISILYHQL	Kb	Thymocyte
432	68477	Rmnd5a	WAVSNREML	Db	EL4 cell line
	68477	Rmnd5a	WAVSNREML	Db	Dendritic cell
	68477	Rmnd5a	WAVSNREML	Db	Thymocyte
433	68505	1110014N23Rik	VITNFSARI	Kb	Dendritic cell
434	68523	1110019N10Rik	AALENTHLL	Db	EL4 cell line
	68523	Fam96b	AALENTHLL	Db	Dendritic cell
	68523	1110019N10Rik	AALENTHLL	Db	Thymocyte
435	68652	Map3k7ip2	SAIHNFYDNI	Db	Dendritic cell
436	68770	Phtf2	AQLLHVHEI	Db	EL4 cell line
437	68795	Zfp650	EQQWVSHTF	Qa2	EL4 cell line
438	68801	Elovl5	TLNSFIHVL	Kb	Dendritic cell
439	68845	Pih1d1	VNSNFYLRM	Kb	EL4 cell line
440	68897	Disp1	SNFTFSHL	Kb	EL4 cell line
441	68975	Crsp8	SGLLNQQSL	Db	Thymocyte
442	68979	Nol11	IAVSFREL	Kb	EL4 cell line
	68979	Nol11	TQLIQTHVL	Qa2	EL4 cell line
	68979	Nol11	TQLIQTHVL	Qa2	Dendritic cell
	68979	Nol11	IAVSFREL	Kb	Thymocyte
	68979	Nol11	TQLIQTHVL	Qa2	Thymocyte
443	68995	Mcts1	IGIENIHYL	Db	Dendritic cell
444	69077	Psmd11	ASIDILHSI	Qa2	Dendritic cell
445	69192	Dhx16	AAIANHQVL	Db	EL4 cell line
	69192	Dhx16	AAIANHQVL	Db	Dendritic cell
446	69237	Gtpbp4	QILSDFPKL	Kb	Thymocyte
447	69482	Nup35	AQYGNILKHVM	Db	EL4 cell line
	69482	Nup35	YGNILKHVM	Qa2	EL4 cell line
	69482	Nup35	AQYGNILKHVM	Db	Dendritic cell
448	69544	Wdr5b	AALENDKTI	Db	EL4 cell line
	69544	Wdr5b	AALENDKTI	Db	Dendritic cell
	69544	Wdr5b	AALENDKTI	Db	Thymocyte
449	69601	Dab2ip	VSPTNPTKL	Db	Thymocyte
450	69608	Sec24d	KVLHFFNV	Kb	EL4 cell line
	69608	Sec24d	KVLHFFNV	Kb	Dendritic cell

	69608	Sec24d	ESQSVIHNL	Qa2	Dendritic cell
	69608	Sec24d	ESQSVIHNL	Qa2	Thymocyte
451	69693	Pof1b	KNVVYERV	Kb	EL4 cell line
452	69719	Cad	GVFSFSRL	Kb	EL4 cell line
	69719	Cad	RQAENGMYI	Db	EL4 cell line
	69719	Cad	RQAENGMYI	Db	Dendritic cell
453	69957	Cdc16	ATYSYKEAL	Kb	Dendritic cell
454	70012	Ccdc21	LSILNSNEHL	Db	EL4 cell line
455	70028	Dopey2	SNLKYSLL	Kb	EL4 cell line
	70028	Dopey2	SNLKYSLL	Kb	Dendritic cell
456	70099	Smc4	AALDFKNV	Kb	EL4 cell line
467	70120	Yars2	SGYEFIHKL	Kb	EL4 cell line
468	70208	Med23	LQIPIPHSL	Qa2	Dendritic cell
469	70349	Copb1	IALRYVAL	Kb	EL4 cell line
	70349	Copb1	KMLEVFHAI	Qa2	EL4 cell line
	70349	Copb1	IALRYVAL	Kb	Dendritic cell
	70349	Copb1	YVHVNQYDI	Db	Dendritic cell
	70349	Copb1	IALRYVAL	Kb	Thymocyte
470	70495	Atp6ap2	SELQVLHDI	Qa2	Dendritic cell
471	70549	Tln2	SVMENSKVLGESM	Db	EL4 cell line
472	70572	Ranbp5	VLSEIMHSF	Qa2	Dendritic cell
473	70603	Mutyh	VIHIFSHI	Kb	EL4 cell line
474	70661	BC033915	QQQQEYHEL	Qa2	Dendritic cell
475	70699	Nup205	VNNEFEKL	Kb	Thymocyte
476	70885	Ints10	ANLLYKYL	Kb	EL4 cell line
477	71409	Fmnl2	LQYEFTKL	Kb	EL4 cell line
	71409	Fmnl2	LQYEFTKL	Kb	Dendritic cell
478	71435	Arhgap21	TGVTNRDLI	Db	EL4 cell line
	71435	Arhgap21	TGVTNRDLI	Db	Dendritic cell
479	71702	Cdc5l	FATNNSEHI	Db	EL4 cell line
480	71728	Stk11ip	SALRFLNL	Kb	EL4 cell line
	71728	Stk11ip	SALRFLNL	Kb	Dendritic cell
	71728	Stk11ip	SALRFLNL	Kb	Thymocyte
481	71732	Vps11	KQILNIYDL	Db	Dendritic cell
482	71745	Cul2	VINSFVHV	Kb	EL4 cell line
	71745	Cul2	VINSFVHV	Kb	Dendritic cell
	71745	Cul2	VINSFVHV	Kb	Thymocyte
483	71778	Klhl5	IQYAYTGRL	Kb	EL4 cell line
484	71911	Bdh1	VINAVTHAL	Qa2	EL4 cell line
485	71919	Rpap3	TNVLFNHL	Kb	EL4 cell line
	71919	Rpap3	TNVLFNHL	Kb	Dendritic cell
	71919	D15Ertd682e	TNVLFNHL	Kb	Thymocyte
486	71941	Cars2	KSLKNYITI	Db	EL4 cell line
487	72042	Cotl1	EVVQNFAKEF	Db	Dendritic cell
488	72154	Zfp157	IQVRNPVAL	Db	EL4 cell line
489	72238	Tbc1d5	KTLLNPEYL	Db	EL4 cell line
490	72313	Fryl	YSGTNTGNVHI	Db	EL4 cell line
491	72368	2310045N01Rik	SSVYFRSV	Kb	EL4 cell line
	72368	2310045N01Rik	SSVYFRSV	Kb	Dendritic cell
	72368	2310045N01Rik	SSVYFRSV	Kb	Thymocyte
492	72416	Lrpprc	AAIENIEHL	Db	EL4 cell line
	72416	Lrpprc	AAIENIEHL	Db	Thymocyte
493	72503	2610507B11Rik	ISLDYQHL	Kb	EL4 cell line
	72503	2610507B11Rik	ISLDYQHL	Kb	Dendritic cell
494	72722	2810405J04Rik	ASPEFTKL	Kb	EL4 cell line
	72722	2810405J04Rik	ASPEFTKL	Kb	Thymocyte
495	72747	Ttc39c	SGYDFENRL	Kb	Dendritic cell

	72747	2810439F02Rik	SGYDFENRL	Kb	Thymocyte
496	72759	Tmem135	KGFTFSAL	Kb	Thymocyte
497	73086	Rps6ka5	QLLTVKHEL	Qa2	EL4 cell line
498	73162	Otud3	QLNVVIHQL	Qa2	EL4 cell line
499	73341	Arhgef6	AIIAFKTL	Kb	EL4 cell line
	73341	Arhgef6	AIIAFKTL	Kb	Dendritic cell
	73341	Arhgef6	AIIAFKTL	Kb	Thymocyte
500	73668	Ttc21b	VNTHFSHL	Kb	EL4 cell line
501	73699	Ppp2r1b	VADKFSEL	Kb	EL4 cell line
	73699	Ppp2r1b	VADKFSEL	Kb	Dendritic cell
	73699	Ppp2r1b	VADKFSEL	Kb	Thymocyte
502	73710	Tubb2b	IREEYPDRI	Kb	EL4 cell line
	73710	Tubb2b	QGFQLTHSL	Qa2	EL4 cell line
	73710	Tubb2b	VQNKNSSYF	Db	EL4 cell line
	73710	Tubb2b	VNMVPFPRL	Kb	Thymocyte
503	73739	Cby1	ASLSNLHSL	Db	EL4 cell line
	73739	Pgea1	ASLSNLHSL	Db	Thymocyte
504	73828	Wdr21	KAPTFEVQM	Kb	EL4 cell line
505	73830	Eif3k	VGITYQHI	Kb	Dendritic cell
	73830	Eif3s12	VGITYQHI	Kb	Thymocyte
506	74015	Fcho1	SALRFQAM	Kb	EL4 cell line
	74015	Fcho1	SALRFQAM	Kb	Dendritic cell
507	74016	Phf19	QGPEYIERL	Kb	EL4 cell line
508	74081	Cep350	SAALNKDFL	Db	EL4 cell line
	74081	Cep350	SAALNKDFL	Db	Dendritic cell
509	74114	Crot	IQLMNTAHL	Db	EL4 cell line
	74114	Crot	IQLMNTAHL	Db	Dendritic cell
510	74123	Foxp4	QQLQQQHLL	Qa2	Dendritic cell
511	74125	Armc8	GAVQNIAHL	Db	Dendritic cell
512	74133	1200011M11Rik	KSYNFHTGL	Db	EL4 cell line
513	74182	Prei4	FGIHNGVETL	Db	EL4 cell line
	74182	Prei4	FGIHNGVETL	Db	Dendritic cell
514	74205	Acsl3	AALKNLPLI	Db	EL4 cell line
515	74246	Gale	AVIHFAGL	Kb	EL4 cell line
516	74338	Slc6a19	NVWRFPYL	Kb	Dendritic cell
517	74383	Ubap2l	KIFTASNV	Kb	EL4 cell line
518	74392	Specc1l	RQIEYFRSL	Kb	EL4 cell line
519	74522	Morc2a	RQVQNTAITL	Db	EL4 cell line
520	74558	Gvin1	VNSIFQHL	Kb	EL4 cell line
	74558	Gvin1	HVYYFAHL	Kb	Dendritic cell
	74558	Gvin1	RQYIFSKL	Kb	Dendritic cell
	74558	Gvin1	ISLKNSQEI	Db	Dendritic cell
	74558	Gvin1	YQLVNSIFQHL	Db	Dendritic cell
	74558	Gvin1	VNSIFQHL	Kb	Dendritic cell
521	74734	Rhoh	YSVANHNSFL	Db	EL4 cell line
	74734	Rhoh	YSVANHNSFL	Db	Dendritic cell
	74734	Rhoh	YSVANHNSFL	Db	Thymocyte
522	74741	5730419I09Rik	AAVLNPRFL	Db	EL4 cell line
523	74781	Wipi2	SGYKFFSL	Kb	EL4 cell line
	74781	Wipi2	SGYKFFSL	Kb	Dendritic cell
	74781	Wipi2	SGYKFFSL	Kb	Thymocyte
524	74841	Usp38	ASLQNAEKTM	Db	EL4 cell line
525	75007	4930504E06Rik	VNVRFTGV	Kb	EL4 cell line
	75007	Fam63a	VNVRFTGV	Kb	Dendritic cell
526	75062	Sf3a3	IIYNPKNL	Kb	EL4 cell line
527	75089	Uhrf1bp1l	SSLLNIQHF	Db	Dendritic cell
528	75292	Prkcn	SQLRNEVAI	Db	EL4 cell line

529	75339	Mphosph8	DAVKNGDYI	Db	EL4 cell line
530	75415	Arhgap12	YGLLNVTKI	Db	EL4 cell line
	75415	Arhgap12	YGLLNVTKI	Db	Dendritic cell
531	75425	2610036D13Rik	QTVENVEHL	Db	EL4 cell line
	75425	2610036D13Rik	QTVENVEHL	Db	Dendritic cell
	75425	2610036D13Rik	QTVENVEHL	Db	Thymocyte
532	75456	Prps1l1	VSYLFSHV	Kb	EL4 cell line
	75456	Prps1l1	VSYLFSHV	Kb	Dendritic cell
533	75547	Akap13	VALAFRHL	Kb	EL4 cell line
534	75565	Ccdc101	ELLTELHQL	Qa2	EL4 cell line
	75565	Ccdc101	ELLTELHQL	Qa2	Thymocyte
535	75627	Snapc1	AAFVFRKL	Kb	EL4 cell line
536	75660	Lin37	STLIYRNM	Kb	EL4 cell line
	75660	Lin37	STLIYRNM	Kb	Dendritic cell
537	75669	Pik3r4	TALRFLEL	Kb	EL4 cell line
538	75725	Phf14	VNYYFERNM	Kb	EL4 cell line
539	75812	Tasp1	SGIKNPVSV	Db	EL4 cell line
540	75965	Zdhhc20	TNYKFFML	Kb	EL4 cell line
541	75974	Dock11	DQIEYHEGL	Kb	Dendritic cell
542	76022	5830417I10Rik	RAAANSETI	Db	EL4 cell line
	76022	5830417I10Rik	NAPQNPESKL	Db	Dendritic cell
543	76041	Ccdc125	NAVLNQRYL	Db	Thymocyte
544	76130	Las1l	ALVRFVNL	Kb	EL4 cell line
545	76131	Depdc1a	FSQENTEKI	Db	EL4 cell line
	76131	Depdc1a	FSQENTEKI	Db	Thymocyte
546	76355	Tgds	RAFEFTYV	Kb	EL4 cell line
547	76582	Ipo11	QQFIYEKL	Kb	EL4 cell line
	76582	Ipo11	TIILFTKV	Kb	EL4 cell line
	76582	Ipo11	TIILFTKV	Kb	Thymocyte
548	76681	Trim12	FISDVEHQL	Qa2	Dendritic cell
549	76788	2410127E18Rik	VQIKNDVFI	Db	EL4 cell line
550	76843	Dtl	SSPENKNWL	Db	EL4 cell line
551	76857	Spopl	KVVKFSYM	Kb	EL4 cell line
552	77048	4921537D05Rik	AQVENVQRI	Db	Thymocyte
553	77480	C330002I19Rik	RANQNFDEI	Db	EL4 cell line
	77480	Kidins220	RANQNFDEI	Db	Dendritic cell
554	77573	Vps33a	GSLANHTSI	Db	EL4 cell line
	77573	Vps33a	GSLANHTSI	Db	Dendritic cell
	77573	Vps33a	GSLANHTSI	Db	Thymocyte
555	77591	Ddx10	VQYLYRVF	Kb	EL4 cell line
556	77700	9130208D14Rik	VNSIFQHL	Kb	EL4 cell line
557	77864	Ypel2	RAYLFNSV	Kb	EL4 cell line
	77864	Ypel2	RAYLFNSV	Kb	Dendritic cell
558	77877	6030458C11Rik	KVLDVLHSL	Qa2	EL4 cell line
	77877	6030458C11Rik	KVLDVLHSL	Qa2	Dendritic cell
559	77987	Ascc3	AMLTILHEI	Qa2	Dendritic cell
560	78251	Zfp712	VMLENYSHL	Db	EL4 cell line
	78251	Zfp712	VMLENYSHL	Db	Dendritic cell
561	78303	Hist3h2ba	VNDIFERI	Kb	EL4 cell line
562	78651	Lsm6	SGVDYRGV	Kb	EL4 cell line
563	78697	Pus7	TSIKNQTQL	Db	EL4 cell line
	78697	Pus7	TSIKNQTQL	Db	Dendritic cell
564	78757	4921505C17Rik	KALSYASL	Kb	EL4 cell line
	78757	4921505C17Rik	LSPINHNTL	Db	EL4 cell line
565	80743	Vps16	VSFTYRYL	Kb	EL4 cell line
	80743	Vps16	VSFTYRYL	Kb	Dendritic cell
	80743	Vps16	VSFTYRYL	Kb	Thymocyte

567	80744	BC003993	ASPIFTHV	Kb	EL4 cell line
	80744	Cwc22	ASPIFTHV	Kb	Dendritic cell
568	80909	Gats	NISGVIHAL	Qa2	Dendritic cell
569	80986	Ckap2	TLNDLIHNI	Qa2	EL4 cell line
	80986	Ckap2	TLNDLIHNI	Qa2	Dendritic cell
570	81702	Ankrd17	ASVLNVNHI	Db	EL4 cell line
	81702	Ankrd17	ASVLNVNHI	Db	Dendritic cell
	81702	Ankrd17	ASVLNVNHI	Db	Thymocyte
571	81897	Tlr9	LGLSNLTHL	Db	Dendritic cell
572	81898	Sf3b1	KAIVNVIGM	Db	EL4 cell line
	81898	Sf3b1	KAIVNVIGM	Db	Dendritic cell
573	83490	Pik3ap1	YGLKNLTAL	Db	Dendritic cell
	83490	Pik3ap1	YGLKNLTAL	Db	Thymocyte
574	83922	Tsga14	KVTTFAQL	Kb	EL4 cell line
575	85031	Pla1a	SAVENVVKL	Db	Dendritic cell
576	93761	Smarca1	RVLIFSQM	Kb	EL4 cell line
	93761	Smarca1	RVLIFSQM	Kb	Dendritic cell
577	93762	Smarca5	RVLIFSQM	Kb	EL4 cell line
	93762	Smarca5	RVLIFSQM	Kb	Dendritic cell
578	94112	Med15	QQQQQQHLI	Qa2	Dendritic cell
579	94176	Dock2	SMVQNRVFL	Db	EL4 cell line
	94176	Dock2	SQFPNAEKM	Db	EL4 cell line
	94176	Dock2	VNQFFKTML	Kb	EL4 cell line
	94176	Dock2	SMVQNRVFL	Db	Dendritic cell
	94176	Dock2	KSVENFVSL	Db	Dendritic cell
	94176	Dock2	SQFPNAEKM	Db	Dendritic cell
	94176	Dock2	SMVQNRVFL	Db	Thymocyte
580	97112	Nmd3	NTYNYKSTF	Kb	Dendritic cell
581	97541	Qars	VQWEYGRL	Kb	EL4 cell line
582	97895	Nlrp4f	TPVKNIDTV	Db	Thymocyte
583	98488	Gtf3c3	IGLTFIHM	Kb	EL4 cell line
584	98758	Hnrpf	FSPLNPVRV	Db	EL4 cell line
	98758	Hnrpf	FSPLNPVRVHI	Db	Dendritic cell
	98758	Hnrpf	FSPLNPVRV	Db	Dendritic cell
	98758	Hnrpf	FSPLNPVRV	Db	Thymocyte
585	98999	Znfx1	VNIPFVRL	Kb	Dendritic cell
586	99382	Abtb2	NTYKYAKI	Kb	EL4 cell line
587	100177	Zmym6	ASIIFEHL	Kb	EL4 cell line
588	100515	Zfp518b	SSVQNKEYL	Db	Dendritic cell
589	100604	Lrrc8c	EIVSFQHL	Kb	Dendritic cell
590	100683	Trrap	QDPVFQKL	Kb	Thymocyte
591	100702	Mpa2l	AGIKNSTEF	Db	Dendritic cell
592	100910	2010209O12Rik	AQIRNLTVL	Db	EL4 cell line
593	101540	Prkd2	SQLRNEVAI	Db	EL4 cell line
594	101706	Numa1	VSILNRQVL	Db	EL4 cell line
	101706	Numa1	VSILNRQVL	Db	Dendritic cell
	101706	Numa1	VSILNRQVL	Db	Thymocyte
595	102566	Tmem16k	KVLVFNFL	Kb	Dendritic cell
596	102680	Slc6a20a	NVWRFPYL	Kb	Dendritic cell
597	102857	Slc6a8	NVWRFPYL	Kb	Dendritic cell
598	103098	Slc6a15	NVWRFPYL	Kb	Dendritic cell
599	103573	Xpo1	LIYKFLNV	Kb	Dendritic cell
600	104245	Slc6a5	NVWRFPYL	Kb	Dendritic cell
601	104662	Tsr1	RAYLFAHV	Kb	EL4 cell line
602	104721	Ddx1	ASVLNKWQM	Db	EL4 cell line
603	104831	Ptpn23	KIYYFAAV	Kb	EL4 cell line
	104831	Ptpn23	RALENPDTASL	Db	EL4 cell line

	104831	Ptpn23	RALENPDTASL	Db	Dendritic cell
604	105203	BC016423	SSSLNQEKI	Db	EL4 cell line
605	106042	Prickle1	LNYKFPGL	Kb	EL4 cell line
606	106143	Cggbp1	VIQDFVKM	Kb	EL4 cell line
607	106298	Rrn3	AAITNKYQL	Db	EL4 cell line
	106298	Rrn3	AAITNKYQL	Db	Dendritic cell
608	106369	Ypel1	RAYLFNSV	Kb	EL4 cell line
	106369	Ypel1	RAYLFNSV	Kb	Dendritic cell
609	106840	Unc119b	HIYEFPQL	Kb	Dendritic cell
610	106894	A630042L21Rik	FAIRNQIKL	Db	EL4 cell line
611	107035	Fbxo38	SAFSFRTL	Kb	EL4 cell line
	107035	Fbxo38	SAFSFRTL	Kb	Dendritic cell
	107035	Fbxo38	SAFSFRTL	Kb	Thymocyte
612	107182	Btaf1	GQIQNKEVL	Db	EL4 cell line
	107182	Btaf1	GQIQNKEVL	Db	Dendritic cell
613	107569	Nt5c3	DGVANVEHI	Db	EL4 cell line
	107569	Nt5c3	GALKNTDYF	Db	Dendritic cell
614	107723	Slc12a6	SAARFALL	Kb	EL4 cell line
	107723	Slc12a6	SAARFALL	Kb	Dendritic cell
615	107769	Tm6sf1	VTYIFNHL	Kb	Dendritic cell
616	107932	Chd4	RVLIFSQM	Kb	EL4 cell line
	107932	Chd4	RVLIFSQM	Kb	Dendritic cell
617	107976	Bre	ATQVYPKL	Kb	EL4 cell line
	107976	Bre	ATQVYPKL	Kb	Dendritic cell
	107976	Bre	ATQVYPKL	Kb	Thymocyte
618	108067	Eif2b3	AQIVNKHLI	Db	EL4 cell line
619	108099	Prkag2	FMKQNLDEL	Db	EL4 cell line
620	108101	Fermt3	KTWRFSNM	Kb	EL4 cell line
621	108143	Taf9	SGLKYVNV	Kb	EL4 cell line
	108143	Taf9	SGLKYVNV	Kb	Dendritic cell
	108143	Taf9	SGLKYVNV	Kb	Thymocyte
622	108655	Foxp1	QQLQQQHLL	Qa2	Dendritic cell
	108655	Foxp1	QQLQQQHLL	Qa2	Thymocyte
623	108911	Rcc2	AAYRNLGQNL	Db	EL4 cell line
	108911	Rcc2	AAYRNLGQNL	Db	Dendritic cell
624	108960	Irak2	VAFAFKKL	Kb	Dendritic cell
625	108989	Tpr	VSYRNIEEL	Db	EL4 cell line
626	109331	Rnf20	SSLQNHNHQL	Db	EL4 cell line
627	109674	Ampd2	VGYRYETL	Kb	EL4 cell line
628	110078	Pygb	SNYRVSLL	Kb	EL4 cell line
	110078	Pygb	SNYRVSLL	Kb	Dendritic cell
629	110095	Pygl	SNYRVSLL	Kb	EL4 cell line
	110095	Pygl	SNYRVSLL	Kb	Dendritic cell
630	110308	Krt5	AAYMNKVEL	Db	Thymocyte
631	110310	Krt7	AAYTNKVEL	Db	Thymocyte
632	110521	Hivep1	GSLTNLHTL	Db	Dendritic cell
633	110606	Fntb	SSYKFNHL	Kb	EL4 cell line
634	110639	Prps2	VSYLFSHV	Kb	EL4 cell line
	110639	Prps2	VSYLFSHV	Kb	Dendritic cell
635	110749	Chaf1b	SNIHYHTL	Kb	EL4 cell line
636	110750	Cse1l	GQMVNNPKIHL	Db	EL4 cell line
637	110816	Pwp2	FAYRFSNL	Kb	EL4 cell line
	110816	Pwp2	FAYRFSNL	Kb	Dendritic cell
638	114741	Supt16h	VSYKNPSLM	Db	EL4 cell line
639	116748	Lsm10	QQLQIIHRV	Qa2	EL4 cell line
	116748	Lsm10	QQLQIIHRV	Qa2	Dendritic cell
640	116848	Baz2a	TIVEFLHSF	Kb	Dendritic cell

641	117599	Helb	VTVDFSKL	Kb	EL4 cell line
642	121022	Mrps6	SAVENILEHL	Db	EL4 cell line
	121022	Mrps6	SAVENILEHL	Db	Dendritic cell
	121022	Mrps6	SAVENILEHL	Db	Thymocyte
643	140580	Elmo1	WSLANHEYF	Db	EL4 cell line
644	140630	Ube4a	EQLNINHMI	Qa2	Dendritic cell
645	140858	Wdr5	AALENDKTI	Db	EL4 cell line
	140858	Wdr5	AALENDKTI	Db	Dendritic cell
646	170439	Elovl6	KSFLFSAL	Kb	EL4 cell line
	170439	Elovl6	KSFLFSAL	Kb	Dendritic cell
	170439	Elovl6	KSFLFSAL	Kb	Thymocyte
647	170742	Sertad3	RSYQQALL	Kb	Dendritic cell
648	170743	Tlr7	KGYVFKEL	Kb	Dendritic cell
649	170749	Mtmr4	HAIRNSFQYL	Db	Dendritic cell
650	170755	Sgk3	SALGYLHSI	Kb	Dendritic cell
651	170763	Zfp87	VMLENYSHL	Db	EL4 cell line
	170763	Zfp87	VMLENYSHL	Db	Dendritic cell
652	170772	Glcci1	SRVSFTSL	Kb	EL4 cell line
653	170826	Ppargc1b	LSVRNGATL	Db	EL4 cell line
	170826	Ppargc1b	LSVRNGATL	Db	Dendritic cell
654	170936	Zfp369	NMISVEHHF	Qa2	EL4 cell line
655	192191	Med9	QQQQQLHSL	Qa2	EL4 cell line
	192191	Med9	QQQQQLHSL	Qa2	Dendritic cell
656	192195	Ash1l	VGLINKDSV	Db	EL4 cell line
	192195	Ash1l	VGLINKDSV	Db	Dendritic cell
	192195	Ash1l	VGLINKDSV	Db	Thymocyte
657	194388	D230004J03Rik	SSYAYTKV	Kb	EL4 cell line
658	195046	Nlrp1a	LSYSFAHL	Kb	EL4 cell line
659	207165	Bptf	KAVDFDGRL	Kb	EL4 cell line
660	207304	Hectd1	IFYYVQKL	Kb	EL4 cell line
661	207728	Pde2a	IKNENQEVI	Db	Thymocyte
662	208146	Yeats2	SGVSNPHVI	Db	EL4 cell line
663	208154	Btla	SQVINSHSV	Db	EL4 cell line
664	210293	Dock10	KNLLNVDKI	Db	EL4 cell line
665	210544	Wdr67	GIMRFVNI	Kb	EL4 cell line
	210544	Wdr67	KVLRFLNV	Kb	EL4 cell line
666	210582	Coq10a	ISFEFRSL	Kb	EL4 cell line
	210582	Coq10a	ISFEFRSL	Kb	Dendritic cell
667	211255	Kbtbd7	AQSFIAHNF	Qa2	Dendritic cell
668	211548	Nomo1	SSLVNKEDV	Db	EL4 cell line
	211548	Nomo1	SSLVNKEDVL	Db	EL4 cell line
	211548	Nomo1	SSLVNKEDVL	Db	Dendritic cell
	211548	Nomo1	SSLVNKEDV	Db	Thymocyte
669	211586	Tfdp2	QQIAFKNL	Kb	EL4 cell line
670	212276	Zfp748	VMLENYSHL	Db	EL4 cell line
	212276	Zfp748	VMLENYSHL	Db	Dendritic cell
671	212281	A530054K11Rik	KAFDYPSRL	Kb	EL4 cell line
672	212307	Mapre2	QLNEQVHSL	Qa2	EL4 cell line
	212307	Mapre2	QLNEQVHSL	Qa2	Dendritic cell
	212307	Mapre2	QLNEQVHSL	Qa2	Thymocyte
673	212377	F730047E07Rik	VGVTYRTL	Kb	EL4 cell line
	212377	F730047E07Rik	VGVTYRTL	Kb	Thymocyte
674	212528	Trmt1	VITEFARI	Kb	EL4 cell line
675	212569	Zfp273	VNLIYHQRI	Kb	EL4 cell line
676	212627	Prpsap2	MSYLFRNI	Kb	EL4 cell line
	212627	Prpsap2	MSYLFRNI	Kb	Dendritic cell
678	213109	Phf3	RAPQFINL	Kb	EL4 cell line

	213109	Phf3	RAPQFINL	Kb	Dendritic cell
679	213550	Dis3l	FSNKNLEEL	Db	Dendritic cell
	213550	AV340375	FSNKNLEEL	Db	Thymocyte
680	213895	Bms1	YQNQEIHNL	Qa2	EL4 cell line
	213895	Bms1	YQNQEIHNL	Qa2	Dendritic cell
681	214230	Pak6	YQHLNVVEM	Db	EL4 cell line
682	214290	Zcchc6	TTYKYFAL	Kb	EL4 cell line
	214290	Zcchc6	TTYKYFAL	Kb	Dendritic cell
683	214459	Fnbp1l	AQQSYERL	Kb	Dendritic cell
684	214572	Prmt7	VIVEFRDL	Kb	EL4 cell line
	214572	Prmt7	VIVEFRDL	Kb	Thymocyte
685	214616	Spata5l1	AVLEVVHEL	Qa2	Dendritic cell
686	214901	Chtf18	QLSDTLHSL	Qa2	EL4 cell line
687	215690	Nav1	SNIQYRSL	Kb	Dendritic cell
688	215900	Fam26f	MSMTNTHEL	Db	Dendritic cell
689	215974	EG215974	YGYSNRVVDLM	Db	EL4 cell line
	215974	EG215974	GLMTTVHAI	Qa2	Dendritic cell
	215974	EG215974	YGYSNRVVDLM	Db	Dendritic cell
690	216131	Tmem1	YTVKNGDSL	Db	Dendritic cell
691	216198	Tcp11l2	KATTNIVEM	Db	Thymocyte
692	216443	Mars	VSPLFQKL	Kb	EL4 cell line
	216443	Mars	VSPLFQKL	Kb	Dendritic cell
693	216445	Arhgap9	SGLLNMTKI	Db	Dendritic cell
694	216825	Usp22	FAVVNHQGTL	Db	EL4 cell line
	216825	Usp22	FAVVNHQGTL	Db	Dendritic cell
	216825	Usp22	FAVVNHQGTL	Db	Thymocyte
695	216848	Chd3	RVLIFSQM	Kb	EL4 cell line
	216848	Chd3	RVLIFSQM	Kb	Dendritic cell
696	216859	Centb1	INQIYEARV	Kb	EL4 cell line
	216859	Centb1	INQIYEARV	Kb	Dendritic cell
	216859	Centb1	INQIYEARV	Kb	Thymocyte
697	217216	BC030867	SALENAENHV	Db	EL4 cell line
698	217351	Tnrc6c	TSPINPQHM	Db	EL4 cell line
699	217353	Tmc6	ASYLFRGL	Kb	EL4 cell line
	217353	Tmc6	ASYLFRGL	Kb	Dendritic cell
	217353	Tmc6	ASYLFRGL	Kb	Thymocyte
700	217431	Nol10	SGFYYKTRI	Kb	EL4 cell line
701	217578	Baz1a	SALENGRYEL	Db	EL4 cell line
	217578	Baz1a	SALENGRYEL	Db	Dendritic cell
702	217615	Mgea6	RNQVYTQL	Kb	Thymocyte
703	218035	Vps41	IGLAYVNHL	Kb	EL4 cell line
704	218314	Zfp595	KAFDYPSRL	Kb	EL4 cell line
705	218490	Btf3	ETIMNQEKL	Db	EL4 cell line
706	218811	Sec24c	KVLHFYNV	Kb	EL4 cell line
707	218952	Fermt2	KTWRFSNM	Kb	EL4 cell line
708	218977	Dlg7	VNQKFNNL	Kb	EL4 cell line
	218977	Dlg7	VNQKFNNL	Kb	Dendritic cell
709	218978	D14Ertd436e	SQHVNLDQL	Db	EL4 cell line
	218978	D14Ertd436e	SQHVNLDQL	Db	Dendritic cell
	218978	D14Ertd436e	SQHVNLDQL	Db	Thymocyte
710	218989	6720456H20Rik	TGIRNLEWL	Db	EL4 cell line
	218989	6720456H20Rik	TGIRNLEWL	Db	Thymocyte
711	219135	Mtmr6	VGIENIHVM	Db	EL4 cell line
	219135	Mtmr6	VGIENIHVM	Db	Dendritic cell
	219135	Mtmr6	SNIRFQFV	Kb	Dendritic cell
	219135	Mtmr6	VGIENIHVM	Db	Thymocyte
712	223499	Wdsof1	SSVKFNPV	Kb	EL4 cell line

713	223664	Lrrc14	ASLRYLGL	Kb	EL4 cell line
714	223672	Apol9a	AAPTGTHVL	Qa2	Dendritic cell
715	223691	Eif3eip	TTYKYEMI	Kb	EL4 cell line
	223691	Eif3eip	TTYKYEMI	Kb	Dendritic cell
	223691	Eif3eip	SVLNVLHSL	Qa2	Dendritic cell
716	223774	Alg12	AAMLNYTHI	Db	EL4 cell line
717	224020	Pi4ka	AILQVLHVL	Qa2	Dendritic cell
718	224045	Eif2b5	RVFQNEVLGTL	Db	EL4 cell line
719	224088	Atp13a3	DAIHNFDFL	Db	Dendritic cell
720	224171	C330027C09Rik	AQNDIEHLF	Qa2	EL4 cell line
	224171	C330027C09Rik	AQNDIEHLF	Qa2	Dendritic cell
	224171	C330027C09Rik	AQNDIEHLF	Qa2	Thymocyte
721	224727	Bat3	SIAAFIQRL	Kb	EL4 cell line
	224727	Bat3	SIAAFIQRL	Kb	Dendritic cell
	224727	Bat3	SIAAFIQRL	Kb	Thymocyte
722	224823	BC011248	KTYQFLNDI	Kb	EL4 cell line
	224823	BC011248	KTYQFLNDI	Kb	Dendritic cell
723	224826	Ubr2	VAYKFPELL	Kb	Dendritic cell
	224826	Ubr2	VAYKFPELL	Kb	Thymocyte
724	224860	Plcl2	AVVSFKEL	Kb	EL4 cell line
	224860	Plcl2	EFIEVFHEL	Qa2	Dendritic cell
	224860	Plcl2	AVVSFKEL	Kb	Dendritic cell
725	226414	Dars	AANINKESI	Db	Dendritic cell
726	226519	Lamc1	EIIKDIHNL	Qa2	EL4 cell line
	226519	Lamc1	EIIKDIHNL	Qa2	Dendritic cell
727	226562	Bat2d	SQLIDTHLL	Qa2	EL4 cell line
728	226747	Ahctf1	KSISNTSKL	Db	EL4 cell line
	226747	Ahctf1	SAYRFSGV	Kb	EL4 cell line
	226747	Ahctf1	TSVENHEFL	Db	EL4 cell line
729	226778	Mark1	TSIAFKNI	Kb	EL4 cell line
	226778	Mark1	TSIAFKNI	Kb	Dendritic cell
730	227197	Ndufs1	AKLVNQEVL	Db	EL4 cell line
	227197	Ndufs1	AKLVNQEVL	Db	Dendritic cell
	227197	Ndufs1	AKLVNQEVL	Db	Thymocyte
731	227446	2310035C23Rik	SSVSNKTTL	Db	EL4 cell line
732	227541	Camk1d	KIFEFKETL	Kb	EL4 cell line
	227541	Camk1d	KIFEFKETL	Kb	Dendritic cell
733	227613	Tubb2c	IREEYPDRI	Kb	EL4 cell line
	227613	Tubb2c	QGFQLTHSL	Qa2	EL4 cell line
	227613	Tubb2c	VQNKNSSYF	Db	EL4 cell line
734	228730	Gm114	AQVRNQGYL	Db	EL4 cell line
735	228829	Phf20	ESPSYRTL	Kb	EL4 cell line
736	228850	B230339M05Rik	KSYVNPTEL	Db	EL4 cell line
737	229841	Cenpe	EQNESAHTL	Qa2	EL4 cell line
	229841	Cenpe	SALQNAESDRL	Db	EL4 cell line
	229841	Cenpe	SALQNAESDRL	Db	Dendritic cell
	229841	Cenpe	SALQNAESDRL	Db	Thymocyte
738	229898	Gbp5	HLVTNQEAL	Db	Dendritic cell
	229898	Gbp5	KSYLMNKL	Kb	Dendritic cell
739	230082	Nol6	SSVRFSYM	Kb	EL4 cell line
740	230700	Foxj3	NTVTNKVTL	Db	EL4 cell line
	230700	Foxj3	NTVTNKVTL	Db	Dendritic cell
741	230721	Pabpc4	IGYAFVHL	Kb	EL4 cell line
742	230770	Tmem39b	RTYSFLNL	Kb	EL4 cell line
743	230866	C230096C10Rik	SQIKNEINI	Db	EL4 cell line
744	230895	Vps13d	INIHYTQL	Kb	EL4 cell line
	230895	Vps13d	INIHYTQL	Kb	Thymocyte

745	231123	BC023882	SQLNELHHL	Qa2	EL4 cell line
	231123	BC023882	TSYRFLAL	Kb	EL4 cell line
746	231128	BC037112	AAPRNSPTGL	Db	EL4 cell line
747	231329	Polr2b	IGPTYYQRL	Kb	EL4 cell line
	231329	Polr2b	IGPTYYQRL	Kb	Dendritic cell
	231329	Polr2b	IGPTYYQRL	Kb	Thymocyte
748	231549	Lrrc8d	EIISFQHL	Kb	EL4 cell line
	231549	Lrrc8d	SQMTNLQELHL	Db	EL4 cell line
	231549	Lrrc8d	SQMTNLQELHL	Db	Dendritic cell
749	231841	AA881470	SALEFLTHL	Kb	Dendritic cell
750	231874	AU022870	KIQSFINRM	Kb	EL4 cell line
751	232333	Slc6a1	NVWRFPYL	Kb	Dendritic cell
752	232339	Ankrd26	AVYSYKRL	Kb	EL4 cell line
753	232341	Wnk1	KSISNPPGSNL	Db	EL4 cell line
	232341	Wnk1	KSISNPPGSNL	Db	Dendritic cell
754	232853	5730403M16Rik	SSYNFIRHM	Kb	EL4 cell line
755	232906	Grlf1	SQLQAEHTL	Qa2	EL4 cell line
756	233056	Zfp790	VMLENYSHL	Db	EL4 cell line
	233056	Zfp790	VMLENYSHL	Db	Dendritic cell
757	233115	Dpy19l3	SVVAFHNL	Kb	EL4 cell line
	233115	Dpy19l3	SVVAFHNL	Kb	Thymocyte
758	233280	Nipa1	IIVQFRYI	Kb	Dendritic cell
759	233405	Vps33b	ASLVNADKL	Db	EL4 cell line
	233405	Vps33b	ASLVNADKL	Db	Dendritic cell
	233405	Vps33b	ASLVNADKL	Db	Thymocyte
760	233489	Picalm	VAFDFTKV	Kb	EL4 cell line
	233489	Picalm	VAFDFTKV	Kb	Dendritic cell
	233489	Picalm	VAFDFTKV	Kb	Thymocyte
761	233575	Frag1	SAPRFLTAF	Kb	Dendritic cell
762	233789	Smg1	ALNNLLHSL	Qa2	Dendritic cell
763	234135	Whsc1l1	KGIGNKTEI	Db	EL4 cell line
764	234309	Cbr4	AAGINRDSL	Db	EL4 cell line
	234309	Cbr4	AAGINRDSL	Db	Dendritic cell
765	234664	Nae1	AAVGNHVAKL	Db	EL4 cell line
766	234740	4932417I16Rik	KIFVFQNQV	Kb	EL4 cell line
767	235461	B230380D07Rik	VNVRFTGV	Kb	EL4 cell line
	235461	B230380D07Rik	VNVRFTGV	Kb	Dendritic cell
	235461	B230380D07Rik	VNVRFTGV	Kb	Thymocyte
768	235527	Plscr4	AQLDNIHVL	Db	Dendritic cell
769	235623	Scap	SGYDFSRL	Kb	EL4 cell line
	235623	Scap	SGYDFSRL	Kb	Dendritic cell
	235623	Scap	SGYDFSRL	Kb	Thymocyte
770	235626	Setd2	SSPSNKFFF	Db	EL4 cell line
	235626	Setd2	SSPSNKFFF	Db	Dendritic cell
771	235682	Zfp445	KSIAFQNV	Kb	EL4 cell line
772	235907	Zfp71-rs1	VMLENYSHL	Db	EL4 cell line
	235907	Zfp71-rs1	VMLENYSHL	Db	Dendritic cell
773	237615	Ankrd52	SSLSNEHVL	Db	EL4 cell line
774	238690	Zfp458	KAFDYPSRL	Kb	EL4 cell line
775	238693	Zfp817	VMLENYSHL	Db	EL4 cell line
	238693	Zfp817	VMLENYSHL	Db	Dendritic cell
776	239554	Foxred2	LGVTNFVHM	Db	EL4 cell line
	239554	Foxred2	LGVTNFVHM	Db	Dendritic cell
777	240066	BC066107	SSFQFHNRM	Kb	EL4 cell line
778	240069	Morc2b	RQVQNTAITL	Db	EL4 cell line
779	240168	Rasgrp3	VITKFINV	Kb	EL4 cell line
780	240641	Mphosph1	QSVAFTKL	Kb	EL4 cell line

781	241035	Pkhd1	ILSVFPKV	Kb	EL4 cell line
782	241296	Lrrc8a	EIISFQHL	Kb	EL4 cell line
783	241525	Ypel4	RAYLFNSV	Kb	EL4 cell line
	241525	Ypel4	RAYLFNSV	Kb	Dendritic cell
784	241568	Lrrc4c	SNLRYLNL	Kb	EL4 cell line
785	241633	Atp8b4	KNFAFTLV	Kb	EL4 cell line
786	242418	Wdr32	VSPRNSLEVL	Db	EL4 cell line
	242418	Wdr32	VSPRNSLEVL	Db	Dendritic cell
787	243616	Slc6a11	NVWRFPYL	Kb	Dendritic cell
788	243764	Chrm2	TVIGYWPL	Kb	Thymocyte
789	244059	Chd2	RVLIFSQM	Kb	EL4 cell line
	244059	Chd2	RVLIFSQM	Kb	Dendritic cell
790	244178	Ubqln3	RALSNLESI	Db	EL4 cell line
791	244879	Npat	KQVNNLTNL	Db	EL4 cell line
792	244962	Snx14	EQLFQEHRL	Qa2	EL4 cell line
	244962	Snx14	IGPKNYEFL	Db	EL4 cell line
793	245240	9930111J21Rik	KAPLNIAVM	Db	Dendritic cell
794	245368	Zfp300	VMLENYSHL	Db	EL4 cell line
	245368	Zfp300	VMLENYSHL	Db	Dendritic cell
795	245423	Gm364	SLYLFNHL	Kb	EL4 cell line
796	267019	Rps15a	VIVRFLTV	Kb	EL4 cell line
	267019	Rps15a	VIVRFLTVM	Kb	EL4 cell line
	267019	Rps15a	VIVRFLTV	Kb	Dendritic cell
	267019	Rps15a	ISPRFDVQL	Kb	Dendritic cell
	267019	Rps15a	ISPRFDVQL	Kb	Thymocyte
	267019	Rps15a	VIVRFLTV	Kb	Thymocyte
797	268697	Ccnb1	VQMKFRLL	Kb	EL4 cell line
798	268721	2310021P13Rik	RAPAFHQL	Kb	EL4 cell line
799	268749	Rnf31	VSLINAHSL	Db	Dendritic cell
800	269254	Setx	VGLLYRLL	Kb	EL4 cell line
801	269610	Chd5	RVLIFSQM	Kb	EL4 cell line
	269610	Chd5	RVLIFSQM	Kb	Dendritic cell
802	271564	Vps13a	VSIQFYHL	Kb	EL4 cell line
	271564	Vps13a	VSIQFYHL	Kb	Thymocyte
803	277360	Prex1	NQVDSIHAL	Qa2	Dendritic cell
804	277939	C2cd3	VITKFDHL	Kb	EL4 cell line
805	319178	Hist1h2bb	SVYVYKVL	Kb	EL4 cell line
	319178	Hist1h2bb	VNDIFERI	Kb	EL4 cell line
	319178	Hist1h2bb	SVYVYKVL	Kb	Dendritic cell
806	319181	Hist1h2bg	SVYVYKVL	Kb	EL4 cell line
	319181	Hist1h2bg	VNDIFERI	Kb	EL4 cell line
	319181	Hist1h2bg	SVYVYKVL	Kb	Dendritic cell
807	319182	Hist1h2bh	SVYVYKVL	Kb	EL4 cell line
	319182	Hist1h2bh	VNDIFERI	Kb	EL4 cell line
	319182	Hist1h2bh	SVYVYKVL	Kb	Dendritic cell
808	319183	Hist1h2bj	SVYVYKVL	Kb	EL4 cell line
	319183	Hist1h2bj	VNDIFERI	Kb	EL4 cell line
	319183	Hist1h2bj	SVYVYKVL	Kb	Dendritic cell
809	319184	Hist1h2bk	SVYVYKVL	Kb	EL4 cell line
	319184	Hist1h2bk	VNDIFERI	Kb	EL4 cell line
	319184	Hist1h2bk	SVYVYKVL	Kb	Dendritic cell
810	319186	Hist1h2bm	SVYVYKVL	Kb	EL4 cell line
	319186	Hist1h2bm	VNDIFERI	Kb	EL4 cell line
	319186	Hist1h2bm	SVYVYKVL	Kb	Dendritic cell
811	319188	Hist1h2bp	SVYVYKVL	Kb	EL4 cell line
	319188	Hist2h2bp	VNDIFERI	Kb	EL4 cell line
	319188	Hist1h2bp	SVYVYKVL	Kb	Dendritic cell

812	319189	Hist1h2bb	VNDIFERI	Kb	EL4 cell line
	319189	Hist2h2bb	SVYVYKVL	Kb	EL4 cell line
	319189	Hist2h2bb	SVYVYKVL	Kb	Dendritic cell
	319189	Hist2h2bb	SVYVYKVL	Kb	Thymocyte
813	319190	Hist2h2be	VNDIFERI	Kb	EL4 cell line
814	319236	9230105E10Rik	FISDVEHQL	Qa2	Thymocyte
815	319448	Fndc3a	TSFRYSSL	Kb	Dendritic cell
816	319491	1110029I05Rik	QQIAFKNL	Kb	EL4 cell line
817	319565	Syne2	TAVLNLHEHL	Db	EL4 cell line
	319565	Syne2	DLIQTIHEL	Qa2	Dendritic cell
	319565	Syne2	DLIQTIHEL	Qa2	Thymocyte
818	319934	Sbf2	QAIHFANL	Kb	EL4 cell line
819	319955	Ercc6	SNYRFEGL	Kb	Dendritic cell
820	320209	Ddx11	SSLKFLLL	Kb	Dendritic cell
821	320487	Heatr5a	IGPRYSSV	Kb	EL4 cell line
822	320571	4930417M19Rik	KNFAFTLV	Kb	EL4 cell line
823	320631	Abca15	VEFFLDAL	Kb	EL4 cell line
824	320632	Ascc3l1	SSLSNAKDV	Db	EL4 cell line
825	320707	Atp2b3	KVYTFNSV	Kb	EL4 cell line
	320707	Atp2b3	KVYTFNSV	Kb	Dendritic cell
826	320714	D030016E14Rik	VSTKFEHL	Kb	EL4 cell line
827	320790	Chd7	RVLIFSQM	Kb	EL4 cell line
	320790	Chd7	RVLIFSQM	Kb	Dendritic cell
828	320817	Atad2b	YGIQNHHEV	Db	EL4 cell line
829	320938	Tnpo3	GLLEIAHSL	Qa2	Dendritic cell
	320938	Tnpo3	GLLEIAHSL	Qa2	Thymocyte
830	326622	Upf2	SAVIFRTL	Kb	EL4 cell line
	326622	Upf2	SAVIFRTL	Kb	Dendritic cell
831	328099	AU021838	VSYLFSHV	Kb	EL4 cell line
	328099	AU021838	VSYLFSHV	Kb	Thymocyte
832	328274	Zfp459	VMLENYSHL	Db	EL4 cell line
	328274	Zfp459	VMLENYSHL	Db	Dendritic cell
833	328572	Ep300	YSYQNRYHF	Db	EL4 cell line
834	329154	Ankrd44	ASVINGHTL	Db	EL4 cell line
	329154	Ankrd44	ASVINGHTL	Db	Dendritic cell
	329154	Ankrd44	ASVINGHTL	Db	Thymocyte
835	330129	EG330129	VQYKFSHL	Kb	EL4 cell line
836	332579	Card9	SSPRNSQEL	Db	Dendritic cell
837	338523	Jhdm1d	SNPEFRQL	Kb	EL4 cell line
	338523	Jhdm1d	SSIQNGKYTL	Db	EL4 cell line
	338523	Jhdm1d	SSIQNGKYTL	Db	Dendritic cell
	338523	Jhdm1d	SNPEFRQL	Kb	Dendritic cell
	338523	A630082K20Rik	SSIQNGKYTL	Db	Thymocyte
838	380959	Alg10b	GVLRFVNL	Kb	EL4 cell line
839	381290	Atp2b4	KVYTFNSV	Kb	EL4 cell line
	381290	Atp2b4	KVYTFNSV	Kb	Dendritic cell
840	382051	4833426J09Rik	MAHVNGVHL	Db	EL4 cell line
841	382252	A830080D01Rik	VSYNHTNI	Kb	EL4 cell line
842	382522	Hist3h2bb	VNDIFERI	Kb	EL4 cell line
843	408067	9630025I21Rik	VMLENYSHL	Db	EL4 cell line
	408067	9630025I21Rik	VMLENYSHL	Db	Dendritic cell
844	431706	Zfp457	KAFDYPSRL	Kb	EL4 cell line
845	432448	EG432448	YVLHNSNTM	Db	EL4 cell line
846	432555	EG432555	KAPLNIAVM	Db	Dendritic cell
	432555	EG432555	KSLLNKEEFL	Db	Dendritic cell
	432555	EG432555	ALSEISHAL	Qa2	Dendritic cell
847	433864	Gm1040	KVVEFSEL	Kb	EL4 cell line

848	433926	Lrrc8b	EIISFQHL	Kb	EL4 cell line
849	433956	Heatr2	VQFLYREL	Kb	EL4 cell line
850	434175	EG434175	VQMKFRLL	Kb	EL4 cell line
851	434215	Lrrc32	TSLRFLNL	Kb	Dendritic cell
852	434223	Gm1966	FVHQNVGEI	Db	EL4 cell line
	434223	Gm1966	VNSIFQHL	Kb	EL4 cell line
853	545216	EG545216	SRVSFTSL	Kb	EL4 cell line
854	545270	LOC545270	YALYNNWEHM	Db	EL4 cell line
855	545486	Tubb1	IREEYPDRI	Kb	EL4 cell line
856	545725	Mterf	KAVTNEQEL	Db	EL4 cell line
857	574437	Xlr3a/b	VAAANREVL	Db	EL4 cell line
858	620913	OTTMUSG00000005523	KSLLNKEEFL	Db	Dendritic cell
859	621205	EG621205	YVVDNIDHL	Db	EL4 cell line
860	627984	Nlrp1c	LSYSFAHL	Kb	EL4 cell line
861	633683	EG633683	VGVYNGKTF	Db	EL4 cell line
862	637515	Nlrp1b	LSYSFAHL	Kb	EL4 cell line
863	638833	EG638833	GLMTTVHAI	Qa2	Dendritic cell
864	640374	LOC640374	YGYSNRVVDLM	Db	EL4 cell line
	640374	LOC640374	GLMTTVHAI	Qa2	Dendritic cell
	640374	LOC640374	YGYSNRVVDLM	Db	Dendritic cell
865	640611	LOC640611	VTLVFEHI	Kb	EL4 cell line
866	641050	LOC641050	VNYLHRNV	Kb	EL4 cell line
867	665596	RP23-38E20.1	SVYVYKVL	Kb	EL4 cell line
	665596	RP23-38E20.1	SVYVYKVL	Kb	Dendritic cell
868	666173	Vps13b	MSFQFAHL	Kb	EL4 cell line
	666173	Vps13b	SNFHFAVL	Kb	EL4 cell line
869	667214	RP23-269N23.3	KAPLNIAVM	Db	Dendritic cell
	667214	RP23-269N23.3	KSLLNKEEFL	Db	Dendritic cell
	667214	RP23-269N23.3	ALSEISHAL	Qa2	Dendritic cell
870	672511	LOC672511	GQIKEYHTL	Qa2	Dendritic cell
871	676923	LOC676923	GLMTTVHAI	Qa2	Dendritic cell
872	100039258	LOC100039258	YGYSNRVVDLM	Db	EL4 cell line
	100039258	LOC100039258	GLMTTVHAI	Qa2	Dendritic cell
	100039258	LOC100039258	YGYSNRVVDLM	Db	Dendritic cell
873	100039840	LOC100039840	YGYSNRVVDLM	Db	EL4 cell line
	100039840	LOC100039840	GLMTTVHAI	Qa2	Dendritic cell
	100039840	LOC100039840	YGYSNRVVDLM	Db	Dendritic cell
874	100039875	LOC100039875	GLMTTVHAI	Qa2	Dendritic cell
875	100040109	LOC100040109	YGYSNRVVDLM	Db	EL4 cell line
	100040109	LOC100040109	GLMTTVHAI	Qa2	Dendritic cell
	100040109	LOC100040109	YGYSNRVVDLM	Db	Dendritic cell
876	100040505	LOC100040505	VSPQNVHHSYL	Db	EL4 cell line
877	100040634	LOC100040634	YGYSNRVVDLM	Db	EL4 cell line
	100040634	LOC100040634	GLMTTVHAI	Qa2	Dendritic cell
	100040634	LOC100040634	YGYSNRVVDLM	Db	Dendritic cell
878	100041236	LOC100041236	YGYSNRVVDLM	Db	EL4 cell line
	100041236	LOC100041236	GLMTTVHAI	Qa2	Dendritic cell
	100041236	LOC100041236	YGYSNRVVDLM	Db	Dendritic cell
879	100041342	LOC100041342	GLMTTVHAI	Qa2	Dendritic cell
	100041342	LOC100041342	YGYSNRVVDLM	Db	Dendritic cell
880	100041399	LOC100041399	YGYSNRVVDLM	Db	EL4 cell line
	100041399	LOC100041399	YGYSNRVVDLM	Db	Dendritic cell
881	100041831	LOC100041831	YGYSNRVVDLM	Db	EL4 cell line
	100041831	LOC100041831	GLMTTVHAI	Qa2	Dendritic cell
	100041831	LOC100041831	YGYSNRVVDLM	Db	Dendritic cell
882	100043998	LOC100043998	VSYRNIEEL	Db	EL4 cell line
883	100044981	LOC100044981	YGYSNRVVDLM	Db	EL4 cell line

	100044981	LOC100044981	GLMTTVHAI	Qa2	Dendritic cell
	100044981	LOC100044981	YGYSNRVVDLM	Db	Dendritic cell
884	100045235	LOC100045235	YVVDNIDHL	Db	EL4 cell line
885	100047129	LOC100047129	YGYSNRVVDLM	Db	EL4 cell line
	100047129	LOC100047129	YGYSNRVVDLM	Db	Dendritic cell
886	100047352	LOC100047352	YGYSNRVVDLM	Db	EL4 cell line
	100047352	LOC100047352	GLMTTVHAI	Qa2	Dendritic cell
	100047352	LOC100047352	YGYSNRVVDLM	Db	Dendritic cell
887	100048117	LOC100048117	YGYSNRVVDLM	Db	EL4 cell line
	100048117	LOC100048117	GLMTTVHAI	Qa2	Dendritic cell
	100048117	LOC100048117	YGYSNRVVDLM	Db	Dendritic cell
888	100048253	LOC100048253	YGYSNRVVDLM	Db	EL4 cell line
	100048253	LOC100048253	YGYSNRVVDLM	Db	Dendritic cell
889	100125587	OTTMUSG00000007002	FSLDNSSSHL	Db	Dendritic cell
890	A2A7B5	Prdm2	SQVRNNVYM	Db	EL4 cell line
891	Q9JKK8	Atr	FQALNAEKL	Db	Thymocyte

Supplementary Table 4

List of components extracted from a comprehensive mTOR interactome and signaling network (Chapitre 5).

Gene ID	Gene symbol	Official full name
11350	Abl1	c-abl oncogene 1, non-receptor tyrosine kinase
11461	Actb	actin, beta
11491	Adam17	a disintegrin and metallopeptidase domain 17
14797	Aes	amino-terminal enhancer of split
67512	Agpat2	1-acylglycerol-3-phosphate O-acyltransferase 2 (lysophosphatidic acid acyltransferase, beta)
11604	Agrp	agouti related protein
11607	Agtr1a	angiotensin II receptor, type 1a
219181	Akap11	A kinase (PRKA) anchor protein 11
75547	Akap13	A kinase (PRKA) anchor protein 13
238276	Akap5	A kinase (PRKA) anchor protein 5
11651	Akt1	thymoma viral proto-oncogene 1
67605	Akt1s1	AKT1 substrate 1 (proline-rich)
11789	Apc	adenomatosis polyposis coli
72993	Appl1	adaptor protein, phosphotyrosine interaction, PH domain and leucine zipper containing 1
11835	Ar	androgen receptor
11836	Araf	v-raf murine sarcoma 3611 viral oncogene homolog
56292	Ard1a	N(alpha)-acetyltransferase 10, NatA catalytic subunitNalpha acetyltransferase 10
228359	Arhgap1	Rho GTPase activating protein 1
192662	Arhgdia	Rho GDP dissociation inhibitor (GDI) alpha
213498	Arhgef11	Rho guanine nucleotide exchange factor (GEF) 11
73341	Arhgef6	Rac/Cdc42 guanine nucleotide exchange factor (GEF) 6
54126	Arhgef7	Rho guanine nucleotide exchange factor (GEF7)
11863	Arnt	aryl hydrocarbon receptor nuclear translocator
216869	Arrb2	arrestin, beta 2
11920	Atm	ataxia telangiectasia mutated homolog (human)
245000	Atr	ataxia telangiectasia and Rad3 related
12005	Axin1	axin 1
12006	Axin2	axin2
12015	Bad	BCL2-associated agonist of cell death
12028	Bax	BCL2-associated X protein
12927	Bcar1	breast cancer anti-estrogen resistance 1
12042	Bcl10	B-cell leukemia/lymphoma 10
12043	Bcl2	B-cell leukemia/lymphoma 2
12048	Bcl2l1	BCL2-like 1
12125	Bcl2l11	BCL2-like 11 (apoptosis facilitator)
12051	Bcl3	B-cell leukemia/lymphoma 3
110279	Bcr	breakpoint cluster region
544971	Bdp1	B double prime 1, subunit of RNA polymerase III transcription initiation factor IIIB
12121	Bicd1	bicaudal D homolog 1 (Drosophila)
11797	Birc2	baculoviral IAP repeat-containing 2
11799	Birc5	baculoviral IAP repeat-containing 5
17060	Blnk	B-cell linker
12176	Bnip3	BCL2/adenovirus E1B interacting protein 3
12177	Bnip3l	BCL2/adenovirus E1B interacting protein 3-like
109880	Braf	Braf transforming gene
72308	Brf1	BRF1 homolog, subunit of RNA polymerase III transcription initiation factor IIIB (S. cerevisiae)
12226	Btg1	B-cell translocation gene 1, anti-proliferative
12234	Btrc	beta-transducin repeat containing protein
19777	C80913	expressed sequence C80913
12283	Cab39	calcium binding protein 39
52163	Camk1	calcium/calmodulin-dependent protein kinase I

12326	Camk4	calcium/calmodulin-dependent protein kinase IV
207565	Camkk2	calcium/calmodulin-dependent protein kinase kinase 2, beta
192160	Casc3	cancer susceptibility candidate 3
12367	Casp3	caspase 3
12370	Casp8	caspase 8
12359	Cat	catalase
12402	Cbl	Casitas B-lineage lymphoma
208650	Cblb	Casitas B-lineage lymphoma b
68339	Ccdc88c	coiled-coil domain containing 88C
12427	Ccna1	cyclin A1
12428	Ccna2	cyclin A2
268697	Ccnb1	cyclin B1
12443	Ccnd1	cyclin D1
12445	Ccnd3	cyclin D3
12447	Ccne1	cyclin E1
12448	Ccne2	cyclin E2
12450	Ccng1	cyclin G1
12455	Ccnt1	cyclin T1
12461	Cct2	chaperonin containing Tcp1, subunit 2 (beta)
12462	Cct3	chaperonin containing Tcp1, subunit 3 (gamma)
12464	Cct4	chaperonin containing Tcp1, subunit 4 (delta)
12465	Cct5	chaperonin containing Tcp1, subunit 5 (epsilon)
12468	Cct7	chaperonin containing Tcp1, subunit 7 (eta)
93671	Cd163	CD163 antigen
12487	Cd28	CD28 antigen
12505	Cd44	CD44 antigen
12534	Cdc2	cyclin-dependent kinase 1
107995	Cdc20	cell division cycle 20 homolog (S. cerevisiae)
12530	Cdc25a	cell division cycle 25 homolog A (S. pombe)
12531	Cdc25b	cell division cycle 25 homolog B (S. pombe)
12539	Cdc37	cell division cycle 37 homolog (S. cerevisiae)
12540	Cdc42	cell division cycle 42 homolog (S. cerevisiae)
12566	Cdk2	cyclin-dependent kinase 2
12567	Cdk4	cyclin-dependent kinase 4
12571	Cdk6	cyclin-dependent kinase 6
12575	Cdkn1a	cyclin-dependent kinase inhibitor 1A (P21)
12576	Cdkn1b	cyclin-dependent kinase inhibitor 1B
12608	Cebpb	CCAAT/enhancer binding protein (C/EBP), beta
12631	Cfl1	cofilin 1, non-muscle
12675	Chuk	conserved helix-loop-helix ubiquitous kinase
12704	Cit	citron
17684	Cited2	Cbp/p300-interacting transactivator, with Glu/Asp-rich carboxy-terminal domain, 2
54124	Cks1b	CDC28 protein kinase 1b
12737	Cldn1	claudin 1
56430	Clip1	CAP-GLY domain containing linker protein 1
194231	Cnksr1	connector enhancer of kinase suppressor of Ras 1
17846	Commd1	COMM domain containing 1
26754	Cops5	COP9 (constitutive photomorphogenic) homolog, subunit 5 (Arabidopsis thaliana)
12914	Crebbp	CREB binding protein
12928	Crk	v-crk sarcoma virus CT10 oncogene homolog (avian)
12929	Crkl	v-crk sarcoma virus CT10 oncogene homolog (avian)-like
12978	Csf1r	colony stimulating factor 1 receptor
12981	Csf2	colony stimulating factor 2 (granulocyte-macrophage)
12988	Csk	c-src tyrosine kinase
104318	Csnk1d	casein kinase 1, delta
27373	Csnk1e	casein kinase 1, epsilon
13000	Csnk2a2	casein kinase 2, alpha prime polypeptide

12387	Ctnnb1	catenin (cadherin associated protein), beta 1
26965	Cul1	cullin 1
99375	Cul4a	cullin 4A
66515	Cul7	cullin 7
208846	Daam1	dishevelled associated activator of morphogenesis 1
13132	Dab2	disabled homolog 2 (Drosophila)
13138	Dag1	dystroglycan 1
13163	Daxx	Fas death domain-associated protein
74747	Ddit4	DNA-damage-inducible transcript 4
13215	Defb2	defensin beta 2
104418	Dgkz	diacylglycerol kinase zeta
13211	Dhx9	DEAH (Asp-Glu-Ala-His) box polypeptide 9
13367	Diap1	diaphanous homolog 1 (Drosophila)
66233	Dmap1	DNA methyltransferase 1-associated protein 1
13429	Dnm1	dynamin 1
330662	Dock1	dedicator of cytokinesis 1
67299	Dock7	dedicator of cytokinesis 7
13490	Drd3	dopamine receptor D3
19252	Dusp1	dual specificity phosphatase 1
240672	Dusp5	dual specificity phosphatase 5
67603	Dusp6	dual specificity phosphatase 6
13542	Dvl1	dishevelled, dsh homolog 1 (Drosophila)
56455	Dynll1	dynein light chain LC8-type 1
13548	Dyrk1a	dual-specificity tyrosine-(Y)-phosphorylation regulated kinase 1a
13555	E2f1	E2F transcription factor 1
242705	E2f2	E2F transcription factor 2
13557	E2f3	E2F transcription factor 3
59022	Edf1	endothelial differentiation-related factor 1
13628	Eef1a2	eukaryotic translation elongation factor 1 alpha 2
55949	Eef1b2	eukaryotic translation elongation factor 1 beta 2
13629	Eef2	eukaryotic translation elongation factor 2
13631	Eef2k	eukaryotic elongation factor-2 kinase
13649	Egfr	epidermal growth factor receptor
112405	Egln1	EGL nine homolog 1 (C. elegans)
112406	Egln2	EGL nine homolog 2 (C. elegans)
112407	Egln3	EGL nine homolog 3 (C. elegans)
209354	Eif2b1	eukaryotic translation initiation factor 2B, subunit 1 (alpha)
67204	Eif2s2	eukaryotic translation initiation factor 2, subunit 2 (beta)
13669	Eif3a	eukaryotic translation initiation factor 3, subunit A
13681	Eif4a1	eukaryotic translation initiation factor 4A1
75705	Eif4b	eukaryotic translation initiation factor 4B
13684	Eif4e	eukaryotic translation initiation factor 4E
13685	Eif4ebp1	eukaryotic translation initiation factor 4E binding protein 1
13688	Eif4ebp2	eukaryotic translation initiation factor 4E binding protein 2
108112	Eif4ebp3	eukaryotic translation initiation factor 4E binding protein 3
74203	Eif4enif1	eukaryotic translation initiation factor 4E nuclear import factor 1
208643	Eif4g1	eukaryotic translation initiation factor 4, gamma 1
13690	Eif4g2	eukaryotic translation initiation factor 4, gamma 2
230861	Eif4g3	eukaryotic translation initiation factor 4 gamma, 3
13712	Elk1	ELK1, member of ETS oncogene family
270162	Elmod1	ELMO domain containing 1
13797	Emx2	empty spiracles homolog 2 (Drosophila)
328572	Ep300	E1A binding protein p300
13823	Epb4.1l3	erythrocyte protein band 4.1-like 3
13836	Epha2	Eph receptor A2
13844	Ephb2	Eph receptor B2
13860	Eps8	epidermal growth factor receptor pathway substrate 8

13866	Erbb2	v-erb-b2 erythroblastic leukemia viral oncogene homolog 2, neuro/glioblastoma derived oncogene homolog (avian)
13982	Esr1	estrogen receptor 1 (alpha)
13983	Esr2	estrogen receptor 2 (beta)
26379	Esrra	estrogen related receptor, alpha
22350	Ezr	ezrin
14082	Fadd	Fas (TNFRSF6)-associated via death domain
14087	Fanca	Fanconi anemia, complementation group A
14102	Fas	Fas (TNF receptor superfamily member 6)
14103	Fasl	Fas ligand (TNF superfamily, member 6)
268882	Fbxo45	F-box protein 45
71538	Fbxo9	f-box protein 9
103583	Fbxw11	F-box and WD-40 domain protein 11
30839	Fbxw5	F-box and WD-40 domain protein 5
50754	Fbxw7	F-box and WD-40 domain protein 7
231672	Fbxw8	F-box and WD-40 domain protein 8
14172	Fgf18	fibroblast growth factor 18
14180	Fgf9	fibroblast growth factor 9
14200	Fhl2	four and a half LIM domains 2
14225	Fkbp1a	FK506 binding protein 1a
30795	Fkbp3	FK506 binding protein 3
14232	Fkbp8	FK506 binding protein 8
14257	Flt4	FMS-like tyrosine kinase 4
216742	Fnip1	folliculin interacting protein 1
14283	Fosl1	fos-like antigen 1
15218	Foxn1	forkhead box N1
56458	Foxo1	forkhead box O1
56484	Foxo3	forkhead box O3
54601	Foxo4	forkhead box O4
56717	Frap1	mechanistic target of rapamycin (serine/threonine kinase)
327826	Frs2	fibroblast growth factor receptor substrate 2
107971	Frs3	fibroblast growth factor receptor substrate 3
14371	Fzd9	frizzled homolog 9 (Drosophila)
14377	G6pc	glucose-6-phosphatase, catalytic
14388	Gab1	growth factor receptor bound protein 2-associated protein 1
14389	Gab2	growth factor receptor bound protein 2-associated protein 2
56486	Gabarap	gamma-aminobutyric acid receptor associated protein
13197	Gadd45a	growth arrest and DNA-damage-inducible 45 alpha
14461	Gata2	GATA binding protein 2
216766	Gemin5	gem (nuclear organelle) associated protein 5
216963	Git1	G protein-coupled receptor kinase-interactor 1
26431	Git2	G protein-coupled receptor kinase-interactor 2
625599	Gml	GPI anchored molecule like protein
14685	Gnat1	guanine nucleotide binding protein, alpha transducing 1
14688	Gnb1	guanine nucleotide binding protein (G protein), beta 1
14702	Gng2	guanine nucleotide binding protein (G protein), gamma 2
66629	Golph3	golgi phosphoprotein 3
268566	Gphn	gephyrin
14783	Grb10	growth factor receptor bound protein 10
50915	Grb14	growth factor receptor bound protein 14
14784	Grb2	growth factor receptor bound protein 2
14786	Grb7	growth factor receptor bound protein 7
232906	Grlf1	glucocorticoid receptor DNA binding factor 1
606496	Gsk3a	glycogen synthase kinase 3 alpha
56637	Gsk3b	glycogen synthase kinase 3 beta
229906	Gtf2b	general transcription factor IIB
66596	Gtf3a	general transcription factor III A

233863	Gtf3c1	general transcription factor III C 1
14961	H2-Ab1	histocompatibility 2, class II antigen A, beta 1
14972	H2-K1	histocompatibility 2, K1, K region
433759	Hdac1	histone deacetylase 1
15182	Hdac2	histone deacetylase 2
15183	Hdac3	histone deacetylase 3
15251	Hif1a	hypoxia inducible factor 1, alpha subunit
319594	Hif1an	hypoxia-inducible factor 1, alpha subunit inhibitor
15461	Hras1	Harvey rat sarcoma virus oncogene 1
15499	Hsf1	heat shock factor 1
15519	Hsp90aa1	heat shock protein 90, alpha (cytosolic), class A member 1
15511	Hspa1b	heat shock protein 1B
14828	Hspa5	heat shock protein 5
15975	Ifnar1	interferon (alpha and beta) receptor 1
15978	Ifng	interferon gamma
16001	Igf1r	insulin-like growth factor I receptor
16009	Igfbp3	insulin-like growth factor binding protein 3
16150	Ikbkb	inhibitor of kappaB kinase beta
16151	Ikbkg	inhibitor of kappaB kinase gamma
16193	Il6	interleukin 6
12765	Il8rb	chemokine (C-X-C motif) receptor 2
16202	Ilk	integrin linked kinase
23918	Impdh2	inosine 5'-phosphate dehydrogenase 2
16331	Inpp5d	inositol polyphosphate-5-phosphatase D
16337	Insr	insulin receptor
29875	Iqgap1	IQ motif containing GTPase activating protein 1
16367	Irs1	insulin receptor substrate 1
384783	Irs2	insulin receptor substrate 2
16399	Itga2b	integrin alpha 2b
16401	Itga4	integrin alpha 4
16412	Itgb1	integrin beta 1 (fibronectin receptor beta)
16438	Itpr1	inositol 1,4,5-triphosphate receptor 1
16443	Itsn1	intersectin 1 (SH3 domain protein 1A)
16449	Jag1	jagged 1
16451	Jak1	Janus kinase 1
16452	Jak2	Janus kinase 2
16476	Jun	Jun oncogene
16490	Kcna2	potassium voltage-gated channel, shaker-related subfamily, member 2
20218	Khdrbs1	KH domain containing, RNA binding, signal transduction associated 1
16590	Kit	kit oncogene
16647	Kpna2	karyopherin (importin) alpha 2
16650	Kpna6	karyopherin (importin) alpha 6
16653	Kras	v-Ki-ras2 Kirsten rat sarcoma viral oncogene homolog
16709	Ktn1	kinectin 1
16797	Lat	linker for activation of T cells
16818	Lck	lymphocyte protein tyrosine kinase
16822	Lcp2	lymphocyte cytosolic protein 2
16842	Lef1	lymphoid enhancer binding factor 1
16905	Lmna	lamin A
16906	Lmnb1	lamin B1
14245	Lpin1	lipin 1
16973	Lrp5	low density lipoprotein receptor-related protein 5
16974	Lrp6	low density lipoprotein receptor-related protein 6
56716	Lst8	MTOR associated protein, LST8 homolog (S. cerevisiae)
16992	Lta	lymphotoxin A
17134	Mafg	v-maf musculoaponeurotic fibrosarcoma oncogene family, protein G (avian)
50791	Magi2	membrane associated guanylate kinase, WW and PDZ domain containing 2

99470	Magi3	membrane associated guanylate kinase, WW and PDZ domain containing 3
26395	Map2k1	mitogen-activated protein kinase kinase 1
26396	Map2k2	mitogen-activated protein kinase kinase 2
26400	Map2k7	mitogen-activated protein kinase kinase 7
53859	Map3k14	mitogen-activated protein kinase kinase kinase 14
26405	Map3k2	mitogen-activated protein kinase kinase kinase 2
26406	Map3k3	mitogen-activated protein kinase kinase kinase 3
26409	Map3k7	mitogen-activated protein kinase kinase kinase 7
26410	Map3k8	mitogen-activated protein kinase kinase kinase 8
26411	Map4k1	mitogen-activated protein kinase kinase kinase kinase 1
225028	Map4k3	mitogen-activated protein kinase kinase kinase kinase 3
26413	Mapk1	mitogen-activated protein kinase 1
26416	Mapk14	mitogen-activated protein kinase 14
26417	Mapk3	mitogen-activated protein kinase 3
23939	Mapk7	mitogen-activated protein kinase 7
26419	Mapk8	mitogen-activated protein kinase 8
30957	Mapk8ip3	mitogen-activated protein kinase 8 interacting protein 3
227743	Mapkap1	mitogen-activated protein kinase associated protein 1
17762	Mapt	microtubule-associated protein tau
546071	Mast3	microtubule associated serine/threonine kinase 3
17220	Mcm7	minichromosome maintenance deficient 7 (S. cerevisiae)
17242	Mdk	midkine
17246	Mdm2	transformed mouse 3T3 cell double minute 2
19014	Med1	mediator complex subunit 1
94112	Med15	mediator complex subunit 15
66999	Med28	mediator of RNA polymerase II transcription, subunit 28 homolog (yeast)
17295	Met	met proto-oncogene
17346	Mknk1	MAP kinase-interacting serine/threonine kinase 1
17347	Mknk2	MAP kinase-interacting serine/threonine kinase 2
19882	Mst1r	macrophage stimulating 1 receptor (c-met-related tyrosine kinase)
116870	Mta1	metastasis associated 1
17756	Mtap2	microtubule-associated protein 2
17829	Muc1	mucin 1, transmembrane
78388	Mvp	major vault protein
17869	Myc	myelocytomatosis oncogene
68092	Ncbp2	nuclear cap binding protein subunit 2
17969	Ncf1	neutrophil cytosolic factor 1
17973	Nck1	non-catalytic region of tyrosine kinase adaptor protein 1
80987	Nckipsd	NCK interacting protein with SH3 domain
17977	Ncoa1	nuclear receptor coactivator 1
27057	Ncoa4	nuclear receptor coactivator 4
56406	Ncoa6	nuclear receptor coactivator 6
20185	Ncor1	nuclear receptor co-repressor 1
20602	Ncor2	nuclear receptor co-repressor 2
17988	Ndrg1	N-myc downstream regulated gene 1
83814	Nedd4l	neural precursor cell expressed, developmentally down-regulated gene 4-like
380684	Nefh	neurofilament, heavy polypeptide
18005	Nek2	NIMA (never in mitosis gene a)-related expressed kinase 2
18015	Nf1	neurofibromatosis 1
18033	Nfkb1	nuclear factor of kappa light polypeptide gene enhancer in B-cells 1, p105
18034	Nfkb2	nuclear factor of kappa light polypeptide gene enhancer in B-cells 2, p49/p100
18035	Nfkbia	nuclear factor of kappa light polypeptide gene enhancer in B-cells inhibitor, alpha
18036	Nfkbib	nuclear factor of kappa light polypeptide gene enhancer in B-cells inhibitor, beta
18037	Nfkbie	nuclear factor of kappa light polypeptide gene enhancer in B-cells inhibitor, epsilon
18044	Nfya	nuclear transcription factor-Y alpha
12070	Ngfrap1	nerve growth factor receptor (TNFRSF16) associated protein 1
18080	Nin	ninein

18126	Nos2	nitric oxide synthase 2, inducible
18128	Notch1	Notch gene homolog 1 (Drosophila)
18129	Notch2	Notch gene homolog 2 (Drosophila)
14815	Nr3c1	nuclear receptor subfamily 3, group C, member 1
18176	Nras	neuroblastoma ras oncogene
18181	Nrf1	nuclear respiratory factor 1
18201	Nsmaf	neutral sphingomyelinase (N-SMase) activation associated factor
216440	Os9	amplified in osteosarcoma
18440	P2rx6	purinergic receptor P2X, ligand-gated ion channel, 6
18458	Pabpc1	poly(A) binding protein, cytoplasmic 1
18472	Pafah1b1	platelet-activating factor acetylhydrolase, isoform 1b, subunit 1
18479	Pak1	p21 protein (Cdc42/Rac)-activated kinase 1
18484	Pam	peptidylglycine alpha-amidating monooxygenase
93742	Pard3	par-3 (partitioning defective 3) homolog (C. elegans)
11545	Parp1	poly (ADP-ribose) polymerase family, member 1
57342	Parva	parvin, alpha
18538	Pcna	proliferating cell nuclear antigen
18569	Pdcd4	programmed cell death 4
18576	Pde3b	phosphodiesterase 3B, cGMP-inhibited
18595	Pdgfra	platelet derived growth factor receptor, alpha polypeptide
18596	Pdgfrb	platelet derived growth factor receptor, beta polypeptide
228026	Pdk1	pyruvate dehydrogenase kinase, isoenzyme 1
18607	Pdpk1	3-phosphoinositide dependent protein kinase 1
18611	Pea15a	phosphoprotein enriched in astrocytes 15A
23980	Pebp1	phosphatidylethanolamine binding protein 1
12034	Phb2	prohibitin 2
83946	Phip	pleckstrin homology domain interacting protein
98432	Phlpp1	PH domain and leucine rich repeat protein phosphatase 1
229615	Pias3	protein inhibitor of activated STAT 3
18693	Pick1	protein interacting with C kinase 1
225326	Pik3c3	phosphoinositide-3-kinase, class 3
18706	Pik3ca	phosphatidylinositol 3-kinase, catalytic, alpha polypeptide
18708	Pik3r1	phosphatidylinositol 3-kinase, regulatory subunit, polypeptide 1 (p85 alpha)
18709	Pik3r2	phosphatidylinositol 3-kinase, regulatory subunit, polypeptide 2 (p85 beta)
18710	Pik3r3	phosphatidylinositol 3 kinase, regulatory subunit, polypeptide 3 (p55)
108083	Pip4k2b	phosphatidylinositol-5-phosphate 4-kinase, type II, beta
320795	Pkn1	protein kinase N1
18803	Plcg1	phospholipase C, gamma 1
234779	Plcg2	phospholipase C, gamma 2
18805	Pld1	phospholipase D1
18806	Pld2	phospholipase D2
18817	Plk1	polo-like kinase 1 (Drosophila)
18854	Pml	promyelocytic leukemia
108767	Pnrc1	proline-rich nuclear receptor coactivator 1
73826	Poldip3	polymerase (DNA-directed), delta interacting protein 3
20017	Polr1b	polymerase (RNA) I polypeptide B
64424	Polr1e	polymerase (RNA) I polypeptide E
18976	Pomc	pro-opiomelanocortin-alpha
19015	Ppard	peroxisome proliferator activator receptor delta
19016	Pparg	peroxisome proliferator activated receptor gamma
19017	Ppargc1a	peroxisome proliferative activated receptor, gamma, coactivator 1 alpha
19041	Ppl	periplakin
53892	Ppm1d	protein phosphatase 1D magnesium-dependent, delta isoform
19047	Ppp1cc	protein phosphatase 1, catalytic subunit, gamma isoform
21981	Ppp1r13b	protein phosphatase 1, regulatory (inhibitor) subunit 13B
333654	Ppp1r13l	protein phosphatase 1, regulatory (inhibitor) subunit 13 like
17872	Ppp1r15a	protein phosphatase 1, regulatory (inhibitor) subunit 15A

243725	Ppp1r9a	protein phosphatase 1, regulatory (inhibitor) subunit 9A
217124	Ppp1r9b	protein phosphatase 1, regulatory subunit 9B
19052	Ppp2ca	protein phosphatase 2 (formerly 2A), catalytic subunit, alpha isoform
51792	Ppp2r1a	protein phosphatase 2 (formerly 2A), regulatory subunit A (PR 65), alpha isoform
110854	Ppp2r4	protein phosphatase 2A, regulatory subunit B (PR 53)
277360	Prex1	phosphatidylinositol-3,4,5-trisphosphate-dependent Rac exchange factor 1
105787	Prkaa1	protein kinase, AMP-activated, alpha 1 catalytic subunit
19079	Prkab1	protein kinase, AMP-activated, beta 1 non-catalytic subunit
108097	Prkab2	protein kinase, AMP-activated, beta 2 non-catalytic subunit
18747	Prkaca	protein kinase, cAMP dependent, catalytic, alpha
241113	Prkag3	protein kinase, AMP-activated, gamma 3 non-catatlytic subunit
18750	Prkca	protein kinase C, alpha
18753	Prkcd	protein kinase C, delta
18762	Prkcz	protein kinase C, zeta
19122	Prnp	prion protein
72446	Protor2	proline rich 5 like
109270	Prr5	proline rich 5 (renal)
19164	Psen1	presenilin 1
19179	Psmc1	protease (prosome, macropain) 26S subunit, ATPase 1
21762	Psmd2	proteasome (prosome, macropain) 26S subunit, non-ATPase, 2
19211	Pten	phosphatase and tensin homolog
14083	Ptk2	PTK2 protein tyrosine kinase 2
19229	Ptk2b	PTK2 protein tyrosine kinase 2 beta
19246	Ptpn1	protein tyrosine phosphatase, non-receptor type 1
19247	Ptpn11	protein tyrosine phosphatase, non-receptor type 11
19248	Ptpn12	protein tyrosine phosphatase, non-receptor type 12
19249	Ptpn13	protein tyrosine phosphatase, non-receptor type 13
545622	Ptpn3	protein tyrosine phosphatase, non-receptor type 3
15170	Ptpn6	protein tyrosine phosphatase, non-receptor type 6
320139	Ptpn7	protein tyrosine phosphatase, non-receptor type 7
19262	Ptpra	protein tyrosine phosphatase, receptor type, A
19268	Ptprf	protein tyrosine phosphatase, receptor type, F
19303	Pxn	paxillin
271457	Rab5a	RAB5A, member RAS oncogene family
54189	Rabep1	rabaptin, RAB GTPase binding effector protein 1
19353	Rac1	RAS-related C3 botulinum substrate 1
110157	Raf1	v-raf-leukemia viral oncogene 1
109905	Rap1a	RAS-related protein-1a
107746	Rapgef1	Rap guanine nucleotide exchange factor (GEF) 1
74370	Raptor	regulatory associated protein of MTOR, complex 1
19401	Rara	retinoic acid receptor, alpha
218397	Rasa1	RAS p21 protein activator 1
19417	Rasgrf1	RAS protein-specific guanine nucleotide-releasing factor 1
19645	Rb1	retinoblastoma 1
12421	Rb1cc1	RB1-inducible coiled-coil 1
19651	Rbl2	retinoblastoma-like 2
56438	Rbx1	ring-box 1
19696	Rel	reticuloendotheliosis oncogene
19697	Rela	v-rel reticuloendotheliosis viral oncogene homolog A (avian)
19713	Ret	ret proto-oncogene
19744	Rheb	Ras homolog enriched in brain
69159	Rhebl1	Ras homolog enriched in brain like 1
212541	Rho	rhodopsin
11848	Rhoa	ras homolog gene family, member A
52428	Rhpn2	rhophilin, Rho GTPase binding protein 2
78757	Rictor	RPTOR independent companion of MTOR, complex 2
225870	Rin1	Ras and Rab interactor 1

19766	Ripk1	receptor (TNFRSF)-interacting serine-threonine kinase 1
19769	Rit1	Ras-like without CAAX 1
84585	Rnf123	ring finger protein 123
57751	Rnf25	ring finger protein 25
54197	Rnf5	ring finger protein 5
19877	Rock1	Rho-associated coiled-coil containing protein kinase 1
110954	Rpl10	ribosomal protein 10
19921	Rpl19	ribosomal protein L19
68193	Rpl24	ribosomal protein L24
19951	Rpl32	ribosomal protein L32
19989	Rpl7	ribosomal protein L7
20005	Rpl9	ribosomal protein L9
20068	Rps17	ribosomal protein S17
20088	Rps24	ribosomal protein S24
78294	Rps27a	ribosomal protein S27A
20090	Rps29	ribosomal protein S29
27050	Rps3	ribosomal protein S3
20104	Rps6	ribosomal protein S6
20111	Rps6ka1	ribosomal protein S6 kinase polypeptide 1
20112	Rps6ka2	ribosomal protein S6 kinase, polypeptide 2
110651	Rps6ka3	ribosomal protein S6 kinase polypeptide 3
72508	Rps6kb1	ribosomal protein S6 kinase, polypeptide 1
68441	Rraga	Ras-related GTP binding A
245670	Rragb	Ras-related GTP binding B
54170	Rragc	Ras-related GTP binding C
52187	Rragd	Ras-related GTP binding D
66922	Rras2	related RAS viral (r-ras) oncogene homolog 2
106298	Rrn3	RRN3 RNA polymerase I transcription factor homolog (yeast)
20166	Rtkn	rhotekin
20181	Rxra	retinoid X receptor alpha
20190	Ryr1	ryanodine receptor 1, skeletal muscle
60406	Sap30	sin3 associated polypeptide
219151	Scara3	scavenger receptor class A, member 3
20971	Sdc4	syndecan 4
20339	Sele	selectin, endothelial cell
53860	Sept9	septin 9
56086	Set	SET translocation
84505	Setdb1	SET domain, bifurcated 1
20393	Sgk1	serum/glucocorticoid regulated kinase 1
20399	Sh2b1	SH2B adaptor protein 1
58194	Sh3kbp1	SH3-domain kinase binding protein 1
20416	Shc1	src homology 2 domain-containing transforming protein C1
20466	Sin3a	transcriptional regulator, SIN3A (yeast)
21402	Skp1a	S-phase kinase-associated protein 1A
27401	Skp2	S-phase kinase-associated protein 2 (p45)
20539	Slc7a5	solute carrier family 7 (cationic amino acid transporter, y+ system), member 5
20544	Slc9a1	solute carrier family 9 (sodium/hydrogen exchanger), member 1
26941	Slc9a3r1	solute carrier family 9 (sodium/hydrogen exchanger), member 3 regulator 1
65962	Slc9a3r2	solute carrier family 9 (sodium/hydrogen exchanger), member 3 regulator 2
17126	Smad2	MAD homolog 2 (Drosophila)
75788	Smurf1	SMAD specific E3 ubiquitin protein ligase 1
12703	Socs1	suppressor of cytokine signaling 1
216233	Socs2	suppressor of cytokine signaling 2
12702	Socs3	suppressor of cytokine signaling 3
20656	Sod2	superoxide dismutase 2, mitochondrial
234214	Sorbs2	sorbin and SH3 domain containing 2
20662	Sos1	son of sevenless homolog 1 (Drosophila)

20663	Sos2	son of sevenless homolog 2 (Drosophila)
20683	Sp1	trans-acting transcription factor 1
24064	Spry2	sprouty homolog 2 (Drosophila)
20779	Src	Rous sarcoma oncogene
20787	Srebf1	sterol regulatory element binding transcription factor 1
106766	Stap2	signal transducing adaptor family member 2
20846	Stat1	signal transducer and activator of transcription 1
20848	Stat3	signal transducer and activator of transcription 3
20850	Stat5a	signal transducer and activator of transcription 5A
20851	Stat5b	signal transducer and activator of transcription 5B
20853	Stau1	staufen (RNA binding protein) homolog 1 (Drosophila)
20869	Stk11	serine/threonine kinase 11
58231	Stk4	serine/threonine kinase 4
227154	Stradb	STE20-related kinase adaptor beta
22218	Sumo1	SMT3 suppressor of mif two 3 homolog 1 (yeast)
20963	Syk	spleen tyrosine kinase
20964	Syn1	synapsin I
20975	Synj2	synaptojanin 2
270627	Taf1	TAF1 RNA polymerase II, TATA box binding protein (TBP)-associated factor
21339	Taf1a	TATA box binding protein (Tbp)-associated factor, RNA polymerase I, A
21340	Taf1b	TATA box binding protein (Tbp)-associated factor, RNA polymerase I, B
24074	Taf7	TAF7 RNA polymerase II, TATA box binding protein (TBP)-associated factor
57915	Tbc1d1	TBC1 domain family, member 1
21374	Tbp	TATA box binding protein
21414	Tcf7	transcription factor 7, T-cell specific
21432	Tcl1	T-cell lymphoma breakpoint 1
21454	Tcp1	t-complex protein 1
21687	Tek	endothelial-specific receptor tyrosine kinase
71718	Telo2	TEL2, telomere maintenance 2, homolog (S. cerevisiae)
21752	Tert	telomerase reverse transcriptase
21754	Tesk1	testis specific protein kinase 1
21802	Tgfa	transforming growth factor alpha
21812	Tgfbr1	transforming growth factor, beta receptor I
21681	Thoc4	THO complex 4
21894	Tln1	talin 1
21926	Tnf	tumor necrosis factor
21929	Tnfaip3	tumor necrosis factor, alpha-induced protein 3
21933	Tnfrsf10b	tumor necrosis factor receptor superfamily, member 10b
21937	Tnfrsf1a	tumor necrosis factor receptor superfamily, member 1a
21938	Tnfrsf1b	tumor necrosis factor receptor superfamily, member 1b
57783	Tnip1	TNFAIP3 interacting protein 1
231130	Tnip2	TNFAIP3 interacting protein 2
51789	Tnk2	tyrosine kinase, non-receptor, 2
22057	Tob1	transducer of ErbB-2.1
21987	Tpd52l1	tumor protein D52-like 1
22070	Tpt1	tumor protein, translationally-controlled 1
71609	Tradd	TNFRSF1A-associated via death domain
22030	Traf2	TNF receptor-associated factor 2
223435	Trio	triple functional domain (PTPRF interacting)
22059	Trp53	transformation related protein 53
209456	Trp53bp2	transformation related protein 53 binding protein 2
22062	Trp73	transformation related protein 73
64930	Tsc1	tuberous sclerosis 1
22084	Tsc2	tuberous sclerosis 2
22143	Tuba1b	tubulin, alpha 1B
22144	Tuba3a	tubulin, alpha 3A
22145	Tuba4a	tubulin, alpha 4A

53857	Tuba8	tubulin, alpha 8
227613	Tubb2c	tubulin, beta 2C
103733	Tubg1	tubulin, gamma 1
103768	Tubg2	tubulin, gamma 2
93765	Ube2n	ubiquitin-conjugating enzyme E2N
56085	Ubqln1	ubiquilin 1
21429	Ubtf	upstream binding transcription factor, RNA polymerase I
16589	Uhmk1	U2AF homology motif (UHM) kinase 1
22241	Ulk1	Unc-51 like kinase 1 (C. elegans)
22294	Uxt	ubiquitously expressed transcript
229658	Vangl1	vang-like 1 (van gogh, Drosophila)
22324	Vav1	vav 1 oncogene
22330	Vcl	vinculin
269523	Vcp	valosin containing protein
22339	Vegfa	vascular endothelial growth factor A
22346	Vhl	von Hippel-Lindau tumor suppressor
22376	Was	Wiskott-Aldrich syndrome homolog (human)
245880	Wasf3	WAS protein family, member 3
73828	Wdr21	DDB1 and CUL4 associated factor 4
83669	Wdr6	WD repeat domain 6
22390	Wee1	WEE 1 homolog 1 (S. pombe)
22408	Wnt1	wingless-related MMTV integration site 1
103573	Xpo1	exportin 1, CRM1 homolog (yeast)
22608	Ybx1	Y box protein 1
54401	Ywhab	tyrosine 3-monooxygenase/tryptophan 5-monooxygenase activation protein, beta polypeptide
22627	Ywhae	tyrosine 3-monooxygenase/tryptophan 5-monooxygenase activation protein, epsilon polypeptide
22628	Ywhag	tyrosine 3-monooxygenase/tryptophan 5-monooxygenase activation protein, gamma polypeptide
22629	Ywhah	tyrosine 3-monooxygenase/tryptophan 5-monooxygenase activation protein, eta polypeptide
22630	Ywhaq	tyrosine 3-monooxygenase/tryptophan 5-monooxygenase activation protein, theta polypeptide
22631	Ywhaz	tyrosine 3-monooxygenase/tryptophan 5-monooxygenase activation protein, zeta polypeptide
22632	Yy1	YY1 transcription factor
235320	Zbtb16	zinc finger and BTB domain containing 16
22401	Zmat3	zinc finger matrin type 3

Supplementary Table 5

Relative expression of DEM source genes (blue) at multiple regulatory layers (see also Fig. 3b). Fold change (FC) represents the rapamycin/ctrl abundance ratio. Overexpressed (red) and underexpressed (green): P<0.05, no change (grey). n.d.: not determined. (n=3, Student t-test).

	mRNA		Normalized polysomal mRNA		Protein		MIP	
Gene symbol	FC	p value	FC	p value	FC	p value	FC	p value
Ap2a2	0.77	0.09	0.78	0.17	n.d.	n.d.	3.39	0.007
Ap2a1	1.17	0.18	0.64	0.047	n.d.	n.d.	2.58	0.01
Bptf	1.42	0.06	1.12	0.12	n.d.	n.d.	4.70	0.004
Bub1b	1.66	0.02	0.64	0.002	n.d.	n.d.	3.62	0.05
Ccnf	3.07	0.01	0.92	0.04	n.d.	n.d.	6.05	0.02
Cenpm	1.15	0.16	1.25	0.21	n.d.	n.d.	3.90	0.01
Chaf1b	1.71	0.01	0.66	0.02	n.d.	n.d.	2.62	0.03
Chtf18	2.46	0.004	0.61	0.002	n.d.	n.d.	4.47	0.04
Dhcr7	3.74	0.01	0.75	0.07	n.d.	n.d.	3.81	0.009
Dtl	1.47	0.048	0.80	0.03	n.d.	n.d.	2.52	0.02
Erbb2ip	0.95	0.83	0.81	0.13	n.d.	n.d.	4.64	0.03
Hivep2	0.87	0.30	1.17	0.47	n.d.	n.d.	2.94	0.03
Igf2r	1.08	0.61	1.40	0.67	n.d.	n.d.	3.18	0.002
Mnat1	0.65	0.04	0.79	0.002	n.d.	n.d.	3.56	0.01
Myb	1.54	0.04	0.98	0.08	2.16	0.01	4.34	0.01
Nsmaf	0.98	0.88	1.05	0.81	n.d.	n.d.	3.47	0.004
Pabpc1	1.25	0.06	1.77	0.03	0.96	0.23	3.41	0.001
Pin1	0.92	0.08	1.21	0.23	n.d.	n.d.	3.02	0.02
Psma3	0.89	0.053	1.02	0.61	n.d.	n.d.	2.60	0.02
Psmb8	1.05	0.34	0.96	0.54	1.01	0.44	5.39	0.02
Psmb9	0.96	0.11	1.00	0.46	0.97	0.24	4.67	0.01
Psmd2	0.98	0.92	0.54	0.001	n.d.	n.d.	3.46	0.02
Ptpn11	0.84	0.22	1.20	0.42	n.d.	n.d.	2.79	0.02
Rcc2	1.09	0.43	0.76	0.02	n.d.	n.d.	3.24	0.07
Rfc2	1.25	0.19	0.88	0.03	1.06	0.18	5.31	0.02
Rictor	1.26	0.02	1.15	0.17	1.06	0.28	9.73	0.003
Rpl27	0.91	0.47	1.10	0.53	n.d.	n.d.	4.63	0.001
Rps15	1.07	0.64	1.14	0.44	n.d.	n.d.	2.52	0.02
Sgk1	2.30	0.04	1.16	0.07	0.9	0.13	9.21	0.03
Supt16h	1.31	0.09	0.59	0.004	n.d.	n.d.	8.91	0.01
Taf6	1.08	0.42	0.77	0.04	n.d.	n.d.	4.07	0.003
Tfdp2	2.65	0.03	1.11	0.87	1.29	0.04	7.92	0.004
Tnfsf10	4.58	0.02	2.03	0.04	n.d.	n.d.	8.97	0.01

Supplementary Table 6

List of primers for quantitative real-time PCR analyses

Gene symbol	Gene ID	Primer_A	Primer_B	Probe
Ap2a1	11772	CCTGGCTGTGTCTCGCTTA	TGTAGTCCTGGAGGTCAGTGG	Universal Library probe: #73
Ap2a2	11771	CTGTCTCGCTAGCTGTCTCG	CCTGAAGATCTGTTGATGCAGA	Universal Library probe: #15
Bptf	207165	CACCGTACGATGAGTCCAAA	CCCGTGGTACCAATTCTGAC	Universal Library probe: #76
Bub1b	12236	GTGTCGGAGGTGCTCTGAA	TGGGGAACTGCATTTAGGAA	Universal Library probe: #85
Ccnf	12449	GGCTTTCTGTTGGGGACAT	CCAGGTACTTGAGGTGGGAGT	Universal Library probe: #56
Cenpm	66570	TTGTGTTTGTGATTAACCTGCAC	AGCTGCTGTCCACGTGCT	Universal Library probe: #25
Chaf1b	110749	GCAGATCGCCTTTCAGGA	TTGCCCAGCAAATATCATACA	Universal Library probe: #63
Chtf18	214901	CACCTGATGGGCAGTACCTC	CTTTCGGGCAGGTAGTTCAG	Universal Library probe: #78
Dhcr7	13360	CCTTGTGGGTCAGCTTCC	CCACATAACCTGGCAGAAATC	Universal Library probe: #29
Dtl	76843	GCTGCCTACATTTGGAAGGT	AGAATGACCCAGGAGCACAG	Universal Library probe: #88
Erbb2ip	59079	AAATGGTGCTTACTAATTACATGTTCC	GCAGGATTAAAACTTTCATTATCTGA	Universal Library probe: #66
Hivep2	15273	ATTGATTTCATTGGAACATTCTCTC	ATGATTGTCCTGACGCTTCC	Universal Library probe: #20
Igf2r	16004	TCAGTATGCAAAGTTCCTGTGG	TTGAATATTGGAGGGCCTGT	Universal Library probe: #53
Mnat1	17420	TGCAGCAGGCTCTGAAAAG	AGCAGAGCAACAGGGAGGT	Universal Library probe: #78
Myb*	17863	Mm00501741		
Nsmaf	18201	CTTGCAATGGCTCTTCAGTCT	TCTTTGTAGCATTTTGGATTCCT	Universal Library probe: #10
Pabpc1	18458	GGTGCCAGACCTCATCCA	TGTGAGGAAGCTGGTCTCATC	Universal Library probe: #68
Pin1**	23988	ACAGTTCAGTGATTGCAGCTCTGCCA	AAAGATCACCAGGAGCAAGGAGGA	TGGTTTCTGCATCTGACCTCTGCT
Psma3	19167	GAAGCAGAGAAATATGCCAAGG	GCAACTGTTACAGAAATGTAAACCA	Universal Library probe: #60
Psmb8	16913	CACACTCGCCTTCAAGTTCC	TCTCGATCACTTTGTTCATCCTT	Universal Library probe: #81
Psmb9	16912	GCCCAAGCCATAGCTGAC	GATGTTCTTCACCACGTTTGC	Universal Library probe: #78
Psmd2	21762	AATGGGAGATTCCAAGTCCA	TGACATCTCCATTGCAGGAC	Universal Library probe: #10
Ptpn11	19247	GAACATGACATCGCGGAGA	AACTGCCATCGACTCCTCTG	Universal Library probe: #18
Rcc2	108911	CTATCAGTTGGGGTCCATCG	AGAAGATGCCATCCAGAGTCTT	Universal Library probe: #79
Rfc2	19718	TTGAAGCTCAACGAAATAGTGG	GGGCACATTGCCTTCTCTT	Universal Library probe: #100
Rictor	78757	TTCCACTACAGACACAGTCCAGA	TGGCTAGAAATCGTGCTTCTC	Universal Library probe: #41
Rpl27	19942	TGAAAGGTTAGCGGAAGTGC	TTTCATGAACTTGCCCATCTC	Universal Library probe: #40
Rps15	20054	TCGACCAACTGCTCGACAT	GCGCTTGAGCAGTGAGTGT	Universal Library probe: #82
Sgk1	20393	TGCCAGCAACACCTATGC	GAGGGGTTAGCGTTCATAAGC	Universal Library probe: #92
Supt16h	114741	TCATGAAGACCATTGTTGATGAC	CGTCCTCAGCGTCACTCC	Universal Library probe: #83
Taf6	21343	GGATGTCTGCCTCAAAGCTC	CTCAGCCTTCTGCTGCTCTT	Universal Library probe: #20
Tfdp2	211586	CGCAATGGTCACTCAGACTC	TCTCTAGCTCGTTTTCTATCACTGG	Universal Library probe: #66
Tnfsf10	22035	TGAGAACCTTTCAGGACACCA	GAGCTGCCACTTTCTGAGGT	Universal Library probe: #52

* Pre-designed Taqman gene expression assay from Applied Biosystems

** Custom Taqman probe (Integrated DNA Technologies) specific assay

CHAPITRE 5

MISE EN SITUATION:

À la section 4.3 du chapitre précédent, nous avons émis l'hypothèse que les changements dans l'immunopeptidome induits par la rapamycine pouvaient être fonctionnellement reliés au réseau de signalisation mTOR. Pour évaluer cette hypothèse, il devenait important de construire une carte illustrant de manière exhaustive l'ensemble des composantes du réseau de signalisation mTOR.

Dans ce chapitre, nous avons utilisé le logiciel CellDesigner, un logiciel de modélisation, pour représenter une carte complète du réseau de signalisation mTOR. Cette carte comprend 964 molécules liées par 777 réactions en plus d'être conforme au language SBML (de l'anglais *Systems Biology Markup Language*) et SBGN (de l'anglais *Systems Biology Graphical Notation*). Cette carte est également disponible sur la plate-forme Web 2.0 *Payao*. La carte du réseau mTOR présentée dans ce chapitre représente une référence importante pour la communauté mTOR en plus d'être un outil précieux pour plusieurs types d'analyses en biologie des systèmes. Finalement, l'utilisation de cette carte dans le cadre du chapitre 4 nous aura permis de démontrer que les changements dans l'immunopeptidome induits par la rapamycine sont fonctionnellement reliés au réseau de signalisation mTOR.

5. ARTICLE 4:

A comprehensive map of the mTOR signaling network

Etienne Caron[1,2], Samik Ghosh[4], Yukiko Matsuoka[4,5], Dariel Ashton-Beaucage[1], Marc Therrien[1,3], Sébastien Lemieux[1], Claude Perreault[1,2], Philippe P. Roux[1,3,*], Hiroaki Kitano[4,6,7,8,*]

Institute for Research in Immunology and Cancer (IRIC), Université de Montréal, Montreal, Canada[1], Department of Medicine, Faculty of Medicine, Université de Montréal, Montreal, Quebec, Canada[2], Department of Pathology and Cell biology, Faculty of Medicine, Université de Montréal, Montreal, Quebec, Canada[3], The Systems Biology Institute, Minato-ku, Tokyo, Japan[4], JST ERATO KAWAOKA Infection-induced Host Responses Project, Tokyo, Japan[5], Sony Computer Science Laboratories, Shinagawa-ku, Tokyo, Japan[6], Division of Systems Biology, Cancer Institute, Tokyo, Japan[7], Open Biology Unit, Okinawa Institute of Science and Technology, Kunigami, Okinawa, Japan[8]

Manuscript information: Abstract: 172 words
Total length: characters 71 333 (incl. spaces)
Introduction, Main text and Perspectives section: 5 437 words

Running title: The mTOR map

*Corresponding authors:

Dr. Philippe P. Roux
Dr. Hiroaki Kitano

Article de revue publié dans: **Molecular Systems Biology, Volume 6, Numéro 453 (2010).**

CONTRIBUTIONS DES AUTEURS:

Etienne Caron a participé à la conception du projet, à l'ensemble des figures et à l'écriture du manuscrit. Samik Ghosh a participé à l'écriture du manuscrit. Yukiko Matsuoka a participé à la conception des figures 2 et 3. Dariel Ashton-Beaucage a participé à la figure supplémentaire 1. Marc Therrien, Sébastien Lemieux, Claude Perreault et Hiroaki Kitano ont commenté le manuscrit. Philippe Roux a participé à la conception du projet et à l'écriture du manuscrit.

5.1 Abstract

The mammalian target of rapamycin (mTOR) is a central regulator of cell growth and proliferation. mTOR signaling is frequently dysregulated in oncogenic cells, and thus an attractive target for anti-cancer therapy. Using CellDesigner, a modeling support software for graphical notation, we present herein a comprehensive map of the mTOR signaling network, which includes 964 species connected by 777 reactions. The map complies with both the systems biology markup language (SBML) and graphical notation (SBGN) for computational analysis and graphical representation, respectively. As captured in the mTOR map, we review and discuss our current understanding of the mTOR signaling network and highlight the impact of mTOR feedback and crosstalk regulations on drug-based cancer therapy. This map is available on the *Payao* platform, a Web 2.0 based community-wide interactive process for creating more accurate and information-rich databases. Thus, this comprehensive map of the mTOR network will serve as a tool to facilitate systems-level study of up-to-date mTOR network components and signaling events toward the discovery of novel regulatory processes and therapeutic strategies for cancer.

5.2 Introduction

The tale of the drug rapamycin and its functional target TOR (target of rapamycin) has attracted monumental scientific and clinical interest over the past few decades. Rapamycin was first identified as a potent antifungal metabolite produced by *Streptomyces hygroscopicus* (Vezina *et al*, 1975), a bacterial strain originally isolated from a soil sample collected on Easter Island in the South Pacific. Surprisingly, rapamycin was subsequently found to possess immunosuppressive and anti-tumorigenic properties (Chiang and Abraham, 2007; Guertin and Sabatini, 2007). The mode of action of rapamycin involves its interaction with the immunophilin FKBP12 (FK-binding protein 12) (Harding *et al*, 1989). Studies in budding yeast determined that a FKBP12-rapamycin complex directly inhibits a ~290 kDa Ser/Thr kinase termed "target of rapamycin" (TOR) (Heitman *et al*, 1991). Subsequently, the mammalian ortholog of TOR was identified and termed FRAP (FKBP-rapamycin-associated protein) and RAFT (rapamycin and FKBP12 target) (Brown *et al*, 1994; Sabatini *et al*, 1994), and is commonly referred to as mammalian TOR (mTOR). In the last two decades, scientists have used rapamycin to decipher mTOR's complex biological functions, which include the regulation of cell growth, proliferation and survival in response to nutrients, growth factors and hormones (Corradetti and Guan, 2006; Foster and Fingar, 2010b; Wullschleger *et al*, 2006). mTOR has also attracted broad interest because of its involvement in many human diseases, including type II diabetes and several types of cancer (Efeyan and Sabatini, 2010). These observations have guided the development of additional mTOR inhibiting drugs (rapalogs and second generation inhibitors), many of which are currently being evaluated for their therapeutic efficacy (Easton and Houghton, 2006).

Over the past few years, intense efforts have revealed many new mTOR regulatory proteins across a complex network of positive and negative regulatory mechanisms (Dunlop and Tee, 2009; Efeyan *et al*, 2010). This increased complexity impacts our ability to interpret and predict the regulation of the mTOR network, which is essential to better understand mTOR-related diseases. To unravel this complexity, computational approaches combined with mathematical modeling techniques have emerged as a solution (Karlebach and Shamir, 2008). To this end, a crucial task involves the reconstruction of networks in a

biologically meaningful manner by manual curation from literature or automated curation from pathway databases (Adriaens *et al*, 2008; Bauer-Mehren *et al*, 2009). Some of these databases represent pathways in computer-readable standard formats, such as Biological Pathway Exchange (BioPAX) (www.biopax.org) and Systems Biology Markup Language (SBML) (Hucka *et al*, 2003), allowing exchange between different software platforms and further processing by network analysis, visualization and modeling tools. However, a recent evaluation conducted to determine the accuracy and completeness of current pathway databases concluded that manual intervention is still needed to obtain a comprehensive and accurate view of a particular signaling network (Bauer-Mehren *et al*, 2009). Furthermore, manual reconstruction of such networks has been shown to be crucial in analyzing and interpreting structural features and global properties of signaling pathways (Calzone *et al*, 2008; Kitano and Oda, 2006; Oda and Kitano, 2006; Oda *et al*, 2005).

Based on the current scientific and clinical interest in understanding the precise regulation and function of mTOR, we set out to communicate the mTOR network in both human- and computer-readable formats. Using CellDesigner (http://celldesigner.org), a modeling support software (Funahashi *et al*, 2007), we present a manually assembled map of the mTOR signaling network. This map complies with SBML and the Systems Biology Graphical Notation (SBGN) process diagram (Kitano *et al*, 2005; Le Novere *et al*, 2009) for machine readable and graphical representation, respectively. Despite its static nature, a comprehensive map of molecular interactions would serve as a valuable working model to gain a systems-level understanding of the mTOR network. The map would also serve as a useful reference, and greatly help research on mTOR signaling. In this regard, we have reviewed our current understanding of the mTOR signaling network and discuss its particular relevance to cancer therapy. In addition, we elaborate on future directions to ensure a community-based effort in updating the mTOR network accurately through concurrent interventions.

5.3 Graphical notations for network representation

Standardizing the visual representation is crucial for more efficient and accurate transmission of biological knowledge between different communities. Recently, a group of biochemists, modelers, and computer scientists proposed the Systems Biology Graphical Notation (SBGN), a visual convention for graphical representation of biological networks (Le Novere *et al*, 2009) (www.sbgn.org). The SBGN aims at standardizing a systematic and unambiguous graphical notation and enables software tool support for computational analysis. SBGN defines three complementary types of visual languages: 1) process diagram, 2) entity relationship diagram, and 3) activity flow diagram. In order to stimulate implementation of SBGN support and the use of the notation, the symbols used to represent molecules and interactions related to the mTOR signaling network are based on the process diagram (Figures 2 and 3) and the activity flow diagram (Figure 4).

Process diagram

In Figure 1A, the process diagram is exemplified with the TSC1-TSC2 complex, a critical negative regulator of the rapamycin-sensitive mTOR complex 1 (mTORC1). In this diagram, the multiple phosphorylation states of TSC1-TSC2 are represented in a system of active or inactive transitive nodes. Using the unphosphorylated form as the initial node, we show that the TSC1-TSC2 complex is phosphorylated, altering it's ability to act as a GAP toward Rheb in vivo. More precisely, the catalysis arrows show that the transition of TSC2 from an active to an inactive state is mediated by the protein kinases AKT, ERK1/2, RSK1/2, IKKβ and CDK1, whereas AMPK and GSK3 positively regulate TSC1-TSC2 function. In addition, the process diagram language used to illustrate the mTOR signaling network was created using the CellDesigner software, which enables users to store data for each molecule and reaction in the protein and reaction notes, respectively. Moreover, the CellDesigner software allows users to access references that are used for individual reaction using PubMed ID (PMID) (Figure 1). For the purpose of this review, we used the process diagram language to draw the comprehensive mTOR network map (Figure 2) and to describe upstream regulators of mTORC1 signaling (Figure 3).

Activity flow diagram

The activity flow diagram language is essentially similar to traditional notation used by molecular biologists in the current literature. It depicts the flow of information between biochemical entities in a network and it omits information about the state transitions of entities. As exemplified in Figure 1B, activity flow diagrams only show influences such as “activation” or “inhibition” of the TSC1-TSC2 complex by different protein kinases. By ignoring biochemical details of processes in a network, the number of nodes in an activity flow diagram is greatly reduced compared to an equivalent process diagram. In Figure 4, the activity flow diagram has been used to represent a simplified version of the mTOR map based on key players of the mTOR signaling network.

5.4 General characteristics of the mTOR map

In Figure 2, we present a comprehensive map of the mTOR signaling network that was manually assembled based on the published literature. To facilitate map exploration, it was organized in different functional modules including regulation of mTORC1 and mTORC2, hypoxia, energy content, growth factor, nutrient, Wnt and TNF signaling, ribosome and rRNA biogenesis, cap-dependent translation, autophagy, protein folding, mitochondrial metabolism, cytoskeleton dynamics, transcription and cell cycle. The map was created using CellDesigner 4.0.1 (http://celldesigner.org/), a modeling software tool that enable users to describe molecular interactions using the process diagram language, as described above. Also, the map complies with the SBML, a standard machine-readable format for computational analysis (Hucka *et al*, 2003).

The map comprises 964 species and 777 reactions. "Species" are defined in SBML as "an entity that takes part in reactions" and it is used to distinguish the different states that are caused by enzymatic modification, association, dissociation, and translocation. In the comprehensive mTOR map, species were categorized as follows: 380 proteins (241 unique proteins), 319 complexes, 20 simple molecules, 80 genes, 87 RNA, 2 ions, 24 degraded products, 6 unknown molecules, and 46 phenotypes. Among all species, 602 were located in the cytoplasm and at the plasma membrane, 298 in the nucleus, 22 in endomembranes, 17 in the mitochondria, 12 in Rab7 vesicular structure, 6 in the extracellular environment, 4 at the centrosome, and 3 in the ER-golgi network. The reactions were categorized as follows: 210 heterodimer associations, 251 state transitions, 224 known transitions omitted, 43 dissociations, 32 transports, and 17 unknown transitions. The criteria for inclusion into the map are similar to those for the previously described maps of the epidermal growth factor receptor (EGFR) and Toll-like receptor (TLR) (Oda *et al*, 2006; Oda *et al*, 2005). The map was manually constructed based on 522 publications available in the Supplementary information section. This approach provides better quality in terms of coverage over major pathway and protein-protein interaction (PPI) databases (Table S2) (Bauer-Mehren *et al*, 2009). As illustrated in Figure 1, users can directly access references for individual reaction represented in the map.

In order to achieve a better coverage of all proteins involved in the mTOR signaling network and to identify potential modulators, we constructed an mTOR protein interaction network (PIN) from a set of 85 central mTOR pathway proteins and physical interaction data from multiple protein interaction databases using APID2NET (Hernandez-Toro *et al*, 2007) (Supplementary Figure 1). In the PIN, we identified 317 additional proteins not present in the current version of the mTOR map. Thus, integration of proteins and reactions from the curated mTOR signaling network and the constructed PIN from public databases offers opportunities to formulate and test new hypotheses. These are essential if we wish to expand the current mTOR map and continuously benefit to the community.

5.5 Description of the mTOR signaling network

In the following section, we review and highlight our current knowledge of the mechanisms regulating the mTOR signaling network, as captured in the comprehensive mTOR map (Figure 2). As mentioned earlier, the comprehensive map was organized in functional modules and includes annotations for the specific reactions and molecular species (PubMed ID of the relevant literature, outlinks to gene and protein databases, etc) to facilitate navigation by researchers.

Upstream regulators of mTORC1 signaling

mTORC1 is a rapamycin-sensitive multi-protein complex that contains mTOR, Raptor, and mLST8 (also known as GβL) (mTORC1 module in Figure 2) (Bhaskar and Hay, 2007; Wullschleger *et al*, 2006). When part of mTORC1, mTOR associates with FKBP38, PRAS40, and Deptor (Laplante and Sabatini, 2009). Most recent studies also suggest that Raptor binds to PRAS40 (Sancak et al, 2007; Yip et al., 2010). Raptor positively regulates mTOR activity and is thought to function as a scaffold that recruits mTORC1 substrates (Hara *et al*, 2002; Kim *et al*, 2002), whereas PRAS40, Deptor and FKBP38 negatively regulate mTOR activity (Bai *et al*, 2007; Peterson *et al*, 2009; Sancak *et al*, 2007; Vander Haar *et al*, 2007). The role of mLST8 in mTORC1 function is currently unclear, as the chronic loss of this protein does not affect mTORC1 activity in vivo (Guertin et al., 2006b). mTORC1 senses and integrates various environmental cues and intracellular signals to regulate cellular processes involved in the promotion of cell growth (Jacinto, 2008). To facilitate interpretation of the major signaling inputs to mTORC1 described below, and to encourage the use of the SBGN notation, we have drawn from the mTOR map a small-scale scheme of mTORC1 signaling events using the SBGN process diagram language (Figure 3). This simplified mTORC1 map comprises 110 species, 77 reactions and 4 cellular compartments and highlights positive and negative regulatory signals to mTORC1.

mTORC1 signaling is positively regulated by growth factors through the PI3K-AKT pathway (Growth factor/Nutrient module in Figure 2 and Figure 3). The binding of insulin to its cell surface receptor leads to the recruitment and phosphorylation of IRS-1,

which promotes the recruitment and activation of PI3K at the cell surface membrane. Active PI3K converts phosphatidylinositol-4,5-phosphate (PIP2) to phosphatidylinositol-3,4,5-phosphate (PIP3), a process antagonized by the lipid phosphatase PTEN. When produced at the plasma membrane, PIP3 recruits both PDK1 and AKT, resulting in the phosphorylation and partial activation of AKT. Whereas PDK1 phosphorylates AKT at Thr308, additional phosphorylation at Ser473 by mTORC2 (see below) is necessary for optimal activation of AKT in vitro (Sarbassov *et al*, 2005). mTORC1 is thought to be activated in part by AKT through the tuberous sclerosis complex proteins, TSC1 and TSC2. The TSC1-TSC2 complex is a critical negative regulator of mTORC1 (Huang and Manning, 2008b). Because of its central role in regulating mTORC1, 34 species depicting extensive details about the TSC1-TSC2 complex (post-translation modifications, interactors, cellular locations) were represented in the comprehensive mTOR map. In response to growth factors, TSC2 is phosphorylated and functionally inactivated by AKT (Inoki *et al*, 2002; Manning *et al*, 2002). ERK1/2 and RSK1/2 were also shown to phosphorylate and inactivate TSC2 in response to growth factors (Ballif *et al*, 2005; Ma *et al*, 2005; Roux *et al*, 2004), suggesting that PI3K and Ras/MAPK pathways collaborate to inhibit TSC1-TSC2 function in response to growth factors. Whereas TSC2 functions as a GAP towards the small Ras-related GTPase Rheb, TSC1 is required to stabilize TSC2 and prevent its proteasomal degradation (Huang *et al*, 2008b). While the active GTP-bound form of Rheb was shown to directly interact with mTOR to stimulate its catalytic activity (Long *et al*, 2005), Rheb may also promote substrate recognition by mTORC1 (Sancak *et al*, 2007; Sato *et al*, 2009).

Nutrients, such as amino acids, regulate mTORC1 signaling via different mechanisms. Amino acid availability regulates mTORC1 in a TSC2-independent but Rheb-dependent manner (Gulati and Thomas, 2007; Smith *et al*, 2005), but the exact mechanism remains poorly understood (Growth factor/Nutrient module in Figure 2 and Figure 3). Two complementary studies have provided compelling evidence that the Rag family of small GTPases is both necessary and sufficient to transmit a positive signal from amino acids to mTOR (Kim *et al*, 2008; Sancak *et al*, 2008). The current model proposes that amino acids induce the movement of mTORC1 to lysosomal membranes, where Rag proteins reside. More precisely, a complex encoded by the MAPKSP1, ROBLD3, and

c11orf59 genes, interacts with the Rag GTPases, recruits them to lysosomes, and was shown to be essential for mTORC1 activation (Sancak et al, 2010).

mTORC1 activity is sensitive to oxygen deprivation and one pathway by which this occurs involves activation of the TSC1-TSC2 complex by REDD1, a hypoxia-inducible protein (Hypoxia module in Figure 2 and Figure 3) (Brugarolas *et al*, 2004). Newly synthesized REDD1 was found to interact with 14-3-3 and relieve TSC2 from 14-3-3-dependent repression (DeYoung *et al*, 2008). mTORC1 also senses insufficient cellular energy levels through AMPK, a protein kinase activated in response to a low ATP/AMP ratio (Inoki *et al*, 2003) and by LKB1-mediated phosphorylation (Low energy module in Figure 2 and Figure 3) (Lizcano *et al*, 2004; Shaw *et al*, 2004). Upon energy depletion, AMPK phosphorylates and activates TSC2, resulting in the inhibition of mTORC1 (Inoki *et al*, 2003). The glycogen synthase kinase 3 (GSK3) may also be involved in the activation of TSC1-TSC2, as it was shown to phosphorylate TSC2 at Ser1337 and Ser1341 in response to AMPK-mediated TSC2 phosphorylation (Wnt module in Figure 2 and Figure 3) (Inoki *et al*, 2006). Site-specific phosphorylation of Raptor also plays an important role in the activation of mTORC1 in response to energy depletion. Indeed, low energy status promotes Raptor phosphorylation at Ser722 and Ser792 by AMPK, thereby providing binding sites for 14-3-3 which attenuates mTORC1 signaling (mTORC1 module in Figure 2 and Figure 3) (Gwinn *et al*, 2008). In contrast, insulin- and Rheb-stimulated mTOR phosphorylates Raptor on Ser863 to promote mTORC1 signaling (Foster *et al*, 2010a; Wang *et al*, 2009). The Ras/MAPK pathway activated protein kinase RSK was also shown to directly phosphorylate Raptor on Ser719, Ser721, and Ser722, thereby promoting mTORC1 signaling (Carriere *et al*, 2008a; Carriere *et al*, 2008b). Four mTOR phosphorylation sites have been identified so far: Ser1261, Ser2448, Ser2481 (an autophosphorylation site), and Thr2446 (Foster *et al*, 2010b). While Ser1261 is the only site demonstrated to affect mTOR activity (Acosta-Jaquez *et al*, 2009), phosphorylation of Ser2481 was shown to correlate with the activation status of mTOR (Soliman *et al*, 2010). Phosphorylation of Ser2448 was originally found to be regulated by Akt (Nave *et al*, 1999), but more recent studies demonstrated that S6K1 phosphorylates this site as part of a feedback loop with unknown functions (Chiang and Abraham, 2005; Holz and Blenis, 2005). The phosphorylation status of PRAS40 and

Deptor were also found to affect mTORC1 signaling. Indeed, phosphorylation of PRAS40 by both AKT (on Thr246) and mTORC1 (on Ser183, Ser212, Ser221) and subsequent association of PRAS40 to 14-3-3 is critical for the activation of mTORC1 (Fonseca *et al*, 2007; Oshiro *et al*, 2007; Vander Haar *et al*, 2007; Wang *et al*, 2008). Upon activation, mTORC1 also directly phosphorylates Deptor to promote its degradation which further activates mTORC1 signaling (Peterson *et al*, 2009). Although 13 specific phosphorylation sites have been identified on Deptor (see protein notes from the SBML-format file of the comprehensive mTOR map), functional role for individual phosphorylated residues have yet to be characterized. Collectively, these reports suggest that multiple phosphorylation events on mTORC1 components cooperate to regulate mTORC1 signaling in response to a wide variety of upstream signals.

Downstream targets of mTORC1 signaling

As described above, mTORC1 responds to diverse external and intracellular signals to promote anabolic and inhibit catabolic cellular processes (Foster *et al*, 2010b). Under favorable conditions, mTORC1 promotes protein synthesis, cell growth and proliferation (Ma and Blenis, 2009). Conversely, various cellular stresses inhibit mTORC1 signaling to reduce biosynthetic rates and allow initiation of macroautophagy. To review major output responses from mTORC1, we have drawn a reduced version of the mTOR map based on central mTOR network components using the SBGN activity flow diagram language (Figure 4). This simplified map also highlights the architecture of mTORC1 signaling and underscores the flow of positive and negative regulatory signals which are briefly discussed in the last section.

mTORC1 regulates protein synthesis via phosphorylation of both S6K1 and 4E-BP1 (Cap-dependent translation module in Figure 2, Figure 3 and 4). Upon growth factor or nutrient stimulations, mTORC1-mediated phosphorylation of 4E-BP1 induces its dissociation from eIF4E, which enables assembly of the eIF4F complex for competent translation initiation (Ma *et al*, 2009). When activated by mTORC1, S6K1 phosphorylates both PDCD4 and eIF4B, resulting in activation of the eIF4A RNA helicase, which unwinds secondary structures in the 5' untranslated region of mRNA to facilitate scanning of the ribosome (Ma *et al*, 2009). S6K1 also controls translation elongation by regulating

the activity of eEF2K. SKAR-mediated recruitment of activated S6K1 also increases the translation efficiency of spliced mRNA during the pioneer round of translation (Ma *et al*, 2009). While both 4E-BP1 and S6K1 regulate protein synthesis, 4E-BP1 appears to be mainly involved in cell proliferation while S6K1 regulates cell size (Dowling *et al*, 2010). Recently, S6K1 and RSK were found to phosphorylate the beta subunit of CCT (Abe *et al*, 2009). CCT is part of a chaperone network linked to protein synthesis and has been shown to facilitate folding of newly translated proteins *in vivo* (Protein folding module in Figure 2 and Figure 4) (Albanese *et al*, 2006; Camasses *et al*, 2003). Although the functional role of S6K1-mediated phosphorylation of CCTβ remains elusive, these findings suggest that mTORC1 may play roles in optimizing folding of newly synthesized proteins during or shortly after translation of polypeptides.

While rapamycin treatment has been shown many years ago to promote macroautophagy in yeast (Noda and Ohsumi, 1998), mTORC1 was recently demonstrated to regulate this process through a protein complex composed of ULK1, ATG13 and FIP200 (Jung *et al*, 2009). Under nutrient-rich conditions, mTORC1 inhibits autophagy through phosphorylation and inactivation of ULK1/2 and ATG13 (Autophagy module in Figure 2 and Figure 4). Upon nutrient starvation or following rapamycin treatment, inactivation of mTORC1 results in the activation of ULK1/2, which promotes phosphorylation of FIP200 and induces macroautophagy (Jung *et al*, 2009). Intriguingly, FIP200 was also shown to interact with the TSC1-TSC2 complex in response to nutrients, resulting in increased S6K1 activity and cell growth (Growth factor/Nutrient module in Figure 2) (Gan *et al*, 2005). Taken together, these observations raise the possibility that FIP200 binds distinct protein complexes both upstream and downstream of mTORC1 to regulate macroautophagy in response to nutrient status.

Gene expression profiling experiments have shown that ~5% of the transcriptome was differentially expressed in response to rapamycin-mediated mTOR inhibition (Guertin *et al*, 2006a), suggesting a role for mTORC1 in regulating gene expression. Additional studies have demonstrated that mTORC1 controls lipid biosynthesis by activating PPAR-γ and SREBP-1, two transcription factors that control expression of many lipogenic and adipogenic genes (Transcription module in Figure 2 and Figure 4) (Laplante *et al*, 2009).

mTORC1 also targets Lipin1, which was shown to play a key role in adipogenesis by promoting triglyceride synthesis and serving as a coactivator of PPAR-γ (Laplante *et al*, 2009). A recent study also identified mTORC1 as an important regulator of mitochondrial gene expression by altering the physical interaction of YY1 and PGC1-α (Cunningham *et al*, 2007), two transcription factors that play key roles in mitochondrial biogenesis (Mitochondrial metabolism module in Figure 2 and Figure 4). In the transcription module of the comprehensive mTOR map, we have drawn several mTOR network-related genes that were shown to be differentially expressed in response to various stimulations. Although most regulatory mechanisms involved in mTOR-dependent gene expression remain to be determined, these studies highlight the important roles played by mTORC1 in regulating the transcriptome.

Regulation of mTORC2 signaling

The second mTOR complex, mTORC2, controls cell survival, metabolism, and proliferation in part by phosphorylating both AKT and SGK1 (mTORC2 module in Figure 2 and Figure 4) (Garcia-Martinez and Alessi, 2008; Guertin *et al*, 2006b; Jacinto *et al*, 2006). Some studies have also suggested a role for mTORC2 in the control of cytoskeleton organization by promoting PKCα and paxillin phosphorylation (Cytoskeleton dynamic module in Figure 2 and Figure 4) (Jacinto *et al*, 2004; Sarbassov *et al*, 2004). mTORC2 is comprised of mTOR, Rictor, mSin1, mLST8, and is often accompanied with PROTOR-1/PPR5 and Deptor (Bhaskar *et al*, 2007; Wullschleger *et al*, 2006). Similar to its role in mTORC1 signaling, Deptor negatively regulates mTORC2 activity (Peterson *et al*, 2009). Deletion or knockdown of the mTORC2 components mTOR, Rictor, mSin1 and mLST8 has a dramatic effect on mTORC2 assembly and activation of AKT and SGK1 (Guertin *et al*, 2006b; Jacinto *et al*, 2006). To be fully activated, AKT requires phosphorylation of both Ser308 and Ser473 by PDK1 and mTORC2, respectively (Bhaskar *et al*, 2007). While phosphorylation of both AKT sites is required for full AKT activity in vitro, Ser473 phosphorylation is dispensable for phosphorylation of most AKT substrates in vivo with the exception of FOXO3 and PKCα (Guertin *et al*, 2006b). The mechanisms leading to PDK1-mediated phosphorylation of AKT are well described but the functional interaction between mTORC2 and AKT is incompletely understood (Jacinto, 2008). One possibility hinges on the presence of a PH-

like domain in mSIN1, which would promote the translocation of mTORC2 to the plasma membrane much like what was found for PDK1 (Schroder *et al*, 2007).

In contrast to mTORC1, recent work revealed that the TSC1–TSC2 complex promotes mTORC2 activity (Huang *et al*, 2008a; Huang *et al*, 2009). Interestingly, a physical interaction between these two complexes was identified, but the exact role for this new interaction is not currently known. mTORC2 is also generally described as being rapamycin-insensitive, but it is now becoming apparent that while short-term rapamycin treatment does not inhibit mTORC2, longer treatments suppress the assembly and function of mTORC2 through a mechanism that may involve dephosphorylation and delocalization of Rictor and mSin1 (Rosner and Hengstschlager, 2008; Sarbassov *et al*, 2006). Although we still know very little about the function and regulation of mTORC2, the availability of competitive ATP antagonists against mTOR will likely help deciphering mTORC2-mediated cellular processes.

5.6 Inhibition of mTOR in drug-based cancer therapy

Inappropriate amplification of the mTOR signaling pathway, as a result of diverse genetic lesions, is implicated in a variety of human cancers (Shaw and Cantley, 2006). Consequently, mTOR has emerged as a key target for the treatment of cancer. Rapamycin has initially been shown to possess strong cytostatic activities against a wide range of tumor cells *in vitro*, and was found to be effective at suppressing growth of cancer cells *in vivo* (Gibbons *et al*, 2009). A number of clinical trials using rapalogs as anticancer drugs have been performed, and in the case of renal cell carcinoma, has led to FDA approval. However, the overall efficacy of rapamycin analogs as single agents for cancer therapy did not meet expectations (Dowling *et al*, 2009a; Guertin and Sabatini, 2009). As highlighted in Figure 4, one notable architectural feature of mTORC1 signaling is the possible existence of a bow-tie structure. Typically, bow-tie networks are composed of a highly conserved core part of the network connected by diverse and redundant input and output subnetworks with various feedback control loops (Csete and Doyle, 2004; Oda *et al*, 2006; Oda *et al*, 2005). In this section, we briefly review key mTOR regulatory mechanisms within the architecture of the mTOR network and discuss their implications in cancer therapy.

Impact of mTOR feedback and crosstalk regulations in rapamycin-based therapy

In recent years, mTORC1 was shown to be involved in the initiation of several negative feedback regulatory mechanisms (Efeyan *et al*, 2010) (Figure 4). Many of the described feedback and crosstalk reactions have not been confirmed in vivo and may be cell- and stimuli-dependent. Nonetheless, upon growth factor stimulation, mTORC1 activates S6K1, which in turn phosphorylates IRS-1 at the plasma membrane, and ultimately suppresses PI3K-mediated activation of AKT (Harrington *et al*, 2005; Manning, 2004). Rapamycin-mediated mTORC1 inhibition results in the attenuation of this negative feedback loop, leading to increased AKT activity and activation of pro-survival signals, which would be a possible explanation for the relative inefficacy of rapamycin in cancer treatment (Harrington *et al*, 2005; Manning, 2004). Activation of elements in collateral pathways has been observed in the bow-tie architecture of the Toll-like receptor signaling network (Oda *et al*, 2006). As illustrated in Figure 4, mTORC1-mediated S6K1 activation

might engage mTORC2 in regulating collateral signals that modulate upstream components of the main bow-tie network. Indeed, two independent studies have recently found a new crosstalk between the two mTOR complexes that could also promote cell survival signaling in rapamycin-based cancer therapy. Thus, mTORC2-dependent AKT activation in the upper wing of the bow-tie was found to be negatively regulated through S6K1-mediated phosphorylation of Rictor on Thr1135 (Dibble *et al*, 2009; Julien *et al*, 2009). In addition, inhibition of mTORC1 was found to stimulate Ras-dependent activation of the MAPK pathway, a signaling cascade frequently activated in human cancers (Carracedo *et al*, 2008). While the exact molecular mechanisms underlying this negative feedback loop remain elusive, these results demonstrate the potential benefit of using combinatorial mTOR and MEK inhibitors for the treatment of certain cancer types.

Recent studies have also shown that rapamycin, previously thought to completely inhibit mTORC1 activity, does not equally suppress mTORC1 signaling to its substrates (Choo and Blenis, 2009; Thoreen et al., 2009; Choo et al., 2008). While rapamycin treatment completely and sustainably inhibits S6K1 activation, it only partly and variably inhibits 4E-BP1 phosphorylation (Choo *et al*, 2008). Because 4E-BP1 is critically involved in cap-dependent translation via regulation of eIF4E, rapamycin-resistant mTORC1 signaling towards 4E-BP1 is a plausible explanation for failed rapamycin-based cancer therapies.

The mTOR signaling map outlined in this review provides a picture of the intricate maze of regulatory interactions and feedback control loops mediated by mTOR both within a bow-tie architecture and between components of different pathways.

Combination therapies and second-generation of mTOR inhibitors

The implication of mTOR signaling in oncogenesis and the interaction of mTOR with other pathway components suggests the potential benefit of combination therapy (Dancey, 2010). Indeed, properly designed multicomponent therapies are the first step in controlling robustness to achieve clinical efficacy (Kitano, 2007). Efforts to combine the anti-tumor effects of therapeutic agents targeting different molecular components have been studied by several groups (Lehar *et al*, 2008a; Lehar *et al*, 2008b; Nelander *et al*, 2008). With

respect to mTOR, synergisms between rapalogs and conventional therapeutics have already been explored (reviewed in Abraham and Eng, 2008). The ability of mTOR inhibitors to down-regulate HIF1 and VEGF have made them interesting combination partners with VEGFR inhibitors like Sorafenib and Sunitinib (El-Hashemite *et al*, 2003; Hudson *et al*, 2002). The feedback interaction between MAPK and mTOR pathways also makes them potential combination partners. MEK inhibitors, such as CI-1040, in combination with rapalogs exhibit dose-dependent synergism in human lung cancer cell lines (Legrier *et al*, 2007). Targeting mTOR/AKT and MEK/ERK pathways have shown synergistic anti-growth phenotypes in androgen-dependent prostate tumors in the mouse (Kinkade *et al*, 2008). Combination therapies with IGF-1 or MAPK2 inhibitors and rapalogs are currently in various stages of clinical evaluation (Dancey, 2010). Combination therapies with an mTOR inhibitor provide a promising avenue in eliciting *synergistic efficacy* by exploiting regulatory interaction between different pathways, which might not be possible in mono-therapy. However, combination of therapeutic agents can also lead to *synergistic toxicity*. Thus, strategies for evaluation of toxicity and side-effects need to be systematically explored, and as signaling pathway interactions are context specific, different dosage regimen need to be evaluated based on cancer sub-types or patient sub-grouping.

While combination therapies with rapamycin or a rapalog may turn out to be efficacious in controlling deregulated mTOR signaling, several groups have developed small molecule active-site inhibitors of mTOR (reviewed in Dowling *et al*, 2009b; Guertin *et al*, 2009). This research has been bolstered by the fact that acute rapamycin treatment does not inhibit mTORC2 and incompletely inhibits mTORC1 signaling (Thoreen et al., 2009; Choo et al., 2008). Several ATP-competitive mTOR inhibitors have been described (Torin1, WYE-125132, PP242, KU-0063794) that inhibit mTOR irrespective of whether it is within mTORC1 or mTORC2 (Growth factor/Nutrient module in Figure 2 and Figure 4) (Feldman *et al*, 2009; Garcia-Martinez *et al*, 2009; Janes *et al*, 2010; Thoreen *et al*, 2009; Yu *et al*, 2009). Generally, these inhibitors are more potent suppressors of protein synthesis and 4E-BP1 phosphorylation, and strongly promote autophagy. Some of these have already been tested for their anti-tumor activities in various cancer sub-types (breast

cancer, glioma, lung and renal tumors) which generally appears to be more potent than what was found for rapamycin (Mayer *et al*; Yu *et al*, 2009).

The comprehensive machine-readable interaction map presented in this review will likely facilitate computational modeling and systems-level study of mTOR pathway components and interacting partners toward the discovery of novel targets and therapeutic intervention strategies for cancer.

5.7 Perspectives

We foresee the comprehensive mTOR network to be a *guidance map* in the study of mTOR signaling and its regulation. Akin to a geographical map which facilitates explorers to navigate new territories, the mTOR signaling map will provide researchers with a tool to quickly and efficiently manoeuvre through the complexity of mTOR interactions in their quest for novel interactions and potential pharmacological targets. Further, the availability of the map in standardized formats (SBML and SBGN) renders the network amenable to computational analyses based on various SBML compliant tools (http://sbml.org/SBML_Software_Guide/SBML_Software_Summary).

Our knowledge of the mTOR signaling network evolves rapidly. Thus, a key feature to the construction of large scale biological networks is the ability to enrich the product with up-to-date information curated from the latest scientific literature. Further, it is of paramount importance to allow this knowledge to be available for community-wide curation and collaboration - allowing researchers to not only access the information, but also to curate the reactions and share comments on possible scientific implications, hypotheses, in a community-wide collaborative manner (Web 2.0). In this direction, we have developed a platform for community-based curation and enrichment of biological pathways called *Payao* (Matsuoka *et al., 2010*). *Payao* is a community-based, collaborative web service platform for gene-regulatory and biochemical pathway model curation, based on SBML and uses CellDesigner for rendering the network. The *Payao* system (www.payaologue.org) enables a community to work on the same models simultaneously, insert tags as pop-up balloon to the parts of the model, exchange comments, record the discussions and eventually update the models accurately and concurrently. The current mTOR network elucidated in this review as well as the maps in Figure 3 and Figure 4 have been published on the *Payao* platform. From the *Payao* site (http://sblab.celldesigner.org/Payao10/bin/), search for mTOR in the “Search Models” field to access the models (a snapshot of the map on *Payao* is available in Supplementary Figure 2).

We envision the comprehensive mTOR map presented in this review to provide researchers with access to up-to-date and annotated mTOR knowledge base, share information through comment tags and subsequently enrich the network in a continuous cycle of open-flow community-collaborative framework.

5.8 Acknowledgments

The authors would like to thank Valeria de Azcoitia and Martin Giroux for critically reading this manuscript and for helpful discussions. E.C. is supported by training grants from the Japan Society for the Promotion of Science and the Canadian Institutes of Health Research. P.P.R. holds a Canada Research Chair in Signal Transduction and Proteomics, and a Career Development Award (CDA) from the Human Frontier Science Program (HFSP). Research in P.P.R. laboratory is funded by a Terry Fox Foundation grant provided through the Canadian Cancer Society Research Institute. C.P. holds a Canada Research Chair in Immunobiology. M.T. holds a Canada Research Chair in Intracellular Signaling.

5.9 References

Abe Y, Yoon SO, Kubota K, Mendoza MC, Gygi SP, Blenis J (2009) p90 ribosomal S6 kinase and p70 ribosomal S6 kinase link phosphorylation of the eukaryotic chaperonin containing TCP-1 to growth factor, insulin, and nutrient signaling. *J Biol Chem* **284:** 14939-14948.

Abraham RT, Eng CH (2008) Mammalian target of rapamycin as a therapeutic target in oncology. *Expert Opin Ther Targets* **12:** 209-222.

Acosta-Jaquez HA, Keller JA, Foster KG, Ekim B, Soliman GA, Feener EP, Ballif BA, Fingar DC (2009) Site-specific mTOR phosphorylation promotes mTORC1-mediated signaling and cell growth. *Mol Cell Biol* **29:** 4308-4324.

Adriaens ME, Jaillard M, Waagmeester A, Coort SL, Pico AR, Evelo CT (2008) The public road to high-quality curated biological pathways. *Drug Discov Today* **13:** 856-862.

Albanese V, Yam AY, Baughman J, Parnot C, Frydman J (2006) Systems analyses reveal two chaperone networks with distinct functions in eukaryotic cells. *Cell* **124:** 75-88.

Bai X, Ma D, Liu A, Shen X, Wang QJ, Liu Y, Jiang Y (2007) Rheb activates mTOR by antagonizing its endogenous inhibitor, FKBP38. *Science* **318:** 977-980.

Ballif BA, Roux PP, Gerber SA, MacKeigan JP, Blenis J, Gygi SP (2005) Quantitative phosphorylation profiling of the ERK/p90 ribosomal S6 kinase-signaling cassette and its targets, the tuberous sclerosis tumor suppressors. *Proc Natl Acad Sci U S A* **102:** 667-672.

Bauer-Mehren A, Furlong LI, Sanz F (2009) Pathway databases and tools for their exploitation: benefits, current limitations and challenges. *Mol Syst Biol* **5:** 290.

Bhaskar PT, Hay N (2007) The two TORCs and Akt. *Dev Cell* **12:** 487-502.

Brown EJ, Albers MW, Shin TB, Ichikawa K, Keith CT, Lane WS, Schreiber SL (1994) A mammalian protein targeted by G1-arresting rapamycin-receptor complex. *Nature* **369:** 756-758.

Brugarolas J, Lei K, Hurley RL, Manning BD, Reiling JH, Hafen E, Witters LA, Ellisen LW, Kaelin WG, Jr. (2004) Regulation of mTOR function in response to hypoxia by REDD1 and the TSC1/TSC2 tumor suppressor complex. *Genes Dev* **18:** 2893-2904.

Calzone L, Gelay A, Zinovyev A, Radvanyi F, Barillot E (2008) A comprehensive modular map of molecular interactions in RB/E2F pathway. *Mol Syst Biol* **4:** 173.

Camasses A, Bogdanova A, Shevchenko A, Zachariae W (2003) The CCT chaperonin promotes activation of the anaphase-promoting complex through the generation of functional Cdc20. *Mol Cell* **12:** 87-100.

Carracedo A, Ma L, Teruya-Feldstein J, Rojo F, Salmena L, Alimonti A, Egia A, Sasaki AT, Thomas G, Kozma SC, Papa A, Nardella C, Cantley LC, Baselga J, Pandolfi PP (2008) Inhibition of mTORC1 leads to MAPK pathway activation through a PI3K-dependent feedback loop in human cancer. *J Clin Invest* **118:** 3065-3074.

Carriere A, Cargnello M, Julien LA, Gao H, Bonneil E, Thibault P, Roux PP (2008a) Oncogenic MAPK signaling stimulates mTORC1 activity by promoting RSK-mediated raptor phosphorylation. *Curr Biol* **18:** 1269-1277.

Carriere A, Ray H, Blenis J, Roux PP (2008b) The RSK factors of activating the Ras/MAPK signaling cascade. *Front Biosci* **13:** 4258-4275.

Chiang GG, Abraham RT (2005) Phosphorylation of mammalian target of rapamycin (mTOR) at Ser-2448 is mediated by p70S6 kinase. *J Biol Chem* **280:** 25485-25490.

Chiang GG, Abraham RT (2007) Targeting the mTOR signaling network in cancer. *Trends Mol Med* **13:** 433-442.

Choo AY, Blenis J (2009) Not all substrates are treated equally: implications for mTOR, rapamycin-resistance and cancer therapy. *Cell Cycle* **8:** 567-572.

Choo AY, Yoon SO, Kim SG, Roux PP, Blenis J (2008) Rapamycin differentially inhibits S6Ks and 4E-BP1 to mediate cell-type-specific repression of mRNA translation. *Proc Natl Acad Sci U S A* **105:** 17414-17419.

Corradetti MN, Guan KL (2006) Upstream of the mammalian target of rapamycin: do all roads pass through mTOR? *Oncogene* **25:** 6347-6360.

Csete M, Doyle J (2004) Bow ties, metabolism and disease. *Trends Biotechnol* **22:** 446-450.

Cunningham JT, Rodgers JT, Arlow DH, Vazquez F, Mootha VK, Puigserver P (2007) mTOR controls mitochondrial oxidative function through a YY1-PGC-1alpha transcriptional complex. *Nature* **450:** 736-740.

Dancey J (2010) mTOR signaling and drug development in cancer. *Nat Rev Clin Oncol* **7:** 209-219.

DeYoung MP, Horak P, Sofer A, Sgroi D, Ellisen LW (2008) Hypoxia regulates TSC1/2-mTOR signaling and tumor suppression through REDD1-mediated 14-3-3 shuttling. *Genes Dev* **22:** 239-251.

Dibble CC, Asara JM, Manning BD (2009) Characterization of Rictor phosphorylation sites reveals direct regulation of mTOR complex 2 by S6K1. *Mol Cell Biol* **29:** 5657-5670.

Dowling RJ, Pollak M, Sonenberg N (2009a) Current status and challenges associated with targeting mTOR for cancer therapy. *BioDrugs* **23:** 77-91.

Dowling RJ, Topisirovic I, Alain T, Bidinosti M, Fonseca BD, Petroulakis E, Wang X, Larsson O, Selvaraj A, Liu Y, Kozma SC, Thomas G, Sonenberg N (2010) mTORC1-mediated cell proliferation, but not cell growth, controlled by the 4E-BPs. *Science* **328:** 1172-1176.

Dowling RJ, Topisirovic I, Fonseca BD, Sonenberg N (2009b) Dissecting the role of mTOR: Lessons from mTOR inhibitors. *Biochim Biophys Acta*.

Dunlop EA, Tee AR (2009) Mammalian target of rapamycin complex 1: signaling inputs, substrates and feedback mechanisms. *Cell Signal* **21:** 827-835.

Easton JB, Houghton PJ (2006) mTOR and cancer therapy. *Oncogene* **25:** 6436-6446.

Efeyan A, Sabatini DM (2010) mTOR and cancer: many loops in one pathway. *Curr Opin Cell Biol* **22:** 169-176.

El-Hashemite N, Walker V, Zhang H, Kwiatkowski DJ (2003) Loss of Tsc1 or Tsc2 induces vascular endothelial growth factor production through mammalian target of rapamycin. *Cancer Res* **63:** 5173-5177.

Feldman ME, Apsel B, Uotila A, Loewith R, Knight ZA, Ruggero D, Shokat KM (2009) Active-site inhibitors of mTOR target rapamycin-resistant outputs of mTORC1 and mTORC2. *PLoS Biol* **7:** e38.

Fonseca BD, Smith EM, Lee VH, MacKintosh C, Proud CG (2007) PRAS40 is a target for mammalian target of rapamycin complex 1 and is required for signaling downstream of this complex. *J Biol Chem* **282:** 24514-24524.

Foster KG, Acosta-Jaquez HA, Romeo Y, Ekim B, Soliman GA, Carriere A, Roux PP, Ballif BA, Fingar DC (2010a) Regulation of mTOR complex 1 (mTORC1) by raptor Ser863 and multisite phosphorylation. *J Biol Chem* **285:** 80-94.

Foster KG, Fingar DC (2010b) Mammalian target of rapamycin (mTOR): conducting the cellular signaling symphony. *J Biol Chem* **285:** 14071-14077.

Funahashi A, Jouraku A, Matsuoka Y, Kitano H (2007) Integration of CellDesigner and SABIO-RK. *In Silico Biol* **7:** S81-90.

Gan B, Melkoumian ZK, Wu X, Guan KL, Guan JL (2005) Identification of FIP200 interaction with the TSC1-TSC2 complex and its role in regulation of cell size control. *J Cell Biol* **170:** 379-389.

Garcia-Martinez JM, Alessi DR (2008) mTOR complex 2 (mTORC2) controls hydrophobic motif phosphorylation and activation of serum- and glucocorticoid-induced protein kinase 1 (SGK1). *Biochem J* **416:** 375-385.

Garcia-Martinez JM, Moran J, Clarke RG, Gray A, Cosulich SC, Chresta CM, Alessi DR (2009) Ku-0063794 is a specific inhibitor of the mammalian target of rapamycin (mTOR). *Biochem J* **421:** 29-42.

Gibbons JJ, Abraham RT, Yu K (2009) Mammalian target of rapamycin: discovery of rapamycin reveals a signaling pathway important for normal and cancer cell growth. *Semin Oncol* **36 Suppl 3:** S3-S17.

Guertin DA, Guntur KV, Bell GW, Thoreen CC, Sabatini DM (2006a) Functional genomics identifies TOR-regulated genes that control growth and division. *Curr Biol* **16:** 958-970.

Guertin DA, Sabatini DM (2007) Defining the role of mTOR in cancer. *Cancer Cell* **12:** 9-22.

Guertin DA, Sabatini DM (2009) The pharmacology of mTOR inhibition. *Sci Signal* **2:** pe24.

Guertin DA, Stevens DM, Thoreen CC, Burds AA, Kalaany NY, Moffat J, Brown M, Fitzgerald KJ, Sabatini DM (2006b) Ablation in mice of the mTORC components raptor, rictor, or mLST8 reveals that mTORC2 is required for signaling to Akt-FOXO and PKCalpha, but not S6K1. *Dev Cell* **11:** 859-871.

Gwinn DM, Shackelford DB, Egan DF, Mihaylova MM, Mery A, Vasquez DS, Turk BE, Shaw RJ (2008) AMPK phosphorylation of raptor mediates a metabolic checkpoint. *Mol Cell* **30:** 214-226.

Hara K, Maruki Y, Long X, Yoshino K, Oshiro N, Hidayat S, Tokunaga C, Avruch J, Yonezawa K (2002) Raptor, a binding partner of target of rapamycin (TOR), mediates TOR action. *Cell* **110:** 177-189.

Harding MW, Galat A, Uehling DE, Schreiber SL (1989) A receptor for the immunosuppressant FK506 is a cis-trans peptidyl-prolyl isomerase. *Nature* **341:** 758-760.

Harrington LS, Findlay GM, Lamb RF (2005) Restraining PI3K: mTOR signaling goes back to the membrane. *Trends Biochem Sci* **30:** 35-42.

Heitman J, Movva NR, Hall MN (1991) Targets for cell cycle arrest by the immunosuppressant rapamycin in yeast. *Science* **253:** 905-909.

Hernandez-Toro J, Prieto C, De las Rivas J (2007) APID2NET: unified interactome graphic analyzer. *Bioinformatics* **23:** 2495-2497.

Holz MK, Blenis J (2005) Identification of S6 kinase 1 as a novel mammalian target of rapamycin (mTOR)-phosphorylating kinase. *J Biol Chem* **280:** 26089-26093.

Huang J, Dibble CC, Matsuzaki M, Manning BD (2008a) The TSC1-TSC2 complex is required for proper activation of mTOR complex 2. *Mol Cell Biol* **28:** 4104-4115.

Huang J, Manning BD (2008b) The TSC1-TSC2 complex: a molecular switchboard controlling cell growth. *Biochem J* **412:** 179-190.

Huang J, Wu S, Wu CL, Manning BD (2009) Signaling events downstream of mammalian target of rapamycin complex 2 are attenuated in cells and tumors deficient for the tuberous sclerosis complex tumor suppressors. *Cancer Res* **69:** 6107-6114.

Hucka M, Finney A, Sauro HM, Bolouri H, Doyle JC, Kitano H, Arkin AP, Bornstein BJ, Bray D, Cornish-Bowden A, Cuellar AA, Dronov S, Gilles ED, Ginkel M, Gor V, Goryanin, II, Hedley WJ, Hodgman TC, Hofmeyr JH, Hunter PJ, Juty NS, Kasberger JL, Kremling A, Kummer U, Le Novere N, Loew LM, Lucio D, Mendes P, Minch E, Mjolsness ED, Nakayama Y, Nelson MR, Nielsen PF, Sakurada T, Schaff JC, Shapiro BE, Shimizu TS, Spence HD, Stelling J, Takahashi K, Tomita M, Wagner J, Wang J (2003) The systems biology markup language (SBML): a medium for representation and exchange of biochemical network models. *Bioinformatics* **19:** 524-531.

Hudson CC, Liu M, Chiang GG, Otterness DM, Loomis DC, Kaper F, Giaccia AJ, Abraham RT (2002) Regulation of hypoxia-inducible factor 1alpha expression and function by the mammalian target of rapamycin. *Mol Cell Biol* **22:** 7004-7014.

Inoki K, Li Y, Zhu T, Wu J, Guan KL (2002) TSC2 is phosphorylated and inhibited by Akt and suppresses mTOR signaling. *Nat Cell Biol* **4:** 648-657.

Inoki K, Ouyang H, Zhu T, Lindvall C, Wang Y, Zhang X, Yang Q, Bennett C, Harada Y, Stankunas K, Wang CY, He X, MacDougald OA, You M, Williams BO, Guan KL (2006) TSC2 integrates Wnt and energy signals via a coordinated phosphorylation by AMPK and GSK3 to regulate cell growth. *Cell* **126:** 955-968.

Inoki K, Zhu T, Guan KL (2003) TSC2 mediates cellular energy response to control cell growth and survival. *Cell* **115:** 577-590.

Jacinto E (2008) What controls TOR? *IUBMB Life* **60:** 483-496.

Jacinto E, Facchinetti V, Liu D, Soto N, Wei S, Jung SY, Huang Q, Qin J, Su B (2006) SIN1/MIP1 maintains rictor-mTOR complex integrity and regulates Akt phosphorylation and substrate specificity. *Cell* **127:** 125-137.

Jacinto E, Loewith R, Schmidt A, Lin S, Ruegg MA, Hall A, Hall MN (2004) Mammalian TOR complex 2 controls the actin cytoskeleton and is rapamycin insensitive. *Nat Cell Biol* **6:** 1122-1128.

Janes MR, Limon JJ, So L, Chen J, Lim RJ, Chavez MA, Vu C, Lilly MB, Mallya S, Ong ST, Konopleva M, Martin MB, Ren P, Liu Y, Rommel C, Fruman DA (2010) Effective and selective targeting of leukemia cells using a TORC1/2 kinase inhibitor. *Nat Med* **16:** 205-213.

Julien LA, Carriere A, Moreau J, Roux PP (2010) mTORC1-Activated S6K1 Phosphorylates Rictor on Threonine 1135 and Regulates mTORC2 Signaling. *Mol Cell Biol*. **30**: 908-921.

Jung CH, Jun CB, Ro SH, Kim YM, Otto NM, Cao J, Kundu M, Kim DH (2009) ULK-Atg13-FIP200 complexes mediate mTOR signaling to the autophagy machinery. *Mol Biol Cell* **20:** 1992-2003.

Karlebach G, Shamir R (2008) Modelling and analysis of gene regulatory networks. *Nat Rev Mol Cell Biol* **9:** 770-780.

Kim DH, Sarbassov DD, Ali SM, King JE, Latek RR, Erdjument-Bromage H, Tempst P, Sabatini DM (2002) mTOR interacts with raptor to form a nutrient-sensitive complex that signals to the cell growth machinery. *Cell* **110:** 163-175.

Kim E, Goraksha-Hicks P, Li L, Neufeld TP, Guan KL (2008) Regulation of TORC1 by Rag GTPases in nutrient response. *Nat Cell Biol* **10:** 935-945.

Kinkade CW, Castillo-Martin M, Puzio-Kuter A, Yan J, Foster TH, Gao H, Sun Y, Ouyang X, Gerald WL, Cordon-Cardo C, Abate-Shen C (2008) Targeting AKT/mTOR and ERK MAPK signaling inhibits hormone-refractory prostate cancer in a preclinical mouse model. *J Clin Invest* **118:** 3051-3064.

Kitano H (2007) A robustness-based approach to systems-oriented drug design. *Nat Rev Drug Discov* **6:** 202-210.

Kitano H, Funahashi A, Matsuoka Y, Oda K (2005) Using process diagrams for the graphical representation of biological networks. *Nat Biotechnol* **23:** 961-966.

Kitano H, Oda K (2006) Robustness trade-offs and host-microbial symbiosis in the immune system. *Mol Syst Biol* **2:** 2006 0022.

Laplante M, Sabatini DM (2009) An emerging role of mTOR in lipid biosynthesis. *Curr Biol* **19:** R1046-1052.

Le Novere N, Hucka M, Mi H, Moodie S, Schreiber F, Sorokin A, Demir E, Wegner K, Aladjem MI, Wimalaratne SM, Bergman FT, Gauges R, Ghazal P, Kawaji H, Li L, Matsuoka Y, Villeger A, Boyd SE, Calzone L, Courtot M, Dogrusoz U, Freeman TC, Funahashi A, Ghosh S, Jouraku A, Kim S, Kolpakov F, Luna A, Sahle S, Schmidt E, Watterson S, Wu G, Goryanin I, Kell DB, Sander C, Sauro H, Snoep JL, Kohn K, Kitano H (2009) The Systems Biology Graphical Notation. *Nat Biotechnol* **27:** 735-741.

Legrier ME, Yang CP, Yan HG, Lopez-Barcons L, Keller SM, Perez-Soler R, Horwitz SB, McDaid HM (2007) Targeting protein translation in human non small cell lung cancer via combined MEK and mammalian target of rapamycin suppression. *Cancer Res* **67:** 11300-11308.

Lehar J, Krueger A, Zimmermann G, Borisy A (2008a) High-order combination effects and biological robustness. *Mol Syst Biol* **4:** 215.

Lehar J, Stockwell BR, Giaever G, Nislow C (2008b) Combination chemical genetics. *Nat Chem Biol* **4:** 674-681.

Lizcano JM, Goransson O, Toth R, Deak M, Morrice NA, Boudeau J, Hawley SA, Udd L, Makela TP, Hardie DG, Alessi DR (2004) LKB1 is a master kinase that activates 13 kinases of the AMPK subfamily, including MARK/PAR-1. *EMBO J* **23:** 833-843.

Long X, Lin Y, Ortiz-Vega S, Yonezawa K, Avruch J (2005) Rheb binds and regulates the mTOR kinase. *Curr Biol* **15:** 702-713.

Ma L, Chen Z, Erdjument-Bromage H, Tempst P, Pandolfi PP (2005) Phosphorylation and functional inactivation of TSC2 by Erk implications for tuberous sclerosis and cancer pathogenesis. *Cell* **121:** 179-193.

Ma XM, Blenis J (2009) Molecular mechanisms of mTOR-mediated translational control. *Nat Rev Mol Cell Biol* **10:** 307-318.

Manning BD (2004) Balancing Akt with S6K: implications for both metabolic diseases and tumorigenesis. *J Cell Biol* **167:** 399-403.

Manning BD, Tee AR, Logsdon MN, Blenis J, Cantley LC (2002) Identification of the tuberous sclerosis complex-2 tumor suppressor gene product tuberin as a target of the phosphoinositide 3-kinase/akt pathway. *Mol Cell* **10:** 151-162.

Matsuoka Y, Ghosh S, Kikuchi N, Kitano H (2010) Payao: a community platform for SBML pathway model curation. *Bioinformatics* **26:** 1381-1383.

Mayer C, Zhao J, Yuan X, Grummt I (2004) mTOR-dependent activation of the transcription factor TIF-IA links rRNA synthesis to nutrient availability. *Genes Dev* **18:** 423-434.

Nave BT, Ouwens M, Withers DJ, Alessi DR, Shepherd PR (1999) Mammalian target of rapamycin is a direct target for protein kinase B: identification of a convergence point for opposing effects of insulin and amino-acid deficiency on protein translation. *Biochem J* **344 Pt 2:** 427-431.

Nelander S, Wang W, Nilsson B, She QB, Pratilas C, Rosen N, Gennemark P, Sander C (2008) Models from experiments: combinatorial drug perturbations of cancer cells. *Mol Syst Biol* **4:** 216.

Noda T, Ohsumi Y (1998) Tor, a phosphatidylinositol kinase homologue, controls autophagy in yeast. *J Biol Chem* **273:** 3963-3966.

Oda K, Kitano H (2006) A comprehensive map of the toll-like receptor signaling network. *Mol Syst Biol* **2:** 2006 0015.

Oda K, Matsuoka Y, Funahashi A, Kitano H (2005) A comprehensive pathway map of epidermal growth factor receptor signaling. *Mol Syst Biol* **1:** 2005 0010.

Oshiro N, Takahashi R, Yoshino K, Tanimura K, Nakashima A, Eguchi S, Miyamoto T, Hara K, Takehana K, Avruch J, Kikkawa U, Yonezawa K (2007) The proline-rich Akt substrate of 40 kDa (PRAS40) is a physiological substrate of mammalian target of rapamycin complex 1. *J Biol Chem* **282:** 20329-20339.

Peterson TR, Laplante M, Thoreen CC, Sancak Y, Kang SA, Kuehl WM, Gray NS, Sabatini DM (2009) DEPTOR is an mTOR inhibitor frequently overexpressed in multiple myeloma cells and required for their survival. *Cell* **137:** 873-886.

Rosner M, Hengstschlager M (2008) Cytoplasmic and nuclear distribution of the protein complexes mTORC1 and mTORC2: rapamycin triggers dephosphorylation and delocalization of the mTORC2 components rictor and sin1. *Hum Mol Genet* **17:** 2934-2948.

Roux PP, Ballif BA, Anjum R, Gygi SP, Blenis J (2004) Tumor-promoting phorbol esters and activated Ras inactivate the tuberous sclerosis tumor suppressor complex via p90 ribosomal S6 kinase. *Proc Natl Acad Sci U S A* **101:** 13489-13494.

Sabatini DM, Erdjument-Bromage H, Lui M, Tempst P, Snyder SH (1994) RAFT1: a mammalian protein that binds to FKBP12 in a rapamycin-dependent fashion and is homologous to yeast TORs. *Cell* **78:** 35-43.

Sancak Y, Peterson TR, Shaul YD, Lindquist RA, Thoreen CC, Bar-Peled L, Sabatini DM (2008) The Rag GTPases bind raptor and mediate amino acid signaling to mTORC1. *Science* **320:** 1496-1501.

Sancak Y, Thoreen CC, Peterson TR, Lindquist RA, Kang SA, Spooner E, Carr SA, Sabatini DM (2007) PRAS40 is an insulin-regulated inhibitor of the mTORC1 protein kinase. *Mol Cell* **25:** 903-915.

Sancak Y, Bar-Peled L, Zoncu R, Markhard AL, Nada S, Sabatini DM (2010) Ragulator-Rag complex targets mTORC1 to the lysosomal surface and is necessary for its activation by amino acids. *Cell* **141**:290-303.

Sarbassov DD, Ali SM, Kim DH, Guertin DA, Latek RR, Erdjument-Bromage H, Tempst P, Sabatini DM (2004) Rictor, a novel binding partner of mTOR, defines a rapamycin-insensitive and raptor-independent pathway that regulates the cytoskeleton. *Curr Biol* **14:** 1296-1302.

Sarbassov DD, Ali SM, Sengupta S, Sheen JH, Hsu PP, Bagley AF, Markhard AL, Sabatini DM (2006) Prolonged rapamycin treatment inhibits mTORC2 assembly and Akt/PKB. *Mol Cell* **22:** 159-168.

Sarbassov DD, Guertin DA, Ali SM, Sabatini DM (2005) Phosphorylation and regulation of Akt/PKB by the rictor-mTOR complex. *Science* **307:** 1098-1101.

Sato T, Nakashima A, Guo L, Tamanoi F (2009) Specific activation of mTORC1 by Rheb G-protein in vitro involves enhanced recruitment of its substrate protein. *J Biol Chem* **284:** 12783-12791.

Schroder WA, Buck M, Cloonan N, Hancock JF, Suhrbier A, Sculley T, Bushell G (2007) Human Sin1 contains Ras-binding and pleckstrin homology domains and suppresses Ras signaling. *Cell Signal* **19:** 1279-1289.

Shaw RJ, Cantley LC (2006) Ras, PI(3)K and mTOR signaling controls tumour cell growth. *Nature* **441:** 424-430.

Shaw RJ, Kosmatka M, Bardeesy N, Hurley RL, Witters LA, DePinho RA, Cantley LC (2004) The tumor suppressor LKB1 kinase directly activates AMP-activated kinase and regulates apoptosis in response to energy stress. *Proc Natl Acad Sci U S A* **101:** 3329-3335.

Smith EM, Finn SG, Tee AR, Browne GJ, Proud CG (2005) The tuberous sclerosis protein TSC2 is not required for the regulation of the mammalian target of rapamycin by amino acids and certain cellular stresses. *J Biol Chem* **280:** 18717-18727.

Soliman GA, Acosta-Jaquez HA, Dunlop EA, Ekim B, Maj NE, Tee AR, Fingar DC (2010) mTOR Ser-2481 autophosphorylation monitors mTORC-specific catalytic activity and clarifies rapamycin mechanism of action. *J Biol Chem* **285:** 7866-7879.

Thoreen CC, Kang SA, Chang JW, Liu Q, Zhang J, Gao Y, Reichling LJ, Sim T, Sabatini DM, Gray NS (2009) An ATP-competitive mammalian target of rapamycin inhibitor reveals rapamycin-resistant functions of mTORC1. *J Biol Chem* **284:** 8023-8032.

Vander Haar E, Lee SI, Bandhakavi S, Griffin TJ, Kim DH (2007) Insulin signaling to mTOR mediated by the Akt/PKB substrate PRAS40. *Nat Cell Biol* **9:** 316-323.

Vezina C, Kudelski A, Sehgal SN (1975) Rapamycin (AY-22,989), a new antifungal antibiotic. I. Taxonomy of the producing streptomycete and isolation of the active principle. *J Antibiot (Tokyo)* **28:** 721-726.

Wang L, Harris TE, Lawrence JC, Jr. (2008) Regulation of proline-rich Akt substrate of 40 kDa (PRAS40) function by mammalian target of rapamycin complex 1 (mTORC1)-mediated phosphorylation. *J Biol Chem* **283:** 15619-15627.

Wang L, Lawrence JC, Jr., Sturgill TW, Harris TE (2009) Mammalian target of rapamycin complex 1 (mTORC1) activity is associated with phosphorylation of raptor by mTOR. *J Biol Chem* **284:** 14693-14697.

Wullschleger S, Loewith R, Hall MN (2006) TOR signaling in growth and metabolism. *Cell* **124:** 471-484.

Yip CK, Murata K, Walz T, Sabatini DM, Kang SA (2010) Structure of the human mTOR complex I and its implications for rapamycin inhibition. *Mol. Cell.* **38**:768-774.

Yu K, Toral-Barza L, Shi C, Zhang WG, Lucas J, Shor B, Kim J, Verheijen J, Curran K, Malwitz DJ, Cole DC, Ellingboe J, Ayral-Kaloustian S, Mansour TS, Gibbons JJ, Abraham RT, Nowak P, Zask A (2009) Biochemical, cellular, and in vivo activity of novel ATP-competitive and selective inhibitors of the mammalian target of rapamycin. *Cancer Res* **69:** 6232-6240.

5.10 Figure Legends

Figure 1: Graphical notations adopted by CellDesigner to illustrate the mTOR signaling network.

(A) Process diagrams, explicitly displaying different phosphorylated forms of the TSC1-TSC2 complex, as well as the processes of phosphorylation on different serine and threonine residues by AKT, ERK1/2, RSK1/2, CDK1, AMPK, GSK3 and IKKβ. The active state of the molecule is indicated by a dashed line surrounding the molecule. Phosphorylation state of the component is represented with target residues and positions. For individual proteins and reactions, specific notes such as PubMed ID (PMID) were added, enabling a direct link to the relevant references. (B) Activity flow diagrams depicting the activation and inhibition of the TSC1-TSC2 complex by the enzymes illustrated in A. In this diagram language, the biochemical details are omitted.

Figure 2: A comprehensive map of the mTOR signaling network. `

This map was created with CellDesigner version 4.0.1. A total number of 777 reactions and 964 species were included. The SBML and PDF files of the mTOR map are available from the Supplementary information. The map can be best viewed in the PDF format (see Supplementary Figure 3). All of the species, proteins, reactions and cellular compartments included in the map are listed in the SBML file when opened by CellDesigner (http://celldesigner.org/). All of the unique proteins were listed in Table S1. A cartoon view of the map (bottom right) depicting different functional modules was drawn to facilitate the exploration of the map . Symbols adopted to build the map are illustrated in the legend.

Figure 3: Upstream regulators of mTORC1 signaling.

Species, proteins, reactions and cellular compartments involved in mTORC1 signaling were extracted from the comprehensive mTOR map and illustrated using the process diagram language. Green and red reactions indicate activation and inhibition of mTORC1, respectively. Size and color of each component are configurable. Symbols are similar to those used in the legend of the Figure 2. The SBML and PDF files (see Supplementary Figure 4) of mTORC1 signaling are available from the Supplementary information.

Figure 4: Activity flow of the mTOR signaling network.

Central components and reactions were extracted from the comprehensive mTOR map and illustrated using the activity flow diagram language. This reduced map focuses on the flow of activation and inhibition and on the architecture of mTORC1 signaling. Components and signaling events related to mTORC1 consist of a possible bow-tie network (pale blue area). In this network architecture, input signals converge to TSC1-TSC2/Rheb/mTORC1, which forms the bow-tie core of the network. Activities of the core components play important roles in controlling diverse downstream responses. Positive and negative feedback loops in the network are represented by the bold lines. Green and red lines indicate activation and inhibition of mTORC1/2, respectively. The inhibition of mTORC1 by rapamycin, the inhibition mTORC1/2 by the ATP-competitive inhibitor Torin1, and the inhibition of MEK by CI-1040 are represented by the bold blue lines. Symbols are similar to those used in the legend of the Figure 1 and 2. The SBML and PDF files (see Supplementary Figure 5) of the reduced mTOR map are available from the Supplementary information.

5.11 Supplementary Figure Legends

Supplementary Figure 1: Overlap of the mTOR signaling network presented in the map and protein interaction network.

An mTOR protein interaction network constructed from a set of 85 (from Figure 4) central mTOR pathway components (blue nodes) and physical interaction data from multiple protein interaction databases using APID2NET (Hernandez-Toro *et al,* 2007). 380 proteins are associated to mTOR components by 3 or more distinct experimental evidences. Among these, 63 components (orange nodes) are represented in the comprehensive mTOR map whereas 317 (purple nodes) additional proteins were identified from protein interactions databases. The cytoscape file including all the components and the physical interactions is available from the Supplementary informations.

Supplementary Figure 2: Comprehensive mTOR map on the web-based collaboration platform Payao.

The Supplementary Figurehows a screen capture of the mTOR comprehensive map as seen on the Payao system. The left hand panel outlines the tagsets already present in the model (model annotations created by the authors). The tags in a tagset appear as bubbles and can be clicked to expand show the tag information (as shown in the bubble dialog expanded the middle portion of the snapshot for reaction no. 472). The bottom panel shows the details for all species and reactions in the map. The top panel (highlighted in black box on the diagram) is the annotation palette which allows the users to add their own tags to the model. Details on the user interface for Payao is available at http://celldesigner.org/payao/doc/PAYAO_Users_GuideE11.pdf. The mTOR comprehensive map as well as the maps in Figure 3 and Figure 4 in the manuscript have been uploaded on Payao for the users through a special account created. The details are: Website access: http://sblab.celldesigner.org/Payao10/bin/; Login name: mTORMap; Password: mappers. Once logged in, if the users click on the “My Favorite Models” tab on the right hand panel (second Tab after MyModels), they can see all the 3 maps and annotate them through tags etc. Details on Payao can be found in (Matsuoka *et al., 2010*).

Figure 1

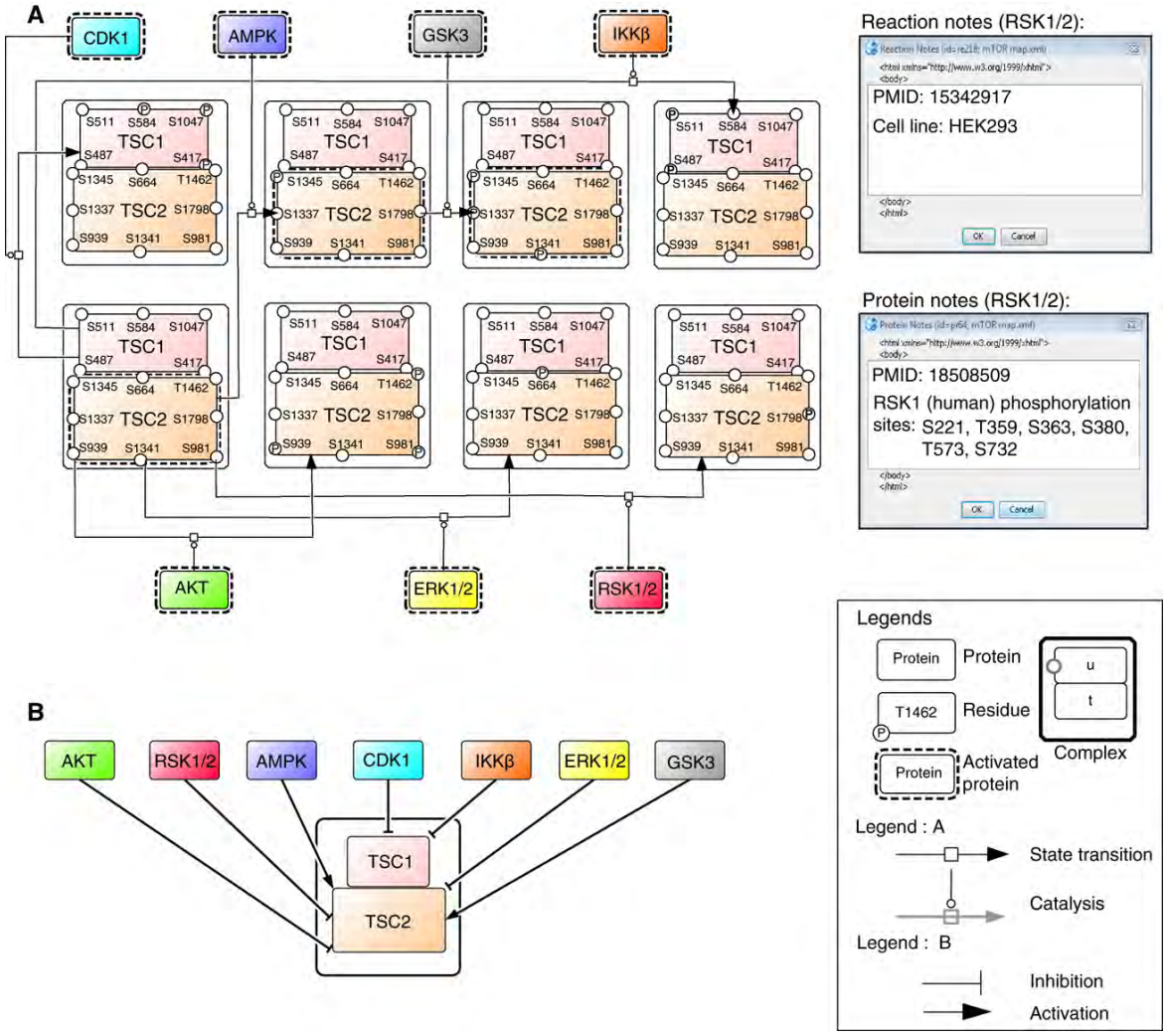
A
CDK1
AMPK
GSK3
IKKβ
TSC1
TSC2
S511 S584 S1047
S487 S417
S1345 S664 T1462
S1337 S1798
S939 S1341 S981
AKT
ERK1/2
RSK1/2
Reaction notes (RSK1/2):
PMID: 15342917
Cell line: HEK293
OK
Cancel
Protein notes (RSK1/2):
PMID: 18508509
RSK1 (human) phosphorylation sites: S221, T359, S363, S380, T573, S732
Legends
Protein
Residue
T1462
Activated protein
u
t
Complex
Legend : A
State transition
Catalysis
Legend : B
Inhibition
Activation
B
AKT
RSK1/2
AMPK
CDK1
IKKβ
ERK1/2
GSK3
TSC1
TSC2

Figure 2

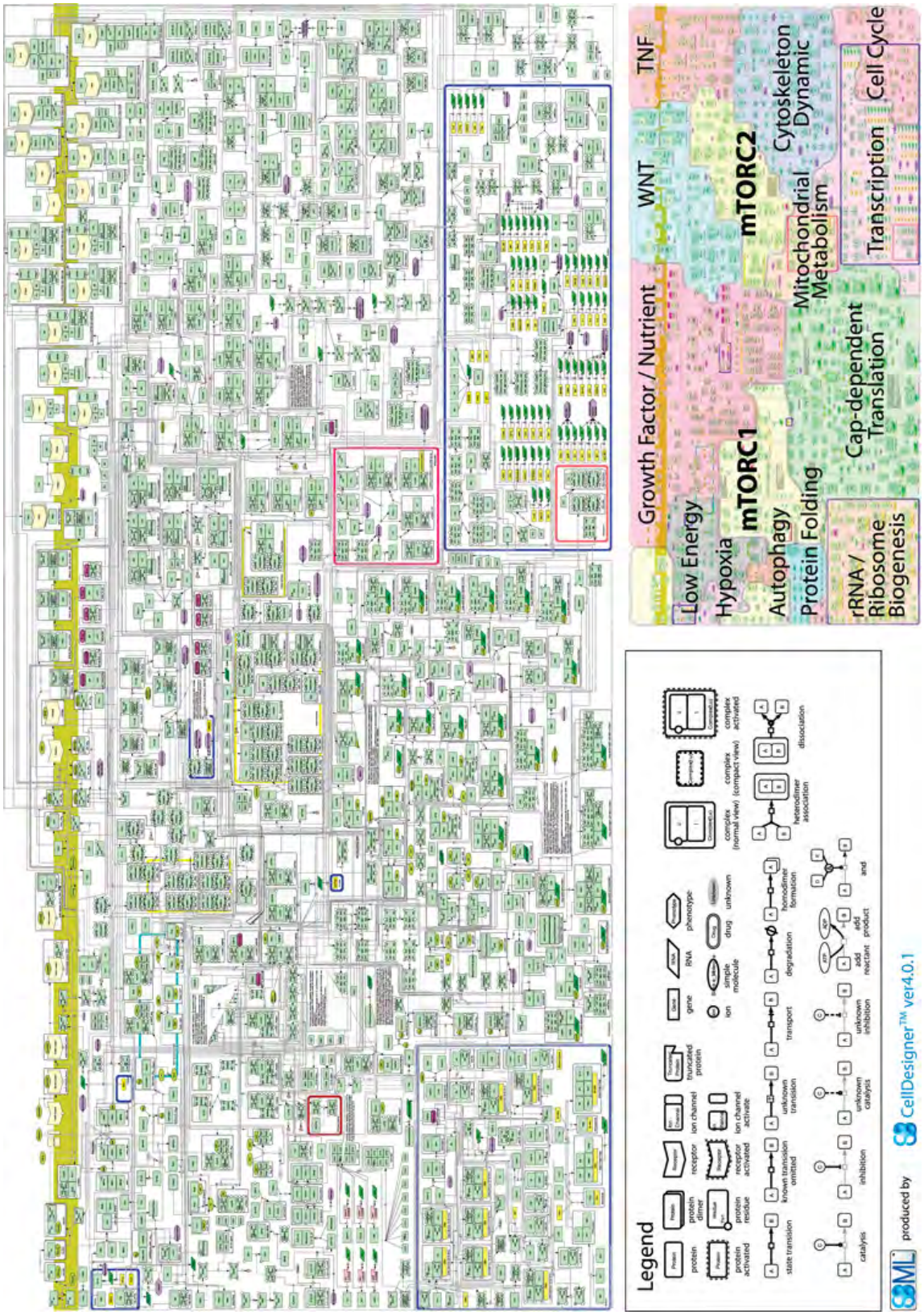
Growth Factor / Nutrient
WNT
TNF
Low Energy
Hypoxia
mTORC1
mTORC2
Autophagy
Protein Folding
Mitochondrial Metabolism
Cytoskeleton Dynamic
Cap-dependent Translation
Transcription
Cell Cycle
rRNA / Ribosome Biogenesis
Legend
produced by
CellDesigner™ ver4.0.1

Figure 3

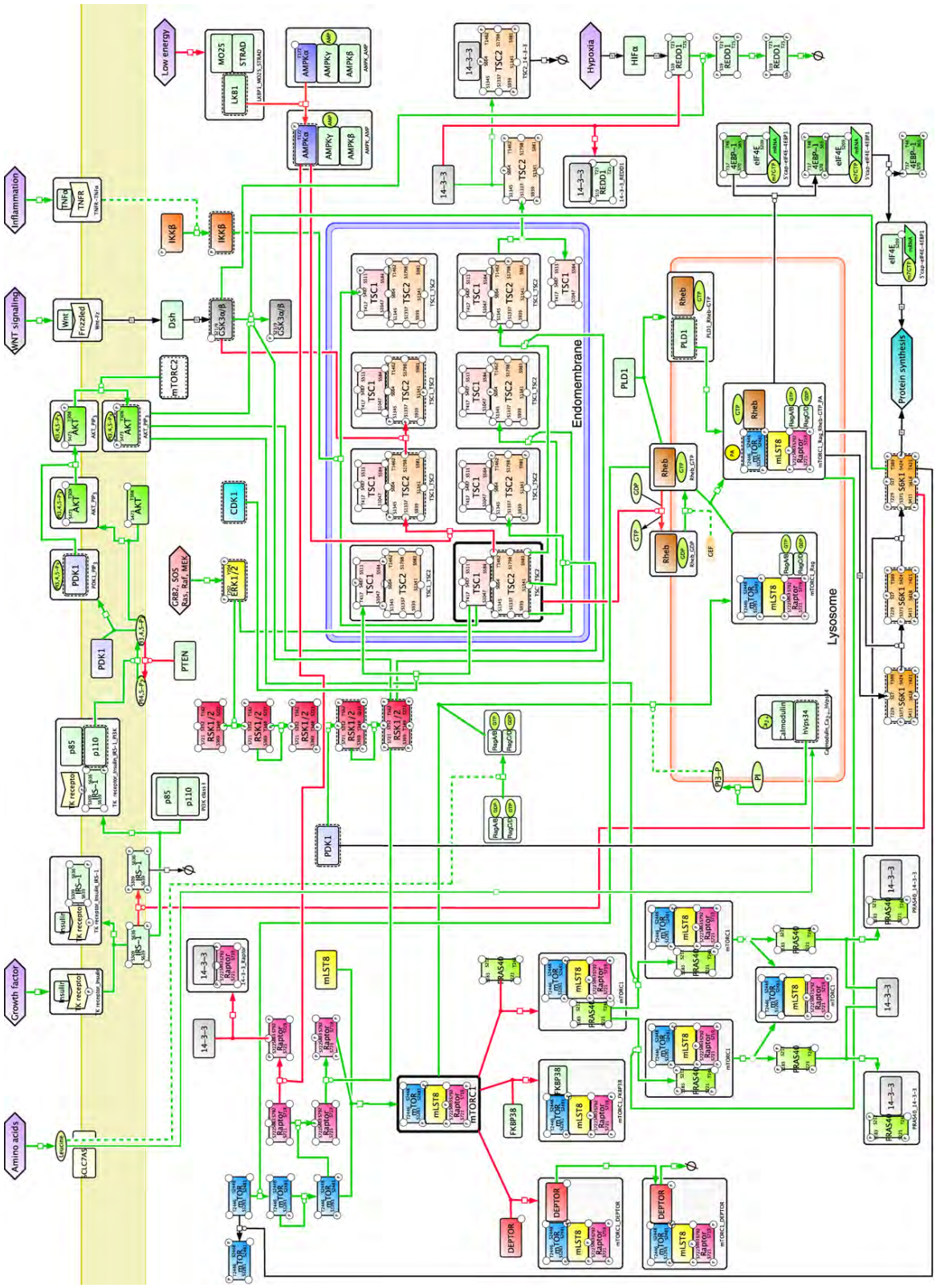
Low energy
MO25
STRAD
LKB1
AMPK
AMPKα
AMPKγ
AMPKβ
Hypoxia
HIF1α
REDD1
14-3-3
TSC2
Inflammation
TNFα
TNFR
IKKβ
WNT signaling
Wnt
Frizzled
Dsh
GSK3α/β
mTORC2
AKT
PDK1
PTEN
CDK1
GRB2, SOS
Ras, Raf, MEK
ERK1/2
RSK1/2
p85
p110
IRS-1
TK receptor
Insulin
Growth factor
Amino acids
SLC7A5
TSC1
Endomembrane
Lysosome
Rheb
PLD1
Protein synthesis
4EBP-1
eIF4E
S6K1
mLST8
Raptor
mTORC1
FKBP38
DEPTOR
RagA/B
RagC/D
Ragulator
Calmodulin
Vps34
PI3-4
PRAS40
14-3-3

Figure 4

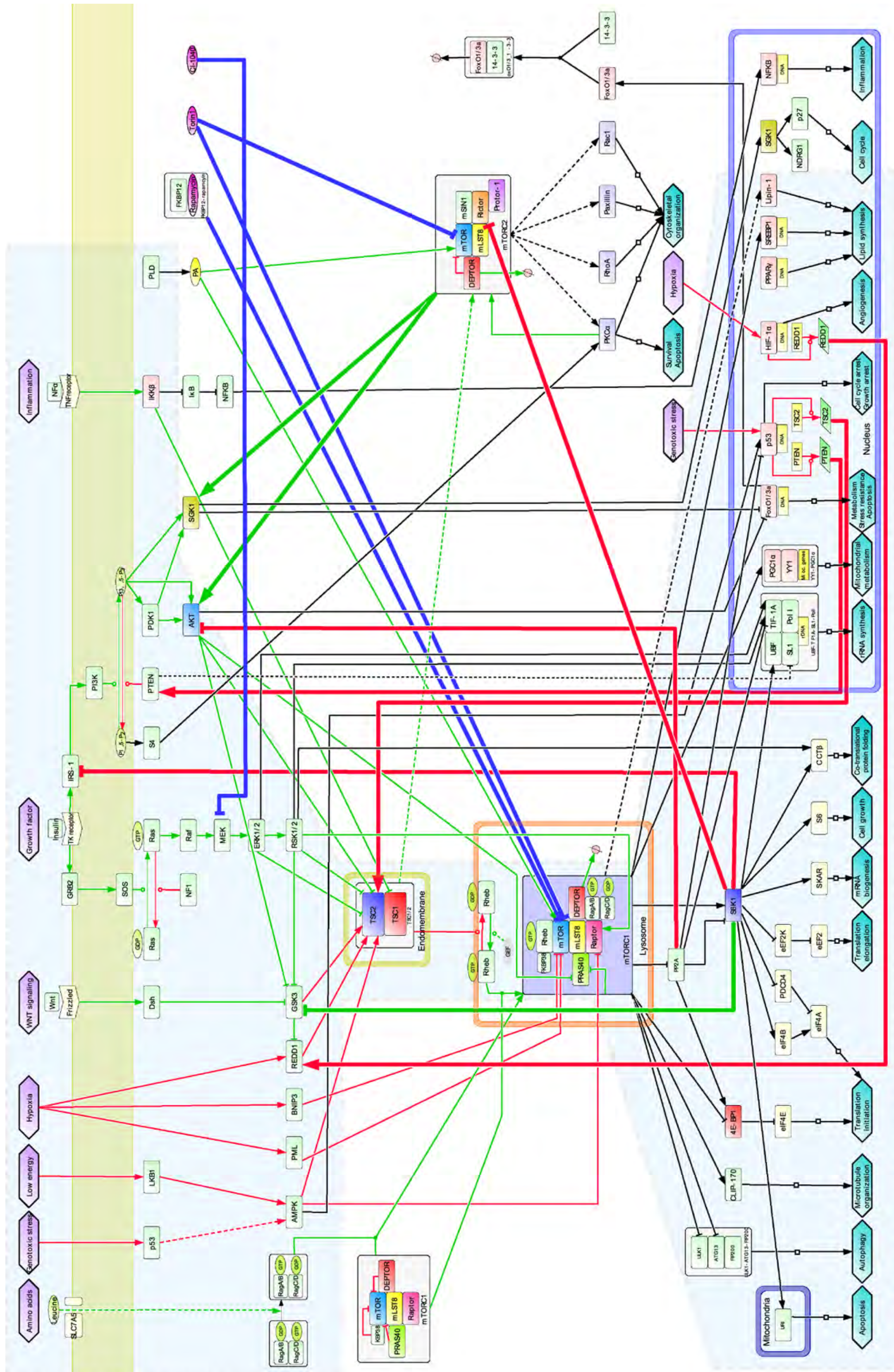
Inflammation
Growth factor
WNT signaling
Hypoxia
Low energy
Genotoxic stress
Amino acids
Insulin
TK receptor
Wnt
Frizzled
IRS-1
PI3K
PDK1
AKT
SGK1
PTEN
PLD
PA
GRB2
SOS
Ras
Raf
MEK
ERK1/2
RSK1/2
NF1
Dsh
GSK3
REDD1
BNIP3
PML
LKB1
AMPK
p53
IKKβ
IκB
NFKB
FKBP12
Rapamycin
Torin1
mTORC2
mTOR
mSIN1
mLST8
Rictor
DEPTOR
Protor-1
Rac1
Paxillin
RhoA
PKCα
Cytoskeletal organization
Survival Apoptosis
TSC2
TSC1
Endomembrane
Rheb
mTORC1
Raptor
PRAS40
Lysosome
S6K1
PP2A
eEF2K
eEF2
PDCD4
eIF4B
eIF4A
4E-BP1
eIF4E
CLIP-170
SKAR
S6
CCTβ
Translation elongation
Translation initiation
mRNA biogenesis
Cell growth
Co-translational protein folding
Microtubule organization
Autophagy
Apoptosis
Mitochondria
Nucleus
FoxO1/3a
14-3-3
HIF-1α
PPARγ
SREBP1
Lipin-1
NDRG1
p27
Angiogenesis
Lipid synthesis
Cell cycle
Cell cycle arrest Growth arrest
Metabolism Stress resistance Apoptosis
Mitochondrial metabolism
RNA synthesis
PGC1α
YY1
TIF-1A
Pol I
UBF
SL1

320

Supplementary Figure 1

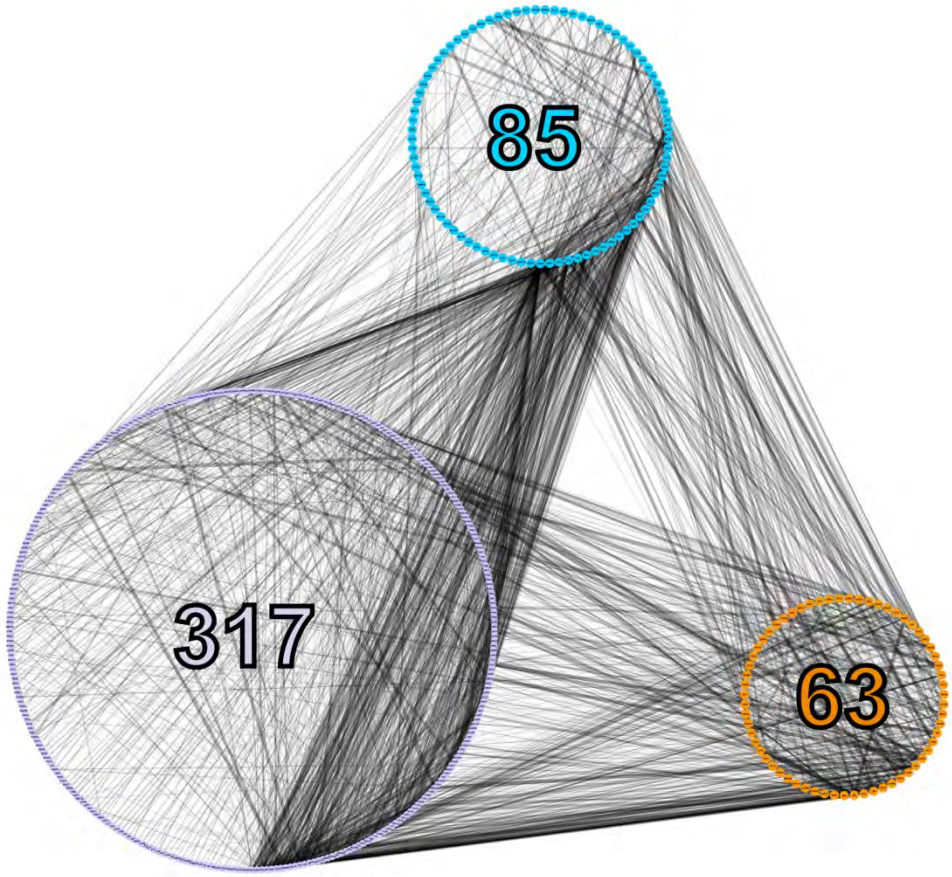

Supplementary Figure 2

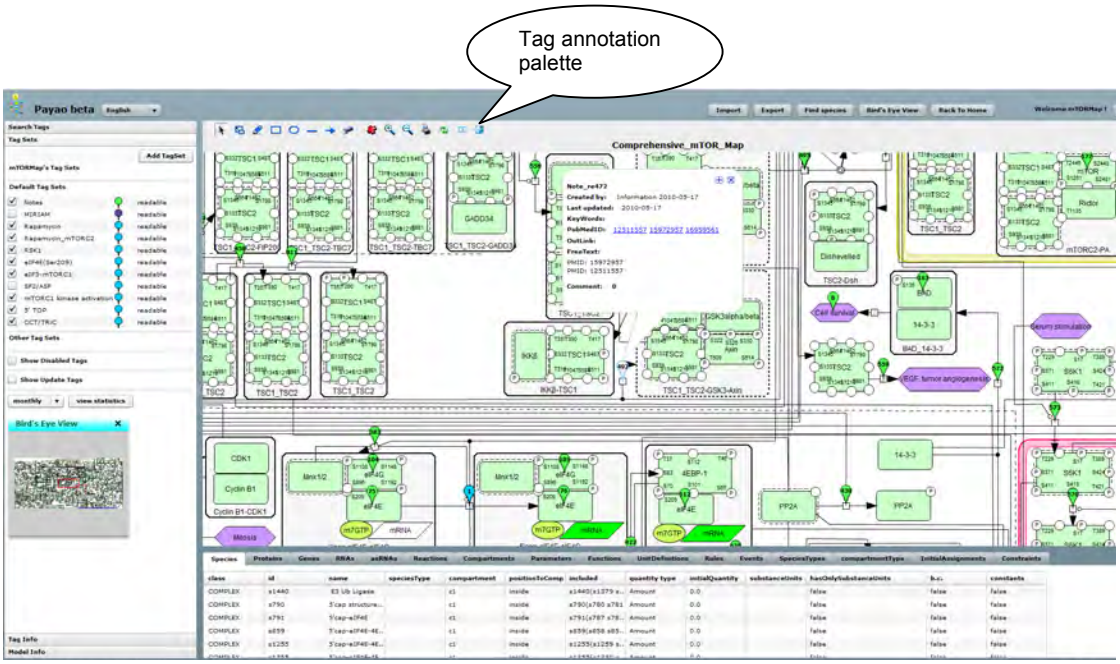

Supplementary Figure 3, 4, 5: see the online version at

http://www.nature.com/msb/journal/v6/n1/suppinfo/msb2010108_S1.html

Supplementary Table 1

List of protein names used in the mTOR map and the corresponding Gene ID and official gene symbols.

Cell designer name	Gene ID (homo sapiens)	Gene symbol
14-3-3_beta	7529	YWHAB
4EBP-1	1978	EIF4EBP1
ABL	25	ABL1
Actin	60	ACTB
AKT	207	AKT1
alpha-4	3476	IGBP1
AMPK_alpha	5562	PRKAA1
AMPK_beta	5564	PRKAB1
AMPK_gamma	53632	PRKAG3
APC	324	APC
ATG13	9776	KIAA0652
ATM	472	ATM
ATR	545	ATR
Axin	8312	AXIN1
BAD	572	BAD
Bdp1	55814	BDP1
beta_Catenin	1499	CTNNB1
beta_TrCP	8945	BTRC
Bnip3	664	BNIP3
Brf1	2972	BRF1
Calmodulin	801	CALM1
CaMKK_beta	10645	CAMKK2
CBP	1387	CREBBP
CBP20	22916	NCBP2
CBP80	4686	NCBP1
CCT_alpha	6950	TCP1
CCT_beta	10576	CCT2
CCT_delta	10575	CCT4
CCT_epsilon	22948	CCT5
CCT_eta	10574	CCT7
CCT_gamma	7203	CCT3
CCT_theta	10694	CCT8
CCT_zeta	908	CCT6A
cdc2	983	CDC2
cdc20	991	CDC20
Cdc42	998	CDC42
CDK1	983	CDC2
CDK2	1017	CDK2
Cdk2	1017	CDK2
Cdk4	1019	CDK4
CDK6	1021	CDK6
CK1	1454	CSNK1E
CK2	1459	CSNK2A2
CKII	1457	CSNK2A1

CKS1B	1163	CKS1B
CLIP-170	6249	CLIP1
CRKII	1398	CRK
CRM1	7514	XPO1
CUL1	8454	CUL1
CUL4	26094	DCAF4
CUL4A	8451	CUL4A
CUL7	9820	CUL7
Cyclin A	890	CCNA2
Cyclin B1	891	CCNB1
Cyclin D1	595	CCND1
Cyclin E	898	CCNE1
DDB1	1642	DDB1
DEPTOR	64798	DEPDC6
DGK_zeta	8525	DGKZ
Dishevelled	1855	DVL1
DOCK180	1793	DOCK1
DOCK7	85440	DOCK7
DYRK	1859	DYRK1A
eEF1A	1917	EEF1A2
eEF1B_gamma	644820	EEF1B4
eEF2	1938	EEF2
eEF2K	29904	EEF2K
eIF1B_beta	10289	EIF1B
eIF2_alpha	1965	EIF2S1
eIF2_beta	8894	EIF2S2
eIF2_gamma	1968	EIF2S3
eIF2B_epsilon	8893	EIF2B5
eIF3	8661	EIF3A
eIF4A	1973	EIF4A1
eIF4B	1975	EIF4B
eIF4E	1977	EIF4E
eIF4G	1981	EIF4G1
ELMO	9844	ELMO1
ERK1/2	5595	MAPK3
ERK1/2	5594	MAPK1
FADD	8772	FADD
FAK	5747	PTK2
FBW5	54461	FBXW5
FBW8	26259	FBXW8
FBXW7	55294	FBXW7
FIP200	9821	RB1CC1
FKBP12	2280	FKBP1A
FKBP38	23770	FKBP8
FoxO1/3a	2308	FOXO1
FoxO1/3a	2309	FOXO3
G_alpha	2771	GNAI2
G_beta	2782	GNB1
G_gamma	2792	GNGT1
GADD34	23645	PPP1R15A

GIT1/2	28964	GIT1
GIT1/2	9815	GIT2
GOLPH3	606496	GOLPH3
GSK3alpha/beta	2931	GSK3A
GSK3alpha/beta	2932	GSK3B
HDAC1	3065	HDAC1
HIF-1_alpha	3091	HIF1A
HSP70	3308	HSPA4
HSP90	3320	HSP90AA1
hVps34	5289	PIK3C3
I_kappa_B_alpha_	4792	NFKBIA
IKK_alpha	1147	CHUK
IKK_beta	3551	IKBKB
IKK_gamma_/NEMO	8517	IKBKG
Insulin receptor	3643	INSR
IRS-1	3667	IRS1
JNK	5599	MAPK8
KIS	127933	UHMK1
KPC1	63891	RNF123
LEF	51176	LEF1
Lipin-1	23175	LPIN1
LKB1	6794	STK11
LPAAT_beta	10555	AGPAT2
LRP5/6	4041	LRP5
LRP5/6	4040	LRP6
MAP4K3	8491	MAP4K3
Mdm2	4193	MDM2
MEK	5604	MAP2K1
MEKK2	10746	MAP3K2
MEKK3	4215	MAP3K3
MK2	9261	MAPKAPK2
mLST8	64223	MLST8
Mnk1/2	2872	MKNK2
Mnk1/2	27250	PDCD4
MO25	51719	CAB39
mTOR	2475	MTOR
Myc	4609	MYC
NCK	4690	NCK1
NDRG1	10397	NDRG1
Nedd4-2	23327	NEDD4L
NF-Y	4800	NFYA
p110	5290	PIK3CA
p120RasGAP	5921	RASA1
p130	5934	RBL2
p190RhoGAP	2909	GRLF1
p27	1027	CDKN1B
p38	1432	MAPK14
p50 (NF_kappa_B)	4790	NFKB1
p53	7157	TP53
p65(NF_kappa_B)	5970	RELA

p73	7161	TP73
p85	5296	PIK3R2
PABP	26986	PABPC1
PAK	5058	PAK1
Pak2	5062	PAK2
PAM-E3 Ligase	23077	MYCBP2
Paxillin	5829	PXN
PCK_delta	5580	PRKCD
PDCD4	27250	PDCD4
PDGFR_beta	5159	PDGFRB
PDK1	5163	PDK1
PGC-1_alpha	10891	PPARGC1A
PHLPP	23239	PHLPP1
PIX	8874	ARHGEF7
PKC_alpha	5578	PRKCA
PLD1	5337	PLD1
Plk1	5347	PLK1
PML	5371	PML
Pol I	84172	POLR1B
Pol III	10621	POLR3F
PP1/2A	5499	PPP1CA
PP1/2A	5524	PPP2R4
PP1_gamma_	5501	PPP1CC
PP2A	5524	PPP2R4
PPAR_gamma	5468	PPARG
PPR5	55615	PRR5
PPR5L	79899	PRR5L
PRAS40	84335	AKT1S1
PTEN	11191	PTENP1
PTP-PEST	5782	PTPN12
Rac	9459	ARHGEF6
RagA	10670	RRAGA
RagB	10325	RRAGB
RagC	64121	RRAGC
RagD	58528	RRAGD
Raptor	57521	RPTOR
Rb	5925	RB1
RBX1	9978	RBX1
REDD1	54541	DDIT4
Rheb	6009	RHEB
RhebL1	121268	RHEBL1
Rho A	387	RHOA
Rictor	253260	RICTOR
RIP1	8737	RIPK1
ROC1	9978	RBX1
rpS6/40S subunit	6194	RPS6
RSK1/2	6197	RPS6KA3
RSK1/2	6195	RPS6KA1
S4	6385	SDC4
S6K1	6198	RPS6KB1

S6K2	6199	RPS6KB2
SAPK4/p38	5603	MAPK13
SF2/ASF	6426	SFRS1
SGK1	6446	SGK1
SHP-2	5781	PTPN11
Sin1.1	79109	MAPKAP1
SKAR	84271	POLDIP3
SKP1	6500	SKP1
SKP2	6502	SKP2
SOCS-1	8651	SOCS1
SOCS-2	8835	SOCS2
Sp1	6667	SP1
Src	6714	SRC
SREBP	6720	SREBF1
Stat3	6774	STAT3
STRAD	92335	STRADA
TAF1	6872	TAF1
TAK1	6885	MAP3K7
TBC7	51256	TBC1D7
TBP	6908	TBP
TCF	6932	TCF7
TCTP	7178	TPT1
Tel2	51513	ETV7
TFIIIA	2971	GTF3A
TFIIIC	2975	GTF3C1
TIF-1A	9015	TAF1A
TIF-1B/SL1	9014	TAF1B
TNF_alpha	7124	TNF
TNFR	7132	TNFRSF1A
TRADD	8717	TRADD
TRAF2/5	7186	TRAF2
TRAF2/5	7188	TRAF5
TSC1	7248	TSC1
TSC2	7249	TSC2
Tubulin	27175	TUBG2
Ubc13	7334	UBE2N
UBF	7343	UBTF
Uev1A	7335	UBE2V1
ULK1/2	9706	ULK2
ULK1/2	8408	ULK1
URI	8725	C19orf2
Vav	7409	VAV1
VHL	7428	VHL
Wnt	7471	WNT1
YY1	7528	YY1
Frizzled	-	Frizzled family
GRB2	2885	GRB2
NF1	4763	NF1
Raf	5894	RAF1
Ras	-	Ras family

SL1	9015	TAF1A
SLC7A4	6545	SLC7A4
SOS	6654	SOS1

Supplementary Table 2

Comparison between the mTOR map and other pathway and PPI databases. To evaluate the degree of overlap and the coverage of the mTOR map relative to other databases, we queried major pathway and PPI databases with the term "mTOR" and visualized the retrieved pathways.

Pathway and PPI database	Web link	Number of components	Components depicted in the mTOR map	Coverage relative to the mTOR map
Reactome	http://www.reactome.org	19	89% (17/19)	7%
KEGG	http://www.genome.jp/kegg/pathway.html	28	93% (26/28)	11%
WikiPathways	http://www.wikipathways.org	34	82% (28/34)	12%
NCI/Nature Pathway Interaction Database (PID)	http://pid.nci.nih.gov	39	97% (38/39)	16%
Nature Signaling Gateways	http://www.signaling-gateway.org/	16	100% (16/16)	7%
Biocarta	http://www.biocarta.com	21	95% (20/21)	8%

5.12 Datasets

SBML-format file 1. A comprehensive map of the mTOR signaling network

SBML-format file 1. A comprehensive map of the mTOR signaling network -Download xml (4.44MB)

SBML-format file 2. Upstream regulators of mTORC1 signaling

SBML-format file 2. Upstream regulators of mTORC1 signaling -Download xml (482KB)

SBML-format file 3. Activity flow of the mTOR signaling network

SBML-format file 3. Activity flow of the mTOR signaling network -Download xml (384KB)

Cytoscape format file

The Cytoscape session file includes 2 networks: 1) APID 1 evidence: proteins are associated to mTOR components by 1 or more distinct experimental evidence 2) APID 3 evidences: proteins are associated to mTOR components by 3 or more distinct experimental evidences

Cytoscape format file -Download Zip file (1.06MB)

5.13 Supplementary References for the mTOR network map

Abe Y, Yoon SO, Kubota K, Mendoza MC, Gygi SP, Blenis J (2009) p90 ribosomal S6 kinase and p70 ribosomal S6 kinase link phosphorylation of the eukaryotic chaperonin containing TCP-1 to growth factor, insulin, and nutrient signaling. *J Biol Chem* **284:** 14939-14948.

Acosta-Jaquez HA, Keller JA, Foster KG, Ekim B, Soliman GA, Feener EP, Ballif BA, Fingar DC (2009) Site-specific mTOR phosphorylation promotes mTORC1-mediated signaling and cell growth. *Mol Cell Biol* **29:** 4308-4324.

Albers MW, Williams RT, Brown EJ, Tanaka A, Hall FL, Schreiber SL (1993) FKBP-rapamycin inhibits a cyclin-dependent kinase activity and a cyclin D1-Cdk association in early G1 of an osteosarcoma cell line. *J Biol Chem* **268:** 22825-22829.

Alessi DR, Andjelkovic M, Caudwell B, Cron P, Morrice N, Cohen P, Hemmings BA (1996) Mechanism of activation of protein kinase B by insulin and IGF-1. *Embo J* **15:** 6541-6551.

Alessi DR, Deak M, Casamayor A, Caudwell FB, Morrice N, Norman DG, Gaffney P, Reese CB, MacDougall CN, Harbison D, Ashworth A, Bownes M (1997a) 3-Phosphoinositide-dependent protein kinase-1 (PDK1): structural and functional homology with the Drosophila DSTPK61 kinase. *Curr Biol* **7:** 776-789.

Alessi DR, James SR, Downes CP, Holmes AB, Gaffney PR, Reese CB, Cohen P (1997b) Characterization of a 3-phosphoinositide-dependent protein kinase which phosphorylates and activates protein kinase Balpha. *Curr Biol* **7:** 261-269.

Andjelkovic M, Jakubowicz T, Cron P, Ming XF, Han JW, Hemmings BA (1996) Activation and phosphorylation of a pleckstrin homology domain containing protein kinase (RAC-PK/PKB) promoted by serum and protein phosphatase inhibitors. *Proc Natl Acad Sci U S A* **93:** 5699-5704.

Angers S, Moon RT (2009) Proximal events in Wnt signal transduction. *Nat Rev Mol Cell Biol* **10:** 468-477.

Anjum R, Roux PP, Ballif BA, Gygi SP, Blenis J (2005) The tumor suppressor DAP kinase is a target of RSK-mediated survival signaling. *Curr Biol* **15:** 1762-1767.

Astrinidis A, Senapedis W, Coleman TR, Henske EP (2003) Cell cycle-regulated phosphorylation of hamartin, the product of the tuberous sclerosis complex 1 gene, by cyclin-dependent kinase 1/cyclin B. *J Biol Chem* **278:** 51372-51379.

Astrinidis A, Senapedis W, Henske EP (2006) Hamartin, the tuberous sclerosis complex 1 gene product, interacts with polo-like kinase 1 in a phosphorylation-dependent manner. *Hum Mol Genet* **15:** 287-297.

Avila-Flores A, Santos T, Rincon E, Merida I (2005) Modulation of the mammalian target of rapamycin pathway by diacylglycerol kinase-produced phosphatidic acid. *J Biol Chem* **280:** 10091-10099.

Avruch J, Long X, Lin Y, Ortiz-Vega S, Rapley J, Papageorgiou A, Oshiro N, Kikkawa U (2009a) Activation of mTORC1 in two steps: Rheb-GTP activation of catalytic function and increased binding of substrates to raptor. *Biochem Soc Trans* **37:** 223-226.

Avruch J, Long X, Ortiz-Vega S, Rapley J, Papageorgiou A, Dai N (2009b) Amino acid regulation of TOR complex 1. *Am J Physiol Endocrinol Metab* **296:** E592-602.

Bai X, Ma D, Liu A, Shen X, Wang QJ, Liu Y, Jiang Y (2007) Rheb activates mTOR by antagonizing its endogenous inhibitor, FKBP38. *Science* **318:** 977-980.

Balciunaite G, Keller MP, Balciunaite E, Piali L, Zuklys S, Mathieu YD, Gill J, Boyd R, Sussman DJ, Hollander GA (2002) Wnt glycoproteins regulate the expression of FoxN1, the gene defective in nude mice. *Nat Immunol* **3:** 1102-1108.

Balendran A, Biondi RM, Cheung PC, Casamayor A, Deak M, Alessi DR (2000a) A 3-phosphoinositide-dependent protein kinase-1 (PDK1) docking site is required for the phosphorylation of protein kinase Czeta (PKCzeta) and PKC-related kinase 2 by PDK1. *J Biol Chem* **275:** 20806-20813.

Balendran A, Hare GR, Kieloch A, Williams MR, Alessi DR (2000b) Further evidence that 3-phosphoinositide-dependent protein kinase-1 (PDK1) is required for the stability and phosphorylation of protein kinase C (PKC) isoforms. *FEBS Lett* **484:** 217-223.

Bellis SL, Miller JT, Turner CE (1995) Characterization of tyrosine phosphorylation of paxillin in vitro by focal adhesion kinase. *J Biol Chem* **270:** 17437-17441.

Beretta L, Gingras AC, Svitkin YV, Hall MN, Sonenberg N (1996) Rapamycin blocks the phosphorylation of 4E-BP1 and inhibits cap-dependent initiation of translation. *Embo J* **15:** 658-664.

Bernardi R, Guernah I, Jin D, Grisendi S, Alimonti A, Teruya-Feldstein J, Cordon-Cardo C, Simon MC, Rafii S, Pandolfi PP (2006) PML inhibits HIF-1alpha translation and neoangiogenesis through repression of mTOR. *Nature* **442:** 779-785.

Bhanot P, Brink M, Samos CH, Hsieh JC, Wang Y, Macke JP, Andrew D, Nathans J, Nusse R (1996) A new member of the frizzled family from Drosophila functions as a Wingless receptor. *Nature* **382:** 225-230.

Bilic J, Huang YL, Davidson G, Zimmermann T, Cruciat CM, Bienz M, Niehrs C (2007) Wnt induces LRP6 signalosomes and promotes dishevelled-dependent LRP6 phosphorylation. *Science* **316:** 1619-1622.

Biondi RM, Kieloch A, Currie RA, Deak M, Alessi DR (2001) The PIF-binding pocket in PDK1 is essential for activation of S6K and SGK, but not PKB. *Embo J* **20:** 4380-4390.

Birge RB, Fajardo JE, Reichman C, Shoelson SE, Songyang Z, Cantley LC, Hanafusa H (1993) Identification and characterization of a high-affinity interaction between v-Crk and tyrosine-phosphorylated paxillin in CT10-transformed fibroblasts. *Mol Cell Biol* **13:** 4648-4656.

Blank JL, Gerwins P, Elliott EM, Sather S, Johnson GL (1996) Molecular cloning of mitogen-activated protein/ERK kinase kinases (MEKK) 2 and 3. Regulation of sequential phosphorylation pathways involving mitogen-activated protein kinase and c-Jun kinase. *J Biol Chem* **271:** 5361-5368.

Blonska M, You Y, Geleziunas R, Lin X (2004) Restoration of NF-kappaB activation by tumor necrosis factor alpha receptor complex-targeted MEKK3 in receptor-interacting protein-deficient cells. *Mol Cell Biol* **24:** 10757-10765.

Boehm M, Yoshimoto T, Crook MF, Nallamshetty S, True A, Nabel GJ, Nabel EG (2002) A growth factor-dependent nuclear kinase phosphorylates p27(Kip1) and regulates cell cycle progression. *Embo J* **21:** 3390-3401.

Bokoch GM (2003) Biology of the p21-activated kinases. *Annu Rev Biochem* **72:** 743-781.

Bonni A, Brunet A, West AE, Datta SR, Takasu MA, Greenberg ME (1999) Cell survival promoted by the Ras-MAPK signaling pathway by transcription-dependent and -independent mechanisms. *Science* **286:** 1358-1362.

Boudeau J, Baas AF, Deak M, Morrice NA, Kieloch A, Schutkowski M, Prescott AR, Clevers HC, Alessi DR (2003) MO25alpha/beta interact with STRADalpha/beta enhancing their ability to bind, activate and localize LKB1 in the cytoplasm. *Embo J* **22:** 5102-5114.

Brickley DR, Mikosz CA, Hagan CR, Conzen SD (2002) Ubiquitin modification of serum and glucocorticoid-induced protein kinase-1 (SGK-1). *J Biol Chem* **277:** 43064-43070.

Brown MC, Cary LA, Jamieson JS, Cooper JA, Turner CE (2005) Src and FAK kinases cooperate to phosphorylate paxillin kinase linker, stimulate its focal adhesion localization, and regulate cell spreading and protrusiveness. *Mol Biol Cell* **16:** 4316-4328.

Brown MC, Turner CE (2004) Paxillin: adapting to change. *Physiol Rev* **84:** 1315-1339.

Browne GJ, Finn SG, Proud CG (2004a) Stimulation of the AMP-activated protein kinase leads to activation of eukaryotic elongation factor 2 kinase and to its phosphorylation at a novel site, serine 398. *J Biol Chem* **279:** 12220-12231.

Browne GJ, Proud CG (2004b) A novel mTOR-regulated phosphorylation site in elongation factor 2 kinase modulates the activity of the kinase and its binding to calmodulin. *Mol Cell Biol* **24:** 2986-2997.

Brugarolas J, Lei K, Hurley RL, Manning BD, Reiling JH, Hafen E, Witters LA, Ellisen LW, Kaelin WG, Jr. (2004) Regulation of mTOR function in response to hypoxia by REDD1 and the TSC1/TSC2 tumor suppressor complex. *Genes Dev* **18:** 2893-2904.

Brugnera E, Haney L, Grimsley C, Lu M, Walk SF, Tosello-Trampont AC, Macara IG, Madhani H, Fink GR, Ravichandran KS (2002) Unconventional Rac-GEF activity is mediated through the Dock180-ELMO complex. *Nat Cell Biol* **4:** 574-582.

Bruick RK (2000) Expression of the gene encoding the proapoptotic Nip3 protein is induced by hypoxia. *Proc Natl Acad Sci U S A* **97:** 9082-9087.

Brunet A, Bonni A, Zigmond MJ, Lin MZ, Juo P, Hu LS, Anderson MJ, Arden KC, Blenis J, Greenberg ME (1999) Akt promotes cell survival by phosphorylating and inhibiting a Forkhead transcription factor. *Cell* **96:** 857-868.

Brunet A, Park J, Tran H, Hu LS, Hemmings BA, Greenberg ME (2001) Protein kinase SGK mediates survival signals by phosphorylating the forkhead transcription factor FKHRL1 (FOXO3a). *Mol Cell Biol* **21:** 952-965.

Bruning JC, Gillette JA, Zhao Y, Bjorbaeck C, Kotzka J, Knebel B, Avci H, Hanstein B, Lingohr P, Moller DE, Krone W, Kahn CR, Muller-Wieland D (2000) Ribosomal subunit kinase-2 is required for growth factor-stimulated transcription of the c-Fos gene. *Proc Natl Acad Sci U S A* **97:** 2462-2467.

Bryant SS, Briggs S, Smithgall TE, Martin GA, McCormick F, Chang JH, Parsons SJ, Jove R (1995) Two SH2 domains of p120 Ras GTPase-activating protein bind synergistically to tyrosine phosphorylated p190 Rho GTPase-activating protein. *J Biol Chem* **270:** 17947-17952.

Budde A, Grummt I (1999) p53 represses ribosomal gene transcription. *Oncogene* **18:** 1119-1124.

Busch S, Renaud SJ, Schleussner E, Graham CH, Markert UR (2009) mTOR mediates human trophoblast invasion through regulation of matrix-remodeling enzymes and is associated with serine phosphorylation of STAT3. *Exp Cell Res* **315:** 1724-1733.

Buse P, Tran SH, Luther E, Phu PT, Aponte GW, Firestone GL (1999) Cell cycle and hormonal control of nuclear-cytoplasmic localization of the serum- and glucocorticoid-inducible protein kinase, Sgk, in mammary tumor cells. A novel convergence point of anti-proliferative and proliferative cell signaling pathways. *J Biol Chem* **274:** 7253-7263.

Byfield MP, Murray JT, Backer JM (2005) hVps34 is a nutrient-regulated lipid kinase required for activation of p70 S6 kinase. *J Biol Chem* **280:** 33076-33082.

Cai SL, Tee AR, Short JD, Bergeron JM, Kim J, Shen J, Guo R, Johnson CL, Kiguchi K, Walker CL (2006) Activity of TSC2 is inhibited by AKT-mediated phosphorylation and membrane partitioning. *J Cell Biol* **173:** 279-289.

Calnan DR, Brunet A (2008) The FoxO code. *Oncogene* **27:** 2276-2288.
Camasses A, Bogdanova A, Shevchenko A, Zachariae W (2003) The CCT chaperonin promotes activation of the anaphase-promoting complex through the generation of functional Cdc20. *Mol Cell* **12:** 87-100.

Carlberg U, Nilsson A, Nygard O (1990) Functional properties of phosphorylated elongation factor 2. *Eur J Biochem* **191:** 639-645.

Carriere A, Cargnello M, Julien LA, Gao H, Bonneil E, Thibault P, Roux PP (2008a) Oncogenic MAPK signaling stimulates mTORC1 activity by promoting RSK-mediated raptor phosphorylation. *Curr Biol* **18:** 1269-1277.

Carriere A, Ray H, Blenis J, Roux PP (2008b) The RSK factors of activating the Ras/MAPK signaling cascade. *Front Biosci* **13:** 4258-4275.

Catania MG, Mischel PS, Vinters HV (2001) Hamartin and tuberin interaction with the G2/M cyclin-dependent kinase CDK1 and its regulatory cyclins A and B. *J Neuropathol Exp Neurol* **60:** 711-723.

Cavanaugh AH, Hempel WM, Taylor LJ, Rogalsky V, Todorov G, Rothblum LI (1995) Activity of RNA polymerase I transcription factor UBF blocked by Rb gene product. *Nature* **374:** 177-180.

Cavet ME, Lehoux S, Berk BC (2003) 14-3-3beta is a p90 ribosomal S6 kinase (RSK) isoform 1-binding protein that negatively regulates RSK kinase activity. *J Biol Chem* **278:** 18376-18383.

Chang M, Lingner J (2008) Cell signaling. Tel2 finally tells one story. *Science* **320:** 60-61.

Chen RH, Abate C, Blenis J (1993) Phosphorylation of the c-Fos transrepression domain by mitogen-activated protein kinase and 90-kDa ribosomal S6 kinase. *Proc Natl Acad Sci U S A* **90:** 10952-10956.

Chen RH, Sarnecki C, Blenis J (1992) Nuclear localization and regulation of erk- and rsk-encoded protein kinases. *Mol Cell Biol* **12:** 915-927.

Chen ZJ (2005) Ubiquitin signaling in the NF-kappaB pathway. *Nat Cell Biol* **7:** 758-765.

Cheng G, Feng Z, He B (2005a) Herpes simplex virus 1 infection activates the endoplasmic reticulum resident kinase PERK and mediates eIF-2alpha dephosphorylation by the gamma(1)34.5 protein. *J Virol* **79:** 1379-1388.

Cheng J, Yang J, Xia Y, Karin M, Su B (2000) Synergistic interaction of MEK kinase 2, c-Jun N-terminal kinase (JNK) kinase 2, and JNK1 results in efficient and specific JNK1 activation. *Mol Cell Biol* **20:** 2334-2342.

Cheng J, Zhang D, Kim K, Zhao Y, Zhao Y, Su B (2005b) Mip1, an MEKK2-interacting protein, controls MEKK2 dimerization and activation. *Mol Cell Biol* **25:** 5955-5964.

Cheng SW, Fryer LG, Carling D, Shepherd PR (2004) Thr2446 is a novel mammalian target of rapamycin (mTOR) phosphorylation site regulated by nutrient status. *J Biol Chem* **279:** 15719-15722.

Chiang GG, Abraham RT (2005) Phosphorylation of mammalian target of rapamycin (mTOR) at Ser-2448 is mediated by p70S6 kinase. *J Biol Chem* **280:** 25485-25490.

Choi JH, Bertram PG, Drenan R, Carvalho J, Zhou HH, Zheng XF (2002) The FKBP12-rapamycin-associated protein (FRAP) is a CLIP-170 kinase. *EMBO Rep* **3:** 988-994.

Choo AY, Roux PP, Blenis J (2006) Mind the GAP: Wnt steps onto the mTORC1 train. *Cell* **126:** 834-836.

Chou MM, Blenis J (1996) The 70 kDa S6 kinase complexes with and is activated by the Rho family G proteins Cdc42 and Rac1. *Cell* **85:** 573-583.

Chou MM, Hou W, Johnson J, Graham LK, Lee MH, Chen CS, Newton AC, Schaffhausen BS, Toker A (1998) Regulation of protein kinase C zeta by PI 3-kinase and PDK-1. *Curr Biol* **8:** 1069-1077.

Chu I, Sun J, Arnaout A, Kahn H, Hanna W, Narod S, Sun P, Tan CK, Hengst L, Slingerland J (2007) p27 phosphorylation by Src regulates inhibition of cyclin E-Cdk2. *Cell* **128:** 281-294.

Chu IM, Hengst L, Slingerland JM (2008) The Cdk inhibitor p27 in human cancer: prognostic potential and relevance to anticancer therapy. *Nat Rev Cancer* **8:** 253-267.

Ciarmatori S, Scott PH, Sutcliffe JE, McLees A, Alzuherri HM, Dannenberg JH, te Riele H, Grummt I, Voit R, White RJ (2001) Overlapping functions of the pRb family in the regulation of rRNA synthesis. *Mol Cell Biol* **21:** 5806-5814.

Cohen MS, Hadjivassiliou H, Taunton J (2007) A clickable inhibitor reveals context-dependent autoactivation of p90 RSK. *Nat Chem Biol* **3:** 156-160.

Cohen P, Frame S (2001) The renaissance of GSK3. *Nat Rev Mol Cell Biol* **2:** 769-776.

Colthurst DR, Campbell DG, Proud CG (1987) Structure and regulation of eukaryotic initiation factor eIF-2. Sequence of the site in the alpha subunit phosphorylated by the haem-controlled repressor and by the double-stranded RNA-activated inhibitor. *Eur J Biochem* **166:** 357-363.

Connor MK, Kotchetkov R, Cariou S, Resch A, Lupetti R, Beniston RG, Melchior F, Hengst L, Slingerland JM (2003) CRM1/Ran-mediated nuclear export of p27(Kip1) involves a nuclear export signal and links p27 export and proteolysis. *Mol Biol Cell* **14:** 201-213.

Coon M, Ball A, Pound J, Ap S, Hollenback D, White T, Tulinsky J, Bonham L, Morrison DK, Finney R, Singer JW (2003) Inhibition of lysophosphatidic acid acyltransferase beta disrupts proliferative and survival signals in normal cells and induces apoptosis of tumor cells. *Mol Cancer Ther* **2:** 1067-1078.

Cote JF, Turner CE, Tremblay ML (1999) Intact LIM 3 and LIM 4 domains of paxillin are required for the association to a novel polyproline region (Pro 2) of protein-tyrosine phosphatase-PEST. *J Biol Chem* **274:** 20550-20560.

Cross DA, Alessi DR, Cohen P, Andjelkovich M, Hemmings BA (1995) Inhibition of glycogen synthase kinase-3 by insulin mediated by protein kinase B. *Nature* **378:** 785-789.

Cunningham JT, Rodgers JT, Arlow DH, Vazquez F, Mootha VK, Puigserver P (2007) mTOR controls mitochondrial oxidative function through a YY1-PGC-1alpha transcriptional complex. *Nature* **450:** 736-740.

Dalby KN, Morrice N, Caudwell FB, Avruch J, Cohen P (1998) Identification of regulatory phosphorylation sites in mitogen-activated protein kinase (MAPK)-activated protein kinase-1a/p90rsk that are inducible by MAPK. *J Biol Chem* **273:** 1496-1505.

Dan HC, Sun M, Yang L, Feldman RI, Sui XM, Ou CC, Nellist M, Yeung RS, Halley DJ, Nicosia SV, Pledger WJ, Cheng JQ (2002) Phosphatidylinositol 3-kinase/Akt pathway regulates tuberous sclerosis tumor suppressor complex by phosphorylation of tuberin. *J Biol Chem* **277:** 35364-35370.

Davidson G, Wu W, Shen J, Bilic J, Fenger U, Stannek P, Glinka A, Niehrs C (2005) Casein kinase 1 gamma couples Wnt receptor activation to cytoplasmic signal transduction. *Nature* **438:** 867-872.

Davies SP, Helps NR, Cohen PT, Hardie DG (1995) 5'-AMP inhibits dephosphorylation, as well as promoting phosphorylation, of the AMP-activated protein kinase. Studies using bacterially expressed human protein phosphatase-2C alpha and native bovine protein phosphatase-2AC. *FEBS Lett* **377:** 421-425.

Davis IJ, Hazel TG, Chen RH, Blenis J, Lau LF (1993) Functional domains and phosphorylation of the orphan receptor Nur77. *Mol Endocrinol* **7:** 953-964.

Deacon K, Blank JL (1997) Characterization of the mitogen-activated protein kinase kinase 4 (MKK4)/c-Jun NH2-terminal kinase 1 and MKK3/p38 pathways regulated by MEK kinases 2 and 3. MEK kinase 3 activates MKK3 but does not cause activation of p38 kinase in vivo. *J Biol Chem* **272:** 14489-14496.

Deakin NO, Turner CE (2008) Paxillin comes of age. *J Cell Sci* **121:** 2435-2444.

Delgoffe GM, Kole TP, Cotter RJ, Powell JD (2009) Enhanced interaction between Hsp90 and raptor regulates mTOR signaling upon T cell activation. *Mol Immunol* **46:** 2694-2698.

Deng X, Mercer SE, Shah S, Ewton DZ, Friedman E (2004) The cyclin-dependent kinase inhibitor p27Kip1 is stabilized in G(0) by Mirk/dyrk1B kinase. *J Biol Chem* **279:** 22498-22504.

Dennis PB, Pullen N, Kozma SC, Thomas G (1996) The principal rapamycin-sensitive p70(s6k) phosphorylation sites, T-229 and T-389, are differentially regulated by rapamycin-insensitive kinase kinases. *Mol Cell Biol* **16:** 6242-6251.

Dennis PB, Pullen N, Pearson RB, Kozma SC, Thomas G (1998) Phosphorylation sites in the autoinhibitory domain participate in p70(s6k) activation loop phosphorylation. *J Biol Chem* **273:** 14845-14852.

Devin A, Cook A, Lin Y, Rodriguez Y, Kelliher M, Liu Z (2000) The distinct roles of TRAF2 and RIP in IKK activation by TNF-R1: TRAF2 recruits IKK to TNF-R1 while RIP mediates IKK activation. *Immunity* **12:** 419-429.

DeYoung MP, Horak P, Sofer A, Sgroi D, Ellisen LW (2008) Hypoxia regulates TSC1/2-mTOR signaling and tumor suppression through REDD1-mediated 14-3-3 shuttling. *Genes Dev* **22:** 239-251.

Dibble CC, Asara JM, Manning BD (2009) Characterization of Rictor phosphorylation sites reveals direct regulation of mTOR complex 2 by S6K1. *Mol Cell Biol* **29:** 5657-5670.

Diggle TA, Redpath NT, Heesom KJ, Denton RM (1998) Regulation of protein-synthesis elongation-factor-2 kinase by cAMP in adipocytes. *Biochem J* **336 (Pt 3):** 525-529.

Diggle TA, Subkhankulova T, Lilley KS, Shikotra N, Willis AE, Redpath NT (2001) Phosphorylation of elongation factor-2 kinase on serine 499 by cAMP-dependent protein kinase induces Ca2+/calmodulin-independent activity. *Biochem J* **353:** 621-626.

Ding VW, Chen RH, McCormick F (2000) Differential regulation of glycogen synthase kinase 3beta by insulin and Wnt signaling. *J Biol Chem* **275:** 32475-32481.

Djouder N, Metzler SC, Schmidt A, Wirbelauer C, Gstaiger M, Aebersold R, Hess D, Krek W (2007) S6K1-mediated disassembly of mitochondrial URI/PP1gamma complexes activates a negative feedback program that counters S6K1 survival signaling. *Mol Cell* **28:** 28-40.

Doble BW, Woodgett JR (2003) GSK-3: tricks of the trade for a multi-tasking kinase. *J Cell Sci* **116:** 1175-1186.

Dorrello NV, Peschiaroli A, Guardavaccaro D, Colburn NH, Sherman NE, Pagano M (2006) S6K1- and betaTRCP-mediated degradation of PDCD4 promotes protein translation and cell growth. *Science* **314:** 467-471.

Drenan RM, Liu X, Bertram PG, Zheng XF (2004) FKBP12-rapamycin-associated protein or mammalian target of rapamycin (FRAP/mTOR) localization in the endoplasmic reticulum and the Golgi apparatus. *J Biol Chem* **279:** 772-778.

DuRose JB, Scheuner D, Kaufman RJ, Rothblum LI, Niwa M (2009) Phosphorylation of eukaryotic translation initiation factor 2alpha coordinates rRNA transcription and translation inhibition during endoplasmic reticulum stress. *Mol Cell Biol* **29:** 4295-4307.
Dutil EM, Toker A, Newton AC (1998) Regulation of conventional protein kinase C isozymes by phosphoinositide-dependent kinase 1 (PDK-1). *Curr Biol* **8:** 1366-1375.

Ea CK, Deng L, Xia ZP, Pineda G, Chen ZJ (2006) Activation of IKK by TNFalpha requires site-specific ubiquitination of RIP1 and polyubiquitin binding by NEMO. *Mol Cell* **22:** 245-257.

Ellisen LW, Ramsayer KD, Johannessen CM, Yang A, Beppu H, Minda K, Oliner JD, McKeon F, Haber DA (2002) REDD1, a developmentally regulated transcriptional target of p63 and p53, links p63 to regulation of reactive oxygen species. *Mol Cell* **10:** 995-1005.

Exton JH (1999) Regulation of phospholipase D. *Biochim Biophys Acta* **1439:** 121-133.

Facchinetti V, Ouyang W, Wei H, Soto N, Lazorchak A, Gould C, Lowry C, Newton AC, Mao Y, Miao RQ, Sessa WC, Qin J, Zhang P, Su B, Jacinto E (2008) The mammalian target of rapamycin complex 2 controls folding and stability of Akt and protein kinase C. *Embo J* **27:** 1932-1943.

Fang Y, Vilella-Bach M, Bachmann R, Flanigan A, Chen J (2001) Phosphatidic acid-mediated mitogenic activation of mTOR signaling. *Science* **294:** 1942-1945.

Feldman DE, Thulasiraman V, Ferreyra RG, Frydman J (1999) Formation of the VHL-elongin BC tumor suppressor complex is mediated by the chaperonin TRiC. *Mol Cell* **4:** 1051-1061.

Feldman ME, Apsel B, Uotila A, Loewith R, Knight ZA, Ruggero D, Shokat KM (2009) Active-site inhibitors of mTOR target rapamycin-resistant outputs of mTORC1 and mTORC2. *PLoS Biol* **7:** e38.

Feng Z, Zhang H, Levine AJ, Jin S (2005) The coordinate regulation of the p53 and mTOR pathways in cells. *Proc Natl Acad Sci U S A* **102:** 8204-8209.

Ferguson G, Mothe-Satney I, Lawrence JC, Jr. (2003) Ser-64 and Ser-111 in PHAS-I are dispensable for insulin-stimulated dissociation from eIF4E. *J Biol Chem* **278:** 47459-47465.

Ferrari S, Bannwarth W, Morley SJ, Totty NF, Thomas G (1992) Activation of p70s6k is associated with phosphorylation of four clustered sites displaying Ser/Thr-Pro motifs. *Proc Natl Acad Sci U S A* **89:** 7282-7286.

Findlay GM, Yan L, Procter J, Mieulet V, Lamb RF (2007) A MAP4 kinase related to Ste20 is a nutrient-sensitive regulator of mTOR signaling. *Biochem J* **403:** 13-20.

Fisher TL, Blenis J (1996) Evidence for two catalytically active kinase domains in pp90rsk. *Mol Cell Biol* **16:** 1212-1219.

Fonseca BD, Smith EM, Lee VH, MacKintosh C, Proud CG (2007) PRAS40 is a target for mammalian target of rapamycin complex 1 and is required for signaling downstream of this complex. *J Biol Chem* **282:** 24514-24524.

Fornace AJ, Jr., Nebert DW, Hollander MC, Luethy JD, Papathanasiou M, Fargnoli J, Holbrook NJ (1989) Mammalian genes coordinately regulated by growth arrest signals and DNA-damaging agents. *Mol Cell Biol* **9:** 4196-4203.

Foster KG, Acosta-Jaquez HA, Romeo Y, Ekim B, Soliman GA, Carriere A, Roux PP, Ballif BA, Fingar DC Regulation of mTOR complex 1 (mTORC1) by raptor Ser863 and multisite phosphorylation. *J Biol Chem* **285:** 80-94.

Frias MA, Thoreen CC, Jaffe JD, Schroder W, Sculley T, Carr SA, Sabatini DM (2006) mSin1 is necessary for Akt/PKB phosphorylation, and its isoforms define three distinct mTORC2s. *Curr Biol* **16:** 1865-1870.

Frodin M, Antal TL, Dummler BA, Jensen CJ, Deak M, Gammeltoft S, Biondi RM (2002) A phosphoserine/threonine-binding pocket in AGC kinases and PDK1 mediates activation by hydrophobic motif phosphorylation. *Embo J* **21:** 5396-5407.

Frodin M, Jensen CJ, Merienne K, Gammeltoft S (2000) A phosphoserine-regulated docking site in the protein kinase RSK2 that recruits and activates PDK1. *Embo J* **19:** 2924-2934.

Frohman MA, Sung TC, Morris AJ (1999) Mammalian phospholipase D structure and regulation. *Biochim Biophys Acta* **1439:** 175-186.

Fuchs SY, Spiegelman VS, Kumar KG (2004) The many faces of beta-TrCP E3 ubiquitin ligases: reflections in the magic mirror of cancer. *Oncogene* **23:** 2028-2036.

Fujita N, Sato S, Tsuruo T (2003) Phosphorylation of p27Kip1 at threonine 198 by p90 ribosomal protein S6 kinases promotes its binding to 14-3-3 and cytoplasmic localization. *J Biol Chem* **278:** 49254-49260.

Fukunaga R, Hunter T (1997) MNK1, a new MAP kinase-activated protein kinase, isolated by a novel expression screening method for identifying protein kinase substrates. *Embo J* **16:** 1921-1933.

Gan B, Melkoumian ZK, Wu X, Guan KL, Guan JL (2005) Identification of FIP200 interaction with the TSC1-TSC2 complex and its role in regulation of cell size control. *J Cell Biol* **170:** 379-389.

Gao T, Furnari F, Newton AC (2005) PHLPP: a phosphatase that directly dephosphorylates Akt, promotes apoptosis, and suppresses tumor growth. *Mol Cell* **18:** 13-24.

Gao T, Newton AC (2002) The turn motif is a phosphorylation switch that regulates the binding of Hsp70 to protein kinase C. *J Biol Chem* **277:** 31585-31592.

Gao T, Newton AC (2006) Invariant Leu preceding turn motif phosphorylation site controls the interaction of protein kinase C with Hsp70. *J Biol Chem* **281:** 32461-32468.

Gao Y, Thomas JO, Chow RL, Lee GH, Cowan NJ (1992) A cytoplasmic chaperonin that catalyzes beta-actin folding. *Cell* **69:** 1043-1050.

Garcia-Martinez JM, Alessi DR (2008) mTOR complex 2 (mTORC2) controls hydrophobic motif phosphorylation and activation of serum- and glucocorticoid-induced protein kinase 1 (SGK1). *Biochem J* **416:** 375-385.

Garcia-Martinez JM, Moran J, Clarke RG, Gray A, Cosulich SC, Chresta CM, Alessi DR (2009) Ku-0063794 is a specific inhibitor of the mammalian target of rapamycin (mTOR). *Biochem J* **421:** 29-42.

Garcia MA, Meurs EF, Esteban M (2007) The dsRNA protein kinase PKR: virus and cell control. *Biochimie* **89:** 799-811.

Garrington TP, Ishizuka T, Papst PJ, Chayama K, Webb S, Yujiri T, Sun W, Sather S, Russell DM, Gibson SB, Keller G, Gelfand EW, Johnson GL (2000) MEKK2 gene disruption causes loss of cytokine production in response to IgE and c-Kit ligand stimulation of ES cell-derived mast cells. *Embo J* **19:** 5387-5395.

Gavin AC, Nebreda AR (1999) A MAP kinase docking site is required for phosphorylation and activation of p90(rsk)/MAPKAP kinase-1. *Curr Biol* **9:** 281-284.

Ghosh P, Wu M, Zhang H, Sun H (2008) mTORC1 signaling requires proteasomal function and the involvement of CUL4-DDB1 ubiquitin E3 ligase. *Cell Cycle* **7:** 373-381.

Gingras AC, Kennedy SG, O'Leary MA, Sonenberg N, Hay N (1998) 4E-BP1, a repressor of mRNA translation, is phosphorylated and inactivated by the Akt(PKB) signaling pathway. *Genes Dev* **12:** 502-513.

Gingras AC, Raught B, Gygi SP, Niedzwiecka A, Miron M, Burley SK, Polakiewicz RD, Wyslouch-Cieszynska A, Aebersold R, Sonenberg N (2001) Hierarchical phosphorylation of the translation inhibitor 4E-BP1. *Genes Dev* **15:** 2852-2864.

Gingras AC, Raught B, Sonenberg N (1999) eIF4 initiation factors: effectors of mRNA recruitment to ribosomes and regulators of translation. *Annu Rev Biochem* **68:** 913-963.

Gingras AC, Raught B, Sonenberg N (2004) mTOR signaling to translation. *Curr Top Microbiol Immunol* **279:** 169-197.

Gottlieb TM, Leal JF, Seger R, Taya Y, Oren M (2002) Cross-talk between Akt, p53 and Mdm2: possible implications for the regulation of apoptosis. *Oncogene* **21:** 1299-1303.

Greer EL, Oskoui PR, Banko MR, Maniar JM, Gygi MP, Gygi SP, Brunet A (2007) The energy sensor AMP-activated protein kinase directly regulates the mammalian FOXO3 transcription factor. *J Biol Chem* **282:** 30107-30119.

Grimmler M, Wang Y, Mund T, Cilensek Z, Keidel EM, Waddell MB, Jakel H, Kullmann M, Kriwacki RW, Hengst L (2007) Cdk-inhibitory activity and stability of p27Kip1 are directly regulated by oncogenic tyrosine kinases. *Cell* **128:** 269-280.

Grimsley CM, Kinchen JM, Tosello-Trampont AC, Brugnera E, Haney LB, Lu M, Chen Q, Klingele D, Hengartner MO, Ravichandran KS (2004) Dock180 and ELMO1 proteins cooperate to promote evolutionarily conserved Rac-dependent cell migration. *J Biol Chem* **279:** 6087-6097.

Grummt I (2003) Life on a planet of its own: regulation of RNA polymerase I transcription in the nucleolus. *Genes Dev* **17:** 1691-1702.

Gstaiger M, Luke B, Hess D, Oakeley EJ, Wirbelauer C, Blondel M, Vigneron M, Peter M, Krek W (2003) Control of nutrient-sensitive transcription programs by the unconventional prefoldin URI. *Science* **302:** 1208-1212.

Guertin DA, Sabatini DM (2009) The pharmacology of mTOR inhibition. *Sci Signal* **2:** pe24.

Guertin DA, Stevens DM, Thoreen CC, Burds AA, Kalaany NY, Moffat J, Brown M, Fitzgerald KJ, Sabatini DM (2006) Ablation in mice of the mTORC components raptor, rictor, or mLST8 reveals that mTORC2 is required for signaling to Akt-FOXO and PKCalpha, but not S6K1. *Dev Cell* **11:** 859-871.

Gulati P, Gaspers LD, Dann SG, Joaquin M, Nobukuni T, Natt F, Kozma SC, Thomas AP, Thomas G (2008) Amino acids activate mTOR complex 1 via Ca2+/CaM signaling to hVps34. *Cell Metab* **7:** 456-465.

Guo K, Searfoss G, Krolikowski D, Pagnoni M, Franks C, Clark K, Yu KT, Jaye M, Ivashchenko Y (2001) Hypoxia induces the expression of the pro-apoptotic gene BNIP3. *Cell Death Differ* **8:** 367-376.

Gwinn DM, Shackelford DB, Egan DF, Mihaylova MM, Mery A, Vasquez DS, Turk BE, Shaw RJ (2008) AMPK phosphorylation of raptor mediates a metabolic checkpoint. *Mol Cell* **30:** 214-226.

Hackzell A, Uramoto H, Izumi H, Kohno K, Funa K (2002) p73 independent of c-Myc represses transcription of platelet-derived growth factor beta-receptor through interaction with NF-Y. *J Biol Chem* **277:** 39769-39776.

Han J, Luby-Phelps K, Das B, Shu X, Xia Y, Mosteller RD, Krishna UM, Falck JR, White MA, Broek D (1998) Role of substrates and products of PI 3-kinase in regulating activation of Rac-related guanosine triphosphatases by Vav. *Science* **279:** 558-560.

Han S, Witt RM, Santos TM, Polizzano C, Sabatini BL, Ramesh V (2008) Pam (Protein associated with Myc) functions as an E3 ubiquitin ligase and regulates TSC/mTOR signaling. *Cell Signal* **20:** 1084-1091.

Hannan KM, Brandenburger Y, Jenkins A, Sharkey K, Cavanaugh A, Rothblum L, Moss T, Poortinga G, McArthur GA, Pearson RB, Hannan RD (2003) mTOR-dependent regulation of ribosomal gene transcription requires S6K1 and is mediated by phosphorylation of the carboxy-terminal activation domain of the nucleolar transcription factor UBF. *Mol Cell Biol* **23:** 8862-8877.

Hannan KM, Hannan RD, Smith SD, Jefferson LS, Lun M, Rothblum LI (2000) Rb and p130 regulate RNA polymerase I transcription: Rb disrupts the interaction between UBF and SL-1. *Oncogene* **19:** 4988-4999.

Hara K, Maruki Y, Long X, Yoshino K, Oshiro N, Hidayat S, Tokunaga C, Avruch J, Yonezawa K (2002) Raptor, a binding partner of target of rapamycin (TOR), mediates TOR action. *Cell* **110:** 177-189.

Hara K, Yonezawa K, Kozlowski MT, Sugimoto T, Andrabi K, Weng QP, Kasuga M, Nishimoto I, Avruch J (1997) Regulation of eIF-4E BP1 phosphorylation by mTOR. *J Biol Chem* **272:** 26457-26463.

Harada H, Andersen JS, Mann M, Terada N, Korsmeyer SJ (2001) p70S6 kinase signals cell survival as well as growth, inactivating the pro-apoptotic molecule BAD. *Proc Natl Acad Sci U S A* **98:** 9666-9670.

Hardie DG (2007) AMP-activated/SNF1 protein kinases: conserved guardians of cellular energy. *Nat Rev Mol Cell Biol* **8:** 774-785.

Harding HP, Zhang Y, Ron D (1999) Protein translation and folding are coupled by an endoplasmic-reticulum-resident kinase. *Nature* **397:** 271-274.

Harrington LS, Findlay GM, Gray A, Tolkacheva T, Wigfield S, Rebholz H, Barnett J, Leslie NR, Cheng S, Shepherd PR, Gout I, Downes CP, Lamb RF (2004) The TSC1-2 tumor suppressor controls insulin-PI3K signaling via regulation of IRS proteins. *J Cell Biol* **166:** 213-223.

Harris TE, Chi A, Shabanowitz J, Hunt DF, Rhoads RE, Lawrence JC, Jr. (2006) mTOR-dependent stimulation of the association of eIF4G and eIF3 by insulin. *Embo J* **25:** 1659-1668.

Haruta T, Uno T, Kawahara J, Takano A, Egawa K, Sharma PM, Olefsky JM, Kobayashi M (2000) A rapamycin-sensitive pathway down-regulates insulin signaling via phosphorylation and proteasomal degradation of insulin receptor substrate-1. *Mol Endocrinol* **14:** 783-794.

Hasegawa T, Xiao H, Hamajima F, Isobe K (2000) Interaction between DNA-damage protein GADD34 and a new member of the Hsp40 family of heat shock proteins that is induced by a DNA-damaging reagent. *Biochem J* **352 Pt 3:** 795-800.

Hawley SA, Boudeau J, Reid JL, Mustard KJ, Udd L, Makela TP, Alessi DR, Hardie DG (2003) Complexes between the LKB1 tumor suppressor, STRAD alpha/beta and MO25 alpha/beta are upstream kinases in the AMP-activated protein kinase cascade. *J Biol* **2:** 28.

Hawley SA, Pan DA, Mustard KJ, Ross L, Bain J, Edelman AM, Frenguelli BG, Hardie DG (2005) Calmodulin-dependent protein kinase kinase-beta is an alternative upstream kinase for AMP-activated protein kinase. *Cell Metab* **2:** 9-19.

Hay N, Sonenberg N (2004) Upstream and downstream of mTOR. *Genes Dev* **18:** 1926-1945.

He TC, Chan TA, Vogelstein B, Kinzler KW (1999) PPARdelta is an APC-regulated target of nonsteroidal anti-inflammatory drugs. *Cell* **99:** 335-345.

He TC, Sparks AB, Rago C, Hermeking H, Zawel L, da Costa LT, Morin PJ, Vogelstein B, Kinzler KW (1998) Identification of c-MYC as a target of the APC pathway. *Science* **281:** 1509-1512.

Hempel WM, Cavanaugh AH, Hannan RD, Taylor L, Rothblum LI (1996) The species-specific RNA polymerase I transcription factor SL-1 binds to upstream binding factor. *Mol Cell Biol* **16:** 557-563.

Hendrix ND, Wu R, Kuick R, Schwartz DR, Fearon ER, Cho KR (2006) Fibroblast growth factor 9 has oncogenic activity and is a downstream target of Wnt signaling in ovarian endometrioid adenocarcinomas. *Cancer Res* **66:** 1354-1362.

Hengst L, Reed SI (1998) Inhibitors of the Cip/Kip family. *Curr Top Microbiol Immunol* **227:** 25-41.

Hinoi T, Yamamoto H, Kishida M, Takada S, Kishida S, Kikuchi A (2000) Complex formation of adenomatous polyposis coli gene product and axin facilitates glycogen synthase kinase-3 beta-dependent phosphorylation of beta-catenin and down-regulates beta-catenin. *J Biol Chem* **275:** 34399-34406.

Holz MK, Ballif BA, Gygi SP, Blenis J (2005a) mTOR and S6K1 mediate assembly of the translation preinitiation complex through dynamic protein interchange and ordered phosphorylation events. *Cell* **123:** 569-580.

Holz MK, Blenis J (2005b) Identification of S6 kinase 1 as a novel mammalian target of rapamycin (mTOR)-phosphorylating kinase. *J Biol Chem* **280:** 26089-26093.

Hong F, Larrea MD, Doughty C, Kwiatkowski DJ, Squillace R, Slingerland JM (2008) mTOR-raptor binds and activates SGK1 to regulate p27 phosphorylation. *Mol Cell* **30:** 701-711.

Horowitz A, Murakami M, Gao Y, Simons M (1999) Phosphatidylinositol-4,5-bisphosphate mediates the interaction of syndecan-4 with protein kinase C. *Biochemistry* **38:** 15871-15877.

Horowitz A, Simons M (1998) Regulation of syndecan-4 phosphorylation in vivo. *J Biol Chem* **273:** 10914-10918.

Horowitz A, Tkachenko E, Simons M (2002) Fibroblast growth factor-specific modulation of cellular response by syndecan-4. *J Cell Biol* **157:** 715-725.

Hresko RC, Mueckler M (2005) mTOR.RICTOR is the Ser473 kinase for Akt/protein kinase B in 3T3-L1 adipocytes. *J Biol Chem* **280:** 40406-40416.

Hsiao KM, Chou SY, Shih SJ, Ferrell JE, Jr. (1994) Evidence that inactive p42 mitogen-activated protein kinase and inactive Rsk exist as a heterodimer in vivo. *Proc Natl Acad Sci U S A* **91:** 5480-5484.

Hsu H, Shu HB, Pan MG, Goeddel DV (1996) TRADD-TRAF2 and TRADD-FADD interactions define two distinct TNF receptor 1 signal transduction pathways. *Cell* **84:** 299-308.

Hsu YC, Chern JJ, Cai Y, Liu M, Choi KW (2007) Drosophila TCTP is essential for growth and proliferation through regulation of dRheb GTPase. *Nature* **445:** 785-788.

Hu J, Zacharek S, He YJ, Lee H, Shumway S, Duronio RJ, Xiong Y (2008) WD40 protein FBW5 promotes ubiquitination of tumor suppressor TSC2 by DDB1-CUL4-ROC1 ligase. *Genes Dev* **22:** 866-871.

Hu KQ, Settleman J (1997) Tandem SH2 binding sites mediate the RasGAP-RhoGAP interaction: a conformational mechanism for SH3 domain regulation. *Embo J* **16:** 473-483.

Hu MC, Lee DF, Xia W, Golfman LS, Ou-Yang F, Yang JY, Zou Y, Bao S, Hanada N, Saso H, Kobayashi R, Hung MC (2004) IkappaB kinase promotes tumorigenesis through inhibition of forkhead FOXO3a. *Cell* **117:** 225-237.

Huang C, Borchers CH, Schaller MD, Jacobson K (2004) Phosphorylation of paxillin by p38MAPK is involved in the neurite extension of PC-12 cells. *J Cell Biol* **164:** 593-602.

Huang C, Rajfur Z, Borchers C, Schaller MD, Jacobson K (2003) JNK phosphorylates paxillin and regulates cell migration. *Nature* **424:** 219-223.

Huang H, Regan KM, Wang F, Wang D, Smith DI, van Deursen JM, Tindall DJ (2005) Skp2 inhibits FOXO1 in tumor suppression through ubiquitin-mediated degradation. *Proc Natl Acad Sci U S A* **102:** 1649-1654.

Huang J, Dibble CC, Matsuzaki M, Manning BD (2008) The TSC1-TSC2 complex is required for proper activation of mTOR complex 2. *Mol Cell Biol* **28:** 4104-4115.

Huffman TA, Mothe-Satney I, Lawrence JC, Jr. (2002) Insulin-stimulated phosphorylation of lipin mediated by the mammalian target of rapamycin. *Proc Natl Acad Sci U S A* **99:** 1047-1052.

Hurley RL, Anderson KA, Franzone JM, Kemp BE, Means AR, Witters LA (2005) The Ca2+/calmodulin-dependent protein kinase kinases are AMP-activated protein kinase kinases. *J Biol Chem* **280:** 29060-29066.

Ikenoue T, Inoki K, Yang Q, Zhou X, Guan KL (2008) Essential function of TORC2 in PKC and Akt turn motif phosphorylation, maturation and signaling. *Embo J* **27:** 1919-1931.

Inoki K, Li Y, Zhu T, Wu J, Guan KL (2002) TSC2 is phosphorylated and inhibited by Akt and suppresses mTOR signaling. *Nat Cell Biol* **4:** 648-657.
Inoki K, Ouyang H, Zhu T, Lindvall C, Wang Y, Zhang X, Yang Q, Bennett C, Harada Y, Stankunas K, Wang CY, He X, MacDougald OA, You M, Williams BO, Guan KL (2006) TSC2 integrates Wnt and energy signals via a coordinated phosphorylation by AMPK and GSK3 to regulate cell growth. *Cell* **126:** 955-968.

Inoki K, Zhu T, Guan KL (2003) TSC2 mediates cellular energy response to control cell growth and survival. *Cell* **115:** 577-590.

Ishibe S, Joly D, Zhu X, Cantley LG (2003) Phosphorylation-dependent paxillin-ERK association mediates hepatocyte growth factor-stimulated epithelial morphogenesis. *Mol Cell* **12:** 1275-1285.

Ishida N, Hara T, Kamura T, Yoshida M, Nakayama K, Nakayama KI (2002) Phosphorylation of p27Kip1 on serine 10 is required for its binding to CRM1 and nuclear export. *J Biol Chem* **277:** 14355-14358.

Isotani S, Hara K, Tokunaga C, Inoue H, Avruch J, Yonezawa K (1999) Immunopurified mammalian target of rapamycin phosphorylates and activates p70 S6 kinase alpha in vitro. *J Biol Chem* **274:** 34493-34498.

Ito A, Kataoka TR, Watanabe M, Nishiyama K, Mazaki Y, Sabe H, Kitamura Y, Nojima H (2000) A truncated isoform of the PP2A B56 subunit promotes cell motility through paxillin phosphorylation. *Embo J* **19:** 562-571.

Itoh K, Antipova A, Ratcliffe MJ, Sokol S (2000) Interaction of dishevelled and Xenopus axin-related protein is required for wnt signal transduction. *Mol Cell Biol* **20:** 2228-2238.

Izumi H, Molander C, Penn LZ, Ishisaki A, Kohno K, Funa K (2001) Mechanism for the transcriptional repression by c-Myc on PDGF beta-receptor. *J Cell Sci* **114:** 1533-1544.

Jacinto E (2008) What controls TOR? *IUBMB Life* **60:** 483-496.

Jacinto E, Facchinetti V, Liu D, Soto N, Wei S, Jung SY, Huang Q, Qin J, Su B (2006) SIN1/MIP1 maintains rictor-mTOR complex integrity and regulates Akt phosphorylation and substrate specificity. *Cell* **127:** 125-137.

Jacinto E, Loewith R, Schmidt A, Lin S, Ruegg MA, Hall A, Hall MN (2004) Mammalian TOR complex 2 controls the actin cytoskeleton and is rapamycin insensitive. *Nat Cell Biol* **6:** 1122-1128.

Jacinto E, Lorberg A (2008) TOR regulation of AGC kinases in yeast and mammals. *Biochem J* **410:** 19-37.

Jackson JL, Young MR (2003) Protein phosphatase-2A regulates protein tyrosine phosphatase activity in Lewis lung carcinoma tumor variants. *Clin Exp Metastasis* **20:** 357-364.

James MJ, Zomerdijk JC (2004) Phosphatidylinositol 3-kinase and mTOR signaling pathways regulate RNA polymerase I transcription in response to IGF-1 and nutrients. *J Biol Chem* **279:** 8911-8918.

James MK, Ray A, Leznova D, Blain SW (2008) Differential modification of p27Kip1 controls its cyclin D-cdk4 inhibitory activity. *Mol Cell Biol* **28:** 498-510.

Jamieson JS, Tumbarello DA, Halle M, Brown MC, Tremblay ML, Turner CE (2005) Paxillin is essential for PTP-PEST-dependent regulation of cell spreading and motility: a role for paxillin kinase linker. *J Cell Sci* **118:** 5835-5847.

Jefferies HB, Fumagalli S, Dennis PB, Reinhard C, Pearson RB, Thomas G (1997) Rapamycin suppresses 5'TOP mRNA translation through inhibition of p70s6k. *Embo J* **16:** 3693-3704.

Jefferies HB, Reinhard C, Kozma SC, Thomas G (1994) Rapamycin selectively represses translation of the "polypyrimidine tract" mRNA family. *Proc Natl Acad Sci U S A* **91:** 4441-4445.

Jensen CJ, Buch MB, Krag TO, Hemmings BA, Gammeltoft S, Frodin M (1999) 90-kDa ribosomal S6 kinase is phosphorylated and activated by 3-phosphoinositide-dependent protein kinase-1. *J Biol Chem* **274:** 27168-27176.

Jho E, Lomvardas S, Costantini F (1999) A GSK3beta phosphorylation site in axin modulates interaction with beta-catenin and Tcf-mediated gene expression. *Biochem Biophys Res Commun* **266:** 28-35.

Jho EH, Zhang T, Domon C, Joo CK, Freund JN, Costantini F (2002) Wnt/beta-catenin/Tcf signaling induces the transcription of Axin2, a negative regulator of the signaling pathway. *Mol Cell Biol* **22:** 1172-1183.

Joel PB, Smith J, Sturgill TW, Fisher TL, Blenis J, Lannigan DA (1998) pp90rsk1 regulates estrogen receptor-mediated transcription through phosphorylation of Ser-167. *Mol Cell Biol* **18:** 1978-1984.

Jones RG, Plas DR, Kubek S, Buzzai M, Mu J, Xu Y, Birnbaum MJ, Thompson CB (2005) AMP-activated protein kinase induces a p53-dependent metabolic checkpoint. *Mol Cell* **18:** 283-293.

Jope RS, Johnson GV (2004) The glamour and gloom of glycogen synthase kinase-3. *Trends Biochem Sci* **29:** 95-102.

Joshi-Barve S, Rychlik W, Rhoads RE (1990) Alteration of the major phosphorylation site of eukaryotic protein synthesis initiation factor 4E prevents its association with the 48 S initiation complex. *J Biol Chem* **265:** 2979-2983.

Jung CH, Jun CB, Ro SH, Kim YM, Otto NM, Cao J, Kundu M, Kim DH (2009) ULK-Atg13-FIP200 complexes mediate mTOR signaling to the autophagy machinery. *Mol Biol Cell* **20:** 1992-2003.

Kahn BB, Alquier T, Carling D, Hardie DG (2005) AMP-activated protein kinase: ancient energy gauge provides clues to modern understanding of metabolism. *Cell Metab* **1:** 15-25.

Kanayama A, Seth RB, Sun L, Ea CK, Hong M, Shaito A, Chiu YH, Deng L, Chen ZJ (2004) TAB2 and TAB3 activate the NF-kappaB pathway through binding to polyubiquitin chains. *Mol Cell* **15:** 535-548.

Karin M, Ben-Neriah Y (2000) Phosphorylation meets ubiquitination: the control of NF-[kappa]B activity. *Annu Rev Immunol* **18:** 621-663.

Karin M, Greten FR (2005) NF-kappaB: linking inflammation and immunity to cancer development and progression. *Nat Rev Immunol* **5:** 749-759.

Karuman P, Gozani O, Odze RD, Zhou XC, Zhu H, Shaw R, Brien TP, Bozzuto CD, Ooi D, Cantley LC, Yuan J (2001) The Peutz-Jegher gene product LKB1 is a mediator of p53-dependent cell death. *Mol Cell* **7:** 1307-1319.

Katanaev VL, Ponzielli R, Semeriva M, Tomlinson A (2005) Trimeric G protein-dependent frizzled signaling in Drosophila. *Cell* **120:** 111-122.

Katiyar S, Liu E, Knutzen CA, Lang ES, Lombardo CR, Sankar S, Toth JI, Petroski MD, Ronai Z, Chiang GG (2009) REDD1, an inhibitor of mTOR signaling, is regulated by the CUL4A-DDB1 ubiquitin ligase. *EMBO Rep* **10:** 866-872.

Keum E, Kim Y, Kim J, Kwon S, Lim Y, Han I, Oh ES (2004) Syndecan-4 regulates localization, activity and stability of protein kinase C-alpha. *Biochem J* **378:** 1007-1014.

Kihm AJ, Hershey JC, Haystead TA, Madsen CS, Owens GK (1998) Phosphorylation of the rRNA transcription factor upstream binding factor promotes its association with TATA binding protein. *Proc Natl Acad Sci U S A* **95:** 14816-14820.

Kim DH, Sarbassov DD, Ali SM, King JE, Latek RR, Erdjument-Bromage H, Tempst P, Sabatini DM (2002) mTOR interacts with raptor to form a nutrient-sensitive complex that signals to the cell growth machinery. *Cell* **110:** 163-175.

Kim DH, Sarbassov DD, Ali SM, Latek RR, Guntur KV, Erdjument-Bromage H, Tempst P, Sabatini DM (2003) GbetaL, a positive regulator of the rapamycin-sensitive pathway required for the nutrient-sensitive interaction between raptor and mTOR. *Mol Cell* **11:** 895-904.

Kim E, Goraksha-Hicks P, Li L, Neufeld TP, Guan KL (2008) Regulation of TORC1 by Rag GTPases in nutrient response. *Nat Cell Biol* **10:** 935-945.

Kim JE, Chen J (2000) Cytoplasmic-nuclear shuttling of FKBP12-rapamycin-associated protein is involved in rapamycin-sensitive signaling and translation initiation. *Proc Natl Acad Sci U S A* **97:** 14340-14345.

Kim JE, Chen J (2004) regulation of peroxisome proliferator-activated receptor-gamma activity by mammalian target of rapamycin and amino acids in adipogenesis. *Diabetes* **53:** 2748-2756.

Kinchen JM, Doukoumetzidis K, Almendinger J, Stergiou L, Tosello-Trampont A, Sifri CD, Hengartner MO, Ravichandran KS (2008) A pathway for phagosome maturation during engulfment of apoptotic cells. *Nat Cell Biol* **10:** 556-566.

Kleijn M, Scheper GC, Voorma HO, Thomas AA (1998) Regulation of translation initiation factors by signal transduction. *Eur J Biochem* **253:** 531-544.

Knebel A, Morrice N, Cohen P (2001) A novel method to identify protein kinase substrates: eEF2 kinase is phosphorylated and inhibited by SAPK4/p38delta. *Embo J* **20:** 4360-4369.

Knight ZA, Gonzalez B, Feldman ME, Zunder ER, Goldenberg DD, Williams O, Loewith R, Stokoe D, Balla A, Toth B, Balla T, Weiss WA, Williams RL, Shokat KM (2006) A pharmacological map of the PI3-K family defines a role for p110alpha in insulin signaling. *Cell* **125:** 733-747.

Kobayashi T, Cohen P (1999) Activation of serum- and glucocorticoid-regulated protein kinase by agonists that activate phosphatidylinositide 3-kinase is mediated by 3-phosphoinositide-dependent protein kinase-1 (PDK1) and PDK2. *Biochem J* **339 (Pt 2):** 319-328.

Kong M, Fox CJ, Mu J, Solt L, Xu A, Cinalli RM, Birnbaum MJ, Lindsten T, Thompson CB (2004) The PP2A-associated protein alpha4 is an essential inhibitor of apoptosis. *Science* **306:** 695-698.

Krieg J, Hofsteenge J, Thomas G (1988) Identification of the 40 S ribosomal protein S6 phosphorylation sites induced by cycloheximide. *J Biol Chem* **263:** 11473-11477.

Kubota H, Obata T, Ota K, Sasaki T, Ito T (2003) Rapamycin-induced translational derepression of GCN4 mRNA involves a novel mechanism for activation of the eIF2 alpha kinase GCN2. *J Biol Chem* **278:** 20457-20460.

Kwiatkowski DJ, Manning BD (2005) Tuberous sclerosis: a GAP at the crossroads of multiple signaling pathways. *Hum Mol Genet* **14 Spec No. 2:** R251-258.

Lachance PE, Miron M, Raught B, Sonenberg N, Lasko P (2002) Phosphorylation of eukaryotic translation initiation factor 4E is critical for growth. *Mol Cell Biol* **22:** 1656-1663.

Lamphear BJ, Panniers R (1990) Cap binding protein complex that restores protein synthesis in heat-shocked Ehrlich cell lysates contains highly phosphorylated eIF-4E. *J Biol Chem* **265:** 5333-5336.

Larrea MD, Liang J, Da Silva T, Hong F, Shao SH, Han K, Dumont D, Slingerland JM (2008) Phosphorylation of p27Kip1 regulates assembly and activation of cyclin D1-Cdk4. *Mol Cell Biol* **28:** 6462-6472.

Le Hir H, Seraphin B (2008) EJCs at the heart of translational control. *Cell* **133:** 213-216.

Le Sourd F, Boulben S, Le Bouffant R, Cormier P, Morales J, Belle R, Mulner-Lorillon O (2006) eEF1B: At the dawn of the 21st century. *Biochim Biophys Acta* **1759:** 13-31.

Lee DF, Kuo HP, Chen CT, Hsu JM, Chou CK, Wei Y, Sun HL, Li LY, Ping B, Huang WC, He X, Hung JY, Lai CC, Ding Q, Su JL, Yang JY, Sahin AA, Hortobagyi GN, Tsai FJ, Tsai CH, Hung MC (2007) IKK beta suppression of TSC1 links inflammation and tumor angiogenesis via the mTOR pathway. *Cell* **130:** 440-455.

Lee E, Salic A, Kruger R, Heinrich R, Kirschner MW (2003) The roles of APC and Axin derived from experimental and theoretical analysis of the Wnt pathway. *PLoS Biol* **1:** E10.

Lei M, Lu W, Meng W, Parrini MC, Eck MJ, Mayer BJ, Harrison SC (2000) Structure of PAK1 in an autoinhibited conformation reveals a multistage activation switch. *Cell* **102:** 387-397.

Levine AJ, Feng Z, Mak TW, You H, Jin S (2006) Coordination and communication between the p53 and IGF-1-AKT-TOR signal transduction pathways. *Genes Dev* **20:** 267-275.

Li J, Tewari M, Vidal M, Lee SS (2007a) The 14-3-3 protein FTT-2 regulates DAF-16 in Caenorhabditis elegans. *Dev Biol* **301:** 82-91.

Li Y, Inoki K, Vacratsis P, Guan KL (2003) The p38 and MK2 kinase cascade phosphorylates tuberin, the tuberous sclerosis 2 gene product, and enhances its interaction with 14-3-3. *J Biol Chem* **278:** 13663-13671.

Li Y, Wang Y, Kim E, Beemiller P, Wang CY, Swanson J, You M, Guan KL (2007b) Bnip3 mediates the hypoxia-induced inhibition on mammalian target of rapamycin by interacting with Rheb. *J Biol Chem* **282:** 35803-35813.

Liang JL, Huang JS, Yu XQ, Zhu N, Che CM (2002) Metalloporphyrin-mediated asymmetric nitrogen-atom transfer to hydrocarbons: aziridination of alkenes and amidation of saturated C-H bonds catalyzed by chiral ruthenium and manganese porphyrins. *Chemistry* **8:** 1563-1572.

Lim ST, Longley RL, Couchman JR, Woods A (2003) Direct binding of syndecan-4 cytoplasmic domain to the catalytic domain of protein kinase C alpha (PKC alpha) increases focal adhesion localization of PKC alpha. *J Biol Chem* **278:** 13795-13802.

Lin CY, Tuan J, Scalia P, Bui T, Comai L (2002) The cell cycle regulatory factor TAF1 stimulates ribosomal DNA transcription by binding to the activator UBF. *Curr Biol* **12:** 2142-2146.

Ling J, Morley SJ, Traugh JA (2005) Inhibition of cap-dependent translation via phosphorylation of eIF4G by protein kinase Pak2. *Embo J* **24:** 4094-4105.

Liu T, Liu X, Wang H, Moon RT, Malbon CC (1999) Activation of rat frizzled-1 promotes Wnt signaling and differentiation of mouse F9 teratocarcinoma cells via pathways that require Galpha(q) and Galpha(o) function. *J Biol Chem* **274:** 33539-33544.

Liu X, Lin CY, Lei M, Yan S, Zhou T, Erikson RL (2005a) CCT chaperonin complex is required for the biogenesis of functional Plk1. *Mol Cell Biol* **25:** 4993-5010.

Liu X, Rubin JS, Kimmel AR (2005b) Rapid, Wnt-induced changes in GSK3beta associations that regulate beta-catenin stabilization are mediated by Galpha proteins. *Curr Biol* **15:** 1989-1997.

Liu X, Zheng XF (2007) Endoplasmic reticulum and Golgi localization sequences for mammalian target of rapamycin. *Mol Biol Cell* **18:** 1073-1082.

Liu ZX, Yu CF, Nickel C, Thomas S, Cantley LG (2002) Hepatocyte growth factor induces ERK-dependent paxillin phosphorylation and regulates paxillin-focal adhesion kinase association. *J Biol Chem* **277:** 10452-10458.

Lizcano JM, Goransson O, Toth R, Deak M, Morrice NA, Boudeau J, Hawley SA, Udd L, Makela TP, Hardie DG, Alessi DR (2004) LKB1 is a master kinase that activates 13 kinases of the AMPK subfamily, including MARK/PAR-1. *Embo J* **23:** 833-843.

Loewith R, Jacinto E, Wullschleger S, Lorberg A, Crespo JL, Bonenfant D, Oppliger W, Jenoe P, Hall MN (2002) Two TOR complexes, only one of which is rapamycin sensitive, have distinct roles in cell growth control. *Mol Cell* **10:** 457-468.

Long X, Lin Y, Ortiz-Vega S, Yonezawa K, Avruch J (2005) Rheb binds and regulates the mTOR kinase. *Curr Biol* **15:** 702-713.

Loo TH, Ng YW, Lim L, Manser E (2004) GIT1 activates p21-activated kinase through a mechanism independent of p21 binding. *Mol Cell Biol* **24:** 3849-3859.

Lou D, Griffith N, Noonan DJ (2001) The tuberous sclerosis 2 gene product can localize to nuclei in a phosphorylation-dependent manner. *Mol Cell Biol Res Commun* **4:** 374-380.

Lu L, Airey DC, Williams RW (2001) Complex trait analysis of the hippocampus: mapping and biometric analysis of two novel gene loci with specific effects on hippocampal structure in mice. *J Neurosci* **21:** 3503-3514.

Lustig B, Jerchow B, Sachs M, Weiler S, Pietsch T, Karsten U, van de Wetering M, Clevers H, Schlag PM, Birchmeier W, Behrens J (2002) Negative feedback loop of Wnt signaling through upregulation of conductin/axin2 in colorectal and liver tumors. *Mol Cell Biol* **22:** 1184-1193.

Ma L, Chen Z, Erdjument-Bromage H, Tempst P, Pandolfi PP (2005) Phosphorylation and functional inactivation of TSC2 by Erk implications for tuberous sclerosis and cancer pathogenesis. *Cell* **121:** 179-193.

Ma L, Teruya-Feldstein J, Bonner P, Bernardi R, Franz DN, Witte D, Cordon-Cardo C, Pandolfi PP (2007) Identification of S664 TSC2 phosphorylation as a marker for extracellular signal-regulated kinase mediated mTOR activation in tuberous sclerosis and human cancer. *Cancer Res* **67:** 7106-7112.

Ma XM, Blenis J (2009) Molecular mechanisms of mTOR-mediated translational control. *Nat Rev Mol Cell Biol* **10:** 307-318.

Ma XM, Yoon SO, Richardson CJ, Julich K, Blenis J (2008) SKAR links pre-mRNA splicing to mTOR/S6K1-mediated enhanced translation efficiency of spliced mRNAs. *Cell* **133:** 303-313.

Mader S, Lee H, Pause A, Sonenberg N (1995) The translation initiation factor eIF-4E binds to a common motif shared by the translation factor eIF-4 gamma and the translational repressors 4E-binding proteins. *Mol Cell Biol* **15:** 4990-4997.

Maira SM, Stauffer F, Brueggen J, Furet P, Schnell C, Fritsch C, Brachmann S, Chene P, De Pover A, Schoemaker K, Fabbro D, Gabriel D, Simonen M, Murphy L, Finan P, Sellers W, Garcia-Echeverria C (2008) Identification and characterization of NVP-BEZ235, a new orally available dual phosphatidylinositol 3-kinase/mammalian target of rapamycin inhibitor with potent in vivo antitumor activity. *Mol Cancer Ther* **7:** 1851-1863.

Maiyar AC, Leong ML, Firestone GL (2003) Importin-alpha mediates the regulated nuclear targeting of serum- and glucocorticoid-inducible protein kinase (Sgk) by recognition of a nuclear localization signal in the kinase central domain. *Mol Biol Cell* **14:** 1221-1239.

Mak BC, Kenerson HL, Aicher LD, Barnes EA, Yeung RS (2005) Aberrant beta-catenin signaling in tuberous sclerosis. *Am J Pathol* **167:** 107-116.

Mak BC, Takemaru K, Kenerson HL, Moon RT, Yeung RS (2003) The tuberin-hamartin complex negatively regulates beta-catenin signaling activity. *J Biol Chem* **278:** 5947-5951.

Manes S, Mira E, Gomez-Mouton C, Zhao ZJ, Lacalle RA, Martinez AC (1999) Concerted activity of tyrosine phosphatase SHP-2 and focal adhesion kinase in regulation of cell motility. *Mol Cell Biol* **19:** 3125-3135.

Manning BD, Cantley LC (2003) Rheb fills a GAP between TSC and TOR. *Trends Biochem Sci* **28:** 573-576.

Manning BD, Tee AR, Logsdon MN, Blenis J, Cantley LC (2002) Identification of the tuberous sclerosis complex-2 tumor suppressor gene product tuberin as a target of the phosphoinositide 3-kinase/akt pathway. *Mol Cell* **10:** 151-162.
Mao JH, Kim IJ, Wu D, Climent J, Kang HC, DelRosario R, Balmain A (2008) FBXW7 targets mTOR for degradation and cooperates with PTEN in tumor suppression. *Science* **321:** 1499-1502.

Martin J, Masri J, Bernath A, Nishimura RN, Gera J (2008) Hsp70 associates with Rictor and is required for mTORC2 formation and activity. *Biochem Biophys Res Commun* **372:** 578-583.

Martin KA, Schalm SS, Romanelli A, Keon KL, Blenis J (2001) Ribosomal S6 kinase 2 inhibition by a potent C-terminal repressor domain is relieved by mitogen-activated protein-extracellular signal-regulated kinase kinase-regulated phosphorylation. *J Biol Chem* **276:** 7892-7898.

Matsuzawa A, Tseng PH, Vallabhapurapu S, Luo JL, Zhang W, Wang H, Vignali DA, Gallagher E, Karin M (2008) Essential cytoplasmic translocation of a cytokine receptor-assembled signaling complex. *Science* **321:** 663-668.

Mayer C, Grummt I (2006) Ribosome biogenesis and cell growth: mTOR coordinates transcription by all three classes of nuclear RNA polymerases. *Oncogene* **25:** 6384-6391.

Mayer C, Zhao J, Yuan X, Grummt I (2004) mTOR-dependent activation of the transcription factor TIF-IA links rRNA synthesis to nutrient availability. *Genes Dev* **18:** 423-434.

McKay LI, Cidlowski JA (1999) Molecular control of immune/inflammatory responses: interactions between nuclear factor-kappa B and steroid receptor-signaling pathways. *Endocr Rev* **20:** 435-459.

McKendrick L, Morley SJ, Pain VM, Jagus R, Joshi B (2001) Phosphorylation of eukaryotic initiation factor 4E (eIF4E) at Ser209 is not required for protein synthesis in vitro and in vivo. *Eur J Biochem* **268:** 5375-5385.

McManus EJ, Collins BJ, Ashby PR, Prescott AR, Murray-Tait V, Armit LJ, Arthur JS, Alessi DR (2004) The in vivo role of PtdIns(3,4,5)P3 binding to PDK1 PH domain defined by knockin mutation. *Embo J* **23:** 2071-2082.

McManus EJ, Sakamoto K, Armit LJ, Ronaldson L, Shpiro N, Marquez R, Alessi DR (2005) Role that phosphorylation of GSK3 plays in insulin and Wnt signaling defined by knockin analysis. *Embo J* **24:** 1571-1583.

McNally FJ (2001) Cytoskeleton: CLASPing the end to the edge. *Curr Biol* **11:** R477-480.

Micheau O, Tschopp J (2003) Induction of TNF receptor I-mediated apoptosis via two sequential signaling complexes. *Cell* **114:** 181-190.

Michlewski G, Sanford JR, Caceres JF (2008) The splicing factor SF2/ASF regulates translation initiation by enhancing phosphorylation of 4E-BP1. *Mol Cell* **30:** 179-189.

Mieulet V, Lamb RF (2008) Shooting the messenger: CULLIN' insulin signaling with Fbw8. *Dev Cell* **14:** 816-817.

Mikawa M, Kato H, Okumura M, Narazaki M, Kanazawa Y, Miwa N, Shinohara H (2001) Paramagnetic water-soluble metallofullerenes having the highest relaxivity for MRI contrast agents. *Bioconjug Chem* **12:** 510-514.

Minami T, Hara K, Oshiro N, Ueoku S, Yoshino K, Tokunaga C, Shirai Y, Saito N, Gout I, Yonezawa K (2001) Distinct regulatory mechanism for p70 S6 kinase beta from that for p70 S6 kinase alpha. *Genes Cells* **6:** 1003-1015.

Mitsui K, Brady M, Palfrey HC, Nairn AC (1993) Purification and characterization of calmodulin-dependent protein kinase III from rabbit reticulocytes and rat pancreas. *J Biol Chem* **268:** 13422-13433.

Miwa N, Furuse M, Tsukita S, Niikawa N, Nakamura Y, Furukawa Y (2001) Involvement of claudin-1 in the beta-catenin/Tcf signaling pathway and its frequent upregulation in human colorectal cancers. *Oncol Res* **12:** 469-476.

Momcilovic M, Hong SP, Carlson M (2006) Mammalian TAK1 activates Snf1 protein kinase in yeast and phosphorylates AMP-activated protein kinase in vitro. *J Biol Chem* **281:** 25336-25343.

Moon RT, Bowerman B, Boutros M, Perrimon N (2002) The promise and perils of Wnt signaling through beta-catenin. *Science* **296:** 1644-1646.

Mora A, Komander D, van Aalten DM, Alessi DR (2004) PDK1, the master regulator of AGC kinase signal transduction. *Semin Cell Dev Biol* **15:** 161-170.

Moran MF, Polakis P, McCormick F, Pawson T, Ellis C (1991) Protein-tyrosine kinases regulate the phosphorylation, protein interactions, subcellular distribution, and activity of p21ras GTPase-activating protein. *Mol Cell Biol* **11:** 1804-1812.

Morley SJ, Dever TE, Etchison D, Traugh JA (1991) Phosphorylation of eIF-4F by protein kinase C or multipotential S6 kinase stimulates protein synthesis at initiation. *J Biol Chem* **266:** 4669-4672.

Moser BA, Dennis PB, Pullen N, Pearson RB, Williamson NA, Wettenhall RE, Kozma SC, Thomas G (1997) Dual requirement for a newly identified phosphorylation site in p70s6k. *Mol Cell Biol* **17:** 5648-5655.

Motti ML, De Marco C, Califano D, Fusco A, Viglietto G (2004) Akt-dependent T198 phosphorylation of cyclin-dependent kinase inhibitor p27kip1 in breast cancer. *Cell Cycle* **3:** 1074-1080.

Murakami M, Horowitz A, Tang S, Ware JA, Simons M (2002) Protein kinase C (PKC) delta regulates PKCalpha activity in a Syndecan-4-dependent manner. *J Biol Chem* **277:** 20367-20371.

Murray JT, Campbell DG, Morrice N, Auld GC, Shpiro N, Marquez R, Peggie M, Bain J, Bloomberg GB, Grahammer F, Lang F, Wulff P, Kuhl D, Cohen P (2004) Exploitation of KESTREL to identify NDRG family members as physiological substrates for SGK1 and GSK3. *Biochem J* **384:** 477-488.

Nader GA, McLoughlin TJ, Esser KA (2005) mTOR function in skeletal muscle hypertrophy: increased ribosomal RNA via cell cycle regulators. *Am J Physiol Cell Physiol* **289:** C1457-1465.

Nakajima T, Fukamizu A, Takahashi J, Gage FH, Fisher T, Blenis J, Montminy MR (1996) The signal-dependent coactivator CBP is a nuclear target for pp90RSK. *Cell* **86:** 465-474.

Nakashima A, Yoshino K, Miyamoto T, Eguchi S, Oshiro N, Kikkawa U, Yonezawa K (2007) Identification of TBC7 having TBC domain as a novel binding protein to TSC1-TSC2 complex. *Biochem Biophys Res Commun* **361:** 218-223.

Nakayama KI, Nakayama K (2006) Ubiquitin ligases: cell-cycle control and cancer. *Nat Rev Cancer* **6:** 369-381.

Nayal A, Webb DJ, Brown CM, Schaefer EM, Vicente-Manzanares M, Horwitz AR (2006) Paxillin phosphorylation at Ser273 localizes a GIT1-PIX-PAK complex and regulates adhesion and protrusion dynamics. *J Cell Biol* **173:** 587-589.

Nellist M, Burgers PC, van den Ouweland AM, Halley DJ, Luider TM (2005) Phosphorylation and binding partner analysis of the TSC1-TSC2 complex. *Biochem Biophys Res Commun* **333:** 818-826.

Nigg EA (2002) Centrosome aberrations: cause or consequence of cancer progression? *Nat Rev Cancer* **2:** 815-825.

Nobukuni T, Joaquin M, Roccio M, Dann SG, Kim SY, Gulati P, Byfield MP, Backer JM, Natt F, Bos JL, Zwartkruis FJ, Thomas G (2005) Amino acids mediate mTOR/raptor signaling through activation of class 3 phosphatidylinositol 3OH-kinase. *Proc Natl Acad Sci U S A* **102:** 14238-14243.

Noonan DJ, Lou D, Griffith N, Vanaman TC (2002) A calmodulin binding site in the tuberous sclerosis 2 gene product is essential for regulation of transcription events and is altered by mutations linked to tuberous sclerosis and lymphangioleiomyomatosis. *Arch Biochem Biophys* **398:** 132-140.

Noordermeer J, Klingensmith J, Perrimon N, Nusse R (1994) dishevelled and armadillo act in the wingless signaling pathway in Drosophila. *Nature* **367:** 80-83.

Novoa I, Zeng H, Harding HP, Ron D (2001) Feedback inhibition of the unfolded protein response by GADD34-mediated dephosphorylation of eIF2alpha. *J Cell Biol* **153:** 1011-1022.

Obsilova V, Vecer J, Herman P, Pabianova A, Sulc M, Teisinger J, Boura E, Obsil T (2005) 14-3-3 Protein interacts with nuclear localization sequence of forkhead transcription factor FoxO4. *Biochemistry* **44:** 11608-11617.

Oh ES, Woods A, Couchman JR (1997a) Multimerization of the cytoplasmic domain of syndecan-4 is required for its ability to activate protein kinase C. *J Biol Chem* **272:** 11805-11811.

Oh ES, Woods A, Couchman JR (1997b) Syndecan-4 proteoglycan regulates the distribution and activity of protein kinase C. *J Biol Chem* **272:** 8133-8136.

Ohi R, Gould KL (1999) Regulating the onset of mitosis. *Curr Opin Cell Biol* **11:** 267-273.

Oshiro N, Takahashi R, Yoshino K, Tanimura K, Nakashima A, Eguchi S, Miyamoto T, Hara K, Takehana K, Avruch J, Kikkawa U, Yonezawa K (2007) The proline-rich Akt substrate of 40 kDa (PRAS40) is a physiological substrate of mammalian target of rapamycin complex 1. *J Biol Chem* **282:** 20329-20339.

Panasyuk G, Nemazanyy I, Filonenko V, Gout I (2008) Ribosomal protein S6 kinase 1 interacts with and is ubiquitinated by ubiquitin ligase ROC1. *Biochem Biophys Res Commun* **369:** 339-343.

Panasyuk G, Nemazanyy I, Zhyvoloup A, Bretner M, Litchfield DW, Filonenko V, Gout IT (2006) Nuclear export of S6K1 II is regulated by protein kinase CK2 phosphorylation at Ser-17. *J Biol Chem* **281:** 31188-31201.

Park J, Leong ML, Buse P, Maiyar AC, Firestone GL, Hemmings BA (1999) Serum and glucocorticoid-inducible kinase (SGK) is a target of the PI 3-kinase-stimulated signaling pathway. *Embo J* **18:** 3024-3033.

Partovian C, Ju R, Zhuang ZW, Martin KA, Simons M (2008) Syndecan-4 regulates subcellular localization of mTOR Complex2 and Akt activation in a PKCalpha-dependent manner in endothelial cells. *Mol Cell* **32:** 140-149.

Patel S, Doble B, Woodgett JR (2004) Glycogen synthase kinase-3 in insulin and Wnt signaling: a double-edged sword? *Biochem Soc Trans* **32:** 803-808.

Pearce LR, Huang X, Boudeau J, Pawlowski R, Wullschleger S, Deak M, Ibrahim AF, Gourlay R, Magnuson MA, Alessi DR (2007) Identification of Protor as a novel Rictor-binding component of mTOR complex-2. *Biochem J* **405:** 513-522.

Pearson RB, Dennis PB, Han JW, Williamson NA, Kozma SC, Wettenhall RE, Thomas G (1995) The principal target of rapamycin-induced p70s6k inactivation is a novel phosphorylation site within a conserved hydrophobic domain. *Embo J* **14:** 5279-5287.

Pelletier G, Stefanovsky VY, Faubladier M, Hirschler-Laszkiewicz I, Savard J, Rothblum LI, Cote J, Moss T (2000) Competitive recruitment of CBP and Rb-HDAC regulates UBF acetylation and ribosomal transcription. *Mol Cell* **6:** 1059-1066.

Pende M, Um SH, Mieulet V, Sticker M, Goss VL, Mestan J, Mueller M, Fumagalli S, Kozma SC, Thomas G (2004) S6K1(-/-)/S6K2(-/-) mice exhibit perinatal lethality and rapamycin-sensitive 5'-terminal oligopyrimidine mRNA translation and reveal a mitogen-activated protein kinase-dependent S6 kinase pathway. *Mol Cell Biol* **24:** 3112-3124.

Peterson RT, Beal PA, Comb MJ, Schreiber SL (2000) FKBP12-rapamycin-associated protein (FRAP) autophosphorylates at serine 2481 under translationally repressive conditions. *J Biol Chem* **275:** 7416-7423.

Peterson RT, Desai BN, Hardwick JS, Schreiber SL (1999) Protein phosphatase 2A interacts with the 70-kDa S6 kinase and is activated by inhibition of FKBP12-rapamycinassociated protein. *Proc Natl Acad Sci U S A* **96:** 4438-4442.

Peterson TR, Laplante M, Thoreen CC, Sancak Y, Kang SA, Kuehl WM, Gray NS, Sabatini DM (2009) DEPTOR is an mTOR inhibitor frequently overexpressed in multiple myeloma cells and required for their survival. *Cell* **137:** 873-886.

Petit V, Boyer B, Lentz D, Turner CE, Thiery JP, Valles AM (2000) Phosphorylation of tyrosine residues 31 and 118 on paxillin regulates cell migration through an association with CRK in NBT-II cells. *J Cell Biol* **148:** 957-970.

Phin S, Kupferwasser D, Lam J, Lee-Fruman KK (2003) Mutational analysis of ribosomal S6 kinase 2 shows differential regulation of its kinase activity from that of ribosomal S6 kinase 1. *Biochem J* **373:** 583-591.

Porstmann T, Santos CR, Griffiths B, Cully M, Wu M, Leevers S, Griffiths JR, Chung YL, Schulze A (2008) SREBP activity is regulated by mTORC1 and contributes to Akt-dependent cell growth. *Cell Metab* **8:** 224-236.

Potter CJ, Pedraza LG, Xu T (2002) Akt regulates growth by directly phosphorylating Tsc2. *Nat Cell Biol* **4:** 658-665.

Proud CG (2007a) Cell signaling. mTOR, unleashed. *Science* **318:** 926-927.

Proud CG (2007b) Signaling to translation: how signal transduction pathways control the protein synthetic machinery. *Biochem J* **403:** 217-234.

Pullen N, Dennis PB, Andjelkovic M, Dufner A, Kozma SC, Hemmings BA, Thomas G (1998) Phosphorylation and activation of p70s6k by PDK1. *Science* **279:** 707-710.

Pyronnet S, Imataka H, Gingras AC, Fukunaga R, Hunter T, Sonenberg N (1999) Human eukaryotic translation initiation factor 4G (eIF4G) recruits mnk1 to phosphorylate eIF4E. *Embo J* **18:** 270-279.

Raught B, Gingras AC, Gygi SP, Imataka H, Morino S, Gradi A, Aebersold R, Sonenberg N (2000) Serum-stimulated, rapamycin-sensitive phosphorylation sites in the eukaryotic translation initiation factor 4GI. *Embo J* **19:** 434-444.

Raught B, Peiretti F, Gingras AC, Livingstone M, Shahbazian D, Mayeur GL, Polakiewicz RD, Sonenberg N, Hershey JW (2004) Phosphorylation of eucaryotic translation initiation factor 4B Ser422 is modulated by S6 kinases. *Embo J* **23:** 1761-1769.

Redpath NT, Proud CG (1993a) Cyclic AMP-dependent protein kinase phosphorylates rabbit reticulocyte elongation factor-2 kinase and induces calcium-independent activity. *Biochem J* **293 (Pt 1):** 31-34.

Redpath NT, Proud CG (1993b) Purification and phosphorylation of elongation factor-2 kinase from rabbit reticulocytes. *Eur J Biochem* **212:** 511-520.

Reiling JH, Hafen E (2004) The hypoxia-induced paralogs Scylla and Charybdis inhibit growth by down-regulating S6K activity upstream of TSC in Drosophila. *Genes Dev* **18:** 2879-2892.

Richards SA, Dreisbach VC, Murphy LO, Blenis J (2001) Characterization of regulatory events associated with membrane targeting of p90 ribosomal S6 kinase 1. *Mol Cell Biol* **21:** 7470-7480.

Richards SA, Fu J, Romanelli A, Shimamura A, Blenis J (1999) Ribosomal S6 kinase 1 (RSK1) activation requires signals dependent on and independent of the MAP kinase ERK. *Curr Biol* **9:** 810-820.

Richardson CJ, Broenstrup M, Fingar DC, Julich K, Ballif BA, Gygi S, Blenis J (2004) SKAR is a specific target of S6 kinase 1 in cell growth control. *Curr Biol* **14:** 1540-1549.

Rickard JE, Kreis TE (1991) Binding of pp170 to microtubules is regulated by phosphorylation. *J Biol Chem* **266:** 17597-17605.

Rinner O, Mueller LN, Hubalek M, Muller M, Gstaiger M, Aebersold R (2007) An integrated mass spectrometric and computational framework for the analysis of protein interaction networks. *Nat Biotechnol* **25:** 345-352.

Rivera VM, Miranti CK, Misra RP, Ginty DD, Chen RH, Blenis J, Greenberg ME (1993) A growth factor-induced kinase phosphorylates the serum response factor at a site that regulates its DNA-binding activity. *Mol Cell Biol* **13:** 6260-6273.

Rodier G, Montagnoli A, Di Marcotullio L, Coulombe P, Draetta GF, Pagano M, Meloche S (2001) p27 cytoplasmic localization is regulated by phosphorylation on Ser10 and is not a prerequisite for its proteolysis. *Embo J* **20:** 6672-6682.

Rodilla V, Villanueva A, Obrador-Hevia A, Robert-Moreno A, Fernandez-Majada V, Grilli A, Lopez-Bigas N, Bellora N, Alba MM, Torres F, Dunach M, Sanjuan X, Gonzalez S, Gridley T, Capella G, Bigas A, Espinosa L (2009) Jagged1 is the pathological link between Wnt and Notch pathways in colorectal cancer. *Proc Natl Acad Sci U S A* **106:** 6315-6320.

Roig J, Traugh JA (2001) Cytostatic p21 G protein-activated protein kinase gamma-PAK. *Vitam Horm* **62:** 167-198.

Rolfe M, McLeod LE, Pratt PF, Proud CG (2005) Activation of protein synthesis in cardiomyocytes by the hypertrophic agent phenylephrine requires the activation of ERK and involves phosphorylation of tuberous sclerosis complex 2 (TSC2). *Biochem J* **388:** 973-984.

Roose J, Huls G, van Beest M, Moerer P, van der Horn K, Goldschmeding R, Logtenberg T, Clevers H (1999) Synergy between tumor suppressor APC and the beta-catenin-Tcf4 target Tcf1. *Science* **285:** 1923-1926.

Rosner M, Freilinger A, Hengstschlager M (2007) Akt regulates nuclear/cytoplasmic localization of tuberin. *Oncogene* **26:** 521-531.

Rossi R, Pester JM, McDowell M, Soza S, Montecucco A, Lee-Fruman KK (2007) Identification of S6K2 as a centrosome-located kinase. *FEBS Lett* **581:** 4058-4064.

Rothwarf DM, Karin M (1999) The NF-kappa B activation pathway: a paradigm in information transfer from membrane to nucleus. *Sci STKE* **1999:** RE1.

Roux PP, Ballif BA, Anjum R, Gygi SP, Blenis J (2004a) Tumor-promoting phorbol esters and activated Ras inactivate the tuberous sclerosis tumor suppressor complex via p90 ribosomal S6 kinase. *Proc Natl Acad Sci U S A* **101:** 13489-13494.

Roux PP, Blenis J (2004b) ERK and p38 MAPK-activated protein kinases: a family of protein kinases with diverse biological functions. *Microbiol Mol Biol Rev* **68:** 320-344.

Roux PP, Richards SA, Blenis J (2003) Phosphorylation of p90 ribosomal S6 kinase (RSK) regulates extracellular signal-regulated kinase docking and RSK activity. *Mol Cell Biol* **23:** 4796-4804.

Roux PP, Shahbazian D, Vu H, Holz MK, Cohen MS, Taunton J, Sonenberg N, Blenis J (2007) RAS/ERK signaling promotes site-specific ribosomal protein S6 phosphorylation via RSK and stimulates cap-dependent translation. *J Biol Chem* **282:** 14056-14064.

Rui L, Yuan M, Frantz D, Shoelson S, White MF (2002) SOCS-1 and SOCS-3 block insulin signaling by ubiquitin-mediated degradation of IRS1 and IRS2. *J Biol Chem* **277:** 42394-42398.

Ruvinsky I, Sharon N, Lerer T, Cohen H, Stolovich-Rain M, Nir T, Dor Y, Zisman P, Meyuhas O (2005) Ribosomal protein S6 phosphorylation is a determinant of cell size and glucose homeostasis. *Genes Dev* **19:** 2199-2211.

Sabe H, Hata A, Okada M, Nakagawa H, Hanafusa H (1994) Analysis of the binding of the Src homology 2 domain of Csk to tyrosine-phosphorylated proteins in the suppression and mitotic activation of c-Src. *Proc Natl Acad Sci U S A* **91:** 3984-3988.

Saghir AN, Tuxworth WJ, Jr., Hagedorn CH, McDermott PJ (2001) Modifications of eukaryotic initiation factor 4F (eIF4F) in adult cardiocytes by adenoviral gene transfer: differential effects on eIF4F activity and total protein synthesis rates. *Biochem J* **356:** 557-566.

Saitoh M, Pullen N, Brennan P, Cantrell D, Dennis PB, Thomas G (2002) Regulation of an activated S6 kinase 1 variant reveals a novel mammalian target of rapamycin phosphorylation site. *J Biol Chem* **277:** 20104-20112.

Salgia R, Uemura N, Okuda K, Li JL, Pisick E, Sattler M, de Jong R, Druker B, Heisterkamp N, Chen LB, et al. (1995) CRKL links p210BCR/ABL with paxillin in chronic myelogenous leukemia cells. *J Biol Chem* **270:** 29145-29150.

Sancak Y, Peterson TR, Shaul YD, Lindquist RA, Thoreen CC, Bar-Peled L, Sabatini DM (2008) The Rag GTPases bind raptor and mediate amino acid signaling to mTORC1. *Science* **320:** 1496-1501.

Sancak Y, Thoreen CC, Peterson TR, Lindquist RA, Kang SA, Spooner E, Carr SA, Sabatini DM (2007) PRAS40 is an insulin-regulated inhibitor of the mTORC1 protein kinase. *Mol Cell* **25:** 903-915.

Sanders MJ, Grondin PO, Hegarty BD, Snowden MA, Carling D (2007) Investigating the mechanism for AMP activation of the AMP-activated protein kinase cascade. *Biochem J* **403:** 139-148.

Sarbassov DD, Ali SM, Kim DH, Guertin DA, Latek RR, Erdjument-Bromage H, Tempst P, Sabatini DM (2004) Rictor, a novel binding partner of mTOR, defines a rapamycin-insensitive and raptor-independent pathway that regulates the cytoskeleton. *Curr Biol* **14:** 1296-1302.

Sarbassov DD, Ali SM, Sengupta S, Sheen JH, Hsu PP, Bagley AF, Markhard AL, Sabatini DM (2006) Prolonged rapamycin treatment inhibits mTORC2 assembly and Akt/PKB. *Mol Cell* **22:** 159-168.

Sarbassov DD, Guertin DA, Ali SM, Sabatini DM (2005) Phosphorylation and regulation of Akt/PKB by the rictor-mTOR complex. *Science* **307:** 1098-1101.

Sastry SK, Lyons PD, Schaller MD, Burridge K (2002) PTP-PEST controls motility through regulation of Rac1. *J Cell Sci* **115:** 4305-4316.

Sato S, Fujita N, Tsuruo T (2000) Modulation of Akt kinase activity by binding to Hsp90. *Proc Natl Acad Sci U S A* **97:** 10832-10837.

Schaefer BC, Ware MF, Marrack P, Fanger GR, Kappler JW, Johnson GL, Monks CR (1999) Live cell fluorescence imaging of T cell MEKK2: redistribution and activation in response to antigen stimulation of the T cell receptor. *Immunity* **11:** 411-421.

Schaller MD, Parsons JT (1995) pp125FAK-dependent tyrosine phosphorylation of paxillin creates a high-affinity binding site for Crk. *Mol Cell Biol* **15:** 2635-2645.

Scheid MP, Marignani PA, Woodgett JR (2002) Multiple phosphoinositide 3-kinase-dependent steps in activation of protein kinase B. *Mol Cell Biol* **22:** 6247-6260.

Scheper GC, van Kollenburg B, Hu J, Luo Y, Goss DJ, Proud CG (2002) Phosphorylation of eukaryotic initiation factor 4E markedly reduces its affinity for capped mRNA. *J Biol Chem* **277:** 3303-3309.

Schlosser A, Bodem J, Bossemeyer D, Grummt I, Lehmann WD (2002) Identification of protein phosphorylation sites by combination of elastase digestion, immobilized metal affinity chromatography, and quadrupole-time of flight tandem mass spectrometry. *Proteomics* **2:** 911-918.

Schroder W, Bushell G, Sculley T (2005) The human stress-activated protein kinase-interacting 1 gene encodes JNK-binding proteins. *Cell Signal* **17:** 761-767.

Schuyler SC, Pellman D (2001) Microtubule "plus-end-tracking proteins": The end is just the beginning. *Cell* **105:** 421-424.

Scott KL, Kabbarah O, Liang MC, Ivanova E, Anagnostou V, Wu J, Dhakal S, Wu M, Chen S, Feinberg T, Huang J, Saci A, Widlund HR, Fisher DE, Xiao Y, Rimm DL, Protopopov A, Wong KK, Chin L (2009) GOLPH3 modulates mTOR signaling and rapamycin sensitivity in cancer. *Nature* **459:** 1085-1090.

Settleman J, Albright CF, Foster LC, Weinberg RA (1992) Association between GTPase activators for Rho and Ras families. *Nature* **359:** 153-154.

Shahbazian D, Roux PP, Mieulet V, Cohen MS, Raught B, Taunton J, Hershey JW, Blenis J, Pende M, Sonenberg N (2006) The mTOR/PI3K and MAPK pathways converge on eIF4B to control its phosphorylation and activity. *Embo J* **25:** 2781-2791.

Shaw M, Cohen P, Alessi DR (1997) Further evidence that the inhibition of glycogen synthase kinase-3beta by IGF-1 is mediated by PDK1/PKB-induced phosphorylation of Ser-9 and not by dephosphorylation of Tyr-216. *FEBS Lett* **416:** 307-311.

Shaw RJ (2008) mTOR signaling: RAG GTPases transmit the amino acid signal. *Trends Biochem Sci* **33:** 565-568.

Shaw RJ, Kosmatka M, Bardeesy N, Hurley RL, Witters LA, DePinho RA, Cantley LC (2004) The tumor suppressor LKB1 kinase directly activates AMP-activated kinase and regulates apoptosis in response to energy stress. *Proc Natl Acad Sci U S A* **101:** 3329-3335.

Sherr CJ, Roberts JM (1999) CDK inhibitors: positive and negative regulators of G1-phase progression. *Genes Dev* **13:** 1501-1512.

Shih AH, Holland EC (2006) Platelet-derived growth factor (PDGF) and glial tumorigenesis. *Cancer Lett* **232:** 139-147.

Shimamura A, Ballif BA, Richards SA, Blenis J (2000) Rsk1 mediates a MEK-MAP kinase cell survival signal. *Curr Biol* **10:** 127-135.

Shimokawa T, Furukawa Y, Sakai M, Li M, Miwa N, Lin YM, Nakamura Y (2003) Involvement of the FGF18 gene in colorectal carcinogenesis, as a novel downstream target of the beta-catenin/T-cell factor complex. *Cancer Res* **63:** 6116-6120.

Shin I, Yakes FM, Rojo F, Shin NY, Bakin AV, Baselga J, Arteaga CL (2002) PKB/Akt mediates cell-cycle progression by phosphorylation of p27(Kip1) at threonine 157 and modulation of its cellular localization. *Nat Med* **8:** 1145-1152.

Shiota C, Woo JT, Lindner J, Shelton KD, Magnuson MA (2006) Multiallelic disruption of the rictor gene in mice reveals that mTOR complex 2 is essential for fetal growth and viability. *Dev Cell* **11:** 583-589.

Shoshani T, Faerman A, Mett I, Zelin E, Tenne T, Gorodin S, Moshel Y, Elbaz S, Budanov A, Chajut A, Kalinski H, Kamer I, Rozen A, Mor O, Keshet E, Leshkowitz D, Einat P, Skaliter R, Feinstein E (2002) Identification of a novel hypoxia-inducible factor 1-responsive gene, RTP801, involved in apoptosis. *Mol Cell Biol* **22:** 2283-2293.

Shtutman M, Zhurinsky J, Simcha I, Albanese C, D'Amico M, Pestell R, Ben-Ze'ev A (1999) The cyclin D1 gene is a target of the beta-catenin/LEF-1 pathway. *Proc Natl Acad Sci U S A* **96:** 5522-5527.

Silva RL, Wendel HG (2008) MNK, EIF4E and targeting translation for therapy. *Cell Cycle* **7:** 553-555.

Simons M, Horowitz A (2001) Syndecan-4-mediated signaling. *Cell Signal* **13:** 855-862.

Smalley MJ, Sara E, Paterson H, Naylor S, Cook D, Jayatilake H, Fryer LG, Hutchinson L, Fry MJ, Dale TC (1999) Interaction of axin and Dvl-2 proteins regulates Dvl-2-stimulated TCF-dependent transcription. *Embo J* **18:** 2823-2835.

Smith EM, Finn SG, Tee AR, Browne GJ, Proud CG (2005) The tuberous sclerosis protein TSC2 is not required for the regulation of the mammalian target of rapamycin by amino acids and certain cellular stresses. *J Biol Chem* **280:** 18717-18727.

Smith EM, Proud CG (2008) cdc2-cyclin B regulates eEF2 kinase activity in a cell cycle- and amino acid-dependent manner. *Embo J* **27:** 1005-1016.

Smith JA, Poteet-Smith CE, Malarkey K, Sturgill TW (1999) Identification of an extracellular signal-regulated kinase (ERK) docking site in ribosomal S6 kinase, a sequence critical for activation by ERK in vivo. *J Biol Chem* **274:** 2893-2898.

Sonnenburg ED, Gao T, Newton AC (2001) The phosphoinositide-dependent kinase, PDK-1, phosphorylates conventional protein kinase C isozymes by a mechanism that is independent of phosphoinositide 3-kinase. *J Biol Chem* **276:** 45289-45297.

Stambolic V, MacPherson D, Sas D, Lin Y, Snow B, Jang Y, Benchimol S, Mak TW (2001) Regulation of PTEN transcription by p53. *Mol Cell* **8:** 317-325.

Stein MP, Feng Y, Cooper KL, Welford AM, Wandinger-Ness A (2003) Human VPS34 and p150 are Rab7 interacting partners. *Traffic* **4:** 754-771.

Sternlicht H, Farr GW, Sternlicht ML, Driscoll JK, Willison K, Yaffe MB (1993) The t-complex polypeptide 1 complex is a chaperonin for tubulin and actin in vivo. *Proc Natl Acad Sci U S A* **90:** 9422-9426.

Stokoe D, Stephens LR, Copeland T, Gaffney PR, Reese CB, Painter GF, Holmes AB, McCormick F, Hawkins PT (1997) Dual role of phosphatidylinositol-3,4,5-trisphosphate in the activation of protein kinase B. *Science* **277:** 567-570.

Sun Y, Chen J (2008a) mTOR signaling: PLD takes center stage. *Cell Cycle* **7:** 3118-3123.

Sun Y, Fang Y, Yoon MS, Zhang C, Roccio M, Zwartkruis FJ, Armstrong M, Brown HA, Chen J (2008b) Phospholipase D1 is an effector of Rheb in the mTOR pathway. *Proc Natl Acad Sci U S A* **105:** 8286-8291.

Sutherland C, Alterio J, Campbell DG, Le Bourdelles B, Mallet J, Haavik J, Cohen P (1993a) Phosphorylation and activation of human tyrosine hydroxylase in vitro by mitogen-activated protein (MAP) kinase and MAP-kinase-activated kinases 1 and 2. *Eur J Biochem* **217:** 715-722.

Sutherland C, Leighton IA, Cohen P (1993b) Inactivation of glycogen synthase kinase-3 beta by phosphorylation: new kinase connections in insulin and growth-factor signaling. *Biochem J* **296 (Pt 1):** 15-19.

Takai H, Wang RC, Takai KK, Yang H, de Lange T (2007) Tel2 regulates the stability of PI3K-related protein kinases. *Cell* **131:** 1248-1259.

Takano A, Usui I, Haruta T, Kawahara J, Uno T, Iwata M, Kobayashi M (2001) Mammalian target of rapamycin pathway regulates insulin signaling via subcellular redistribution of insulin receptor substrate 1 and integrates nutritional signals and metabolic signals of insulin. *Mol Cell Biol* **21:** 5050-5062.

Tallquist M, Kazlauskas A (2004) PDGF signaling in cells and mice. *Cytokine Growth Factor Rev* **15:** 205-213.

Tamai K, Semenov M, Kato Y, Spokony R, Liu C, Katsuyama Y, Hess F, Saint-Jeannet JP, He X (2000) LDL-receptor-related proteins in Wnt signal transduction. *Nature* **407:** 530-535.

Tamai K, Zeng X, Liu C, Zhang X, Harada Y, Chang Z, He X (2004) A mechanism for Wnt coreceptor activation. *Mol Cell* **13:** 149-156.

Tange TO, Nott A, Moore MJ (2004) The ever-increasing complexities of the exon junction complex. *Curr Opin Cell Biol* **16:** 279-284.

Tee AR, Blenis J (2005a) mTOR, translational control and human disease. *Semin Cell Dev Biol* **16:** 29-37.

Tee AR, Blenis J, Proud CG (2005b) Analysis of mTOR signaling by the small G-proteins, Rheb and RhebL1. *FEBS Lett* **579:** 4763-4768.

Tessier M, Woodgett JR (2006) Serum and glucocorticoid-regulated protein kinases: variations on a theme. *J Cell Biochem* **98:** 1391-1407.

Thedieck K, Polak P, Kim ML, Molle KD, Cohen A, Jeno P, Arrieumerlou C, Hall MN (2007) PRAS40 and PRR5-like protein are new mTOR interactors that regulate apoptosis. *PLoS One* **2:** e1217.

Thoreen CC, Kang SA, Chang JW, Liu Q, Zhang J, Gao Y, Reichling LJ, Sim T, Sabatini DM, Gray NS (2009) An ATP-competitive mammalian target of rapamycin inhibitor reveals rapamycin-resistant functions of mTORC1. *J Biol Chem* **284:** 8023-8032.

Thulasiraman V, Yang CF, Frydman J (1999) In vivo newly translated polypeptides are sequestered in a protected folding environment. *Embo J* **18:** 85-95.

Tkachenko E, Rhodes JM, Simons M (2005) Syndecans: new kids on the signaling block. *Circ Res* **96:** 488-500.

Tokino T, Nakamura Y (2000) The role of p53-target genes in human cancer. *Crit Rev Oncol Hematol* **33:** 1-6.

Torres MA, Eldar-Finkelman H, Krebs EG, Moon RT (1999) Regulation of ribosomal S6 protein kinase-p90(rsk), glycogen synthase kinase 3, and beta-catenin in early Xenopus development. *Mol Cell Biol* **19:** 1427-1437.

Toschi A, Lee E, Xu L, Garcia A, Gadir N, Foster DA (2009) Regulation of mTORC1 and mTORC2 complex assembly by phosphatidic acid: competition with rapamycin. *Mol Cell Biol* **29:** 1411-1420.

Tsubouchi A, Sakakura J, Yagi R, Mazaki Y, Schaefer E, Yano H, Sabe H (2002) Localized suppression of RhoA activity by Tyr31/118-phosphorylated paxillin in cell adhesion and migration. *J Cell Biol* **159:** 673-683.

Tuan JC, Zhai W, Comai L (1999) Recruitment of TATA-binding protein-TAFI complex SL1 to the human ribosomal DNA promoter is mediated by the carboxy-terminal activation domain of upstream binding factor (UBF) and is regulated by UBF phosphorylation. *Mol Cell Biol* **19:** 2872-2879.

Tuazon PT, Merrick WC, Traugh JA (1989) Comparative analysis of phosphorylation of translational initiation and elongation factors by seven protein kinases. *J Biol Chem* **264:** 2773-2777.

Tuazon PT, Morley SJ, Dever TE, Merrick WC, Rhoads RE, Traugh JA (1990) Association of initiation factor eIF-4E in a cap binding protein complex (eIF-4F) is critical for and enhances phosphorylation by protein kinase C. *J Biol Chem* **265:** 10617-10621.

Ueda T, Watanabe-Fukunaga R, Fukuyama H, Nagata S, Fukunaga R (2004) Mnk2 and Mnk1 are essential for constitutive and inducible phosphorylation of eukaryotic initiation factor 4E but not for cell growth or development. *Mol Cell Biol* **24:** 6539-6549.

Um SH, Frigerio F, Watanabe M, Picard F, Joaquin M, Sticker M, Fumagalli S, Allegrini PR, Kozma SC, Auwerx J, Thomas G (2004) Absence of S6K1 protects against age- and diet-induced obesity while enhancing insulin sensitivity. *Nature* **431:** 200-205.

Ursic D, Sedbrook JC, Himmel KL, Culbertson MR (1994) The essential yeast Tcp1 protein affects actin and microtubules. *Mol Biol Cell* **5:** 1065-1080.

Vallabhapurapu S, Karin M (2009) Regulation and function of NF-kappaB transcription factors in the immune system. *Annu Rev Immunol* **27:** 693-733.

Valles AM, Beuvin M, Boyer B (2004) Activation of Rac1 by paxillin-Crk-DOCK180 signaling complex is antagonized by Rap1 in migrating NBT-II cells. *J Biol Chem* **279:** 44490-44496.

Valovka T, Verdier F, Cramer R, Zhyvoloup A, Fenton T, Rebholz H, Wang ML, Gzhegotsky M, Lutsyk A, Matsuka G, Filonenko V, Wang L, Proud CG, Parker PJ, Gout IT (2003) Protein kinase C phosphorylates ribosomal protein S6 kinase betaII and regulates its subcellular localization. *Mol Cell Biol* **23:** 852-863.

Vander Haar E, Lee SI, Bandhakavi S, Griffin TJ, Kim DH (2007) Insulin signaling to mTOR mediated by the Akt/PKB substrate PRAS40. *Nat Cell Biol* **9:** 316-323.

Viglietto G, Motti ML, Fusco A (2002) Understanding p27(kip1) deregulation in cancer: down-regulation or mislocalization. *Cell Cycle* **1:** 394-400.

Vik TA, Ryder JW (1997) Identification of serine 380 as the major site of autophosphorylation of Xenopus pp90rsk. *Biochem Biophys Res Commun* **235:** 398-402.

Voit R, Grummt I (2001) Phosphorylation of UBF at serine 388 is required for interaction with RNA polymerase I and activation of rDNA transcription. *Proc Natl Acad Sci U S A* **98:** 13631-13636.

Voit R, Hoffmann M, Grummt I (1999) Phosphorylation by G1-specific cdk-cyclin complexes activates the nucleolar transcription factor UBF. *Embo J* **18:** 1891-1899.

Voit R, Schafer K, Grummt I (1997) Mechanism of repression of RNA polymerase I transcription by the retinoblastoma protein. *Mol Cell Biol* **17:** 4230-4237.

Voit R, Schnapp A, Kuhn A, Rosenbauer H, Hirschmann P, Stunnenberg HG, Grummt I (1992) The nucleolar transcription factor mUBF is phosphorylated by casein kinase II in the C-terminal hyperacidic tail which is essential for transactivation. *Embo J* **11:** 2211-2218.

Vousden KH, Lane DP (2007) p53 in health and disease. *Nat Rev Mol Cell Biol* **8:** 275-283.

Wang L, Harris TE, Lawrence JC, Jr. (2008) Regulation of proline-rich Akt substrate of 40 kDa (PRAS40) function by mammalian target of rapamycin complex 1 (mTORC1)-mediated phosphorylation. *J Biol Chem* **283:** 15619-15627.

Wang L, Harris TE, Roth RA, Lawrence JC, Jr. (2007) PRAS40 regulates mTORC1 kinase activity by functioning as a direct inhibitor of substrate binding. *J Biol Chem* **282:** 20036-20044.

Wang L, Lawrence JC, Jr., Sturgill TW, Harris TE (2009) Mammalian target of rapamycin complex 1 (mTORC1) activity is associated with phosphorylation of raptor by mTOR. *J Biol Chem* **284:** 14693-14697.

Wang X, Beugnet A, Murakami M, Yamanaka S, Proud CG (2005) Distinct signaling events downstream of mTOR cooperate to mediate the effects of amino acids and insulin on initiation factor 4E-binding proteins. *Mol Cell Biol* **25:** 2558-2572.

Wang X, Li W, Parra JL, Beugnet A, Proud CG (2003a) The C terminus of initiation factor 4E-binding protein 1 contains multiple regulatory features that influence its function and phosphorylation. *Mol Cell Biol* **23:** 1546-1557.

Wang X, Li W, Williams M, Terada N, Alessi DR, Proud CG (2001a) Regulation of elongation factor 2 kinase by p90(RSK1) and p70 S6 kinase. *Embo J* **20:** 4370-4379.

Wang X, Paulin FE, Campbell LE, Gomez E, O'Brien K, Morrice N, Proud CG (2001b) Eukaryotic initiation factor 2B: identification of multiple phosphorylation sites in the epsilon-subunit and their functions in vivo. *Embo J* **20:** 4349-4359.

Wang Z, Zhang B, Wang M, Carr BI (2003b) Persistent ERK phosphorylation negatively regulates cAMP response element-binding protein (CREB) activity via recruitment of CREB-binding protein to pp90RSK. *J Biol Chem* **278:** 11138-11144.

Waskiewicz AJ, Flynn A, Proud CG, Cooper JA (1997) Mitogen-activated protein kinases activate the serine/threonine kinases Mnk1 and Mnk2. *Embo J* **16:** 1909-1920.

Waskiewicz AJ, Johnson JC, Penn B, Mahalingam M, Kimball SR, Cooper JA (1999) Phosphorylation of the cap-binding protein eukaryotic translation initiation factor 4E by protein kinase Mnk1 in vivo. *Mol Cell Biol* **19:** 1871-1880.

Watanabe R, Tambe Y, Inoue H, Isono T, Haneda M, Isobe K, Kobayashi T, Hino O, Okabe H, Chano T (2007) GADD34 inhibits mammalian target of rapamycin signaling via tuberous sclerosis complex and controls cell survival under bioenergetic stress. *Int J Mol Med* **19:** 475-483.

Webster KA, Graham RM, Bishopric NH (2005) BNip3 and signal-specific programmed death in the heart. *J Mol Cell Cardiol* **38:** 35-45.

Wehrli M, Dougan ST, Caldwell K, O'Keefe L, Schwartz S, Vaizel-Ohayon D, Schejter E, Tomlinson A, DiNardo S (2000) arrow encodes an LDL-receptor-related protein essential for Wingless signaling. *Nature* **407:** 527-530.

Welcker M, Clurman BE (2008) FBW7 ubiquitin ligase: a tumour suppressor at the crossroads of cell division, growth and differentiation. *Nat Rev Cancer* **8:** 83-93.

Welsh GI, Miller CM, Loughlin AJ, Price NT, Proud CG (1998) Regulation of eukaryotic initiation factor eIF2B: glycogen synthase kinase-3 phosphorylates a conserved serine which undergoes dephosphorylation in response to insulin. *FEBS Lett* **421:** 125-130.

Welsh GI, Proud CG (1993) Glycogen synthase kinase-3 is rapidly inactivated in response to insulin and phosphorylates eukaryotic initiation factor eIF-2B. *Biochem J* **294 (Pt 3):** 625-629.

Wendel HG, Silva RL, Malina A, Mills JR, Zhu H, Ueda T, Watanabe-Fukunaga R, Fukunaga R, Teruya-Feldstein J, Pelletier J, Lowe SW (2007) Dissecting eIF4E action in tumorigenesis. *Genes Dev* **21:** 3232-3237.

Wertz IE, O'Rourke KM, Zhou H, Eby M, Aravind L, Seshagiri S, Wu P, Wiesmann C, Baker R, Boone DL, Ma A, Koonin EV, Dixit VM (2004) De-ubiquitination and ubiquitin ligase domains of A20 downregulate NF-kappaB signaling. *Nature* **430:** 694-699.

White MF (1998) The IRS-signaling system: a network of docking proteins that mediate insulin action. *Mol Cell Biochem* **182:** 3-11.

White RJ (2008) RNA polymerases I and III, non-coding RNAs and cancer. *Trends Genet* **24:** 622-629.

Wielenga VJ, Smits R, Korinek V, Smit L, Kielman M, Fodde R, Clevers H, Pals ST (1999) Expression of CD44 in Apc and Tcf mutant mice implies regulation by the WNT pathway. *Am J Pathol* **154:** 515-523.

Wilker EW, van Vugt MA, Artim SA, Huang PH, Petersen CP, Reinhardt HC, Feng Y, Sharp PA, Sonenberg N, White FM, Yaffe MB (2007) 14-3-3sigma controls mitotic translation to facilitate cytokinesis. *Nature* **446:** 329-332.

Willert K, Shibamoto S, Nusse R (1999) Wnt-induced dephosphorylation of axin releases beta-catenin from the axin complex. *Genes Dev* **13:** 1768-1773.

Williams MR, Arthur JS, Balendran A, van der Kaay J, Poli V, Cohen P, Alessi DR (2000) The role of 3-phosphoinositide-dependent protein kinase 1 in activating AGC kinases defined in embryonic stem cells. *Curr Biol* **10:** 439-448.

Wilson NS, Dixit V, Ashkenazi A (2009) Death receptor signal transducers: nodes of coordination in immune signaling networks. *Nat Immunol* **10:** 348-355.

Wingate AD, Campbell DG, Peggie M, Arthur JS (2006) Nur77 is phosphorylated in cells by RSK in response to mitogenic stimulation. *Biochem J* **393:** 715-724.

Woiwode A, Johnson SA, Zhong S, Zhang C, Roeder RG, Teichmann M, Johnson DL (2008) PTEN represses RNA polymerase III-dependent transcription by targeting the TFIIIB complex. *Mol Cell Biol* **28:** 4204-4214.

Won KA, Schumacher RJ, Farr GW, Horwich AL, Reed SI (1998) Maturation of human cyclin E requires the function of eukaryotic chaperonin CCT. *Mol Cell Biol* **18:** 7584-7589.

Woo SY, Kim DH, Jun CB, Kim YM, Haar EV, Lee SI, Hegg JW, Bandhakavi S, Griffin TJ, Kim DH (2007) PRR5, a novel component of mTOR complex 2, regulates platelet-derived growth factor receptor beta expression and signaling. *J Biol Chem* **282:** 25604-25612.

Woods A, Dickerson K, Heath R, Hong SP, Momcilovic M, Johnstone SR, Carlson M, Carling D (2005) Ca2+/calmodulin-dependent protein kinase kinase-beta acts upstream of AMP-activated protein kinase in mammalian cells. *Cell Metab* **2:** 21-33.

Woods A, Johnstone SR, Dickerson K, Leiper FC, Fryer LG, Neumann D, Schlattner U, Wallimann T, Carlson M, Carling D (2003) LKB1 is the upstream kinase in the AMP-activated protein kinase cascade. *Curr Biol* **13:** 2004-2008.

Woods AJ, Roberts MS, Choudhary J, Barry ST, Mazaki Y, Sabe H, Morley SJ, Critchley DR, Norman JC (2002) Paxillin associates with poly(A)-binding protein 1 at the dense endoplasmic reticulum and the leading edge of migrating cells. *J Biol Chem* **277:** 6428-6437.

Woods YL, Cohen P, Becker W, Jakes R, Goedert M, Wang X, Proud CG (2001) The kinase DYRK phosphorylates protein-synthesis initiation factor eIF2Bepsilon at Ser539 and the microtubule-associated protein tau at Thr212: potential role for DYRK as a glycogen synthase kinase 3-priming kinase. *Biochem J* **355:** 609-615.

Wouters BG, Koritzinsky M (2008) Hypoxia signaling through mTOR and the unfolded protein response in cancer. *Nat Rev Cancer* **8:** 851-864.

Wu J, Janknecht R (2002) Regulation of the ETS transcription factor ER81 by the 90-kDa ribosomal S6 kinase 1 and protein kinase A. *J Biol Chem* **277:** 42669-42679.

Wu M, Hemesath TJ, Takemoto CM, Horstmann MA, Wells AG, Price ER, Fisher DZ, Fisher DE (2000) c-Kit triggers dual phosphorylations, which couple activation and degradation of the essential melanocyte factor Mi. *Genes Dev* **14:** 301-312.

Wullschleger S, Loewith R, Hall MN (2006) TOR signaling in growth and metabolism. *Cell* **124:** 471-484.

Xu X, Sarikas A, Dias-Santagata DC, Dolios G, Lafontant PJ, Tsai SC, Zhu W, Nakajima H, Nakajima HO, Field LJ, Wang R, Pan ZQ (2008) The CUL7 E3 ubiquitin ligase targets insulin receptor substrate 1 for ubiquitin-dependent degradation. *Mol Cell* **30:** 403-414.

Yam AY, Xia Y, Lin HT, Burlingame A, Gerstein M, Frydman J (2008) Defining the TRiC/CCT interactome links chaperonin function to stabilization of newly made proteins with complex topologies. *Nat Struct Mol Biol* **15:** 1255-1262.

Yamamoto H, Kishida S, Kishida M, Ikeda S, Takada S, Kikuchi A (1999) Phosphorylation of axin, a Wnt signal negative regulator, by glycogen synthase kinase-3beta regulates its stability. *J Biol Chem* **274:** 10681-10684.

Yan L, Mieulet V, Lamb RF (2008) mTORC2 is the hydrophobic motif kinase for SGK1. *Biochem J* **416:** e19-21.

Yan Y, Backer JM (2007) Regulation of class III (Vps34) PI3Ks. *Biochem Soc Trans* **35:** 239-241.

Yang-Snyder J, Miller JR, Brown JD, Lai CJ, Moon RT (1996) A frizzled homolog functions in a vertebrate Wnt signaling pathway. *Curr Biol* **6:** 1302-1306.

Yang HS, Cho MH, Zakowicz H, Hegamyer G, Sonenberg N, Colburn NH (2004) A novel function of the MA-3 domains in transformation and translation suppressor Pdcd4 is essential for its binding to eukaryotic translation initiation factor 4A. *Mol Cell Biol* **24:** 3894-3906.

Yang HS, Jansen AP, Komar AA, Zheng X, Merrick WC, Costes S, Lockett SJ, Sonenberg N, Colburn NH (2003) The transformation suppressor Pdcd4 is a novel eukaryotic translation initiation factor 4A binding protein that inhibits translation. *Mol Cell Biol* **23:** 26-37.

Yang J, Cron P, Thompson V, Good VM, Hess D, Hemmings BA, Barford D (2002) Molecular mechanism for the regulation of protein kinase B/Akt by hydrophobic motif phosphorylation. *Mol Cell* **9:** 1227-1240.

Yang J, Lin Y, Guo Z, Cheng J, Huang J, Deng L, Liao W, Chen Z, Liu Z, Su B (2001) The essential role of MEKK3 in TNF-induced NF-kappaB activation. *Nat Immunol* **2:** 620-624.

Yang Q, Inoki K, Ikenoue T, Guan KL (2006) Identification of Sin1 as an essential TORC2 component required for complex formation and kinase activity. *Genes Dev* **20:** 2820-2832.

Yang TT, Xiong Q, Graef IA, Crabtree GR, Chow CW (2005) Recruitment of the extracellular signal-regulated kinase/ribosomal S6 kinase signaling pathway to the NFATc4 transcription activation complex. *Mol Cell Biol* **25:** 907-920.

Yap TA, Garrett MD, Walton MI, Raynaud F, de Bono JS, Workman P (2008) Targeting the PI3K-AKT-mTOR pathway: progress, pitfalls, and promises. *Curr Opin Pharmacol* **8:** 393-412.

York B, Lou D, Noonan DJ (2006) Tuberin nuclear localization can be regulated by phosphorylation of its carboxyl terminus. *Mol Cancer Res* **4:** 885-897.

York B, Lou D, Panettieri RA, Jr., Krymskaya VP, Vanaman TC, Noonan DJ (2005) Cross-talk between tuberin, calmodulin, and estrogen signaling pathways. *Faseb J* **19:** 1202-1204.

Young MR, Liu SW, Meisinger J (2003) Protein phosphatase-2A restricts migration of Lewis lung carcinoma cells by modulating the phosphorylation of focal adhesion proteins. *Int J Cancer* **103:** 38-44.

Zeng X, Huang H, Tamai K, Zhang X, Harada Y, Yokota C, Almeida K, Wang J, Doble B, Woodgett J, Wynshaw-Boris A, Hsieh JC, He X (2008) Initiation of Wnt signaling: control of Wnt coreceptor Lrp6 phosphorylation/activation via frizzled, dishevelled and axin functions. *Development* **135:** 367-375.

Zeng X, Tamai K, Doble B, Li S, Huang H, Habas R, Okamura H, Woodgett J, He X (2005) A dual-kinase mechanism for Wnt co-receptor phosphorylation and activation. *Nature* **438:** 873-877.

Zenke FT, King CC, Bohl BP, Bokoch GM (1999) Identification of a central phosphorylation site in p21-activated kinase regulating autoinhibition and kinase activity. *J Biol Chem* **274:** 32565-32573.

Zhai W, Comai L (2000) Repression of RNA polymerase I transcription by the tumor suppressor p53. *Mol Cell Biol* **20:** 5930-5938.

Zhang C, Comai L, Johnson DL (2005) PTEN represses RNA Polymerase I transcription by disrupting the SL1 complex. *Mol Cell Biol* **25:** 6899-6911.

Zhang H, Bajraszewski N, Wu E, Wang H, Moseman AP, Dabora SL, Griffin JD, Kwiatkowski DJ (2007) PDGFRs are critical for PI3K/Akt activation and negatively regulated by mTOR. *J Clin Invest* **117:** 730-738.

Zhang HH, Huang J, Duvel K, Boback B, Wu S, Squillace RM, Wu CL, Manning BD (2009) Insulin stimulates adipogenesis through the Akt-TSC2-mTORC1 pathway. *PLoS One* **4:** e6189.

Zhang HH, Lipovsky AI, Dibble CC, Sahin M, Manning BD (2006) S6K1 regulates GSK3 under conditions of mTOR-dependent feedback inhibition of Akt. *Mol Cell* **24:** 185-197.

Zhang P, McGrath BC, Reinert J, Olsen DS, Lei L, Gill S, Wek SA, Vattem KM, Wek RC, Kimball SR, Jefferson LS, Cavener DR (2002) The GCN2 eIF2alpha kinase is required for adaptation to amino acid deprivation in mice. *Mol Cell Biol* **22:** 6681-6688.

Zhang SQ, Kovalenko A, Cantarella G, Wallach D (2000) Recruitment of the IKK signalosome to the p55 TNF receptor: RIP and A20 bind to NEMO (IKKgamma) upon receptor stimulation. *Immunity* **12:** 301-311.

Zhang T, Otevrel T, Gao Z, Gao Z, Ehrlich SM, Fields JZ, Boman BM (2001) Evidence that APC regulates survivin expression: a possible mechanism contributing to the stem cell origin of colon cancer. *Cancer Res* **61:** 8664-8667.

Zhao J, Yuan X, Frodin M, Grummt I (2003) ERK-dependent phosphorylation of the transcription initiation factor TIF-IA is required for RNA polymerase I transcription and cell growth. *Mol Cell* **11:** 405-413.

Zhao Y, Bjorbaek C, Moller DE (1996) Regulation and interaction of pp90(rsk) isoforms with mitogen-activated protein kinases. *J Biol Chem* **271:** 29773-29779.

Ziegler WH, Parekh DB, Le Good JA, Whelan RD, Kelly JJ, Frech M, Hemmings BA, Parker PJ (1999) Rapamycin-sensitive phosphorylation of PKC on a carboxy-terminal site by an atypical PKC complex. *Curr Biol* **9:** 522-529.

CHAPITRE 6

6. DISCUSSION

L'étude de l'immunopeptidome est un sujet de recherche qui reste encore peu développé. Dans le cadre de la présente thèse, nous avons orienté nos efforts pour tenter de mieux comprendre la nature, l'origine et la plasticité de l'immunopeptidome.

6.1 UNE NOUVELLE MÉTHODE POUR DÉFINIR LA NATURE DE L'IMMUNOPEPTIDOME

Aujourd'hui, la spectrométrie de masse est devenue indispensable pour appréhender la complexité et l'abondance des peptides composant l'immunopeptidome (Mester *et al*, 2011b). Au cours des dernières années, les progrès technologiques réalisés dans le domaine de la protéomique ont permis le développement d'approches quantitatives performantes pour mesurer l'abondance relative ou absolue des protéines et des peptides composant la cellule (Lu *et al*, 2007; Ong and Mann, 2005). La quantification des protéines et des peptides par marquage isotopique est maintenant largement utilisée. La quantification des peptides sans marquage est également possible à l'aide de l'utilisation d'outils bio-informatiques (Kearney and Thibault, 2003). En combinant l'isolation des peptides par élution acide douce à l'approche de quantification sans marquage, nous avons défini la nature et l'abondance relative des peptides composant l'immunopeptidome de cellules thymiques normales et néoplasiques (cellules EL4). L'utilisation de cette technique a également permis à notre groupe de déceler, lors d'une étude parallèle, l'immunopeptidome de cellules dendritiques cultivées *in vitro* (de Verteuil *et al*, 2010). Les peptides de faible abondance (< 100 copies par cellule) demeurent toutefois indiscernables. Notre incapacité à identifier les peptides faiblement abondants est liée à l'insuffisance de la sensibilité des spectromètres de masse dont nous disposons actuellement. C'est pour ça que pour l'instant, on s'accorde unanimement à dire que les peptides identifiés sur chaque population cellulaire ne représentent vraisemblablement que la partie émergée de l'iceberg.

L'élution acide douce permet d'isoler l'ensemble des peptides composant l'immunopeptidome. Plusieurs peptides contaminants sont également obtenus par cette technique d'isolation. Pour discerner les peptides contaminants des peptides spécifiquement liés aux molécules du CMH de classe I, nous avons utilisé des cellules contrôles EL4 déficientes pour la molécule β2m. Nous avons curieusement observé une proportion élevée de peptides contaminants provenant de l'extrémité C-terminale, de leur protéine d'origine (ces données ne sont pas illustrées dans cette thèse). Une autre étude indépendante appuie fortement cette observation (Gebreselassie *et al*, 2006). Nous avons également noté que plusieurs peptides contaminants avaient antérieurement été considérés à tort comme des peptides spécifiques pour les molécules du CMH de classe I (Gebreselassie *et al*, 2006; Suri *et al*, 2006). L'utilisation d'une lignée déficiente en β2m représente par conséquent une approche appropriée pour discriminer les peptides contaminants obtenus par élution acide douce. Cette approche nous a permis de déduire que le taux de faux-négatifs dans l'immunopeptidome des thymocytes était d'environ 3%. Autrement dit, 3% des peptides ont été exclu à tord dans l'analyse de l'immunopeptidome des thymocytes. Ce faible taux devrait donc avoir des conséquences peu prononcées sur les conclusions de notre étude. Néanmoins, considérant qu'environ 10 000 peptides différents peuvent être présents dans l'immunopeptidome d'une cellule (Mester *et al*, 2011a), on peut estimer qu'environ 300 peptides spécifiques aux molécules du CMH I seraient exclus à partir de notre approche. Il est également considérable de croire que ce taux de faux-négatifs pourraient varier d'un type cellulaire à l'autre.

6.2 LA PLASTICITÉ DE L'IMMUNOPEPTIDOME

Les premières études en protéomique indiquaient que la composition de l'immunopeptidome entre plusieurs types cellulaires était pratiquement invariable (Engelhard *et al*, 2002; Marrack *et al*, 1993). Les spectromètres de masse de l'époque étaient cependant bien inférieurs en matière de précision et de sensibilité.

Au chapitre 3, nous démontrons que 17 % des peptides identifiés à la surface de cellules thymiques proviennent de gènes préférentiellement surexprimés dans ce type

cellulaire, suggérant ainsi la présence d'une signature tissu-spécifique dans la composition de l'immunopeptidome. Une étude parallèle nous a permis de comparer la nature des peptides présentés sur des cellules thymiques et des cellules dendritiques (de Verteuil *et al*, 2010). Cette étude démontre que 40 % des peptides identifiés sont spécifiques pour chacun des types cellulaires comparés, appuyant ainsi la notion de tissu-spécificité. À partir de ces résultats, il est raisonnablement permis de penser que la composition de l'immunopeptidome puisse diverger entre chaque type cellulaire composant l'organisme. Autrement dit, la composition de l'immunopeptidome serait modulable dans l'espace.

La plasticité de l'immunopeptidome se définit par des variations dans sa composition en réponse à différentes perturbations environnementales. Pour étudier la plasticité de l'immunopeptidome, il est nécessaire de mesurer quantitativement et de manière dynamique l'ensemble des peptides présentés par les CMH de classe I. Au chapitre 4, nous démontrons que l'abondance de 53 % des peptides (222 sur 422) augmente progressivement (de 2 à 15 fois) en fonction du niveau de modification du métabolisme cellulaire. De plus, 1.5 % (6 sur 422) des peptides sont uniquement détectés à la surface des cellules dont le métabolisme est plus longuement perturbé. D'où nous concluons que la composition de l'immunopeptidome est plastique, c'est-à-dire modulable à travers le temps.

Nos analyses quantitatives ont permis de démontrer que 25 % des peptides quantifiés dans l'immunopeptidome de cellules thymiques normales et néoplasiques étaient différentiellement exprimés. L'équipe de Stefan Stevanovic a, par ailleurs, démontré qu'environ 20 % des peptides composant l'immunopeptidome des tissus rénaux humains sains et cancéreux étaient différentiellement exprimés (Stickel *et al*, 2009; Weinzierl *et al*, 2007). L'infection de cellules par HIV provoque également des changements dans le répertoire peptidique à la surface cellulaire (Hickman *et al*, 2003; Wahl *et al*, 2010). Il est particulièrement intéressant de relever que la majorité des peptides surexprimés sur les cellules infectées par HIV ne proviennent pas de protéines virales. Ces peptides proviennent plutôt de protéines du « soi » et sont vraisemblablement en rapport avec le stress métabolique provoqué par HIV. Ces résultats suggèrent donc que les perturbations métaboliques à l'intérieur des cellules infectées et des cellules

cancéreuses provoquent plusieurs changements dans la composition de l'immunopeptidome. Considérant la modulation de l'immunopeptidome dans l'espace et le temps, il serait opportun d'évaluer de façon dynamique la composition de l'immunopeptidome pour plusieurs types cellulaires à la suite d'une transformation néoplasique ou d'une infection déterminée. Puisque le cancer est d'origine et de nature hétérogène (Visvader, 2011), il serait également judicieux, lorsque la technologie le permettra, d'évaluer la composition de l'immunopeptidome au niveau des cellules cancéreuses individuelles.

6.2.1 Avantage évolutif de la plasticité de l'immunopeptidome du « soi »

La complexité et la plasticité de l'immunopeptidome constituent une notion fondamentale comportant d'importantes implications pour le système immunitaire. Tel que nous l'avons exposé au chapitre 4, nous avons observé que des peptides présentés *de novo* à la surface de cellules métaboliquement perturbées étaient immunogènes, suggérant ainsi que la plasticité de l'immunopeptidome peut être perçue par le système immunitaire. La génération de peptides de « soi » devenant immunogène, en réponse à différents stress cellulaires, représente un risque considérable pour le développement de maladies auto-immunes (Todd *et al*, 2008).

La plasticité de l'immunopeptidome du « soi » pourrait par ailleurs conférer un avantage évolutif au système immunitaire en favorisant l'élimination des virus et des pathogènes. Plusieurs preuves expérimentales suggèrent en effet que la génération de peptides du « soi » aiderait les lymphocytes T CD8+ à reconnaître les peptides étrangers (Anikeeva *et al*, 2006; Krogsgaard *et al*, 2005; Yachi *et al*, 2005; Yachi *et al*, 2007). Ceci est particulièrement frappant quand les peptides étrangers sont en quantité limitée, ce qui pourrait d'ailleurs expliquer pourquoi les lymphocytes T peuvent détecter d'infimes quantités de peptides étrangers (Irvine *et al*, 2002; Purbhoo *et al*, 2004; Sykulev *et al*, 1996). Le rôle des peptides du « soi » serait de concentrer et de favoriser l'interaction des molécules du CMH I et des molécules CD8 (et par conséquent Lck) à la synapse immunologique (Figure 21) (Yachi *et al*, 2005). La coopération entre les complexes CMH I-peptide du « soi » et les complexes CMH I-peptide du « non-soi » augmenterait ainsi la

rapidité et l'efficacité d'un RCT à identifier le peptide étranger parmi la masse des peptides du « soi ».

Comme nous l'avons mentionné ci-dessus, l'infection d'une cellule peut augmenter la présentation des peptides du « soi » relié au stress métabolique (Hickman *et al*, 2003). Plusieurs peptides reliés au stress sont immunogènes et provoquent une réaction des lymphocytes T CD8+ (Gleimer and Parham, 2003; Hickman-Miller and Hildebrand, 2004). Ces peptides immunogènes proviennent plus précisément de la protéine vinculine chez des patients infectés par HIV (di Marzo Veronese *et al*, 1996), de HSP90 et IFI-6-16 succédant à l'infection de la rougeole (Herberts *et al*, 2003) et de HSP70 chez des patients atteints de cancers épithéliaux (Azuma *et al*, 2003; Faure *et al*, 2004). La plasticité de l'immunopeptidome pourrait hypothétiquement favoriser la présentation de peptides reliés au stress métabolique. La reconnaissance des peptides du stress par les lymphocytes T CD8+ faciliterait l'élimination des cellules stressées par une infection ou encore une transformation néoplasique. Par ailleurs, la concentration à la synapse immunologique des complexes CMH I-Peptides du « soi » relié au stress métabolique, et des complexes CMH I-peptide du « non-soi » relié aux protéines virales, pourrait ultimement faire entrer en synergie l'efficacité du système immunitaire adaptatif et l'élimination des cellules infectées.

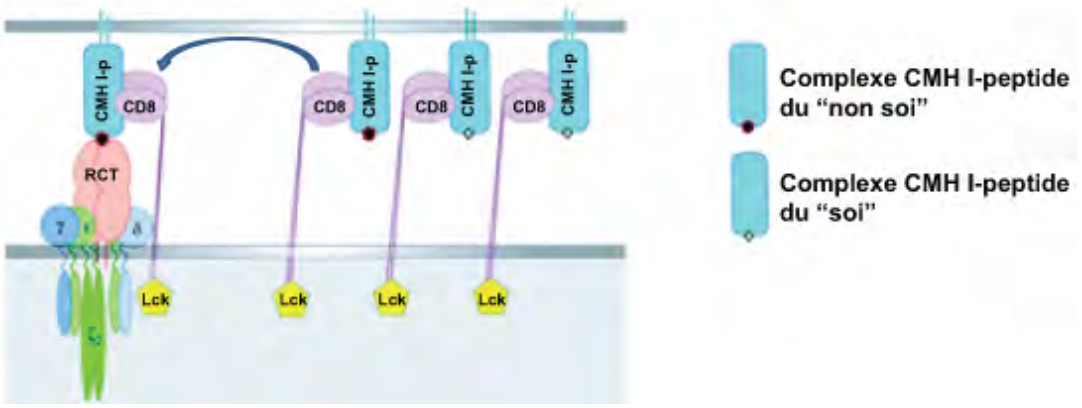

Figure 21. Modèle de « concentration » à la synapse immunologique. L'interaction des CD8 avec les complexes CMH I-peptide du « soi » et du « non-soi » provoque une concentration des co-récepteurs CD8, des complexes CMH I-peptide et des protéines Lck à la synapse immunologique.

6.3 L'ORIGINE DE L'IMMUNOPEPTIDOME

Dans le cadre de cette thèse, des analyses qualitatives, quantitatives et intégratives sur l'origine de l'immunopeptidome ont été effectuées pour mieux comprendre les règles qui sont à la base de sa composition.

6.3.1 La nature des protéines sources de peptides

Nos travaux suggèrent que certaines protéines contribuent plus activement que d'autres à la composition de l'immunopeptidome. Nos analyses qualitatives sur l'origine de l'immunopeptidome indiquent en effet que les peptides composant l'immunopeptidome de cellules thymiques proviennent préférentiellement des hélicases, des cyclines et des kinases dépendantes des cyclines. Dans une étude indépendante, il a été souligné que ce sont les composantes du ribosome et les chaperonnes qui contribuent préférentiellement à l'immunopeptidome (Hickman *et al*, 2004). Les protéines régulant la transcription, la traduction, la progression du cycle cellulaire et le repliement des protéines sont ainsi surreprésentées dans l'immunopeptidome.

On estime que les peptides du « soi » se présentent généralement entre 10 et 100 copies par cellule (den Haan *et al*, 1995; Henderson *et al*, 1993; Levitsky *et al*, 1996; Mendoza *et al*, 1997; Uenaka *et al*, 1994; Zuberi *et al*, 1998). Or, on retrouve ~1700 copies du peptide KAPDNRETL (provenant de la protéine SIMP/STT3B) à la surface des splénocytes (Pion *et al*, 1997). Le peptide SFFPEITHII (provenant de la protéine JAK 1 kinase) est présenté à ~10 000 copies à la surface de cellules p815 (Rammensee *et al*, 1993). Ces deux protéines contribuent donc fortement à la composition de l'immunopeptidome. Nos résultats suggèrent qu'au moins trois caractéristiques intrinsèques de la protéine SIMP/STT3B pourraient expliquer sa forte contribution à l'immunopeptidome : 1) la présence d'un dégron (signal de dégradation), 2) sa localisation intracellulaire dans la membrane du RE et, 3) sa forte propension à être incorrectement repliée (c.-à-d. à être une source de DRiPs). La présence d'un dégron dans la séquence primaire de la protéine JAK 1 kinase serait également responsable de sa forte contribution à l'immunopeptidome (Realini *et al*, 1994).

Le développement d'utiles stratégies en spectrométrie de masse nous permettant de quantifier de manière absolue chacun des peptides composant l'immunopeptidome représentera indéniablement une avancée majeure. Ceci nous permettra d'investiguer davantage les caractéristiques intrinsèques des protéines responsables de leur forte ou faible contribution à la composition de l'immunopeptidome. Puisque l'efficacité de la réponse cytotoxique d'un lymphocyte T CD8+ est influencée par l'abondance du peptide ciblé (Bullock *et al*, 2000; Bullock *et al*, 2003; Fontaine *et al*, 2001; Meunier *et al*, 2005; Reay *et al*, 2000; Tobery and Siliciano, 1997; Wherry *et al*, 1999), la contribution des protéines sources de peptides à la génération de l'immunopeptidome représente une notion essentielle pour l'élaboration de stratégies immunothérapeutiques.

6.3.1.1 Autres caractéristiques intrinsèques possibles

La transcription, la traduction et la dégradation cellulaire affectent la production des peptides présentés par les CMH de classe I (Dolan *et al*, 2010). L'efficacité de ces différents processus de régulation peut être influencée, dans une certaine mesure, par la présence de caractéristiques dans la séquence primaire des gènes et des protéines (Tableau 3) (Lackner *et al*, 2007; Vogel *et al*, 2010). La présence de ces caractéristiques dans la séquence des gènes sources de peptides pourrait hypothétiquement favoriser leur contribution à la composition de l'immunopeptidome. Il serait par conséquente intéressant d'évaluer si les gènes sources de peptides sont enrichis pour certaines des caractéristiques illustrées au Tableau 3.

Tableau 3. Caractéristiques reconnues pour affecter la régulation des gènes et des protéines au niveau de la transcription, de la traduction et de la dégradation. La section commentaire décrit la méthode à suivre pour analyser les séquences d'acides nucléiques ou d'acides aminés. Tiré de (Vogel *et al*, 2010).

Caractéristique	Commentaire
Longueur de la séquence	Utiliser R (seqinR) (Charif *et al*, 2005) pour mesurer la longueur.
Nucléotide, dinucléotide, composition en acides aminés	Utiliser R(seqinR) (Charif *et al*, 2005) pour déterminer la fréquence des résidus et (Karlin and Cardon, 1994) pour chercher les dinucléotide sur - ou sous- représentés.
Propriétés des acides aminés	Utiliser AA index (http://www.genome.jp/aaindex/) pour déterminer la fréquence relative des groupes d'acides aminés et leurs propriétés physico-chimiques.
Index de biais de codon	Utiliser Codon W (http://codonw.sourceforge.net/) : plus l'index de biais de codon est élevé, plus l'utilisation du codon est biaisée dans la séquence.
Contenu en G+C	Utiliser R (seqinR) (Charif *et al*, 2005) pour mesurer le contenu de la séquence en G+C.
Présence de cadre de lecture dans la région 5' UTR	Utiliser un script pour déterminer la présence de codon START et STOP dans la région 5'UTR.
Degré de désorganisation (séquence non structurée)	Utiliser DisoPred (Ward *et al*, 2004) pour prédire les séquences non structurées. Plus la valeur est élevée, plus les régions dans la séquence sont non structurées, et plus la protéine peut être instable.
Structures secondaires dans les régions 5' et 3' UTR	Utiliser Vienna RNA (Gruber *et al*, 2008) pour prédire l'énergie de repliement potentiel des séquences. Plus l'énergie est basse, plus la structure secondaire de la séquence est stable. Utiliser SEGFOLD/SIGSTB (Le *et al*, 1990) pour prédire l'UFR (« unusual folding regions »).
Sites de Poly-adénylation	Utiliser http://rulai.cshl.org/tools/polyadq/polyadq_form.html pour prédire les sites de Poly-adénylation (Tabaska and Zhang, 1999).
miRNA	Utiliser www.microRNA.org pour obtenir l'expression des miRNA dans différentes lignées cellulaires. Utiliser miRBase (Griffiths-Jones *et al*, 2008) et TargetScan (Grimson *et al*, 2007) pour obtenir les cibles des miRNAs.
Index de stabilité des protéines (PSI : « Protein Stability Index »)	À extraire de (Yen *et al*, 2008). Plus le PSI est élevé, plus la protéine est stable.
Taux du déclin de l'ARNm	Extraire en molécules/heure à partir de (Yang *et al*, 2003). Plus le taux de déclin est grand, moins l'ARN est stable.
Sites de phosphorylation	Utiliser PhosphoPep (Bodenmiller *et al*, 2008).
Fonction des protéines	Utiliser DAVID (Huang da *et al*, 2009).
Séquence Kozak	À partir d'un script, déterminer la composition des 10 acides aminés avant et après le codon d'initiation de la traduction AUG (Kozak, 1987).

6.3.2 La régulation des gènes sources de peptides

Nos analyses quantitatives et intégratives ont permis d'améliorer notre niveau de connaissance sur l'origine des variations dans la composition de l'immunopeptidome.

6.3.2.1 Contribution de la transcription sur l'immunopeptidome

Nos résultats indiquent que l'activation transcriptionnelle pourrait expliquer l'augmentation de l'abondance de 36 % des peptides sur les cellules EL4 traitées à la rapamycine. De plus, nous avons observé une corrélation modérée (r = 0.63) entre l'abondance relative de 47 paires de peptides et ARNm sources provenant de thymocytes normaux et néoplasiques. En comparaison, le groupe de Stevanovic n'a observé aucune corrélation stricte (r = 0.32) entre l'abondance relative de 273 paires de peptides et ARNm sources provenant de tissus rénaux sains et cancéreux (Figure 20) (Weinzierl *et al*, 2007). L'approche méthodologique utilisée est cependant bien différente entre notre équipe de recherche et celle de Stevanovic, ce qui pourrait expliquer la divergence de ces mesures de corrélation. L'équipe de Stevanovic a : 1) utilisé un nombre de paires plus élevé, 2) effectué la quantification relative de l'ARNm par puces d'ADN, 3) procédé à l'isolation des peptides par immunoaffinité, 4) procédé à la quantification des peptides par nicotinylation et, 5) utilisé un Q-TOF comme analyseur de masse. Néanmoins, ces deux études de corrélation indiquent que la surexpression de la majorité des peptides (74 % dans notre étude) sur les cellules néoplasiques n'aurait pu être prédite à partir de la quantification des transcrits. Ces études indiquent dans l'ensemble que les changements survenant dans la composition de l'immunopeptidome entre deux populations cellulaires proviennent majoritairement de modifications post-transcriptionnelles.

L'intégration de nos données peptidomiques au profil transcriptionnel de cellules thymiques nous a permis de démontrer que les peptides présentés par les CMH de classe I provenaient préférentiellement d'ARNm abondants. Cette démonstration a été récemment corroborée par une étude indépendante (Juncker *et al*, 2009). À partir de 1372 gènes humains sources de peptides, Juncker et ses collaborateurs ont noté une relation entre l'abondance des ARNm et leurs probabilités de générer des peptides présentés par les

CMH de classe I. Leurs résultats montrent plus précisément que 41 % des peptides analysés proviennent des ARNm fortement abondants alors que 3.2 % proviennent des ARNm faiblement abondants. Ces deux études indiquent donc que l'immunopeptidome provient préférentiellement, mais non exclusivement des ARNm plus abondants. Chez la levure, les ARNm les plus abondants sont plus efficacement traduits (Lackner *et al*, 2007) en plus d'être enrichis en transcrits sous exprimés lors d'un stress environnemental (Chen *et al*, 2003). Advenant que ces observations soient transposables chez l'humain, la forte activité traductionnelle pourrait favoriser la génération de peptides en condition physiologique normale, alors qu'une diminution de la transcription pourrait défavoriser la génération de peptides à la suite d'un stress environnemental.

Actuellement, le séquençage de l'ARN offre des avantages sans précédent pour la caractérisation et la quantification des transcriptomes (Ozsolak and Milos, 2011). L'utilisation de cette technologie nous permettra assurément d'étudier en profondeur et avec précision la contribution du transcriptome à la composition de l'immunopeptidome.

6.3.2.2 Contribution de la traduction sur l'immunopeptidome

Les travaux dirigés par Jonathan Yewdell ont démontré que l'inhibition complète de la traduction des ARNm, suivant un traitement des cellules à la cycloheximide, provoquait une chute drastique de la présentation des peptides associés aux CMH de classe I (Qian *et al*, 2006; Yewdell *et al*, 2003). Quelle est cependant l'influence de l'activité traductionnelle sur la génération de peptides? L'activité traductionnelle se mesure en nombre de protéines produites par molécules d'ARNm à travers le temps (Inada *et al*, 2002). On mesure l'activité traductionnelle par la densité ribosomale, c.-à.-d : le nombre de ribosomes par unité de transcrits, ou encore par l'occupation des ribosomes, c.-à.-d : l'enrichissement spécifique de chaque espèce d'ARNm sur les ribosomes (Maier *et al*, 2009). L'occupation des ribosomes est déterminée par purifications de polysomes, suivies d'analyses par PCR (de l'anglais *Polymerase Chain Reaction*) quantitative ou par puces d'ADN (Inada *et al*, 2002). Nos résultats ont indiqué que l'activation traductionnelle pourrait expliquer l'augmentation de l'abondance de seulement 6 % des peptides identifiés sur les cellules EL4 traitées à la rapamycine. Nos résultats indiquent également que le

niveau d'expression plus élevé des protéines sources pourrait expliquer l'augmentation de l'abondance de 25 % (2 sur 8) des peptides sur les cellules EL4 traitées à la rapamycine. En quantifiant 51 peptides et protéines sources par l'approche SILAC, le groupe d'Arie Admon a également retrouvé une corrélation limitée (environ 6 %) entre la quantité de peptides présentés et la quantité relative des protéines sources correspondantes (Milner *et al*, 2006). L'activité traductionnelle et les niveaux d'expression relatifs des protéines sources de peptides possèdent donc un faible pouvoir prédictif sur l'abondance des peptides présentés à la surface cellulaire.

Une nouvelle approche de séquençage de fragments d'ARNm protégés par les ribosomes a récemment été développée pour évaluer l'activité traductionnelle de tous les ARNm cellulaires (Ingolia *et al*, 2009). Le développement de la spectrométrie de masse et de la microscopie à grande échelle permet également de mesurer l'abondance et le taux de dégradation de l'ensemble des protéines cellulaires (Doherty *et al*, 2009; Eden *et al*, 2011; Yen *et al*, 2008). Une compréhension en profondeur de la relation entre le traductome, le protéome, le dégradome et l'immunpeptidome nécessitera l'utilisation de ces approches.

6.3.2.3 Contribution de la dégradation co -et/ou- post-traductionnelle sur l'immunopeptidome

De la manière dont cela était conçu précédemment, l'augmentation de l'abondance des peptides présents à la surface des cellules traitées à la rapamycine corrèle faiblement l'activité traductionnelle des ARNm. Nos résultats suggèrent que cette augmentation serait plutôt provoquée par un niveau plus élevé de protéines acheminées vers le protéasome. L'activation de la dégradation co-traductionnelle par un rapprochement des mécanismes de traduction et de dégradation pourrait expliquer ce résultat. L'activation d'immunoribosomes, telle qu'elle est présentée par Jonathan Yewdell, favoriserait la dégradation immédiate des protéines nouvellement synthétisées (Yewdell and Nicchitta, 2006). De manière remarquable, une analyse détaillée du réseau d'interaction du protéasome chez la levure a récemment révélé plusieurs protéines impliquées dans la traduction (Guerrero *et al*, 2008). Les protéines eIF3 et EGD ont été décrites pour interagir avec les ribosomes et le protéasome (Figure 22) (Panasenko *et al*, 2006; Sha *et al*, 2009).

Il a de plus été démontré qu'eIF1A interagit avec la sous-unité Rpt1 du protéasome pour faciliter la dégradation co-traductionnelle des protéines incorrectement repliées (Chuang *et al*, 2005). Chez les mammifères, eIF2 et eIF1α ont également été reportés pour s'associer au protéasome (Besche *et al*, 2009). Afin d'approfondir nos connaissances de la contribution de la dégradation co-traductionnelle sur l'immunopeptidome, il serait particulièrement intéressant d'examiner la dynamique des interactions entre le protéasome et certaines protéines de la machinerie traductionnelle.

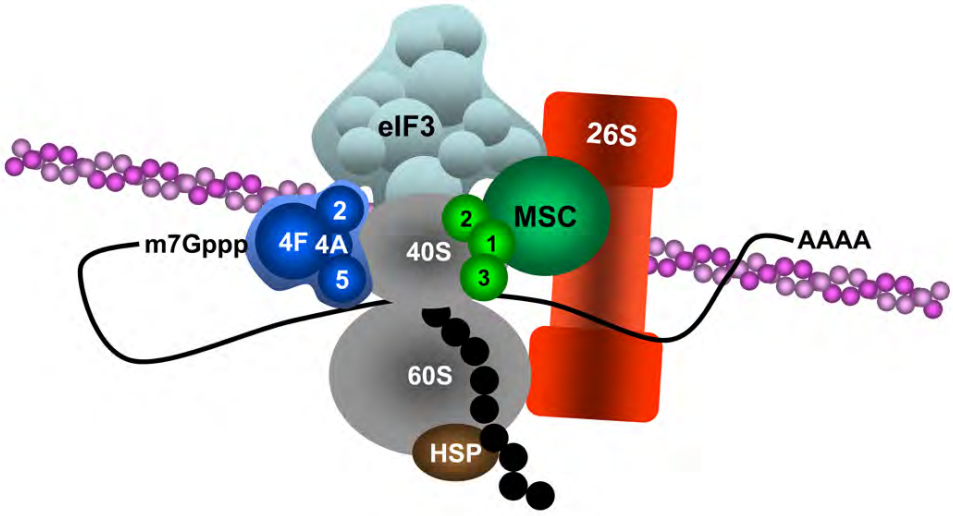

Figure 22. L'interactome d'eIF3 révèle un supercomplexe liant la synthèse et la dégradation des protéines. Les cercles verts représentent les facteurs d'élongation eEF1, 2 et 3. Un filament d'actine est illustré en mauve. Les boules noires représentent un polypeptide naissant. MSC (de l'anglais *Multi-Synthetase Complex*).

Certaines chaperonnes impliquées dans le repliement co-traductionnel des protéines, pourraient également influencer la génération de peptides. Une étude récente a démontré que S6K1, un substrat de mTORC1, phosphoryle la sous-unité β de CCT (de l'anglais *Chaperonin Containing TCP-1*) (Abe *et al*, 2009). CCT fait partie d'un réseau de chaperonnes et facilite le repliement des protéines naissantes (Albanese *et al*, 2006; Camasses *et al*, 2003). Les résultats obtenus par Abe et ses collaborateurs suggèrent que l'activation de mTORC1 favoriserait le repliement des protéines nouvellement synthétisées via la phosphorylation de CCTβ par S6K1. Suivant l'inactivation de S6K1 par le traitement des cellules à la rapamycine, les niveaux de phosphorylation de CCTβ

pourraient être grandement diminués. Une proportion plus élevée de protéines incorrectement repliées (c.-à-d. DRiPs) serait alors générée (Annexe 2, Figure 1).

L'augmentation des substrats du protéasome suivant l'inhibition de mTOR par la rapamycine pourrait également s'expliquer par un défaut dans la réponse UPR (de l'anglais *Unfolded Protein Response*) (Annexe 2, Figure 1). Lors d'un stress cellulaire, l'accumulation de protéines dans la lumière du RE va entraîner l'activation de l'UPR (Wouters and Koritzinsky, 2008). L'UPR mène à l'activation de la machinerie cellulaire impliquée dans le repliement des protéines. Cette réponse se met en place par l'activation de trois protéines transmembranaires du RE : PERK (de l'anglais *PKR-like ER protein Kinase*), ATF6 (de l'anglais *Activating Transcription Factor 6*) et IRE-1 (de l'anglais *Inositol Requiring Enzyme 1*). Nos résultats sur puce d'ADN indiquent de manière intéressante que les acteurs clés impliqués dans l'activation de l'UPR sont sous-exprimés suivant le traitement des cellules à la rapamycine (Annexe 2, Figure 2). L'incapacité des cellules traitées à la rapamycine d'activer l'UPR pourrait provoquer une augmentation du taux de DRiPs, et par conséquent hausser le nombre de protéines acheminées vers le système ubiquitine-protéasome.

6.3.2.4 Contribution des réseaux de régulation sur l'immunopeptidome

La collecte de données à grande échelle est rarement suffisante pour l'élaboration d'un nouveau concept au niveau des systèmes. Les données doivent être replacées dans leur propre contexte biologique, une étape qui implique fréquemment l'intégration des données en réseau d'interaction biomoléculaire. L'analyse des réseaux permettra d'obtenir une vision globale des interactions physiques ou fonctionnelles entre gènes, ARNs, protéines, et/ou autres molécules (Gardy *et al*, 2009). Le développement de la cartographie des interactomes a conduit à l'explosion du volume des bases de données de réseaux et de voies de signalisation (Charbonnier *et al*, 2008). Parmi les bases de données non commerciales les plus populaires, Int (Kerrien *et al*, 2007), MINT (Chatr-aryamontri *et al*, 2007) et BioGRID (Stark *et al*, 2011) contiennent plus de 100 000 interactions. Les bases de données d'interactions STRING (de l'anglais S*earch Tool for the Retrieval of Interacting Genes*) (Szklarczyk *et al*, 2011) et STITCH (de l'anglais *Search Tool for*

Interactions of Chemicals) (Kuhn *et al*, 2010) intègrent de multiples bases de données d'interactions, et ce pour plus de 1100 espèces différentes.

Dans le cadre de cette thèse, nous avons démontré que la plasticité de l'immunopeptidome provenait de certains réseaux intracellulaires. Plus précisément, nos analyses au niveau des systèmes ont montré que les variations provoquées par la rapamycine dans l'immunopeptidome des cellules EL4 étaient fonctionnellement reliées à la signalisation mTOR. D'autres analyses seraient nécessaires afin d'évaluer si la connectivité observée entre l'immunopeptidome et la voie mTOR est une réponse spécifique à la lignée EL4 ou représente plutôt une réponse généralisable aux autres types cellulaires. Il serait par exemple intéressant d'évaluer si le peptide surexprimé provenant de la protéine Rictor serait également surexprimé à partir de différentes lignées cellulaires traitées à la rapamycine. Dans ce même ordre d'idée, il a été démontré que l'assemblage du complexe mTORC2 (impliquant Rictor) pouvait être perturbé par la rapamycine, et que cette réponse était dépendante du type cellulaire étudié (Sarbassov *et al*, 2006). Il serait donc plausible que le peptide surexprimé provenant de Rictor soit une réponse spécifique à certains types cellulaires traités à la rapamycine.

De la même façon, il serait intéressant d'évaluer si les peptides surexprimés dans cette étude sont spécifiques à la rapamycine ou s'ils représentent plutôt une réponse généralisable à d'autres types de stress cellulaires. Dans une étude précédente, notre équipe de recherche a évalué l'effet de différents stress (tunicamycine, palmitate ou déprivation en glucose) sur l'expression des complexes CMH I – peptide à la surface des cellules EL4 (Granados *et al*, 2009). Cette étude montre que le stress cellulaire induit par la tunicamycin, le palmitate et la déprivation en glucose mène à une diminution de la génération des peptides et une diminution de la présentation des molécules du CMH I. Ces effets sont donc à l'opposé de ce qui est observé suivant le traitement des cellules EL4 à la rapamycine : une augmentation de l'abondance des peptides à la surface cellulaire et une surexpression des molécules du CMH I. Il est par conséquent raisonnable de conclure que les variations induites dans l'immunopeptidome par la rapamycine ne sont pas des changements non-spécifiques reliés à tous les types de stress cellulaires. De plus, la connectivité élevée entre les variations dans l'immunopeptidome de cellules traitées à la

rapamycine et le réseau de signalisation mTOR suggère que l'immunopeptidome pourrait représenter une réflexion de l'état des voies de signalisation intracellulaire. Pour démontrer cette notion avec certitude, il serait pertinent d'analyser la composition et l'origine de l'immunopeptidome sous différentes conditions environnementales. En ce sens, mTOR est un régulateur clé intégrant plusieurs voies de signalisation, telle que la voie Wnt (Caron *et al*, 2010; Inoki *et al*, 2006). Par conséquent, il est considérable de croire que des perturbations de mTOR par d'autres stimuli/inhibiteurs pourraient apporter dans une certaine mesure des changements similaires à ceux induits par la rapamycine au niveau de la nature des peptides.

Nos travaux montrent également que 82 % des gènes responsables de la plasticité de l'immunopeptidome proviennent de sous-réseaux transcriptionnellement perturbés par la rapamycine. La réorganisation transcriptionnelle de sous-réseaux de régulation est fréquemment observée à la suite d'un stress cellulaire [ex. infection par un agent pathogène (Kumar *et al*, 2010)]. L'identification des différentes composantes à l'intérieur des sous-réseaux perturbés pourrait possiblement permettre de prédire la nature des gènes responsables de la plasticité de l'immunopeptidome.

PERSPECTIVES

Modéliser la genèse de l'immunopeptidome pour simuler et prédire sa composition

L'immunopeptidome représente une vision intégrative de la régulation cellulaire (Chapitre 4). Nous proposons ainsi que l'acquisition et l'intégration de données biologiques quantitatives à grande échelle (c.-à-d. – omics), dans l'espace et dans le temps, pourrait nous permettre de modéliser la composition de l'immunopeptidome. Grâce aux énormes progrès technologiques réalisés au cours de ces dernières années, il est maintenant possible de quantifier à différentes étapes de leur régulation, l'ensemble des ARNm et des protéines cellulaire (Figure 23) (Beynon and Pratt, 2005; Ishihama *et al*, 2008; Lu *et al*, 2007; Malmstrom *et al*, 2009; Ong *et al*, 2005; t Hoen *et al*, 2008; Taniguchi *et al*, 2010; Yewdell *et al*, 2011). À partir de l'ensemble des données biologiques générées, la création de modèle cinétique computationnelle sur la genèse de l'immunopeptidome permettrait de simuler les changements dans sa composition. Nous croyons ainsi que nos travaux ouvrent de nouveaux horizons dans le domaine de l'immunologie des systèmes (Germain *et al*, 2011). Modéliser, simuler et prédire la composition de l'immunopeptidome à la suite d'une infection ou d'un événement de transformation néoplasique nous permettront d'accélérer le développement de stratégies immunothérapeutiques.

L'immunopeptidome : un niveau intégré de la génomique fonctionnelle

L'immunopeptidome projette à la surface de la cellule une vision intégrative de la régulation cellulaire (Chapitre 4). L'immunopeptidome représente ainsi un niveau intégré de la génomique fonctionnelle. L'utilisation de données immunopeptidomiques dans le domaine de la biologie des systèmes nous permettra d'améliorer assurément notre compréhension du fonctionnement cellulaire.

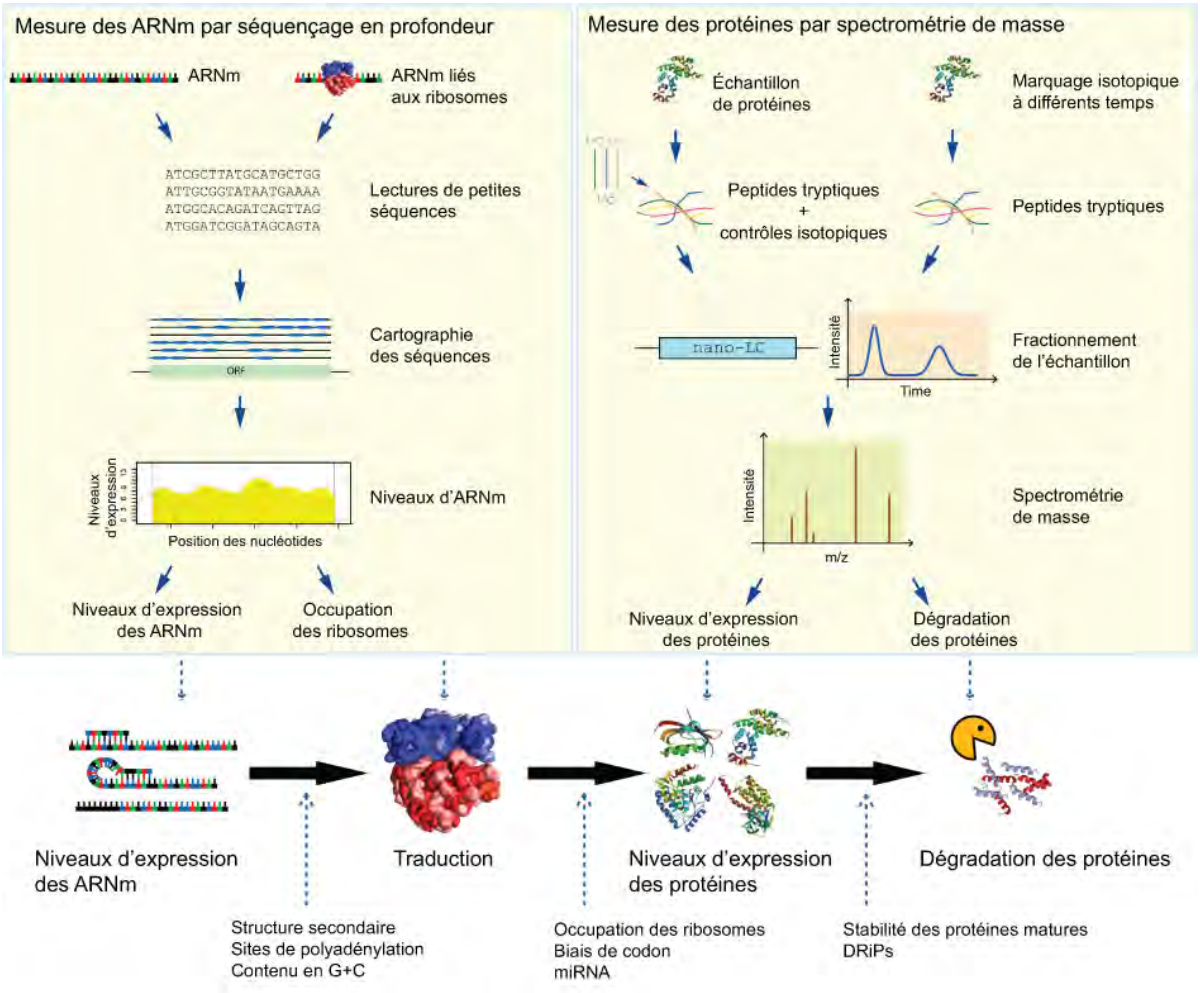

Figure 23. Approches expérimentales pour mesurer le niveau d'expression des ARNm et des protéines à différents stades de leur régulation. Les longues flèches bleues pointillées indiquent les paramètres influençant ou pouvant influencer la composition de l'immunopeptidome.

CONCLUSION

Dans le cadre de cette thèse, nous avons développé une nouvelle approche par spectrométrie de masse pour définir et quantifier à grande échelle la nature et l'abondance relative des peptides présentés par les molécules du CMH de classe I.

Nos analyses sur l'origine de l'immunopeptidome ont révélé que les peptides présents au niveau des cellules thymiques primaires proviennent préférentiellement de transcrits fortement abondants. L'immunopeptidome de ces cellules est enrichi en plus, de peptides provenant : d'hélicases, de cyclines et de kinases dépendantes des cyclines. Nos travaux sur la protéine SIMP/STT3B nous laissent également suggérer que la contribution d'une protéine à la composition de l'immunopeptidome résulte d'au moins trois facteurs : 1) la présence d'un signal de dégradation, 2) la tendance d'une protéine à être incorrectement repliée et, 3) sa localisation intracellulaire.

Nos analyses quantitatives et intégratives ont permis de démontrer que : 1) l'altération du métabolisme cellulaire via l'inhibition de mTOR provoque des changements dynamiques dans la composition de l'immunopeptidome, 2) 25 % des peptides quantifiés dans l'immunopeptidome de cellules thymiques normales et néoplasiques sont différentiellement exprimés et, 3) l'immunopeptidome dissimule une signature tissu-spécifique. Nous fournissons en outre la première évidence au niveau des systèmes que l'immunopeptidome représente une projection de réseaux biochimiques et d'événements métaboliques régulés à différents niveaux à l'intérieur de la cellule. Ces résultats indiquent conjointement que l'immunopeptidome est plastique, c'est-à-dire modulable dans l'espace et le temps. Nos résultats suggèrent par ailleurs que cette plasticité peut être perçue par le système immunitaire.

Nous avons également identifié deux peptides (VAAANREVL et STLTYSRM) TAAs (de l'anglais *Tumor-Associated Antigens*) permettant d'induire une réaction cytotoxique par les lymphocytes T CD8+ contre les cellules néoplasiques EL4. L'analyse à grande échelle de l'immunopeptidome par spectrométrie de masse représente donc une plateforme très intéressante pour l'identification de TAAs immunogènes.

RÉFÉRENCES BIBLIOGRAPHIQUES

Abe Y, Yoon SO, Kubota K, Mendoza MC, Gygi SP, Blenis J (2009) p90 ribosomal S6 kinase and p70 ribosomal S6 kinase link phosphorylation of the eukaryotic chaperonin containing TCP-1 to growth factor, insulin, and nutrient signaling. *J Biol Chem* **284:** 14939-14948

Ackerman AL, Kyritsis C, Tampe R, Cresswell P (2003) Early phagosomes in dendritic cells form a cellular compartment sufficient for cross presentation of exogenous antigens. *Proc Natl Acad Sci U S A* **100:** 12889-12894

Ackerman AL, Kyritsis C, Tampe R, Cresswell P (2005) Access of soluble antigens to the endoplasmic reticulum can explain cross-presentation by dendritic cells. *Nat Immunol* **6:** 107-113

Aki M, Shimbara N, Takashina M, Akiyama K, Kagawa S, Tamura T, Tanahashi N, Yoshimura T, Tanaka K, Ichihara A (1994) Interferon-gamma induces different subunit organizations and functional diversity of proteasomes. *J Biochem* **115:** 257-269

Akiyama K, Yokota K, Kagawa S, Shimbara N, Tamura T, Akioka H, Nothwang HG, Noda C, Tanaka K, Ichihara A (1994) cDNA cloning and interferon gamma down-regulation of proteasomal subunits X and Y. *Science* **265:** 1231-1234

Albanese V, Yam AY, Baughman J, Parnot C, Frydman J (2006) Systems analyses reveal two chaperone networks with distinct functions in eukaryotic cells. *Cell* **124:** 75-88

Alberts B (2008) *Molecular biology of the cell*, 5e éd. edn. New York, N.Y. ;: Garkand Science.

Allen PM, Strydom DJ, Unanue ER (1984) Processing of lysozyme by macrophages: identification of the determinant recognized by two T-cell hybridomas. *Proc Natl Acad Sci U S A* **81:** 2489-2493

Andersen MH, Bonfill JE, Neisig A, Arsequell G, Sondergaard I, Valencia G, Neefjes J, Zeuthen J, Elliott T, Haurum JS (1999) Phosphorylated peptides can be transported by TAP molecules, presented by class I MHC molecules, and recognized by phosphopeptide-specific CTL. *J Immunol* **163:** 3812-3818

Anikeeva N, Lebedeva T, Clapp AR, Goldman ER, Dustin ML, Mattoussi H, Sykulev Y (2006) Quantum dot/peptide-MHC biosensors reveal strong CD8-dependent cooperation between self and viral antigens that augment the T cell response. *Proc Natl Acad Sci U S A* **103:** 16846-16851

Annacker O, Pimenta-Araujo R, Burlen-Defranoux O, Bandeira A (2001) On the ontogeny and physiology of regulatory T cells. *Immunol Rev* **182:** 5-17

Arora S, Lapinski PE, Raghavan M (2001) Use of chimeric proteins to investigate the role of transporter associated with antigen processing (TAP) structural domains in peptide binding and translocation. *Proc Natl Acad Sci U S A* **98:** 7241-7246

Azuma K, Shichijo S, Takedatsu H, Komatsu N, Sawamizu H, Itoh K (2003) Heat shock cognate protein 70 encodes antigenic epitopes recognised by HLA-B4601-restricted cytotoxic T lymphocytes from cancer patients. *Br J Cancer* **89:** 1079-1085

Bacik I, Snyder HL, Anton LC, Russ G, Chen W, Bennink JR, Urge L, Otvos L, Dudkowska B, Eisenlohr L, Yewdell JW (1997) Introduction of a glycosylation site into a secreted protein provides evidence for an alternative antigen processing pathway: transport of precursors of major histocompatibility complex class I-restricted peptides from the endoplasmic reticulum to the cytosol. *J Exp Med* **186:** 479-487

Bancroft GJ, Kelly JP, Kaye PM, McDonald V, Cross CE (1994) Pathways of macrophage activation and innate immunity. *Immunol Lett* **43:** 67-70

Bangia N, Lehner PJ, Hughes EA, Surman M, Cresswell P (1999) The N-terminal region of tapasin is required to stabilize the MHC class I loading complex. *Eur J Immunol* **29:** 1858-1870

Barnden MJ, Purcell AW, Gorman JJ, McCluskey J (2000) Tapasin-mediated retention and optimization of peptide ligands during the assembly of class I molecules. *J Immunol* **165:** 322-330

Bauer D, Tampe R (2002) Herpes viral proteins blocking the transporter associated with antigen processing TAP--from genes to function and structure. *Curr Top Microbiol Immunol* **269:** 87-99

Bays NW, Gardner RG, Seelig LP, Joazeiro CA, Hampton RY (2001) Hrd1p/Der3p is a membrane-anchored ubiquitin ligase required for ER-associated degradation. *Nat Cell Biol* **3:** 24-29

Beninga J, Rock KL, Goldberg AL (1998) Interferon-gamma can stimulate post-proteasomal trimming of the N terminus of an antigenic peptide by inducing leucine aminopeptidase. *J Biol Chem* **273:** 18734-18742

Bennink JR, Yewdell JW, Smith GL, Moller C, Moss B (1984) Recombinant vaccinia virus primes and stimulates influenza haemagglutinin-specific cytotoxic T cells. *Nature* **311:** 578-579

Berman HM, Westbrook J, Feng Z, Gilliland G, Bhat TN, Weissig H, Shindyalov IN, Bourne PE (2000) The Protein Data Bank. *Nucleic Acids Res* **28:** 235-242

Besche HC, Haas W, Gygi SP, Goldberg AL (2009) Isolation of mammalian 26S proteasomes and p97/VCP complexes using the ubiquitin-like domain from HHR23B reveals novel proteasome-associated proteins. *Biochemistry* **48:** 2538-2549

Beynon RJ, Pratt JM (2005) Metabolic labeling of proteins for proteomics. *Mol Cell Proteomics* **4:** 857-872

Bjorkman PJ, Saper MA, Samraoui B, Bennett WS, Strominger JL, Wiley DC (1987) Structure of the human class I histocompatibility antigen, HLA-A2. *Nature* **329:** 506-512

Bluestone JA, Jameson S, Miller S, Dick R, 2nd (1992) Peptide-induced conformational changes in class I heavy chains alter major histocompatibility complex recognition. *J Exp Med* **176:** 1757-1761

Bochtler M, Ditzel L, Groll M, Hartmann C, Huber R (1999) The proteasome. *Annu Rev Biophys Biomol Struct* **28:** 295-317

Bodenmiller B, Campbell D, Gerrits B, Lam H, Jovanovic M, Picotti P, Schlapbach R, Aebersold R (2008) PhosphoPep--a database of protein phosphorylation sites in model organisms. *Nat Biotechnol* **26:** 1339-1340

Boes B, Hengel H, Ruppert T, Multhaup G, Koszinowski UH, Kloetzel PM (1994) Interferon gamma stimulation modulates the proteolytic activity and cleavage site preference of 20S mouse proteasomes. *J Exp Med* **179:** 901-909

Bonifacino JS, Rojas R (2006) Retrograde transport from endosomes to the trans-Golgi network. *Nat Rev Mol Cell Biol* **7:** 568-579

Bonneil E, Jaitly, G., Jaitly, N., Pomiès, C., and Thibault, P. (2007) Comprehensive expression profiling and trace-level identification of unlabeled peptide ions in 2DLC-MS proteomics experiments using integrated detection and clustering software. *Proceedings of 55th ASMS conference on Mass Spectrometry & Allied Topics, Indianapolis, IN*

Borden KL (2000) RING domains: master builders of molecular scaffolds? *J Mol Biol* **295:** 1103-1112

Braciale TJ, Braciale VL, Henkel TJ, Sambrook J, Gething MJ (1984) Cytotoxic T lymphocyte recognition of the influenza hemagglutinin gene product expressed by DNA-mediated gene transfer. *J Exp Med* **159:** 341-354

Bromme D, Rossi AB, Smeekens SP, Anderson DC, Payan DG (1996) Human bleomycin hydrolase: molecular cloning, sequencing, functional expression, and enzymatic characterization. *Biochemistry* **35:** 6706-6714

Bramoullé A (2010) Identification des peptides du complexe majeur d'histocompatibilité de classe I par spectrométrie de masse [En ligne]. Mémoire en Bioinformatique. Université de Montréal : http://hdl.handle.net/1866/5255

Brooks P, Murray RZ, Mason GG, Hendil KB, Rivett AJ (2000) Association of immunoproteasomes with the endoplasmic reticulum. *Biochem J* **352 Pt 3:** 611-615

Brown MG, Driscoll J, Monaco JJ (1991) Structural and serological similarity of MHC-linked LMP and proteasome (multicatalytic proteinase) complexes. *Nature* **353:** 355-357

Bullock TN, Colella TA, Engelhard VH (2000) The density of peptides displayed by dendritic cells affects immune responses to human tyrosinase and gp100 in HLA-A2 transgenic mice. *J Immunol* **164:** 2354-2361

Bullock TN, Eisenlohr LC (1996) Ribosomal scanning past the primary initiation codon as a mechanism for expression of CTL epitopes encoded in alternative reading frames. *J Exp Med* **184:** 1319-1329

Bullock TN, Mullins DW, Engelhard VH (2003) Antigen density presented by dendritic cells in vivo differentially affects the number and avidity of primary, memory, and recall CD8+ T cells. *J Immunol* **170:** 1822-1829

Bullock TN, Patterson AE, Franlin LL, Notidis E, Eisenlohr LC (1997) Initiation codon scanthrough versus termination codon readthrough demonstrates strong potential for major histocompatibility complex class I-restricted cryptic epitope expression. *J Exp Med* **186:** 1051-1058

Cagney G, Emili A (2002) De novo peptide sequencing and quantitative profiling of complex protein mixtures using mass-coded abundance tagging. *Nat Biotechnol* **20:** 163-170

Camasses A, Bogdanova A, Shevchenko A, Zachariae W (2003) The CCT chaperonin promotes activation of the anaphase-promoting complex through the generation of functional Cdc20. *Mol Cell* **12:** 87-100

Cardinaud S, Moris A, Fevrier M, Rohrlich PS, Weiss L, Langlade-Demoyen P, Lemonnier FA, Schwartz O, Habel A (2004) Identification of cryptic MHC I-restricted epitopes encoded by HIV-1 alternative reading frames. *J Exp Med* **199:** 1053-1063

Caron E, Ghosh S, Matsuoka Y, Ashton-Beaucage D, Therrien M, Lemieux S, Perreault C, Roux PP, Kitano H (2010) A comprehensive map of the mTOR signaling network. *Mol Syst Biol* **6:** 453

Cascio P, Hilton C, Kisselev AF, Rock KL, Goldberg AL (2001) 26S proteasomes and immunoproteasomes produce mainly N-extended versions of an antigenic peptide. *EMBO J* **20:** 2357-2366

Castellino F, Han R, Germain RN (2001) The transmembrane segment of invariant chain mediates binding to MHC class II molecules in a CLIP-independent manner. *Eur J Immunol* **31:** 841-850

Chang SC, Momburg F, Bhutani N, Goldberg AL (2005) The ER aminopeptidase, ERAP1, trims precursors to lengths of MHC class I peptides by a "molecular ruler" mechanism. *Proc Natl Acad Sci U S A* **102:** 17107-17112

Charbonnier S, Gallego O, Gavin AC (2008) The social network of a cell: recent advances in interactome mapping. *Biotechnol Annu Rev* **14:** 1-28

Charif D, Thioulouse J, Lobry JR, Perriere G (2005) Online synonymous codon usage analyses with the ade4 and seqinR packages. *Bioinformatics* **21:** 545-547

Chatr-aryamontri A, Ceol A, Palazzi LM, Nardelli G, Schneider MV, Castagnoli L, Cesareni G (2007) MINT: the Molecular INTeraction database. *Nucleic Acids Res* **35:** D572-574

Chemali M, Radtke K, Desjardins M, English L (2011) Alternative pathways for MHC class I presentation: a new function for autophagy. *Cell Mol Life Sci*

Chen D, Toone WM, Mata J, Lyne R, Burns G, Kivinen K, Brazma A, Jones N, Bahler J (2003) Global transcriptional responses of fission yeast to environmental stress. *Mol Biol Cell* **14:** 214-229

Chen W, Norbury CC, Cho Y, Yewdell JW, Bennink JR (2001) Immunoproteasomes shape immunodominance hierarchies of antiviral CD8(+) T cells at the levels of T cell repertoire and presentation of viral antigens. *J Exp Med* **193:** 1319-1326

Chen X, Reed-Loisel LM, Karlsson L, Jensen PE (2006) H2-O expression in primary dendritic cells. *J Immunol* **176:** 3548-3556

Chicz RM, Urban RG, Gorga JC, Vignali DA, Lane WS, Strominger JL (1993) Specificity and promiscuity among naturally processed peptides bound to HLA-DR alleles. *J Exp Med* **178:** 27-47

Choe L, D'Ascenzo M, Relkin NR, Pappin D, Ross P, Williamson B, Guertin S, Pribil P, Lee KH (2007) 8-plex quantitation of changes in cerebrospinal fluid protein expression in subjects undergoing intravenous immunoglobulin treatment for Alzheimer's disease. *Proteomics* **7:** 3651-3660

Chuang SM, Chen L, Lambertson D, Anand M, Kinzy TG, Madura K (2005) Proteasome-mediated degradation of cotranslationally damaged proteins involves translation elongation factor 1A. *Mol Cell Biol* **25:** 403-413

Coico R, Sunshine G, Benjamini E (2009) *Immunology : a short course*, 6th edn. Hoboken, N.J.: Wiley-Blackwell.

Cox AL, Skipper J, Chen Y, Henderson RA, Darrow TL, Shabanowitz J, Engelhard VH, Hunt DF, Slingluff CL, Jr. (1994) Identification of a peptide recognized by five melanoma-specific human cytotoxic T cell lines. *Science* **264:** 716-719

Craig R, Beavis RC (2003) A method for reducing the time required to match protein sequences with tandem mass spectra. *Rapid Commun Mass Spectrom* **17:** 2310-2316

Crotty S, Ahmed R (2004) Immunological memory in humans. *Semin Immunol* **16:** 197-203

Crotzer VL, Blum JS (2009) Autophagy and its role in MHC-mediated antigen presentation. *J Immunol* **182:** 3335-3341

Dalet A, Vigneron N, Stroobant V, Hanada K, Van den Eynde BJ (2010) Splicing of distant peptide fragments occurs in the proteasome by transpeptidation and produces the spliced antigenic peptide derived from fibroblast growth factor-5. *J Immunol* **184:** 3016-3024

De Groot AS (2006) Immunomics: discovering new targets for vaccines and therapeutics. *Drug Discov Today* **11:** 203-209

de Verteuil D, Muratore-Schroeder TL, Granados DP, Fortier MH, Hardy MP, Bramoulle A, Caron E, Vincent K, Mader S, Lemieux S, Thibault P, Perreault C (2010) Deletion of immunoproteasome subunits imprints on the transcriptome and has a broad impact on peptides presented by major histocompatibility complex I molecules. *Mol Cell Proteomics* **9:** 2034-2047

de Virgilio M, Weninger H, Ivessa NE (1998) Ubiquitination is required for the retro-translocation of a short-lived luminal endoplasmic reticulum glycoprotein to the cytosol for degradation by the proteasome. *J Biol Chem* **273:** 9734-9743

DeMartino GN, Moomaw CR, Zagnitko OP, Proske RJ, Chu-Ping M, Afendis SJ, Swaffield JC, Slaughter CA (1994) PA700, an ATP-dependent activator of the 20 S proteasome, is an ATPase containing multiple members of a nucleotide-binding protein family. *J Biol Chem* **269:** 20878-20884

den Haan JM, Meadows LM, Wang W, Pool J, Blokland E, Bishop TL, Reinhardus C, Shabanowitz J, Offringa R, Hunt DF, Engelhard VH, Goulmy E (1998) The minor histocompatibility antigen HA-1: a diallelic gene with a single amino acid polymorphism. *Science* **279:** 1054-1057

den Haan JM, Sherman NE, Blokland E, Huczko E, Koning F, Drijfhout JW, Skipper J, Shabanowitz J, Hunt DF, Engelhard VH, et al. (1995) Identification of a graft versus host disease-associated human minor histocompatibility antigen. *Science* **268:** 1476-1480

Dengjel J, Schoor O, Fischer R, Reich M, Kraus M, Muller M, Kreymborg K, Altenberend F, Brandenburg J, Kalbacher H, Brock R, Driessen C, Rammensee HG, Stevanovic S (2005) Autophagy promotes MHC class II presentation of peptides from intracellular source proteins. *Proc Natl Acad Sci U S A* **102:** 7922-7927

Denic V, Quan EM, Weissman JS (2006) A luminal surveillance complex that selects misfolded glycoproteins for ER-associated degradation. *Cell* **126:** 349-359

di Marzo Veronese F, Arnott D, Barnaba V, Loftus DJ, Sakaguchi K, Thompson CB, Salemi S, Mastroianni C, Sette A, Shabanowitz J, Hunt DF, Appella E (1996)

Autoreactive cytotoxic T lymphocytes in human immunodeficiency virus type 1-infected subjects. *J Exp Med* **183:** 2509-2516

DiBrino M, Tsuchida T, Turner RV, Parker KC, Coligan JE, Biddison WE (1993) HLA-A1 and HLA-A3 T cell epitopes derived from influenza virus proteins predicted from peptide binding motifs. *J Immunol* **151:** 5930-5935

Doherty MK, Hammond DE, Clague MJ, Gaskell SJ, Beynon RJ (2009) Turnover of the human proteome: determination of protein intracellular stability by dynamic SILAC. *J Proteome Res* **8:** 104-112

Dolan BP, Knowlton JJ, David A, Bennink JR, Yewdell JW (2010a) RNA polymerase II inhibitors dissociate antigenic peptide generation from normal viral protein synthesis: a role for nuclear translation in defective ribosomal product synthesis? *J Immunol* **185:** 6728-6733

Dolan BP, Li L, Takeda K, Bennink JR, Yewdell JW (2010b) Defective ribosomal products are the major source of antigenic peptides endogenously generated from influenza A virus neuraminidase. *J Immunol* **184:** 1419-1424

Dolan BP, Li L, Veltri CA, Ireland CM, Bennink JR, Yewdell JW (2011) Distinct pathways generate peptides from defective ribosomal products for CD8+ T cell immunosurveillance. *J Immunol* **186:** 2065-2072

Dongre AR, Kovats S, deRoos P, McCormack AL, Nakagawa T, Paharkova-Vatchkova V, Eng J, Caldwell H, Yates JR, 3rd, Rudensky AY (2001) In vivo MHC class II presentation of cytosolic proteins revealed by rapid automated tandem mass spectrometry and functional analyses. *Eur J Immunol* **31:** 1485-1494

Dorfel D, Appel S, Grunebach F, Weck MM, Muller MR, Heine A, Brossart P (2005) Processing and presentation of HLA class I and II epitopes by dendritic cells after transfection with in vitro-transcribed MUC1 RNA. *Blood* **105:** 3199-3205

Dubiel W, Pratt G, Ferrell K, Rechsteiner M (1992) Purification of an 11 S regulator of the multicatalytic protease. *J Biol Chem* **267:** 22369-22377

Dunn GP, Old LJ, Schreiber RD (2004) The immunobiology of cancer immunosurveillance and immunoediting. *Immunity* **21:** 137-148

Eden E, Geva-Zatorsky N, Issaeva I, Cohen A, Dekel E, Danon T, Cohen L, Mayo A, Alon U (2011) Proteome half-life dynamics in living human cells. *Science* **331:** 764-768

Edman P (1949) A method for the determination of amino acid sequence in peptides. *Arch Biochem* **22:** 475

Engelhard VH (1994a) Structure of peptides associated with class I and class II MHC molecules. *Annu Rev Immunol* **12:** 181-207

Engelhard VH (1994b) Structure of peptides associated with MHC class I molecules. *Curr Opin Immunol* **6:** 13-23

Engelhard VH, Altrich-Vanlith M, Ostankovitch M, Zarling AL (2006) Post-translational modifications of naturally processed MHC-binding epitopes. *Curr Opin Immunol* **18:** 92-97

Engelhard VH, Appella E, Benjamin DC, Bodnar WM, Cox AL, Chen Y, Henderson RA, Huczko EL, Michel H, Sakaguichi K, et al. (1993) Mass spectrometric analysis of peptides associated with the human class I MHC molecules HLA-A2.1 and HLA-B7 and identification of structural features that determine binding. *Chem Immunol* **57:** 39-62

Engelhard VH, Brickner AG, Zarling AL (2002) Insights into antigen processing gained by direct analysis of the naturally processed class I MHC associated peptide repertoire. *Mol Immunol* **39:** 127-137

English L, Chemali M, Desjardins M (2009) Nuclear membrane-derived autophagy, a novel process that participates in the presentation of endogenous viral antigens during HSV-1 infection. *Autophagy* **5:** 1026-1029

Esquivel F, Yewdell J, Bennink J (1992) RMA/S cells present endogenously synthesized cytosolic proteins to class I-restricted cytotoxic T lymphocytes. *J Exp Med* **175:** 163-168

Fairchild PJ, Austyn JM (1990) Thymic dendritic cells: phenotype and function. *Int Rev Immunol* **6:** 187-196

Falk K, Rotzschke O, Stevanovic S, Jung G, Rammensee HG (1991) Allele-specific motifs revealed by sequencing of self-peptides eluted from MHC molecules. *Nature* **351:** 290-296

Fallas JL, Yi W, Draghi NA, O'Rourke HM, Denzin LK (2007) Expression patterns of H2-O in mouse B cells and dendritic cells correlate with cell function. *J Immunol* **178:** 1488-1497

Farmery MR, Allen S, Allen AJ, Bulleid NJ (2000) The role of ERp57 in disulfide bond formation during the assembly of major histocompatibility complex class I in a synchronized semipermeabilized cell translation system. *J Biol Chem* **275:** 14933-14938

Faure O, Graff-Dubois S, Bretaudeau L, Derre L, Gross DA, Alves PM, Cornet S, Duffour MT, Chouaib S, Miconnet I, Gregoire M, Jotereau F, Lemonnier FA, Abastado JP, Kosmatopoulos K (2004) Inducible Hsp70 as target of anticancer immunotherapy: Identification of HLA-A*0201-restricted epitopes. *Int J Cancer* **108:** 863-870

Fehling HJ, Swat W, Laplace C, Kuhn R, Rajewsky K, Muller U, von Boehmer H (1994) MHC class I expression in mice lacking the proteasome subunit LMP-7. *Science* **265:** 1234-1237

Fenn JB, Mann M, Meng CK, Wong SF, Whitehouse CM (1989) Electrospray ionization for mass spectrometry of large biomolecules. *Science* **246:** 64-71

Fontaine P, Roy-Proulx G, Knafo L, Baron C, Roy DC, Perreault C (2001) Adoptive transfer of minor histocompatibility antigen-specific T lymphocytes eradicates leukemia cells without causing graft-versus-host disease. *Nat Med* **7:** 789-794

Fortier MH (2009) Développement de méthodes analytiques pour la protéomique et l'identification de peptides MHC I issus de cellules leucémiques. [En ligne]. Thèse en Chimie. Université de Montréal : http://hdl.handle.net/1866/6563

Fu H, Sadis S, Rubin DM, Glickman M, van Nocker S, Finley D, Vierstra RD (1998) Multiubiquitin chain binding and protein degradation are mediated by distinct domains within the 26 S proteasome subunit Mcb1. *J Biol Chem* **273:** 1970-1981

Gaczynska M, Goldberg AL, Tanaka K, Hendil KB, Rock KL (1996) Proteasome subunits X and Y alter peptidase activities in opposite ways to the interferon-gamma-induced subunits LMP2 and LMP7. *J Biol Chem* **271:** 17275-17280

Gagnon E, Duclos S, Rondeau C, Chevet E, Cameron PH, Steele-Mortimer O, Paiement J, Bergeron JJ, Desjardins M (2002) Endoplasmic reticulum-mediated phagocytosis is a mechanism of entry into macrophages. *Cell* **110:** 119-131

Gardy JL, Lynn DJ, Brinkman FS, Hancock RE (2009) Enabling a systems biology approach to immunology: focus on innate immunity. *Trends Immunol* **30:** 249-262

Garrett TP, Saper MA, Bjorkman PJ, Strominger JL, Wiley DC (1989) Specificity pockets for the side chains of peptide antigens in HLA-Aw68. *Nature* **342:** 692-696

Gebreselassie D, Spiegel H, Vukmanovic S (2006) Sampling of major histocompatibility complex class I-associated peptidome suggests relatively looser global association of HLA-B*5101 with peptides. *Hum Immunol* **67:** 894-906

Geier E, Pfeifer G, Wilm M, Lucchiari-Hartz M, Baumeister W, Eichmann K, Niedermann G (1999) A giant protease with potential to substitute for some functions of the proteasome. *Science* **283:** 978-981

Germain RN, Meier-Schellersheim M, Nita-Lazar A, Fraser ID (2011) Systems biology in immunology: a computational modeling perspective (*). *Annu Rev Immunol* **29:** 527-585

Ghosh P, Amaya M, Mellins E, Wiley DC (1995) The structure of an intermediate in class II MHC maturation: CLIP bound to HLA-DR3. *Nature* **378:** 457-462

Gingras AC, Gstaiger M, Raught B, Aebersold R (2007) Analysis of protein complexes using mass spectrometry. *Nat Rev Mol Cell Biol* **8:** 645-654

Gleimer M, Parham P (2003) Stress management: MHC class I and class I-like molecules as reporters of cellular stress. *Immunity* **19:** 469-477

Glickman MH, Rubin DM, Coux O, Wefes I, Pfeifer G, Cjeka Z, Baumeister W, Fried VA, Finley D (1998a) A subcomplex of the proteasome regulatory particle required for ubiquitin-conjugate degradation and related to the COP9-signalosome and eIF3. *Cell* **94:** 615-623

Glickman MH, Rubin DM, Fried VA, Finley D (1998b) The regulatory particle of the Saccharomyces cerevisiae proteasome. *Mol Cell Biol* **18:** 3149-3162

Golovina TN, Wherry EJ, Bullock TN, Eisenlohr LC (2002) Efficient and qualitatively distinct MHC class I-restricted presentation of antigen targeted to the endoplasmic reticulum. *J Immunol* **168:** 2667-2675

Granados DP, Tanguay PL, Hardy MP, Caron E, de Verteuil D, Meloche S, Perreault C (2009) ER stress affects processing of MHC class I-associated peptides. *BMC Immunol* **10:** 10

Griffiths-Jones S, Saini HK, van Dongen S, Enright AJ (2008) miRBase: tools for microRNA genomics. *Nucleic Acids Res* **36:** D154-158

Grimson A, Farh KK, Johnston WK, Garrett-Engele P, Lim LP, Bartel DP (2007) MicroRNA targeting specificity in mammals: determinants beyond seed pairing. *Mol Cell* **27:** 91-105

Groettrup M, Kirk CJ, Basler M (2010) Proteasomes in immune cells: more than peptide producers? *Nat Rev Immunol* **10:** 73-78

Groettrup M, Kraft R, Kostka S, Standera S, Stohwasser R, Kloetzel PM (1996a) A third interferon-gamma-induced subunit exchange in the 20S proteasome. *Eur J Immunol* **26:** 863-869

Groettrup M, Soza A, Eggers M, Kuehn L, Dick TP, Schild H, Rammensee HG, Koszinowski UH, Kloetzel PM (1996b) A role for the proteasome regulator PA28alpha in antigen presentation. *Nature* **381:** 166-168

Groll M, Ditzel L, Lowe J, Stock D, Bochtler M, Bartunik HD, Huber R (1997) Structure of 20S proteasome from yeast at 2.4 A resolution. *Nature* **386:** 463-471

Grossman SR, Deato ME, Brignone C, Chan HM, Kung AL, Tagami H, Nakatani Y, Livingston DM (2003) Polyubiquitination of p53 by a ubiquitin ligase activity of p300. *Science* **300:** 342-344

Gruber AR, Lorenz R, Bernhart SH, Neubock R, Hofacker IL (2008) The Vienna RNA websuite. *Nucleic Acids Res* **36:** W70-74

Guermonprez P, Ladant D, Karimova G, Ullmann A, Leclerc C (1999) Direct delivery of the Bordetella pertussis adenylate cyclase toxin to the MHC class I antigen presentation pathway. *J Immunol* **162:** 1910-1916

Guermonprez P, Saveanu L, Kleijmeer M, Davoust J, Van Endert P, Amigorena S (2003) ER-phagosome fusion defines an MHC class I cross-presentation compartment in dendritic cells. *Nature* **425:** 397-402

Guermonprez P, Valladeau J, Zitvogel L, Thery C, Amigorena S (2002) Antigen presentation and T cell stimulation by dendritic cells. *Annu Rev Immunol* **20:** 621-667

Guerrero C, Milenkovic T, Przulj N, Kaiser P, Huang L (2008) Characterization of the proteasome interaction network using a QTAX-based tag-team strategy and protein interaction network analysis. *Proc Natl Acad Sci U S A* **105:** 13333-13338

Gygi SP, Rist B, Gerber SA, Turecek F, Gelb MH, Aebersold R (1999) Quantitative analysis of complex protein mixtures using isotope-coded affinity tags. *Nat Biotechnol* **17:** 994-999

Haglund K, Di Fiore PP, Dikic I (2003) Distinct monoubiquitin signals in receptor endocytosis. *Trends Biochem Sci* **28:** 598-603

Hammer GE, Gonzalez F, James E, Nolla H, Shastri N (2007a) In the absence of aminopeptidase ERAAP, MHC class I molecules present many unstable and highly immunogenic peptides. *Nat Immunol* **8:** 101-108

Hammer GE, Kanaseki T, Shastri N (2007b) The final touches make perfect the peptide-MHC class I repertoire. *Immunity* **26:** 397-406

Hampton RY (2002) ER-associated degradation in protein quality control and cellular regulation. *Curr Opin Cell Biol* **14:** 476-482

Han X, Aslanian A, Yates JR, 3rd (2008) Mass spectrometry for proteomics. *Curr Opin Chem Biol* **12:** 483-490

Hanada K, Yewdell JW, Yang JC (2004) Immune recognition of a human renal cancer antigen through post-translational protein splicing. *Nature* **427:** 252-256

Hatakeyama S, Yada M, Matsumoto M, Ishida N, Nakayama KI (2001) U box proteins as a new family of ubiquitin-protein ligases. *J Biol Chem* **276:** 33111-33120

Haurum JS, Hoier IB, Arsequell G, Neisig A, Valencia G, Zeuthen J, Neefjes J, Elliott T (1999) Presentation of cytosolic glycosylated peptides by human class I major histocompatibility complex molecules in vivo. *J Exp Med* **190:** 145-150

Heath WR, Carbone FR (2001) Cross-presentation in viral immunity and self-tolerance. *Nat Rev Immunol* **1:** 126-134

Heath WR, Carbone FR (2005) Coupling and cross-presentation. *Nature* **434:** 27-28

Heemels MT, Ploegh H (1995) Generation, translocation, and presentation of MHC class I-restricted peptides. *Annu Rev Biochem* **64:** 463-491

Helliwell SB, Losko S, Kaiser CA (2001) Components of a ubiquitin ligase complex specify polyubiquitination and intracellular trafficking of the general amino acid permease. *J Cell Biol* **153:** 649-662

Henderson RA, Cox AL, Sakaguchi K, Appella E, Shabanowitz J, Hunt DF, Engelhard VH (1993) Direct identification of an endogenous peptide recognized by multiple HLA-A2.1-specific cytotoxic T cells. *Proc Natl Acad Sci U S A* **90:** 10275-10279

Hendil KB, Khan S, Tanaka K (1998) Simultaneous binding of PA28 and PA700 activators to 20 S proteasomes. *Biochem J* **332 (Pt 3):** 749-754

Herberts CA, van Gaans-van den Brink J, van der Heeft E, van Wijk M, Hoekman J, Jaye A, Poelen MC, Boog CJ, Roholl PJ, Whittle H, de Jong AP, van Els CA (2003) Autoreactivity against induced or upregulated abundant self-peptides in HLA-A*0201 following measles virus infection. *Hum Immunol* **64:** 44-55

Hershko A, Heller H, Elias S, Ciechanover A (1983) Components of ubiquitin-protein ligase system. Resolution, affinity purification, and role in protein breakdown. *J Biol Chem* **258:** 8206-8214

Hicke L (2001) Protein regulation by monoubiquitin. *Nat Rev Mol Cell Biol* **2:** 195-201

Hickman HD, Luis AD, Bardet W, Buchli R, Battson CL, Shearer MH, Jackson KW, Kennedy RC, Hildebrand WH (2003) Cutting edge: class I presentation of host peptides following HIV infection. *J Immunol* **171:** 22-26

Hickman HD, Luis AD, Buchli R, Few SR, Sathiamurthy M, VanGundy RS, Giberson CF, Hildebrand WH (2004) Toward a definition of self: proteomic evaluation of the class I peptide repertoire. *J Immunol* **172:** 2944-2952

Hickman-Miller HD, Hildebrand WH (2004) The immune response under stress: the role of HSP-derived peptides. *Trends Immunol* **25:** 427-433

Hillen N, Stevanovic S (2006) Contribution of mass spectrometry-based proteomics to immunology. *Expert Rev Proteomics* **3:** 653-664

Hisamatsu H, Shimbara N, Saito Y, Kristensen P, Hendil KB, Fujiwara T, Takahashi E, Tanahashi N, Tamura T, Ichihara A, Tanaka K (1996) Newly identified pair of proteasomal subunits regulated reciprocally by interferon gamma. *J Exp Med* **183:** 1807-1816

Hoppe T (2005) Multiubiquitylation by E4 enzymes: 'one size' doesn't fit all. *Trends Biochem Sci* **30:** 183-187

Hoppe T, Cassata G, Barral JM, Springer W, Hutagalung AH, Epstein HF, Baumeister R (2004) Regulation of the myosin-directed chaperone UNC-45 by a novel E3/E4-multiubiquitylation complex in C. elegans. *Cell* **118:** 337-349

Hornell TM, Burster T, Jahnsen FL, Pashine A, Ochoa MT, Harding JJ, Macaubas C, Lee AW, Modlin RL, Mellins ED (2006) Human dendritic cell expression of HLA-DO is subset specific and regulated by maturation. *J Immunol* **176:** 3536-3547

Houde M, Bertholet S, Gagnon E, Brunet S, Goyette G, Laplante A, Princiotta MF, Thibault P, Sacks D, Desjardins M (2003) Phagosomes are competent organelles for antigen cross-presentation. *Nature* **425:** 402-406

Huang AY, Gulden PH, Woods AS, Thomas MC, Tong CD, Wang W, Engelhard VH, Pasternack G, Cotter R, Hunt D, Pardoll DM, Jaffee EM (1996) The immunodominant major histocompatibility complex class I-restricted antigen of a murine colon tumor derives from an endogenous retroviral gene product. *Proc Natl Acad Sci U S A* **93:** 9730-9735

Huang da W, Sherman BT, Lempicki RA (2009) Systematic and integrative analysis of large gene lists using DAVID bioinformatics resources. *Nat Protoc* **4:** 44-57

Huczko EL, Bodnar WM, Benjamin D, Sakaguchi K, Zhu NZ, Shabanowitz J, Henderson RA, Appella E, Hunt DF, Engelhard VH (1993) Characteristics of endogenous peptides eluted from the class I MHC molecule HLA-B7 determined by mass spectrometry and computer modeling. *J Immunol* **151:** 2572-2587

Hughes EA, Cresswell P (1998) The thiol oxidoreductase ERp57 is a component of the MHC class I peptide-loading complex. *Curr Biol* **8:** 709-712

Hunt DF, Henderson RA, Shabanowitz J, Sakaguchi K, Michel H, Sevilir N, Cox AL, Appella E, Engelhard VH (1992) Characterization of peptides bound to the class I MHC molecule HLA-A2.1 by mass spectrometry. *Science* **255:** 1261-1263

Huseby ES, White J, Crawford F, Vass T, Becker D, Pinilla C, Marrack P, Kappler JW (2005) How the T cell repertoire becomes peptide and MHC specific. *Cell* **122:** 247-260

Imai J, Hasegawa H, Maruya M, Koyasu S, Yahara I (2005) Exogenous antigens are processed through the endoplasmic reticulum-associated degradation (ERAD) in cross-presentation by dendritic cells. *Int Immunol* **17:** 45-53

Imai Y, Soda M, Hatakeyama S, Akagi T, Hashikawa T, Nakayama KI, Takahashi R (2002) CHIP is associated with Parkin, a gene responsible for familial Parkinson's disease, and enhances its ubiquitin ligase activity. *Mol Cell* **10:** 55-67

Inada T, Winstall E, Tarun SZ, Jr., Yates JR, 3rd, Schieltz D, Sachs AB (2002) One-step affinity purification of the yeast ribosome and its associated proteins and mRNAs. *RNA* **8:** 948-958

Ingolia NT, Ghaemmaghami S, Newman JR, Weissman JS (2009) Genome-wide analysis in vivo of translation with nucleotide resolution using ribosome profiling. *Science* **324:** 218-223

Inoki K, Ouyang H, Zhu T, Lindvall C, Wang Y, Zhang X, Yang Q, Bennett C, Harada Y, Stankunas K, Wang CY, He X, MacDougald OA, You M, Williams BO, Guan KL (2006) TSC2 integrates Wnt and energy signals via a coordinated phosphorylation by AMPK and GSK3 to regulate cell growth. *Cell* **126:** 955-968

Irvine DJ, Purbhoo MA, Krogsgaard M, Davis MM (2002) Direct observation of ligand recognition by T cells. *Nature* **419:** 845-849

Ishihama Y, Schmidt T, Rappsilber J, Mann M, Hartl FU, Kerner MJ, Frishman D (2008) Protein abundance profiling of the Escherichia coli cytosol. *BMC Genomics* **9:** 102

Istrail S, Florea L, Halldorsson BV, Kohlbacher O, Schwartz RS, Yap VB, Yewdell JW, Hoffman SL (2004) Comparative immunopeptidomics of humans and their pathogens. *Proc Natl Acad Sci U S A* **101:** 13268-13272

Jacobson S, Sekaly RP, Jacobson CL, McFarland HF, Long EO (1989) HLA class II-restricted presentation of cytoplasmic measles virus antigens to cytotoxic T cells. *J Virol* **63:** 1756-1762

Jarosch E, Geiss-Friedlander R, Meusser B, Walter J, Sommer T (2002a) Protein dislocation from the endoplasmic reticulum--pulling out the suspect. *Traffic* **3:** 530-536

Jarosch E, Taxis C, Volkwein C, Bordallo J, Finley D, Wolf DH, Sommer T (2002b) Protein dislocation from the ER requires polyubiquitination and the AAA-ATPase Cdc48. *Nat Cell Biol* **4:** 134-139

Jasanoff A, Wagner G, Wiley DC (1998) Structure of a trimeric domain of the MHC class II-associated chaperonin and targeting protein Ii. *EMBO J* **17:** 6812-6818

Jensen PE (2007) Recent advances in antigen processing and presentation. *Nat Immunol* **8:** 1041-1048

Jensen PE, Weber DA, Thayer WP, Chen X, Dao CT (1999) HLA-DM and the MHC class II antigen presentation pathway. *Immunol Res* **20:** 195-205

Johnson ES, Ma PC, Ota IM, Varshavsky A (1995) A proteolytic pathway that recognizes ubiquitin as a degradation signal. *J Biol Chem* **270:** 17442-17456

Johnson GD, Hersh LB (1990) Studies on the subsite specificity of the rat brain puromycin-sensitive aminopeptidase. *Arch Biochem Biophys* **276:** 305-309

Johnson RS, Martin SA, Biemann K, Stults JT, Watson JT (1987) Novel fragmentation process of peptides by collision-induced decomposition in a tandem mass spectrometer: differentiation of leucine and isoleucine. *Anal Chem* **59** : 2621-2625

Juncker AS, Larsen MV, Weinhold N, Nielsen M, Brunak S, Lund O (2009) Systematic characterisation of cellular localisation and expression profiles of proteins containing MHC ligands. *PLoS One* **4:** e7448

Kapsenberg ML (2003) Dendritic-cell control of pathogen-driven T-cell polarization. *Nat Rev Immunol* **3:** 984-993

Karas M, Hillenkamp F (1988) Laser desorption ionization of proteins with molecular masses exceeding 10,000 daltons. *Anal Chem* **60:** 2299-2301

Karlin S, Cardon LR (1994) Computational DNA sequence analysis. *Annu Rev Microbiol* **48:** 619-654

Karlsson L, Surh CD, Sprent J, Peterson PA (1991) A novel class II MHC molecule with unusual tissue distribution. *Nature* **351:** 485-488

Kearney P, Thibault P (2003) Bioinformatics meets proteomics--bridging the gap between mass spectrometry data analysis and cell biology. *J Bioinform Comput Biol* **1:** 183-200

Kelly A, Powis SH, Glynne R, Radley E, Beck S, Trowsdale J (1991) Second proteasome-related gene in the human MHC class II region. *Nature* **353:** 667-668

Kerrien S, Alam-Faruque Y, Aranda B, Bancarz I, Bridge A, Derow C, Dimmer E, Feuermann M, Friedrichsen A, Huntley R, Kohler C, Khadake J, Leroy C, Liban A, Lieftink C, Montecchi-Palazzi L, Orchard S, Risse J, Robbe K, Roechert B et al (2007) IntAct--open source resource for molecular interaction data. *Nucleic Acids Res* **35:** D561-565

Kienast A, Preuss M, Winkler M, Dick TP (2007) Redox regulation of peptide receptivity of major histocompatibility complex class I molecules by ERp57 and tapasin. *Nat Immunol* **8:** 864-872

Kisselev AF, Akopian TN, Goldberg AL (1998) Range of sizes of peptide products generated during degradation of different proteins by archaeal proteasomes. *J Biol Chem* **273:** 1982-1989

Klein J, Sato A (2000) The HLA system. First of two parts. *N Engl J Med* **343:** 702-709

Kloetzel PM (2001) Antigen processing by the proteasome. *Nat Rev Mol Cell Biol* **2:** 179-187

Knittler MR, Dirks S, Haas IG (1995) Molecular chaperones involved in protein degradation in the endoplasmic reticulum: quantitative interaction of the heat shock cognate protein BiP with partially folded immunoglobulin light chains that are degraded in the endoplasmic reticulum. *Proc Natl Acad Sci U S A* **92:** 1764-1768

Knowlton JR, Johnston SC, Whitby FG, Realini C, Zhang Z, Rechsteiner M, Hill CP (1997) Structure of the proteasome activator REGalpha (PA28alpha). *Nature* **390:** 639-643

Koegl M, Hoppe T, Schlenker S, Ulrich HD, Mayer TU, Jentsch S (1999) A novel ubiquitination factor, E4, is involved in multiubiquitin chain assembly. *Cell* **96:** 635-644

Kondo A, Sidney J, Southwood S, del Guercio MF, Appella E, Sakamoto H, Grey HM, Celis E, Chesnut RW, Kubo RT, Sette A (1997) Two distinct HLA-A*0101-specific submotifs illustrate alternative peptide binding modes. *Immunogenetics* **45:** 249-258

Konig R (2002) Interactions between MHC molecules and co-receptors of the TCR. *Curr Opin Immunol* **14:** 75-83

Koopmann JO, Post M, Neefjes JJ, Hammerling GJ, Momburg F (1996) Translocation of long peptides by transporters associated with antigen processing (TAP). *Eur J Immunol* **26:** 1720-1728

Kovacsovics-Bankowski M, Rock KL (1995) A phagosome-to-cytosol pathway for exogenous antigens presented on MHC class I molecules. *Science* **267:** 243-246

Kozak M (1987) An analysis of 5'-noncoding sequences from 699 vertebrate messenger RNAs. *Nucleic Acids Res* **15:** 8125-8148

Krogsgaard M, Li QJ, Sumen C, Huppa JB, Huse M, Davis MM (2005) Agonist/endogenous peptide-MHC heterodimers drive T cell activation and sensitivity. *Nature* **434:** 238-243

Kropshofer H, Vogt AB, Thery C, Armandola EA, Li BC, Moldenhauer G, Amigorena S, Hammerling GJ (1998) A role for HLA-DO as a co-chaperone of HLA-DM in peptide loading of MHC class II molecules. *EMBO J* **17:** 2971-2981

Kruger M, Moser M, Ussar S, Thievessen I, Luber CA, Forner F, Schmidt S, Zanivan S, Fassler R, Mann M (2008) SILAC mouse for quantitative proteomics uncovers kindlin-3 as an essential factor for red blood cell function. *Cell* **134:** 353-364

Kubo RT, Sette A, Grey HM, Appella E, Sakaguchi K, Zhu NZ, Arnott D, Sherman N, Shabanowitz J, Michel H, et al. (1994) Definition of specific peptide motifs for four major HLA-A alleles. *J Immunol* **152:** 3913-3924

Kuhn M, Szklarczyk D, Franceschini A, Campillos M, von Mering C, Jensen LJ, Beyer A, Bork P (2010) STITCH 2: an interaction network database for small molecules and proteins. *Nucleic Acids Res* **38:** D552-556

Kumar D, Nath L, Kamal MA, Varshney A, Jain A, Singh S, Rao KV (2010) Genome-wide analysis of the host intracellular network that regulates survival of Mycobacterium tuberculosis. *Cell* **140:** 731-743

Kunisawa J, Shastri N (2003) The group II chaperonin TRiC protects proteolytic intermediates from degradation in the MHC class I antigen processing pathway. *Mol Cell* **12:** 565-576

Lackner DH, Beilharz TH, Marguerat S, Mata J, Watt S, Schubert F, Preiss T, Bahler J (2007) A network of multiple regulatory layers shapes gene expression in fission yeast. *Mol Cell* **26:** 145-155

Larsen CN, Finley D (1997) Protein translocation channels in the proteasome and other proteases. *Cell* **91:** 431-434

Larsson J, Karlsson S (2005) The role of Smad signaling in hematopoiesis. *Oncogene* **24:** 5676-5692

Le SY, Malim MH, Cullen BR, Maizel JV (1990) A highly conserved RNA folding region coincident with the Rev response element of primate immunodeficiency viruses. *Nucleic Acids Res* **18:** 1613-1623

Lechler R, Aichinger G, Lightstone L (1996) The endogenous pathway of MHC class II antigen presentation. *Immunol Rev* **151:** 51-79

Lehner PJ, Surman MJ, Cresswell P (1998) Soluble tapasin restores MHC class I expression and function in the tapasin-negative cell line .220. *Immunity* **8:** 221-231

Leinders-Zufall T, Ishii T, Mombaerts P, Zufall F, Boehm T (2009) Structural requirements for the activation of vomeronasal sensory neurons by MHC peptides. *Nat Neurosci* **12:** 1551-1558

Lelouard H, Ferrand V, Marguet D, Bania J, Camosseto V, David A, Gatti E, Pierre P (2004) Dendritic cell aggresome-like induced structures are dedicated areas for ubiquitination and storage of newly synthesized defective proteins. *J Cell Biol* **164:** 667-675

Lelouard H, Gatti E, Cappello F, Gresser O, Camosseto V, Pierre P (2002) Transient aggregation of ubiquitinated proteins during dendritic cell maturation. *Nature* **417:** 177-182

Lelouard H, Schmidt EK, Camosseto V, Clavarino G, Ceppi M, Hsu HT, Pierre P (2007) Regulation of translation is required for dendritic cell function and survival during activation. *J Cell Biol* **179:** 1427-1439

Lemmel C, Weik S, Eberle U, Dengjel J, Kratt T, Becker HD, Rammensee HG, Stevanovic S (2004) Differential quantitative analysis of MHC ligands by mass spectrometry using stable isotope labeling. *Nat Biotechnol* **22:** 450-454

Lev A, Princiotta MF, Zanker D, Takeda K, Gibbs JS, Kumagai C, Waffarn E, Dolan BP, Burgevin A, Van Endert P, Chen W, Bennink JR, Yewdell JW (2010) Compartmentalized MHC class I antigen processing enhances immunosurveillance by circumventing the law of mass action. *Proc Natl Acad Sci U S A* **107:** 6964-6969

Levine B, Deretic V (2007) Unveiling the roles of autophagy in innate and adaptive immunity. *Nat Rev Immunol* **7:** 767-777

Levitsky V, Zhang QJ, Levitskaya J, Masucci MG (1996) The life span of major histocompatibility complex-peptide complexes influences the efficiency of presentation

and immunogenicity of two class I-restricted cytotoxic T lymphocyte epitopes in the Epstein-Barr virus nuclear antigen 4. *J Exp Med* **183:** 915-926

Li S, Paulsson KM, Chen S, Sjogren HO, Wang P (2000) Tapasin is required for efficient peptide binding to transporter associated with antigen processing. *J Biol Chem* **275:** 1581-1586

Liblau RS, Wong FS, Mars LT, Santamaria P (2002) Autoreactive CD8 T cells in organ-specific autoimmunity: emerging targets for therapeutic intervention. *Immunity* **17:** 1-6

Lilley BN, Ploegh HL (2004) A membrane protein required for dislocation of misfolded proteins from the ER. *Nature* **429:** 834-840

Lin ML, Zhan Y, Villadangos JA, Lew AM (2008) The cell biology of cross-presentation and the role of dendritic cell subsets. *Immunol Cell Biol* **86:** 353-362

Lin WC, Desiderio S (1995) V(D)J recombination and the cell cycle. *Immunol Today* **16:** 279-289

Lippolis JD, White FM, Marto JA, Luckey CJ, Bullock TN, Shabanowitz J, Hunt DF, Engelhard VH (2002) Analysis of MHC class II antigen processing by quantitation of peptides that constitute nested sets. *J Immunol* **169:** 5089-5097

Lizee G, Basha G, Jefferies WA (2005) Tails of wonder: endocytic-sorting motifs key for exogenous antigen presentation. *Trends Immunol* **26:** 141-149

Lu P, Vogel C, Wang R, Yao X, Marcotte EM (2007) Absolute protein expression profiling estimates the relative contributions of transcriptional and translational regulation. *Nat Biotechnol* **25:** 117-124

Luber CA, Cox J, Lauterbach H, Fancke B, Selbach M, Tschopp J, Akira S, Wiegand M, Hochrein H, O'Keeffe M, Mann M (2010) Quantitative proteomics reveals subset-specific viral recognition in dendritic cells. *Immunity* **32:** 279-289

Ma CP, Slaughter CA, DeMartino GN (1992) Identification, purification, and characterization of a protein activator (PA28) of the 20 S proteasome (macropain). *J Biol Chem* **267:** 10515-10523

Maattanen P, Kozlov G, Gehring K, Thomas DY (2006) ERp57 and PDI: multifunctional protein disulfide isomerases with similar domain architectures but differing substrate-partner associations. *Biochem Cell Biol* **84:** 881-889

Macek B, Waanders LF, Olsen JV, Mann M (2006) Top-down protein sequencing and MS3 on a hybrid linear quadrupole ion trap-orbitrap mass spectrometer. *Mol Cell Proteomics* **5:** 949-958

Madden DR, Gorga JC, Strominger JL, Wiley DC (1991) The structure of HLA-B27 reveals nonamer self-peptides bound in an extended conformation. *Nature* **353:** 321-325

Maier T, Guell M, Serrano L (2009) Correlation of mRNA and protein in complex biological samples. *FEBS Lett* **583:** 3966-3973

Makarov A (2000) Electrostatic axially harmonic orbital trapping: a high-performance technique of mass analysis. *Anal Chem* **72:** 1156-1162

Makarov A, Denisov E, Kholomeev A, Balschun W, Lange O, Strupat K, Horning S (2006a) Performance evaluation of a hybrid linear ion trap/orbitrap mass spectrometer. *Anal Chem* **78:** 2113-2120

Makarov A, Denisov E, Lange O, Horning S (2006b) Dynamic range of mass accuracy in LTQ Orbitrap hybrid mass spectrometer. *J Am Soc Mass Spectrom* **17:** 977-982

Malarkannan S, Horng T, Shih PP, Schwab S, Shastri N (1999) Presentation of out-of-frame peptide/MHC class I complexes by a novel translation initiation mechanism. *Immunity* **10:** 681-690

Malmstrom J, Beck M, Schmidt A, Lange V, Deutsch EW, Aebersold R (2009) Proteome-wide cellular protein concentrations of the human pathogen Leptospira interrogans. *Nature* **460:** 762-765

Marrack P, Ignatowicz L, Kappler JW, Boymel J, Freed JH (1993) Comparison of peptides bound to spleen and thymus class II. *J Exp Med* **178:** 2173-2183

Marrack P, Kappler J (2004) Control of T cell viability. *Annu Rev Immunol* **22:** 765-787

Mason DE, Liebler DC (2003) Quantitative analysis of modified proteins by LC-MS/MS of peptides labeled with phenyl isocyanate. *J Proteome Res* **2:** 265-272

Masopust D, Ahmed R (2004) Reflections on CD8 T-cell activation and memory. *Immunol Res* **29:** 151-160

Mathews M, Sonenberg N, Hershey JWB (2007) *Translational control in biology and medicine*, 3rd edn. Cold Spring Harbor, N.Y.: Cold Spring Harbor Laboratory Press.

Matsuki Y, Ohmura-Hoshino M, Goto E, Aoki M, Mito-Yoshida M, Uematsu M, Hasegawa T, Koseki H, Ohara O, Nakayama M, Toyooka K, Matsuoka K, Hotta H, Yamamoto A, Ishido S (2007) Novel regulation of MHC class II function in B cells. *EMBO J* **26:** 846-854

Matsumoto M, Yada M, Hatakeyama S, Ishimoto H, Tanimura T, Tsuji S, Kakizuka A, Kitagawa M, Nakayama KI (2004) Molecular clearance of ataxin-3 is regulated by a mammalian E4. *EMBO J* **23:** 659-669

Mayrand SM, Green WR (1998) Non-traditionally derived CTL epitopes: exceptions that prove the rules? *Immunol Today* **19:** 551-556

Meadows L, Wang W, den Haan JM, Blokland E, Reinhardus C, Drijfhout JW, Shabanowitz J, Pierce R, Agulnik AI, Bishop CE, Hunt DF, Goulmy E, Engelhard VH (1997) The HLA-A*0201-restricted H-Y antigen contains a posttranslationally modified cysteine that significantly affects T cell recognition. *Immunity* **6:** 273-281

Meiring HD, Soethout EC, Poelen MC, Mooibroek D, Hoogerbrugge R, Timmermans H, Boog CJ, Heck AJ, de Jong AP, van Els CA (2006) Stable isotope tagging of epitopes: a highly selective strategy for the identification of major histocompatibility complex class I-associated peptides induced upon viral infection. *Mol Cell Proteomics* **5:** 902-913

Mendoza LM, Paz P, Zuberi A, Christianson G, Roopenian D, Shastri N (1997) Minors held by majors: the H13 minor histocompatibility locus defined as a peptide/MHC class I complex. *Immunity* **7:** 461-472

Mester G, Hoffmann V, Stevanovic S (2011a) Insights into MHC class I antigen processing gained from large-scale analysis of class I ligands. *Cell Mol Life Sci*

Mester G, Hoffmann V, Stevanovic S (2011b) Insights into MHC class I antigen processing gained from large-scale analysis of class I ligands. *Cell Mol Life Sci* **68:** 1521-1532

Meunier MC, Delisle JS, Bergeron J, Rineau V, Baron C, Perreault C (2005) T cells targeted against a single minor histocompatibility antigen can cure solid tumors. *Nat Med* **11:** 1222-1229

Michalek MT, Grant EP, Gramm C, Goldberg AL, Rock KL (1993) A role for the ubiquitin-dependent proteolytic pathway in MHC class I-restricted antigen presentation. *Nature* **363:** 552-554

Milner E, Barnea E, Beer I, Admon A (2006) The turnover kinetics of major histocompatibility complex peptides of human cancer cells. *Mol Cell Proteomics* **5:** 357-365

Mohammed F, Cobbold M, Zarling AL, Salim M, Barrett-Wilt GA, Shabanowitz J, Hunt DF, Engelhard VH, Willcox BE (2008) Phosphorylation-dependent interaction between antigenic peptides and MHC class I: a molecular basis for the presentation of transformed self. *Nat Immunol* **9:** 1236-1243

Moise L, De Groot AS (2006) Putting immunoinformatics to the test. *Nat Biotechnol* **24:** 791-792

Molinari M, Calanca V, Galli C, Lucca P, Paganetti P (2003) Role of EDEM in the release of misfolded glycoproteins from the calnexin cycle. *Science* **299:** 1397-1400

Momburg F, Roelse J, Howard JC, Butcher GW, Hammerling GJ, Neefjes JJ (1994) Selectivity of MHC-encoded peptide transporters from human, mouse and rat. *Nature* **367:** 648-651

Mosse CA, Meadows L, Luckey CJ, Kittlesen DJ, Huczko EL, Slingluff CL, Shabanowitz J, Hunt DF, Engelhard VH (1998) The class I antigen-processing pathway for the membrane protein tyrosinase involves translation in the endoplasmic reticulum and processing in the cytosol. *J Exp Med* **187:** 37-48

Mosyak L, Zaller DM, Wiley DC (1998) The structure of HLA-DM, the peptide exchange catalyst that loads antigen onto class II MHC molecules during antigen presentation. *Immunity* **9:** 377-383

Moutaftsi M, Peters B, Pasquetto V, Tscharke DC, Sidney J, Bui HH, Grey H, Sette A (2006) A consensus epitope prediction approach identifies the breadth of murine T(CD8+)-cell responses to vaccinia virus. *Nat Biotechnol* **24:** 817-819

Muchamuel T, Basler M, Aujay MA, Suzuki E, Kalim KW, Lauer C, Sylvain C, Ring ER, Shields J, Jiang J, Shwonek P, Parlati F, Demo SD, Bennett MK, Kirk CJ, Groettrup M (2009) A selective inhibitor of the immunoproteasome subunit LMP7 blocks cytokine production and attenuates progression of experimental arthritis. *Nat Med* **15:** 781-787

Munchbach M, Quadroni M, Miotto G, James P (2000) Quantitation and facilitated de novo sequencing of proteins by isotopic N-terminal labeling of peptides with a fragmentation-directing moiety. *Anal Chem* **72:** 4047-4057

Murata S, Sasaki K, Kishimoto T, Niwa S, Hayashi H, Takahama Y, Tanaka K (2007) Regulation of CD8+ T cell development by thymus-specific proteasomes. *Science* **316:** 1349-1353

Murata S, Udono H, Tanahashi N, Hamada N, Watanabe K, Adachi K, Yamano T, Yui K, Kobayashi N, Kasahara M, Tanaka K, Chiba T (2001) Immunoproteasome assembly and antigen presentation in mice lacking both PA28alpha and PA28beta. *EMBO J* **20:** 5898-5907

Nakagawa T, Roth W, Wong P, Nelson A, Farr A, Deussing J, Villadangos JA, Ploegh H, Peters C, Rudensky AY (1998) Cathepsin L: critical role in Ii degradation and CD4 T cell selection in the thymus. *Science* **280:** 450-453

Nedjic J, Aichinger M, Emmerich J, Mizushima N, Klein L (2008) Autophagy in thymic epithelium shapes the T-cell repertoire and is essential for tolerance. *Nature* **455:** 396-400

Neefjes JJ, Momburg F, Hammerling GJ (1993) Selective and ATP-dependent translocation of peptides by the MHC-encoded transporter. *Science* **261:** 769-771

Neefjes JJ, Ploegh HL (1988) Allele and locus-specific differences in cell surface expression and the association of HLA class I heavy chain with beta 2-microglobulin: differential effects of inhibition of glycosylation on class I subunit association. *Eur J Immunol* **18:** 801-810

Neefjes JJ, Stollorz V, Peters PJ, Geuze HJ, Ploegh HL (1990) The biosynthetic pathway of MHC class II but not class I molecules intersects the endocytic route. *Cell* **61:** 171-183

Neijssen J, Herberts C, Drijfhout JW, Reits E, Janssen L, Neefjes J (2005) Cross-presentation by intercellular peptide transfer through gap junctions. *Nature* **434:** 83-88

Nijenhuis M, Hammerling GJ (1996) Multiple regions of the transporter associated with antigen processing (TAP) contribute to its peptide binding site. *J Immunol* **157:** 5467-5477

Nimmerjahn F, Milosevic S, Behrends U, Jaffee EM, Pardoll DM, Bornkamm GW, Mautner J (2003) Major histocompatibility complex class II-restricted presentation of a cytosolic antigen by autophagy. *Eur J Immunol* **33:** 1250-1259

Nishikawa SI, Fewell SW, Kato Y, Brodsky JL, Endo T (2001) Molecular chaperones in the yeast endoplasmic reticulum maintain the solubility of proteins for retrotranslocation and degradation. *J Cell Biol* **153:** 1061-1070

Nitta T, Murata S, Sasaki K, Fujii H, Ripen AM, Ishimaru N, Koyasu S, Tanaka K, Takahama Y (2010) Thymoproteasome shapes immunocompetent repertoire of CD8+ T cells. *Immunity* **32:** 29-40

Nossal GJ (1994) Negative selection of lymphocytes. *Cell* **76:** 229-239

Oda Y, Hosokawa N, Wada I, Nagata K (2003) EDEM as an acceptor of terminally misfolded glycoproteins released from calnexin. *Science* **299:** 1394-1397

Oh YK, Harding CV, Swanson JA (1997) The efficiency of antigen delivery from macrophage phagosomes into cytoplasm for MHC class I-restricted antigen presentation. *Vaccine* **15:** 511-518

Ohmura-Hoshino M, Matsuki Y, Aoki M, Goto E, Mito M, Uematsu M, Kakiuchi T, Hotta H, Ishido S (2006) Inhibition of MHC class II expression and immune responses by c-MIR. *J Immunol* **177:** 341-354

Ong SE, Blagoev B, Kratchmarova I, Kristensen DB, Steen H, Pandey A, Mann M (2002) Stable isotope labeling by amino acids in cell culture, SILAC, as a simple and accurate approach to expression proteomics. *Mol Cell Proteomics* **1:** 376-386

Ong SE, Mann M (2005) Mass spectrometry-based proteomics turns quantitative. *Nat Chem Biol* **1:** 252-262

Oviedo-Orta E, Evans WH (2002) Gap junctions and connexins: potential contributors to the immunological synapse. *J Leukoc Biol* **72:** 636-642

Owen JJ, Jenkinson EJ, Kingston R, Williams GT, Smith CA (1990) Cell growth and gene rearrangement signals during the development of T lymphocytes within the thymus. *Philos Trans R Soc Lond B Biol Sci* **327:** 111-116

Ozsolak F, Milos PM (2011) RNA sequencing: advances, challenges and opportunities. *Nat Rev Genet* **12:** 87-98

Palmer A, Mason GG, Paramio JM, Knecht E, Rivett AJ (1994) Changes in proteasome localization during the cell cycle. *Eur J Cell Biol* **64:** 163-175

Paludan C, Schmid D, Landthaler M, Vockerodt M, Kube D, Tuschl T, Munz C (2005) Endogenous MHC class II processing of a viral nuclear antigen after autophagy. *Science* **307:** 593-596

Pamer E, Cresswell P (1998) Mechanisms of MHC class I--restricted antigen processing. *Annu Rev Immunol* **16:** 323-358

Panasenko O, Landrieux E, Feuermann M, Finka A, Paquet N, Collart MA (2006) The yeast Ccr4-Not complex controls ubiquitination of the nascent-associated polypeptide (NAC-EGD) complex. *J Biol Chem* **281:** 31389-31398

Papaioannou MD, Lagarrigue M, Vejnar CE, Rolland AD, Kuhne F, Aubry F, Schaad O, Fort A, Descombes P, Neerman-Arbez M, Guillou F, Zdobnov EM, Pineau C, Nef S (2010) Loss of Dicer in Sertoli cells has a major impact on the testicular proteome of mice. *Mol Cell Proteomics*

Park B, Lee S, Kim E, Cho K, Riddell SR, Cho S, Ahn K (2006) Redox regulation facilitates optimal peptide selection by MHC class I during antigen processing. *Cell* **127:** 369-382

Paul WE (2008) *Fundamental immunology*, 6th edn. Philadelphia: Lippincott Williams & Wilkins.

Perkins DN, Pappin DJ, Creasy DM, Cottrell JS (1999) Probability-based protein identification by searching sequence databases using mass spectrometry data. *Electrophoresis* **20:** 3551-3567

Perreault C (2010) The origin and role of MHC class I-associated self-peptides. *Prog Mol Biol Transl Sci* **92:** 41-60

Perreault C, Decary F, Brochu S, Gyger M, Belanger R, Roy D (1990) Minor histocompatibility antigens. *Blood* **76:** 1269-1280

Peters B, Bui HH, Frankild S, Nielson M, Lundegaard C, Kostem E, Basch D, Lamberth K, Harndahl M, Fleri W, Wilson SS, Sidney J, Lund O, Buus S, Sette A (2006) A community resource benchmarking predictions of peptide binding to MHC-I molecules. *PLoS Comput Biol* **2:** e65

Peters B, Sidney J, Bourne P, Bui HH, Buus S, Doh G, Fleri W, Kronenberg M, Kubo R, Lund O, Nemazee D, Ponomarenko JV, Sathiamurthy M, Schoenberger S, Stewart S, Surko P, Way S, Wilson S, Sette A (2005) The immune epitope database and analysis resource: from vision to blueprint. *PLoS Biol* **3:** e91

Pickart CM (2001) Mechanisms underlying ubiquitination. *Annu Rev Biochem* **70:** 503-533

Pickart CM, Eddins MJ (2004) Ubiquitin: structures, functions, mechanisms. *Biochim Biophys Acta* **1695:** 55-72

Pierre P (2005) Dendritic cells, DRiPs, and DALIS in the control of antigen processing. *Immunol Rev* **207:** 184-190

Pierre P (2009) Immunity and the regulation of protein synthesis: surprising connections. *Curr Opin Immunol* **21:** 70-77

Pieters J, Bakke O, Dobberstein B (1993) The MHC class II-associated invariant chain contains two endosomal targeting signals within its cytoplasmic tail. *J Cell Sci* **106 (Pt 3):** 831-846

Pilon M, Schekman R, Romisch K (1997) Sec61p mediates export of a misfolded secretory protein from the endoplasmic reticulum to the cytosol for degradation. *EMBO J* **16:** 4540-4548

Pion S, Fontaine P, Desaulniers M, Jutras J, Filep JG, Perreault C (1997) On the mechanisms of immunodominance in cytotoxic T lymphocyte responses to minor histocompatibility antigens. *Eur J Immunol* **27:** 421-430

Plemper RK, Bohmler S, Bordallo J, Sommer T, Wolf DH (1997) Mutant analysis links the translocon and BiP to retrograde protein transport for ER degradation. *Nature* **388:** 891-895

Prakash S, Tian L, Ratliff KS, Lehotzky RE, Matouschek A (2004) An unstructured initiation site is required for efficient proteasome-mediated degradation. *Nat Struct Mol Biol* **11:** 830-837

Prilliman K, Lindsey M, Zuo Y, Jackson KW, Zhang Y, Hildebrand W (1997) Large-scale production of class I bound peptides: assigning a signature to HLA-B*1501. *Immunogenetics* **45:** 379-385

Purbhoo MA, Irvine DJ, Huppa JB, Davis MM (2004) T cell killing does not require the formation of a stable mature immunological synapse. *Nat Immunol* **5:** 524-530

Purcell AW, Gorman JJ (2001) The use of post-source decay in matrix-assisted laser desorption/ionisation mass spectrometry to delineate T cell determinants. *J Immunol Methods* **249:** 17-31

Purcell AW, Gorman JJ (2004) Immunoproteomics: Mass spectrometry-based methods to study the targets of the immune response. *Mol Cell Proteomics* **3:** 193-208

Qian SB, Princiotta MF, Bennink JR, Yewdell JW (2006a) Characterization of rapidly degraded polypeptides in mammalian cells reveals a novel layer of nascent protein quality control. *J Biol Chem* **281:** 392-400

Qian SB, Reits E, Neefjes J, Deslich JM, Bennink JR, Yewdell JW (2006b) Tight linkage between translation and MHC class I peptide ligand generation implies specialized antigen processing for defective ribosomal products. *J Immunol* **177:** 227-233

Rammensee H, Bachmann J, Emmerich NP, Bachor OA, Stevanovic S (1999) SYFPEITHI: database for MHC ligands and peptide motifs. *Immunogenetics* **50:** 213-219

Rammensee HG, Falk K, Rotzschke O (1993) Peptides naturally presented by MHC class I molecules. *Annu Rev Immunol* **11:** 213-244

Rao M, Rothwell SW, Wassef NM, Pagano RE, Alving CR (1997) Visualization of peptides derived from liposome-encapsulated proteins in the trans-Golgi area of macrophages. *Immunol Lett* **59:** 99-105

Realini C, Rogers SW, Rechsteiner M (1994) KEKE motifs. Proposed roles in protein-protein association and presentation of peptides by MHC class I receptors. *FEBS Lett* **348:** 109-113

Reay PA, Matsui K, Haase K, Wulfing C, Chien YH, Davis MM (2000) Determination of the relationship between T cell responsiveness and the number of MHC-peptide complexes using specific monoclonal antibodies. *J Immunol* **164:** 5626-5634

Rechsteiner M, Realini C, Ustrell V (2000) The proteasome activator 11 S REG (PA28) and class I antigen presentation. *Biochem J* **345 Pt 1:** 1-15

Reits E, Griekspoor A, Neijssen J, Groothuis T, Jalink K, van Veelen P, Janssen H, Calafat J, Drijfhout JW, Neefjes J (2003) Peptide diffusion, protection, and degradation in nuclear and cytoplasmic compartments before antigen presentation by MHC class I. *Immunity* **18:** 97-108

Reits E, Neijssen J, Herberts C, Benckhuijsen W, Janssen L, Drijfhout JW, Neefjes J (2004) A major role for TPPII in trimming proteasomal degradation products for MHC class I antigen presentation. *Immunity* **20:** 495-506

Reits EA, Benham AM, Plougastel B, Neefjes J, Trowsdale J (1997) Dynamics of proteasome distribution in living cells. *EMBO J* **16:** 6087-6094

Reits EA, Griekspoor AC, Neefjes J (2000a) How does TAP pump peptides? insights from DNA repair and traffic ATPases. *Immunol Today* **21:** 598-600

Reits EA, Vos JC, Gromme M, Neefjes J (2000b) The major substrates for TAP in vivo are derived from newly synthesized proteins. *Nature* **404:** 774-778

Riese RJ, Chapman HA (2000) Cathepsins and compartmentalization in antigen presentation. *Curr Opin Immunol* **12:** 107-113

Rock KL, Rothstein L, Gamble S, Fleischacker C (1993) Characterization of antigen-presenting cells that present exogenous antigens in association with class I MHC molecules. *J Immunol* **150:** 438-446

Rock KL, York IA, Saric T, Goldberg AL (2002) Protein degradation and the generation of MHC class I-presented peptides. *Adv Immunol* **80:** 1-70

Rockel B, Peters J, Muller SA, Seyit G, Ringler P, Hegerl R, Glaeser RM, Baumeister W (2005) Molecular architecture and assembly mechanism of Drosophila tripeptidyl peptidase II. *Proc Natl Acad Sci U S A* **102:** 10135-10140

Roelse J, Gromme M, Momburg F, Hammerling G, Neefjes J (1994) Trimming of TAP-translocated peptides in the endoplasmic reticulum and in the cytosol during recycling. *J Exp Med* **180:** 1591-1597

Roepstorff P, Fohlman J (1984) Proposal for a common nomenclature for sequence ions in mass spectra of peptides. *Biomed Mass Spectrom* **11**:601.

Roitt IM (1990) *Immunologie*, Paris: Pradel.

Romagnani S (1999) Th1/Th2 cells. *Inflamm Bowel Dis* **5:** 285-294

Ross PL, Huang YN, Marchese JN, Williamson B, Parker K, Hattan S, Khainovski N, Pillai S, Dey S, Daniels S, Purkayastha S, Juhasz P, Martin S, Bartlet-Jones M, He F, Jacobson A, Pappin DJ (2004) Multiplexed protein quantitation in Saccharomyces cerevisiae using amine-reactive isobaric tagging reagents. *Mol Cell Proteomics* **3:** 1154-1169

Rotzschke O, Falk K (1991) Naturally-occurring peptide antigens derived from the MHC class-I-restricted processing pathway. *Immunol Today* **12:** 447-455

Rotzschke O, Falk K, Stevanovic S, Jung G, Walden P, Rammensee HG (1991) Exact prediction of a natural T cell epitope. *Eur J Immunol* **21:** 2891-2894

Rudensky A, Preston-Hurlburt P, Hong SC, Barlow A, Janeway CA, Jr. (1991) Sequence analysis of peptides bound to MHC class II molecules. *Nature* **353:** 622-627

Rudolph MG, Stanfield RL, Wilson IA (2006) How TCRs bind MHCs, peptides, and coreceptors. *Annu Rev Immunol* **24:** 419-466

Ruppert J, Sidney J, Celis E, Kubo RT, Grey HM, Sette A (1993) Prominent role of secondary anchor residues in peptide binding to HLA-A2.1 molecules. *Cell* **74:** 929-937

Sarbassov DD, Ali SM, Sengupta S, Sheen JH, Hsu PP, Bagley AF, Markhard AL, Sabatini DM (2006) Prolonged rapamycin treatment inhibits mTORC2 assembly and Akt/PKB. *Mol Cell* **22:** 159-168

Saric T, Chang SC, Hattori A, York IA, Markant S, Rock KL, Tsujimoto M, Goldberg AL (2002) An IFN-gamma-induced aminopeptidase in the ER, ERAP1, trims precursors to MHC class I-presented peptides. *Nat Immunol* **3:** 1169-1176

Scheffner M, Nuber U, Huibregtse JM (1995) Protein ubiquitination involving an E1-E2-E3 enzyme ubiquitin thioester cascade. *Nature* **373:** 81-83

Schmid D, Munz C (2007) Innate and adaptive immunity through autophagy. *Immunity* **27:** 11-21

Schmidt A, Kellermann J, Lottspeich F (2005) A novel strategy for quantitative proteomics using isotope-coded protein labels. *Proteomics* **5:** 4-15

Schmitz A, Herrgen H, Winkeler A, Herzog V (2000) Cholera toxin is exported from microsomes by the Sec61p complex. *J Cell Biol* **148:** 1203-1212

Schmitz A, Maintz M, Kehle T, Herzog V (1995) In vivo iodination of a misfolded proinsulin reveals co-localized signals for Bip binding and for degradation in the ER. *EMBO J* **14:** 1091-1098

Schubert U, Anton LC, Gibbs J, Norbury CC, Yewdell JW, Bennink JR (2000) Rapid degradation of a large fraction of newly synthesized proteins by proteasomes. *Nature* **404:** 770-774

Schumacher TN, Kantesaria DV, Heemels MT, Ashton-Rickardt PG, Shepherd JC, Fruh K, Yang Y, Peterson PA, Tonegawa S, Ploegh HL (1994) Peptide length and sequence specificity of the mouse TAP1/TAP2 translocator. *J Exp Med* **179:** 533-540

Schwab SR, Li KC, Kang C, Shastri N (2003) Constitutive display of cryptic translation products by MHC class I molecules. *Science* **301:** 1367-1371

Schwab SR, Shugart JA, Horng T, Malarkannan S, Shastri N (2004) Unanticipated antigens: translation initiation at CUG with leucine. *PLoS Biol* **2:** e366

Seifert U, Bialy LP, Ebstein F, Bech-Otschir D, Voigt A, Schroter F, Prozorovski T, Lange N, Steffen J, Rieger M, Kuckelkorn U, Aktas O, Kloetzel PM, Kruger E (2010) Immunoproteasomes preserve protein homeostasis upon interferon-induced oxidative stress. *Cell* **142:** 613-624

Selby M, Erickson A, Dong C, Cooper S, Parham P, Houghton M, Walker CM (1999) Hepatitis C virus envelope glycoprotein E1 originates in the endoplasmic reticulum and requires cytoplasmic processing for presentation by class I MHC molecules. *J Immunol* **162:** 669-676

Serwold T, Gonzalez F, Kim J, Jacob R, Shastri N (2002) ERAAP customizes peptides for MHC class I molecules in the endoplasmic reticulum. *Nature* **419:** 480-483

Sette A, Rappuoli R (2010) Reverse vaccinology: developing vaccines in the era of genomics. *Immunity* **33:** 530-541

Sha Z, Brill LM, Cabrera R, Kleifeld O, Scheliga JS, Glickman MH, Chang EC, Wolf DA (2009) The eIF3 interactome reveals the translasome, a supercomplex linking protein synthesis and degradation machineries. *Mol Cell* **36:** 141-152

Shamu CE, Flierman D, Ploegh HL, Rapoport TA, Chau V (2001) Polyubiquitination is required for US11-dependent movement of MHC class I heavy chain from endoplasmic reticulum into cytosol. *Mol Biol Cell* **12:** 2546-2555

Shastri N, Nguyen V, Gonzalez F (1995) Major histocompatibility class I molecules can present cryptic translation products to T-cells. *J Biol Chem* **270:** 1088-1091

Shastri N, Schwab S, Serwold T (2002) Producing nature's gene-chips: the generation of peptides for display by MHC class I molecules. *Annu Rev Immunol* **20:** 463-493

Shen L, Sigal LJ, Boes M, Rock KL (2004) Important role of cathepsin S in generating peptides for TAP-independent MHC class I crosspresentation in vivo. *Immunity* **21:** 155-165

Shen Z, Reznikoff G, Dranoff G, Rock KL (1997) Cloned dendritic cells can present exogenous antigens on both MHC class I and class II molecules. *J Immunol* **158:** 2723-2730

Shepherd JC, Schumacher TN, Ashton-Rickardt PG, Imaeda S, Ploegh HL, Janeway CA, Jr., Tonegawa S (1993) TAP1-dependent peptide translocation in vitro is ATP dependent and peptide selective. *Cell* **74:** 577-584

Shi GP, Villadangos JA, Dranoff G, Small C, Gu L, Haley KJ, Riese R, Ploegh HL, Chapman HA (1999) Cathepsin S required for normal MHC class II peptide loading and germinal center development. *Immunity* **10:** 197-206

Shimonkevitz R, Kappler J, Marrack P, Grey H (1983) Antigen recognition by H-2-restricted T cells. I. Cell-free antigen processing. *J Exp Med* **158:** 303-316

Shin JS, Ebersold M, Pypaert M, Delamarre L, Hartley A, Mellman I (2006) Surface expression of MHC class II in dendritic cells is controlled by regulated ubiquitination. *Nature* **444:** 115-118

Sijts EJ, Kloetzel PM (2011) The role of the proteasome in the generation of MHC class I ligands and immune responses. *Cell Mol Life Sci*

Silverstein AM (1995) From the forehead of Zeus: the ontogeny of the immune response. *Eye (Lond)* **9 (Pt 2):** 147-151

Skipper JC, Hendrickson RC, Gulden PH, Brichard V, Van Pel A, Chen Y, Shabanowitz J, Wolfel T, Slingluff CL, Jr., Boon T, Hunt DF, Engelhard VH (1996) An HLA-A2-restricted tyrosinase antigen on melanoma cells results from posttranslational modification and suggests a novel pathway for processing of membrane proteins. *J Exp Med* **183:** 527-534

Slev PR, Nelson AC, Potts WK (2006) Sensory neurons with MHC-like peptide binding properties: disease consequences. *Curr Opin Immunol* **18:** 608-616

Solheim JC, Carreno BM, Smith JD, Gorka J, Myers NB, Wen Z, Martinko JM, Lee DR, Hansen TH (1993) Binding of peptides lacking consensus anchor residue alters H-2Ld serologic recognition. *J Immunol* **151:** 5387-5397

Sprent J, Surh CD (2002) T cell memory. *Annu Rev Immunol* **20:** 551-579

Stark C, Breitkreutz BJ, Chatr-Aryamontri A, Boucher L, Oughtred R, Livstone MS, Nixon J, Van Auken K, Wang X, Shi X, Reguly T, Rust JM, Winter A, Dolinski K, Tyers M (2011) The BioGRID Interaction Database: 2011 update. *Nucleic Acids Res* **39:** D698-704

Starr TK, Jameson SC, Hogquist KA (2003) Positive and negative selection of T cells. *Annu Rev Immunol* **21:** 139-176

Steen H, Mann M (2004) The ABC's (and XYZ's) of peptide sequencing. *Nat Rev Mol Cell Biol* **5:** 699-711

Steinman RM, Witmer MD (1978) Lymphoid dendritic cells are potent stimulators of the primary mixed leukocyte reaction in mice. *Proc Natl Acad Sci U S A* **75:** 5132-5136

Stern LJ (2007) Characterizing MHC-associated peptides by mass spectrometry. *J Immunol* **179:** 2667-2668

Stickel JS, Weinzierl AO, Hillen N, Drews O, Schuler MM, Hennenlotter J, Wernet D, Muller CA, Stenzl A, Rammensee HG, Stevanovic S (2009) HLA ligand profiles of primary renal cell carcinoma maintained in metastases. *Cancer Immunol Immunother* **58:** 1407-1417

Storkus WJ, Zeh HJ, 3rd, Salter RD, Lotze MT (1993) Identification of T-cell epitopes: rapid isolation of class I-presented peptides from viable cells by mild acid elution. *J Immunother Emphasis Tumor Immunol* **14:** 94-103

Sun Y, Sijts AJ, Song M, Janek K, Nussbaum AK, Kral S, Schirle M, Stevanovic S, Paschen A, Schild H, Kloetzel PM, Schadendorf D (2002) Expression of the proteasome activator PA28 rescues the presentation of a cytotoxic T lymphocyte epitope on melanoma cells. *Cancer Res* **62:** 2875-2882

Suri A, Walters JJ, Levisetti MG, Gross ML, Unanue ER (2006) Identification of naturally processed peptides bound to the class I MHC molecule H-2Kd of normal and TAP-deficient cells. *Eur J Immunol* **36:** 544-557

Suzuki T, Park H, Lennarz WJ (2002) Cytoplasmic peptide:N-glycanase (PNGase) in eukaryotic cells: occurrence, primary structure, and potential functions. *FASEB J* **16:** 635-641

Sykulev Y, Joo M, Vturina I, Tsomides TJ, Eisen HN (1996) Evidence that a single peptide-MHC complex on a target cell can elicit a cytolytic T cell response. *Immunity* **4:** 565-571

Szklarczyk D, Franceschini A, Kuhn M, Simonovic M, Roth A, Minguez P, Doerks T, Stark M, Muller J, Bork P, Jensen LJ, von Mering C (2011) The STRING database in 2011: functional interaction networks of proteins, globally integrated and scored. *Nucleic Acids Res* **39:** D561-568

t Hoen PA, Ariyurek Y, Thygesen HH, Vreugdenhil E, Vossen RH, de Menezes RX, Boer JM, van Ommen GJ, den Dunnen JT (2008) Deep sequencing-based expression analysis shows major advances in robustness, resolution and inter-lab portability over five microarray platforms. *Nucleic Acids Res* **36:** e141

Tabaska JE, Zhang MQ (1999) Detection of polyadenylation signals in human DNA sequences. *Gene* **231:** 77-86

Tanahashi N, Murakami Y, Minami Y, Shimbara N, Hendil KB, Tanaka K (2000) Hybrid proteasomes. Induction by interferon-gamma and contribution to ATP-dependent proteolysis. *J Biol Chem* **275:** 14336-14345

Taniguchi Y, Choi PJ, Li GW, Chen H, Babu M, Hearn J, Emili A, Xie XS (2010) Quantifying E. coli proteome and transcriptome with single-molecule sensitivity in single cells. *Science* **329:** 533-538

Tobery TW, Siliciano RF (1997) Targeting of HIV-1 antigens for rapid intracellular degradation enhances cytotoxic T lymphocyte (CTL) recognition and the induction of de novo CTL responses in vivo after immunization. *J Exp Med* **185:** 909-920

Todd DJ, Lee AH, Glimcher LH (2008) The endoplasmic reticulum stress response in immunity and autoimmunity. *Nat Rev Immunol* **8:** 663-674

Toes RE, Nussbaum AK, Degermann S, Schirle M, Emmerich NP, Kraft M, Laplace C, Zwinderman A, Dick TP, Muller J, Schonfisch B, Schmid C, Fehling HJ, Stevanovic S, Rammensee HG, Schild H (2001) Discrete cleavage motifs of constitutive and immunoproteasomes revealed by quantitative analysis of cleavage products. *J Exp Med* **194:** 1-12

Torabi-Pour N, Nouri AM, Saffie R, Oliver RT (2002) Comparative study between direct mild acid extraction and immunobead purification technique for isolation of HLA class I-associated peptides. *Urol Int* **68:** 38-43

Touret N, Paroutis P, Terebiznik M, Harrison RE, Trombetta S, Pypaert M, Chow A, Jiang A, Shaw J, Yip C, Moore HP, van der Wel N, Houben D, Peters PJ, de Chastellier C, Mellman I, Grinstein S (2005) Quantitative and dynamic assessment of the contribution of the ER to phagosome formation. *Cell* **123:** 157-170

Townsend A, Bastin J, Gould K, Brownlee G, Andrew M, Coupar B, Boyle D, Chan S, Smith G (1988) Defective presentation to class I-restricted cytotoxic T lymphocytes in vaccinia-infected cells is overcome by enhanced degradation of antigen. *J Exp Med* **168:** 1211-1224

Townsend AR, Bastin J, Gould K, Brownlee GG (1986a) Cytotoxic T lymphocytes recognize influenza haemagglutinin that lacks a signal sequence. *Nature* **324:** 575-577

Townsend AR, Gotch FM, Davey J (1985) Cytotoxic T cells recognize fragments of the influenza nucleoprotein. *Cell* **42:** 457-467

Townsend AR, Rothbard J, Gotch FM, Bahadur G, Wraith D, McMichael AJ (1986b) The epitopes of influenza nucleoprotein recognized by cytotoxic T lymphocytes can be defined with short synthetic peptides. *Cell* **44:** 959-968

Trombetta ES, Parodi AJ (2003) Quality control and protein folding in the secretory pathway. *Annu Rev Cell Dev Biol* **19:** 649-676

Tsai B, Ye Y, Rapoport TA (2002) Retro-translocation of proteins from the endoplasmic reticulum into the cytosol. *Nat Rev Mol Cell Biol* **3:** 246-255

Turzynski A, Mentlein R (1990) Prolyl aminopeptidase from rat brain and kidney. Action on peptides and identification as leucyl aminopeptidase. *Eur J Biochem* **190:** 509-515

Uenaka A, Ono T, Akisawa T, Wada H, Yasuda T, Nakayama E (1994) Identification of a unique antigen peptide pRL1 on BALB/c RL male 1 leukemia recognized by cytotoxic T lymphocytes and its relation to the Akt oncogene. *J Exp Med* **180:** 1599-1607

Vallejo AN, Davila E, Weyand CM, Goronzy JJ (2004) Biology of T lymphocytes. *Rheum Dis Clin North Am* **30:** 135-157

Van Bleek GM, Nathenson SG (1990) Isolation of an endogenously processed immunodominant viral peptide from the class I H-2Kb molecule. *Nature* **348:** 213-216

van Hall T, Sijts A, Camps M, Offringa R, Melief C, Kloetzel PM, Ossendorp F (2000) Differential influence on cytotoxic T lymphocyte epitope presentation by controlled expression of either proteasome immunosubunits or PA28. *J Exp Med* **192:** 483-494

van Ham SM, Tjin EP, Lillemeier BF, Gruneberg U, van Meijgaarden KE, Pastoors L, Verwoerd D, Tulp A, Canas B, Rahman D, Ottenhoff TH, Pappin DJ, Trowsdale J, Neefjes J (1997) HLA-DO is a negative modulator of HLA-DM-mediated MHC class II peptide loading. *Curr Biol* **7:** 950-957

Van Kaer L, Ashton-Rickardt PG, Eichelberger M, Gaczynska M, Nagashima K, Rock KL, Goldberg AL, Doherty PC, Tonegawa S (1994) Altered peptidase and viral-specific T cell response in LMP2 mutant mice. *Immunity* **1:** 533-541

van Niel G, Wubbolts R, Ten Broeke T, Buschow SI, Ossendorp FA, Melief CJ, Raposo G, van Balkom BW, Stoorvogel W (2006) Dendritic cells regulate exposure of MHC class II at their plasma membrane by oligoubiquitination. *Immunity* **25:** 885-894

Vembar SS, Brodsky JL (2008) One step at a time: endoplasmic reticulum-associated degradation. *Nat Rev Mol Cell Biol* **9:** 944-957

Venable JD, Wohlschlegel J, McClatchy DB, Park SK, Yates JR, 3rd (2007) Relative quantification of stable isotope labeled peptides using a linear ion trap-Orbitrap hybrid mass spectrometer. *Anal Chem* **79:** 3056-3064

Verma R, Aravind L, Oania R, McDonald WH, Yates JR, 3rd, Koonin EV, Deshaies RJ (2002) Role of Rpn11 metalloprotease in deubiquitination and degradation by the 26S proteasome. *Science* **298:** 611-615

Vigneron N, Stroobant V, Chapiro J, Ooms A, Degiovanni G, Morel S, van der Bruggen P, Boon T, Van den Eynde BJ (2004) An antigenic peptide produced by peptide splicing in the proteasome. *Science* **304:** 587-590

Visvader JE (2011) Cells of origin in cancer. *Nature* **469:** 314-322

Vogel C, Abreu Rde S, Ko D, Le SY, Shapiro BA, Burns SC, Sandhu D, Boutz DR, Marcotte EM, Penalva LO (2010) Sequence signatures and mRNA concentration can explain two-thirds of protein abundance variation in a human cell line. *Mol Syst Biol* **6:** 400

Voges D, Zwickl P, Baumeister W (1999) The 26S proteasome: a molecular machine designed for controlled proteolysis. *Annu Rev Biochem* **68:** 1015-1068

Vos JC, Reits EA, Wojcik-Jacobs E, Neefjes J (2000) Head-head/tail-tail relative orientation of the pore-forming domains of the heterodimeric ABC transporter TAP. *Curr Biol* **10:** 1-7

Vos JC, Spee P, Momburg F, Neefjes J (1999) Membrane topology and dimerization of the two subunits of the transporter associated with antigen processing reveal a three-domain structure. *J Immunol* **163:** 6679-6685

Wahl A, Schafer F, Bardet W, Hildebrand WH (2010) HLA class I molecules reflect an altered host proteome after influenza virus infection. *Hum Immunol* **71:** 14-22

Walter J, Urban J, Volkwein C, Sommer T (2001) Sec61p-independent degradation of the tail-anchored ER membrane protein Ubc6p. *EMBO J* **20:** 3124-3131

Wang JH, Reinherz EL (2002) Structural basis of T cell recognition of peptides bound to MHC molecules. *Mol Immunol* **38:** 1039-1049

Wang Q, Chang A (2003) Substrate recognition in ER-associated degradation mediated by Eps1, a member of the protein disulfide isomerase family. *EMBO J* **22:** 3792-3802

Ward JJ, McGuffin LJ, Bryson K, Buxton BF, Jones DT (2004) The DISOPRED server for the prediction of protein disorder. *Bioinformatics* **20:** 2138-2139

Warren EH, Vigneron NJ, Gavin MA, Coulie PG, Stroobant V, Dalet A, Tykodi SS, Xuereb SM, Mito JK, Riddell SR, Van den Eynde BJ (2006) An antigen produced by splicing of noncontiguous peptides in the reverse order. *Science* **313:** 1444-1447

Wearsch PA, Cresswell P (2007) Selective loading of high-affinity peptides onto major histocompatibility complex class I molecules by the tapasin-ERp57 heterodimer. *Nat Immunol* **8:** 873-881

Weinzierl AO, Lemmel C, Schoor O, Muller M, Kruger T, Wernet D, Hennenlotter J, Stenzl A, Klingel K, Rammensee HG, Stevanovic S (2007) Distorted relation between mRNA copy number and corresponding major histocompatibility complex ligand density on the cell surface. *Mol Cell Proteomics* **6:** 102-113

Werlen G, Hausmann B, Naeher D, Palmer E (2003) Signaling life and death in the thymus: timing is everything. *Science* **299:** 1859-1863

Wherry EJ, Golovina TN, Morrison SE, Sinnathamby G, McElhaugh MJ, Shockey DC, Eisenlohr LC (2006) Re-evaluating the generation of a "proteasome-independent" MHC class I-restricted CD8 T cell epitope. *J Immunol* **176:** 2249-2261

Wherry EJ, Puorro KA, Porgador A, Eisenlohr LC (1999) The induction of virus-specific CTL as a function of increasing epitope expression: responses rise steadily until excessively high levels of epitope are attained. *J Immunol* **163:** 3735-3745

Whitby FG, Masters EI, Kramer L, Knowlton JR, Yao Y, Wang CC, Hill CP (2000) Structural basis for the activation of 20S proteasomes by 11S regulators. *Nature* **408:** 115-120

Wolf PR, Ploegh HL (1995) Antigen presentation. DM exchange mechanism. *Nature* **376:** 464-465

Wong P, Pamer EG (2003) CD8 T cell responses to infectious pathogens. *Annu Rev Immunol* **21:** 29-70

Wouters BG, Koritzinsky M (2008) Hypoxia signalling through mTOR and the unfolded protein response in cancer. *Nat Rev Cancer* **8:** 851-864

Yachi PP, Ampudia J, Gascoigne NR, Zal T (2005) Nonstimulatory peptides contribute to antigen-induced CD8-T cell receptor interaction at the immunological synapse. *Nat Immunol* **6:** 785-792

Yachi PP, Lotz C, Ampudia J, Gascoigne NR (2007) T cell activation enhancement by endogenous pMHC acts for both weak and strong agonists but varies with differentiation state. *J Exp Med* **204:** 2747-2757

Yague J, Vazquez J, Lopez de Castro JA (2000) A post-translational modification of nuclear proteins, N(G),N(G)-dimethyl-Arg, found in a natural HLA class I peptide ligand. *Protein Sci* **9:** 2210-2217

Yang E, van Nimwegen E, Zavolan M, Rajewsky N, Schroeder M, Magnasco M, Darnell JE, Jr. (2003) Decay rates of human mRNAs: correlation with functional characteristics and sequence attributes. *Genome Res* **13:** 1863-1872

Yates JR, Cociorva D, Liao L, Zabrouskov V (2006) Performance of a linear ion trap-Orbitrap hybrid for peptide analysis. *Anal Chem* **78:** 493-500

Ye Y, Meyer HH, Rapoport TA (2003) Function of the p97-Ufd1-Npl4 complex in retrotranslocation from the ER to the cytosol: dual recognition of nonubiquitinated polypeptide segments and polyubiquitin chains. *J Cell Biol* **162:** 71-84

Ye Y, Shibata Y, Yun C, Ron D, Rapoport TA (2004) A membrane protein complex mediates retro-translocation from the ER lumen into the cytosol. *Nature* **429:** 841-847

Yen HC, Xu Q, Chou DM, Zhao Z, Elledge SJ (2008) Global protein stability profiling in mammalian cells. *Science* **322:** 918-923

Yewdell JW (2001) Not such a dismal science: the economics of protein synthesis, folding, degradation and antigen processing. *Trends Cell Biol* **11:** 294-297

Yewdell JW (2007) Plumbing the sources of endogenous MHC class I peptide ligands. *Curr Opin Immunol* **19:** 79-86

Yewdell JW, Anton LC, Bennink JR (1996) Defective ribosomal products (DRiPs): a major source of antigenic peptides for MHC class I molecules? *J Immunol* **157:** 1823-1826

Yewdell JW, Bennink JR, Mackett M, Lefrancois L, Lyles DS, Moss B (1986) Recognition of cloned vesicular stomatitis virus internal and external gene products by cytotoxic T lymphocytes. *J Exp Med* **163:** 1529-1538

Yewdell JW, Lacsina JR, Rechsteiner MC, Nicchitta CV (2011) Out with the old, in with the new? Comparing methods for measuring protein degradation. *Cell Biol Int* **35:** 457-462

Yewdell JW, Nicchitta CV (2006) The DRiP hypothesis decennial: support, controversy, refinement and extension. *Trends Immunol* **27:** 368-373

Yewdell JW, Reits E, Neefjes J (2003) Making sense of mass destruction: quantitating MHC class I antigen presentation. *Nat Rev Immunol* **3:** 952-961

York IA, Chang SC, Saric T, Keys JA, Favreau JM, Goldberg AL, Rock KL (2002) The ER aminopeptidase ERAP1 enhances or limits antigen presentation by trimming epitopes to 8-9 residues. *Nat Immunol* **3:** 1177-1184

Zamvil SS, Mitchell DJ, Moore AC, Kitamura K, Steinman L, Rothbard JB (1986) T-cell epitope of the autoantigen myelin basic protein that induces encephalomyelitis. *Nature* **324:** 258-260

Zarling AL, Ficarro SB, White FM, Shabanowitz J, Hunt DF, Engelhard VH (2000) Phosphorylated peptides are naturally processed and presented by major histocompatibility complex class I molecules in vivo. *J Exp Med* **192:** 1755-1762

Zarling AL, Polefrone JM, Evans AM, Mikesh LM, Shabanowitz J, Lewis ST, Engelhard VH, Hunt DF (2006) Identification of class I MHC-associated phosphopeptides as targets for cancer immunotherapy. *Proc Natl Acad Sci U S A* **103:** 14889-14894

Zhang Y, Williams DB (2006) Assembly of MHC class I molecules within the endoplasmic reticulum. *Immunol Res* **35:** 151-162

Zuberi AR, Christianson GJ, Mendoza LM, Shastri N, Roopenian DC (1998) Positional cloning and molecular characterization of an immunodominant cytotoxic determinant of the mouse H3 minor histocompatibility complex. *Immunity* **9:** 687-698

ANNEXES

ANNEXE 1 - ARTICLE:

Identification of two distinct intracellular localization signals in STT3-B

Étienne Caron[a], Caroline Côté[a], Marc Parisien[b], François Major[a,b], and Claude Perreault[a]

Institute of Research in Immunology and Cancer [a], and Computer Science and Operations Research Department [b], University of Montreal, CP 6128, Downtown Station, Montreal, Quebec, Canada, H3C 3J7

Manuscript information: Abstract: 144 words
Total length: characters 26 909 (incl. spaces)
Materials and Methods: 474 words
Introduction, Results and Discussion section: 1 676 words

Running title: Structural differences between STT3 isoforms

*Corresponding authors:

Dr. Claude Perreault

Article publié dans: **Archives of Biochemistry and Biophysics, Volume 445, pages 108-114 (2006)**

Abstract

The STT3 subunit of the oligosaccharyltransferase (OT) complex plays a critical role in the *N*-glycosylation process. From *Arabidopsis thaliana* to *Homo sapiens*, two functional STT3 isoforms have been identified, STT3-A and STT3-B. We report that the last transmembrane (TM) segment of STT3-B corresponds to a topogenic determinant that is sufficient for proper integration and orientation of STT3-B C-terminal domain. Notably, the last TM segment of STT3-A and -B isoforms present major differences in amino acid sequence and predicted 3D-structure. We also identified a bipartite nuclear targeting sequence in the C-terminal tail of STT3-B that is absent in STT3-A. The latter sequence is sufficient to induce nucleolar localization of a reporter protein. Our results show that STT3-A and -B display two structural differences that may have a drastic influence on their function and might account for the remarkable evolutionary conservation of the two *STT3* paralogs.

Introduction

Asparagine-linked protein glycosylation is essential for the viability of all eukaryotic cells and is catalyzed by the OT complex (Yan and Lennarz, 2005). Since it has been found from *Campylobacter jejuni* to *Homo sapiens*, *N*-linked protein glycosylation is the most ubiquitous co-translational modification occurring in the endoplasmic reticulum (ER) (Wacker *et al*, 2002). STT3, the most conserved subunit in the OT complex, plays an essential role in substrate recognition (Nilsson *et al*, 2003; Yan and Lennarz, 2002). In addition to the core catalytic STT3 protein, other OT subunits have been identified in mammalian cells: ribophorin I, ribophorin II, OST48, DAD1, N33 and implantation-associated protein. Their yeast homologs are Ost1p, Swp1p, Wbp1p, Ost2p, Ost3p and Ost6p, respectively (Knauer and Lehle, 1999; Yan *et al*, 2005). Remarkably, two isoforms of the yeast STT3 protein have been identified in higher eukaryotes, STT3-A and STT3-B (Hong *et al*, 1996; Kelleher *et al*, 2003; McBride *et al*, 2002).

Human STT3-A and -B share more than 50% identity with yeast STT3. Both STT3-A and -B isoforms are polytopic ER membrane glycoproteins and contain in their C-terminal domain the active site that is essential for substrate binding and/or catalytic activity of OT (Nilsson *et al*, 2003; Yan *et al*, 2002). The fact that two *STT3* paralogs have been conserved from *Arabidopsis thaliana* to *Homo sapiens* strongly suggest that the isoforms they encode have some distinct properties. Thus, it was found that STT3-A and -B differentially modulate the enzymatic activity of the OT complex and are differentially expressed in various tissues and cell types (Kelleher *et al*, 2003). In addition, Koiwa *et al.* reported that STT3-A but not -B was necessary for cell cycle progression during salt/osmotic stress recovery in plant (Koiwa *et al*, 2003). Recently, a topological model for mouse STT3-A has been proposed through a series of *in vitro* and *in vivo* topology mapping assays (Kim *et al*, 2005). However, structural or topological comparison with mouse STT3-B has not been investigated. Therefore, the main objective of this work was to identify structural disparities between STT3-A and -B that could explain putative functional differences between these two STT3 isoforms. We report on two such disparities. First, we found major differences in the amino acid sequence and predicted 3D-structure of the last TM segment of STT3-A and -B isoforms. We showed that the

latter TM segment behaves as an independent topogenic determinant in STT3-B. Second, the C-terminal domain of STT3-B, but not STT3-A, contains a conserved bipartite nuclear localization signal (bNLS) from *D. melanogaster* to *H. sapiens*.

Materials and Methods

Plasmids

EGFP expression constructs described in this work were prepared using pEGFP-C1 (Clontech). To create EGFP-STT3-B truncated constructs, STT3-$B_{529-556}$, STT3-$B_{529-611}$, STT3-$B_{529-662}$, STT3-$B_{529-714}$, STT3-$B_{529-775}$ STT3-$B_{529-823}$ coding sequences were PCR-amplified from pcDNA3-STT3-B and cloned in-frame to the carboxy-terminal sequence of the EGFP in the pEGFP-C1 vector (Clontech) using the EcoRI/BamHI cloning sites. Specific primers were used to perform PCR amplification using PfuUltra High-Fidelity DNA Polymerase (Stratagene) (5'-GGAATTCCCCCAACATCA-AAGCATTG-3' as sense primer and the following as antisense primers: 5'CGGGATCCTTGCTTGTGACCCACGTGCA-3', 5'-CGGGATCCATGCCAGCAAT-CTGATAGC-3', 5'-CGGGATCCCTCCGAAAATAACCAACACA-3', 5'-CGGGA-TCCCATAAGGCAGTTTAACAGAG-3', 5'-CGGGATCCTGTTGTCAGGTGCTTTC-ACT-3' and 5'-CGGGATCCCGGTTCTCTCAAGGACTGC-3'). pDsRed2-ER (Clontech) was used for fluorescent labeling of the endoplasmic reticulum (Roderick *et al*, 1997).

Cell culture

Cells were maintained in DMEM supplemented with 10% FBS and antibiotics. Transient transfection was performed according to the manufacturer's instructions using FuGENE 6 transfection reagent (Roche) for HEK293 and COS-7 cells. Cells were chemically treated with tunicamycin (Sigma-Aldrich) at a concentration of 10ug/mL for 16h.

Immunoblotting

Cells were lysed in SDS sample buffer (62.5 mM Tris-HCl (pH 6.8), 2.3% SDS, 10% glycerol, 5% -mercaptoethanol, and 0.005% bromphenol blue). Proteins (10-50 µg) from whole cell lysates were separated by SDS-PAGE on 10% gels. Proteins were detected immunologically following electrotransfer onto nitrocellulose membranes (Amersham Biosciences, Inc.). Protein and molecular mass markers (Bio-Rad) were revealed by Ponceau red staining. Membranes were blocked in PBS containing 5% powdered milk and 0.05% Tween 20 for at least 1 h at 25 °C. Membranes were incubated overnight at 4 °C

with anti-GFP (Santa Cruz Biotechnologies) or anti-α-tubulin (Reseach Diagnostics) in blocking solution, and then with horseradish peroxidase-conjugated goat anti-mouse IgG for 1 h. The blots were visualized using the Amersham Biosciences ECL system.

Fluorescence and electron microscopy analysis

To analyze the sub-cellular distribution of EGFP-tagged proteins, transiently transfected cells on coverslips were fixed with 4% formaldehyde in PBS for 20 min at room temperature. Cells were then washed five times in PBS, mounted with Vectashield (Vector Laboratories Inc.) and analyzed under a Zeiss LSM 510 confocal microscope. For electron microscopy analyses, cells were collected in a pellet by centrifugation at 2000 g, fixed in 2.5% glutaraldehyde in 0.1M cacodylate buffer for 1 h at 4°C, postfixed in 1% osmium acid and embedded in epon. Lead citrate stained thin sections were examined under a Hitachi H-7500 transmission electron microscope and photographs were taken with a Hamamatsu digital camera (model C4742-95).

Computer based sequence analysis

Multiple sequence alignment of STT3 was performed by the Vector NTI program (Invitrogen) and the internet Boxshade program (http://www.ch.embnet.org/software/BOX_form.html). NLS were predicted by the PROSITE database (http://www.expasy.org/tools/scanprosite) (Hulo *et al*, 2004; Sigrist *et al*, 2002). Topological model was performed by SOSUI (Hirokawa *et al*, 1998) and TOPO2 (http://www.sacs.ucsf.edu/TOPO2/). Structural 3D models were created with the LEAP module from the AMBER series 4.1. The main chain torsion angles were set to the mean ALA conformation in R-alpha-helices: phi = -63.1°; psi = -41.2° (Ballesteros *et al*, 2000).

Results and discussion

Phylogenic analysis of STT3 isoforms

Genomic analysis revealed that two STT3 isoforms, STT3-A and -B, are conserved from *Arabidopsis thaliana* to *Homo sapiens* (Figure 1A and data not shown). In our search for significant discrepancies between STT3 isoforms, we focused on the C-terminal portion of these molecules (corresponding to residues 530 to 826 of human STT3-B) because it contains OT active site (Nilsson *et al*, 2003; Yan *et al*, 2002). We postulated that biologically relevant differences between STT3-A and -B isoforms should be linked to amino acid stretches sharing two features: high interspecies residue identity among homologs of a given isoform (STT3-A or STT3-B), and low intraspecies residue identity between STT3-A and STT3-B isoforms. We found that two regions displayed these characteristics (Figure 1). For region #1, comparison of amino acid sequences in *D. melanogaster, M. musculus* and *H. sapiens* showed that the mean intraspecies residue identity between STT3-A and -B isoforms is only 22%. In contrast, the percentage of amino acid residue identity from *D. melanogaster* to *H. sapiens* is 61% for STT3-A and 83% for STT3-B. The topological models of STT3-A (Kim *et al*, 2005) and STT3-B (Figure 1B) predict that hydrophobic residues of region #1 belong to STT3 eleventh TM segment. Region #2, a lysine-rich region found at the C-terminus of STT3-B but not STT3-A isoforms, exhibits an average residue identity of 67% from *D. melanogaster* to *H. sapiens.* Search in the PROSITE database (Hulo *et al*, 2004; Sigrist *et al*, 2002) revealed that region #2 contains a bNLS signature (PROSITE 00015) (Figure 1).

The last TM segment of STT3-B has topogenic properties

Polytopic integral membrane proteins acquire proper transmembrane orientation through the action of discrete topogenic determinants encoded within TM segments and their flanking residues (Johnson and van Waes, 1999). Some but not all TM segments are integrated within the membrane independently. Thus, in the case of the Na^+,K^+-ATPase α subunit, TM5 and TM6 together failed to translocate and integrate into the membrane (Homareda *et al*, 1989). Also, the TM1 from the cystic fibrosis transmembrane conductance regulator (CFTR) translocated inefficiently through the ER membrane, whereas TM2 rescued the proper CFTR amino-terminus topology by an efficient and

specific signal sequence activity (Lu *et al*, 1998). We therefore asked whether STT3-B-TM11, which contains region #1, would show topogenic function. To this end, we tested by confocal microscopy the localization of two proteins in COS-7 cells: DsRed2-ER, an exogenous ER resident protein (see materials and methods), and a chimera created by fusion of mouse STT3-$B_{529-556}$ residues to the C-terminus of EGFP. We found that the putative last TM segment of STT3-B was sufficient to target EGFP to the ER (Figure 2). Two fluorescence patterns were found in cells transfected with EGFP-STT3-$B_{529-556}$. About 50% of the cells showed a typical reticular ER pattern, while the other cells showed juxtanuclear accumulation of ER tubules (Figure 2A). Cells transfected with the EGFP vector alone showed EGFP fluorescence throughout the cytoplasm (data not shown). The juxtanuclear ER structures were observed in transfected cells with EGFP-STT3-$B_{529-556}$ alone whereas neither EGFP nor DsRed2-ER was sufficient to induce such ER arrangement (data not shown). Electron microscopy studies showed that the juxtanuclear accretion of EGFP-STT3-$B_{529-556}$ was due to a bulky accumulation of anastomosing smooth ER tubules (Figure 2B). The same two patterns were observed in cells transfected with the whole STT3-B molecule coupled to EGFP or other tags (Caron *et al*, 2005). Bulky accumulation of ER tubules has been observed in mammalian cells overexpressing proteins that are anchored in the ER membrane by at least one TM segment (Ishihara *et al*, 1995; Li *et al*, 2003; Snapp *et al*, 2003). These results strongly suggest that TM11 of STT3-B is sufficient to target and translocate a reporter protein in the ER membrane. They therefore suggest that TM11 could function as a key topogenic determinant to properly orient the C-terminal domain of STT3-B in the ER lumen.

To gain further insight into the membrane topology of STT3-B-TM11, we used truncated constructs coding for different fragments of the C-terminal domain of mouse STT3-B (Figure 3A). Putative endogenous glycosylation sites in the C-terminal domain of STT3-B were used to determine the orientation of the growing polypeptide chain. Following transfection of COS-7 cells with EGFP-STT3-B truncated constructs (529-556, -611, -662, -714, -775, -823), cells were subjected or not to treatment with tunicamycin, a specific inhibitor of *N*-glycosylation. A mobility shift was specifically observed for constructs containing the glycosylation acceptor sites (Figure 3B). Thus, STT3-B reporter domain in the latter constructs was glycosylated. This leads us to infer that TM11 is

sufficient to orient the nascent C-terminal domain of STT3-B in the ER lumen. In addition, the intensities of the protein bands from cells treated with tunicamycin was greater than the corresponding bands from non-treated cells. Since N-linked glycans are necessary to allow efficient protein degradation (Helenius and Aebi, 2004), inhibition of the N-glycosylation process by tunicamycin might explain accumulation of chimeric proteins in treated cells. Together, these results demonstrate that the predicted last TM segment of STT3-B corresponds to an independent topogenic determinant sufficient for the targeting, translocation and integration of the nascent polypeptide chain into the ER membrane.

Kim *et al.* investigated the topology of mouse STT3-A using glycosylation mapping to determine the location of the N- and C-terminal ends of the protein and of the predicted loops (Kim *et al*, 2005). The topogenic model of STT3-A proposed by these authors is consistent with the concept that the last TM segment of STT3 homologs is involved in the orientation of their C-terminal domain in the ER lumen. The present work supports and extends these data by showing that TM11 is sufficient for integration of STT3-B into the ER membrane in the proper orientation, independently of TM1-10. The low identity level between the last TM segment of STT3-A and -B isoforms (Figure 1A) might significantly alter their respective topogenic properties. To determine whether differences in the primary structure might have an impact on their 3D structure, we use computational analysis to generate 3D models of the last TM segment of STT3-A and STT3-B. The key finding that emerged from overlapping of the two 3D models was that they presented a single major structural difference corresponding to the non-conservative Ala/Lys difference at their amino-terminus (Figure 4A). This significant difference is conserved in STT3-A (Ala) and STT3-B (Lys) isoforms from drosophila to human. The hydrophobic moment profile analysis of the 3D models (Figure 4 B,C) suggests that the charged side chain of LYS533 points away from the membrane and can thus interfere in signal sequence activity. It has been shown that mutating Lys to Ala residue improved the signal sequence activity of CFTR-TM1 (Lu *et al*, 1998). Thus, even if STT3-B-TM11 is sufficient for anchoring into the membrane, it would not be surprising to observe a more active integration of the corresponding TM segment from STT3-A. In addition, charges introduced into TM domains diminish their partitioning into the membrane, and TM

segment with charged residues remain associated with the translocon complex for extended periods of time (Do *et al*, 1996; Heinrich *et al*, 2000). Since STT3-B is prone to misfolding (Caron *et al*, 2005), the conserved Lys residue in TM11 might be instrumental in avoiding re-engagement of the translocating channel until the large C-terminal domain of STT3-B is properly folded.

Identification of a conserved nucleolar targeting signal at the C-terminus of STT3-B

Our bioinformatic analyses allowed us to identify a conserved bNLS signature (PROSITE 00015) within the lysine-rich region of STT3-B (region #2 in Figure 1). The significance of that bNLS signature was unclear since STT3-B is an ER membrane resident protein (Kelleher *et al*, 2003) and no STT3-B fragment has been found in the nucleolus of HeLa cells by mass spectrometry analyses (Andersen *et al*, 2005; Andersen *et al*, 2002). However, since this latter technique has technical limitations and has not been perform under a wide range of cellular conditions, we cannot exclude the possibility that STT3-B contains of a functional bNLS. To evaluate the functionality of this nuclear signal, we fused the lysine-rich region of mouse STT3-B (STT3-$B_{790-823}$) at the C-terminus of EGFP and followed the intracellular localization of the chimeric protein. While HEK293 cells transfected with EGFP alone show a cytoplasmic fluorescence pattern (data not shown), the chimeric EGFP-STT3-$B_{790-823}$ protein localized strictly into the nucleus, particularly in the nucleolus (Figure 5). Thus, the lysine-rich region of STT3-B is sufficient to allow nucleolar localization of a reporter protein. Our results are in accordance with bioinformatic analysis showing that nucleolar localization signals usually involve clustered basic amino acids that form bNLS (Hatanaka, 1990).

These data raise intriguing questions on the possible role of STT3-B in the nucleolus. Interestingly, ATF6, an ER membrane-anchored protein, is cleaved posttranslationally in response to cell stress, allowing one of its fragments to enter the nucleoplasm where it acts as a transcription factor (Ye *et al*, 2000). A similar process might lead to transfer of a C-terminal STT3-B fragment from the ER to the nucleolus. In response to cellular stress which leads to accumulation of unfolded proteins, the ER sends signals to downregulate protein translation (Harding *et al*, 2002). Because of its essential function in the *N*-glycosylation process, STT3-B is essential for protein folding in the ER

(Helenius *et al*, 2004). It is therefore tempting to speculate that STT3-B might contribute to the unfolded protein response by acting as a sensor protein that would coordinate ER folding function with ribosomal biosynthesis in the nucleolus (Moss and Stefanovsky, 2002). The absence of a bNLS at the C-terminus of STT3-A suggests that STT3-B would be the sole STT3 isoform able to transmit signals from the ER to the nucleolus.

In summary, we have identified two major conserved differences between STT3-A and STT3-B. The last TM segment of STT3-B has topogenic function and differs from its STT3-A counterpart in terms of primary and 3D-structure. In addition, the C-terminal domain of STT3-B but not STT3-A contains a functional bNLS. Further studies are needed to determine whether STT3-B can transmit signals from the ER to the nucleolus.

Acknowledgements

Grant 014271 (CP) from the National Cancer Institute of Canada supported this work. CP holds a Canada Research Chair in Immunobiology. FM is a Canadian Institutes of Health Research Investigator. We thank Christian Charbonneau and Renée Charbonneau for technical assistance.

References

Andersen JS, Lam YW, Leung AK, Ong SE, Lyon CE, Lamond AI, Mann M (2005) Nucleolar proteome dynamics. *Nature* **433:** 77-83.

Andersen JS, Lyon CE, Fox AH, Leung AK, Lam YW, Steen H, Mann M, Lamond AI (2002) Directed proteomic analysis of the human nucleolus. *Curr Biol* **12:** 1-11.

Ballesteros JA, Deupi X, Olivella M, Haaksma EE, Pardo L (2000) Serine and threonine residues bend alpha-helices in the chi(1) = g(-) conformation. *Biophys J* **79:** 2754-2760.

Caron E, Charbonneau R, Huppe G, Brochu S, Perreault C (2005) The structure and location of SIMP/STT3B account for its prominent imprint on the MHC I immunopeptidome. *Int Immunol* **17:** 1583-1596.

Do H, Falcone D, Lin J, Andrews DW, Johnson AE (1996) The cotranslational integration of membrane proteins into the phospholipid bilayer is a multistep process. *Cell* **85:** 369-378.

Harding HP, Calfon M, Urano F, Novoa I, Ron D (2002) Transcriptional and translational control in the Mammalian unfolded protein response. *Annu Rev Cell Dev Biol* **18:** 575-599.

Hatanaka M (1990) Discovery of the nucleolar targeting signal. *Bioessays* **12:** 143-148.

Heinrich SU, Mothes W, Brunner J, Rapoport TA (2000) The Sec61p complex mediates the integration of a membrane protein by allowing lipid partitioning of the transmembrane domain. *Cell* **102:** 233-244.

Helenius A, Aebi M (2004) Roles of N-linked glycans in the endoplasmic reticulum. *Annu Rev Biochem* **73:** 1019-1049.

Hirokawa T, Boon-Chieng S, Mitaku S (1998) SOSUI: classification and secondary structure prediction system for membrane proteins. *Bioinformatics* **14:** 378-379.

Homareda H, Kawakami K, Nagano K, Matsui H (1989) Location of signal sequences for membrane insertion of the Na+,K+-ATPase alpha subunit. *Mol Cell Biol* **9:** 5742-5745.

Hong G, Deleersnijder W, Kozak CA, Van Marck E, Tylzanowski P, Merregaert J (1996) Molecular cloning of a highly conserved mouse and human integral membrane protein (Itm1) and genetic mapping to mouse chromosome 9. *Genomics* **31:** 295-300.

Hulo N, Sigrist CJ, Le Saux V, Langendijk-Genevaux PS, Bordoli L, Gattiker A, De Castro E, Bucher P, Bairoch A (2004) Recent improvements to the PROSITE database. *Nucleic Acids Res* **32:** D134-137.

Ishihara N, Yamashina S, Sakaguchi M, Mihara K, Omura T (1995) Malfolded cytochrome P-450(M1) localized in unusual membrane structures of the endoplasmic reticulum in cultured animal cells. *J Biochem* **118:** 397-404.

Johnson AE, van Waes MA (1999) The translocon: a dynamic gateway at the ER membrane. *Annu Rev Cell Dev Biol* **15:** 799-842.

Kelleher DJ, Karaoglu D, Mandon EC, Gilmore R (2003) Oligosaccharyltransferase isoforms that contain different catalytic STT3 subunits have distinct enzymatic properties. *Mol Cell* **12:** 101-111.

Kim H, von Heijne G, Nilsson I (2005) Membrane topology of the STT3 subunit of the oligosaccharyl transferase complex. *J Biol Chem* **280:** 20261-20267.

Knauer R, Lehle L (1999) The oligosaccharyltransferase complex from yeast. *Biochim Biophys Acta* **1426:** 259-273.

Koiwa H, Li F, McCully MG, Mendoza I, Koizumi N, Manabe Y, Nakagawa Y, Zhu J, Rus A, Pardo JM, Bressan RA, Hasegawa PM (2003) The STT3a subunit isoform of the Arabidopsis oligosaccharyltransferase controls adaptive responses to salt/osmotic stress. *Plant Cell* **15:** 2273-2284.

Li Y, Dinsdale D, Glynn P (2003) Protein domains, catalytic activity, and subcellular distribution of neuropathy target esterase in Mammalian cells. *J Biol Chem* **278:** 8820-8825.

Lu Y, Xiong X, Helm A, Kimani K, Bragin A, Skach WR (1998) Co- and posttranslational translocation mechanisms direct cystic fibrosis transmembrane conductance regulator N terminus transmembrane assembly. *J Biol Chem* **273:** 568-576.

McBride K, Baron C, Picard S, Martin S, Boismenu D, Bell A, Bergeron J, Perreault C (2002) The model B6(dom1) minor histocompatibility antigen is encoded by a mouse homolog of the yeast STT3 gene. *Immunogenetics* **54:** 562-569.

Moss T, Stefanovsky VY (2002) At the center of eukaryotic life. *Cell* **109:** 545-548.

Nilsson I, Kelleher DJ, Miao Y, Shao Y, Kreibich G, Gilmore R, von Heijne G, Johnson AE (2003) Photocross-linking of nascent chains to the STT3 subunit of the oligosaccharyltransferase complex. *J Cell Biol* **161:** 715-725.

Roderick HL, Campbell AK, Llewellyn DH (1997) Nuclear localisation of calreticulin in vivo is enhanced by its interaction with glucocorticoid receptors. *FEBS Lett* **405:** 181-185.
Sayle RA, Milner-White EJ (1995) RASMOL: biomolecular graphics for all. *Trends Biochem Sci* **20:** 374.

Sigrist CJ, Cerutti L, Hulo N, Gattiker A, Falquet L, Pagni M, Bairoch A, Bucher P (2002) PROSITE: a documented database using patterns and profiles as motif descriptors. *Brief Bioinform* **3:** 265-274.

Snapp EL, Hegde RS, Francolini M, Lombardo F, Colombo S, Pedrazzini E, Borgese N, Lippincott-Schwartz J (2003) Formation of stacked ER cisternae by low affinity protein interactions. *J Cell Biol* **163:** 257-269.

Wacker M, Linton D, Hitchen PG, Nita-Lazar M, Haslam SM, North SJ, Panico M, Morris HR, Dell A, Wren BW, Aebi M (2002) N-linked glycosylation in Campylobacter jejuni and its functional transfer into E. coli. *Science* **298:** 1790-1793.

Yan A, Lennarz WJ (2005) Unraveling the mechanism of protein N-glycosylation. *J Biol Chem* **280:** 3121-3124.

Yan Q, Lennarz WJ (2002) Studies on the function of oligosaccharyl transferase subunits. Stt3p is directly involved in the glycosylation process. *J Biol Chem* **277:** 47692-47700.

Ye J, Rawson RB, Komuro R, Chen X, Dave UP, Prywes R, Brown MS, Goldstein JL (2000) ER stress induces cleavage of membrane-bound ATF6 by the same proteases that process SREBPs. *Mol Cell* **6:** 1355-1364.

Figure legends

Figure 1: **Bioinformatic analysis of STT3-A and -B.**

(**A**) Multiple sequence alignment of STT3 homologs from residue 530 to 826 of the human STT3-B sequence. STT3-B regions studied in this work are boxed. The conserved STT3-B bNLS are in green. (**B**) Proposed mouse STT3-B topology in the ER membrane. The model is based on SOSUI (Hirokawa *et al*, 1998) and TOPO2 (http://www.sacs.ucsf.edu/TOPO2/) prediction methods. The last predicted TM segment of mouse STT3-B (region #1; residues 529-556) and the lysine-rich region (region #2; residues 790-823) are in black. Putative *N*-glycosylation sites are in red.

Figure 2 : STT3-B$_{529-556}$ region anchors reporter protein in the ER and induces an abnormal ER arrangement.

(**A**) COS-7 cells were co-transfected with EGFP-STT3-B$_{529-556}$ and DsRed2-ER and studied by confocal microscopy 48 h post-transfection. Two fluorescence patterns were observed with approximately equal frequencies in transfected cells: diffuse reticular (upper row) and paranuclear (lower row). (**B**) Transmission electron microscopy showed that the paranuclear pattern was due to bulky accumulation of smooth ER tubules. Bar for A = 10 μm and for B = 500 nm.

Figure 3 : STT3-B$_{529-556}$ domain carries out a luminal orientation of the nascent C-terminal domain of STT3-B.

(**A**) Six EGFP-fusion constructs consisting of different portions of the STT3-B C-terminal domain (residues 529-556, 529-611, 529-662, 529-714, 529-775 and 529-823) were used to transfect COS-7 cells. The last TM segment of STT3-B (residues 529-556) is in black and Y signs represent predicted *N*-glycosylation sites. (**B**) COS-7 cells were transfected with the six types of EGFP-fusion constructs and treated or not with tunicamycin for 16h. Using anti-GFP monoclonal antibody, EGFP-fusion constructs were detected by immunobloting. α-tubulin was used as a control for the amount of protein loaded.

Figure 4

(**A**) Superimposition of the 3D model from the predicted last TM segment of mouse STT3-A and -B. Residues 456-477 from mouse STT3-A (V**A**SGMILVMAFFLITYTF**H**STW in green) and residues 532-553 from mouse STT3-B (I**K**SIVTMLMLMLLMMFAV**H**CTW in blue) are shown: small spheres correspond to the heavy atoms of the polar residue side chains, and large spheres to those of charged residues. The image was generated by the RasMol program (Sayle and Milner-White, 1995). Wheel representation of STT3-A (**B**) and STT3-B (**C**). Nonpolar residues are in yellow, polar in green, and basic in blue.

Figure 5: Identification of a functional bNLS in the C-terminal tail of STT3-B.

(**A**) The lysine-rich region of STT3-B (residues 790-823) was fused at the C-terminus of EGFP. The predicted bNLS is underlined. HEK293 cells were transfected for 48h with the EGFP-STT3-$B_{790\text{-}823}$ construct and imaged with fluorescence (**B,D**) and phase contrast (C,D). Bar = 10 μm.

Figure 1

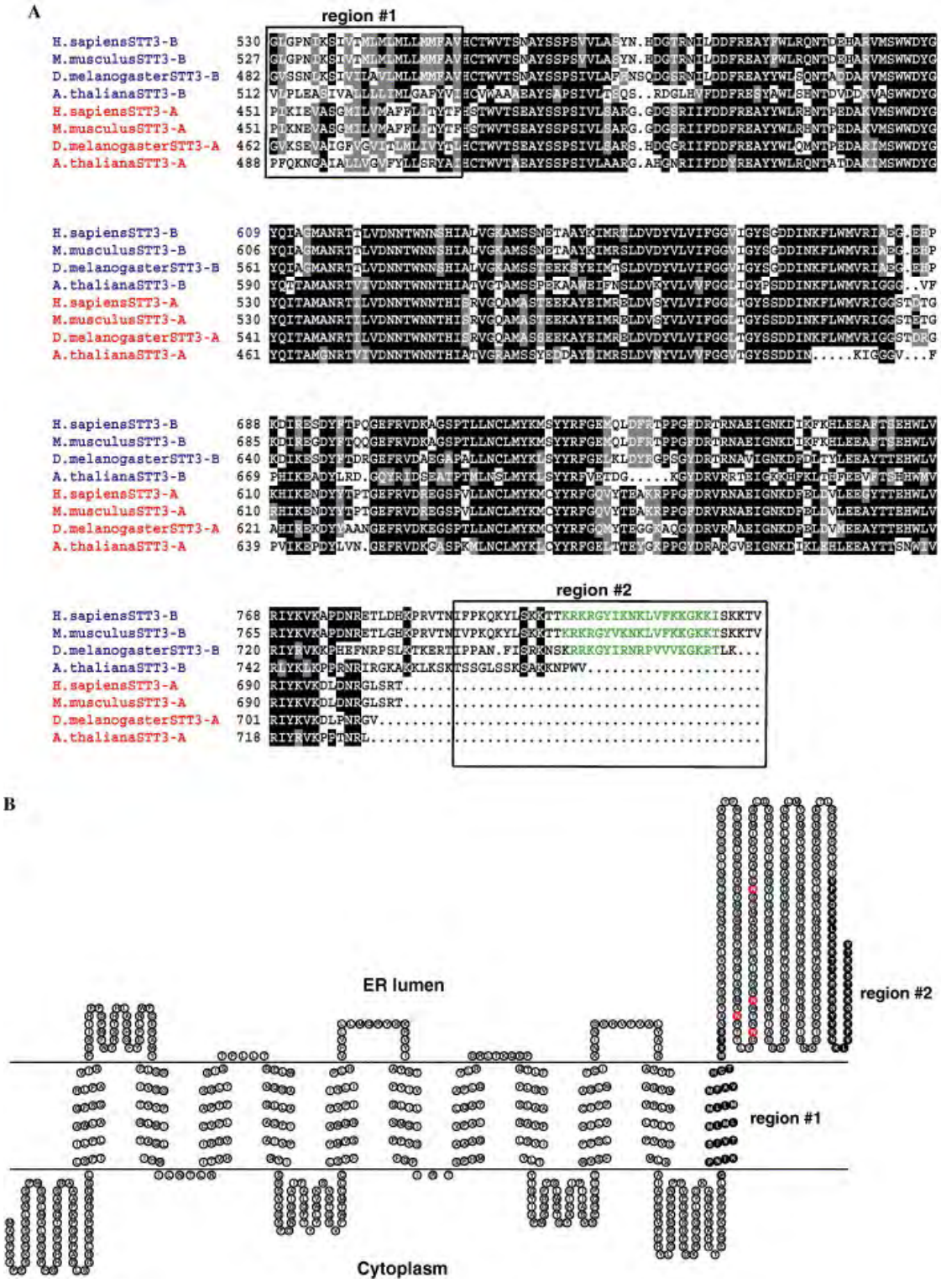
A
region #1
H.sapiensSTT3-B
M.musculusSTT3-B
D.melanogasterSTT3-B
A.thalianaSTT3-B
H.sapiensSTT3-A
M.musculusSTT3-A
D.melanogasterSTT3-A
A.thalianaSTT3-A
region #2
B
ER lumen
region #2
region #1
Cytoplasm

Figure 2

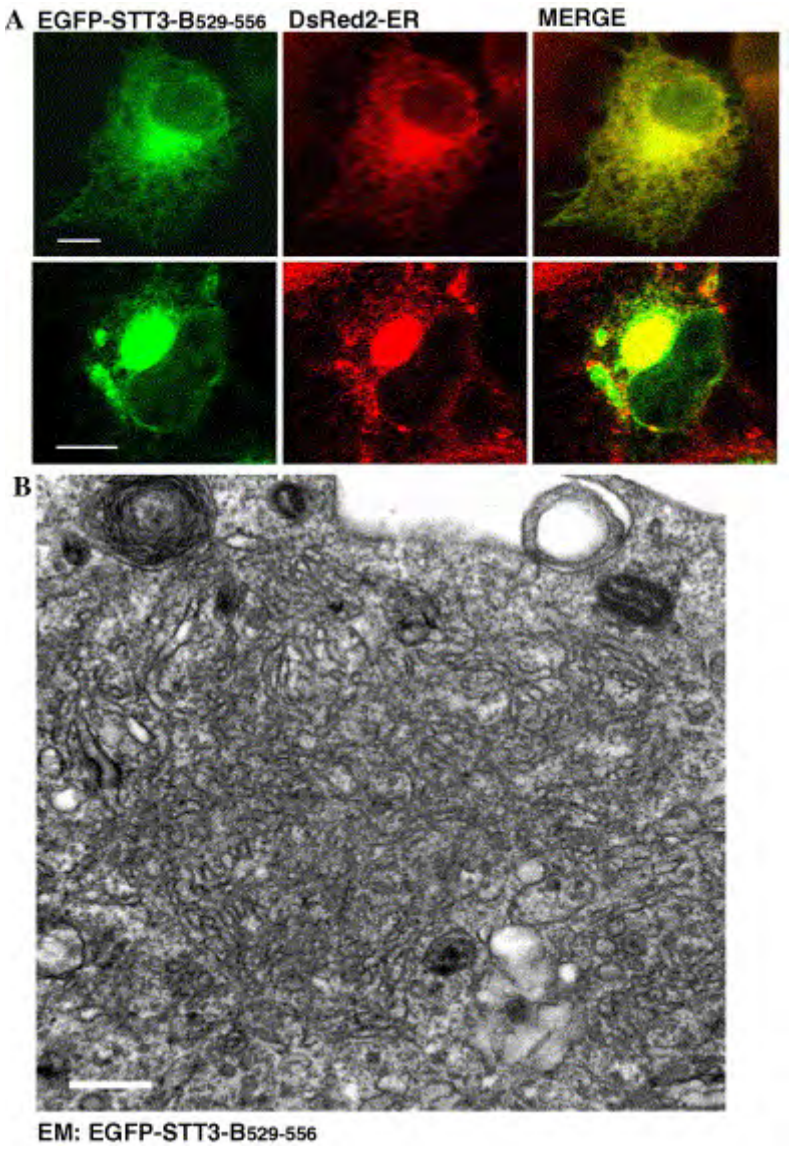

Figure 3

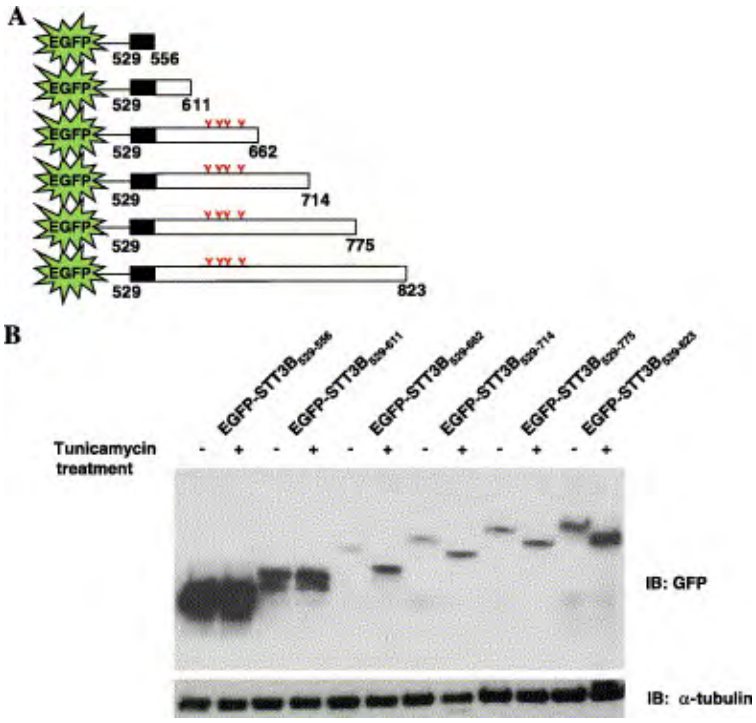
A
EGFP
529 556
EGFP
529 611
EGFP
529 662
EGFP
529 714
EGFP
529 775
EGFP
529 823
B
EGFP-STT3B529-556
EGFP-STT3B529-611
EGFP-STT3B529-662
EGFP-STT3B529-714
EGFP-STT3B529-775
EGFP-STT3B529-823
Tunicamycin treatment
- + - + - + - + - + - +
IB: GFP
IB: α-tubulin

Figure 4

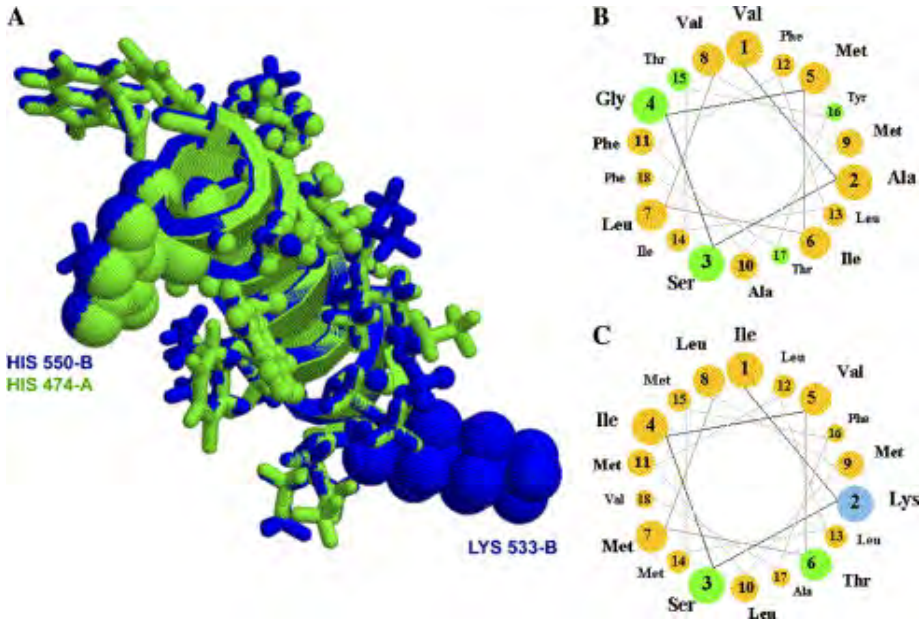
A
HIS 550-B
HIS 474-A
LYS 533-B
B
Val
Val
Phe
Met
Thr
Tyr
Gly
Met
Phe
Ala
Leu
Leu
Ile
Ile
Ser
Thr
Ala
C
Leu
Ile
Leu
Met
Val
Ile
Phe
Met
Met
Lys
Val
Leu
Met
Met
Thr
Ala
Ser
Leu

Figure 5

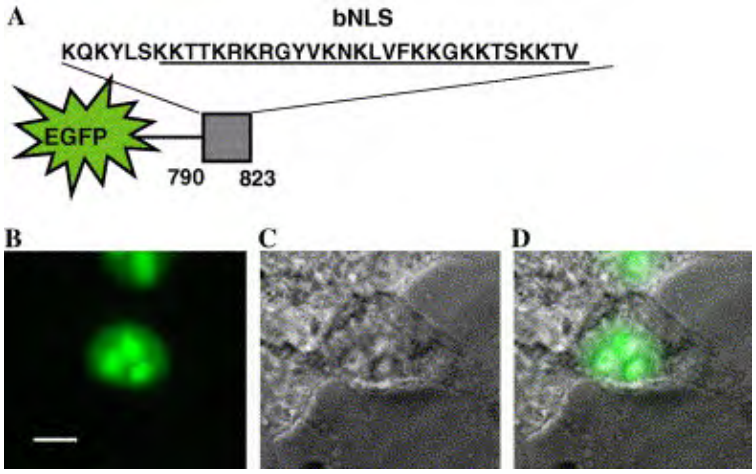
A
bNLS
KQKYLSKKTTKRKRGYVKNKLVFKKGKKTSKKTV
EGFP
790
823
B
C
D

ANNEXE 2-FIGURES:

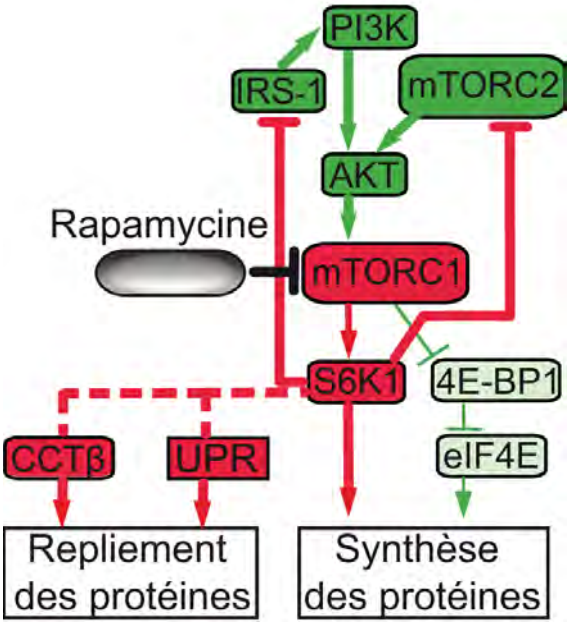

Figure 1. Modèle proposé sur l'effet de la rapamycine dans la signalisation mTOR des cellules EL4 (voir Chapitre 4, Figure 1D). La rapamycine pourrait affecter le repliement des protéines via l'inactivation de S6K1. Les flèches pointillées rouges indiquent l'inhibition hypothétique de CCTβ et de la réponse UPR.

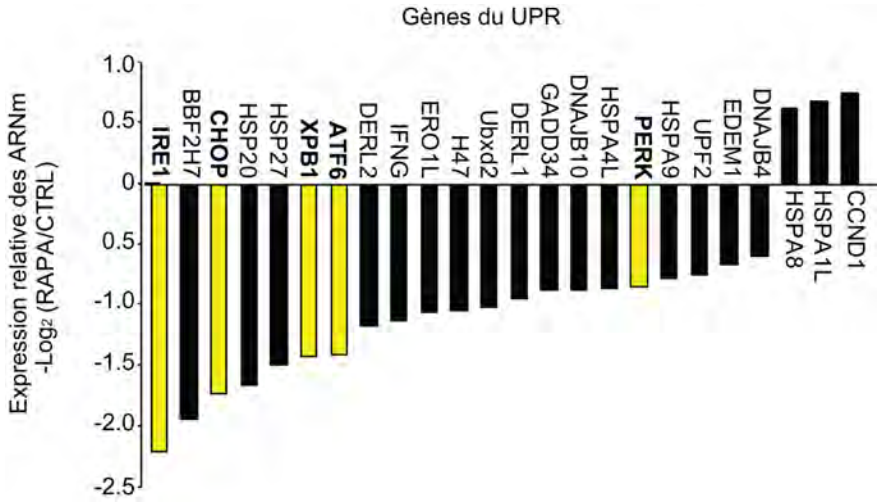

Figure 2. La majorité des gènes impliqués dans la réponse UPR sont sous-exprimés suivant le traitement des cellules à la rapamycine. Les cellules EL4 ont été traitées ou non à la rapamycine pendant 48 h. L'expression relative des ARNm a été obtenue par puces d'ADN. Les barres jaunes indiquent l'expression relative de cinq gènes clés impliqués dans la réponse UPR.